

COMPUSOFT

ENGINEERING

CTV Building

Non-Linear Time History Analysis (NLTHA) Report

Ref: 12026-00

SECOND (INCOMPLETE) DRAFT ISSUE

July 2012



Prepared for: Canterbury Earthquakes Royal Commission
Te Komihana Rūwhenua o Waitaha
PO Box 14053, Christchurch Airport,
Christchurch 8544



Document Control Record

Report Title		CTV Building Non-Linear Time History Analysis (NTHA) Report			
Document ID		12026-00	Project Number		12026
File Path		Z:\01 Projects current\12026 - CTVNL(extended) - RoyalCommission\Report\12026.00 Non-Linear Time History Analysis Report.docx			
Client		Canterbury Earthquakes Royal Commission	Client Contact		Professor Athol Carr
Report prepared by		Compusoft Engineering Limited PO Box 9493, Newmarket Auckland 1149 09 522 1456			
Rev	Date	Revision Details/Status	Author	Verifier	Approver
A	13 July 2012	Draft	DSB/TJS/NJB		BJD
B	24 July 2012	Draft	DSB/TJS/NJB		BJD
Current Revision		0			

Approval

Author Signature		Approver Signature	
Name	Derek Bradley Tony Stuart Dr. Nicholas Brooke	Name	Dr. Barry Davidson
Title	Structural Engineer	Title	Director

Limitations

This report has been prepared for Canterbury Earthquakes Royal Commission, and the findings presented within the report are for their sole use. The findings are not intended for use by other parties, and may not contain sufficient information for the purposes of other parties or other uses. The client will place no reliance on any draft reports, incomplete documents, and/or verbal advice.

Compusoft Engineering Limited undertakes professional services using a degree of care and skill normally exercised, under similar circumstances, by reputable consultants practicing in this field at the current time. No other warranty, expressed or implied, is made as to the professional advice presented in this report.

Contents

Document Control Record.....	i
Approval	i
Limitations.....	i
List of figures.....	iv
List of Tables.....	xvi
Executive Summary	1
Limitations of the Content of this Report.....	2
1. Introduction	3
2. Building description.....	4
3. Analysis Procedure Overview.....	7
3.1. Alterations Made from Previous (DBH) Analysis Model	7
3.2. Analysis Procedure	8
4. Material Properties.....	10
4.1. Concrete	10
4.2. Reinforcement	11
5. Structural Elements.....	13
5.1. Soil Structure Interaction	13
5.2. Foundation Elements	13
5.3. Reinforced Concrete Frames	15
5.3.1. Beams and beam hinges	15
5.3.2. Columns and column hinges	18
5.3.3. Beam-Column Joints	20
5.4. Reinforced Concrete Shear Walls	26
5.5. Floors	27
6. Loadings	30
6.1. Gravity Loadings	30
6.2. Dynamic Mass	31
7. Modal Analysis	33
8. Non-Linear Static (Pushover) Analysis	34
8.1. Methodology	34

8.2.	Force-Displacement Relationships	35
8.3.	Building Displacement Ductility Capacity.	39
9.	Non-linear Dynamic (Time History) Analysis	40
9.1.	Analysis Ground Motions	40
9.2.	Elastic Structural Damping	44
9.3.	Radiation Damping	46
10.	NLTHA Results : Darfield	48
10.1.	Drifts and Displacements	48
10.2.	Diaphragm Connection Forces.	49
10.3.	Inelastic Wall Demands.	54
10.4.	Inelastic Column Actions.	56
10.5.	Inelastic Beam-Column Joint Actions	60
11.	NLTHA Results : Lyttelton	66
11.1.	Drifts and Displacements	66
11.2.	Diaphragm Connection Forces.	68
11.3.	Inelastic Column Actions.	73
11.4.	Beam-Column Joints.	84
11.5.	Beam Bar Pullout.	118
12.	Vertical Earthquake Effects	119
12.1.	Axial Load Effects	119
13.	Conclusions	121
14.	Additional Work	122
15.	References	124
	List of appendices	127
Appendix A	Nonlinear analysis of diagonally reinforced coupling beams	130
Appendix B	Nonlinear analysis of columns with consideration of axial-moment (P-M) interaction	136
Appendix C	Development of a model for beam-column joints of the CTV building	137
Appendix D	Hook anchor capacity	153
Appendix E	Foundation Modelling Properties	155
Appendix F	Acceleration Time History Records.	156

Appendix G	Analysis Results - Darfield Event: CBGS Record	163
Appendix H	Analysis Results - Darfield Event: CCCC Record	178
Appendix I	Analysis Results - Lyttelton Aftershock: CBGS record	194
Appendix J	Analysis Results - Lyttelton Aftershock: CCCC record	217
Appendix K	Analysis Results - Lyttelton Aftershock: CHHC record	242
Appendix L	Analysis Results - Lyttelton Aftershock: REHS record	257

List of figures

Figure 1: Overall view of the CTV structural model (viewed from SW & SE respectively)	5
Figure 2: CTV structural model viewed from the east (slabs omitted for clarity)	5
Figure 3: CTV foundation arrangement viewed from the south-west	6
Figure 4: Building grid system.	6
Figure 5: Time history analysis sequence	9
Figure 6: Concrete stress-strain curve	11
Figure 7: Reinforcing steel stress-strain curve	12
Figure 8: CTV foundation element location plan (Design Engineer 1986a)	14
Figure 9: Typical moment-curvature relationship for beam hinges	17
Figure 10: Reinforcement anchorage in Grid A beam column joint zone (Design Engineer 1986a)	17
Figure 11: Typical bottom reinforcement anchorage in interior beam column joint zone (Design Engineer 1986a)	17
Figure 12: Effective column stiffness relationship	18
Figure 13: Typical column reinforcement. (Design Engineer 1986a)	19
Figure 14: Column at GL 4 D/E (C18) to wall connection detailing at roof level (Design Engineer 1986a)	20
Figure 15: Joint response backbone curve for joint at grid A2, level 3 (exterior E/W, interior N/S)	21
Figure 16: Effective wall stiffness relationship	26
Figure 17: South shear wall typical coupling beam reinforcement arrangement (Design Engineer 1986a)	27
Figure 18: Seismic mass distribution	32
Figure 19: Site spectral displacements.	34

Figure 27: Force-displacement relationship.....	35
Figure 28: Base shear components - east/west direction.....	36
Figure 29: Base shear components - north/south direction.....	36
Figure 30: Level 6 western pushover displacement profile.....	37
Figure 31: Level 6 eastern pushover displacement profile.....	38
Figure 32: Level 6 northern pushover displacement profile.....	38
Figure 33: Level 6 southern pushover displacement profile.....	39
Figure 34: Bi-linear pushover plots.....	39
Figure 20: Darfield N00E 5% damped response spectra (north/south).....	42
Figure 21: Darfield N90E 5% damped response spectra (east/west).....	42
Figure 22: Darfield Vertical 5% damped response spectra.....	42
Figure 23: Lyttelton N00E 5% damped response spectra (north/south).....	43
Figure 24: Lyttelton N90E 5% damped response spectra (east/west).....	43
Figure 25: Lyttelton Vertical 5% damped response spectra.....	43
Figure 26: Equivalent viscous damping vs structure period - Lyttelton.....	46
Figure 35: Frame A north/south storey drifts - Darfield.....	48
Figure 36: Frame F north/south storey drifts - Darfield.....	48
Figure 37: Frame 1 east/west storey drifts - Darfield.....	49
Figure 38: Frame 4 east/west storey drifts - Darfield.....	49
Figure 39: Slab 4 C-C/D section cut line.....	53
Figure 40: Column F3, Level 4 top hinge rotation and elongation vs time, CBGS, Darfield.....	57
Figure 41: Column F3 Level 4 upper hinge strain vs time, CBGS, Darfield.....	57
Figure 42: Column F3 Level 4 upper hinge axial and moments vs time, CBGS, Darfield.....	58
Figure 43: Column F3 Level 4 upper hinge moment axial relationship, CBGS, Darfield.....	58
Figure 44: Column F3 Level 4 upper hinge hysteretic form, CBGS, Darfield.....	59
Figure 45: Column F3 Level 4 upper hinge moment rotation plot, CBGS, Darfield.....	59
Figure 46: Column F3 Level 4 upper hinge bi-axial moment plot, CBGS, Darfield.....	60
Figure 47: Colour coding used to represent different joint deformation states in Figure 48 to Figure 53.....	61
Figure 48: One-way beam-column joint R1 rotations - CBGS, Darfield.....	61
Figure 49: Two-way beam-column joint R1 rotations - CBGS, Darfield.....	62

Figure 50: Two-way beam-column joint R2 rotations - CBGS, Darfield.....	62
Figure 51: One-way beam-column joint R1 rotations - CCCC, Darfield.	63
Figure 52: Two-way beam-column joint R1 rotations - CCCC, Darfield.....	64
Figure 53: Two-way beam-column joint R2 rotations - CCCC, Darfield.....	64
Figure 54: Frame A north/south storey drifts - Lyttelton.	66
Figure 55: Frame F north/south storey drifts - Lyttelton.....	67
Figure 56: Frame 1 east/west storey drifts - Lyttelton.....	67
Figure 57: Frame 4 east/west storey drifts - Lyttelton.....	68
Figure 58: Building level 6 displacements, CBGS, Lyttelton.....	79
Figure 59: Column C2, Level 1 hinge rotation and elongation vs time, CBGS, Lyttelton.	80
Figure 60: Column C2 Level 1 lower hinge strain vs time, CBGS, Lyttelton.	81
Figure 61: Column C2 Level 1 lower hinge axial and moments vs time, CBGS, Lyttelton.....	81
Figure 62: Column C2 Level 1 lower hinge moment axial relationship, CBGS, Lyttelton.	82
Figure 63: Column C2 Level 1 lower hinge hysteretic form, CBGS, Lyttelton.	82
Figure 64: Column C2 Level 1 lower hinge moment rotation, CBGS, Lyttelton.....	83
Figure 65: Column C2 Level 1 lower hinge bi-axial moment, CBGS, Lyttelton.....	83
Figure 66: One-way beam-column joint R1 rotations, CBGS, Lyttelton.....	85
Figure 67: GL A two-way beam-column joint R1 rotations, CBGS, Lyttelton.....	86
Figure 68: GL A two-way beam-column joint R1 rotations, CBGS, Lyttelton, Sequential.	86
Figure 69: GL F two-way beam-column joint R1 rotations, CBGS, Lyttelton.	87
Figure 70: GL F two-way beam-column joint R1 rotations, CBGS, Lyttelton, Sequential.	87
Figure 71: GL A two-way beam-column joint R2 rotations, CBGS, Lyttelton.....	88
Figure 72: GL A two-way beam-column joint R2 rotations, CBGS, Lyttelton, Sequential.	88
Figure 73: GL F two-way beam-column joint R2 rotations, CBGS, Lyttelton.	89
Figure 74: GL F two-way beam-column joint R2 rotations, CBGS, Lyttelton, Sequential.	89
Figure 75: One-way beam-column joint R1 rotations, CCCC, Lyttelton.	90
Figure 76: GL A two-way beam-column joint R1 rotations, CCCC, Lyttelton.	91
Figure 77: GL A two-way beam-column joint R1 rotations, CCCC, Lyttelton, Sequential 91	
Figure 78: GL F two-way beam-column joint R1 rotations, CCCC, Lyttelton.	92
Figure 79: GL F two-way beam-column joint R1 rotations, CCCC, Lyttelton, Sequential..... 92	
Figure 80: GL A two-way beam-column joint R2 rotations, CCCC, Lyttelton.	93

Figure 81: GL A two-way beam-column joint R2 rotations, CCCC, Lyttelton, Sequential	93
Figure 82: GL F two-way beam-column joint R2 rotations, CCCC, Lyttelton.	94
Figure 83: GL F two-way beam-column joint R2 rotations, CCCC, Lyttelton, Sequential.....	94
Figure 84: One-way beam-column joint R1 rotations, CHHC, Lyttelton.	95
Figure 85: GL A two-way beam-column joint R1 rotations, CHHC, Lyttelton.	95
Figure 86: GL F two-way beam-column joint R1 rotations, CHHC, Lyttelton.....	96
Figure 87: GL A two-way beam-column joint R2 rotations, CHHC, Lyttelton.	96
Figure 88: GL F two-way beam-column joint R2 rotations, CHHC, Lyttelton.....	97
Figure 89: One-way beam-column joint R1 rotations, REHS, Lyttelton.	97
Figure 90: GL A two-way beam-column joint R1 rotations, REHS, Lyttelton.	98
Figure 91: GL F two-way beam-column joint R1 rotations, REHS, Lyttelton.....	98
Figure 92: GL A two-way beam-column joint R2 rotations, REHS, Lyttelton.	99
Figure 93: GL F two-way beam-column joint R2 rotations, REHS, Lyttelton.....	99
Figure 94: Max GL A BCJ R1 rotations: Column A2 level 2 hysteretic behaviour - CBGS, Lyttelton	101
Figure 95: Max GL A BCJ R1 rotations: Column A2 level 2 rotations vs time - CBGS, Lyttelton	101
Figure 96: Max GL A BCJ R2 rotations: Column A4 level 3 hysteretic behaviour - CBGS, Lyttelton	102
Figure 97: Max GL A BCJ R2 rotations: Column A4 level 3 rotations vs time - CBGS, Lyttelton	102
Figure 98: Max GL F BCJ R1 rotations: Column F1 level 5 hysteretic behaviour - CBGS, Lyttelton	103
Figure 99: Max GL F BCJ R1 rotations: Column F1 level 5 rotations vs time - CBGS, Lyttelton	103
Figure 100: Max GL F BCJ R2 rotations: Column F1 level 5 hysteretic behaviour - CBGS, Lyttelton	104
Figure 101: Max GL F BCJ R2 rotations: Column F1 level 5 rotations vs time - CBGS, Lyttelton	104
Figure 102: Max GL A BCJ R1 rotations: Column A2 level 4 hysteretic behaviour - CCCC, Lyttelton	105
Figure 103: Max GL A BCJ R1 rotations: Column A2 level 4 rotations vs time - CCCC, Lyttelton	105

Figure 104: Max GL A BCJ R2 rotations: Column A4 level 3 hysteretic behaviour - CCCC, Lyttelton	106
Figure 105: Max GL A BCJ R2 rotations: Column A4 level 3 rotations vs time - CCCC, Lyttelton	106
Figure 106: Max GL F BCJ R1 rotations: Column F2 level 5 hysteretic behaviour - CCCC, Lyttelton	107
Figure 107: Max GL F BCJ R1 rotations: Column F2 level 5 rotations vs time - CCCC, Lyttelton	107
Figure 108: Max GL F BCJ R2 rotations: Column F1 level 5 hysteretic behaviour - CCCC, Lyttelton	108
Figure 109: Max GL F BCJ R2 rotations: Column F1 level 5 rotations vs time - CCCC, Lyttelton	108
Figure 110: Max GL A BCJ R1 rotations: Column A2 level 5 hysteretic behaviour - CHHC, Lyttelton	109
Figure 111: Max GL A BCJ R1 rotations: Column A2 level 5 rotations vs time - CHHC, Lyttelton	109
Figure 112: Max GL A BCJ R2 rotations: Column A4 level 3 hysteretic behaviour - CHHC, Lyttelton	110
Figure 113: Max GL A BCJ R2 rotations: Column A4 level 3 rotations vs time - CHHC, Lyttelton	110
Figure 114: Max GL F BCJ R1 rotations: Column F2 level 6 hysteretic behaviour - CHHC, Lyttelton	111
Figure 115: Max GL F BCJ R1 rotations: Column F2 level 6 rotations vs time - CHHC, Lyttelton	111
Figure 116: Max GL F BCJ R2 rotations: Column F1 level 5 hysteretic behaviour - CHHC, Lyttelton	112
Figure 117: Max GL F BCJ R2 rotations: Column F1 level 5 rotations vs time - CHHC, Lyttelton	112
Figure 118: Max GL A BCJ R1 rotations: Column A2 level 4 hysteretic behaviour - REHS, Lyttelton	113
Figure 119: Max GL A BCJ R1 rotations: Column A2 level 4 rotations vs time - REHS, Lyttelton	113
Figure 120: Max GL A BCJ R2 rotations: Column A4 level 3 hysteretic behaviour - REHS, Lyttelton	114

Figure 121: Max GL A BCJ R2 rotations: Column A4 level 3 rotations vs time - REHS, Lyttelton	114
Figure 122: Max GL F BCJ R1 rotations: Column F2 level 5 hysteretic behaviour - REHS, Lyttelton	115
Figure 123: Max GL F BCJ R1 rotations: Column F2 level 5 rotations vs time - REHS, Lyttelton	115
Figure 124: Max GL F BCJ R2 rotations: Column F1 level 5 hysteretic behaviour - REHS, Lyttelton	116
Figure 125: Max GL F BCJ R2 rotations: Column F1 level 5 rotations vs time - REHS, Lyttelton	116
Figure 126: Max one-way BCJ R1 rotations: Column E2 level 3 hysteretic behaviour - REHS, Lyttelton	117
Figure 127: Max one way BCJ R1 rotations: Column E2 level 3 rotations vs time - REHS, Lyttelton	117
Figure 128: Beam bar pullout demand capacity ratios for north/south translation, CBGS, Lyttelton	118
Figure 129: Beam bar pullout demand capacity ratios for east/west translation, CBGS, Lyttelton	118
Figure 130: Column C2 axial load variation - CBGS (left) & CCCC (right), Lyttelton	119
Figure 131: Column F2 axial load variation - CBGS (left) & CCCC (right), Lyttelton	119
Figure A.1: Proposed model (from Hindi and Hassan 2004)	130
Figure A.2: Example wall reinforcement	131
Figure A.3: SAP2000 analysis model	132
Figure A.4: Reinforcing nonlinear steel stress-strain plot	132
Figure A.5: Concrete nonlinear stress-strain plot	133
Figure A.6: Nonlinear backbone curve	133
Figure A.7: Coupling beam hysteretic response	134
Figure A.8: Coupling beam hysteretic response (Takeda reinforcement)	134
Figure A.9: Reinforcing nonlinear stress-strain plot (modified for strain penetrations)	135
Figure C.1: Backbone curves from various sources (Alire 2002; ASCE 2006; Birely et al. 2012; S. Park 2010; Sharma et al. 2011; Walker 2001; Weng Yuen 2010)	141
Figure C.2: Joint shear stress vs strain until 3% drift for tests by Walker (2001) and Alire (2002) of interior unreinforced joints with axial load of $\approx 0.1A_g f_c$	141

Figure C.3: Joint shear stress-deformation response of deficient beam-column joints (from Kurose 1987).....	142
Figure C.4: Proposed backbone curve for joint deformation.....	142
Figure C.5: Comparison of PEER-4150 (Alire 2002; D. E. Lehman et al. 2004) against proposed backbone curve	143
Figure C.6: Column axial load ratio against joint shear strength coefficient for interior joints	145
Figure C.7: Column axial load ratio against joint shear strength coefficient for exterior joints	145
Figure C.8: Relationship of factor K to curvature ductility for different joint types (after NZSEE 2006).....	146
Figure C.9: Example of beam-column joint finite element model relying on inputs from multiple nodes (from Mitra and Lowes 2007)	147
Figure C.10: Moment diagram assumed for development of joint spring	148
Figure C.11: Damage of exterior joint (left) observed during testing and (right) illustrated schematically (from Pampanin et al. 2002).....	149
Figure C.12: Plan views of CTV Building exterior joints (Design Engineer 1986a).....	149
Figure C.13: Relationship between joint shear capacity and framing member curvature ductility (from NZSEE 2006)	150
Figure D.1: CTV building hook detail (Design Engineer 1986b)	153
Figure D.2: Hooked anchorage failure modes (from Joh and Shibata 1996).....	154
Figure E.1: Expected Soil Stiffness (Sinclair 2011).....	155
Figure F.1: Darfield 20100903_163541_CBGS N00E (top), N90E (middle), and Vertical (bottom) acceleration time history record plots	156
Figure F.2: Darfield 20100903_163541_CCCC N00E (top), N90E (middle), and Vertical (bottom) acceleration time history record plots	157
Figure F.3: Lyttelton 20110221_235142_CBGS N00E (top), N90E (middle), and Vertical (bottom) acceleration time history record plots	159
Figure F.4: Lyttelton 20110221_235142_CCCC N00E (top), N90E (middle), and Vertical (bottom) acceleration time history record plots.....	160
Figure F.5: Lyttelton 20110221_235142_CHHC N00E (top), N90E (middle), and Vertical (bottom) acceleration time history record plots.....	161
Figure F.6: Lyttelton 20110221_235142_REHS N00E (top), N90E (middle), and Vertical (bottom) acceleration time history record plots	162
Figure G.1: Level 6 Southeast corner displacements, Darfield, CBGS	163
Figure G.2: Level 6 Northwest corner displacements, Darfield, CBGS	163

Figure G.3: Frame A north/south inter-storey displacements, Darfield, CBGS	164
Figure G.4: Frame F north/south inter-storey displacements, Darfield, CBGS	165
Figure G.5: Frame 1 east/west inter-storey displacements, Darfield, CBGS	165
Figure G.6: Frame 4 east/west inter-storey displacements, Darfield, CBGS	166
Figure G.7: North core total diaphragm north/south actions, Darfield, CBGS	166
Figure G.8: North core total diaphragm east/west actions, Darfield, CBGS	167
Figure G.9: North core total diaphragm in-plane moments, Darfield, CBGS	167
Figure G.10: North core Wall C diaphragm north/south actions, Darfield, CBGS	168
Figure G.11: North core Wall C/D diaphragm north/south actions, Darfield, CBGS	168
Figure G.12: North core Wall D diaphragm north/south actions, Darfield, CBGS	169
Figure G.13: North core Wall D/E diaphragm north/south actions, Darfield, CBGS	169
Figure G.14: North core Slab 4/C to C/D diaphragm north/south actions, Darfield, CBGS	170
Figure G.15: North core Slab 4/C to C/D diaphragm east/west actions, Darfield, CBGS	170
Figure G.16: North core Slab 4/C to C/D diaphragm in-plane moments, Darfield, CBGS	171
Figure G.17: North core Wall 5 diaphragm east/west actions, Darfield, CBGS	171
Figure G.18: South wall diaphragm east/west actions, Darfield, CBGS	172
Figure G.19: Column F1 Levels 1 (bottom) to 5 (top) hinge actions, Darfield, CBGS	173
Figure G.20: Column F2 Levels 1 (bottom) to 5 (top) hinge actions, Darfield, CBGS	174
Figure G.21: Column F3 Levels 1 (bottom) to 5 (top) hinge actions, Darfield, CBGS	175
Figure G.22: Column C1 Levels 1 (bottom) to 5 (top) hinge actions, Darfield, CBGS	176
Figure G.23: Column C2 Levels 1 (bottom) to 5 (top) hinge actions, Darfield, CBGS	177
Figure H.1: Level 6 Southeast corner displacements, Darfield, CCCC	178
Figure H.2: Level 6 Northwest corner displacements, Darfield, CCCC	179
Figure H.3: Frame A north/south inter-storey displacements, Darfield, CCCC	180
Figure H.4: Frame F north/south inter-storey displacements, Darfield, CCCC	180
Figure H.5: Frame 1 east/west inter-storey displacements, Darfield, CCCC	181
Figure H.6: Frame 4 east/west inter-storey displacements, Darfield, CCCC	181
Figure H.7: North core total diaphragm north/south actions, Darfield, CCCC	182
Figure H.8: North core total diaphragm east/west actions, Darfield, CCCC	182
Figure H.9: North core total diaphragm in-plane moments, Darfield, CCCC	183
Figure H.10: North core Wall C diaphragm north/south actions, Darfield, CCCC	183

Figure H.11: North core Wall C/D diaphragm north/south actions, Darfield, CCCC.....	184
Figure H.12: North core Wall D diaphragm north/south actions, Darfield, CCCC.....	184
Figure H.13: North core Wall D/E diaphragm north/south actions, Darfield, CCCC.....	185
Figure H.14: North core Slab 4/C to C/D diaphragm north/south actions, Darfield, CCCC.....	185
Figure H.15: North core Slab 4/C to C/D diaphragm east/west actions, Darfield, CCCC.....	186
Figure H.16: North core Slab 4/C to C/D diaphragm in-plane moments, Darfield, CCCC.....	186
Figure H.17: North core Wall 5 diaphragm east/west actions, Darfield, CCCC.....	187
Figure H.18: South wall diaphragm east/west actions, Darfield, CCCC.....	187
Figure H.19: Column F1 Levels 1 (bottom) to 5 (top) hinge actions, Darfield, CCCC.....	189
Figure H.20: Column F2 Levels 1 (bottom) to 5 (top) hinge actions, Darfield, CCCC.....	190
Figure H.21: Column F3 Levels 1 (bottom) to 5 (top) hinge actions, Darfield, CCCC.....	191
Figure H.22: Column C1 Levels 1 (bottom) to 5 (top) hinge actions, Darfield, CCCC.....	192
Figure H.23: Column C2 Levels 1 (bottom) to 5 (top) hinge actions, Darfield, CCCC.....	193
Figure I.1: Level 6 Southeast corner displacements, Lyttelton, CBGS.....	194
Figure I.2: Level 6 Southeast corner displacements, Lyttelton, CBGS Sequential.....	194
Figure I.3: Level 6 Northwest corner displacements, Lyttelton, CBGS.....	195
Figure I.4: Level 6 Northwest corner displacements, Lyttelton, CBGS Sequential.....	195
Figure I.5: Frame A north/south inter-storey displacements, Lyttelton, CBGS.....	196
Figure I.6: Frame A north/south inter-storey displacements, Lyttelton, CBGS Sequential.....	197
Figure I.7: Frame F north/south inter-storey displacements, Lyttelton, CBGS.....	197
Figure I.8: Frame F north/south inter-storey displacements, Lyttelton, CBGS Sequential.....	198
Figure I.9: Frame 1 east/west inter-storey displacements, Lyttelton, CBGS.....	198
Figure I.10: Frame 1 east/west inter-storey displacements, Lyttelton, CBGS Sequential.....	199
Figure I.11: Frame 4 east/west inter-storey displacements, Lyttelton, CBGS.....	199
Figure I.12: Frame 4 east/west inter-storey displacements, Lyttelton, CBGS Sequential.....	200
Figure I.13: North core total diaphragm north/south actions, Lyttelton, CBGS.....	200
Figure I.14: North core total diaphragm east/west actions, Lyttelton, CBGS.....	201
Figure I.15: North core total diaphragm in-plane moments, Lyttelton, CBGS.....	201
Figure I.16: North core Wall C diaphragm north/south actions, Lyttelton, CBGS.....	202
Figure I.17: North core Wall C/D diaphragm north/south actions, Lyttelton, CBGS.....	202
Figure I.18: North core Wall D diaphragm north/south actions, Lyttelton, CBGS.....	203

Figure I.19: North core Wall D/E diaphragm north/south actions, Lyttelton, CBGS	203
Figure I.20: North core Slab 4/C to C/D diaphragm north/south actions, Lyttelton, CBGS.....	204
Figure I.21: North core Slab 4/C to C/D diaphragm east/west actions, Lyttelton, CBGS	204
Figure I.22: North core Slab 4/C to C/D diaphragm in-plane moments, Lyttelton, CBGS	205
Figure I.23: North core Wall 5 diaphragm east/west actions, Lyttelton, CBGS.....	205
Figure I.24: South wall diaphragm east/west actions, Lyttelton, CBGS.....	206
Figure I.25: Column F1 Levels 1 (bottom) to 5 (top) hinge actions, Lyttelton, CBGS.....	207
Figure I.26: Column F2 Levels 1 (bottom) to 5 (top) hinge actions, Lyttelton, CBGS.....	208
Figure I.27: Column F3 Levels 1 (bottom) to 5 (top) hinge actions, Lyttelton, CBGS.....	209
Figure I.28: Column C1 Levels 1 (bottom) to 5 (top) hinge actions, Lyttelton, CBGS	210
Figure I.29: Column C2 Levels 1 (bottom) to 5 (top) hinge actions, Lyttelton, CBGS	211
Figure I.30: Column F1 Levels 1 (bottom) to 5 (top) hinge actions, Lyttelton, CBGS Sequential	212
Figure I.31: Column F2 Levels 1 (bottom) to 5 (top) hinge actions, Lyttelton, CBGS Sequential	213
Figure I.32: Column F3 Levels 1 (bottom) to 5 (top) hinge actions, Lyttelton, CBGS Sequential.	214
Figure I.33: Column C1 Levels 1 (bottom) to 5 (top) hinge actions, Lyttelton, CBGS Sequential.	215
Figure I.34: Column C2 Levels 1 (bottom) to 5 (top) hinge actions, Lyttelton, CBGS, Sequential.	216
Figure J.1: Level 6 Southeast corner displacements, Lyttelton, CCCC	217
Figure J.2: Level 6 Southeast corner displacements, Lyttelton, CCCC Sequential.....	217
Figure J.3: Level 6 Northwest corner displacements, Lyttelton, CCCC	218
Figure J.4: Level 6 Northwest corner displacements, Lyttelton, CCCC Sequential.....	218
Figure J.5: Frame A north/south inter-storey displacements, Lyttelton, CCCC.....	219
Figure J.6: Frame A north/south inter-storey displacements, Lyttelton, CCCC Sequential.....	220
Figure J.7: Frame F north/south inter-storey displacements, Lyttelton, CCCC.....	220
Figure J.8: Frame F north/south inter-storey displacements, Lyttelton, CCCC Sequential.	221
Figure J.9: Frame 1 east/west inter-storey displacements, Lyttelton, CCCC.....	221
Figure J.10: Frame 1 east/west inter-storey displacements, Lyttelton, CCCC Sequential.	222
Figure J.11: Frame 4 east/west inter-storey displacements, Lyttelton, CCCC.....	222
Figure J.12: Frame 4 east/west inter-storey displacements, Lyttelton, CCCC Sequential	223
Figure J.13: North core total diaphragm north/south actions, Lyttelton, CCCC	224

Figure J.14: North core total diaphragm north/south actions, Lyttelton, CCCC Sequential	224
Figure J.15: North core total diaphragm east/west actions, Lyttelton, CCCC	225
Figure J.16: North core total diaphragm east/west actions, Lyttelton, CCCC Sequential.....	225
Figure J.17: North core total diaphragm in-plane moments, Lyttelton, CCCC	226
Figure J.18: North core total diaphragm in-plane moments, Lyttelton, CCCC Sequential.....	226
Figure J.19: North core Wall C diaphragm north/south actions, Lyttelton, CCCC.....	227
Figure J.20: North core Wall C diaphragm north/south actions, Lyttelton, CCCC Sequential	227
Figure J.21: North core Wall C/D diaphragm north/south actions, Lyttelton, CCCC.....	228
Figure J.22: North core Wall C/D diaphragm north/south actions, Lyttelton, CCCC Sequential .	228
Figure J.23: North core Wall D diaphragm north/south actions, Lyttelton, CCCC.....	229
Figure J.24: North core Wall D diaphragm north/south actions, Lyttelton, CCCC Sequential	229
Figure J.25: North core Wall D/E diaphragm north/south actions, Lyttelton, CCCC.....	230
Figure J.26: North core Wall D/E diaphragm north/south actions, Lyttelton, CCCC Sequential .	230
Figure J.27: North core Slab 4/C to C/D diaphragm north/south actions, Lyttelton, CCCC	231
Figure J.28: North core Slab 4/C to C/D diaphragm north/south actions, Lyttelton, CCCC Sequential.....	231
Figure J.29: North core Slab 4/C to C/D diaphragm east/west actions, Lyttelton, CCCC.....	232
Figure J.30: North core Slab 4/C to C/D diaphragm east/west actions, Lyttelton, CCCC Sequential	232
Figure J.31: North core Slab 4/C to C/D diaphragm in-plane moments, Lyttelton, CCCC.....	233
Figure J.32: North core Slab 4/C to C/D diaphragm in-plane moments, Lyttelton, CCCC Sequential.....	233
Figure J.33: North core Wall 5 diaphragm east/west actions, Lyttelton, CCCC	234
Figure J.34: North core Wall 5 diaphragm east/west actions, Lyttelton, CCCC Sequential.....	234
Figure J.35: South wall diaphragm east/west actions, Lyttelton, CCCC	235
Figure J.36: South wall diaphragm east/west actions, Lyttelton, CCCC Sequential.....	235
Figure J.37: Column F1 Levels 1 (bottom) to 5 (top) hinge actions, Lyttelton, CCCC	237
Figure J.38: Column F2 Levels 1 (bottom) to 5 (top) hinge actions, Lyttelton, CCCC	238
Figure J.39: Column F3 Levels 1 (bottom) to 5 (top) hinge actions, Lyttelton, CCCC	239
Figure J.40: Column C1 Levels 1 (bottom) to 5 (top) hinge actions, Lyttelton, CCCC.....	240
Figure J.41: Column C2 Levels 1 (bottom) to 5 (top) hinge actions, Lyttelton, CCCC.....	241
Figure K.1: Level 6 Southeast corner displacements, Lyttelton, CHHC	242

Figure K.2: Level 6 Northwest corner displacements, Lyttelton, CHHC	242
Figure K.3: Frame A north/south inter-storey displacements, Lyttelton, CHHC	243
Figure K.4: Frame F north/south inter-storey displacements, Lyttelton, CHHC	244
Figure K.5: Frame 1 east/west inter-storey displacements, Lyttelton, CHHC	244
Figure K.6: Frame 4 east/west inter-storey displacements, Lyttelton, CHHC	245
Figure K.7: North core total diaphragm north/south actions, Lyttelton, CHHC	245
Figure K.8: North core total diaphragm east/west actions, Lyttelton, CHHC	246
Figure K.9: North core total diaphragm in-plane moments, Lyttelton, CHHC	246
Figure K.10: North core Wall C diaphragm north/south actions, Lyttelton, CHHC	247
Figure K.11: North core Wall C/D diaphragm north/south actions, Lyttelton, CHHC	247
Figure K.12: North core Wall D diaphragm north/south actions, Lyttelton, CHHC	248
Figure K.13: North core Wall D/E diaphragm north/south actions, Lyttelton, CHHC	248
Figure K.14: North core Slab 4/C to C/D diaphragm north/south actions, Lyttelton, CHHC	249
Figure K.15: North core Slab 4/C to C/D diaphragm east/west actions, Lyttelton, CHHC	249
Figure K.16: North core Slab 4/C to C/D diaphragm in-plane moments, Lyttelton, CHHC	250
Figure K.17: North core Wall 5 diaphragm east/west actions, Lyttelton, CHHC	250
Figure K.18: South wall diaphragm east/west actions, Lyttelton, CHHC	251
Figure K.19: Column F1 Levels 1 (bottom) to 5 (top) hinge actions, Lyttelton, CHHC	252
Figure K.20: Column F2 Levels 1 (bottom) to 5 (top) hinge actions, Lyttelton, CHHC	253
Figure K.21: Column F3 Levels 1 (bottom) to 5 (top) hinge actions, Lyttelton, CHHC	254
Figure K.22: Column C1 Levels 1 (bottom) to 5 (top) hinge actions, Lyttelton, CHHC	255
Figure K.23: Column C2 Levels 1 (bottom) to 5 (top) hinge actions, Lyttelton, CHHC	256
Figure L.1: Level 6 Southeast corner displacements, Lyttelton, REHS	257
Figure L.2: Level 6 Northwest corner displacements, Lyttelton, REHS	257
Figure L.3: Frame A north/south inter-storey displacements, Lyttelton, REHS	258
Figure L.4: Frame F north/south inter-storey displacements, Lyttelton, REHS	259
Figure L.5: Frame 1 east/west inter-storey displacements, Lyttelton, REHS	259
Figure L.6: Frame 4 east/west inter-storey displacements, Lyttelton, REHS	260
Figure L.7: North core total diaphragm north/south actions, Lyttelton, REHS	260
Figure L.8: North core total diaphragm east/west actions, Lyttelton, REHS	261
Figure L.9: North core total diaphragm in-plane moments, Lyttelton, REHS	261

Figure L.10: North core Wall C diaphragm north/south actions, Lyttelton, REHS	262
Figure L.11: North core Wall C/D diaphragm north/south actions, Lyttelton, REHS	262
Figure L.12: North core Wall D diaphragm north/south actions, Lyttelton, REHS	263
Figure L.13: North core Wall D/E diaphragm north/south actions, Lyttelton, REHS	263
Figure L.14: North core Slab 4/C to C/D diaphragm north/south actions, Lyttelton, REHS.....	264
Figure L.15: North core Slab 4/C to C/D diaphragm east/west actions, Lyttelton, REHS	264
Figure L.16: North core Slab 4/C to C/D diaphragm in-plane moments, Lyttelton, REHS	265
Figure L.17: North core Wall 5 diaphragm east/west actions, Lyttelton, REHS.....	265
Figure L.18: South wall diaphragm east/west actions, Lyttelton, REHS.....	266
Figure L.19: Column F1 Levels 1 (bottom) to 5 (top) hinge actions, Lyttelton, REHS.....	267
Figure L.20: Column F2 Levels 1 (bottom) to 5 (top) hinge actions, Lyttelton, REHS.....	268
Figure L.21: Column F3 Levels 1 (bottom) to 5 (top) hinge actions, Lyttelton, REHS.....	269
Figure L.22: Column C1 Levels 1 (bottom) to 5 (top) hinge actions, Lyttelton, REHS	270
Figure L.23: Column C2 Levels 1 (bottom) to 5 (top) hinge actions, Lyttelton, REHS	271

List of Tables

Table 1: Unconfined concrete stress-strain parameters	10
Table 2: Reinforcing steel stress-strain parameters.....	11
Table 3: Expected soil stiffness	14
Table 4: Stiffness modifiers for elastically responding beam elements	15
Table 5: Column stiffnesses used in the analysis model	19
Table 6: Definition of beam-column joint response backbone curve.....	21
Table 7: Summary details of beam-column joints.....	22
Table 8: Modelled diaphragm (drag bar) connection capacities.....	28
Table 9: Basic load pattern definitions.....	30
Table 10: Global base reactions for basic load patterns (linear).....	31
Table 11: Imposed loading allowances (for derivation of dynamic mass).....	32
Table 12: Modal participating mass ratios	33
Table 13: Seismic event information	40
Table 14: Adopted earthquake record information.....	40
Table 15: Adopted record start and finish times.....	44

Table 16: Rayleigh damping parameters - Darfield	45
Table 17: Rayleigh damping parameters - Lyttelton.....	46
Table 18: Wall C diaphragm connection forces - Darfield.....	50
Table 19: Wall C/D diaphragm connection forces - Darfield.....	50
Table 20: Wall D diaphragm connection forces - Darfield.....	50
Table 21: Wall D/E diaphragm connection forces - Darfield.....	51
Table 22: Wall 5 (C to C/D) diaphragm connection forces - Darfield.....	51
Table 23: North core total diaphragm connection forces - Darfield.....	52
Table 24: North core total diaphragm connection forces - Darfield.....	52
Table 25: Slab 4 C to C/D diaphragm E/W actions - Darfield	53
Table 26: Slab 4 C to C/D diaphragm N/S actions - Darfield.....	53
Table 27: South wall diaphragm connection forces - Darfield	54
Table 28: Wall strains - Darfield	55
Table 29: South Wall Coupling Beam Strain	55
Table 30: CBGS peak column hinge compression strains - Darfield.....	56
Table 31: Wall C diaphragm connection forces - Lyttelton.....	69
Table 32: Wall C/D diaphragm connection forces - Lyttelton.....	69
Table 33: Wall D diaphragm connection forces - Lyttelton.	69
Table 34: Wall D/E diaphragm connection forces - Lyttelton.....	70
Table 35: Wall 5 (C to C/D) diaphragm connection forces - Lyttelton.....	70
Table 36: North core total diaphragm connection E/W forces - Lyttelton.....	71
Table 37: North core total diaphragm connection N/S forces - Lyttelton.	71
Table 38: North core total diaphragm connection forces - Lyttelton.....	71
Table 39: Slab 4 C to C/D diaphragm E/W actions - Lyttelton.....	72
Table 40: Slab 4 C to C/D diaphragm N/S actions - Lyttelton.	72
Table 41: Slab 4 C to C/D diaphragm connection forces - Lyttelton.	73
Table 42: South wall diaphragm connection forces - Lyttelton.....	73
Table 43: Column hinges included in assessment.....	75
Table 44: Time at which $\epsilon > \epsilon_{cu}$ @column centroid.....	78
Table 45: Time at which $\epsilon > \epsilon_y$ @reinforcement.....	78
Table 46: Time at which $\epsilon > \epsilon_{cu}$ @column face	78

Table G.1: Wall D and D/E diaphragm disconnection times, Darfield, CBGS	164
Table H.1: Wall D and D/E diaphragm disconnection times, Darfield, CCCC.....	179
Table I.1: Wall D and D/E diaphragm disconnection times, Lyttelton, CBGS.	196
Table J.1: Wall D and D/E diaphragm disconnection times, Lyttelton, CCCC.....	219
Table K.1: Wall D and D/E diaphragm disconnection times, Lyttelton, CHHC.....	243
Table L.1: Wall D and D/E diaphragm disconnection times, Lyttelton, REHS	258

DRAFT

Executive Summary

This report describes the work performed by Compusoft Engineering Ltd to support the NLTA Expert Committee of the Royal Commission of Inquiry. The work undertaken has been the modification of a SAP2000 computer model of the CTV building developed for the DBH investigation into that building's collapse during the February 2011 earthquake and the rerunning of that model for a range of earthquake events.

The major changes to the model from that used in the DBH analyses are:

- The non-linear beam column joint behaviour has been modelled.
- Plastic hinges at the top and bottom of each column have been modelled to incorporate P-M-M interaction.
- The possibility of non-linear behaviour of the floor diaphragm adjacent to the north and south walls, and beam lines 2 and 3 has been modelled.
- The Rayleigh damping coefficients have been slightly adjusted so that an appropriate level of damping has been assigned to the vertical vibration of the floors.
- The ground motions recorded from the CBGS and CCCC sites have been run sequentially for both the September and February events to investigate whether possible damage from the first event influenced the results of analyses during the February earthquake.

The results of the analyses highlighted a number of effects. Firstly it supported the major findings of the previous analyses reported previously, that is:

1. During the September event it was most likely that one or more floor connections to the north wall failed.

Secondly, then inclusion of the additional modelling features listed above supported the assumptions made in the first (DBH) series of analyses:

1. The building would have collapsed in the February event whether or not there had been damage incurred in the previous earthquakes.

Limitations of the Content of this Report

This report has been produced under significant time pressures, with the analyses described within performed under similar time pressure. As a result, neither the report nor the analyses have been subject to the degree of internal review that Compusoft Engineering Limited typically applies to work of similar complexity. Readers of this draft issue should be aware of this situation, and also be cognisant that information presented in the report may be revised without specific notice between different issues of the report.

It is particularly important to note that the data presented in this report is far from comprehensive. Data is presented for only a limited number of elements within the structure, and not all behavioural types are considered in the presented data. Readers should make no assumptions as to the significance of the data included and omitted. At the date of issue, processing of data has not been completed, and thus there is a possibility that currently unprocessed aspects of behaviour may prove significant to the overall suggested performance of the structure.

1. Introduction

Compusoft Engineering Limited was engaged by the Canterbury Earthquakes Royal Commission as part of the NLTHA Expert Panel to undertake further non-linear seismic analyses of the CTV Building. These analyses are additional to those undertaken for StructureSmith and the Department of Building and Housing that were detailed within the Compusoft report titled 'CTV Non-linear Seismic Analysis Report', reference 11033-00. It is the intent that the analyses outlined within this report further enhance the understanding of the CTV performance during the 4th September 2010 Darfield earthquake, and the February 2011 Lyttelton aftershock.

The non-linear analyses outlined in this report are intended to;

- Assist with the identification of the probable sequence of failure.
- Report displacement and storey drift demands, identifying the onset and progression of damage throughout the structure.
- Monitor and report seismic demands on critical structural elements.

The model used for all analyses have been based on building geometry, record structural drawings (Design Engineer 1986a), material tests (Hyland 2011), along with published guidance on the hysteretic behaviour of detailing present within the CTV building.

2. Building description

The CTV building was a 6 storey structure of reinforced concrete construction with plan dimensions of approximately 31 m by 23 m. An overall impression of the complete structure is shown in Figure 1. Construction consisted of 200 mm thick in-situ composite concrete Hi-Bond floors supported by precast concrete half-beams, shell beams and in-situ concrete columns. A lightweight roof was supported from concrete columns that cantilever above the level 6 floor plate. At the north of the building a series of 300 mm thick reinforced concrete walls were used to support a stair and lift core that projects two storeys above the upper floor plate. A 400 mm thick reinforced concrete coupled shear wall system was situated on the south face of the building. These walls were considered to form the primary seismic resisting system. Frame action was engaged through stiffness compatibility with the walls and contributed to the overall lateral resistance of the structure, particularly the torsional resistance. Figure 2 below indicates the reinforced concrete framing and wall elements that were present (note that the model is presented with north oriented to the right). Foundations comprised pads supporting the internal columns, with a series of in-situ concrete inverted 'tee' beams supporting the perimeter columns and walls as shown in Figure 3. Inter-storey height was typically 3.24 m with 3.70 m for the bottom storey (3.825 m to top of foundations).

The lower 3 levels of the western perimeter frame were in-filled with reinforced concrete masonry panels. An additional feature was a series of precast concrete spandrel panels that were present on the north, east, and south perimeter frames.

Terminology used to describe floor levels within this report has been selected to match that used in the record structural drawings and ongoing investigation reports, with ground floor referred to as level 1, and the level 1 columns spanning between levels 1 and 2.

Figure 4 presents the building grid system used in both the original design and the analysis model.

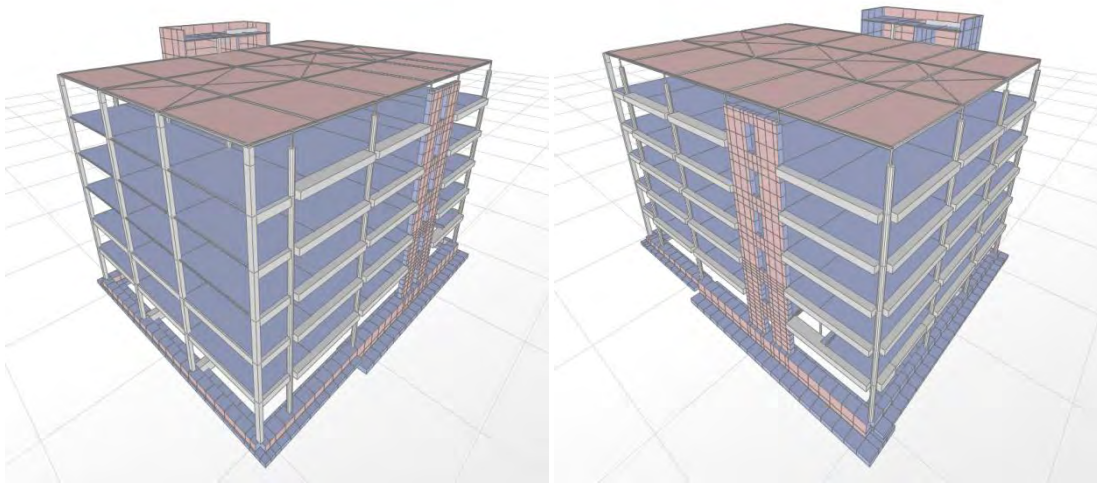


Figure 1: Overall view of the CTV structural model (viewed from SW & SE respectively)

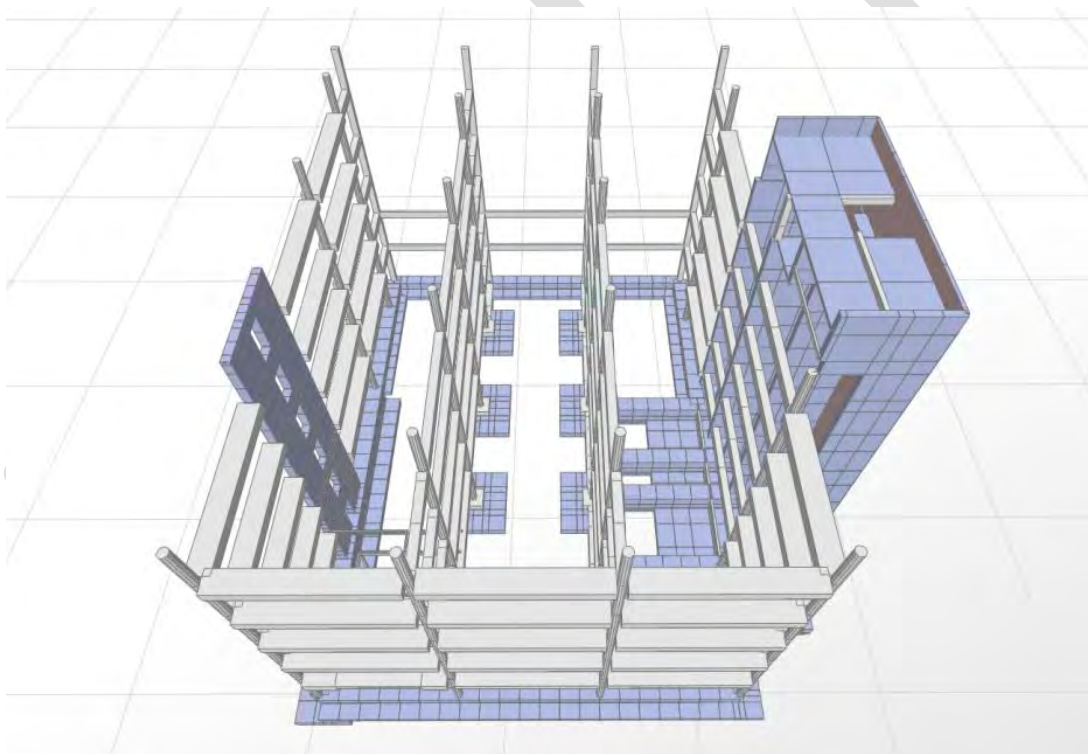


Figure 2: CTV structural model viewed from the east (slabs omitted for clarity)

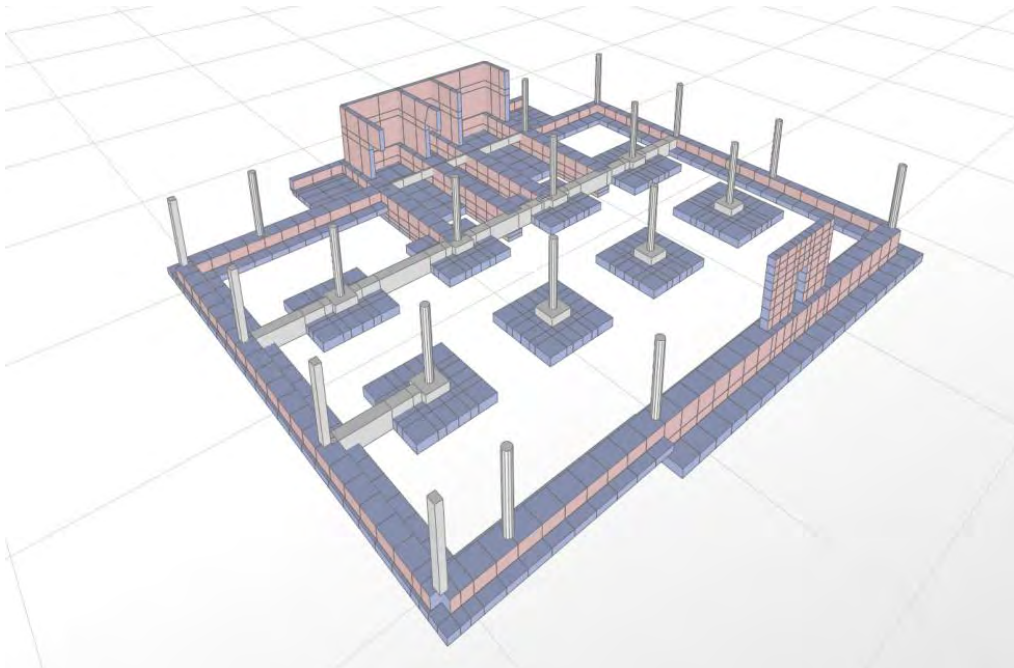


Figure 3: CTV foundation arrangement viewed from the south-west.

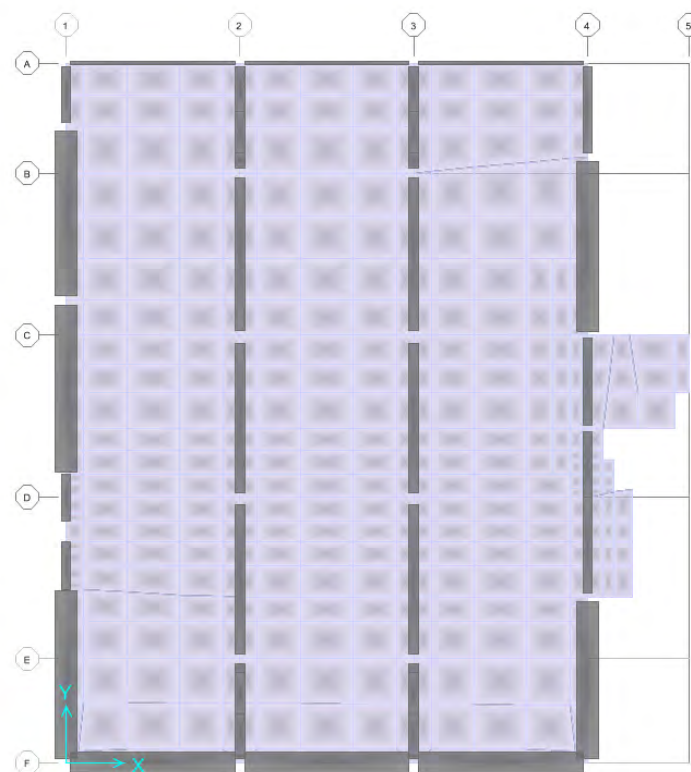


Figure 4: Building grid system.

3. Analysis Procedure Overview

A three dimensional model of the building was formed using the SAP2000 Advanced (v14.2.5, CSI Berkeley 2011) finite element program. This model was used to evaluate the seismic actions using non-linear pushover, and non-linear time history methods in accordance with accepted good practice, and recent advances in the understanding of the seismic performance of structures.

As requested by Royal Commission NLTHA panel the analysis of the CTV building has been conducted based on the assumption that the only structural elements that resist seismic actions are the reinforced concrete frames and shear walls. Masonry infill panels and precast concrete spandrel elements are assumed to be effectively isolated such that they cannot influence the seismic response and performance of the building.

3.1. Alterations Made from Previous (DBH) Analysis Model

The analysis model has been developed from the original analysis model (denoted *Model A*) developed for use in the CTV Building non-linear analyses undertaken for the DBH, the results of which are documented in the Compusoft report titled 'CTV Building Non-Linear Seismic Analysis Report'. Changes/alterations made to the previous Model A include the following;

- Interacting M-M Hinges have been replaced with interacting P-M-M hinges.
- Axial release added to roof purlin.
- Non-linear floor elements included (adjacent to beam lines only).
- Damping parameters have been revised for the Lyttelton analysis runs.
- Non-linear strength and stiffness degradation of the beam column joints has been incorporated into the model.
- Slab stiffness has been revised.
- Minor floor mesh refinements.
- Changes to the concrete strength and corresponding stiffness parameters.
- Adjustment to non-linear link and elastic element stiffness to account for concrete material property changes.

- Analysis run times have been amended.
- Some Lyttelton analyses have been undertaken considering the damaged state present at the end of the Darfield earthquake.
- Inclusion of additional ground motion record (REHS) for the Lyttelton event.

3.2. Analysis Procedure

The overall seismic analysis procedure for the CTV building consisted several different tasks as summarised below.

Non-linear static (Pushover) analyses

Non-linear static pushover analyses of the structure were undertaken for the two primary directions starting from the end state of a gravity analysis. The purpose of these analyses was to aid understanding of the non-linear performance of the structure, and to partially verify assumptions of the adopted analysis parameters.

Non-linear time history analyses for the Darfield event

Non-linear time history were undertaken using the CBGS and CCCC station records of the Darfield event.

Non-linear time history analyses for the Lyttelton event

Two separate sets of non-linear time history analyses were undertaken for the Lyttelton event.

Non-linear time history analyses assuming no pre-existing damage were conducted using four records of the Lyttelton event, namely CBGS, CCCC, CHHC, and REHS.

Two further time history analyses were undertaken to quantify and assess the effect of damage that occurred during the Darfield event on the response of the structure during the Lyttelton event. These analyses used the condition of the CTV building at the end of the Darfield event (CBGS and CCCC analyses) as the starting condition for the Lyttelton event as indicated in Figure 5. For these analyses the CBGS and CCCC records were examined.

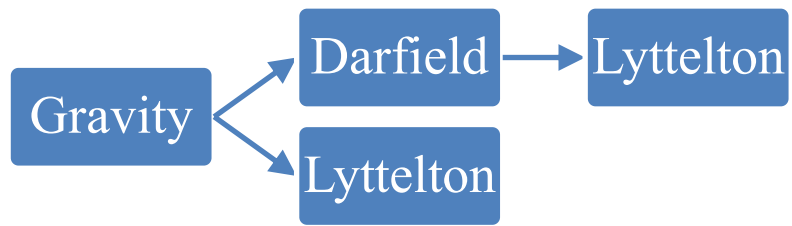


Figure 5: Time history analysis sequence

4. Material Properties

4.1. Concrete

The mean in-situ unconfined compressive strengths of the concrete elements have been evaluated via NZSEE guidelines (NZSEE 2006). In this the mean strength of in-situ concrete can be taken as 1.5 times the specified lower characteristic design strength. The elastic stiffness of the concrete has been derived following the provisions of the New Zealand Concrete Structures Standard (NZS 3101 2006, Clause 5.2.3) as below:

$$E_c = 3320\sqrt{f'_c} + 6900 \text{ (MPa)}$$

Where ' f'_c ' is taken as the mean in-situ unconfined strength of concrete (in MPa).

Table 1 below presents the key input parameters used for the definition of concrete materials.

Table 1: Unconfined concrete stress-strain parameters

Material	f'_c (MPa) Specified	f'_c (MPa) Adopted	ϵ_{cu}	E_c (GPa)
PC Beams	25	37.5	0.00825	27.2
Ground beams	20	30	-NA-	25.1
Columns L1 - L2	35	52.5	0.0065	31.0
Columns L2- L3	30	45	0.0075	29.2
Columns L3- Roof	25	37.5	0.00825	27.2
Floor Slabs	25	37.5	0.00825	27.2
Shear Walls	25	37.5	0.00825	27.2

Definition of the stress-strain curve for unconfined concrete has been based on the model proposed by Karthik and Mander (Karthik and Mander 2011). The nonlinear stress-strain behaviour of unconfined concrete materials is presented in Figure 6 below.

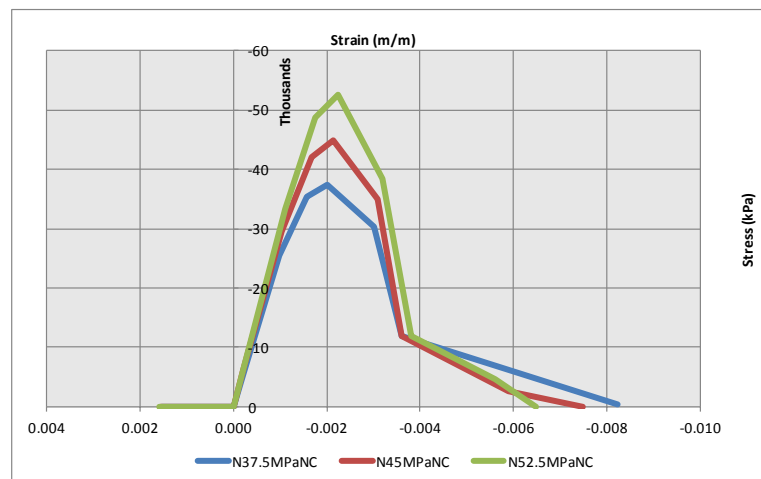


Figure 6: Concrete stress-strain curve

4.2. Reinforcement

Reinforcing steel stress-strain properties have been determined from testing of materials extracted from the as-built structure (Hyland 2011). Where no test data is available, material properties have been adopted which are consistent with the period in which the structure was constructed (Andriono and R. Park 1986). Table 2 below presents the key input parameters used for the definition of reinforcing materials. The non-linear stress-strain behaviour of the reinforcing materials is presented in Figure 7 below.

Table 2: Reinforcing steel stress-strain parameters.

Grade	Es (GPa)	fy (MPa)	ϵ_{sh}	ϵ_{su}	fu (MPa)
G275	205	321.3	0.0220	0.202	451.0
G380	205	448 ¹	0.0097	0.168 ¹	603 ¹
664 Mesh	205	615 ¹	0.01	0.042 ¹	665 ¹

Notes: 1. Mean values obtained via testing (Hyland 2011)

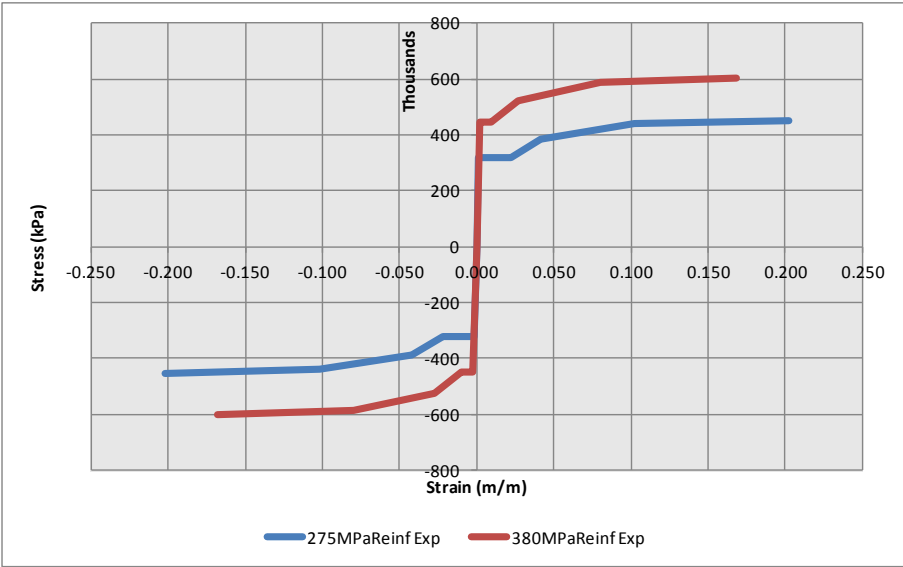


Figure 7: Reinforcing steel stress-strain curve

5. Structural Elements

5.1. Soil Structure Interaction

In order to incorporate the potential lift-off of foundation elements in the model, non-linear link elements have been incorporated that represent the gapping behaviour of the foundations. Soil stiffness was considered to behave in a linear manner for compressive strains, with applied soil stiffness based on values provided by Tonkin and Taylor for the probable soil conditions at the site (Sinclair 2011).

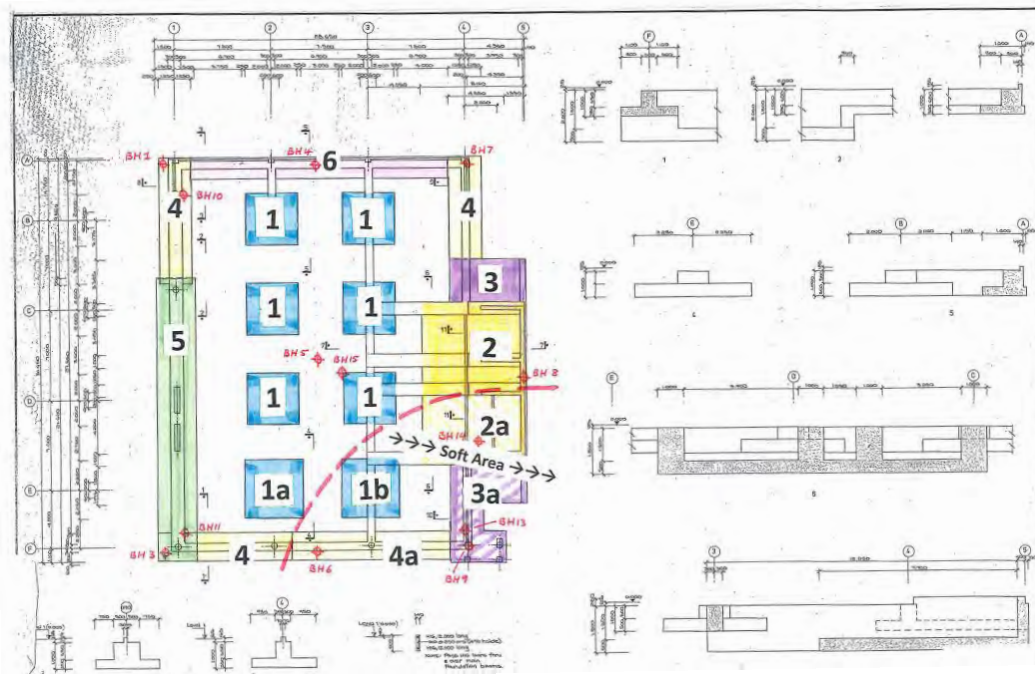
It is expected that modelling the effects of any period shift due to foundation flexibility through gapping would outweigh the potential benefits of modelling the plastic behaviour of the soil (Carr 1994). No allowance was made for any suction that may be present between the soil and underside of the foundation beams. Table 3 and Figure 8 present the soil stiffness and foundation designation used in the analysis, with additional information presented in Appendix C. Based upon post earthquake inspections of the site it has been considered that the level of liquefaction observed would not have had a significantly adverse affect on the performance of the building (Sinclair 2011), and as such the effects of liquefaction have not been considered.

5.2. Foundation Elements

The foundation system consists of a series of large reinforced concrete pads and flanged ground beams. The pads are modelled using shell objects with suitable thickness. The ground beams are typically modelled as an assemblage of shell objects to form the overall section and provide the necessary bearing area. The Effect of backfill present on top of the foundations has been considered assuming that only the soil contained within vertical planes bounding the foundation width is able to be mobilised, and has a soil density of 18 kN/m^3 .

Table 3: Expected soil stiffness

Foundation Element	Compressive Stiffness (MN/m ³)
1	122.7
1a	130.89
1b	65.98
2	85.4
2a	53.14
3	117.22
3a	78.59
4	159.69
4a	73.94
5	104.35
6	185.42

**Figure 8: CTV foundation element location plan (Design Engineer 1986a)**

5.3. Reinforced Concrete Frames

Reinforced concrete frames have been incorporated in the analysis model using elastically responding frame elements to represent the beam and column members, and discrete non-linear elements to account for non-linear behaviour of beams, columns, and beam-column joints. The implementation of these elements are all discussed in the following sections.

5.3.1. Beams and beam hinges

To account for the effects of concrete cracking, the effective elastic stiffness of the reinforced concrete beam sections has been determined based upon the moment-curvature relationship (Priestley et al. 2007) as below:

$$EI_{eff} = \frac{M_y}{\phi'_y}$$

where ' M_y ' is the first yield bending moment, and ' ϕ'_y ' is the curvature at first yield using material strengths as per Section 4, member geometry and reinforcement as specified in the record drawings. Table 4 presents the stiffness modifiers used for a selection of beams.

Table 4: Stiffness modifiers for elastically responding beam elements

Structural Component	Effective Cracked Section Property, I_e
GL C Core Ground Beam (rect)	$0.64 I_g$
GL C/D Core Ground Beam (rect)	$0.25 I_g$
GL D/E Core Ground Beam (rect)	$0.39 I_g$
GL 1 2m Ground Beam (tee)	$0.31-0.39 I_g$
GL 3 Ground Beam (rect)	$0.22-0.49 I_g$
Typical 550x400 Beam (tee)	$0.47 I_g$
Typical 550x960 Beam (L)	$0.17 I_g$

Beam hinges are incorporated in the analysis model as discrete non linear link elements located where inelastic demand is expected to occur. This is taken to be at beam ends.

The adopted beam plastic hinge length (L_p) considers strain penetration (L_{sp}) into the beam-column joint zone and has been determined using the following relationship (Priestley et al. 2007):

$$L_p = kL_c + L_{sp} > 2L_{sp}$$

where,

$$k = 0.2 \left(\frac{f_u}{f_y} - 1 \right) \leq 0.08$$

$$L_{sp} = 0.022f_{ye}d_b$$

and L_c is the length between the critical section and the point of contra-flexure in the member under consideration.

The non-linear moment vs rotation behaviour of the beam hinges has been defined considering a multi-linear backbone curve. The backbone curve for each hinge was determined via moment-curvature analysis of the section including the contribution of the slab where applicable. It should be noted that it has been assumed for analysis purposes that beam hinge formation is not limited by the capacity of bar anchorages. A Takeda hysteresis model (Takeda et al. 1970) was used to consider the degradation of hinge stiffness under cyclic loading. Figure 9 below presents the discretised moment curvature backbone relationship for an example beam hinge along with the actual hinge moment curvature relationship.

For all precast beams, anchorage of positive (bottom) reinforcement occurs via hooks into the beam-column joint zone which can be seen in Figure 10 and Figure 11 below. Top steel anchorage in exterior beam column joints is via hooked bars similar to the typical bottom steel anchorage (as seen in Figure 10). Physical evidence has indicated that the positive reinforcement of the beam along gridline 4 between grids B and C was not effectively anchored into the wall on grid C at levels 3 and 4 (Hyland 2011). To reflect this finding no positive moment capacity has been provided in the model at these locations ¹.

¹ Note that post analyses it has been confirmed that in addition to levels 3 and 4, beam bottom steel (between grids B and C) was not effectively anchored at levels 1, 5, and 6 into the wall at grid C

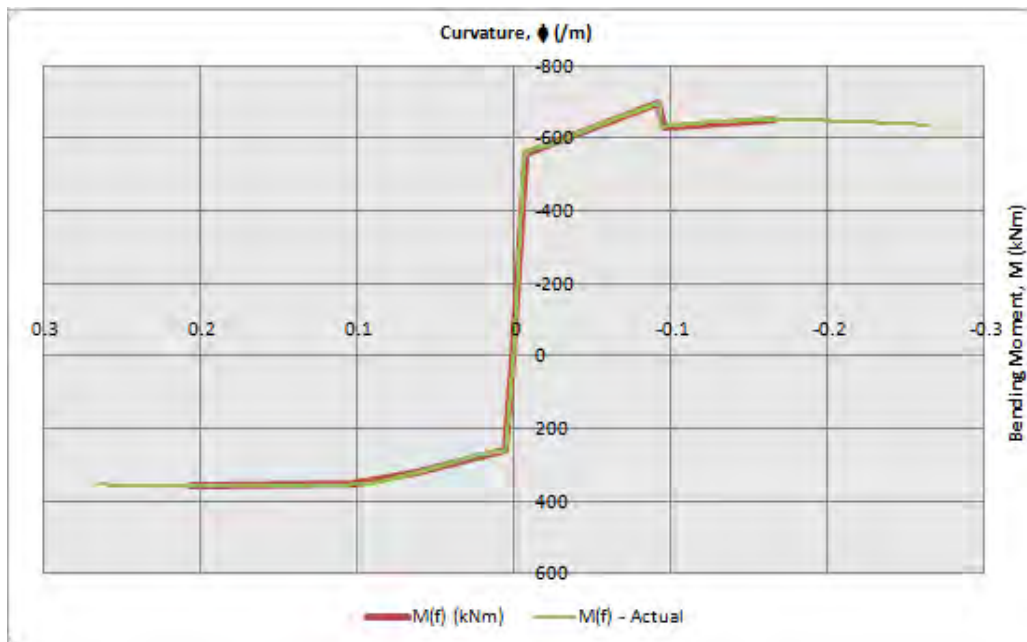


Figure 9: Typical moment-curvature relationship for beam hinges

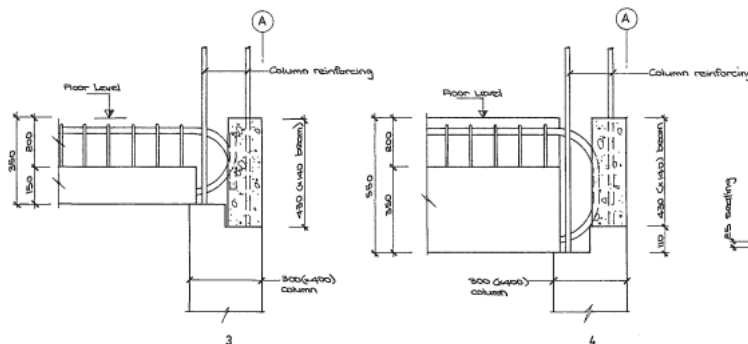


Figure 10: Reinforcement anchorage in Grid A beam column joint zone (Design Engineer 1986a)

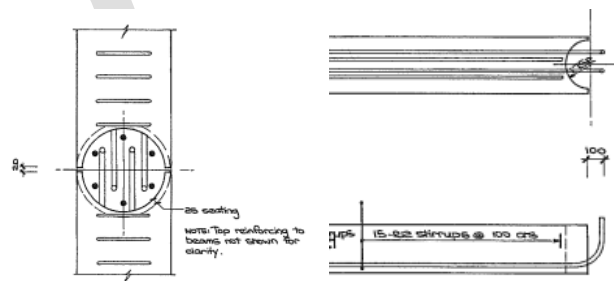


Figure 11: Typical bottom reinforcement anchorage in interior beam column joint zone (Design Engineer 1986a)

Given the limited anchorage of the hooked beam bars into the beam-column joints, a possibility exists that bar pullout will occur and limit the performance of the beams and beam-

column joints. Bar pullout capacity is dependent on column axial load and thus is expected to vary considerably throughout the course of an earthquake. Due to difficulties in accurately modelling the varying pullout capacities it is the intent that the potential for bar pullout to be determined via post processing. Appendix D presents the methodology used to assess bar pullout of the hooked beam reinforcement.

5.3.2. Columns and column hinges

To account for the effect of concrete cracking on the flexural stiffness of the linearly responding frame elements stiffness modifier have been assigned. The stiffness modifiers have been determined in accordance with the New Zealand Concrete Structures Standard (NZS 3101 2006, Section 8.6.3) considering a weighted average of stiffness over the column height.

Figure 12 below presents the effective stiffness relationships used for the columns in the analysis model, with the effective stiffness properties presented in the New Zealand Concrete Structures Standard (NZS 3101 2006, Table C6.6) shown for comparison.

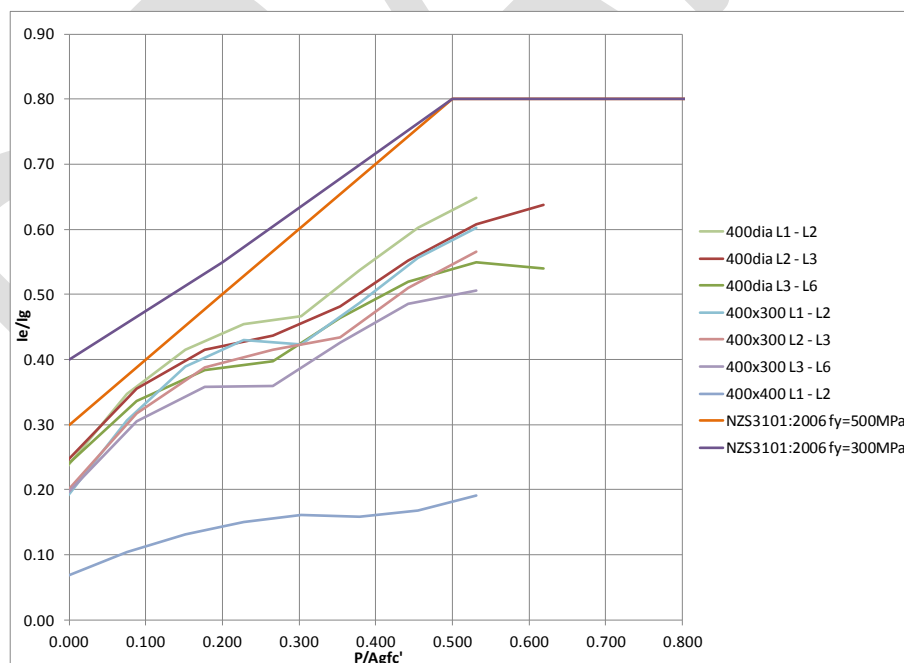


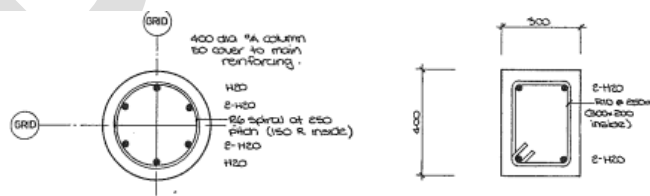
Figure 12: Effective column stiffness relationship.

Table 5: Column stiffnesses used in the analysis model

Grid Ref.	L1			L2			L3			L4			L5		
	N* _{G+Qu} (kN)	I _{cr}	I _{eff}	N* _{G+Qu} (kN)	I _{cr}	I _{eff}	N* _{G+Qu} (kN)	I _{cr}	I _{eff}	N* _{G+Qu} (kN)	I _{cr}	I _{eff}	N* _{G+Qu} (kN)	I _{cr}	I _{eff}
F1	1012	0.41	0.77	807	0.39	0.74	613	0.36	0.71	407	0.34	0.67	201	0.28	0.6
C1	1308	0.44	0.8	1035	0.42	0.78	805	0.38	0.74	544	0.35	0.69	281	0.31	0.64
A/B1	890	0.4	0.75	698	0.38	0.72	544	0.35	0.69	369	0.33	0.66	195	0.29	0.61
A1	241	0.25	0.73	174	0.24	0.71	130	0.24	0.69	88	0.22	0.67	49	0.21	0.66
F2	1194	0.43	0.79	947	0.41	0.77	723	0.37	0.72	482	0.34	0.68	240	0.29	0.62
E2	1429	0.45	0.81	1128	0.42	0.79	878	0.39	0.76	574	0.35	0.69	270	0.31	0.64
D2	1734	0.46	0.85	1372	0.43	0.81	1070	0.39	0.78	703	0.37	0.72	335	0.32	0.65
C2	1802	0.46	0.86	1430	0.43	0.82	1127	0.39	0.78	759	0.37	0.73	390	0.33	0.66
B2	1569	0.46	0.83	1244	0.43	0.8	984	0.39	0.77	655	0.36	0.71	344	0.32	0.65
A2	689	0.34	0.79	508	0.32	0.76	427	0.31	0.75	254	0.27	0.72	135	0.24	0.73
F3	1183	0.43	0.79	933	0.41	0.77	715	0.37	0.73	476	0.34	0.68	237	0.29	0.62
E3	1427	0.45	0.81	1118	0.42	0.78	873	0.39	0.76	570	0.35	0.69	268	0.31	0.64
D3	1734	0.46	0.85	1364	0.43	0.81	1064	0.39	0.78	698	0.37	0.72	332	0.32	0.65
C3	1752	0.46	0.85	1391	0.43	0.81	1096	0.39	0.78	737	0.37	0.73	377	0.33	0.65
B3	1564	0.46	0.83	1240	0.43	0.8	980	0.39	0.77	660	0.36	0.71	342	0.32	0.65
A3	689	0.34	0.79	508	0.32	0.76	427	0.31	0.75	254	0.27	0.72	135	0.24	0.73
F4	970	0.41	0.76	777	0.39	0.74	588	0.36	0.7	391	0.34	0.67	194	0.28	0.6
D/E4	1394	0.14	0.7	1062	0.42	0.78	833	0.38	0.75	560	0.35	0.69	275	0.31	0.64
B4	1095	0.43	0.78	860	0.4	0.75	668	0.36	0.71	450	0.34	0.68	236	0.3	0.62
A4	357	0.28	0.75	267	0.27	0.73	188	0.25	0.71	120	0.23	0.68	71	0.22	0.68

Flexural hinging is anticipated to occur in the columns immediately adjacent to the beam face. To account for this in the analysis model non-linear elements have been incorporated that includes consideration of axial-moment (commonly termed P-M-M) interaction and strength and stiffness degradation. The performance of these hinges is presented in Appendix B.

Figure 13 below indicates the typical reinforcement arrangement for the typical 400 mm diameter circular columns and the 400 mm x 300 mm columns located on grid A.

**Figure 13: Typical column reinforcement. (Design Engineer 1986a)**

Examination of the eccentric column connection between the top of the column located at grid 4 D/E (referenced as C18 on the structural drawings) and the north core wall as seen in Figure 14, has indicated that the detailing present is not capable of transferring the significant axial

forces that would result from moderate seismic demands. As such, this connection has not been included in the analysis model, with column C18 assumed to behave as a cantilever above Level 6.

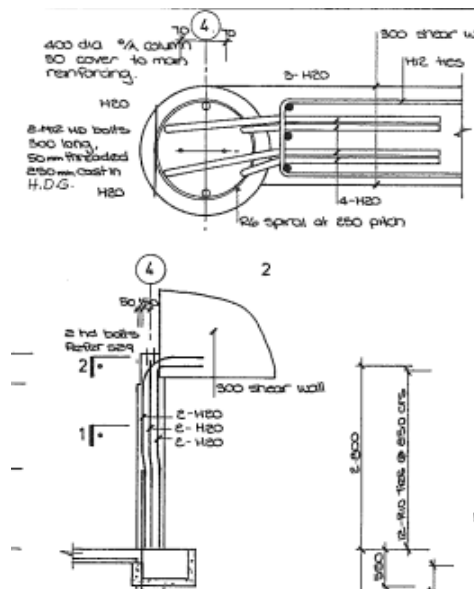


Figure 14: Column at GL 4 D/E (C18) to wall connection detailing at roof level (Design Engineer 1986a)

5.3.3. Beam-Column Joints

Non-linear behaviour of the beam-column joints in the CTV Building has been incorporated in the model by use of a non-linear moment-rotation spring located at the node at the intersection of the beam and column elements. This spring was calibrated to represent the expected shear stress-shear strain response of deficient concrete beam-column joints. The strength of beam column joints was determined based on procedures commonly used in New Zealand practice (NZSEE 2006), while the non-linear backbone curve defining response of the spring has been determined based on review of relevant literature. The definition of this backbone curve is summarised in Table 6, and an example joint response backbone curve can be seen in Figure 15. Table 7 provides summary details of data used to define the response of each beam-column joint in the CTV Building. Detailed discussion of the beam-column joint implementation can be found in Appendix C.

Table 6: Definition of beam-column joint response backbone curve

Joint rotation ($\times 10^{-3}$ radians)	Capacity (M/M_{\max})
0	0.0
2	0.7
7	1.0
10	1.0
30	0.5
100	0.0

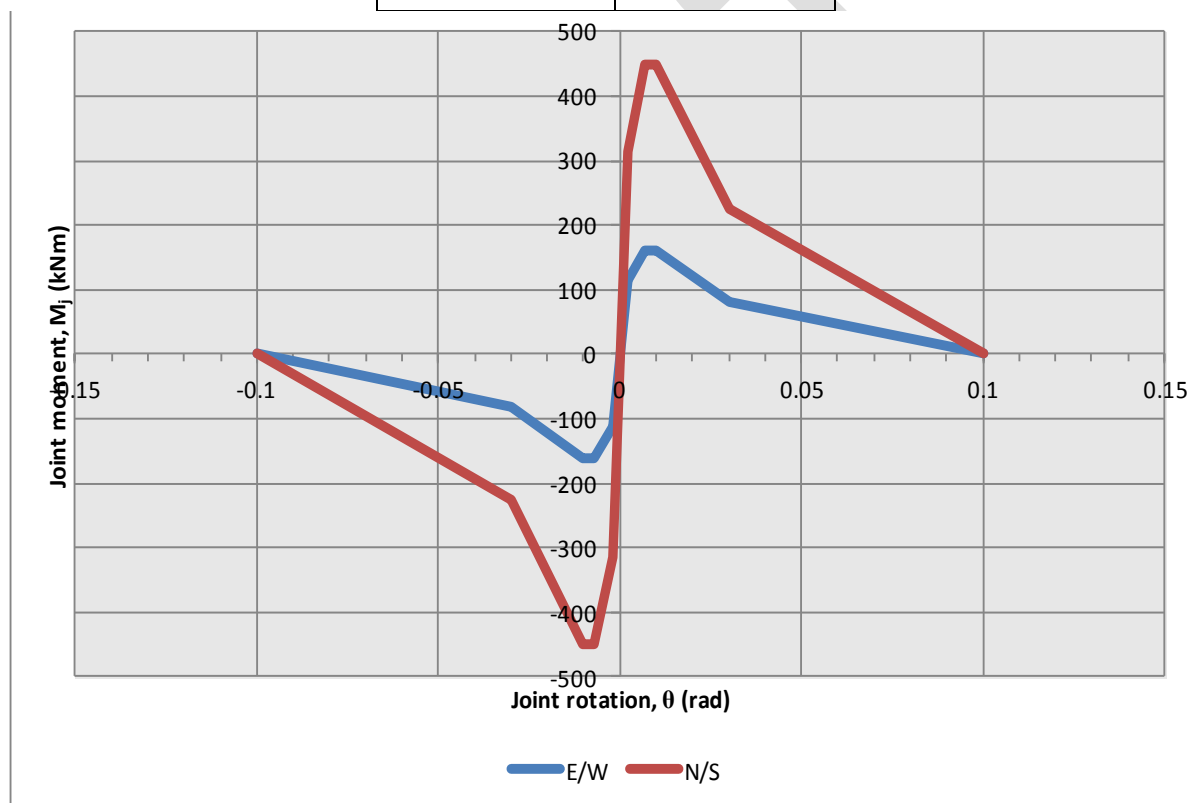
**Figure 15: Joint response backbone curve for joint at grid A2, level 3 (exterior E/W, interior N/S)**

Table 7: Summary details of beam-column joints

Location (grid, level)	Joint axial stress (MPa)	East/West			North/South		
		Type	V_{jh}	M_j/V_{jh}	Type	V_{jh}	M_j/V_{jh}
F1, L2	-3.5	Ext	873	0.584	Ext	873	0.584
C1, L2	-4.5	Int	1842	0.584	-	-	-
B1, L2	-4.4	Int	1282	0.622	-	-	-
A1, L2	-1.5	Ext	371	0.628	Ext	310	0.584
F2, L2	-3.9	Ext	950	0.363	Int	1809	0.584
E2, L2	-7.1	Int	1437	0.599	-	-	-
D2, L2	-8.6	Int	1518	0.587	-	-	-
C2, L2	-8.9	Int	1537	0.587	-	-	-
B2, L2	-7.8	Int	1476	0.597	-	-	-
A2, L2	-4.2	Ext	486	0.352	Int	803	0.584
F2, L2	-3.9	Ext	950	0.363	Int	1809	0.584
E2, L2	-7.1	Int	1437	0.599	-	-	-
D2, L2	-8.6	Int	1518	0.587	-	-	-
C2, L2	-8.9	Int	1537	0.587	-	-	-
B2, L2	-7.8	Int	1476	0.597	-	-	-
A2, L2	-4.2	Ext	486	0.352	Int	803	0.584
F1, L2	-3.5	Ext	873	0.584	Ext	873	0.584
D/E4, L2	-6.6	Int	1414	0.586	-	-	-
B4, L2	-5.4	Int	1343	0.601	-	-	-
A4, L2	-2.2	Ext	406	0.600	Ext	344	0.584
F1, L3	-2.7	Ext	809	0.583	Ext	809	0.583
C1, L3	-3.5	Int	1753	0.583	-	-	-
B1, L3	-3.4	Int	1222	0.620	-	-	-
A1, L3	-1.1	Ext	353	0.626	Ext	293	0.583
F2, L3	-3.0	Ext	878	0.363	Int	1720	0.583

Table 7 (cont.): Summary details of beam-column joints

Location (grid, level)	Joint axial stress (MPa)	East/West			North/South		
		Type	V_{jh}	M_j/V_{jh}	Type	V_{jh}	M_j/V_{jh}
E2, L3	-5.5	Int	1349	0.598	-	-	-
D2, L3	-6.7	Int	1417	0.585	-	-	-
C2, L3	-7.0	Int	1437	0.585	-	-	-
B2, L3	-6.2	Int	1387	0.596	-	-	-
A2, L3	-3.6	Ext	460	0.352	Int	772	0.583
F2, L3	-3.0	Ext	878	0.363	Int	1720	0.583
E2, L3	-5.5	Int	1349	0.598	-	-	-
D2, L3	-6.7	Int	1417	0.585	-	-	-
C2, L3	-7.0	Int	1437	0.585	-	-	-
B2, L3	-6.2	Int	1387	0.596	-	-	-
A2, L3	-3.6	Ext	460	0.352	Int	772	0.583
F1, L3	-2.7	Ext	809	0.583	Ext	809	0.583
D/E4, L3	-5.2	Int	1333	0.584	-	-	-
B4, L3	-4.2	Int	1271	0.600	-	-	-
A4, L3	-1.6	Ext	376	0.598	Ext	315	0.583
F1, L4	-1.8	Ext	734	0.583	Ext	734	0.583
C1, L4	-2.4	Int	1646	0.583	-	-	-
B1, L4	-2.3	Int	1150	0.620	-	-	-
A1, L4	-0.7	Ext	335	0.626	Ext	276	0.583
F2, L4	-2.0	Ext	793	0.363	Int	1619	0.583
E2, L4	-3.6	Int	1234	0.598	-	-	-
D2, L4	-4.4	Int	1284	0.585	-	-	-
C2, L4	-4.7	Int	1305	0.585	-	-	-
B2, L4	-4.1	Int	1266	0.596	-	-	-
A2, L4	-2.1	Ext	401	0.352	Int	704	0.583

Table 7 (cont.): Summary details of beam-column joints

Location (grid, level)	Joint axial stress (MPa)	East/West			North/South		
		Type	V_{jh}	M_j/V_{jh}	Type	V_{jh}	M_j/V_{jh}
F2, L4	-2.0	Ext	793	0.363	Int	1619	0.583
E2, L4	-3.6	Int	1234	0.598	-	-	-
D2, L4	-4.4	Int	1284	0.585	-	-	-
C2, L4	-4.7	Int	1305	0.585	-	-	-
B2, L4	-4.1	Int	1266	0.596	-	-	-
A2, L4	-2.1	Ext	401	0.352	Int	704	0.583
F1, L4	-1.8	Ext	734	0.583	Ext	734	0.583
D/E4, L4	-3.5	Int	1228	0.584	-	-	-
B4, L4	-2.8	Int	1184	0.600	-	-	-
A4, L4	-1.0	Ext	349	0.598	Ext	289	0.583
F1, L5	-0.9	Ext	651	0.583	Ext	651	0.583
C1, L5	-1.2	Int	1530	0.583	-	-	-
B1, L5	-1.2	Int	1073	0.620	-	-	-
A1, L5	-0.4	Ext	317	0.626	Ext	258	0.583
F2, L5	-1.0	Ext	698	0.363	Int	1511	0.583
E2, L5	-1.7	Int	1107	0.598	-	-	-
D2, L5	-2.1	Int	1135	0.585	-	-	-
C2, L5	-2.4	Int	1158	0.585	-	-	-
B2, L5	-2.2	Int	1139	0.596	-	-	-
A2, L5	-1.1	Ext	355	0.352	Int	652	0.583
F2, L5	-1.0	Ext	698	0.363	Int	1511	0.583
E2, L5	-1.7	Int	1107	0.598	-	-	-
D2, L5	-2.1	Int	1135	0.585	-	-	-
C2, L5	-2.4	Int	1158	0.585	-	-	-
B2, L5	-2.2	Int	1139	0.596	-	-	-

Table 7 (cont.): Summary details of beam-column joints

Location (grid, level)	Joint axial stress (MPa)	East/West			North/South		
		Type	V_{jh}	M_j/V_{jh}	Type	V_{jh}	M_j/V_{jh}
A2, L5	-1.1	Ext	355	0.352	Int	652	0.583
F1, L5	-0.9	Ext	651	0.583	Ext	651	0.583
D/E4, L5	-1.7	Int	1109	0.584	-	-	-
B4, L5	-1.5	Int	1091	0.600	-	-	-
A4, L5	-0.6	Ext	328	0.598	Ext	268	0.583
F1, L6	-0.1	Ext	566	0.583	Ext	566	0.583
C1, L6	-0.1	Int	1406	0.583	-	-	-
B1, L6	-0.1	Int	989	0.620	-	-	-
A1, L6	-0.1	Ext	301	0.626	Ext	243	0.583
F2, L6	-0.1	Ext	596	0.363	Int	1404	0.583
E2, L6	-0.1	Int	990	0.598	-	-	-
D2, L6	-0.1	Int	991	0.585	-	-	-
C2, L6	-0.1	Int	991	0.585	-	-	-
B2, L6	-0.1	Int	990	0.596	-	-	-
A2, L6	-0.2	Ext	305	0.352	Int	599	0.583
F2, L6	-0.1	Ext	596	0.363	Int	1404	0.583
E2, L6	-0.1	Int	990	0.598	-	-	-
D2, L6	-0.1	Int	991	0.585	-	-	-
C2, L6	-0.1	Int	991	0.585	-	-	-
B2, L6	-0.1	Int	990	0.596	-	-	-
A2, L6	-0.2	Ext	305	0.352	Int	599	0.583
F1, L6	-0.1	Ext	566	0.583	Ext	566	0.583
D/E4, L6	-0.5	Int	1020	0.584	-	-	-
B4, L6	-0.1	Int	990	0.600	-	-	-
A4, L6	-0.1	Ext	302	0.598	Ext	244	0.583

5.4. Reinforced Concrete Shear Walls

The CTV Building contains two reinforced concrete shear wall systems. Each of these systems was modelled using non-linear layered shell elements, which incorporate inelastic material effects at a fibre level. Where significant inelastic demands were not expected, the wall was modelled using linear elastic shell elements with stiffness modifiers determined from moment curvature analyses similar to those described in Section 5.3.2. The stiffness modifiers determined via these analyses along with those determined following the recommendations presented in the New Zealand Concrete Structures Standard (NZS 3101 2006, Table C6.6) are presented in Figure 16 below based on the gravity axial load.

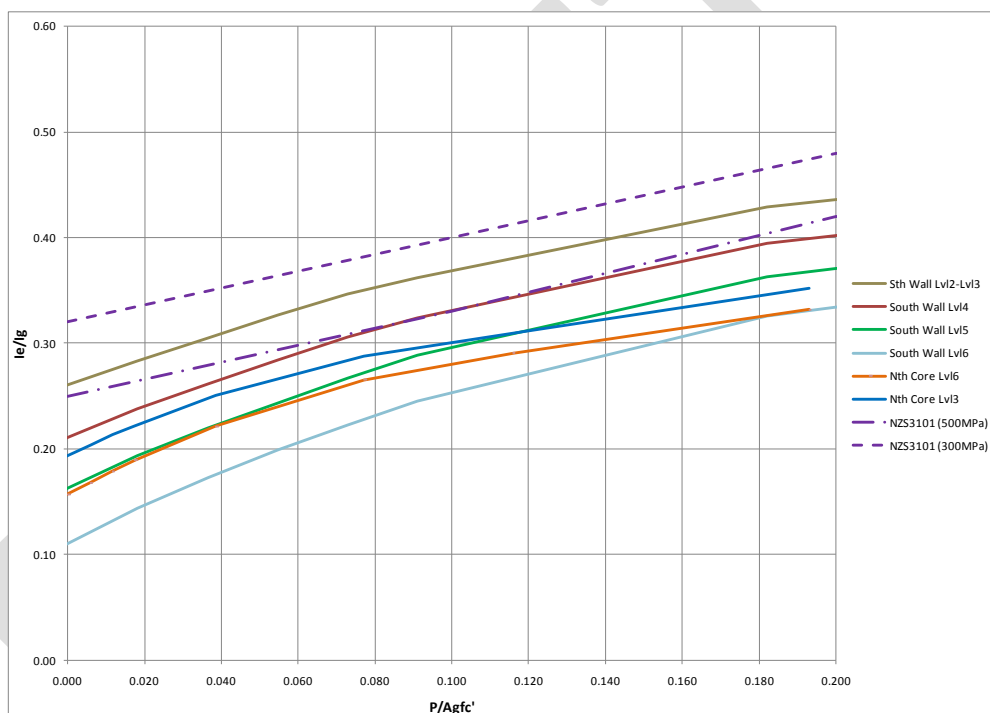


Figure 16: Effective wall stiffness relationship

Confining reinforcement was detailed for the boundary regions of all reinforced concrete shear walls in the lower two storeys. It was considered appropriate to model the non-linear stress strain behaviour of the concrete fibres in these regions based on the Mander confined concrete model (Mander et al. 1988). The concrete material in the layered shell element was assumed to be unconfined between boundary regions and for wall elements above the level 3 floor plate.

Diagonally reinforced coupling beams connected the two portions of south shear wall as seen in Figure 17 below. The typical span to depth aspect ratio of the coupling beams was 0.76 but varied from 0.55 at the bottom to 1.2 at the top of the wall. Modelling of the diagonally reinforced coupling beams has been based upon the approach documented in Appendix A, with non linear links substituted for the fibre elements to reduce computation time.

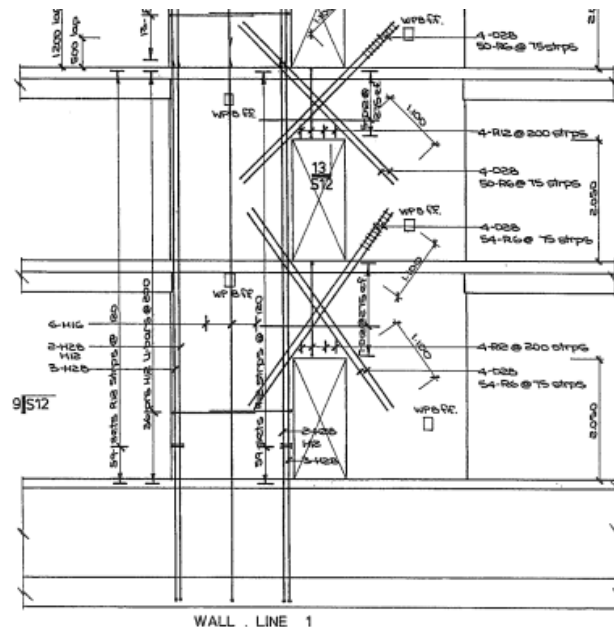


Figure 17: South shear wall typical coupling beam reinforcement arrangement (Design Engineer 1986a)

5.5. Floors

Review of the lateral load paths has indicated that diaphragm integrity at the interface with shear walls may have been an important consideration in the determination of the seismic performance of the structure. As such, the flexibility of each floor level has been modelled with in-plane stiffness based on the average thickness of the concrete slab (173 mm). For the purposes of the analysis the stiffness of the slab elements has been taken as $0.32A_{gross}$ for in-plane actions. In order to capture potential inelastic demand in the slabs at the support locations, non-linear layered shells have been used adjacent to beam lines. Shell properties have been based upon the reinforcement present at the beam face assuming no contribution from the metal decking. Linear elastic shells have been used to represent the remainder of the floor slabs. Diaphragm actions have been monitored at interfaces with shear walls.

The floor diaphragm connections to the north core lift shaft walls on grids D and D/E have been identified as an area of potential connection failure. As a consequence of a lack of specific tie reinforcement it was assumed that there is no tensile or gravity connection between the slab and these walls at levels 2 and 3. At levels 4 to 6 a retrofitted steel angle tie (or 'drag bar') provided limited tensile and gravity connection to the slab at the tips of walls D and D/E. Multi-linear links have been used to provide a 'fuse' that will transfer the expected upper bound tensile capacity of the retrofitted connection only with no limitation on the compressive load transfer capability. Nominal tensile connection capacities for the drag bar and its connections, and the corresponding ultimate displacements have been provided by Hyland Fatigue & Earthquake Engineering and StructureSmith. These are listed in Table 8 below.

Table 8: Modelled diaphragm (drag bar) connection capacities

Wall	Level	Tensile Capacity (kN)	Displacement at Disconnection (mm)	Compressive Capacity (kN)
D	2	0	0	Not limited
	3	0	0	Not limited
	4	320	2.3	Not limited
	5	420	2.4	Not limited
	6	603	2.6	Not limited
D/E	2	0	0	Not limited
	3	0	0	Not limited
	4	403	2.8	Not limited
	5	503	3.0	Not limited
	6	540	3.0	Not limited

Floor diaphragm connections to the other north core walls on grids 5, C and C/D, and to the south wall on grid 1 were assumed to remain connected for the purposes of the seismic analysis. Maximum diaphragm actions at these locations are reported at these locations in Sections 10 and 11 for assessment by others.

For out-of-plane demands (i.e. plate action) the floors have been considered to have stiffness corresponding to $EI_{Effective} = 1872 \text{ kNm}^2/\text{m}$ for the remaining slab (as recommended by Mander 2012, June 14) with the effective stiffness adjacent to beam lines and implicitly considered by the non-linear layered shell element. In the determination of the slab flexural stiffness at beam faces the contribution of the metal decking has been ignored as the decking would not have been effectively anchored at the beam support where the positive (sagging) flexural demands are greatest.

6. Loadings

6.1. Gravity Loadings

For combination with seismic loads a gravity load combination has been developed following the requirements of the New Zealand Design Actions Standard (AS/NZS 1170.0 2002, section 4). This gravity load combination also formed the basis for consideration of P-delta effects in the seismic analyses. In this combination live load allowances have been combined with the initial staged dead load analysis as a separate loading step as follows,

$$E_d = G + \sum \Psi_{C,i} \Psi_{A,i} Q_i$$

Taking ‘G’ as the sum of all dead type loadings incorporating element self weights, plus any superimposed dead load (SDL) allowances that are required to be considered, and ‘ $\sum \Psi_{C,i} \Psi_{A,i} Q_i$ ’ given as the sum product of all individual components of imposed loading as presented in Table 9 below¹.

Table 9: Basic load pattern definitions

Gravity load component	Load allowance (kPa)	Ψ_C	Ψ_A
DL	Self weight	1.0	1.0
SDL	0.55	1.0	1.0
Plant LL	5.0	0.6	1.0
Toilet LL	2.0	0.4	1.0
Office LL	3.0	0.4	1.0
Roof LL	0.25	0	1.0

Note that the use of Ψ_A equal to 1.0 for office live load could slightly over-estimate column compression demand in lower levels of the structure by between 2 and 7 percent. For the purpose of determining gravity actions in the upper levels of the structure it is believed that a Ψ_A equal to 1.0 suitably represents the gravity actions.

¹ It is noted that the recent third amendment to NZS 1170.0 corrected the load combinations for earthquake loading so that the earthquake combination factor Ψ_E is used to factor the live load component rather than the combination factor Ψ_C . This change would have only a minor effect on the calculated gravity loads, resulting in the toilet and office live load factor listed in Table 9 reducing from 0.4 to 0.3.

It should be noted that level 3 and the east side of level 6 of the CTV structure are understood to have been untenanted at the time of the earthquake. No live load allowance has been included at these locations.

Table 10 below presents the global base reaction reported at the model origin (i.e. $\{x,y,z\}=\{0,0,0\}$ c= Level 1 at grid reference F/1) for each load type arising from a linear analysis.

Table 10: Global base reactions for basic load patterns (linear)

Gravity load case	FZ (kN)	MX (kNm)	MY (kNm)
DL	35458	492755	482464
SDL	4647	65608	59200
Plant LL	364	5014	8951
Toilet LL	135	2220	3307
Office LL	7437	119468	87223
Roof LL	0	0	0

6.2. Dynamic Mass

The dynamic mass used in the seismic analyses was determined following the provisions of the New Zealand Design Actions Standard (NZS 1170.5 2004, clause 4.2) where,

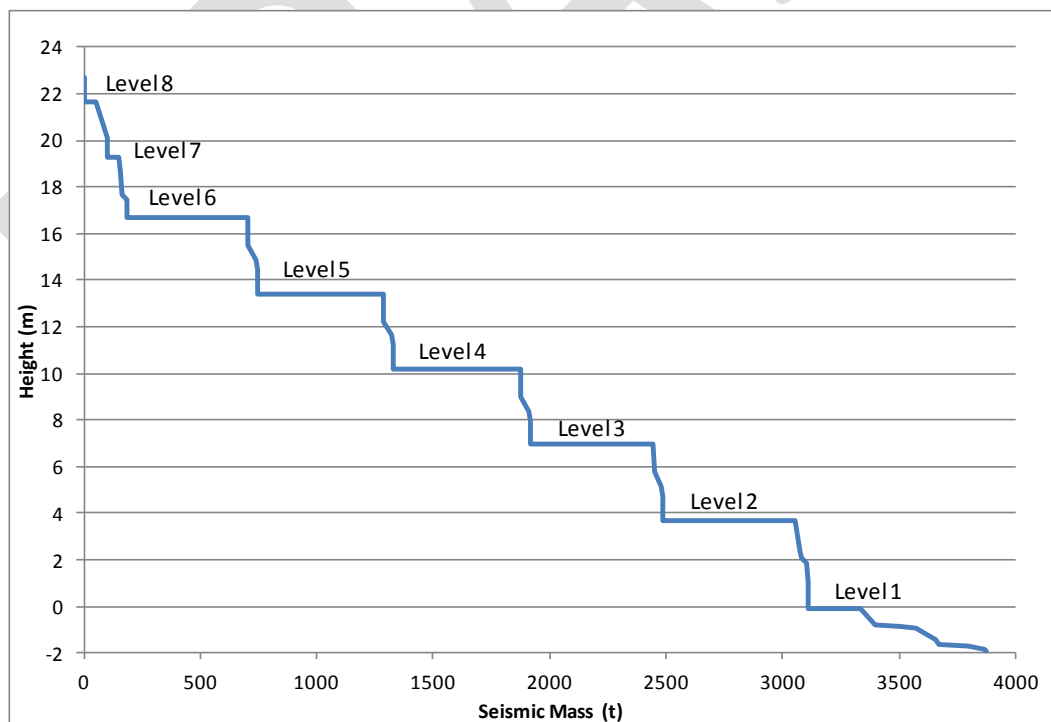
$$W_t = G + \sum \Psi_{E,i} \Psi_{A,i} Q_i$$

taking ‘ G ’ based on all dead loads (plus superimposed dead loads), ‘ $\sum \Psi_{c,i} \Psi_{A,i} Q_i$ ’ as the sum product of the individual imposed loadings as per Table 11 below.

Table 11: Imposed loading allowances (for derivation of dynamic mass)

Gravity load component	Load allowance (kPa)	Ψ_E	Ψ_A
DL	Self weight	NA	NA
SDL	0.55	NA	NA
Plant LL	5.0	0.6	0.74
Toilet LL	2.0	0.3	0.5
Office LL	3.0	0.3	0.5
Roof LL	0.25	0.0	0.0

Seismic mass associated with the load component ‘DL’ has been obtained through explicit modelling of the structural elements. All other tributary masses outlined in Table 11 have been incorporated via distributed loads applied to the floor/roof elements in order to accurately proportion mass for slabs and beams etc. Note that as for Section 6.1 no live load has been included in the development of the dynamic mass for the untenanted levels. The distribution of seismic mass in the analysis model is as presented in Figure 18 below.

**Figure 18: Seismic mass distribution**

7. Modal Analysis

Modal analysis has been carried out considering dynamic mass as outlined in Section 6.2. The results of this analysis are presented in Table 12 below (showing modes with more than 2% mass participating only), with X, Y, and Z representing the north, west, and vertical axes respectively. Note the modal analysis was performed using $EI_{\text{effective}}$ values for all members in the structure.

Table 12: Modal participating mass ratios

Mode	Period (sec)	UX	UY	UZ	ΣUX	ΣUY	ΣUZ	RZ	ΣRZ
1	1.33	0.63	0.01	0.00	0.63	0.00	0.00	0.21	0.21
2	1.00	0.00	0.41	0.00	0.63	0.41	0.00	0.01	0.23
3	0.51	0.00	0.25	0.00	0.63	0.66	0.00	0.42	0.65
7	0.28	0.02	0.03	0.00	0.68	0.71	0.00	0.01	0.68
8	0.27	0.06	0.02	0.00	0.74	0.73	0.00	0.00	0.69
13	0.21	0.00	0.02	0.00	0.77	0.78	0.00	0.05	0.76
14	0.19	0.00	0.00	0.28	0.77	0.78	0.28	0.00	0.76
16	0.19	0.00	0.00	0.08	0.77	0.78	0.38	0.00	0.76
78	0.1	0.00	0.00	0.03	0.81	0.81	0.69	0.00	0.78
81	0.1	0.00	0.00	0.04	0.81	0.81	0.73	0.00	0.78
102	0.05	0.04	0.00	0.00	0.87	0.88	0.85	0.02	0.83
104	0.04	0.01	0.04	0.00	0.88	0.92	0.87	0.07	0.90
105	0.04	0.03	0.00	0.00	0.91	0.93	0.87	0.00	0.91
110	0.03	0.00	0.00	0.03	0.96	0.95	0.93	0.00	0.93
112	0.02	0.00	0.00	0.04	0.96	0.95	0.96	0.00	0.93
115	0.02	0.00	0.00	0.03	0.97	0.97	1.00	0.00	0.94

8. Non-Linear Static (Pushover) Analysis

8.1. Methodology

In order to gain an initial view of the anticipated seismic performance of the building a non-linear static analysis (often referred to as a “Pushover”) was undertaken for the analysis model. This pushover was used to verify that the finite elements employed for each of the structural mechanisms outlined in Section 0 were performing as expected.

Pushover analyses were undertaken in each of the two orthogonal directions i.e. north/south (N/S) & east/west (E/W) independently. The pushover cases consist of a displacement controlled, force based analysis with the load vector based upon a triangular load distribution, and inertia force applied to each mass degree of freedom in the model. Building centre of mass target displacements of 200 mm and 150 mm were taken for the N/S and E/W directions respectively. These values are approximately equivalent to the current Building Code (DBH 2011) elastic displacement demands based upon the fundamental periods of vibration obtained from section 7 and considering subsoil type D, $Z=0.30$, and $S_p=1$ as can be seen in Figure 19 below. It was assumed that the level 6 displacement demand is approximately 1.5 times greater than the building centre of mass demand.



Figure 19: Site spectral displacements.

8.2. Force-Displacement Relationships

Force-displacement plots for the push-over analyses are presented in Figure 20. Displacements have been recorded at a node located at approximately the centre of mass of level 6. Figure 21 and Figure 22 present the base shear components recorded at the top of the foundation beams for each of the primary structural elements.

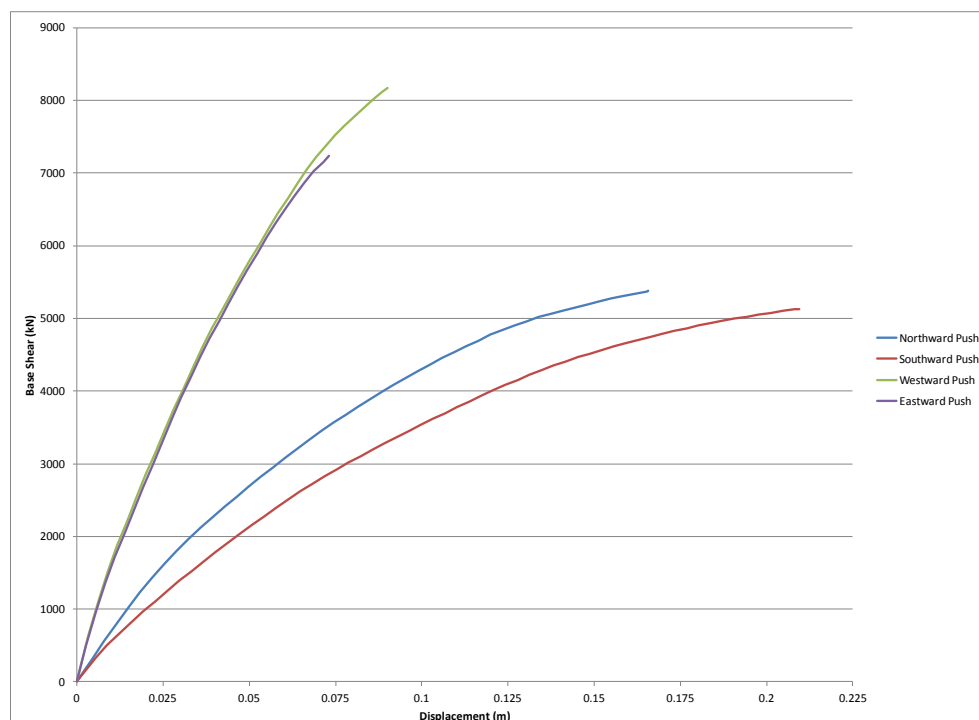


Figure 20: Force-displacement relationship.

It can be seen from the pushover plots that the building responds to the imposed lateral loading in a non-linear manner. Plot profiles for both the east and west directions are almost identical indicating a similar building response in each of these directions. Initial response of the building in the northward direction is stiffer than in the southward direction, which can be attributed to the differences in the foundation behaviour under the north core for these directions.

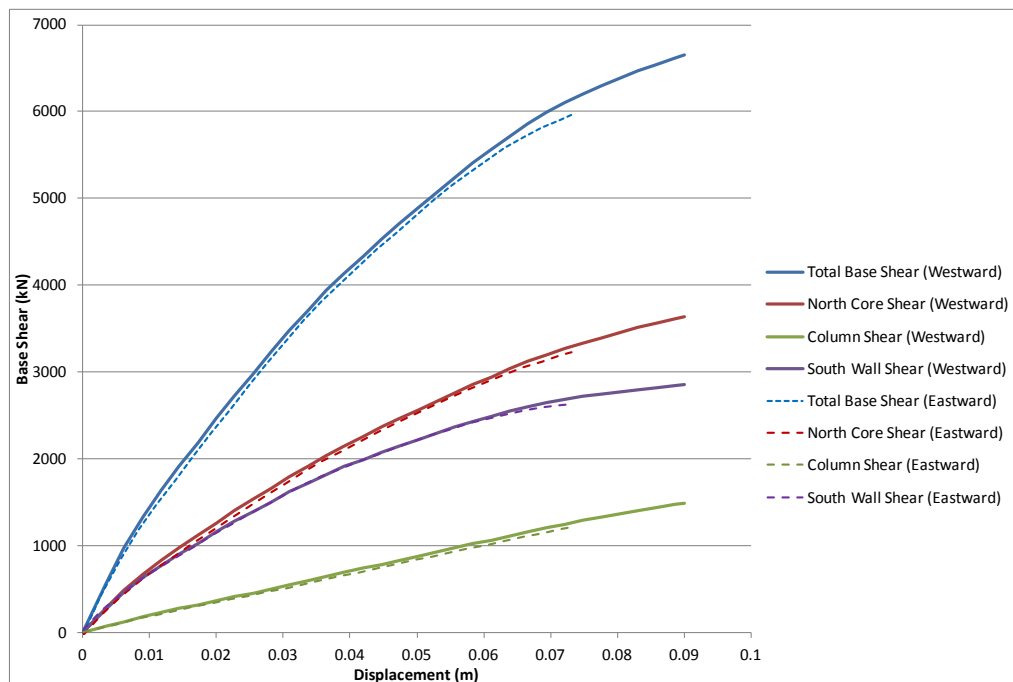


Figure 21: Base shear components - east/west direction.

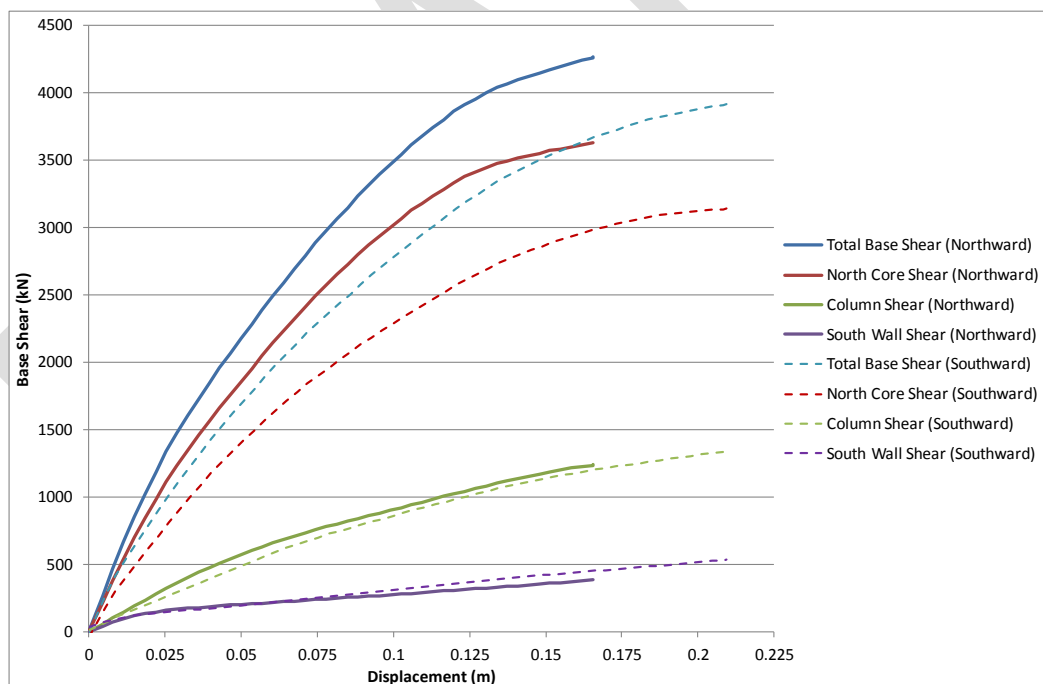


Figure 22: Base shear components - north/south direction.

Components of base shear are similar in each of the directions of loading with the exception of the north core in the north/south direction. As can be seen in Figure 22, more base shear is carried by the core for an applied northward load than for a loading direction toward the south. This is due to the mobilisation of additional gravity load from the beams and slab

along gridline 4 as the southern edge of the core wall webs move upwards with core rotation to the north. These shears provide a restoring force that restrains the wall rotation, requiring higher shears to generate the same centre of mass displacement at level 6.

Pushover analyses have indicated that the response of the building in the east/west direction to be significantly torsional. Figure 23 to Figure 26 present the variation in displacement profile between the approximate centre of mass (at Level 6) and the building perimeter gridlines for each direction under consideration. East/west displacement on gridline 1 is approximately three times greater than that on grid 4, and can be seen in Figure 23 and Figure 24. This is a consequence of the difference in relative stiffness between the north core and the coupled shear wall on grid 1. As the coupled shear wall on gridline 1 yields the torsional response of the building is further exacerbated.

Little torsional behaviour is exhibited through loading in the north/south direction. As can be seen in Figure 25 and Figure 26 there is almost no difference in displacement between grid A and grid F under north/south loading.

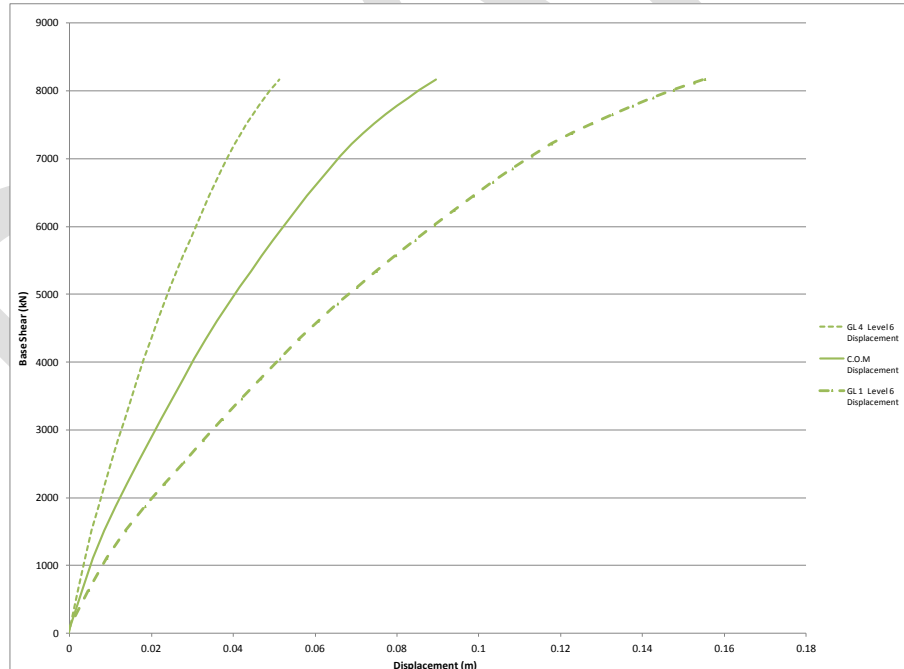


Figure 23: Level 6 western pushover displacement profile.

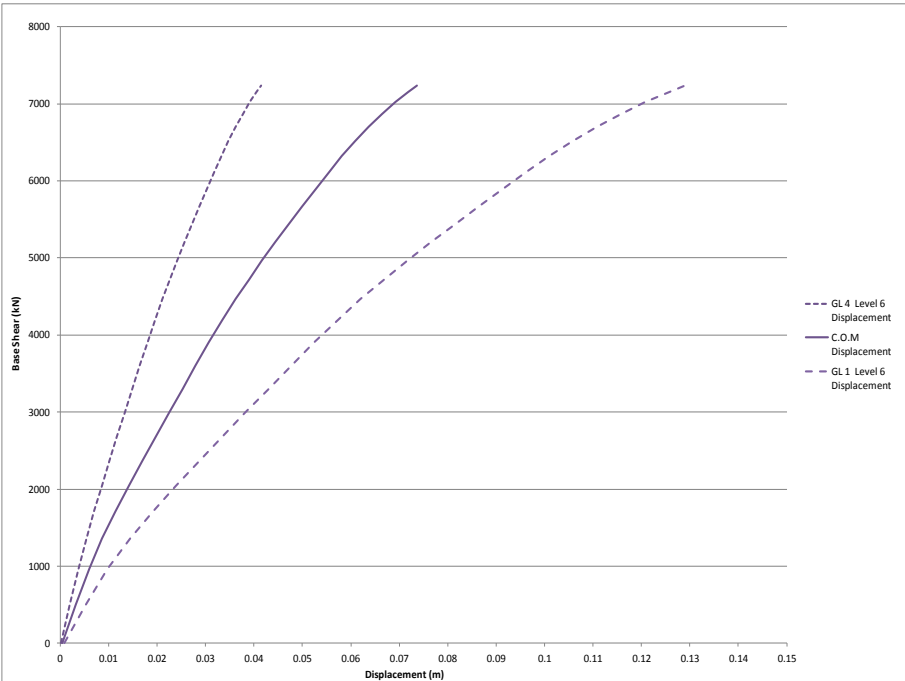


Figure 24: Level 6 eastern pushover displacement profile.

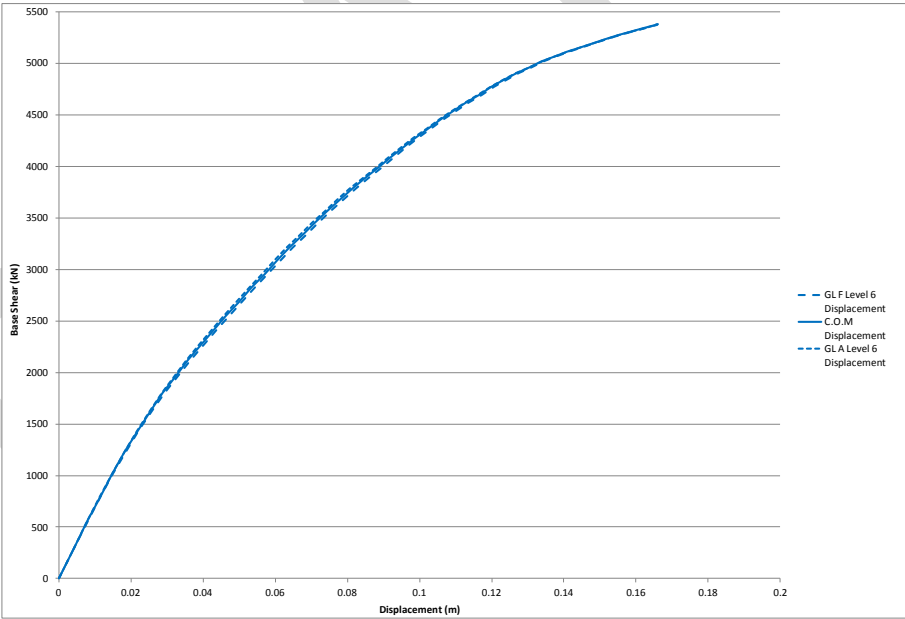


Figure 25: Level 6 northern pushover displacement profile.

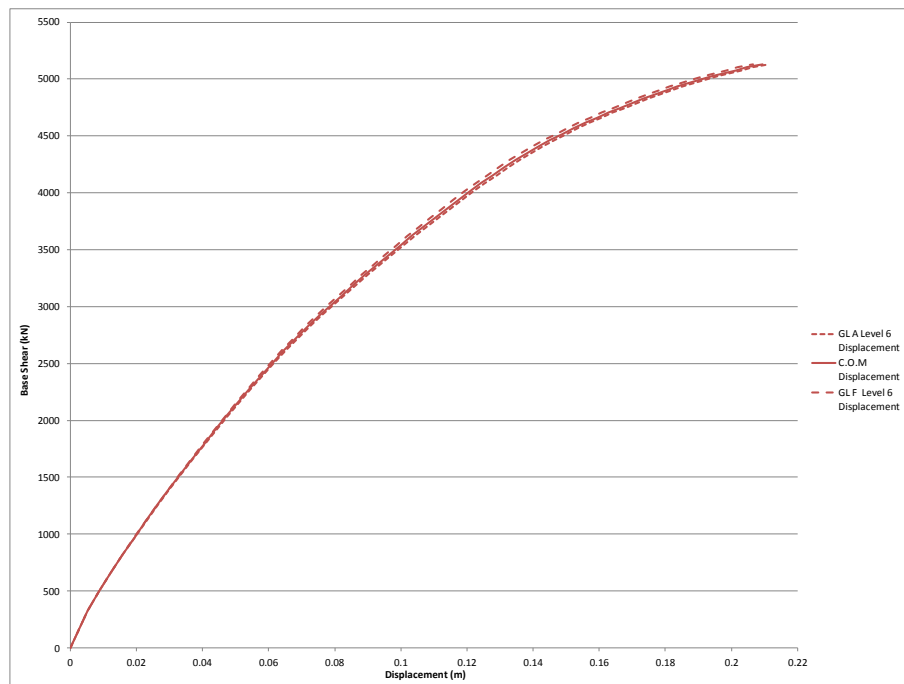


Figure 26: Level 6 southern pushover displacement profile.

8.3. Building Displacement Ductility Capacity.

Figure 27 presents the pushover plots that have been bi-linearised in order to obtain an estimate on the building displacement ductility capacity. From Figure 27 the ductility capacity can be estimated as being approximately two.

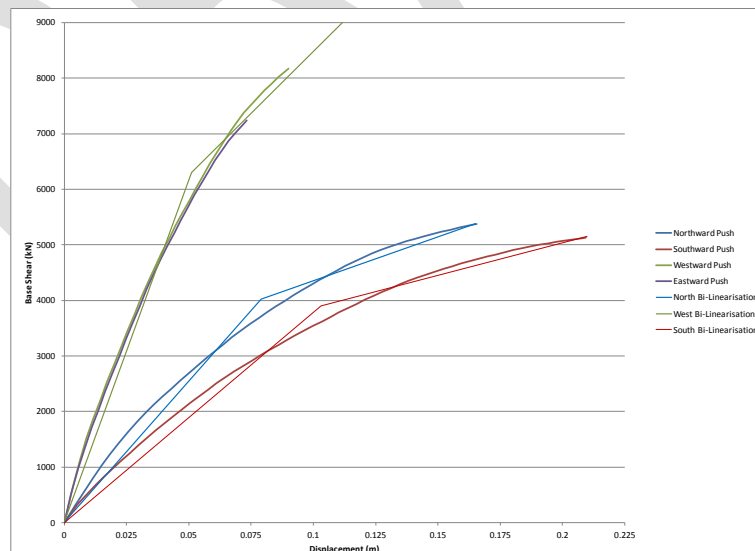


Figure 27: Bi-linear pushover plots

9. Non-linear Dynamic (Time History) Analysis

Non-linear time history analyses (NTHA) have been undertaken incorporating inelastic behaviour for the analysis model as outlined in Section 3. Two seismic event scenarios are considered in these analyses which are denoted as the ‘*Darfield*’ event, and the ‘*Lyttelton*’ event in this report. The details of these events as obtained from GNS Science (Geonet 2010a, 2011a) are presented in Table 13 below.

Table 13: Seismic event information

Event Name	Reference Number	Local Date & Time	Epicenter Location	Magnitude	Focal Depth
Darfield	3366146	04Sept2010, 0435hrs	43.55°S, 172.17°E	M _L 7.1	11 km
Lyttelton	3468575	22Feb2011, 1251hrs	43.60°S, 172.71°E	M _L 6.3	5 km

9.1. Analysis Ground Motions

In an attempt to approximate the ground shaking that was experienced at the CTV site for each of the two events, a suite of four acceleration time history records were adopted following the recommendations of Tonkin and Taylor (Sinclair 2011). These were records recorded at other locations in the Christchurch CBD and are presented in Table 14 below. It is expected that the REHS time history record will produce an upper bound response in the performance of the CTV building (Sinclair 2012).

Table 14: Adopted earthquake record information

Station Name	Station ID	Station Location
Christchurch Cathedral College	CCCC	43.54°S, 172.65°E
Christchurch Hospital	CHHC	43.54°S, 172.63°E
Christchurch Botanic Gardens	CBGS	43.53°S, 172.62°E
Resthaven	REHS	43.52 S, 172.64 E

The acceleration time histories were obtained from GNS Science (Geonet 2010b, 2011b) and have been processed in order to align the axes of the recorded motions to purely north/south (denoted as component N00E) and east/west (denoted as component N90E) components to

coincide with the principle axis of the CTV building. No processing has been undertaken on the vertical components of the records.

Figure 28 through Figure 33 below present the site 5% damped response spectra for the three (processed) components of the Darfield and Lyttelton events respectively. Also presented for reference is the mean of the recorded components and the elastic spectra used for design purposes at the site derived in accordance with New Zealand Standards (NZS 1170.5 2004) considering site subsoil class D, $Z = 0.22$ (i.e. that applicable for a new building design in Christchurch during February 2011), and $S_p = 1.0$.

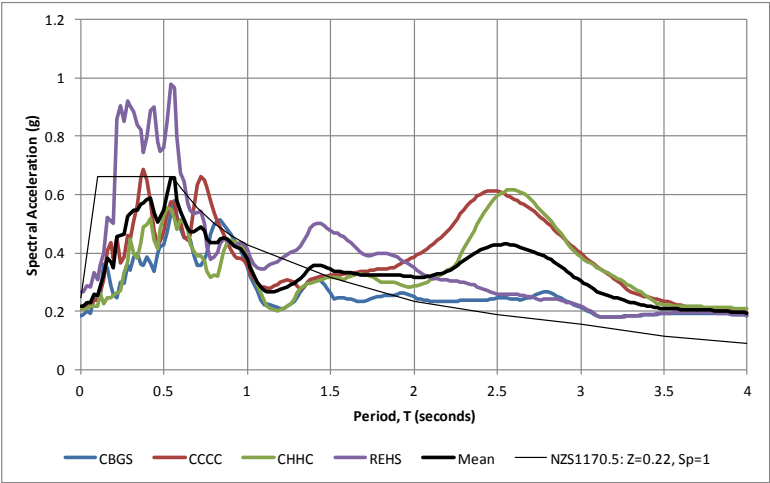


Figure 28: Darfield N00E 5% damped response spectra (north/south)

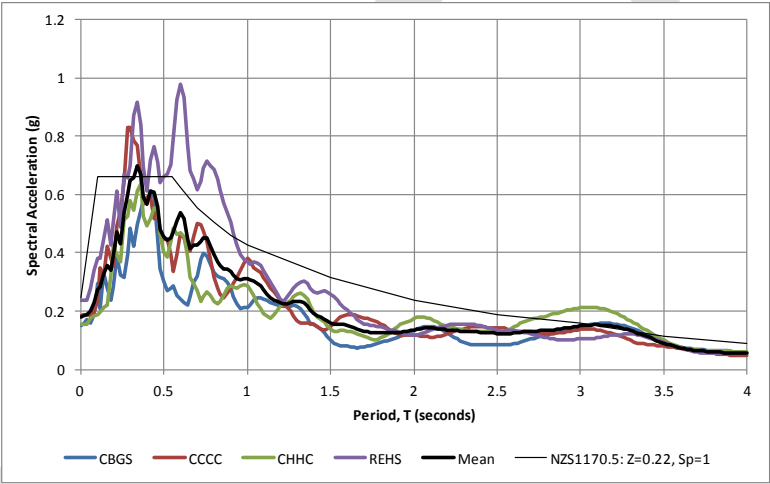


Figure 29: Darfield N90E 5% damped response spectra (east/west)

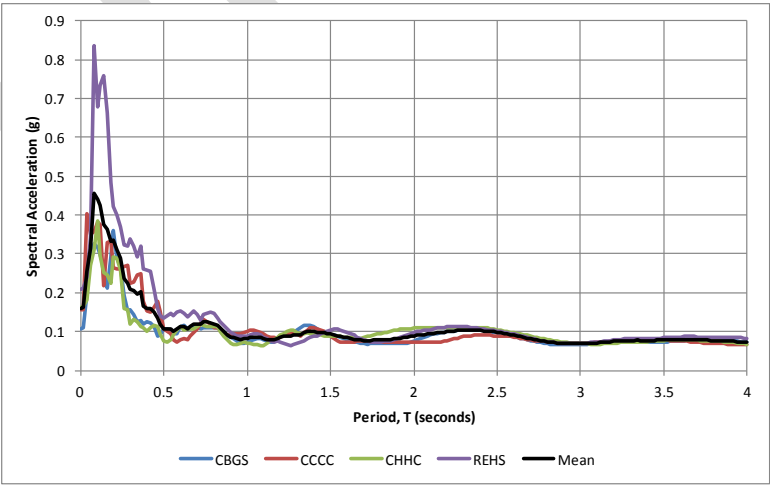


Figure 30: Darfield Vertical 5% damped response spectra

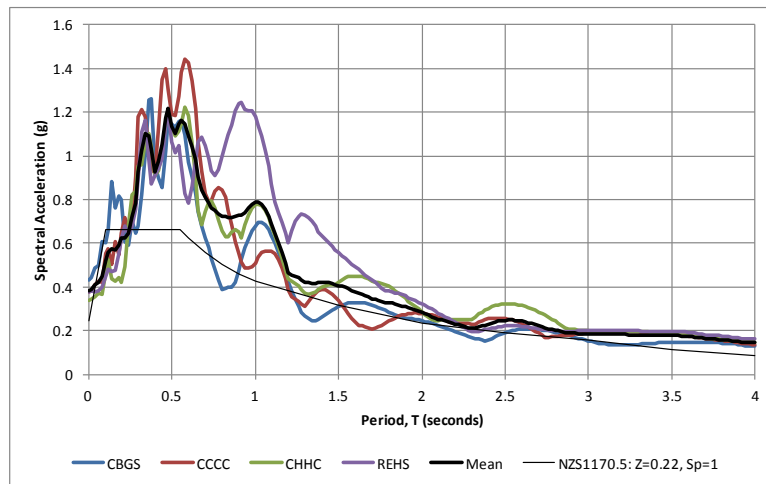


Figure 31: Lyttelton N00E 5% damped response spectra (north/south)

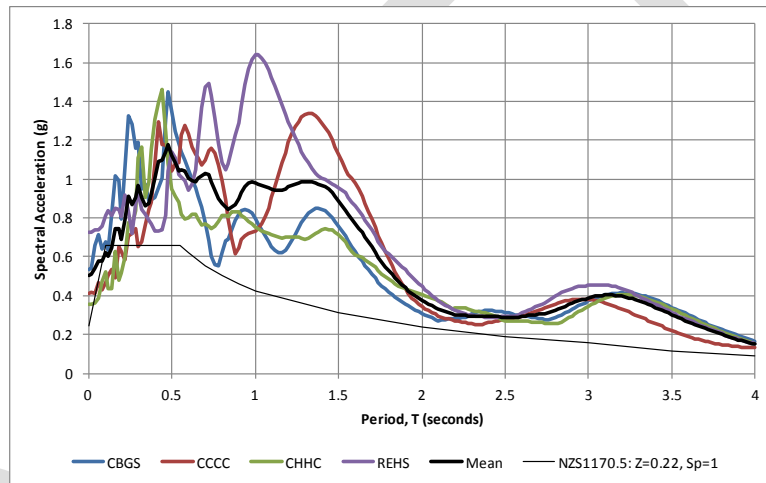


Figure 32: Lyttelton N90E 5% damped response spectra (east/west)

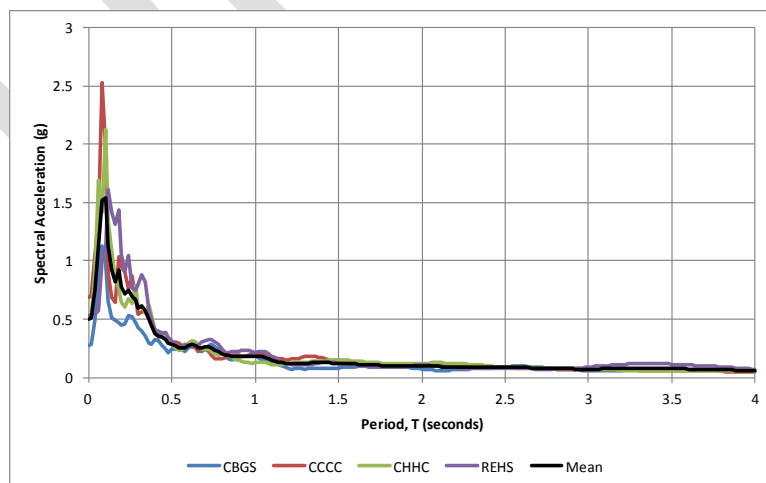


Figure 33: Lyttelton Vertical 5% damped response spectra

The records as supplied by GNS have arbitrary stop and start times that encompass many seconds of very small ground vibration. Incorporation of the entire record into the analysis would add no benefit to the understanding of the structural response or performance, and would only add considerable analysis time. For the purposes of the non linear time history analysis runs, reduced length records have been used to reduce computation times. Record start and finish times have been selected to ensure that all significant shaking is captured by the analysis and are presented in Table 15. All results contained with this document have been presented relative to the adopted start time of each acceleration time history record. Appendix F contains the acceleration time history records used for these analyses.

Acceleration time history records for the Darfield event were much longer in duration than for the Lyttelton event. To reduce analysis time only the CBGS and CCCC record was analysed for Darfield.

Table 15: Adopted record start and finish times

Station Name	Event	Start Time (sec)	Finish Time (sec)
Christchurch Botanic Gardens (CBGS)	Darfield	15	55
Christchurch Cathedral College (CCCC)	Darfield	15	55
Christchurch Cathedral College (CCCC)	Lyttelton	15	25
Christchurch Hospital (CHHC)	Lyttelton	15	25
Christchurch Botanic Gardens (CBGS)	Lyttelton	15	25
Resthaven (REHS)	Lyttelton	9.5	19.5

9.2. Elastic Structural Damping

Elastic damping for the structure has been incorporated in the time history analyses by way of mass (α) and stiffness (β) proportional damping coefficients, commonly referred to as Rayleigh damping. A common criticism of the Rayleigh damping method is that it considers only the initial stiffness in its determination of level of damping. In order to consider the reduced level of damping appropriate during inelastic cycling of structural elements a tangent

stiffness damping model is often considered as being preferable (Priestley et al. 2007). To address this issue, a reduced damping coefficient, ' ξ^* ', for the fundamental period has been specified for use in determining the damping coefficients. This adopted method more closely approximates the tangent stiffness approach.

Observed damage of the CTV building after the Darfield event indicated that the ductility demand of the structure was nominal. On this basis, unmodified Rayleigh damping was adopted for Darfield analysis runs. Table 16 below presents the input parameters adopted in determining the Rayleigh damping coefficients for analyses of the Darfield event.

Table 16: Rayleigh damping parameters - Darfield

	Period, T (sec)	Damping, ξ^* (%)
First	1.33	5
Second	0.05	5

Using the parameters presented in Table 16 the mass and stiffness proportional damping coefficients are determined as follows:

- Mass Proportional Coefficient, α 0.4553
- Stiffness Proportional Coefficient, β 7.669×10^{-4}

For the Lyttelton event it was necessary to estimate the building displacement ductility capacity in order to select an appropriate level of damping. From the bi-linearised pushover plot in Figure 27 of Section **Error! Reference source not found.** the approximate ductility capacity of the structure is between 1.4 and 2.1 depending on the direction of demand. For the purpose of the non-linear time history analyses a ductility of 2 was assumed for the structure. As vertical earthquake effects are assumed to influence the performance of the building it has been necessary to ensure that the damping in the vertical modes is realistically represented. For the purposes of this analysis the targeted damping in the vertical modes is 2%. Table 17 below presents the input parameters adopted in determining the Rayleigh damping coefficients for analyses of the Lyttelton event.

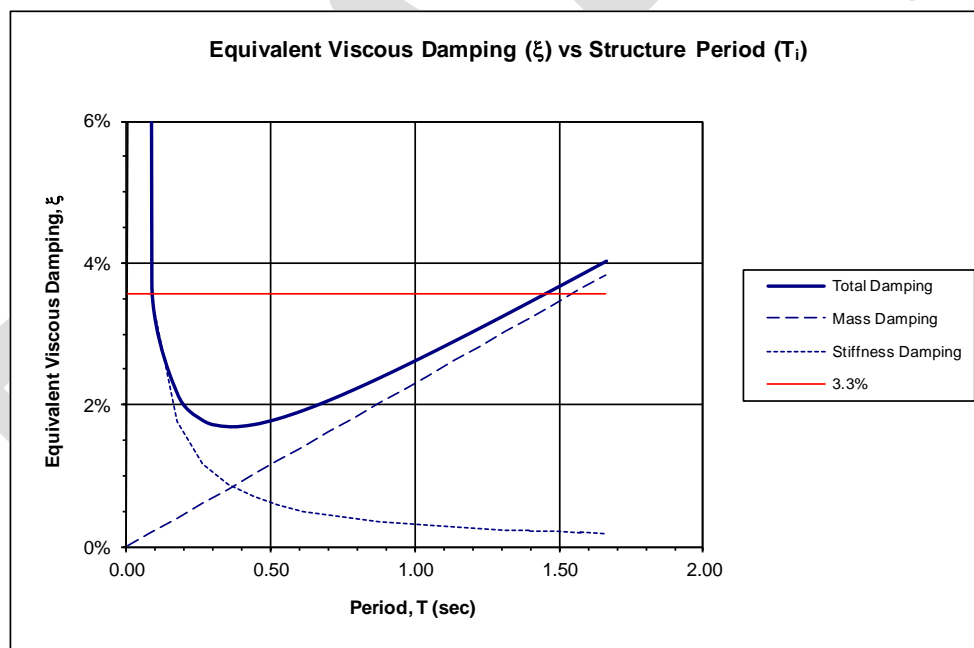
Table 17: Rayleigh damping parameters - Lyttelton

	Period, T (sec)	Damping, $\xi^*(\%)$
First	1.33	3.3
Second	0.20	2.0

Using the parameters presented in Table 17 the mass and stiffness proportional damping coefficients are determined as follows:

- Mass Proportional Coefficient, α 0.2899
- Stiffness Proportional Coefficient, β 9.795×10^{-4}

Figure 34 below presents a plot of equivalent viscous damping vs structure period obtained using the above coefficients.

**Figure 34: Equivalent viscous damping vs structure period - Lyttelton**

9.3. Radiation Damping

It has been considered that the adopted acceleration time histories inherently contain a component of radiation damping and given the uncertainties over the actual site accelerations,

and material properties, the incorporation of additional radiation damping is expected to be insignificant and as such has not been incorporated.

DRAFT

10. NLTHA Results : Darfield

Results presented are a summary of the analyses only. Additional results can be found in Appendix G and Appendix H. All results are presented for the earthquake acceleration time history recorded at the Christchurch Botanic Gardens (CBGS), and the Christchurch Cathedral College (CCCC) using all three components of the record.

10.1. Drifts and Displacements

Figure 35 and Figure 36 indicates the north/south storey drifts for the perimeter frames located on grid A, and grid F for CBGS and CCCC.

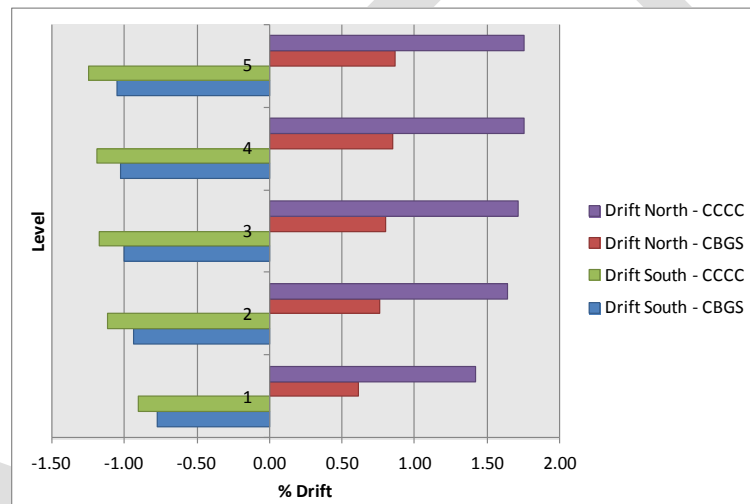


Figure 35: Frame A north/south storey drifts - Darfield.

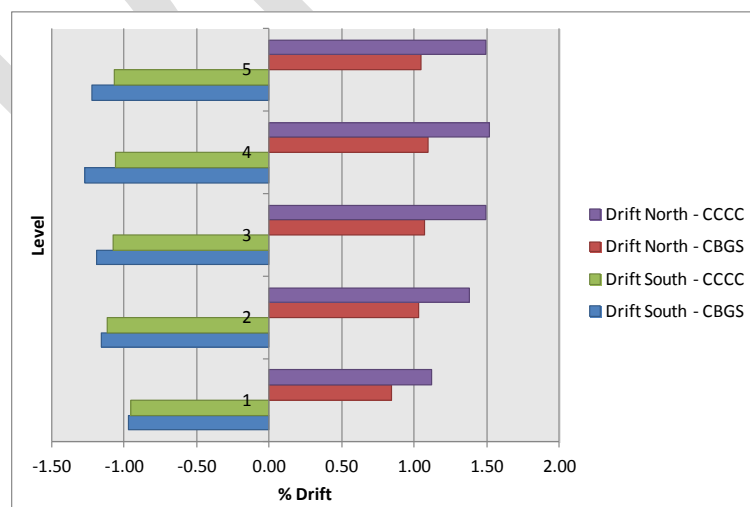


Figure 36: Frame F north/south storey drifts - Darfield.

Figure 37 and Figure 38 indicates the east/west storey drifts for the perimeter frames located on grid 1, and grid 4 for CBGS and CCCC.

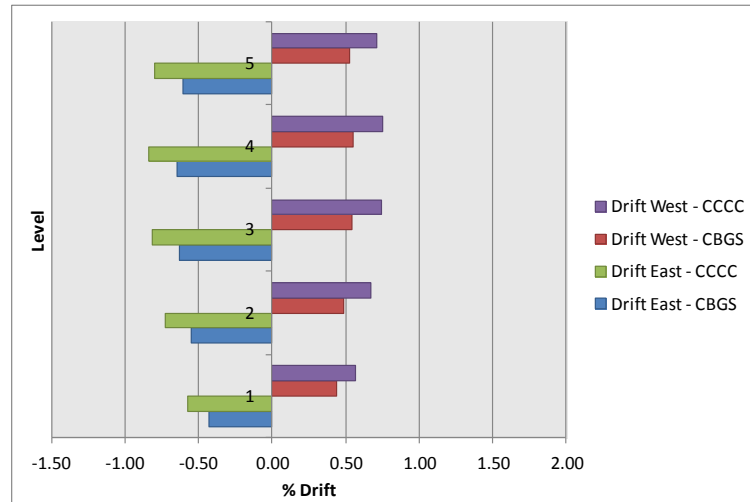


Figure 37: Frame 1 east/west storey drifts - Darfield.

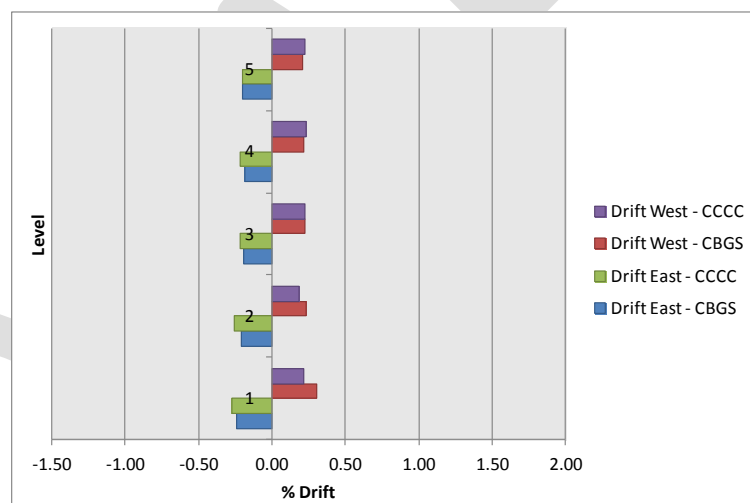


Figure 38: Frame 4 east/west storey drifts - Darfield.

10.2. Diaphragm Connection Forces.

Table 18 to Table 22 present the diaphragm connection forces acting at each of the north core individual wall interfaces. Results presented are the enveloped maxima recorded over the duration of the time-history record analysed.

Table 18: Wall C diaphragm connection forces - Darfield.

Level	North/South Actions			
	CBGS		CCCC	
	Maximum Northward (kN)	Maximum Southward (kN)	Maximum Northward (kN)	Maximum Southward (kN)
Level 6	963	-807	1069	-790
Level 5	624	-421	889	-404
Level 4	487	-529	795	-494
Level 3	623	-495	941	-609
Level 2	584	-694	742	-869

Table 19: Wall C/D diaphragm connection forces - Darfield.

Level	North/South Actions			
	CBGS		CCCC	
	Maximum Northward (kN)	Maximum Southward (kN)	Maximum Northward (kN)	Maximum Southward (kN)
Level 6	593	-500	526	-397
Level 5	548	-495	608	-412
Level 4	487	-461	568	-574
Level 3	427	-479	354	-763
Level 2	677	-577	755	-516

Table 20: Wall D diaphragm connection forces - Darfield.

Level	North/South Actions			
	CBGS		CCCC	
	Maximum Northward (kN)	Maximum Southward (kN)	Maximum Northward (kN)	Maximum Southward (kN)
Level 6	460	-289	427	-322
Level 5	253	-216	267	-267
Level 4	230	-237	263	-320 ¹
Level 3	335	0	341	0
Level 2	335	0	341	0
Notes: 1. Tensile limit of connection was exceeded.				

Table 21: Wall D/E diaphragm connection forces - Darfield.

Level	North/South Actions			
	CBGS		CCCC	
	Maximum Northward (kN)	Maximum Southward (kN)	Maximum Northward (kN)	Maximum Southward (kN)
Level 6	463	-352	404	-442
Level 5	141	-333	212	-485
Level 4	222	-382	277	-403 ¹
Level 3	476	0	443	0
Level 2	577	0	452	0
Notes: 1. Tensile limit of connection was exceeded.				

Table 22: Wall 5 (C to C/D) diaphragm connection forces - Darfield.

Level	East/West Actions			
	CBGS		CCCC	
	Maximum Westward (kN)	Maximum Eastward (kN)	Maximum Westward (kN)	Maximum Eastward (kN)
Level 6	783	-980	820	-745
Level 5	576	-666	500	-672
Level 4	495	-649	484	-693
Level 3	413	-606	451	-798
Level 2	369	-430	566	-508

It can be seen from Table 20 and Table 21 that diaphragm drag bar disconnections is predicted for the CCCC record only at wall D and D/E for the upper bound connection forces analysed. Note that remaining tie forces are shown to be very close to the upper bound capacity at level 4 for the CBGS record, and level 5 and 6 for the CCCC record, indicating that connection failure may occur at these levels.

Once the diaphragms have disconnected at these wall lines any torsion on the north core must be resisted by a couple between walls C and C/D.

Table 23 and Table 24 present the diaphragm connection actions summarised for the entire north core at each floor level. Results presented are the enveloped maxima recorded over the duration of the time-history record analysed.

Table 23: North core total diaphragm connection forces - Darfield.

Level	East/West Actions					
	CBGS			CCCC		
	Maximum Westward (kN)	Maximum Eastward (kN)	Maximum In-Plane Moment (kNm)	Maximum Westward (kN)	Maximum Eastward (kN)	Maximum In-Plane Moment (kNm)
Level 6	1075	-1168	7044	1111	-904	6952
Level 5	962	-841	2566	806	-714	2816
Level 4	831	-821	2050	851	-663	2176
Level 3	740	-671	3739	749	-722	5974
Level 2	451	-463	5351	611	-468	5050

Table 24: North core total diaphragm connection forces - Darfield.

Level	North/South Actions					
	CBGS			CCCC		
	Maximum Northward (kN)	Maximum Southward (kN)	Minimum In-Plane Moment (kNm)	Maximum Northward (kN)	Maximum Southward (kN)	Minimum In-Plane Moment (kNm)
Level 6	1424	-831	-8068	1434	-919	-7063
Level 5	1521	-1105	-4796	1699	-1316	-5548
Level 4	1180	-1061	-4286	1835	-1079	-2893
Level 3	1883	-796	-2107	2000	-1304	-2068
Level 2	1115	-1119	-2616	959	-1061	-2915

Table 25 and Table 26 present the actions acting along the slab interface along gridline 4 between grids C and C/D. Figure 39 indicates (in dark blue) the location of slab elements used to determine the actions presented. Results presented are the enveloped maxima recorded over the duration of the time-history record analysed.

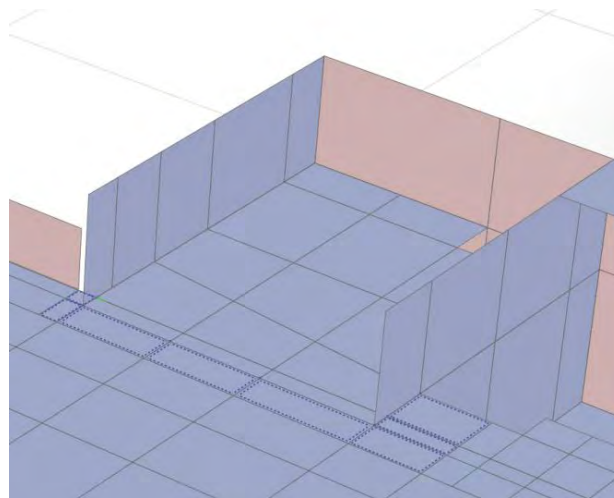


Figure 39: Slab 4 C-C/D section cut line.

Table 25: Slab 4 C to C/D diaphragm E/W actions - Darfield

Level	East/West Actions					
	CBGS			CCCC		
	Maximum Westward (kN)	Maximum Eastward (kN)	Maximum In-Plane Moment (kNm)	Maximum Westward (kN)	Maximum Eastward (kN)	Maximum In-Plane Moment (kNm)
Level 6	1008	-976	5102	766	-935	3509
Level 5	683	-828	3423	597	-672	2553
Level 4	691	-727	2976	553	-729	2721
Level 3	591	-641	2587	626	-639	2575
Level 2	423	-373	1631	430	-560	2223

Table 26: Slab 4 C to C/D diaphragm N/S actions - Darfield

Level	North/South Actions					
	CBGS			CCCC		
	Maximum Northward (kN)	Maximum Southward (kN)	Minimum In-Plane Moment (kNm)	Maximum Northward (kN)	Maximum Southward (kN)	Minimum In-Plane Moment (kNm)
Level 6	1124	-1399	-3719	1149	-1466	-3654
Level 5	759	-1081	-2728	600	-1388	-2618
Level 4	828	-874	-2555	908	-1385	-2278
Level 3	783	-987	-2137	1176	-1233	-1913
Level 2	1097	-850	-2231	1198	-902	-1584

Table 27 presents the diaphragm connection actions at each floor level of the South wall located on grid 1. Results presented are the enveloped maxima recorded over the duration of the time-history record analysed.

Table 27: South wall diaphragm connection forces - Darfield

Level	East/West Actions			
	CBGS		CCCC	
	Maximum Westward (kN)	Maximum Eastward (kN)	Maximum Westward (kN)	Maximum Eastward (kN)
Level 6	667	-557	633	-660
Level 5	654	-824	726	-872
Level 4	605	-669	720	-699
Level 3	663	-541	843	-737
Level 2	612	-480	724	-678

10.3. Inelastic Wall Demands.

Results have shown that inelastic demand for the cantilever bending of the north core and the south wall only occurs in the lower part of level 1. Table 28 below presents the peak strains that occur during the Darfield CBGS and CCCC events. Strains listed have been taken from the bottom shell elements at the extremities of each wall, and have presented as the average strain over the bottom 1 m of wall. Note that $\epsilon_y = 0.00219$ for the wall longitudinal reinforcement.

Table 28: Wall strains - Darfield

Location	Wall Element	CBGS		CCCC	
		Maximum Strain	Residual Displacement per meter (m)	Maximum Strain	Residual Displacement per meter (m)
North Core	Wall C gl 4	0.0070	0.0002	0.0235	0.0003
	Wall C gl 5	0.0035	0.0006	0.0079	0.0020
	Wall C/D gl 4	0.0093	0.0000	0.0207	-0.0001
	Wall C/D gl 5	0.0023	0.0001	0.0049	0.0014
	Wall D gl 4	0.0099	0.0003	0.0201	-0.0002
	Wall D gl 5	0.0023	0.0001	0.0038	0.0012
	Wall D/E gl 4	0.0094	0.0020	0.0155	0.0011
	Wall D/E gl 5	0.0021	0.0000	0.0019	0.0000
South Wall	Pier D gl D	0.0025	0.0001	0.0036	0.0008
	Pier D gl E	0.0065	0.0005	0.0111	0.0008
	Pier E gl D	0.0024	0.0001	0.0041	0.0009
	Pier E gl E	0.0059	0.0000	0.0099	0.0004

Table 29: South Wall Coupling Beam Strain

Level	CBGS Maximum	CCCC Maximum
Level 7	0.00024	0.00027
Level 6	0.00069	0.00070
Level 5	0.00103	0.00119
Level 4	0.00128	0.00147
Level 3	0.00150	0.00176
Level 2	0.00189	0.00247

The analysis results indicate that only the CCCC record produces inelastic demands on the coupling beams. Under CCCC the diagonal bars, located in the level 1 coupling beam are predicted to yield, with a maximum strain of 0.00247 (which corresponds to $1.13\varepsilon_y$) reported.

10.4. Inelastic Column Actions.

Analysis results indicate that column hinging occurs for both the CBGS and CCCC records, with the number of hinges and plastic rotation demand being significantly greater for the CCCC record.

Hinges are predominantly located in the eastern perimeter frame (Frame F), although the CCCC record also predicts hinges in the base of numerous interior columns.

CBGS

The peak CBGS concrete hinge compressive strains generated at the outer face of the column are presented in Table 30 below for a selection of indicator columns.

Table 30: CBGS peak column hinge compression strains - Darfield

Column	Peak strain (mm/m)				
	Level 1	Level 2	Level 3	Level 4	Level 5
C1	1.89	1.83	2.48	2.85	3.21
F1	3.96	1.89	2.14	2.43	3.91
F2	3.50	3.14	3.27	3.67	3.79
F3	3.46	3.31	3.60	4.16	3.85
F4	2.44	1.73	1.70	1.83	3.17

Peak compressive strains are typically less than 0.002 for all levels of the remaining columns. From Table 30 it can be seen that hinging is predicted in gridlines F and 1 for the CBGS record. Maximum concrete strains are predicted for the upper hinge on column F3 at Level 4. Figure 40 to Figure 46 present a selection of plots showing the behaviour of this hinge. Information on further columns can be found in Appendix G.3. It should be noted that 'R1' corresponds to rotation about the north/south axis and 'R2' corresponds to rotation about the east/west axis.

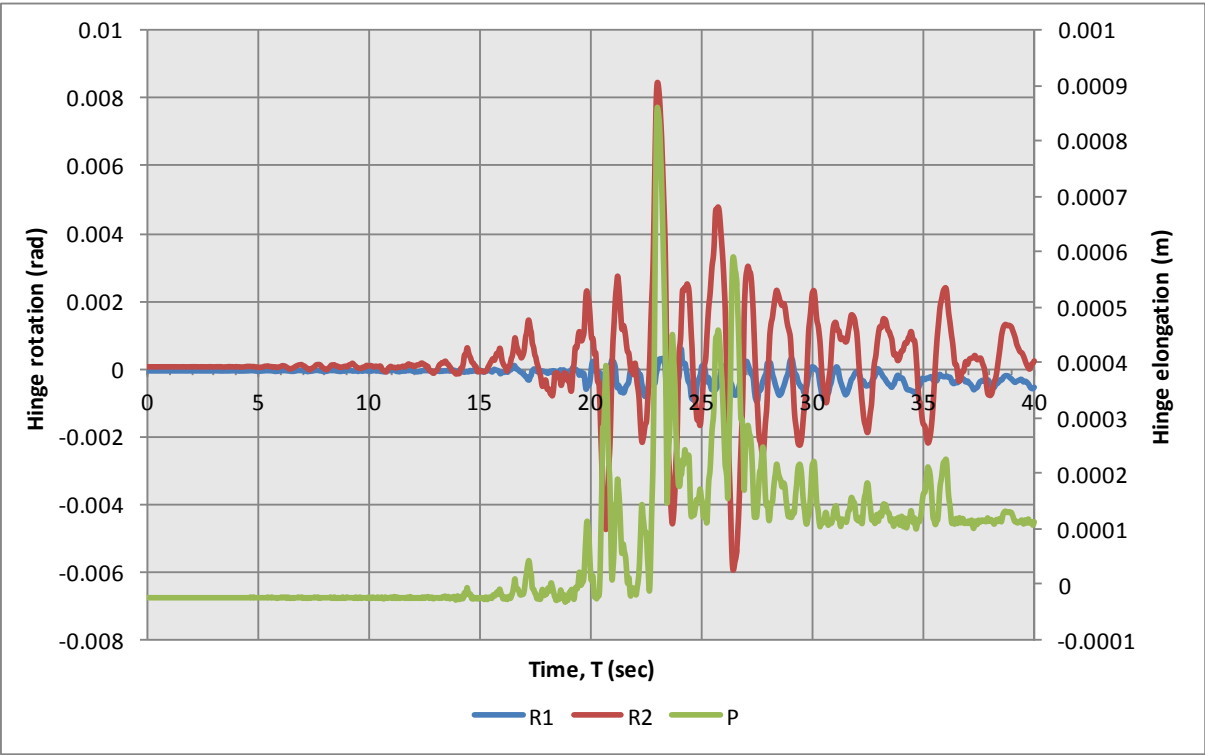


Figure 40: Column F3, Level 4 top hinge rotation and elongation vs time, CBGS, Darfield.

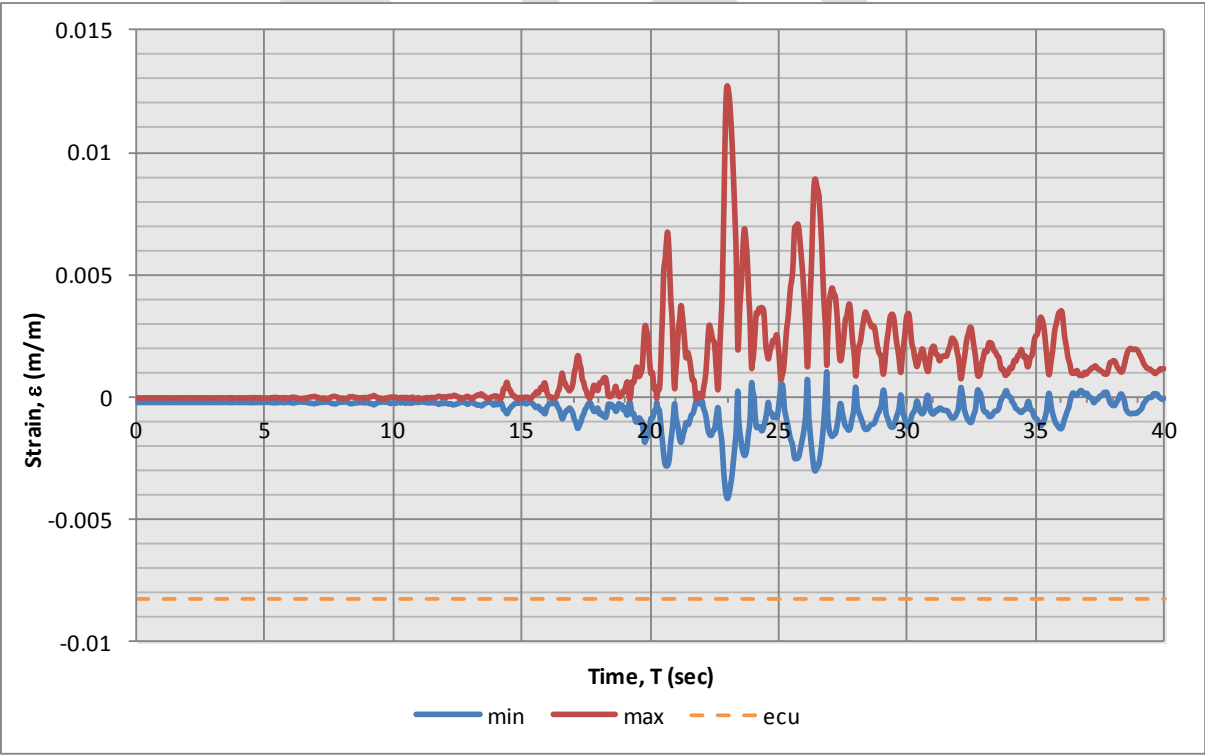


Figure 41: Column F3 Level 4 upper hinge strain vs time, CBGS, Darfield.

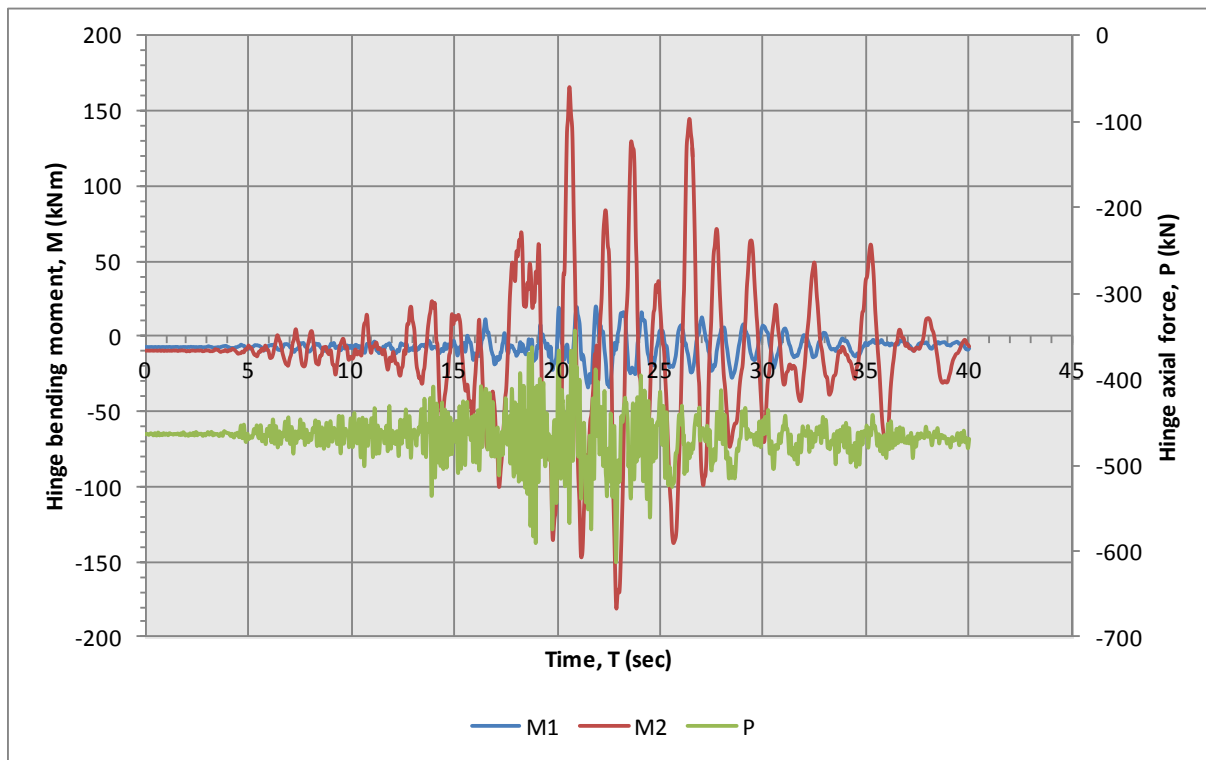


Figure 42: Column F3 Level 4 upper hinge axial and moments vs time, CBGS, Darfield.

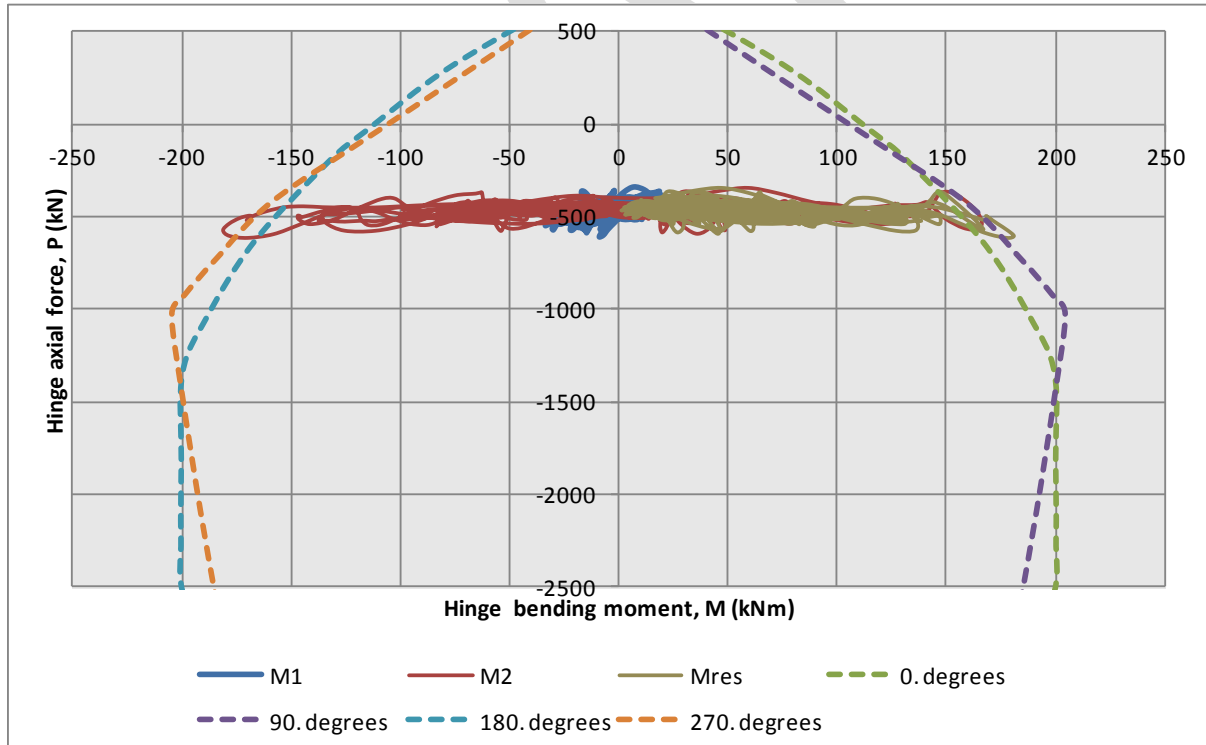


Figure 43: Column F3 Level 4 upper hinge moment axial relationship, CBGS, Darfield.

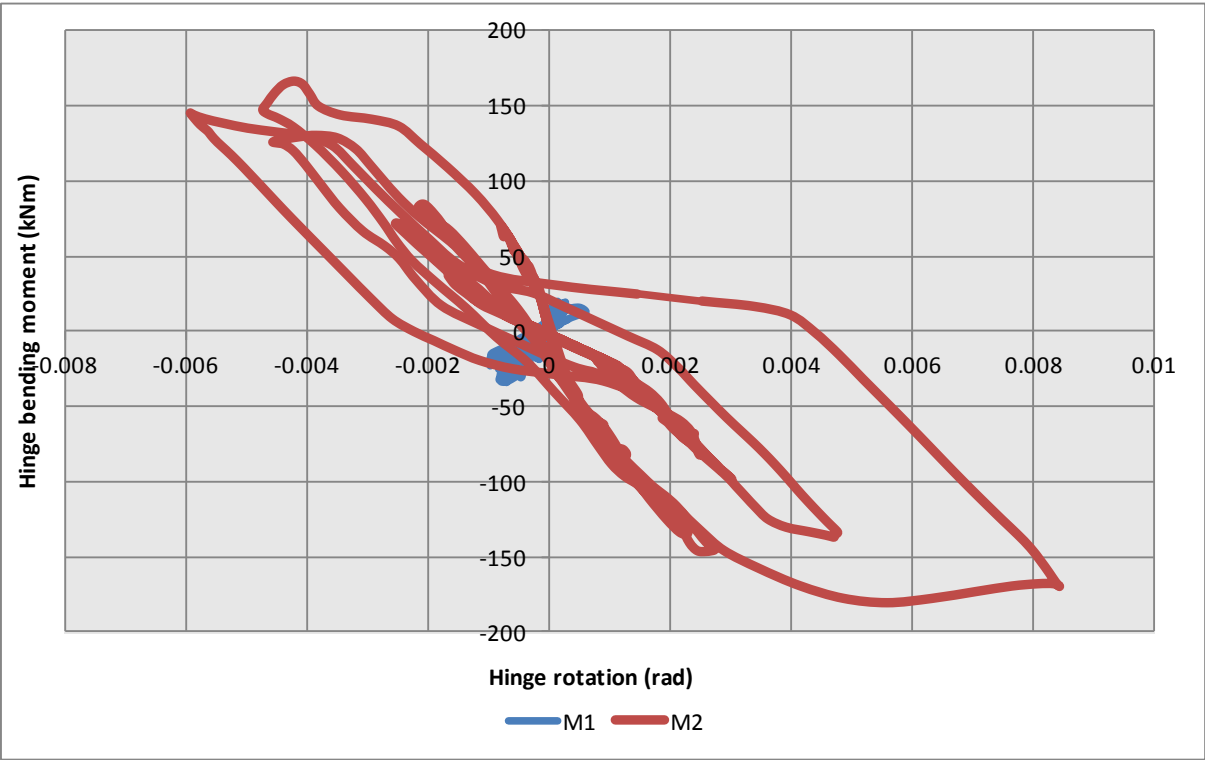


Figure 44: Column F3 Level 4 upper hinge hysteretic form, CBGS, Darfield.

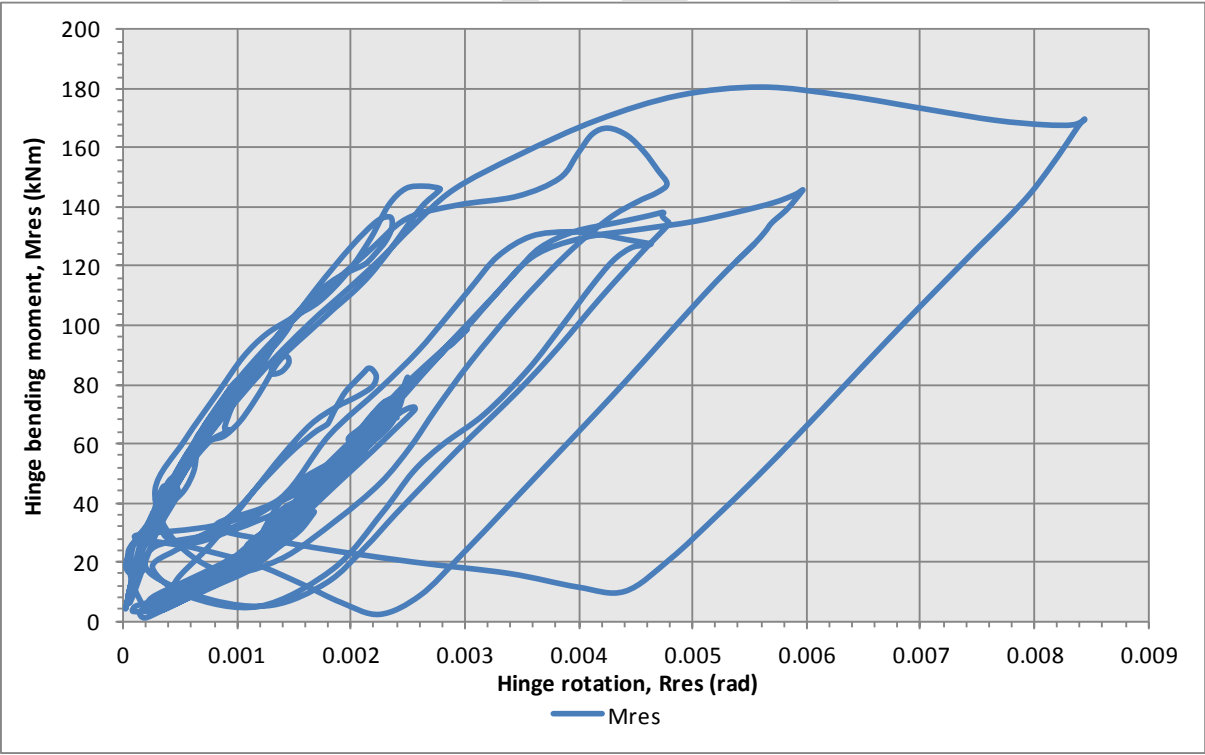


Figure 45: Column F3 Level 4 upper hinge moment rotation plot, CBGS, Darfield.

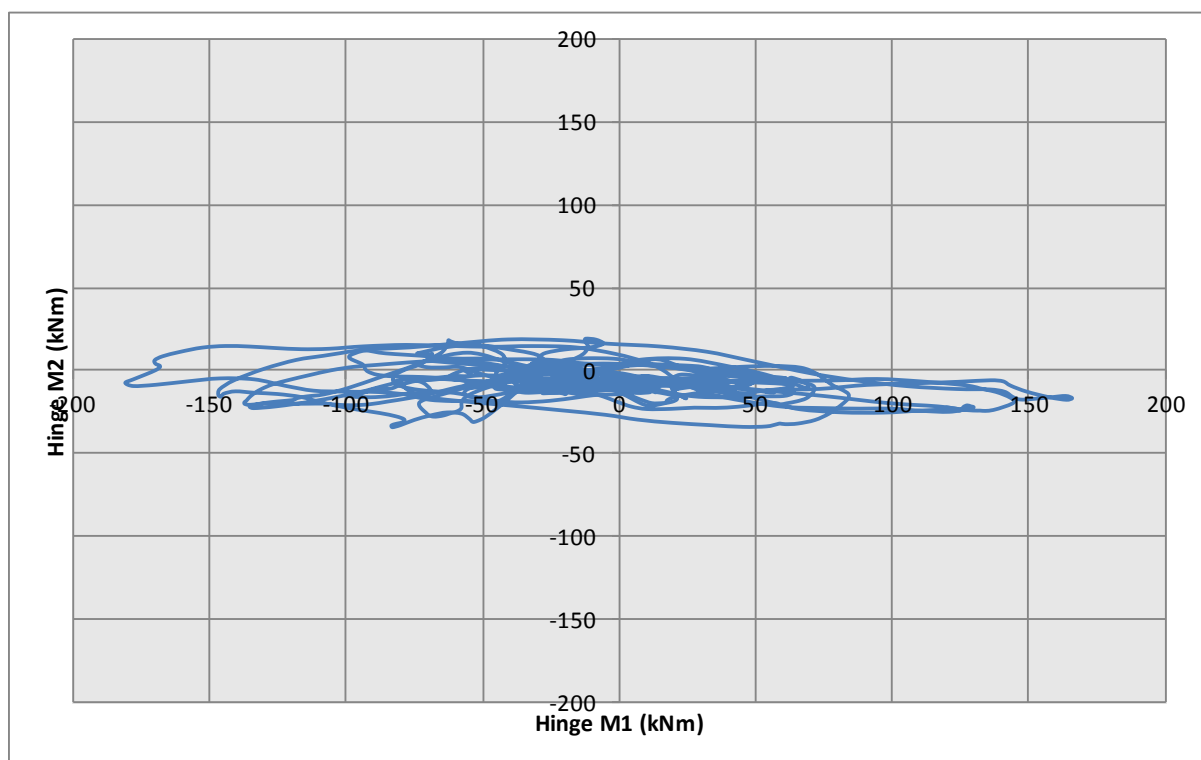


Figure 46: Column F3 Level 4 upper hinge bi-axial moment plot, CBGS, Darfield.

CCCC

The peak CCCC concrete hinge compressive strains generated at the outer face of the column are presented in Appendix H.3. Under Darfield CCCC record demands, several columns are predicted to exceed their ultimate concrete strain limits. Detailed processing of this data has not yet been completed.

10.5. Inelastic Beam-Column Joint Actions

This section presents the cumulative maximum joint deformation states for the Darfield event. Figure 47 defines the colour coding used in the plots to indicate the number of joints that have been subjected to different deformation states as the earthquake event progresses. Note that the blue colour represents elastic behaviour of the joints.

Plots are presented separately for the one-way (joints located on gridlines B to E) and two-way joints (joints located on gridline A and F). It should be noted that 'R1' corresponds to rotation about the north/south axis and 'R2' corresponds to rotation about the east/west axis.

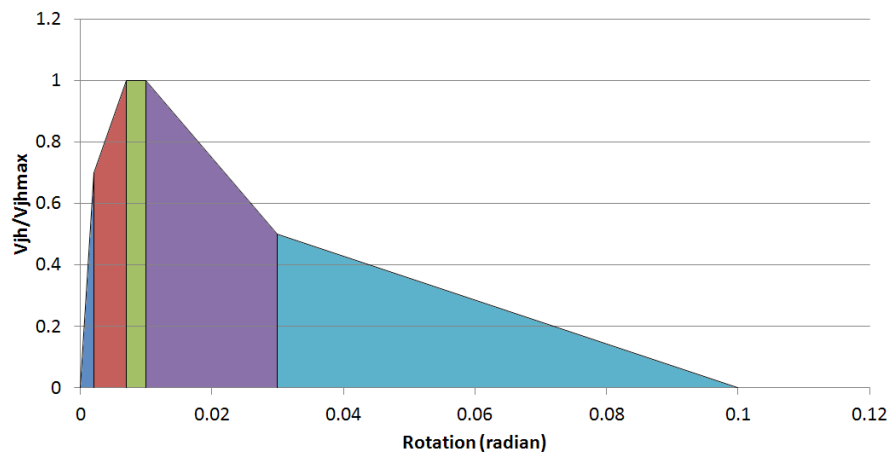


Figure 47: Colour coding used to represent different joint deformation states in Figure 48 to Figure 53

CBGS

Figure 48 to Figure 50 present the behaviour of the beam column joints during the passage of the CBGS Darfield event. These plots present the maximum hinge rotation.

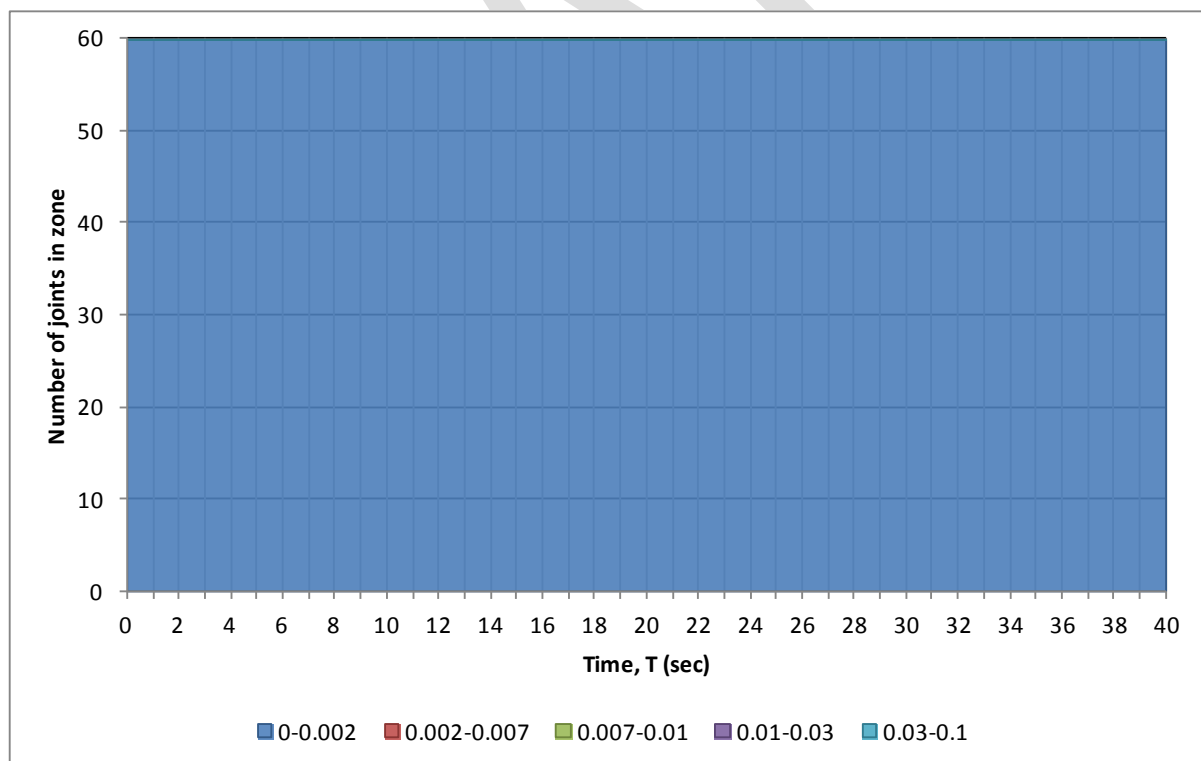


Figure 48: One-way beam-column joint R1 rotations - CBGS, Darfield

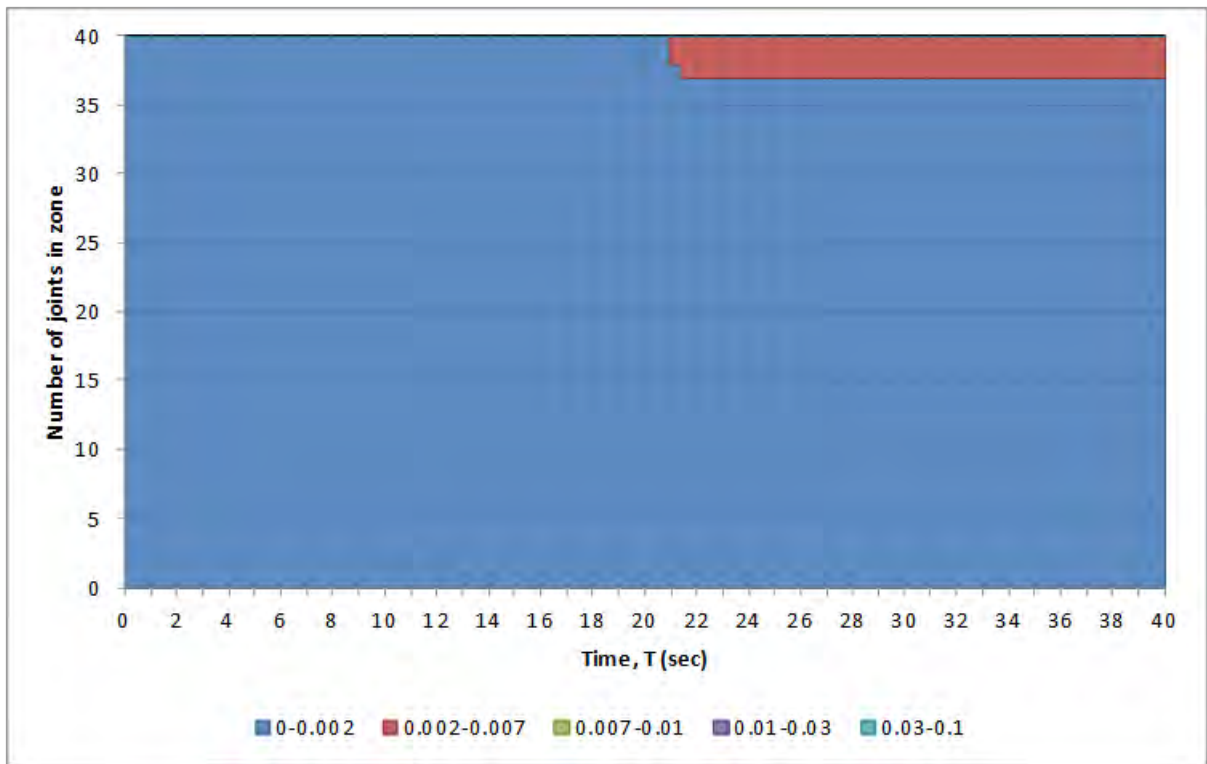


Figure 49: Two-way beam-column joint R1 rotations - C.BGS, Darfield

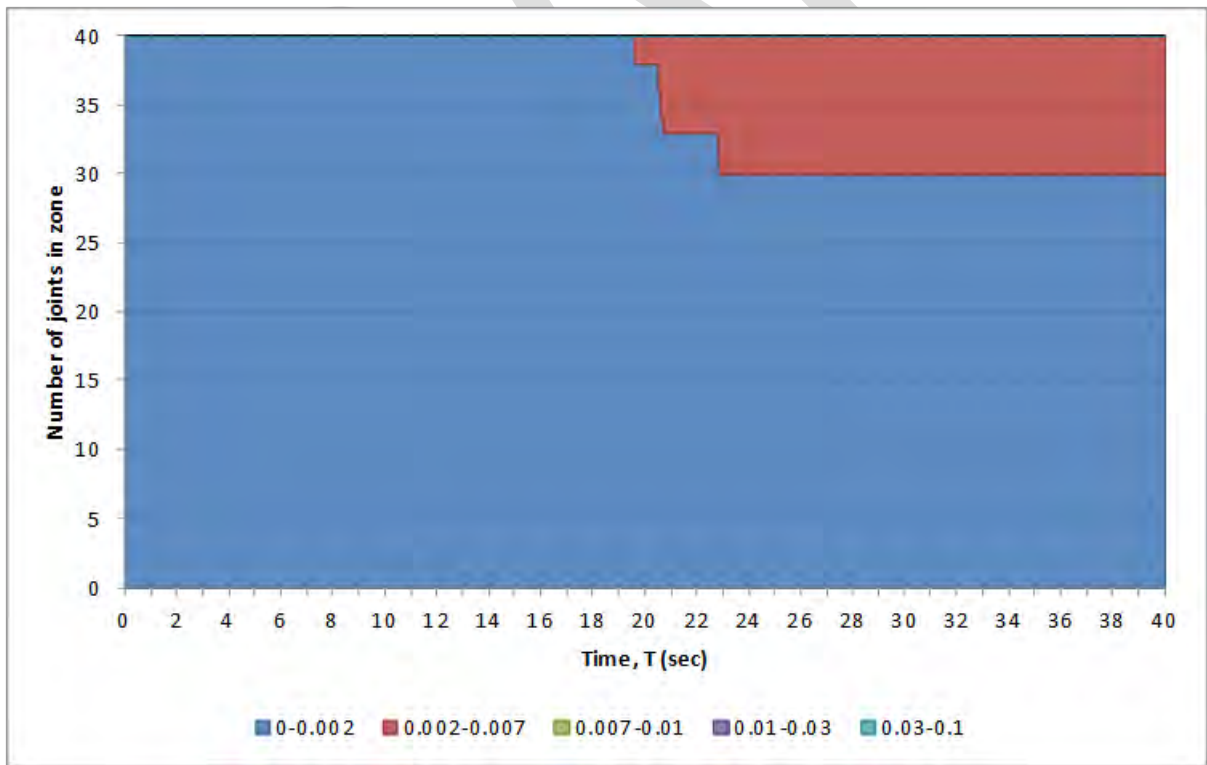


Figure 50: Two-way beam-column joint R2 rotations - C.BGS, Darfield.

As can be seen in the Figure 48 the one-way beam column joints are predicted to remain elastic after the passage of the CBGS Darfield earthquake. Little non-linear response of the two-way beam-column joints is predicted for either axis of rotation during the Darfield event, as can be seen in Figure 49 and Figure 50.

CCCC

Figure 51 to Figure 53 present the behaviour of the beam column joints during the passage of the CCCC Darfield event. These plots present the maximum hinge rotation.

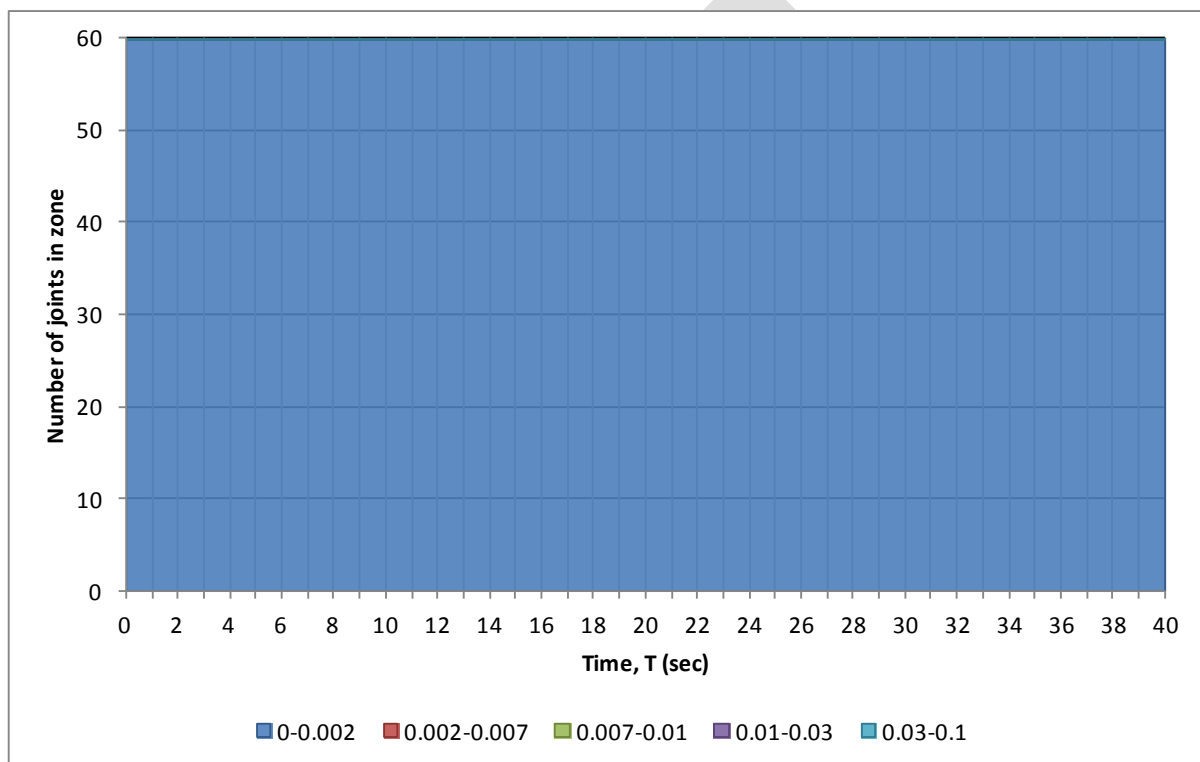


Figure 51: One-way beam-column joint R1 rotations - CCCC, Darfield.

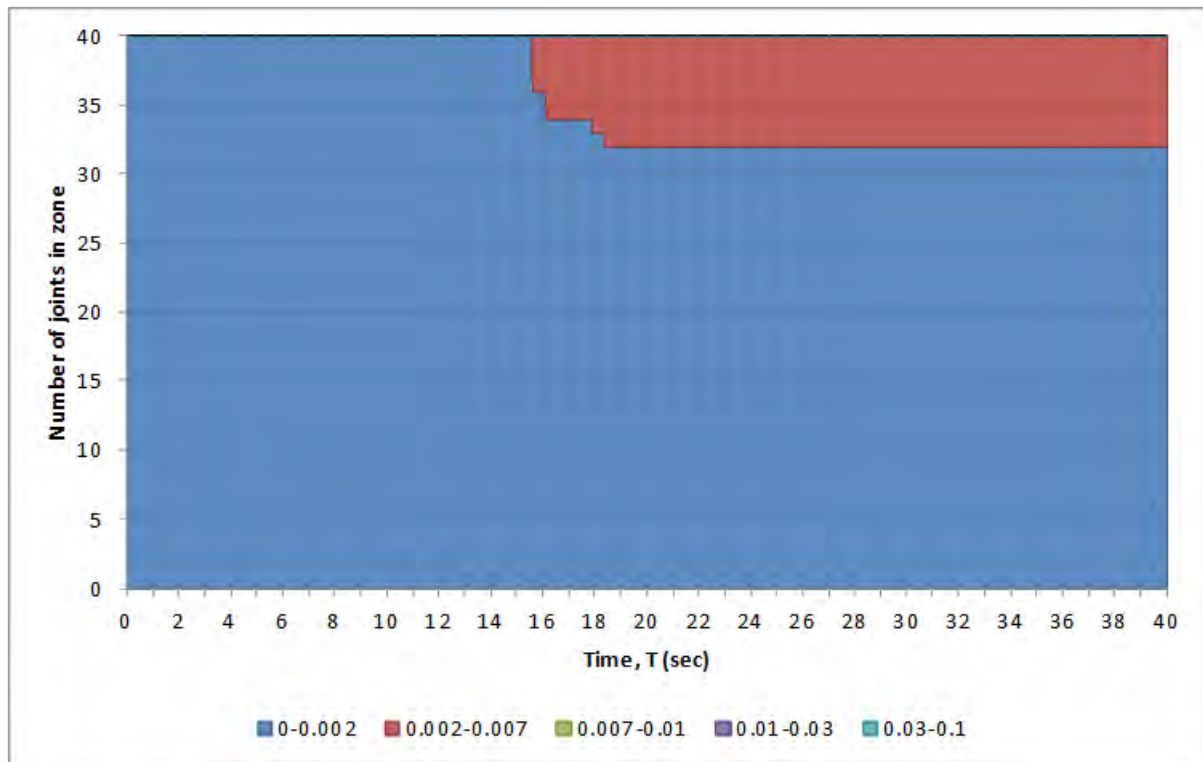


Figure 52: Two-way beam-column joint R1 rotations - CCCC, Darfield.

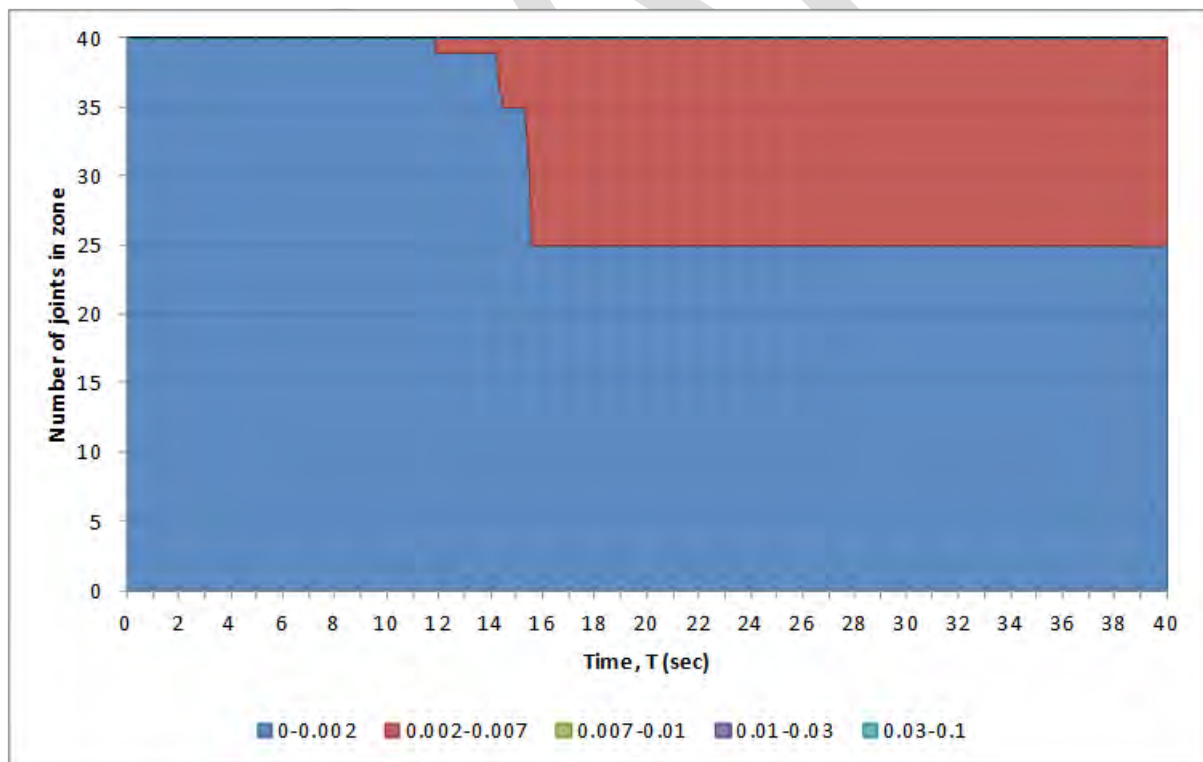


Figure 53: Two-way beam-column joint R2 rotations - CCCC, Darfield.

As can be seen in the Figure 51 the one-way beam column joints are predicted to remain elastic after the passage of the CCCC Darfield earthquake. Figure 52 and Figure 53 show that up to 15 two-way joints are predicted to have undergone some minor cracking during the Darfield event, although their ultimate strength was not attained.

DRAFT

11. NLTHA Results : Lyttelton

Results presented in this section are for the earthquake acceleration time history recorded at the Christchurch Botanical Gardens (CBGS), Christchurch Hospital (CHHC), Christchurch Cathedral College (CCCC), and Resthaven (REHS) stations and are a summary of the analyses only. Additional results for each record can be found in Appendix I to Appendix L. In all cases analyses results include all three components of the appropriate time history record.

Note that all records predict the loss of axial load carrying capacity of some columns during the course of the run record. Results have been presented for time-steps after axial column capacity has been exceeded so that trends can be seen and comparisons can be made between earthquake records. Assumptions in the solution process mean that results subsequent to the occurrence of column axial capacity degradation are not necessarily realistic and should be treated with caution.

11.1. Drifts and Displacements

Figure 54, and Figure 55, below present the maximum north/south percent storey drifts recorded for the perimeter frames located on grids A, and F respectively. Drifts are presented for the CCCC, CBGS, CHHC, and the REHS records.

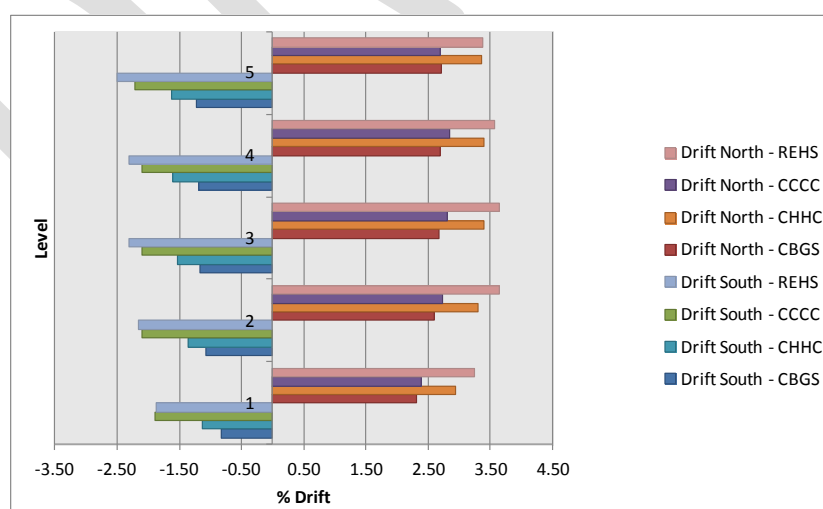


Figure 54: Frame A north/south storey drifts - Lyttelton.

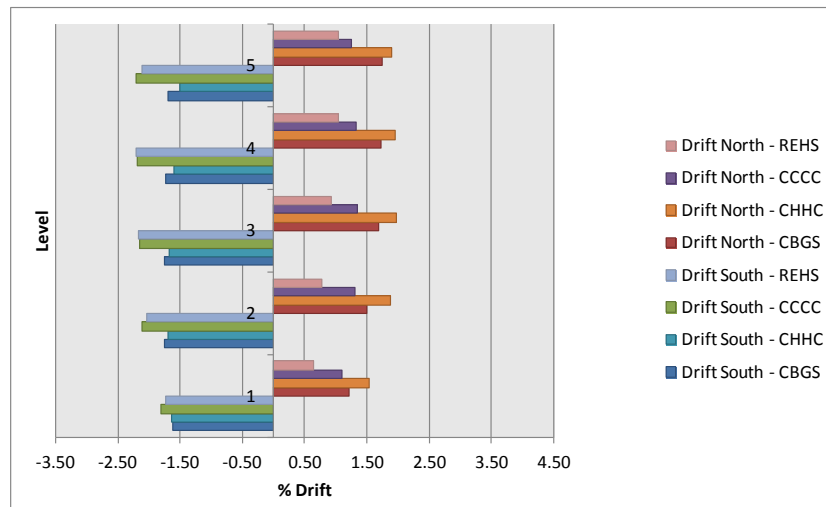


Figure 55: Frame F north/south storey drifts - Lyttelton.

Figure 56, and Figure 57, below present the maximum east/west percentage storey drifts recorded for the perimeter frames located on grids 1, and 4 respectively. Drifts are presented for the CCCC, CBGS, CHHC, and the REHS records.

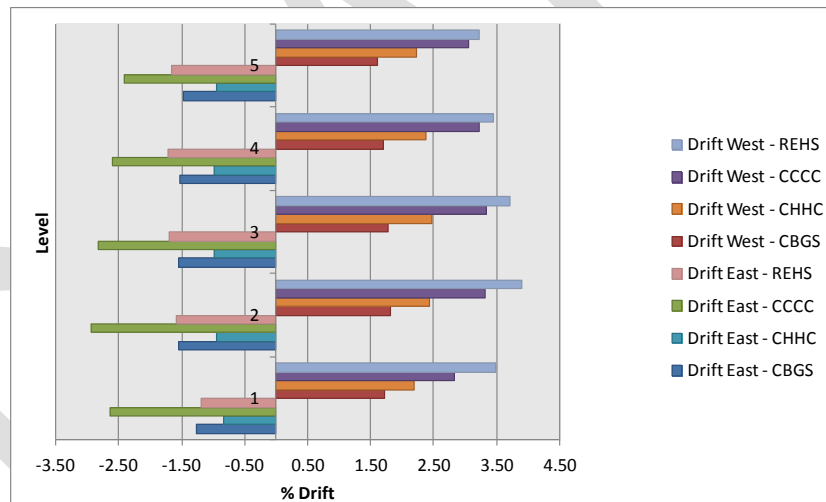


Figure 56: Frame 1 east/west storey drifts - Lyttelton.

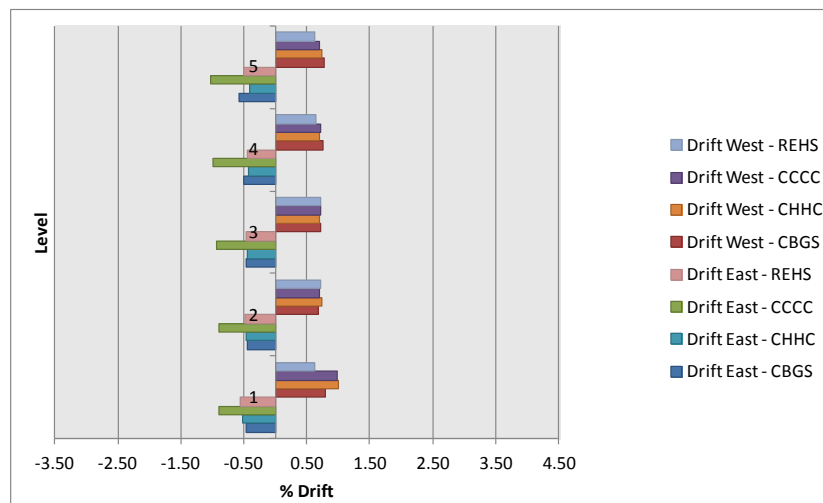


Figure 57: Frame 4 east/west storey drifts - Lyttelton.

It can be seen from the storey drift plots above that the REHS record has larger displacement demands in the westerly direction, with the CCCC record producing the largest easterly drifts by some margin. Drift variations of up to 2.0% are predicted in the easterly direction with the CHHC record producing the smallest drifts. In the westerly direction drifts are similar for Frame 4, although variations of 0.6% are observed between the CCCC (highest drift) the CBGS (lowest drift) records.

Along frame line F all records produce a similar level of drift in the southerly direction with a maximum variation in drift of 0.7% occurring over all records and levels. More variation is seen in the northerly direction where up to 1.1% variation in drifts is seen between the REHS (smallest) and the CHHC records (largest). Frame A drifts exhibit more variation between records in the southward direction (up to 1.3% difference), with the CBGS and CHHC records producing the smallest southward drifts.

Frame A exhibits very high drifts in the northerly direction. Drifts of nearly 3.7% are predicted for the REHS record. In the southerly direction maximum drift predicted is 2.5% at level 6.

11.2. Diaphragm Connection Forces.

Table 31 to Table 35 present the diaphragm connection forces acting at each of the north core individual wall interfaces. Results presented are the enveloped maxima recorded over the duration of the time-history record analysed.

Table 31: Wall C diaphragm connection forces - Lyttelton.

Level	North/South Actions							
	CCCC		CHHC		CBGS		REHS	
	Maximum Northward (kN)	Maximum Southward (kN)	Maximum Northward (kN)	Maximum Southward (kN)	Maximum Northward (kN)	Maximum Southward (kN)	Maximum Northward (kN)	Maximum Southward (kN)
Level 6	3041	-1924	2394	-1835	2882	-2277	3173	-1995
Level 5	1052	-836	974	-726	1055	-829	986	-806
Level 4	973	-1103	1156	-1028	843	-1387	837	-877
Level 3	1035	-1185	1392	-1323	1232	-1449	963	-937
Level 2	879	-2038	982	-1138	1274	-1087	1447	-1272

Table 32: Wall C/D diaphragm connection forces - Lyttelton.

Level	North/South Actions							
	CCCC		CHHC		CBGS		REHS	
	Maximum Northward (kN)	Maximum Southward (kN)	Maximum Northward (kN)	Maximum Southward (kN)	Maximum Northward (kN)	Maximum Southward (kN)	Maximum Northward (kN)	Maximum Southward (kN)
Level 6	804	-2619	1109	-2258	954	-2428	674	-2355
Level 5	731	-1084	826	-1451	747	-1261	866	-1218
Level 4	768	-937	795	-1461	656	-987	724	-870
Level 3	813	-1482	1057	-1293	908	-980	831	-971
Level 2	1308	-1059	1151	-1062	1099	-986	1269	-955

Table 33: Wall D diaphragm connection forces - Lyttelton.

Level	North/South Actions							
	CCCC		CHHC		CBGS		REHS	
	Maximum Northward (kN)	Maximum Southward (kN)	Maximum Northward (kN)	Maximum Southward (kN)	Maximum Northward (kN)	Maximum Southward (kN)	Maximum Northward (kN)	Maximum Southward (kN)
Level 6	909	-603 ¹	720	-603 ¹	889	-603 ¹	718	-603 ¹
Level 5	781	-420 ¹	703	-420 ¹	1129	-420 ¹	542	-420 ¹
Level 4	593	-320 ¹	452	-320 ¹	629	-320 ¹	448	-320 ¹
Level 3	456	0	483	0	501	0	521	0
Level 2	456	0	565	0	534	0	613	0

Notes: 1. Tensile limit of connection was exceeded.

Table 34: Wall D/E diaphragm connection forces - Lyttelton.

Level	North/South Actions							
	CCCC		CHHC		CBGS		REHS	
	Maximum Northward (kN)	Maximum Southward (kN)	Maximum Northward (kN)	Maximum Southward (kN)	Maximum Northward (kN)	Maximum Southward (kN)	Maximum Northward (kN)	Maximum Southward (kN)
Level 6	1237	-603 ¹	743	-603 ¹	1477	-603 ¹	1075	-603 ¹
Level 5	836	-420 ¹	743	-420 ¹	733	-420 ¹	615	-420 ¹
Level 4	568	-320 ¹	564	-320 ¹	500	-320 ¹	600	-320 ¹
Level 3	504	0	662	0	579	0	369	0
Level 2	837	0	678	0	628	0	653	0

Notes: 1. Tensile limit of connection was exceeded.

Table 35: Wall 5 (C to C/D) diaphragm connection forces - Lyttelton.

Level	East/West Actions							
	CCCC		CHHC		CBGS		REHS	
	Maximum Westward (kN)	Maximum Eastward (kN)	Maximum Westward (kN)	Maximum Eastward (kN)	Maximum Westward (kN)	Maximum Eastward (kN)	Maximum Westward (kN)	Maximum Eastward (kN)
Level 6	1516	-1847	1533	-1960	2155	-1863	1380	-1707
Level 5	1531	-2201	1102	-1542	1150	-1487	988	-1669
Level 4	1307	-2180	1143	-1202	1400	-1840	1066	-1458
Level 3	1169	-2001	1179	-1332	1241	-1313	906	-1438
Level 2	893	-1389	771	-1041	1058	-1095	856	-1363

Table 36, Table 37 and Table 38 present the diaphragm connection actions summarised for the entire north core at each floor level. Results presented are the enveloped maxima recorded over the duration of the time-history record analysed.

Table 36: North core total diaphragm connection E/W forces - Lyttelton.

Level	East/West Actions							
	CCCC		CHHC		CBGS		REHS	
	Maximum Westward (kN)	Maximum Eastward (kN)	Maximum Westward (kN)	Maximum Eastward (kN)	Maximum Westward (kN)	Maximum Eastward (kN)	Maximum Westward (kN)	Maximum Eastward (kN)
Level 6	2107	-2178	1920	-2546	2772	-2077	2068	-1717
Level 5	2455	-2097	1719	-1852	1967	-1670	1664	-1575
Level 4	2215	-2005	1838	-1392	2280	-1568	1745	-1493
Level 3	1836	-2014	1848	-1338	1924	-1467	1437	-1667
Level 2	1199	-1396	1129	-1214	1334	-1359	1139	-1714

Table 37: North core total diaphragm connection N/S forces - Lyttelton.

Level	North/South Actions							
	CCCC		CHHC		CBGS		REHS	
	Maximum Northward (kN)	Maximum Southward (kN)	Maximum Northward (kN)	Maximum Southward (kN)	Maximum Northward (kN)	Maximum Southward (kN)	Maximum Northward (kN)	Maximum Southward (kN)
Level 6	2150	-1907	2034	-1700	2137	-1669	2772	-1689
Level 5	1803	-1623	1974	-1982	2189	-1515	1875	-1628
Level 4	1375	-2032	2143	-1793	1835	-2078	1514	-1795
Level 3	1914	-2742	3111	-2339	2581	-2395	2236	-1906
Level 2	2012	-1955	2320	-2005	2820	-1966	2352	-1844

Table 38: North core total diaphragm connection forces - Lyttelton.

Level	In-Plane Moments							
	CCCC		CHHC		CBGS		REHS	
	Maximum +Moment (kNm)	Maximum -Moment (kNm)	Maximum +Moment (kNm)	Maximum -Moment (kNm)	Maximum +Moment (kNm)	Maximum -Moment (kNm)	Maximum +Moment (kNm)	Maximum -Moment (kNm)
Level 6	16127	-14027	16696	-11624	20809	-13254	15775	-15953
Level 5	8232	-7792	5490	-7259	7223	-7125	6590	-6365
Level 4	6149	-7138	5403	-5788	6779	-4918	6540	-4761
Level 3	6779	-6128	5824	-5561	6227	-5315	6313	-5420
Level 2	10378	-4811	8388	-4237	9543	-4857	7739	-6889

Table 39, Table 40, and Table 41 present the actions acting along the slab interface along gridline 4 between grids C and C/D. Results presented are the enveloped maxima recorded over the duration of the time-history record analysed.

Table 39: Slab 4 C to C/D diaphragm E/W actions - Lyttelton.

Level	East/West Actions							
	CCCC		CHHC		CBGS		REHS	
	Maximum Westward (kN)	Maximum Eastward (kN)	Maximum Westward (kN)	Maximum Eastward (kN)	Maximum Westward (kN)	Maximum Eastward (kN)	Maximum Westward (kN)	Maximum Eastward (kN)
Level 6	2009	-1898	2311	-1697	1944	-2572	1523	-1892
Level 5	1790	-2177	1620	-1591	1431	-1739	1325	-1395
Level 4	1633	-1941	1161	-1599	1346	-2059	1276	-1499
Level 3	1686	-1598	1147	-1603	1291	-1700	1427	-1403
Level 2	1248	-1012	1103	-912	1174	-1216	1512	-935

Table 40: Slab 4 C to C/D diaphragm N/S actions - Lyttelton.

Level	North/South Actions							
	CCCC		CHHC		CBGS		REHS	
	Maximum Northward (kN)	Maximum Southward (kN)	Maximum Northward (kN)	Maximum Southward (kN)	Maximum Northward (kN)	Maximum Southward (kN)	Maximum Northward (kN)	Maximum Southward (kN)
Level 6	2300	-1724	2444	-1799	2297	-1956	2179	-3186
Level 5	1464	-1532	1754	-1477	1538	-1749	1432	-1572
Level 4	1948	-1328	1677	-1952	2012	-1448	1513	-1370
Level 3	2551	-1443	2254	-2338	2255	-1690	1832	-1484
Level 2	2118	-1882	1946	-1824	1745	-2157	1842	-2246

Table 41: Slab 4 C to C/D diaphragm connection forces - Lyttelton.

Level	In-Plane Moments							
	CCCC		CHHC		CBGS		REHS	
	Maximum +Moment (kNm)	Maximum -Moment (kNm)	Maximum +Moment (kNm)	Maximum -Moment (kNm)	Maximum +Moment (kNm)	Maximum -Moment (kNm)	Maximum +Moment (kNm)	Maximum -Moment (kNm)
Level 6	15514	-8454	12502	-6496	13223	-7931	13830	-6194
Level 5	9372	-7821	8336	-5425	7653	-7047	8119	-5526
Level 4	9343	-7220	5557	-5754	6177	-7446	7470	-5168
Level 3	7968	-4931	4928	-5329	5194	-5053	5714	-4450
Level 2	5365	-4406	4739	-4615	5119	-3397	5366	-3073

Table 41 presents the diaphragm connection actions at each floor level of the south wall located on grid 1. Results presented are the enveloped maxima recorded over the duration of the time-history record analysed.

Table 42: South wall diaphragm connection forces - Lyttelton.

Level	East/West Actions							
	CCCC		CHHC		CBGS		REHS	
	Maximum Westward (kN)	Maximum Eastward (kN)	Maximum Westward (kN)	Maximum Eastward (kN)	Maximum Westward (kN)	Maximum Eastward (kN)	Maximum Westward (kN)	Maximum Eastward (kN)
Level 6	1080	-979	1001	-1281	845	-1007	865	-1169
Level 5	1298	-1244	1124	-906	1321	-1010	1225	-1118
Level 4	1077	-1063	1265	-1126	1000	-1047	1120	-915
Level 3	1228	-1081	1134	-1364	1110	-1518	1299	-953
Level 2	1651	-1313	1492	-1151	1432	-1568	1460	-1203

11.3. Inelastic Column Actions.

Analyses predict failure of the columns to occur at various times throughout the passage of all earthquake records.

It is important to note that not all column hinges are included in the assessments undertaken to date. Table 43 below presents the list of column hinges in the model and identifies (in blue) which have been included in the assessment at this time. Column hinges are identified by a naming convention that includes the grid location, floor level and location within the column.

An example of this naming convention is the column hinge denoted as “A2L3b” which corresponds to the hinge located at the base of the level 3 column located on grid A2.

DRAFT

Table 43: Column hinges included in assessment

Level	b/t	Grid	1	2	3	4
L1	b	A				
L1	b	B				
L1	b	C				
L1	b	D				
L1	b	E				
L1	b	F				
L1	t	A				
L1	t	B				
L1	t	C				
L1	t	D				
L1	t	E				
L1	t	F				
L2	b	A				
L2	b	B				
L2	b	C				
L2	b	D				
L2	b	E				
L2	b	F				
L2	t	A				
L2	t	B				
L2	t	C				
L2	t	D				
L2	t	E				
L2	t	F				
L3	b	A				
L3	b	B				
L3	b	C				

Table 43: Column hinges included in assessment

Level	b/t	Grid	1	2	3	4
L3	b	D				
L3	b	E				
L3	b	F				
L3	t	A				
L3	t	B				
L3	t	C				
L3	t	D				
L3	t	E				
L3	t	F				
L4	b	A				
L4	b	B				
L4	b	C				
L4	b	D				
L4	b	E				
L4	b	F				
L4	t	A				
L4	t	B				
L4	t	C				
L4	t	D				
L4	t	E				
L4	t	F				
L5	b	A				
L5	b	B				
L5	b	C				
L5	b	D				
L5	b	E				
L5	b	F				

Table 43: Column hinges included in assessment

Level	b/t	Grid	1	2	3	4
L5	t	A				
L5	t	B				
L5	t	C				
L5	t	D				
L5	t	E				
L5	t	F				
L6	b	A				
L6	b	B				
L6	b	C				
L6	b	D				
L6	b	E				
L6	b	F				

The performance of an individual column hinge can be assessed with respect to the time series on the basis of strain levels at various locations within the column cross section. Three strain criteria have been evaluated as follows:

- the time at which the compression strain at the column centroid exceeds the ultimate strain capacity of the concrete (indicative of column gravity load carrying capacity being compromised),
- the time at which the strain at the location of longitudinal reinforcement exceeds the yield strain of the reinforcement in compression (which could be considered to be an indicator for initiation of bar buckling),
- the time at which the strain at the column face exceeds the ultimate strain capacity of the concrete (indicative of concrete spalling).

Where the ultimate strain capacity of the concrete is given in Table 1, and the reinforcement yield strain as given in Table 2.

The time at which these criteria are exceeded for the hinges identified in Table 43 is presented in Table 44 through Table 46 below.

Table 44: Time at which $\epsilon > \epsilon_{cu}$ @column centroid

CBGS		CBGS (SEQ)		CCCC		CCCC (SEQ)		CHHC		REHS	
ID	Time	ID	Time	ID	Time	ID	Time	ID	Time	ID	Time
C2L1b	7.02	C2L1b	7.04	C2L1b	4.26	C2L1b	4.06	C2L1b	6.04	C2L1b	6.70
D2L1b	7.1	B2L1b	7.08	D2L1b	4.3	D2L1b	4.24	D2L1b	6.1	C1L2b	6.94
B2L1b	7.12	D2L1b	7.08	B2L1b	4.44	B2L1b	4.4	C1L1b	6.48	D2L1b	7.02
C1L1b	7.98	E2L1b	7.38	C2L2b	4.76	C1L1b	4.98	B2L1b	6.66	C1L1b	7.04

Table 45: Time at which $\epsilon > \epsilon_y$ @reinforcement

CBGS		CBGS (SEQ)		CCCC		CCCC (SEQ)		CHHC		REHS	
ID	Time	ID	Time	ID	Time	ID	Time	ID	Time	ID	Time
F3L1b	4.04	F1L1b	4.02	F1L5t	2.6	C2L1b	0	F1L5t	3.9	F3L2b	3.84
F4L1b	5.88	F3L1b	4.04	F1L1b	2.62	F2L2t	0.78	F3L1b	3.94	F3L3t	3.86
F2L1b	5.90	F2L1b	4.06	F1L4t	2.62	F2L1b	0.8	F2L1b	3.96	F3L3b	3.88
F1L5t	6.00	C1L5t	4.16	F3L3b	2.64	F2L2b	0.84	F3L2b	3.96	F2L3b	3.90

Table 46: Time at which $\epsilon > \epsilon_{cu}$ @column face

CBGS		CBGS (SEQ)		CCCC		CCCC (SEQ)		CHHC		REHS	
ID	Time	ID	Time	ID	Time	ID	Time	ID	Time	ID	Time
F1L5t	6.02	F1L1b	5.88	F1L5t	2.62	F2L1b	2.14	F3L1b	3.98	F3L3t	3.92
B2L1b	6.36	F3L1b	5.88	F1L1b	2.66	F2L2t	2.16	F2L1b	3.98	F2L3b	3.98
C2L1b	6.38	F2L1b	5.88	F3L3b	2.66	F2L2b	2.16	F3L2b	4.00	F3L2b	4.02
D2L1b	6.38	F4L1b	5.92	F3L1b	2.66	F2L3b	2.16	F3L2t	4.00	F3L2t	4.02

CBGS

A number of column hinges in the base of the level 1 columns are predicted to exceed their ultimate strain limits between 6 and 6.4 seconds into the run CBGS record. These hinges are located along grid lines 1 and 2 e.g. column B1, B2, C1, C2, D2, and E2. Exceedence of the ultimate concrete strain corresponds to a large spike in the east-west displacements of the structure, which can be seen in Figure 58

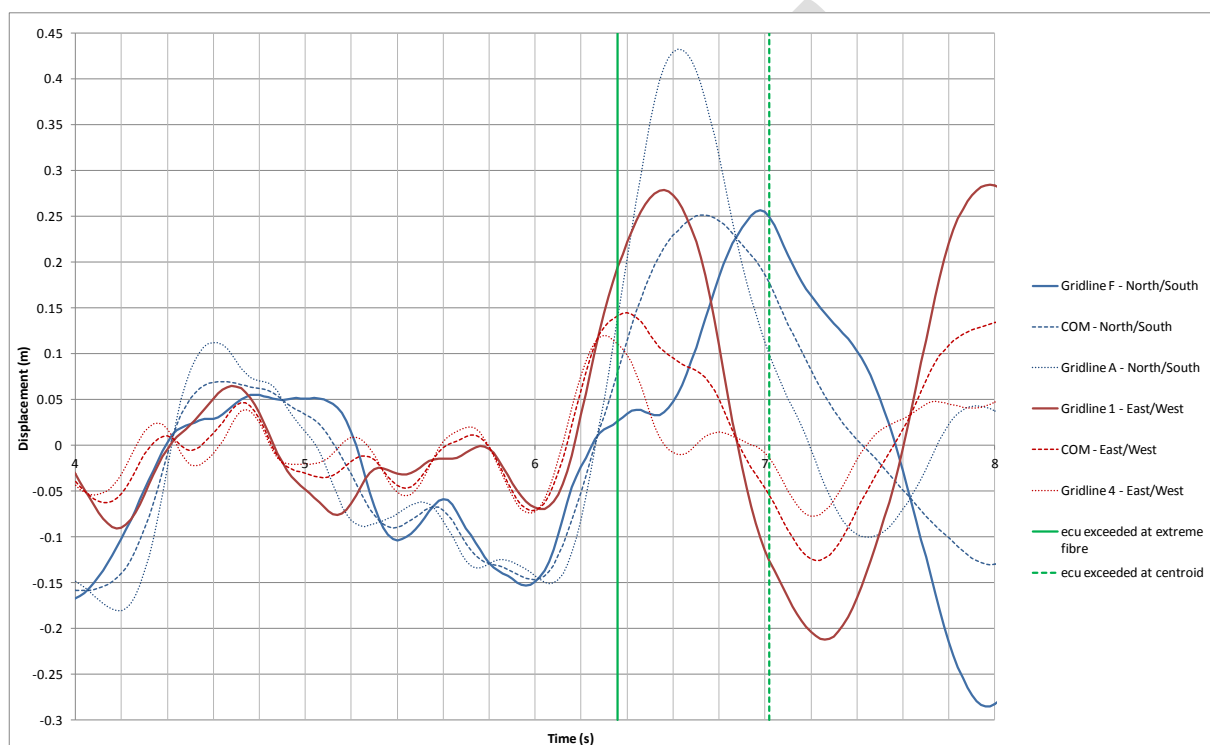


Figure 58: Building level 6 displacements, CBGS, Lyttelton.

Column C2 has been presented in this section as it is predicted to be the first column to exceed its ultimate compression strain capacity at the column centroid under the CBGS record demands, although only by a fraction of a second. A selection of column hinge actions for the hinge located at the base of the column at gridline C2 is presented in Figure 59 to Figure 65 for the CBGS earthquake record.

It can be seen in Figure 59 that the hinge at the bottom of the level 1 gridline C2 column is subject to a significant increase in rotation approximately 6.3 seconds into the run record. This causes a corresponding increase in concrete strains causing the ultimate concrete strain to be exceeded at the extreme compression fibre at 6.36 seconds. At this time concrete spalling

is expected to occur. Shortly after spalling is predicted the column is seen to lose its axial load carrying capacity as can be seen in Figure 60 and Figure 61.

Although columns C2 and D2 are subject to a similar amount of axial load, and the same east/west drift, column C2 is seen to lose its axial load carrying capacity first. This is as a consequence of column C2 being subject to a higher concurrent north/south drift than column D2. Column C2 is offset further from the centre of stiffness in the north/south direction than column D2 so is subject to higher north south displacement demands due to building rotation.

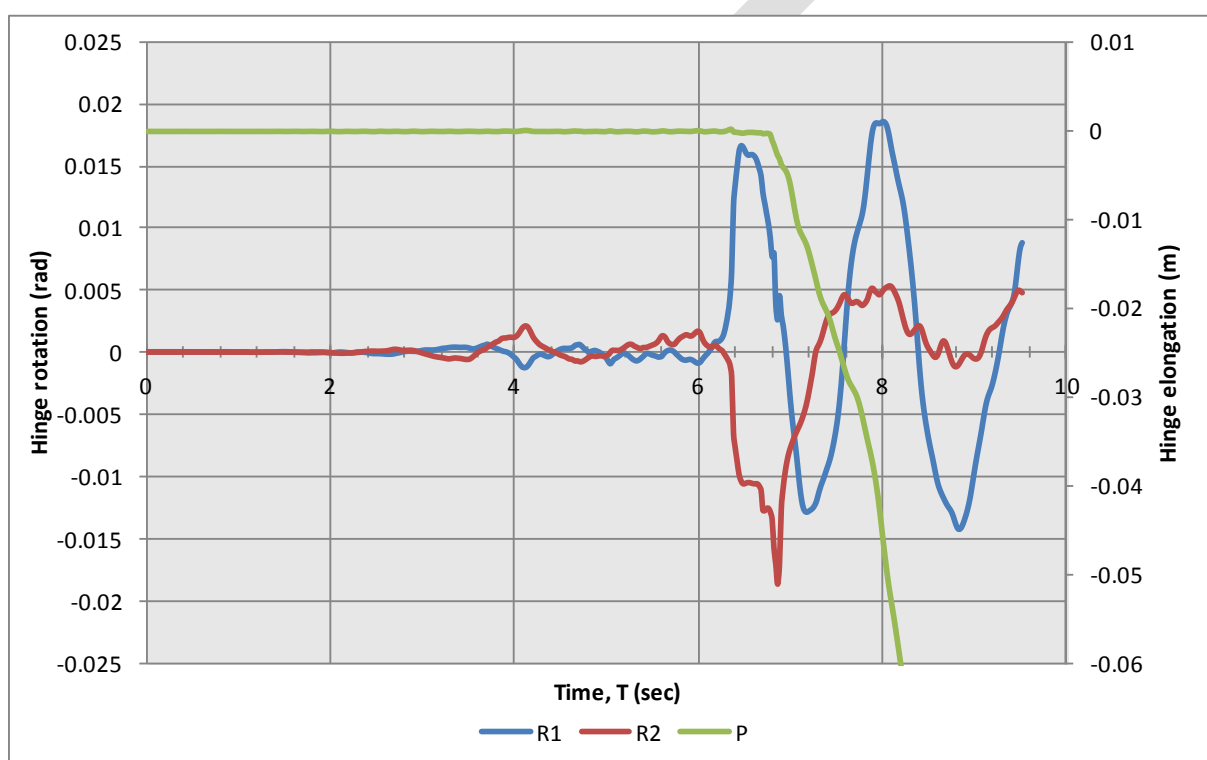


Figure 59: Column C2, Level 1 hinge rotation and elongation vs time, CBGS, Lyttelton.

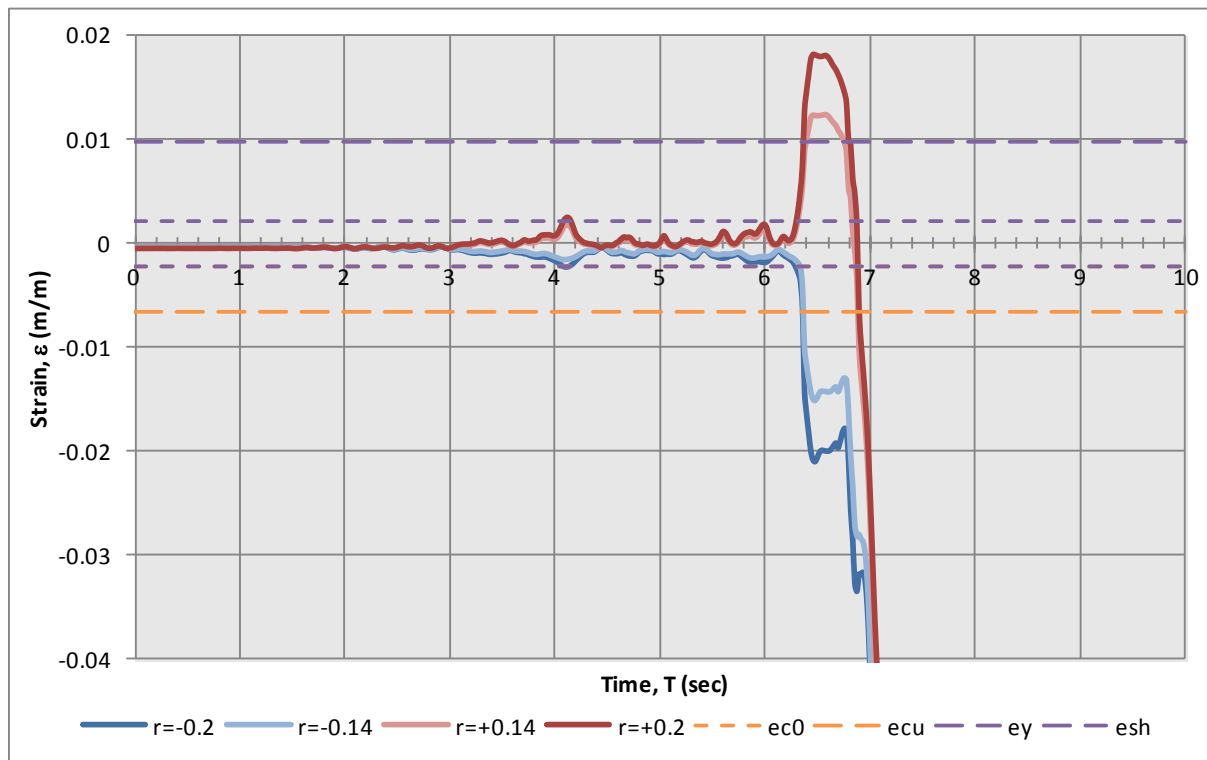


Figure 60: Column C2 Level 1 lower hinge strain vs time, CBGS, Lyttelton.

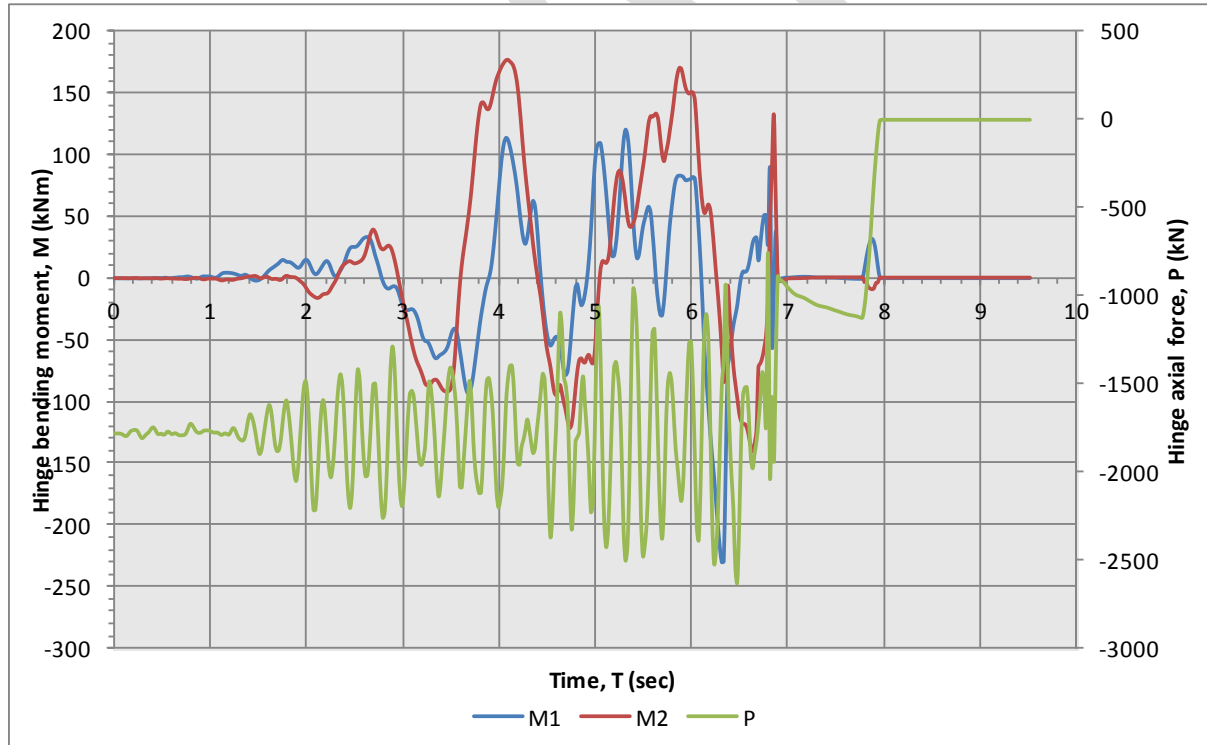


Figure 61: Column C2 Level 1 lower hinge axial and moments vs time, CBGS, Lyttelton.

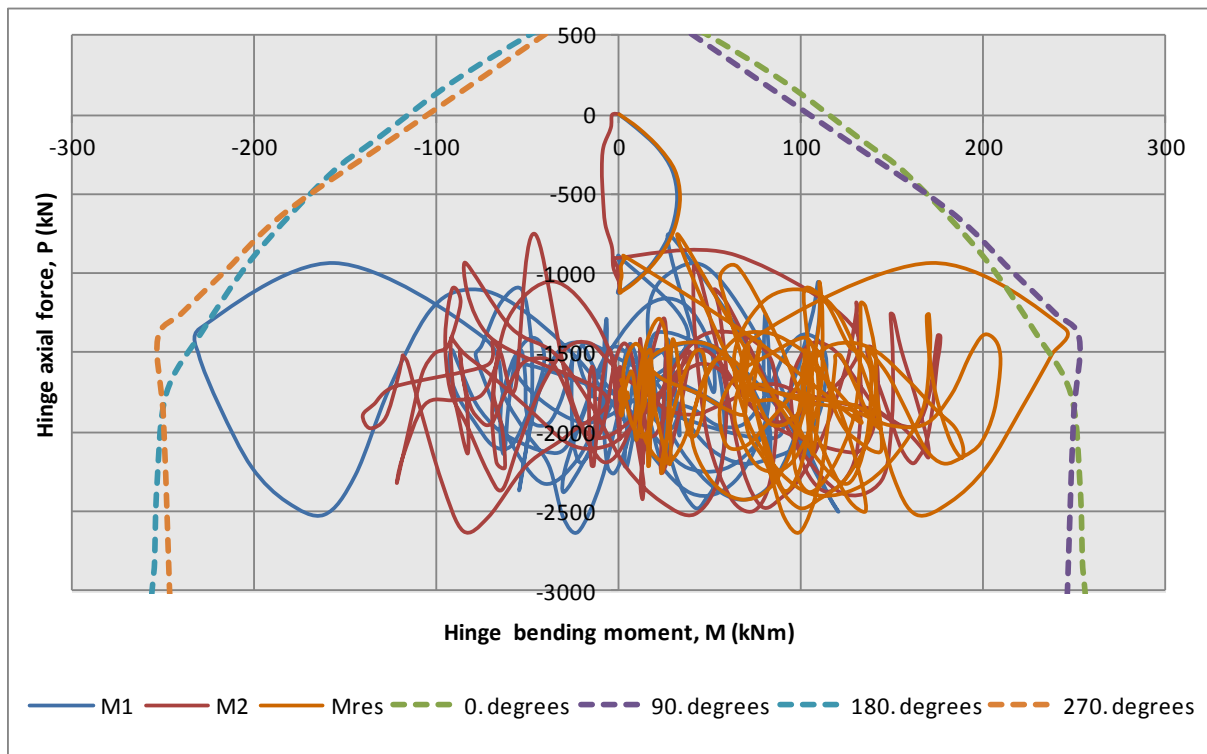


Figure 62: Column C2 Level 1 lower hinge moment axial relationship, CBGS, Lyttelton.

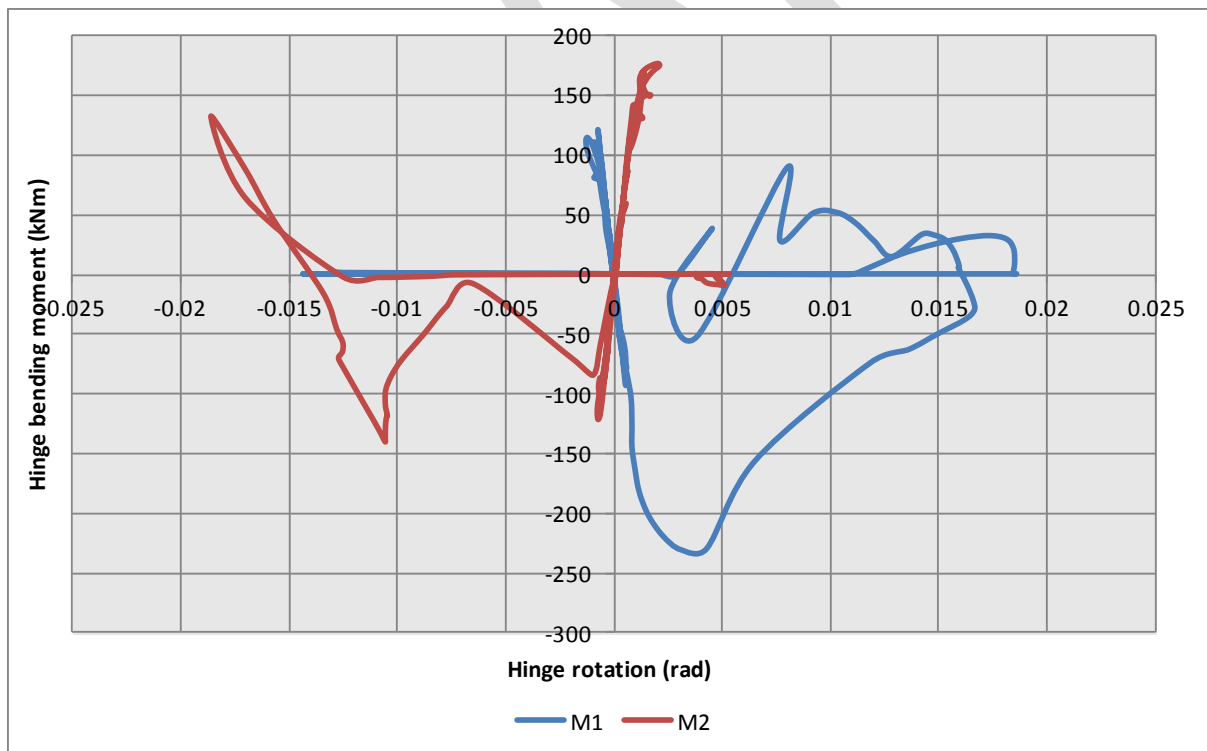


Figure 63: Column C2 Level 1 lower hinge hysteretic form, CBGS, Lyttelton.

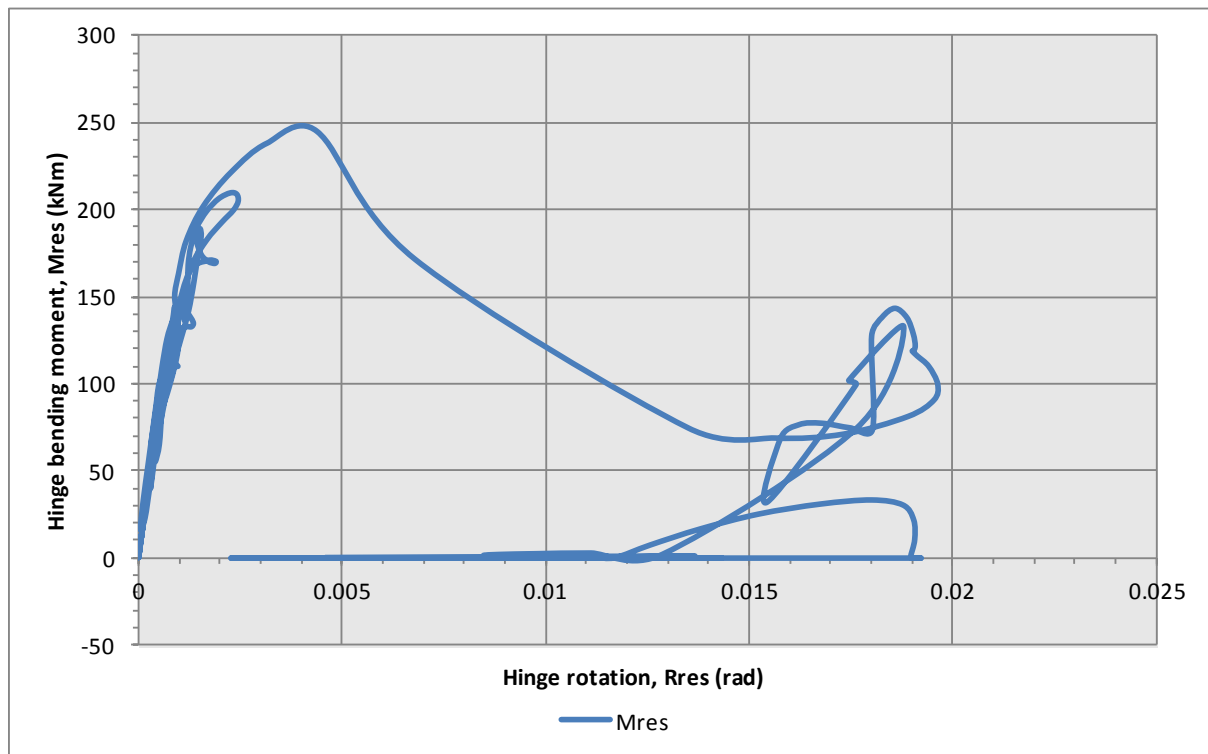


Figure 64: Column C2 Level 1 lower hinge moment rotation, CBGS, Lyttelton.

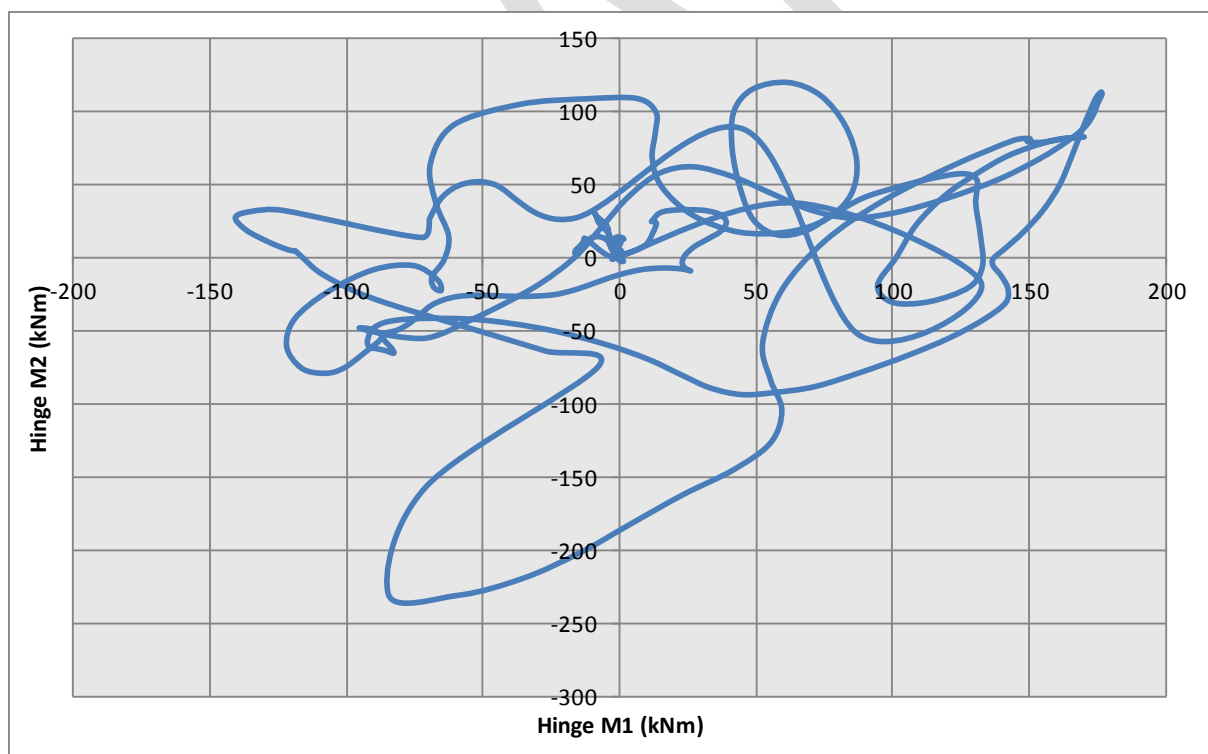


Figure 65: Column C2 Level 1 lower hinge bi-axial moment, CBGS, Lyttelton.

It should be noted that the strain plots indicate that the whilst a number of columns exceed the ultimate concrete compressive strain at similar times, the more heavily loaded columns such as columns C2 and D2 are seen to lose their vertical support more rapidly than the more lightly loaded columns. Appendix I.3 contains more information on the hinge strains for various hinges when subject to the CBGS Lyttelton demands.

CCCC

Results for the CCCC Lyttelton analyses can be found in Appendix J.3.

CHHC

Results for the CHHC Lyttelton analyses can be found in Appendix K.3.

REHS

Results for the REHS Lyttelton analyses can be found in Appendix L.3.

11.4. Beam-Column Joints.

This section presents the cumulative maximum joint deformation states for the Lyttelton event. Figure 47 (represented below) defines the colour coding used in the plots to indicate the number of joints that have been subjected to different deformation states as the earthquake event progresses. Note that the blue colour represents elastic behaviour of the joints.

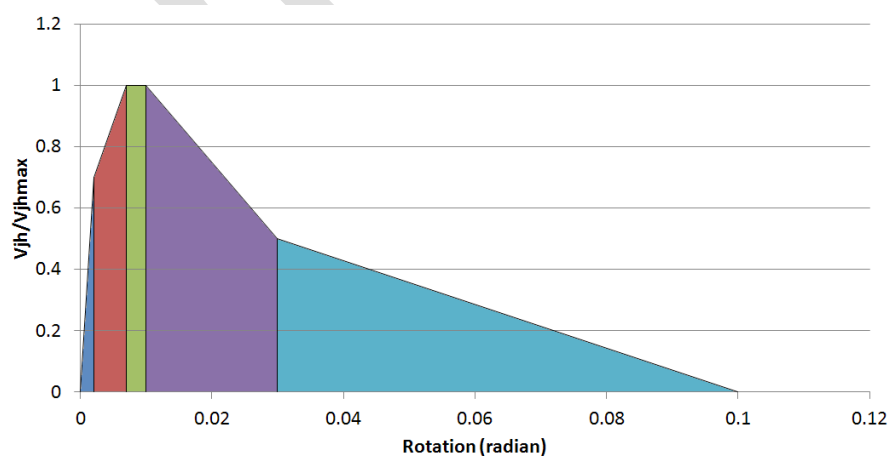


Figure 47: Colour coding used to represent different joint deformation states in Figure 66 to Figure 93

Plots are presented separately for the one-way (joints located on gridlines B to E) and two-way joints (joints located on gridline A and F). It should be noted that 'R1' corresponds to rotation about the north/south axis and 'R2' corresponds to rotation about the east/west axis. Results presented in this section include those assuming that the CTV Building was in an undamaged state at the commencement of the analysis, and those for the sequential analyses following on from stiffness state at the end of the Darfield event (denoted '*sequential*').

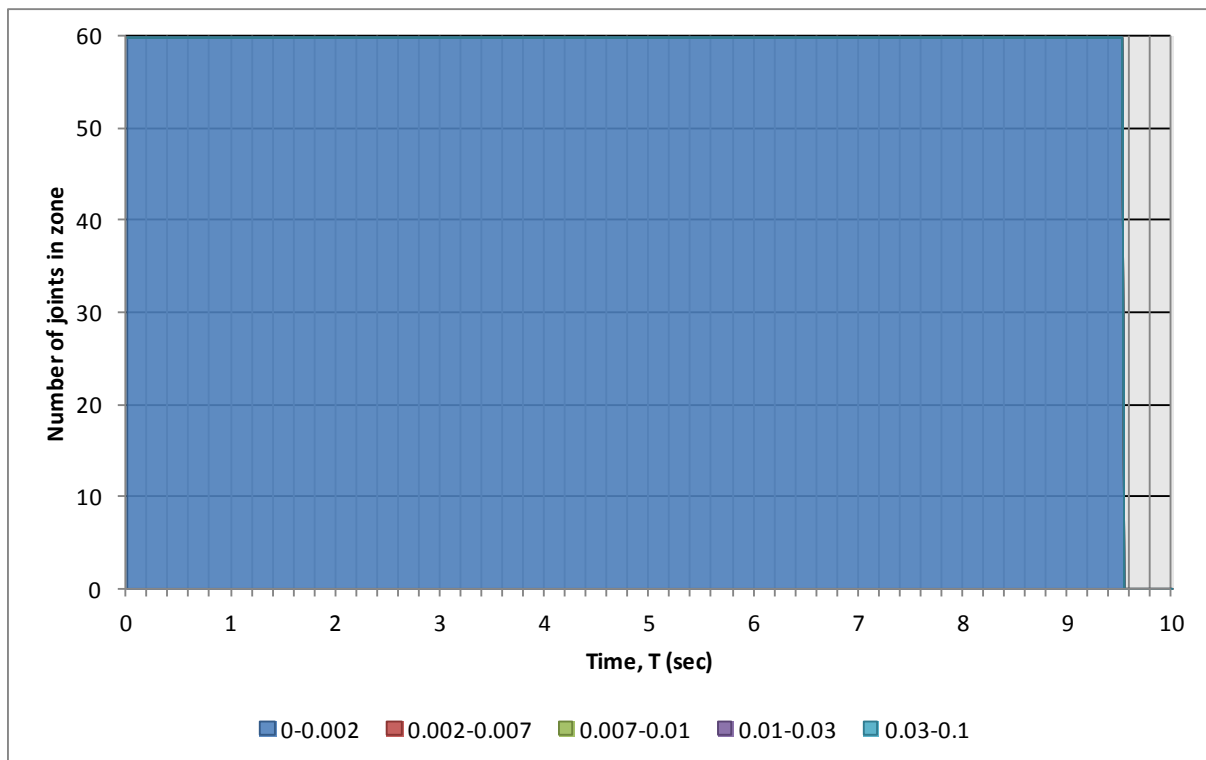


Figure 66: One-way beam-column joint R1 rotations, CBTG, Lyttelton.



Figure 67: GL A two-way beam-column joint R1 rotations, CBGS, Lyttelton.

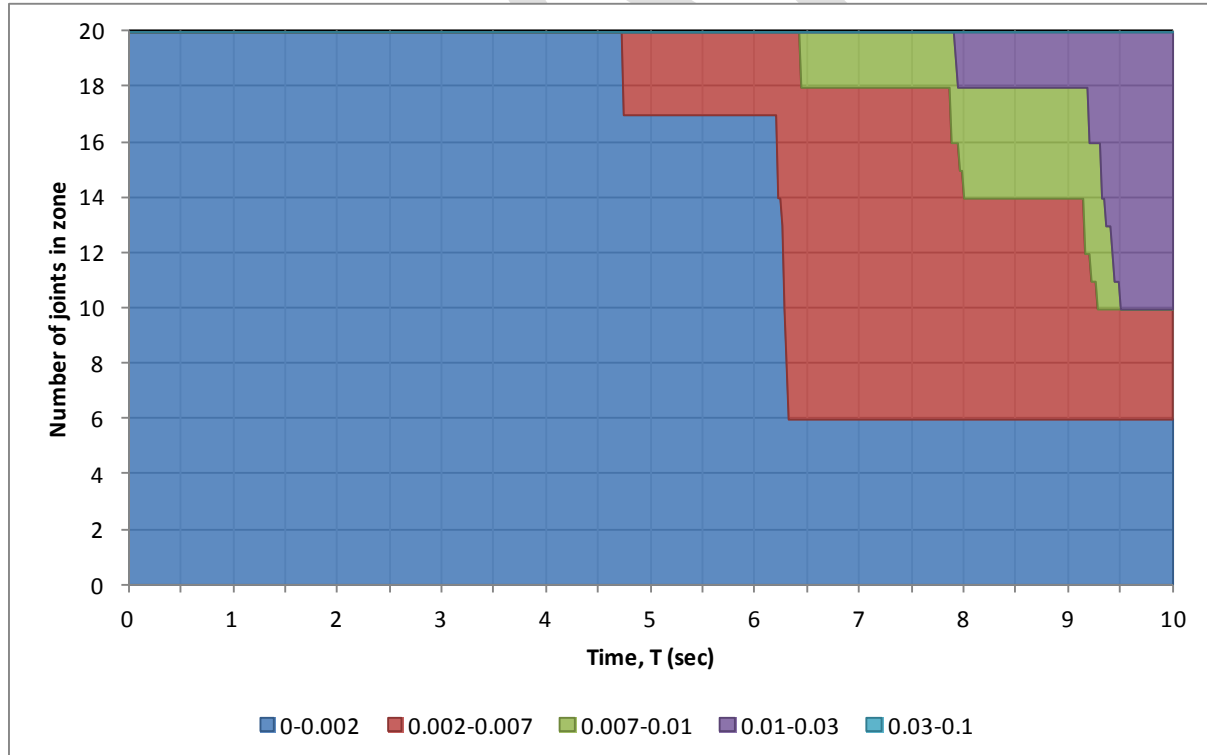


Figure 68: GL A two-way beam-column joint R1 rotations, CBGS, Lyttelton, Sequential.

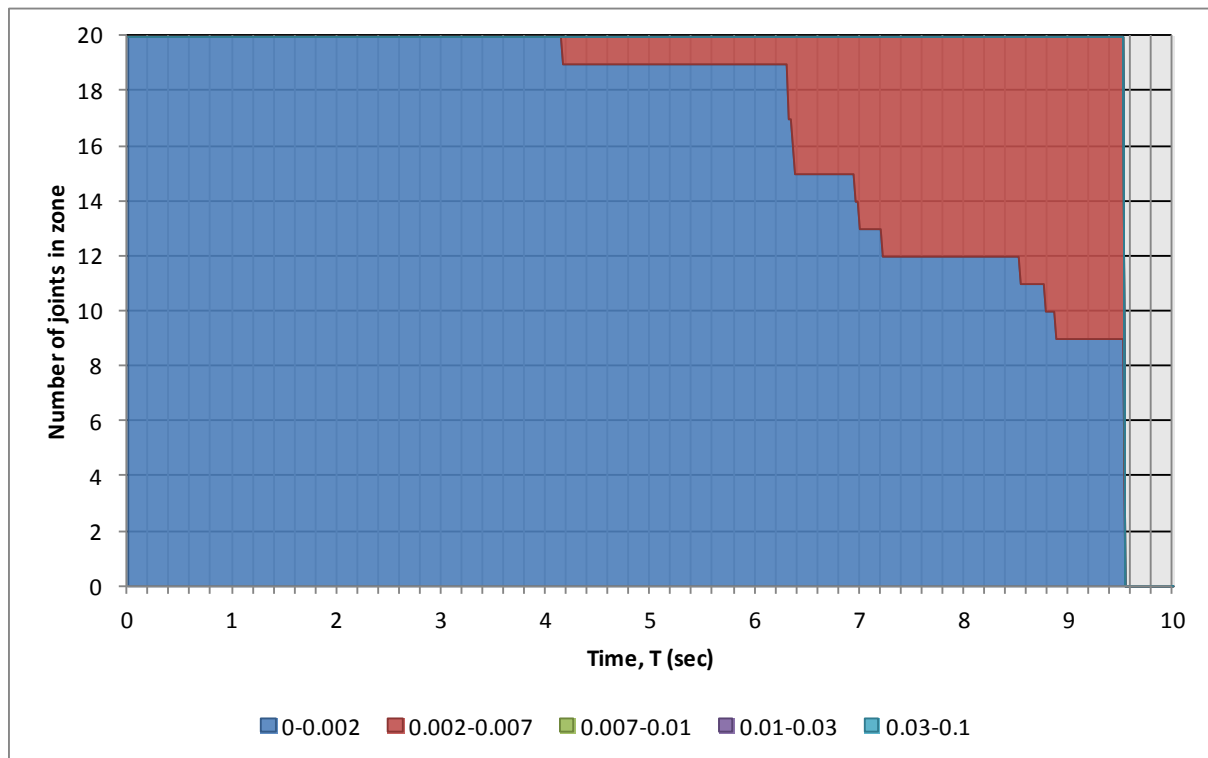


Figure 69: GL F two-way beam-column joint R1 rotations, CBGS, Lyttelton.

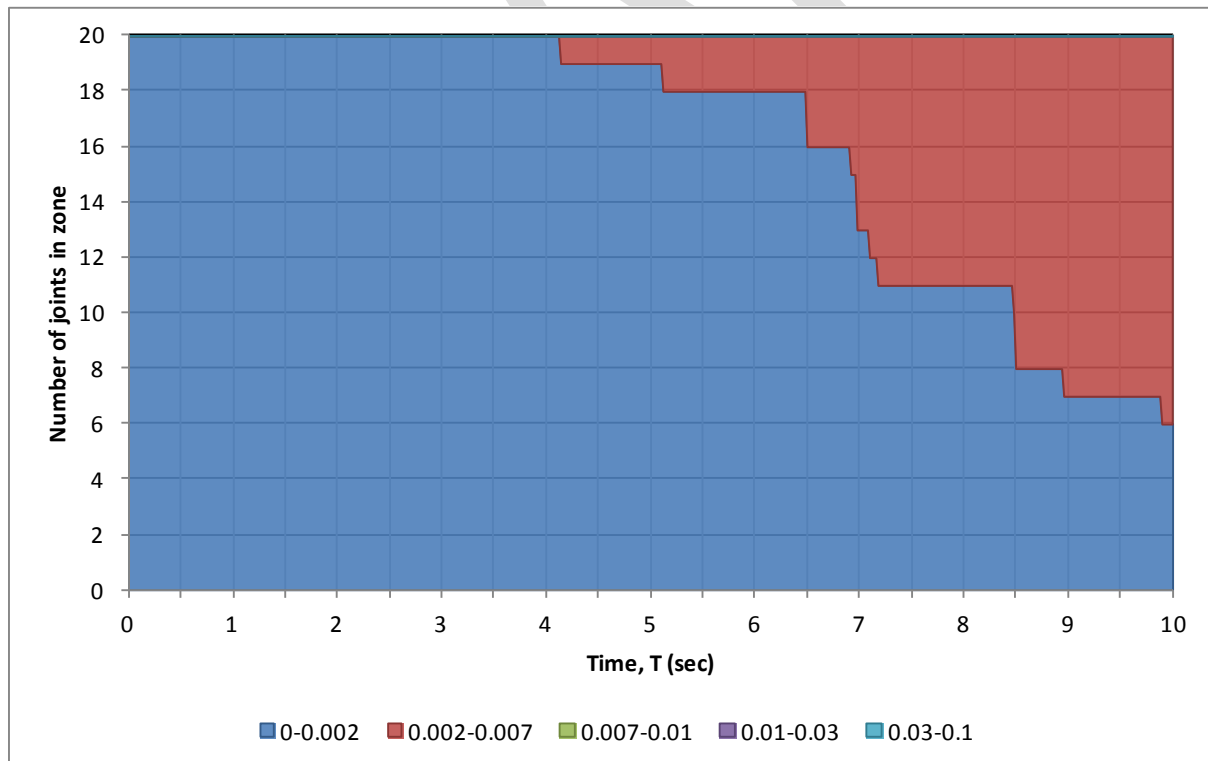


Figure 70: GL F two-way beam-column joint R1 rotations, CBGS, Lyttelton, Sequential.

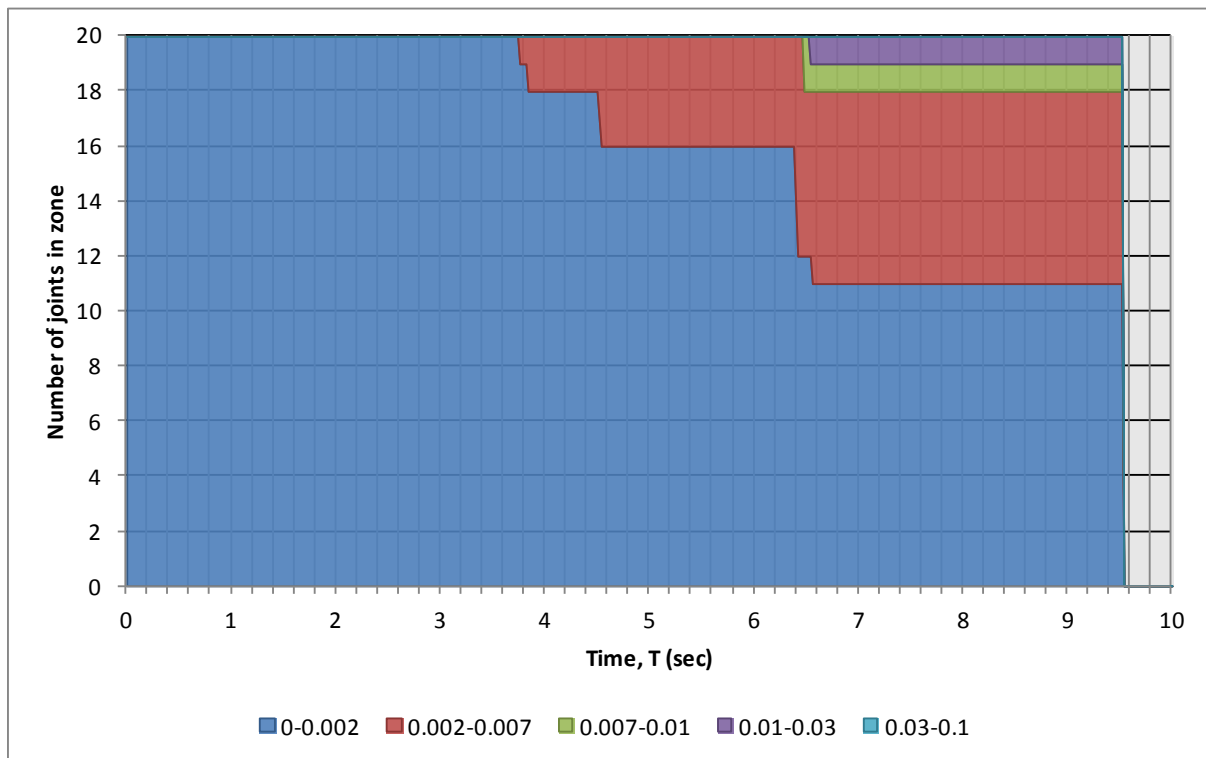


Figure 71: GL A two-way beam-column joint R2 rotations, CBGS, Lyttelton.

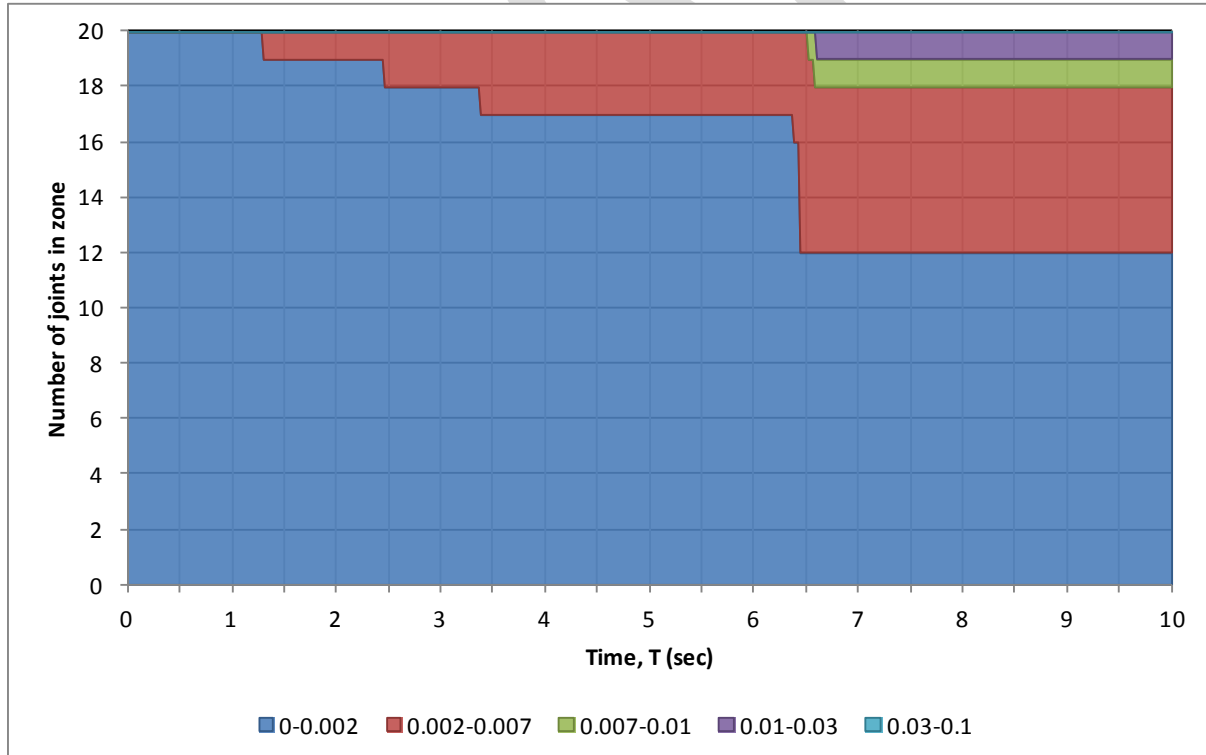


Figure 72: GL A two-way beam-column joint R2 rotations, CBGS, Lyttelton, Sequential.

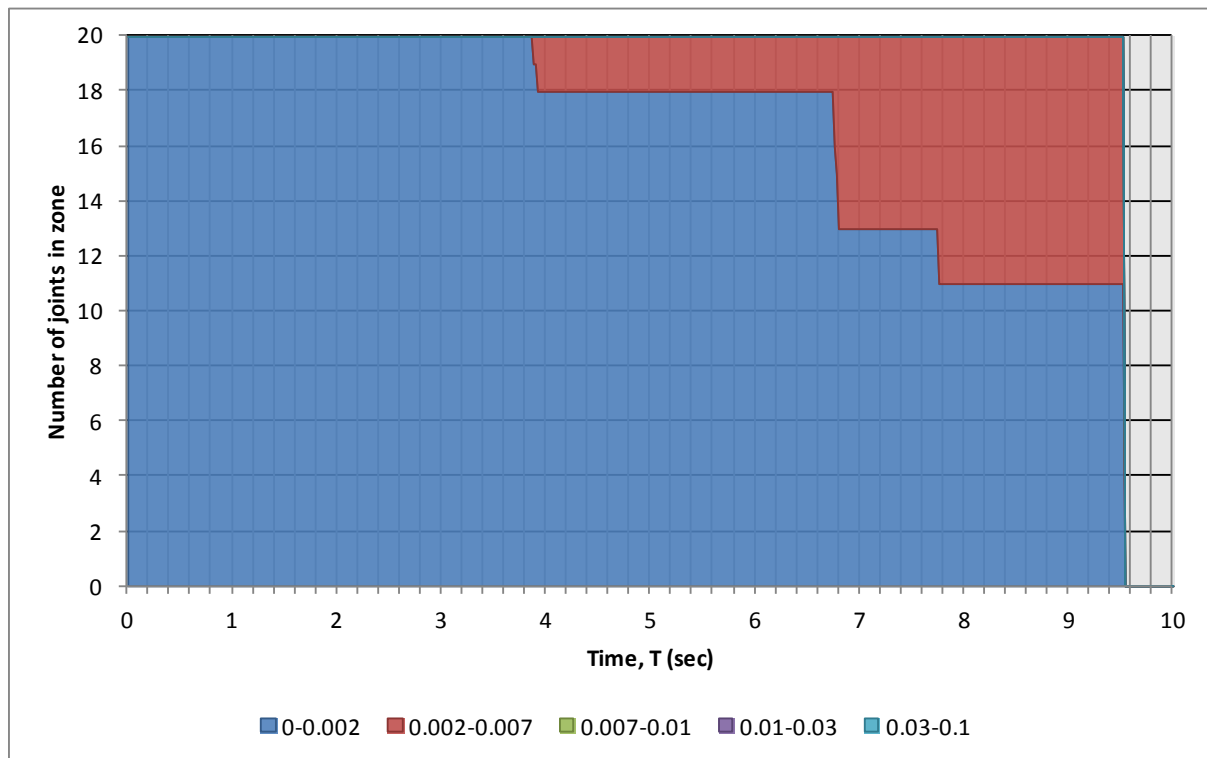


Figure 73: GL F two-way beam-column joint R2 rotations, CBGS, Lyttelton.

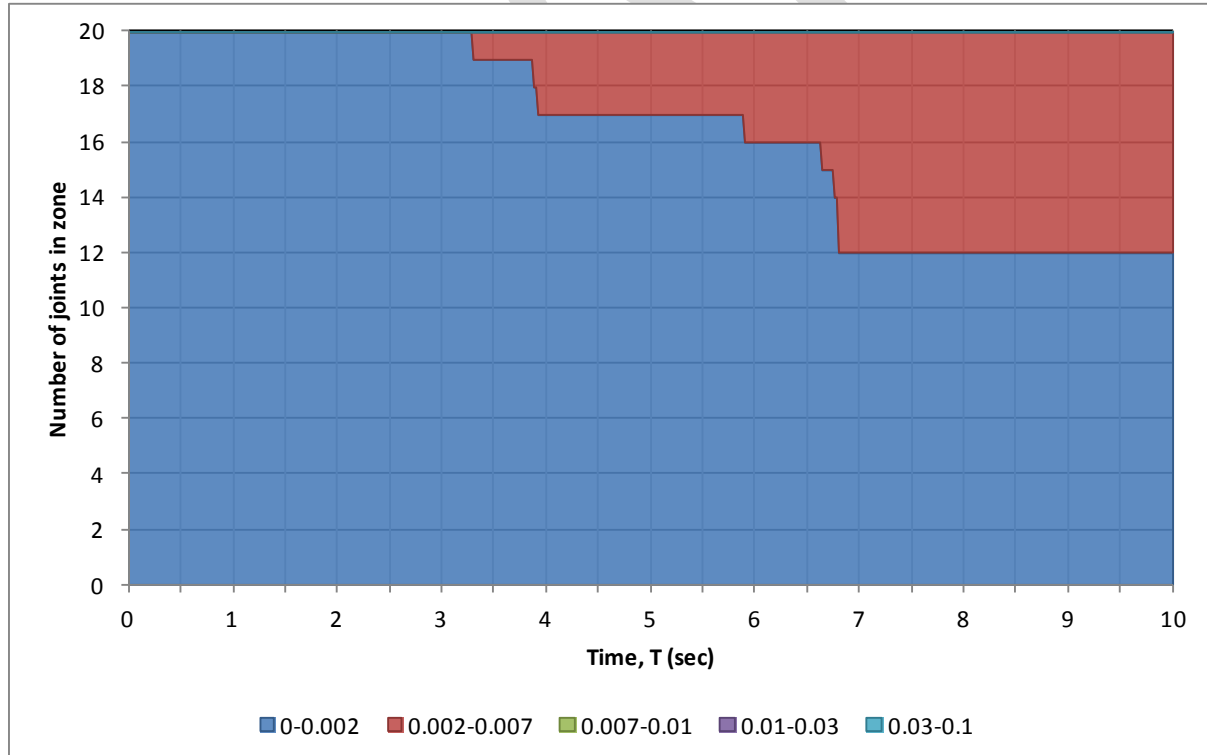


Figure 74: GL F two-way beam-column joint R2 rotations, CBGS, Lyttelton, Sequential.

As can be seen in Figure 66 the interior beam column joints behave elastically when subject to the CBGS record demands. Figure 67 to Figure 74 indicate that the exterior joints are subject to inelastic demand, however joint ultimate capacity is only reached after column hinges located at the base of the column are predicted to have their ultimate concrete strain exceeded i.e. 6.36 seconds.

As can be seen in Figure 75 the interior beam column joints behave elastically when subject to the CCCC record demands. Figure 76 to Figure 83 indicate that the exterior joints are subject to inelastic demand, however joint ultimate capacity is only reached after column hinges are predicted to have their ultimate concrete strain exceeded.

As can be seen in Figure 84 the interior beam column joints behave elastically when subject to the CHHC record demands. Figure 85 and Figure 88 indicate that the exterior joints are subject to inelastic demand, however joint ultimate capacity is only reached after column hinges are predicted to have their ultimate concrete strain exceeded.

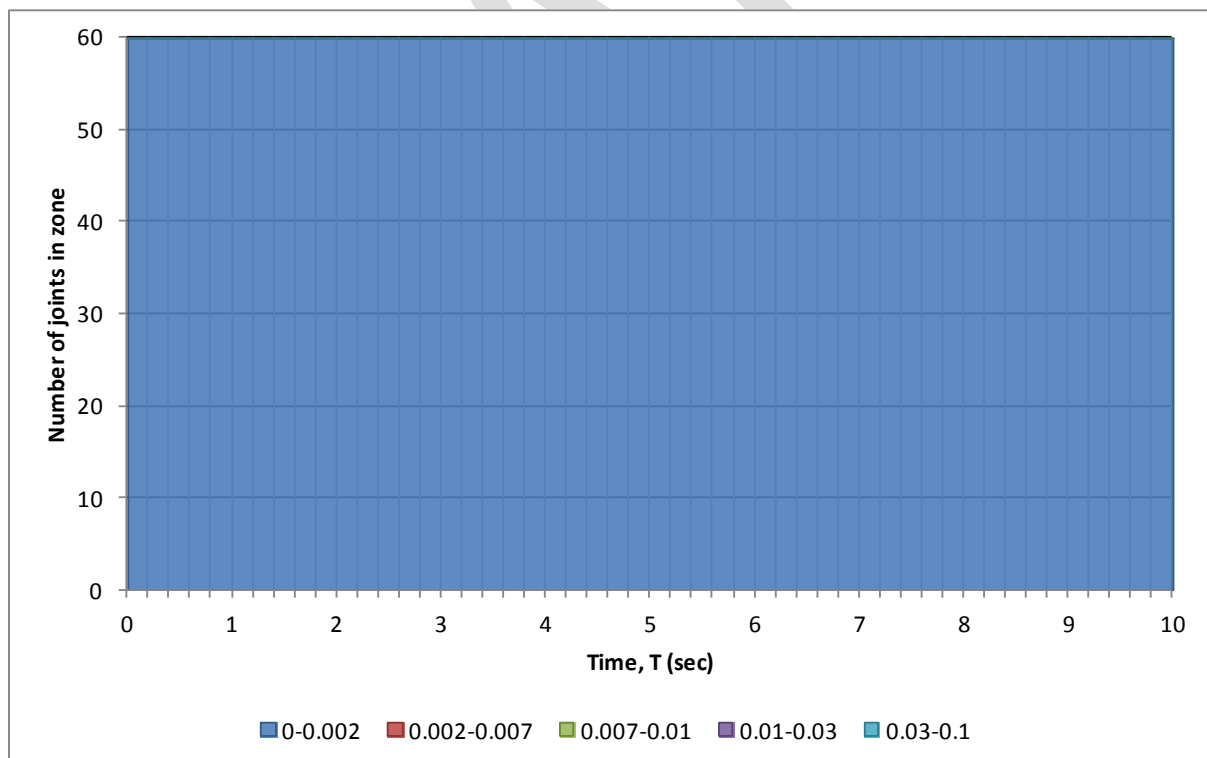


Figure 75: One-way beam-column joint R1 rotations, CCCC, Lyttelton.

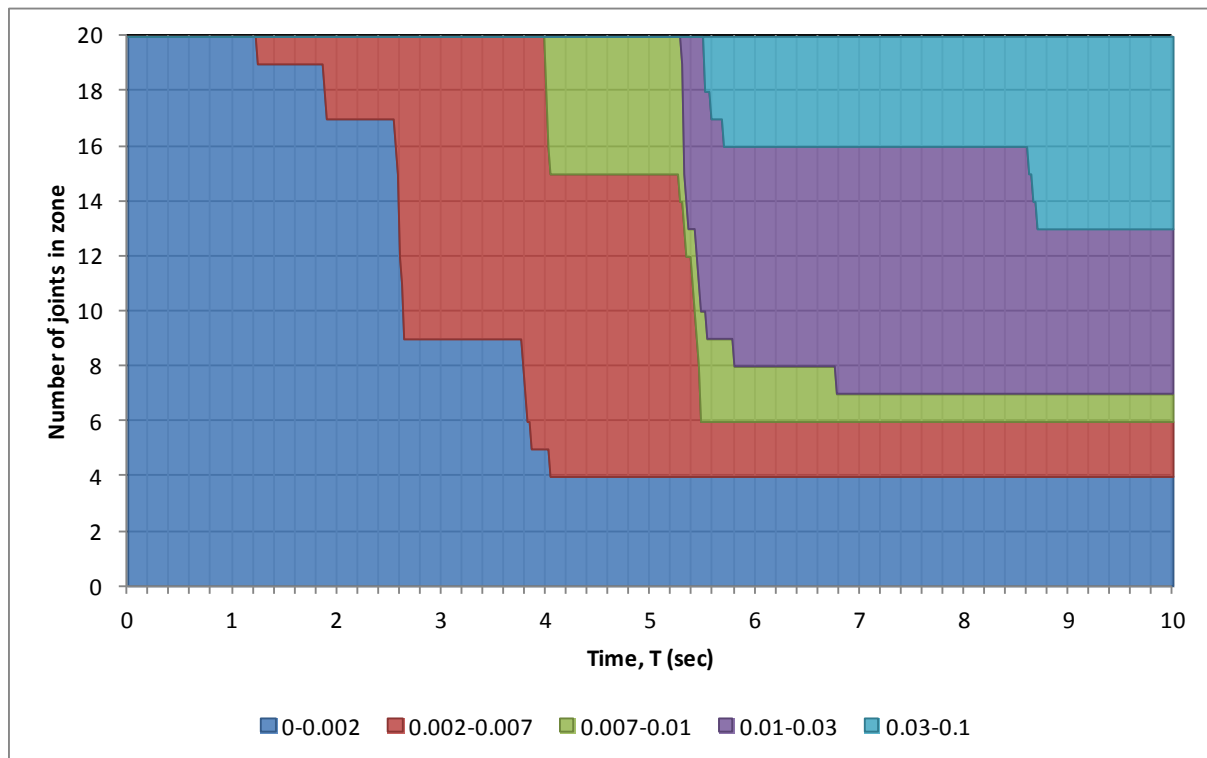


Figure 76: GL A two-way beam-column joint R1 rotations, CCCC, Lyttelton.

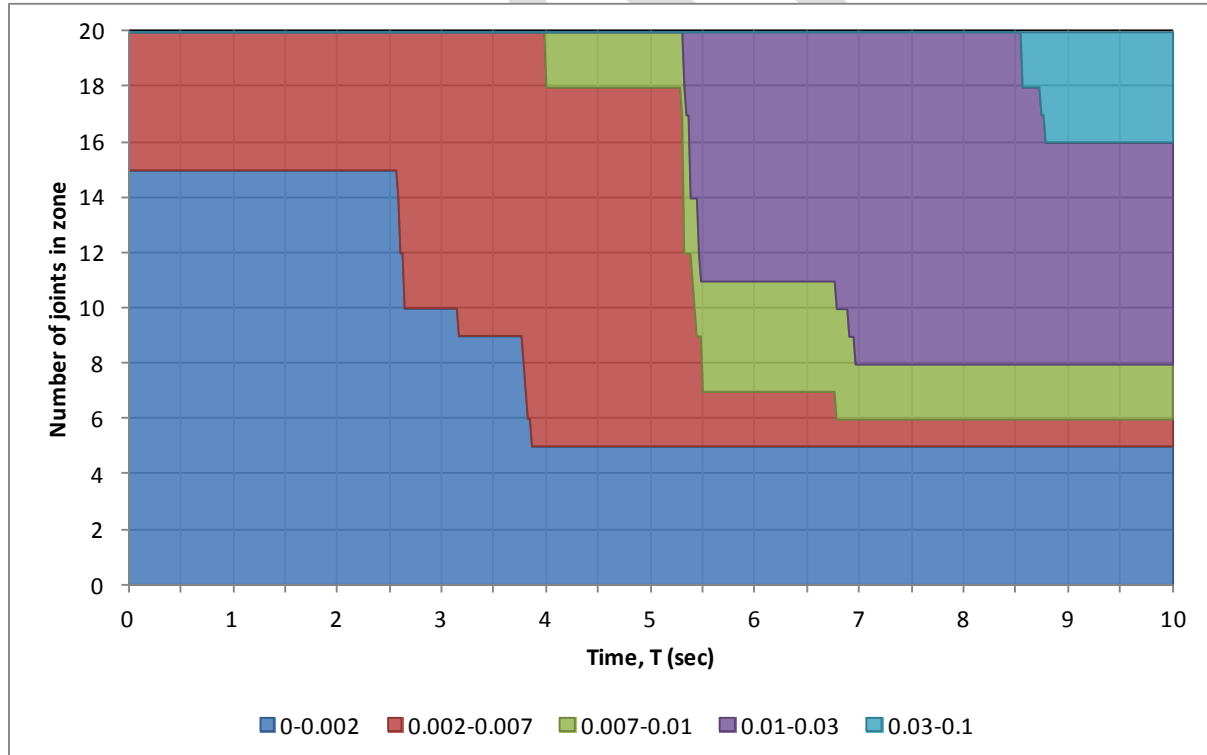


Figure 77: GL A two-way beam-column joint R1 rotations, CCCC, Lyttelton, Sequential

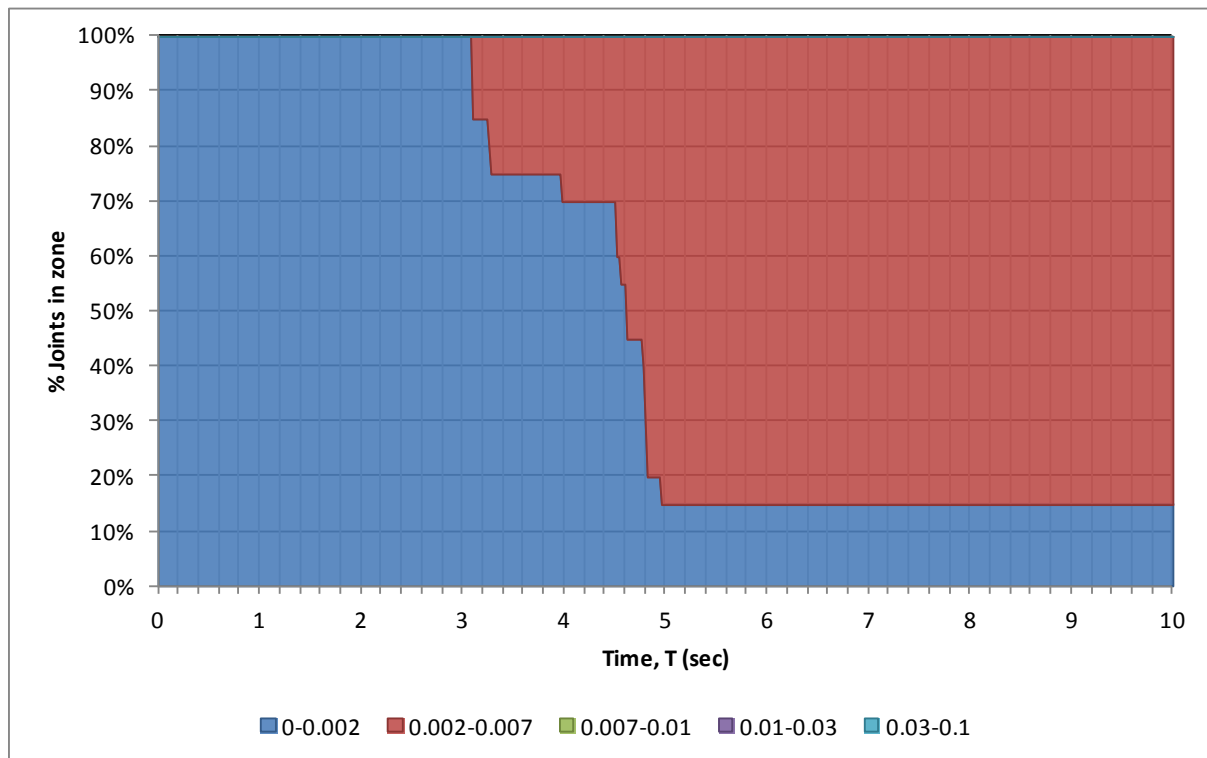


Figure 78: GL F two-way beam-column joint R1 rotations, CCCC, Lyttelton.

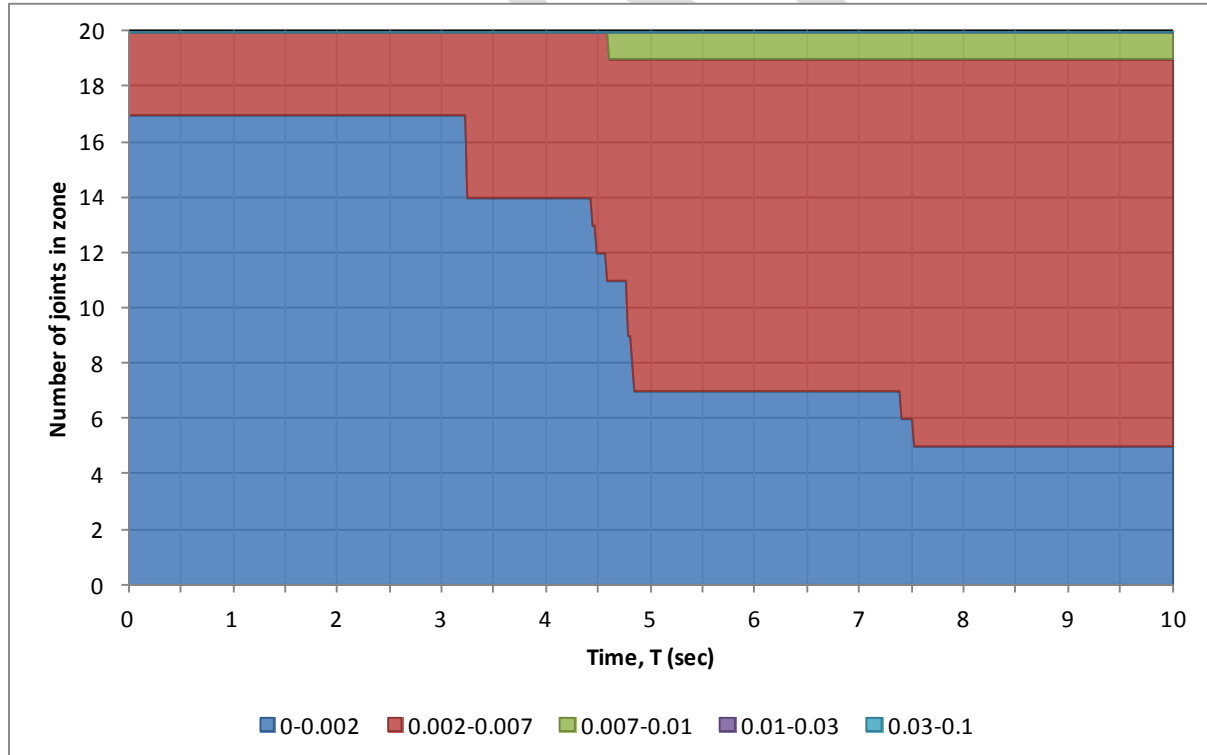


Figure 79: GL F two-way beam-column joint R1 rotations, CCCC, Lyttelton, Sequential

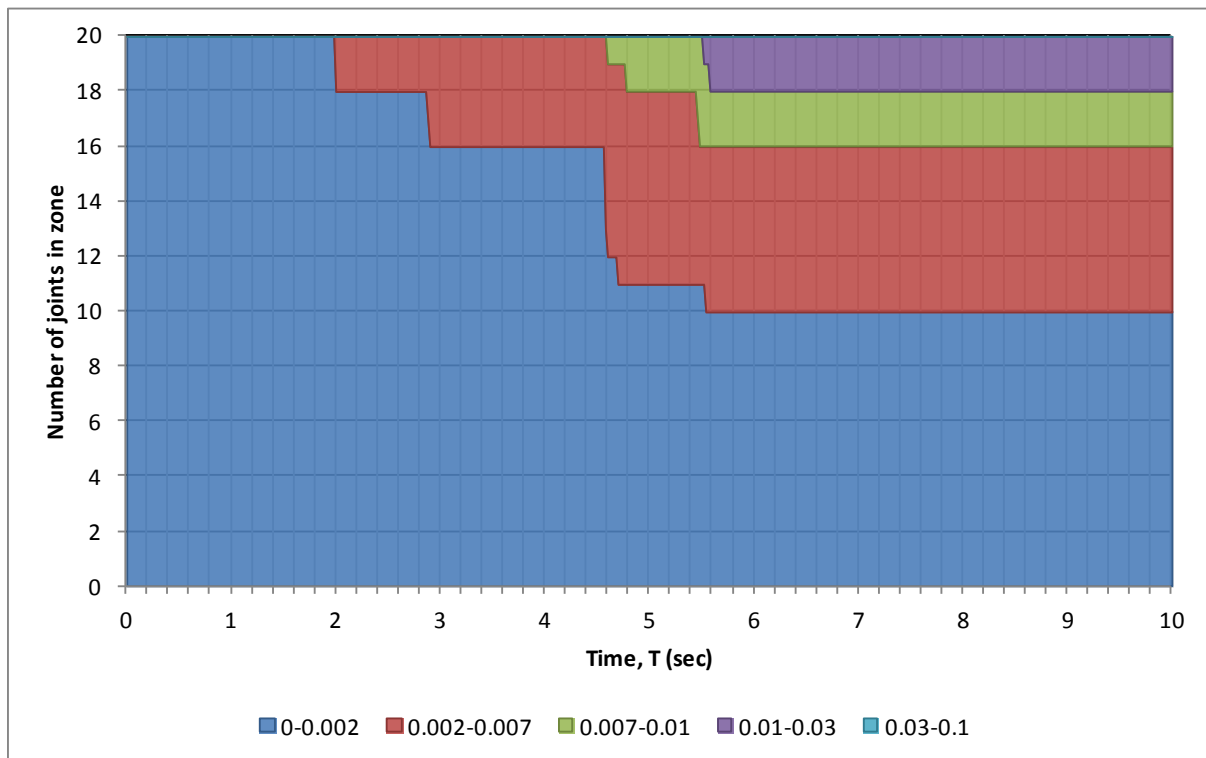


Figure 80: GL A two-way beam-column joint R2 rotations, CCCC, Lyttelton.

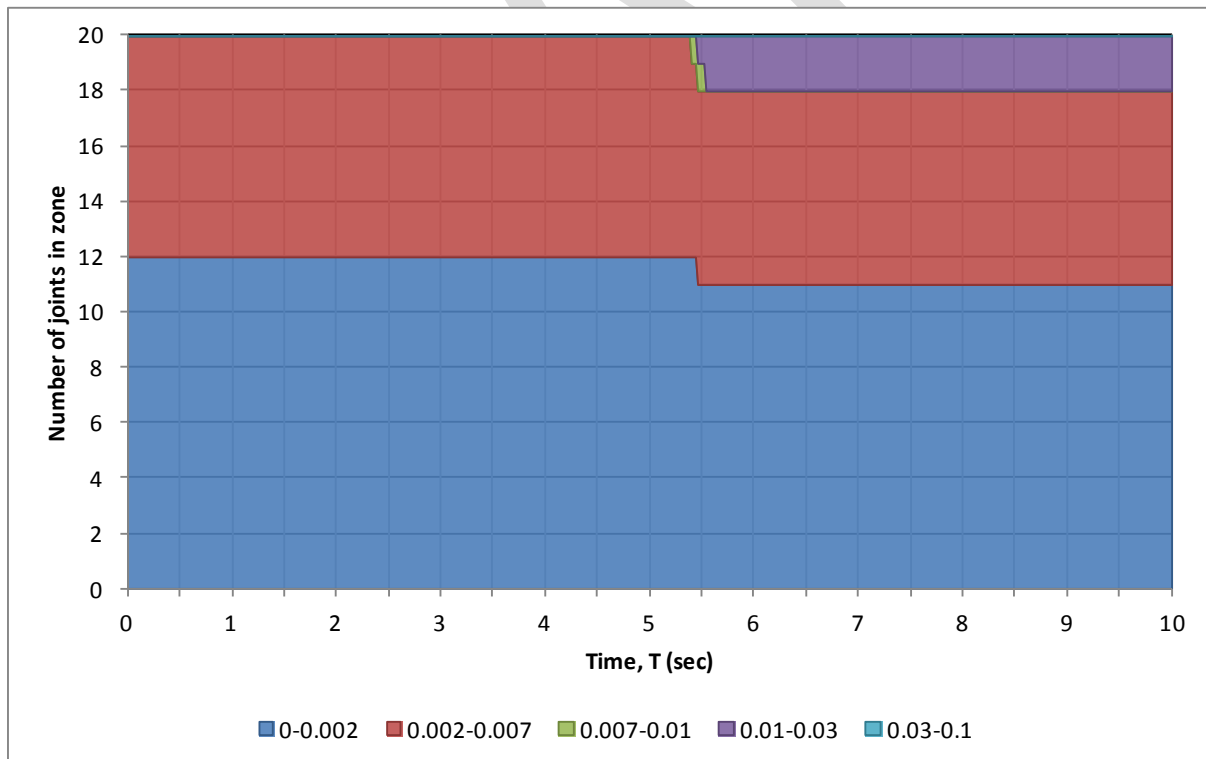


Figure 81: GL A two-way beam-column joint R2 rotations, CCCC, Lyttelton, Sequential

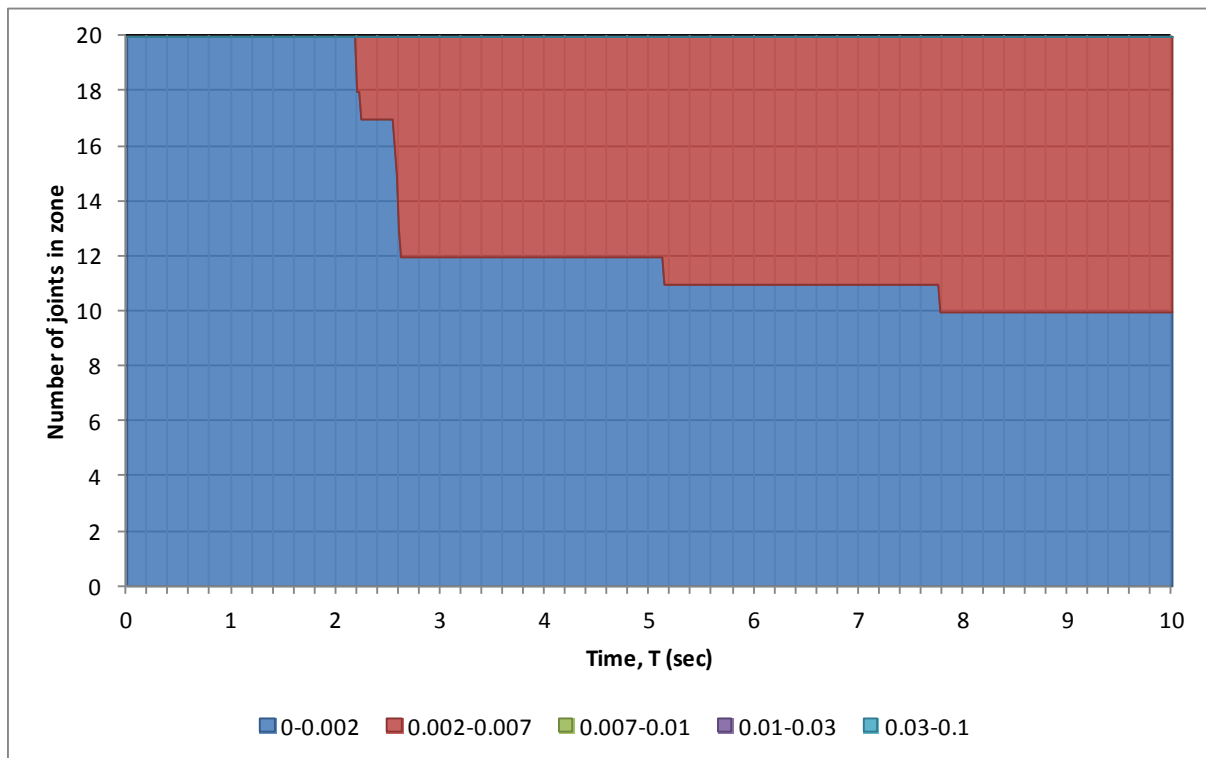


Figure 82: GL F two-way beam-column joint R2 rotations, CCCC, Lyttelton.

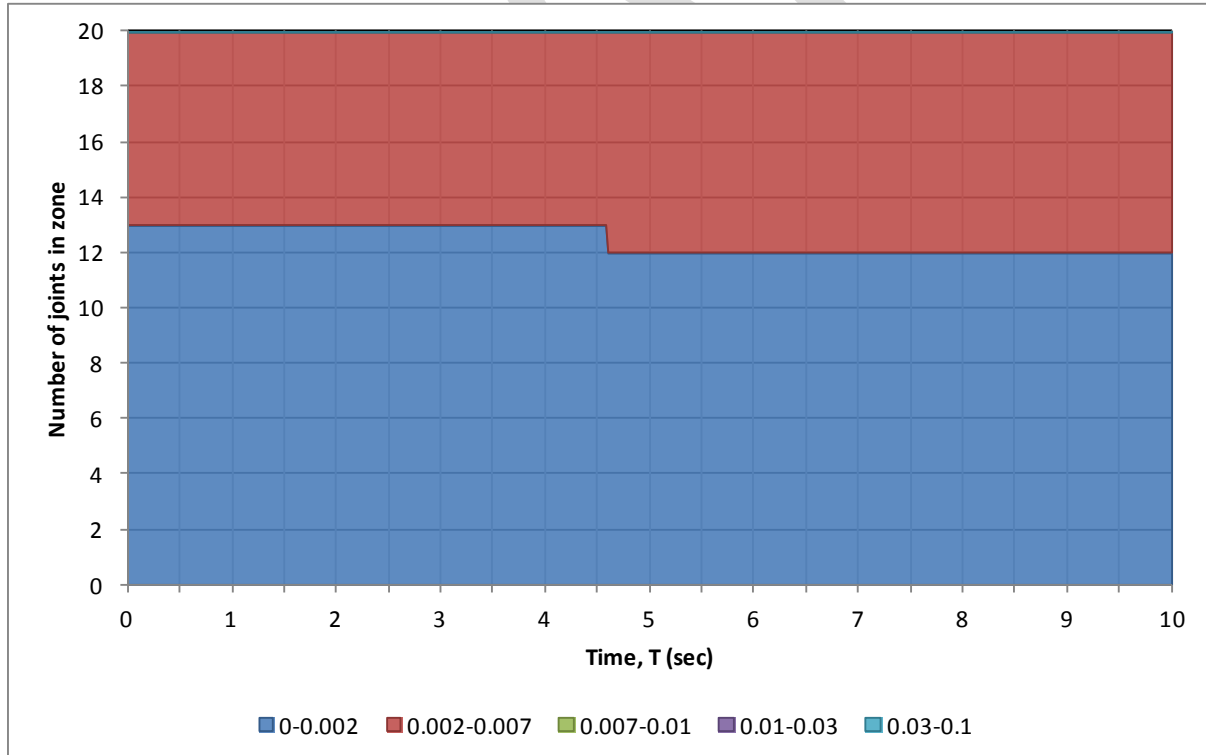


Figure 83: GL F two-way beam-column joint R2 rotations, CCCC, Lyttelton, Sequential

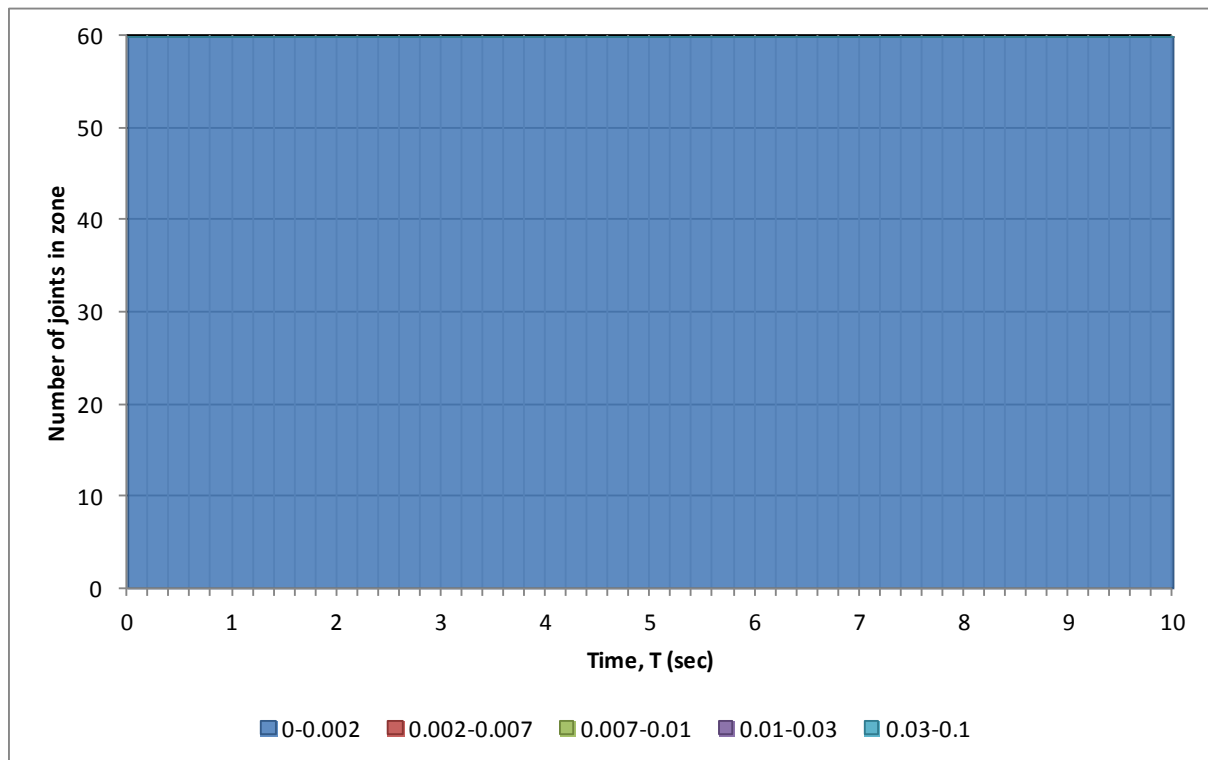


Figure 84: One-way beam-column joint R1 rotations, CHHC, Lyttelton.



Figure 85: GL A two-way beam-column joint R1 rotations, CHHC, Lyttelton.

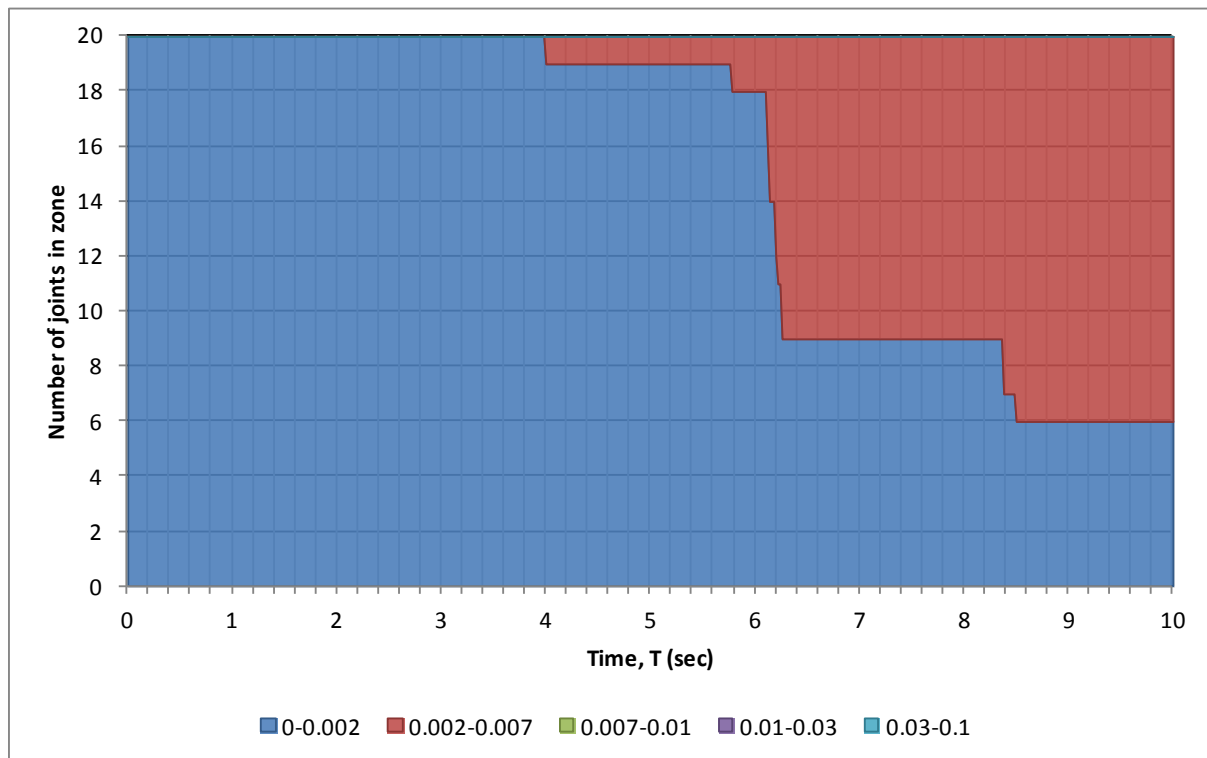


Figure 86: GL F two-way beam-column joint R1 rotations, CHHC, Lyttelton.

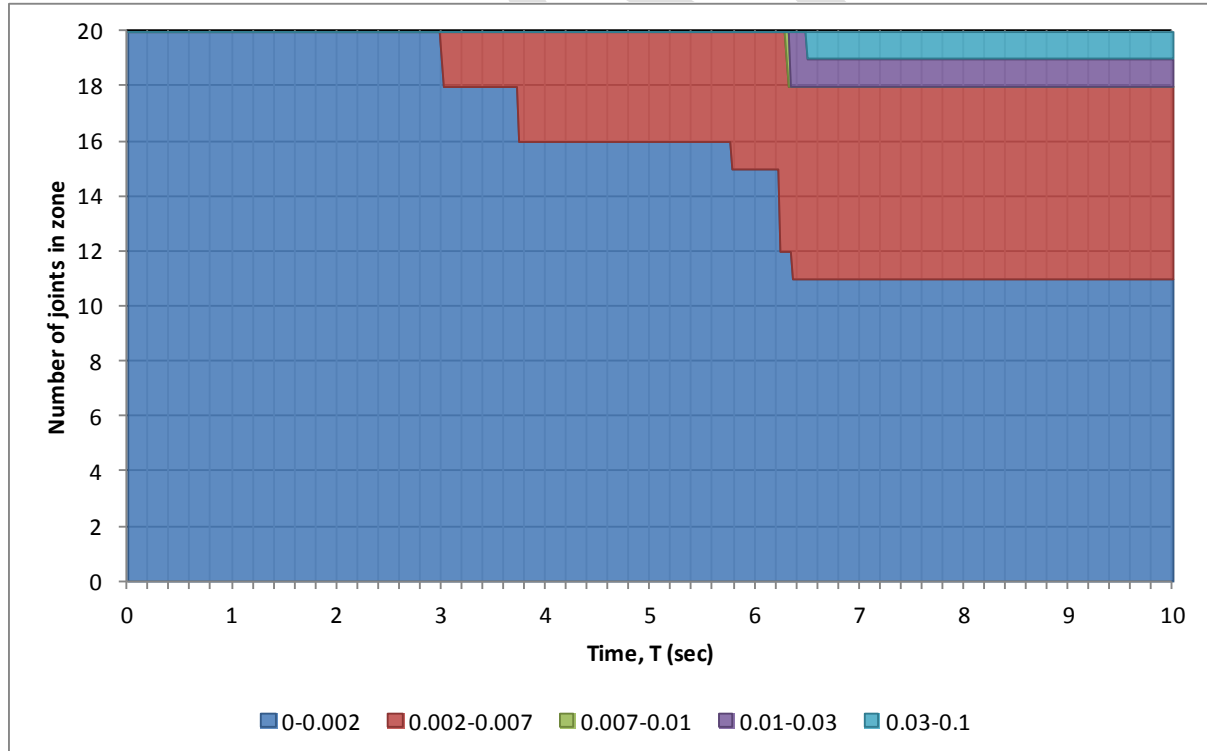


Figure 87: GL A two-way beam-column joint R2 rotations, CHHC, Lyttelton.

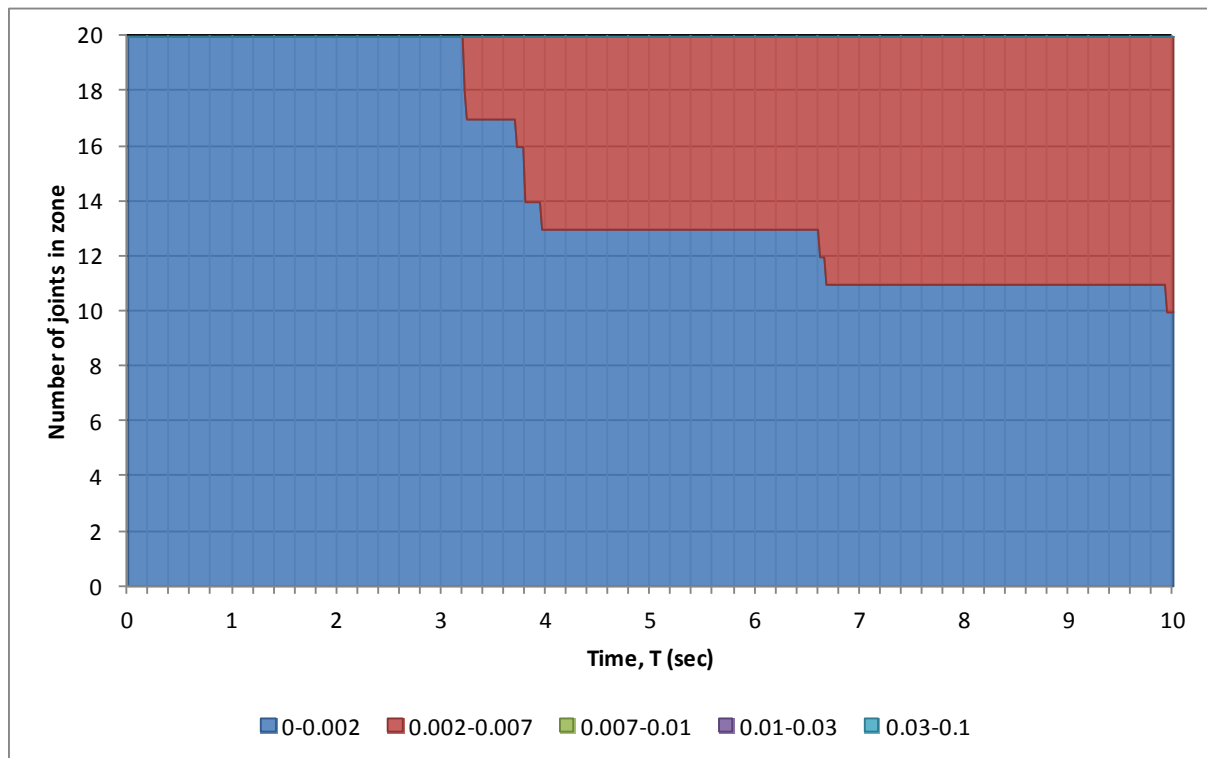


Figure 88: GL F two-way beam-column joint R2 rotations, CHHC, Lyttelton.

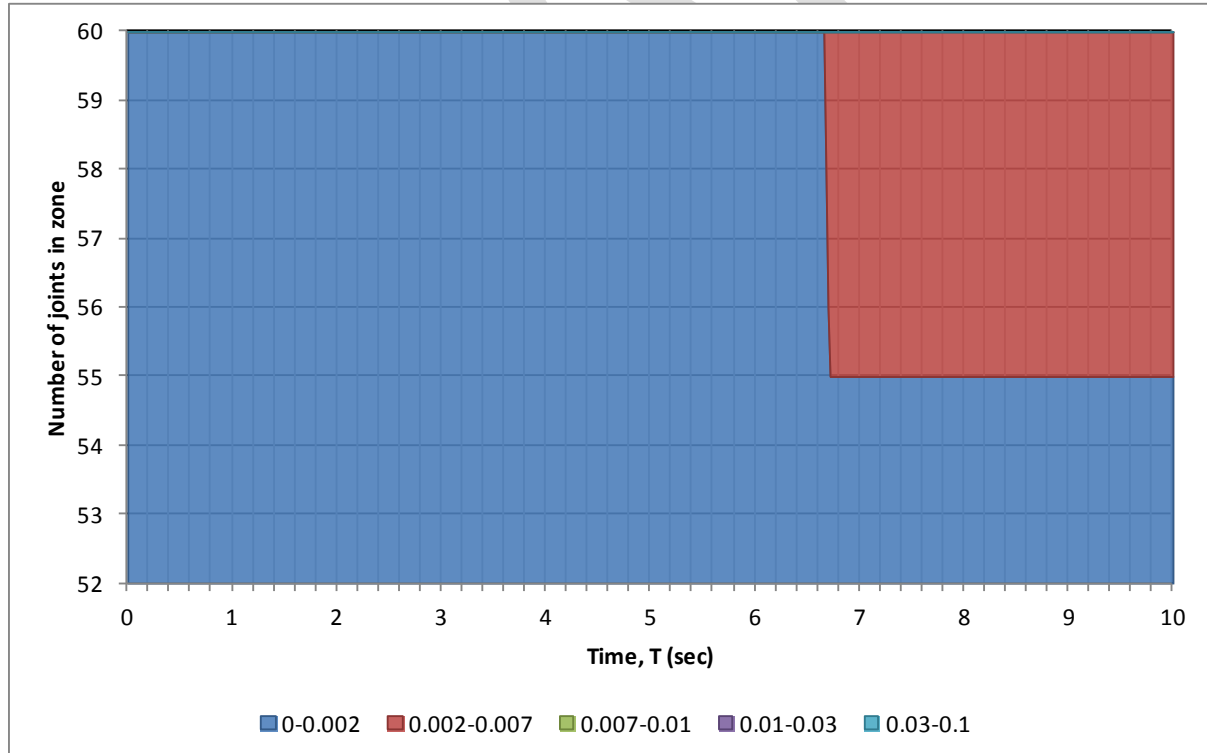


Figure 89: One-way beam-column joint R1 rotations, REHS, Lyttelton.

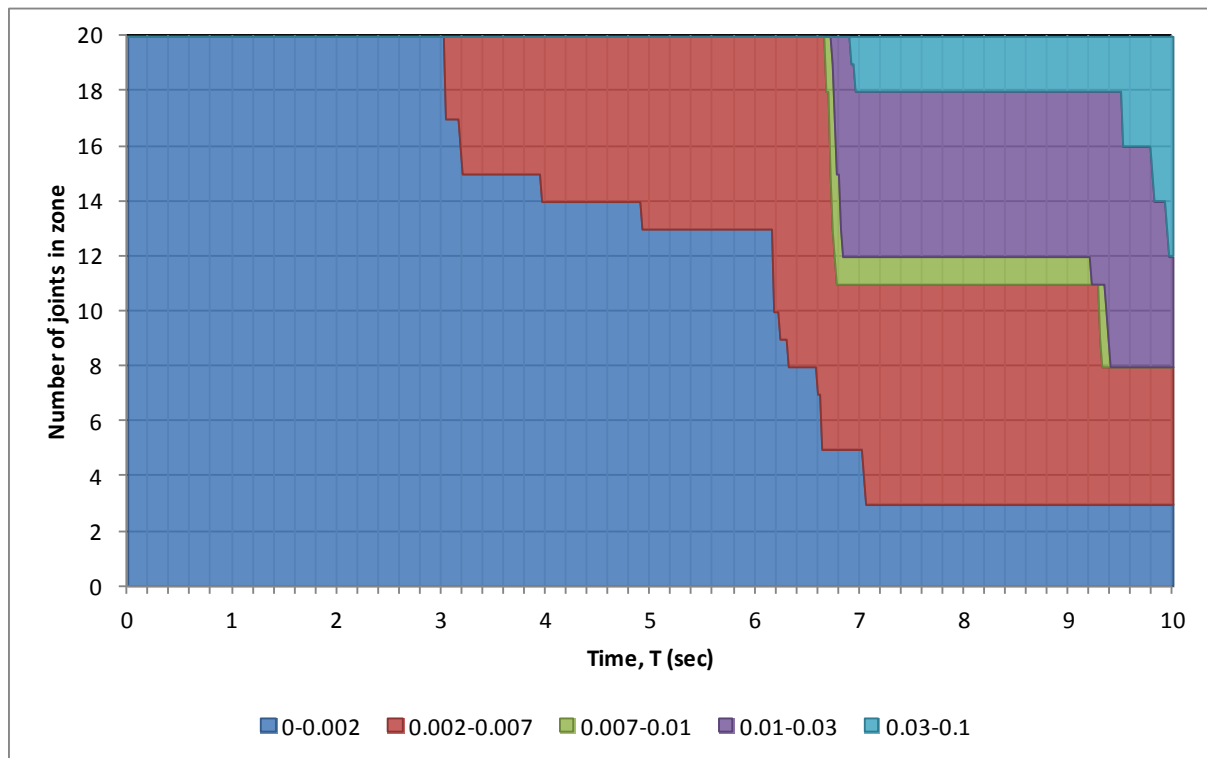


Figure 90: GL A two-way beam-column joint R1 rotations, REHS, Lyttelton.

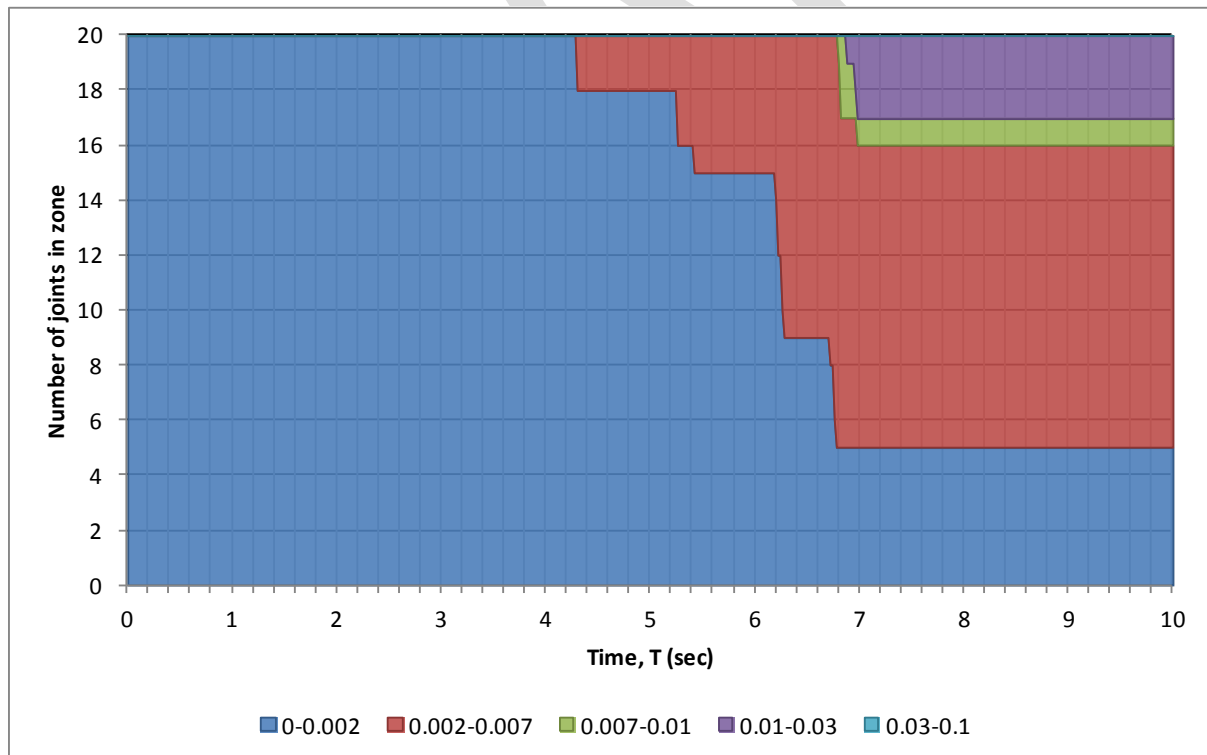


Figure 91: GL F two-way beam-column joint R1 rotations, REHS, Lyttelton.

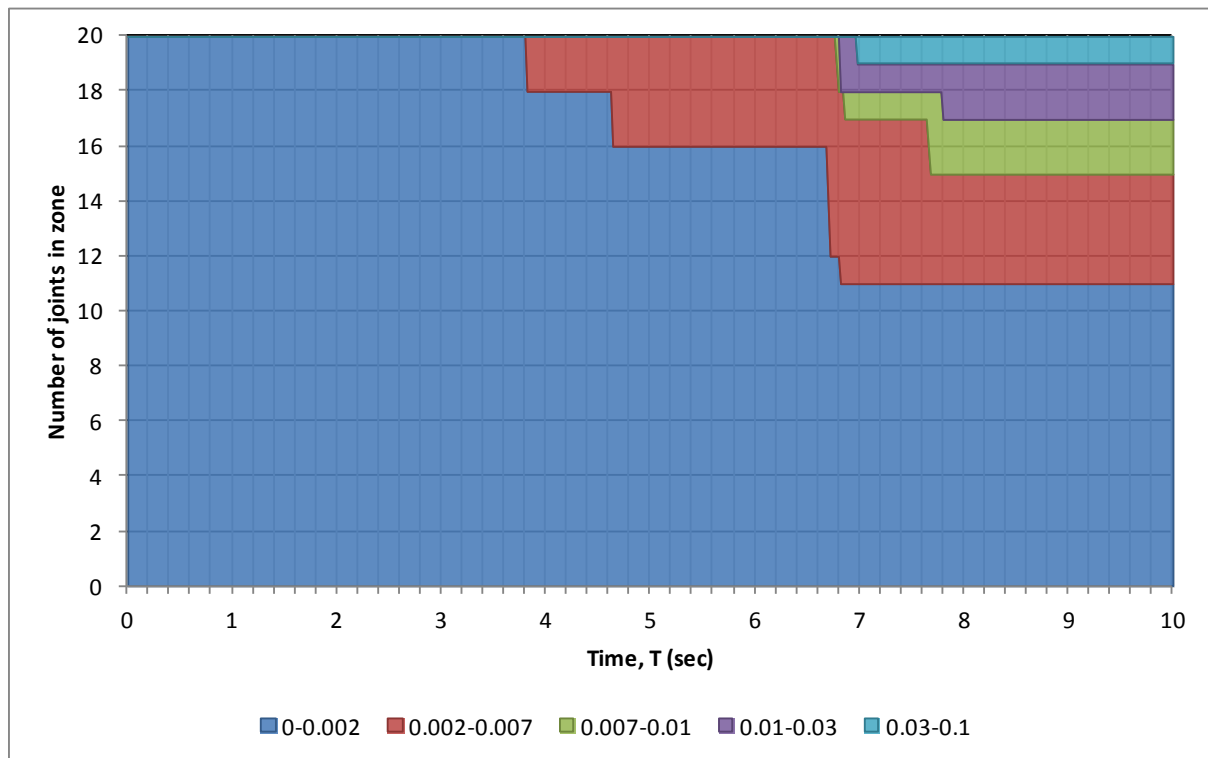


Figure 92: GL A two-way beam-column joint R2 rotations, REHS, Lyttelton.

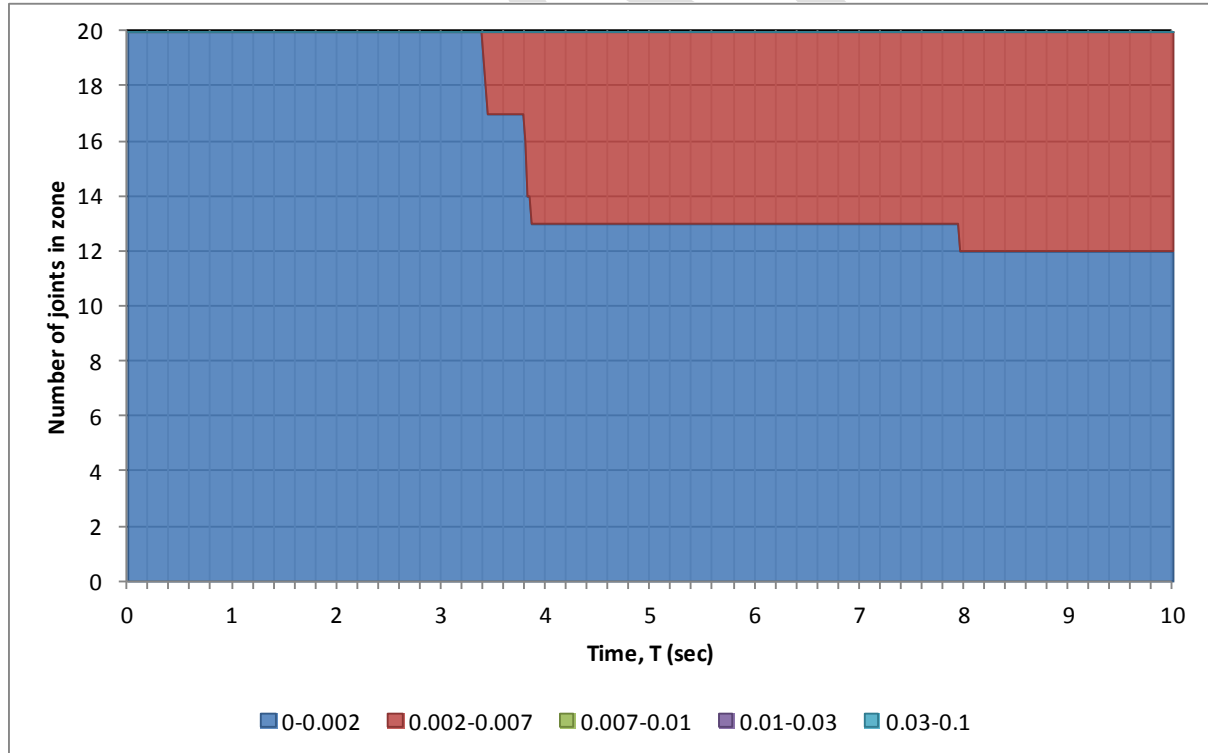


Figure 93: GL F two-way beam-column joint R2 rotations, REHS, Lyttelton.

As can be seen in Figure 89 the interior beam column joints exhibit some minor in-elastic behaviour when subject to the REHS record demands, with up to five joints indicating rotations between 0.002 and 0.007 radians. Figure 90 to Figure 93 indicate that the exterior joints are subject to inelastic demand with strength degradation occurring in up to 11 joints after 6.7 seconds. It should be noted that degradation in the joint strength only occurs after column hinges are predicted to have their ultimate concrete strain exceeded.

Results show that the interior joints behaved elastically in the CBGS, CCCC, and CHHC records. The REHS record produced some minor inelastic behaviour in the joints towards the end of significant shaking. The results indicate that the interior beam-column joint strengths were not reached for all records.

Exterior beam-column joints were subject to inelastic demand for all records.

Figure 94 to Figure 125 present the beam column joint hysteretic form and rotations for the joints with the largest rotation about R1 and R2 axes on gridlines A and F, for each ground motion record. Figure 126 and Figure 127 present the beam column joint hysteretic form and rotations for the one way joint with the largest inelastic behaviour for the REHS record.

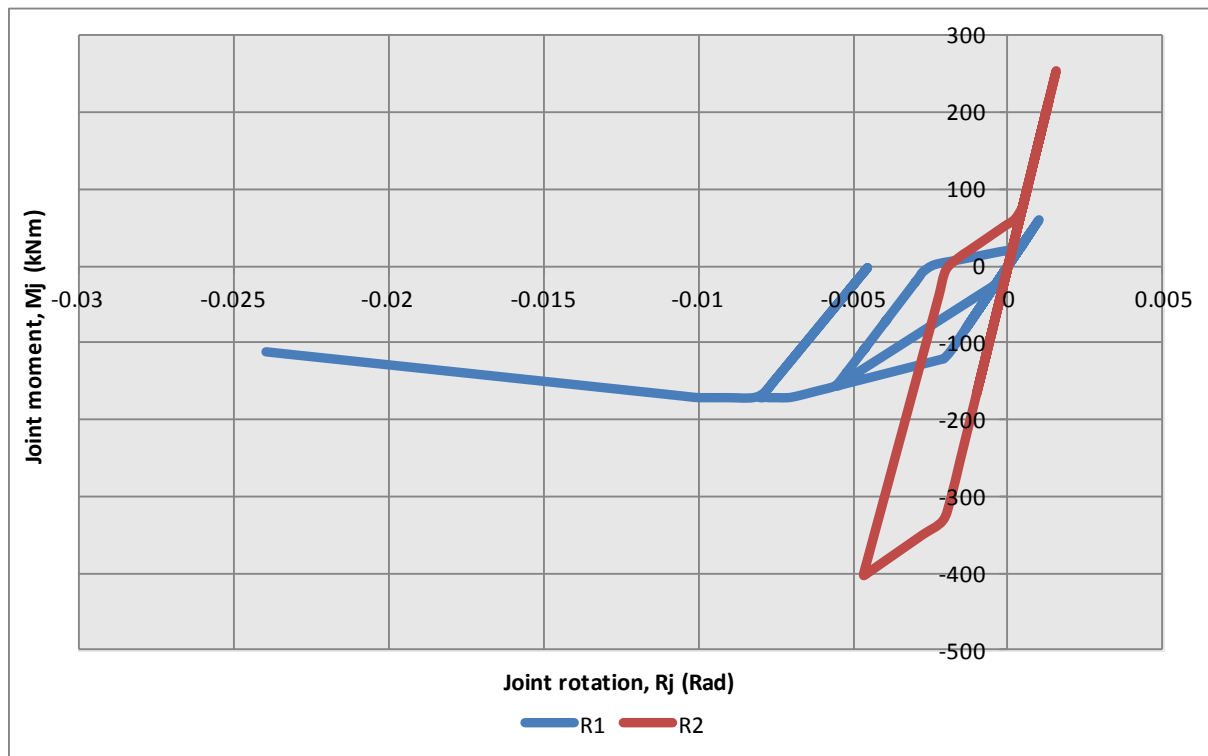


Figure 94: Max GL A BCJ R1 rotations: Column A2 level 2 hysteretic behaviour - CBUGS, Lyttelton

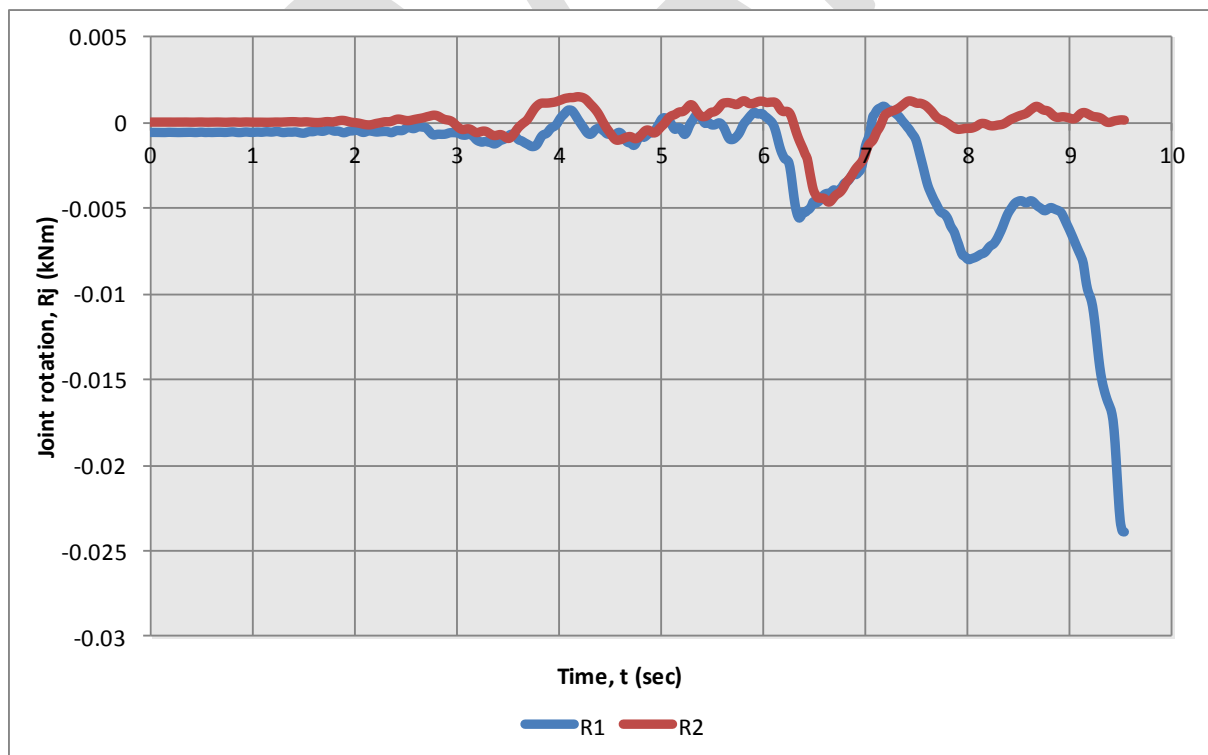


Figure 95: Max GL A BCJ R1 rotations: Column A2 level 2 rotations vs time - CBUGS, Lyttelton

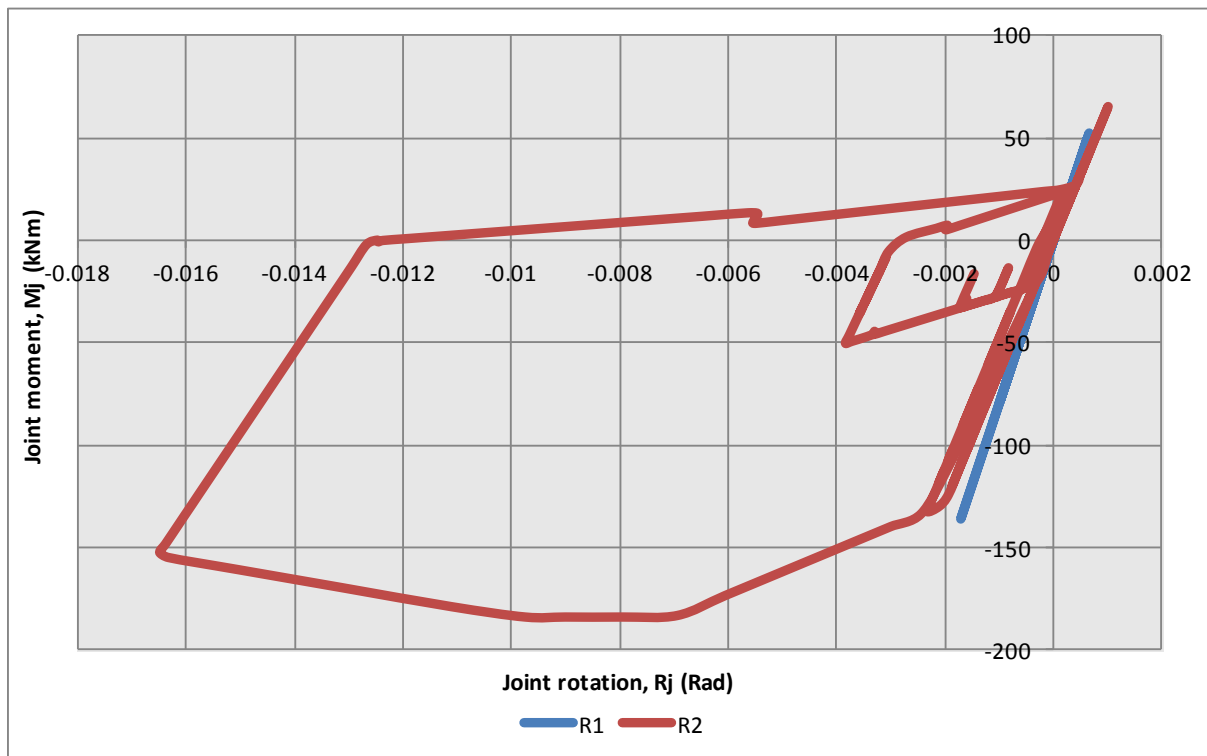


Figure 96: Max GL A BCJ R2 rotations: Column A4 level 3 hysteretic behaviour - CBUGS, Lyttelton

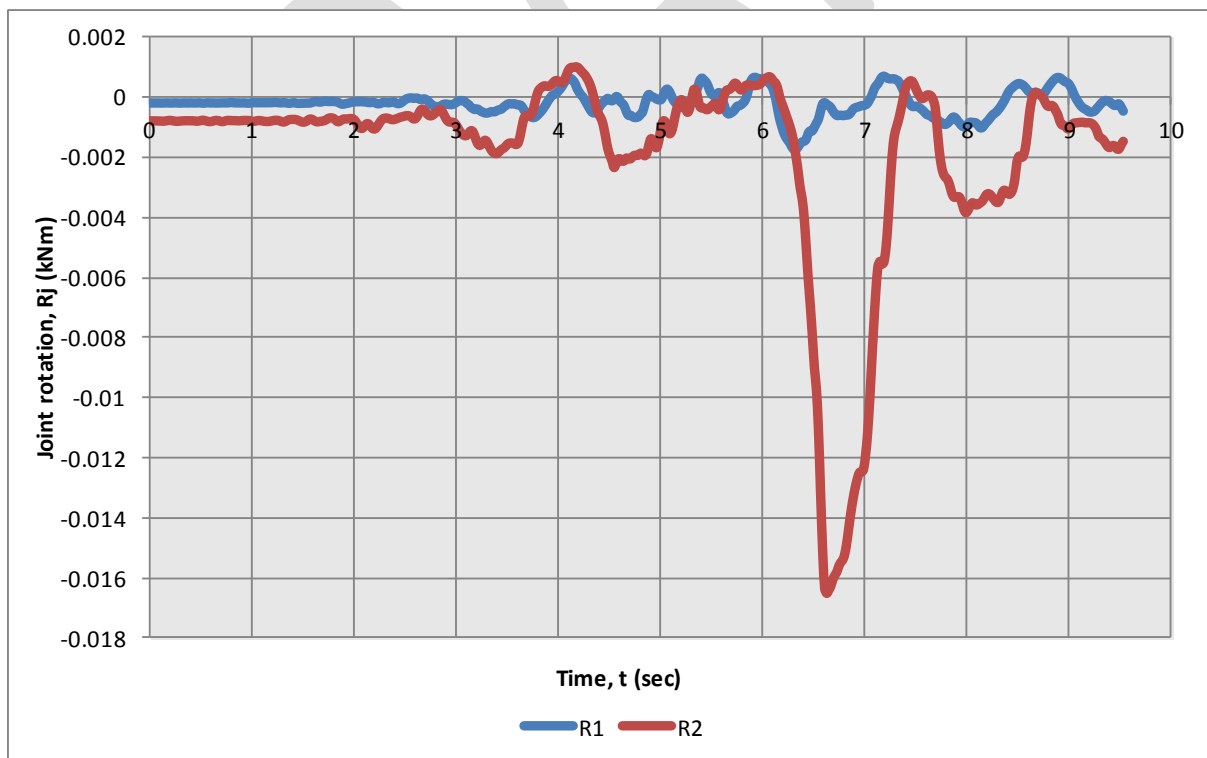


Figure 97: Max GL A BCJ R2 rotations: Column A4 level 3 rotations vs time - CBUGS, Lyttelton

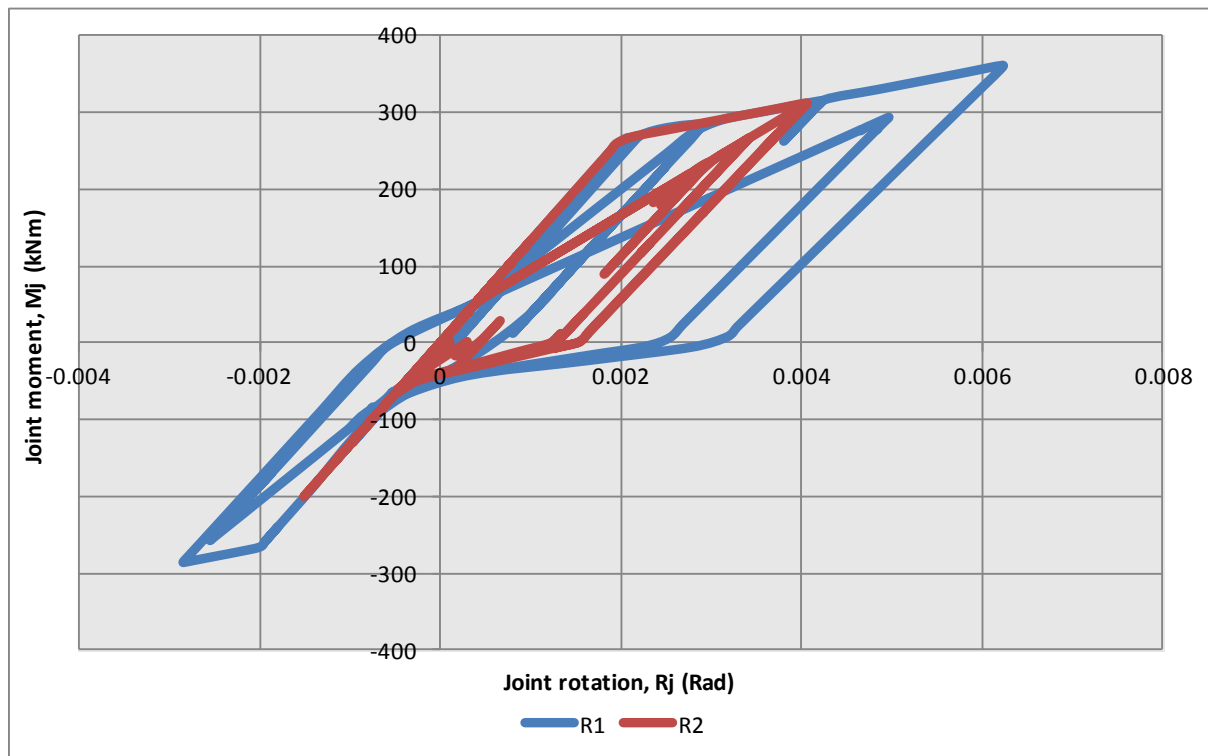


Figure 98: Max GL F BCJ R1 rotations: Column F1 level 5 hysteretic behaviour - CBUGS, Lyttelton

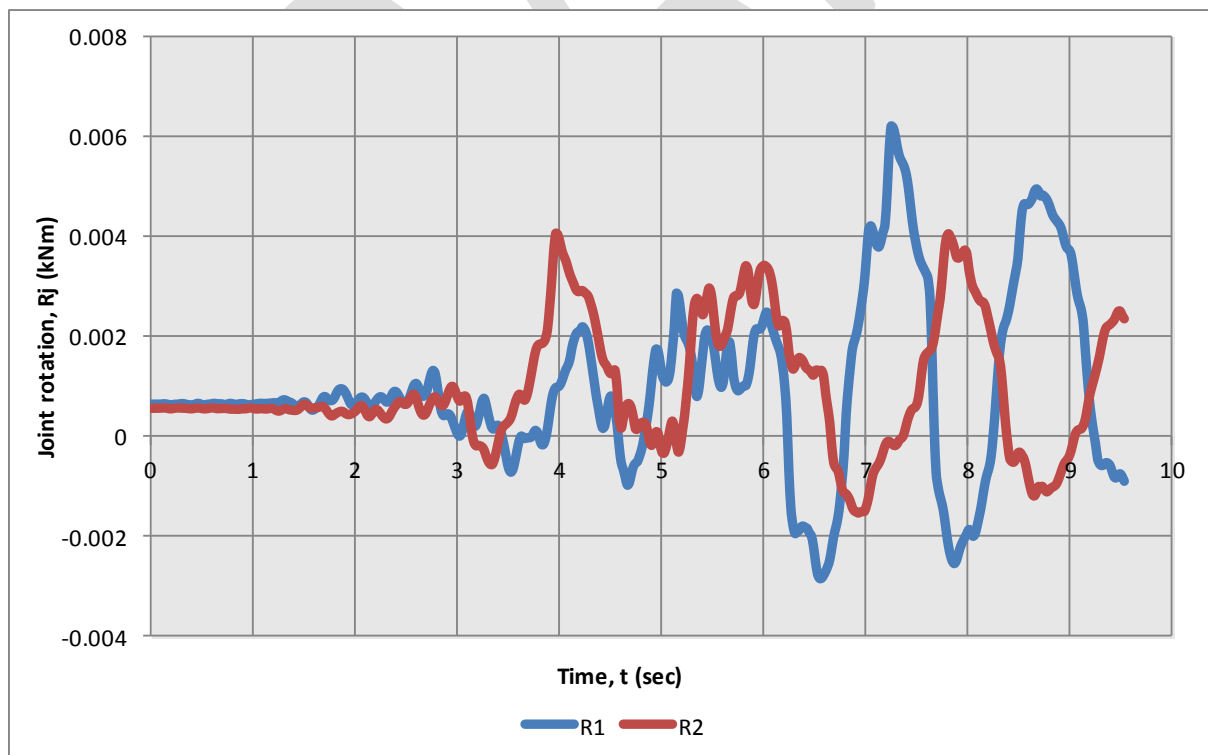


Figure 99: Max GL F BCJ R1 rotations: Column F1 level 5 rotations vs time - CBUGS, Lyttelton

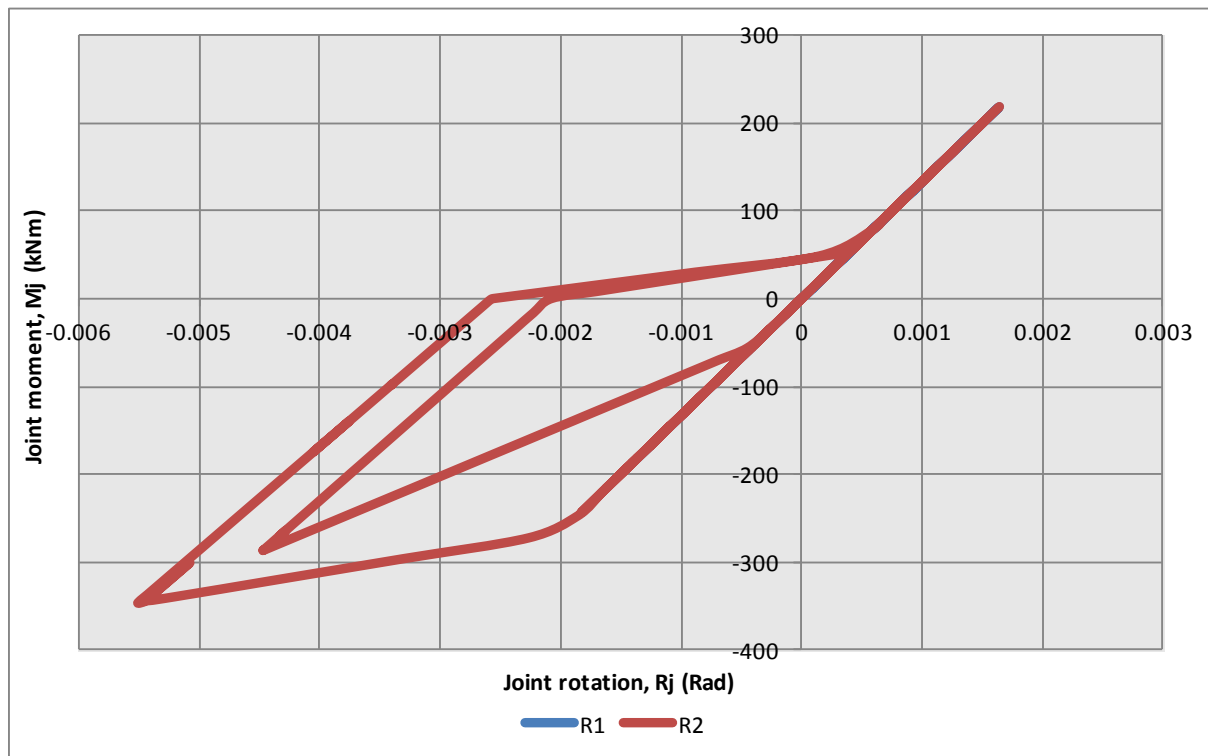


Figure 100: Max GL F BCJ R2 rotations: Column F1 level 5 hysteretic behaviour - CBUGS, Lyttelton

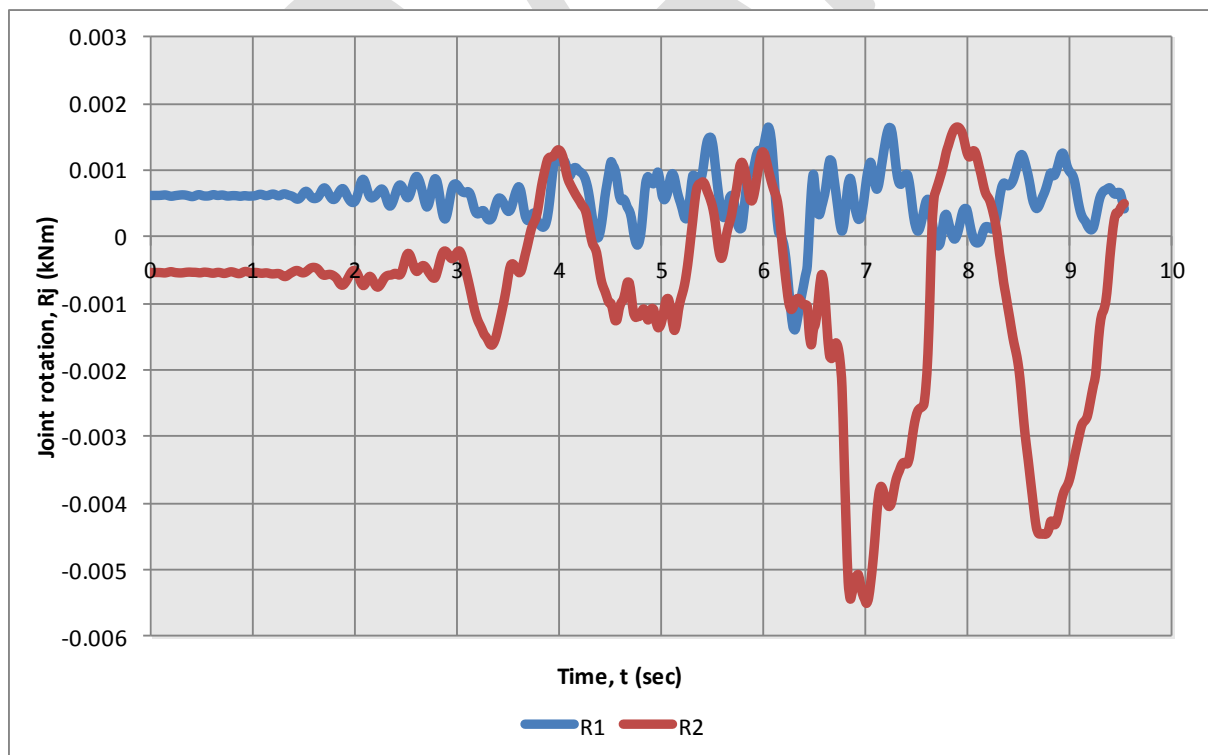


Figure 101: Max GL F BCJ R2 rotations: Column F1 level 5 rotations vs time - CBUGS, Lyttelton

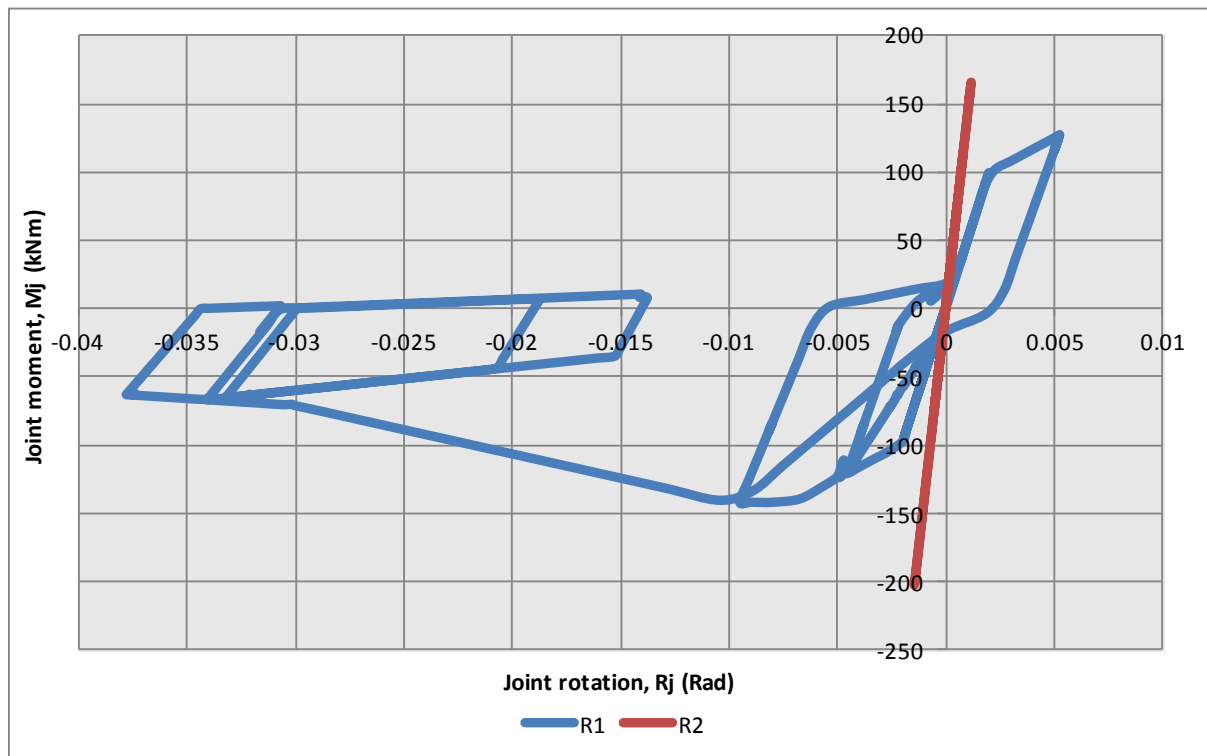


Figure 102: Max GL A BCJ R1 rotations: Column A2 level 4 hysteretic behaviour - CCCC, Lyttelton

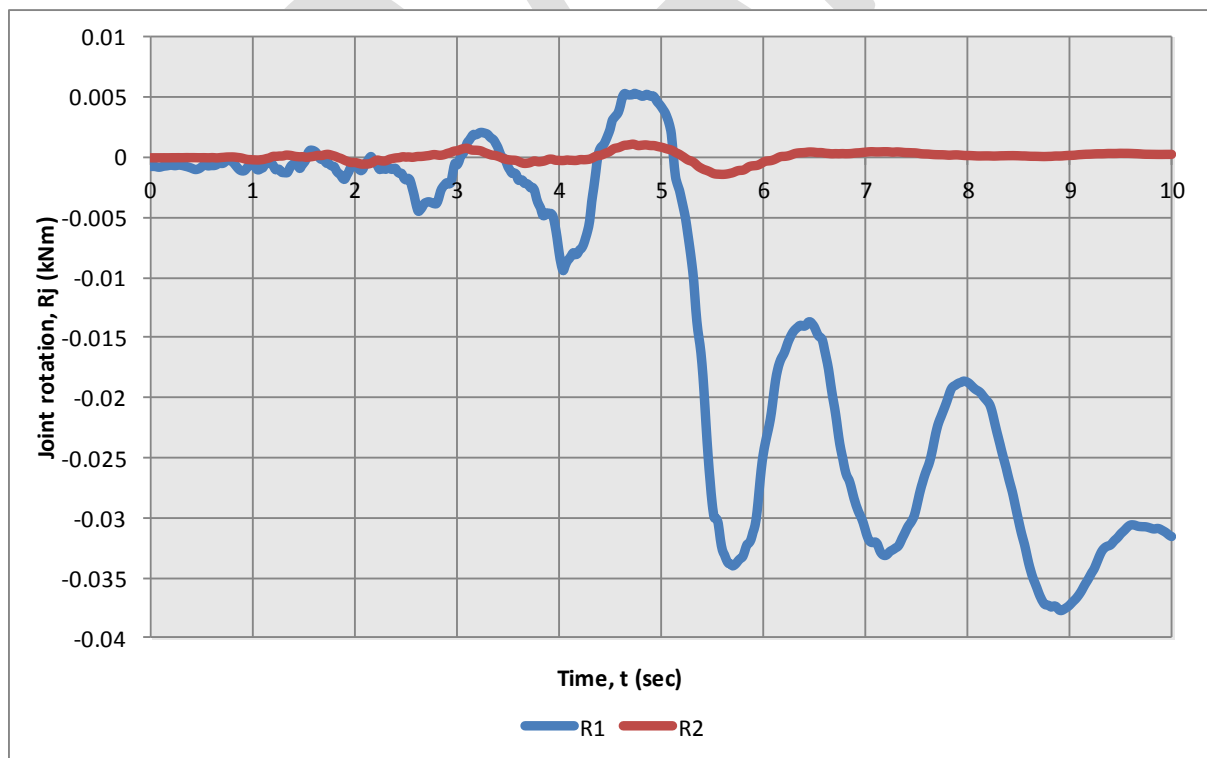


Figure 103: Max GL A BCJ R1 rotations: Column A2 level 4 rotations vs time - CCCC, Lyttelton

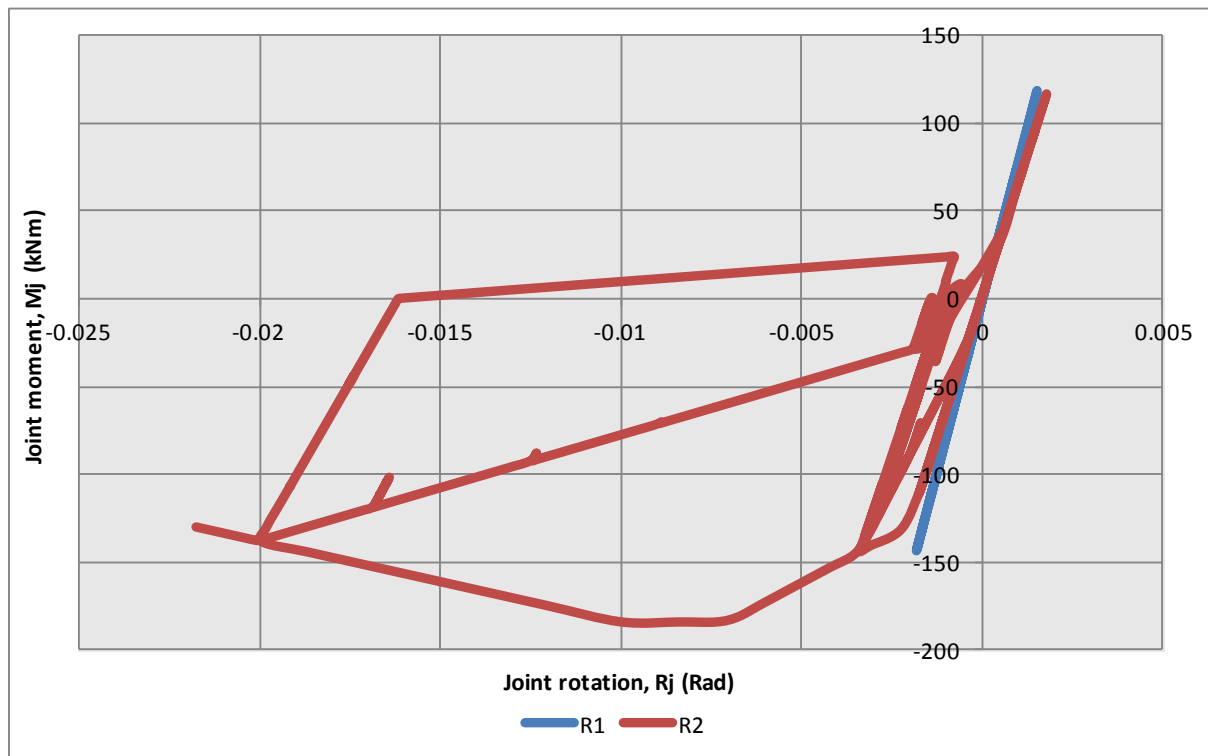


Figure 104: Max GL A BCJ R2 rotations: Column A4 level 3 hysteretic behaviour - CCCC, Lyttelton

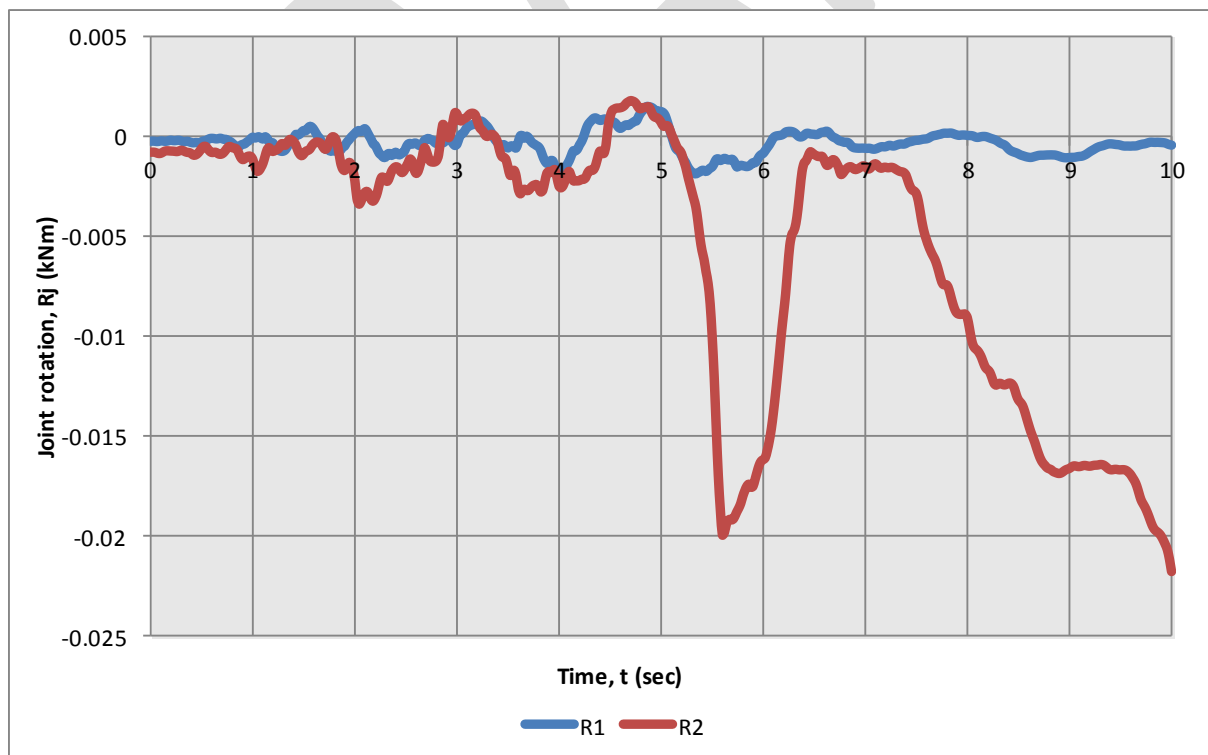


Figure 105: Max GL A BCJ R2 rotations: Column A4 level 3 rotations vs time - CCCC, Lyttelton

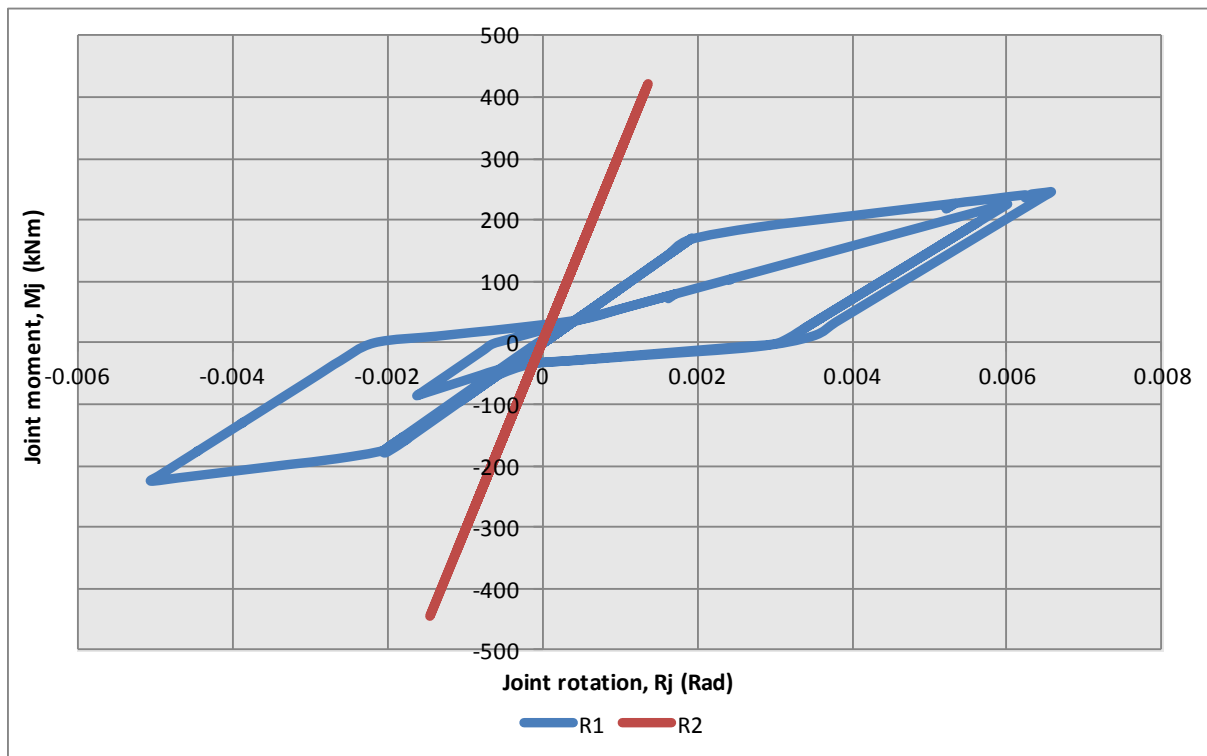


Figure 106: Max GL F BCJ R1 rotations: Column F2 level 5 hysteretic behaviour - CCCC, Lyttelton

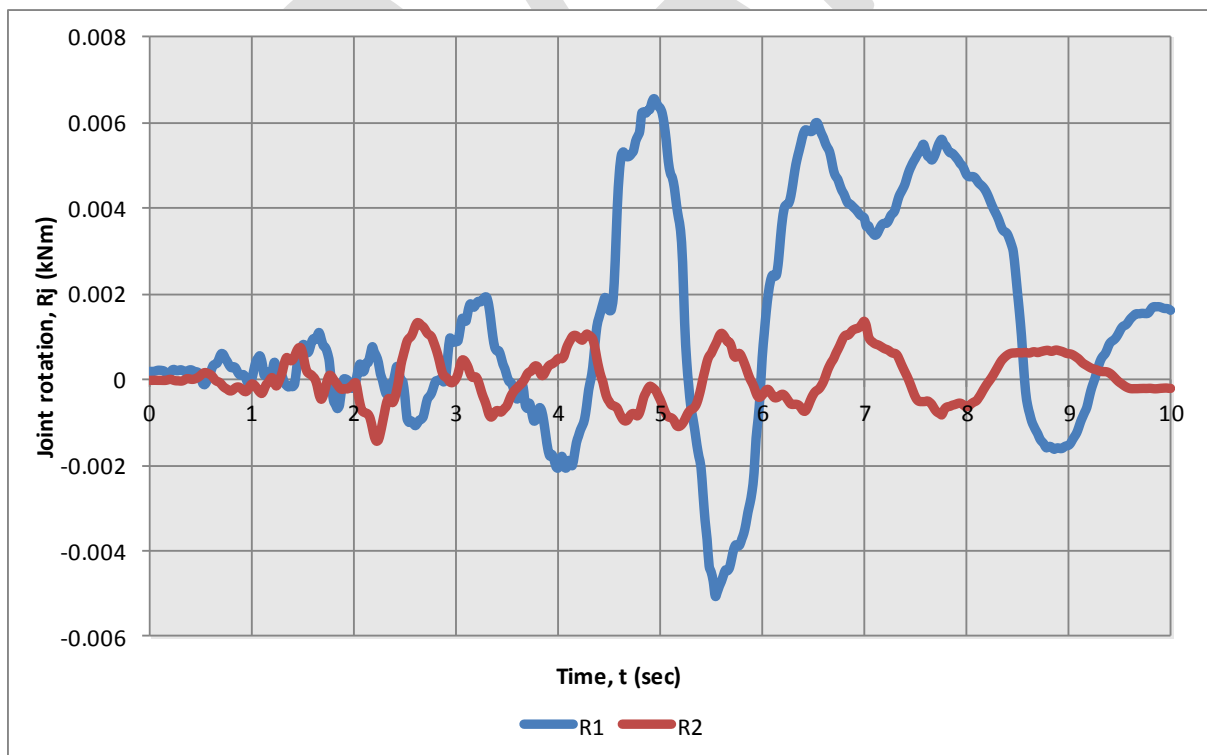


Figure 107: Max GL F BCJ R1 rotations: Column F2 level 5 rotations vs time - CCCC, Lyttelton

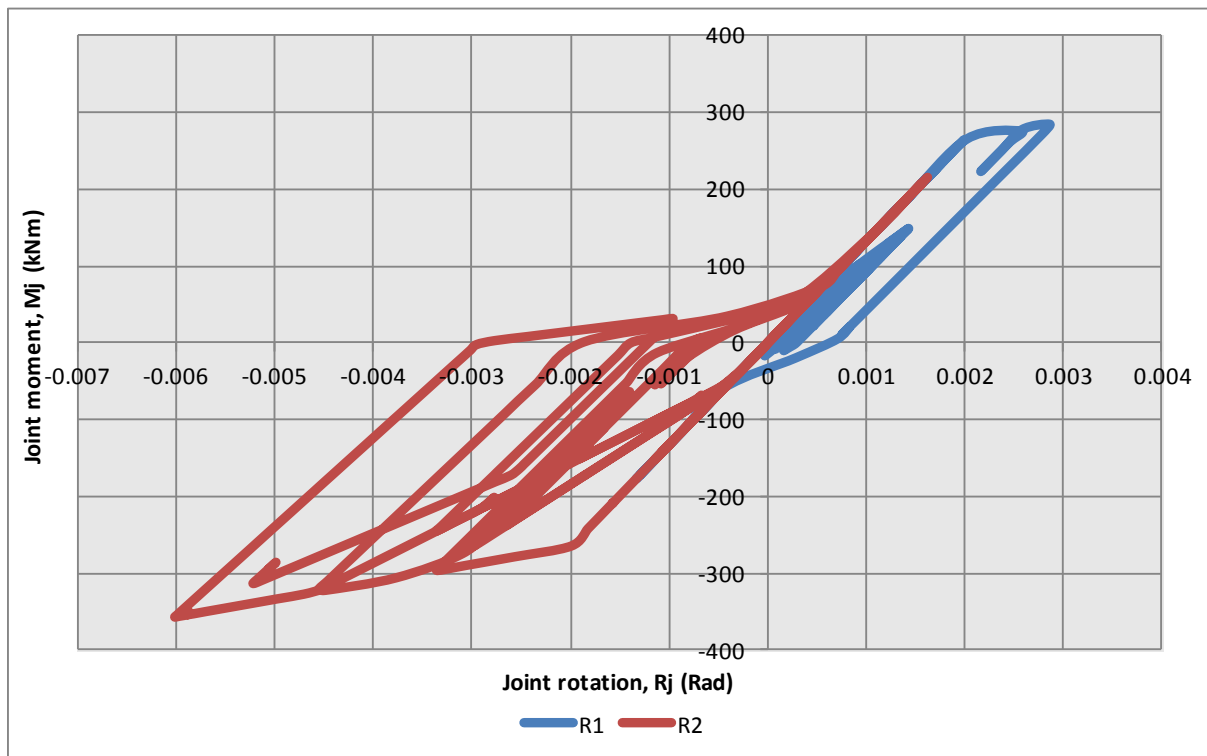


Figure 108: Max GL F BCJ R2 rotations: Column F1 level 5 hysteretic behaviour - CCCC, Lyttelton

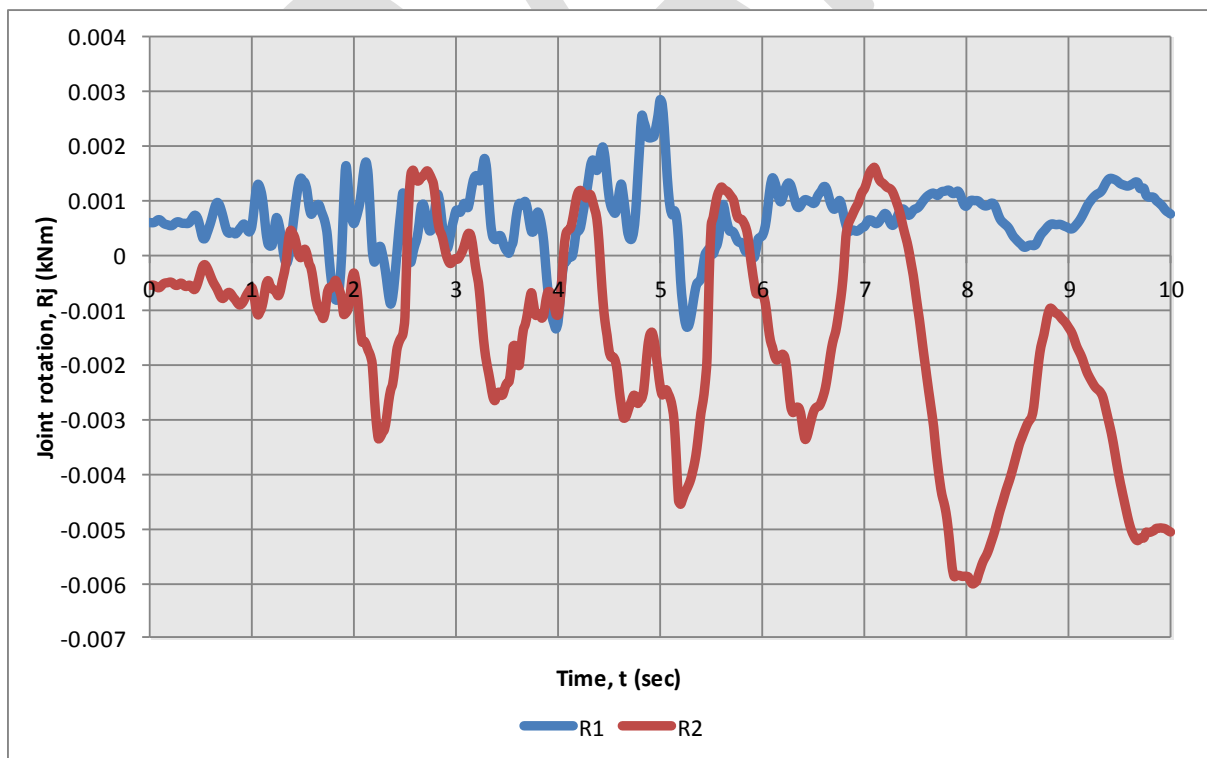


Figure 109: Max GL F BCJ R2 rotations: Column F1 level 5 rotations vs time - CCCC, Lyttelton

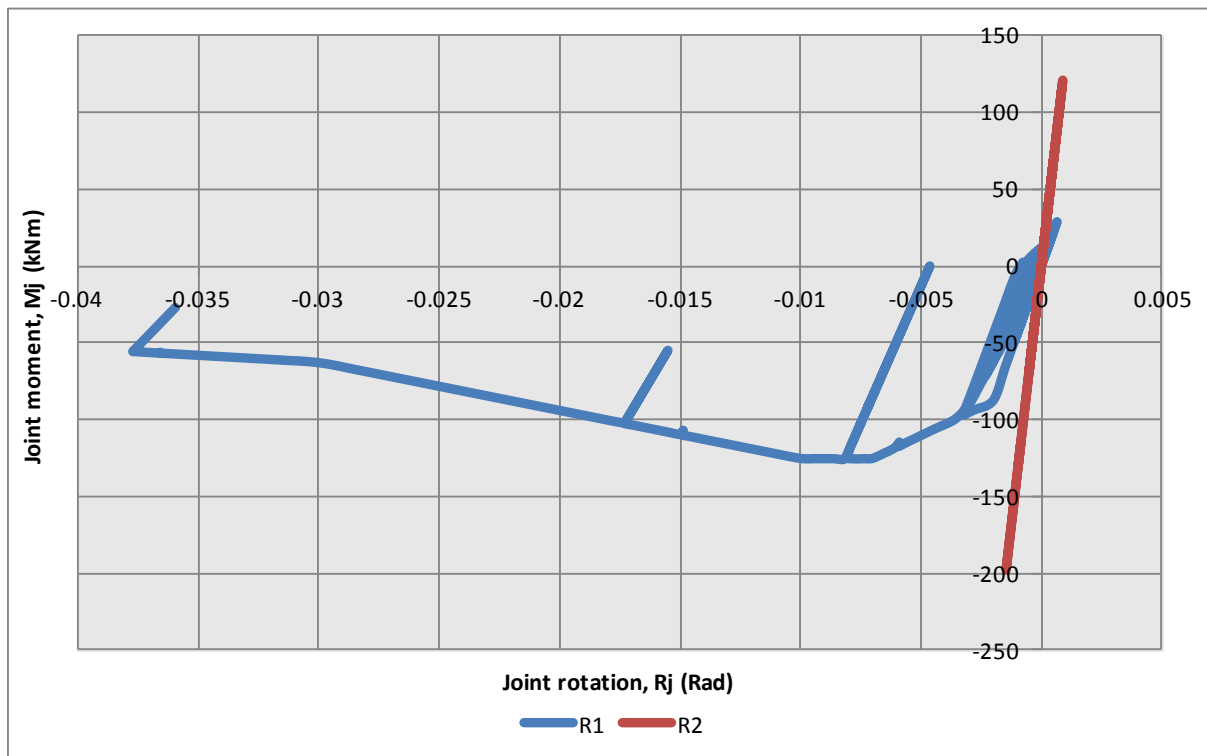


Figure 110: Max GL A BCJ R1 rotations: Column A2 level 5 hysteretic behaviour - CHHC, Lyttelton

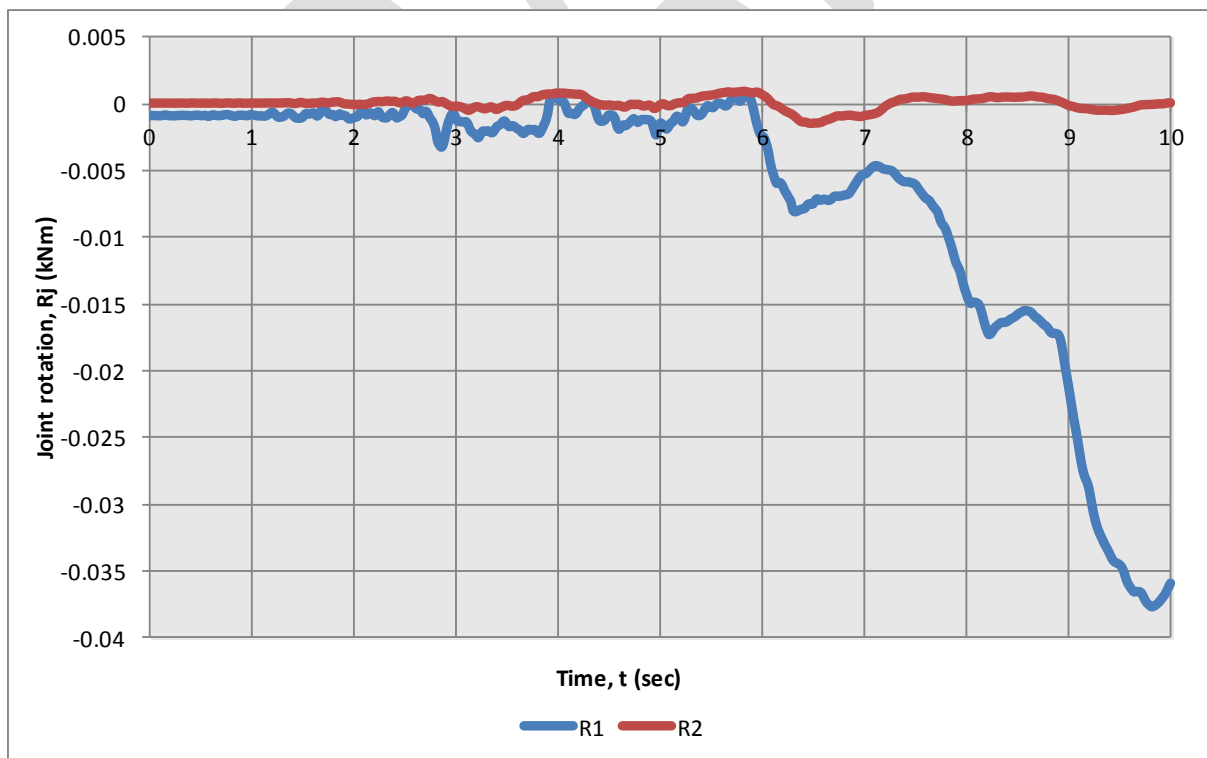


Figure 111: Max GL A BCJ R1 rotations: Column A2 level 5 rotations vs time - CHHC, Lyttelton

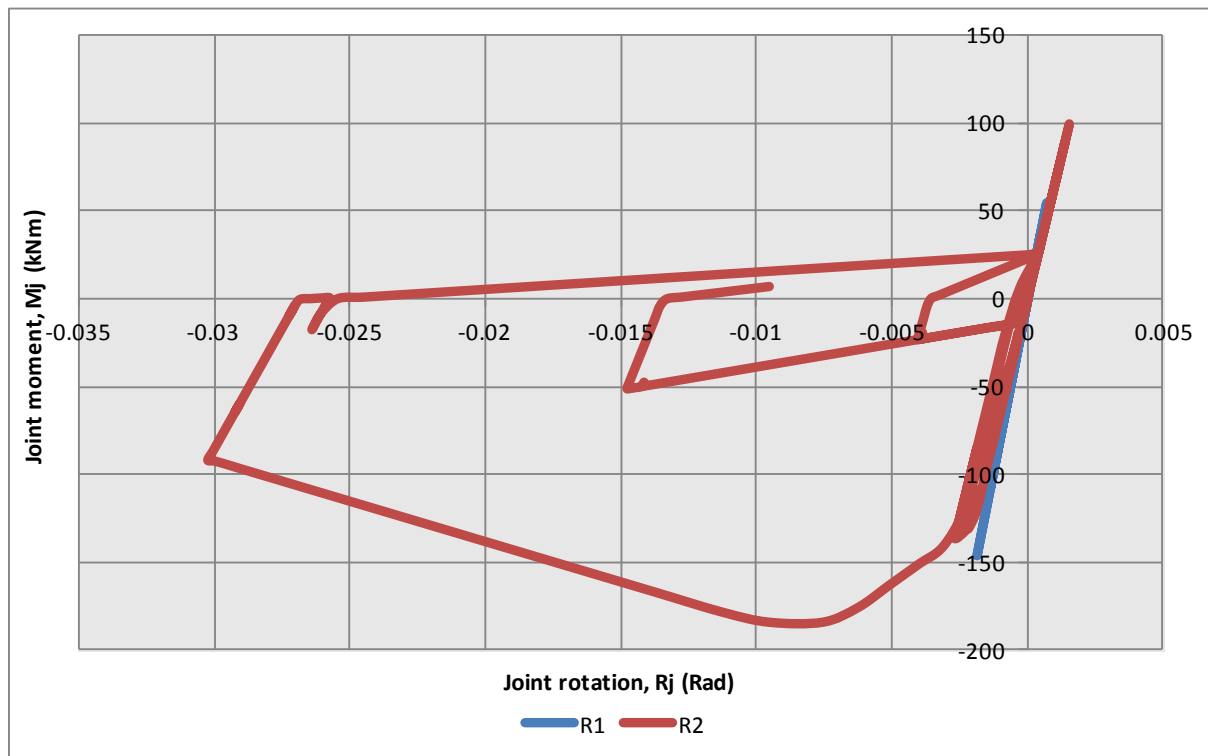


Figure 112: Max GL A BCJ R2 rotations: Column A4 level 3 hysteretic behaviour - CHHC, Lyttelton

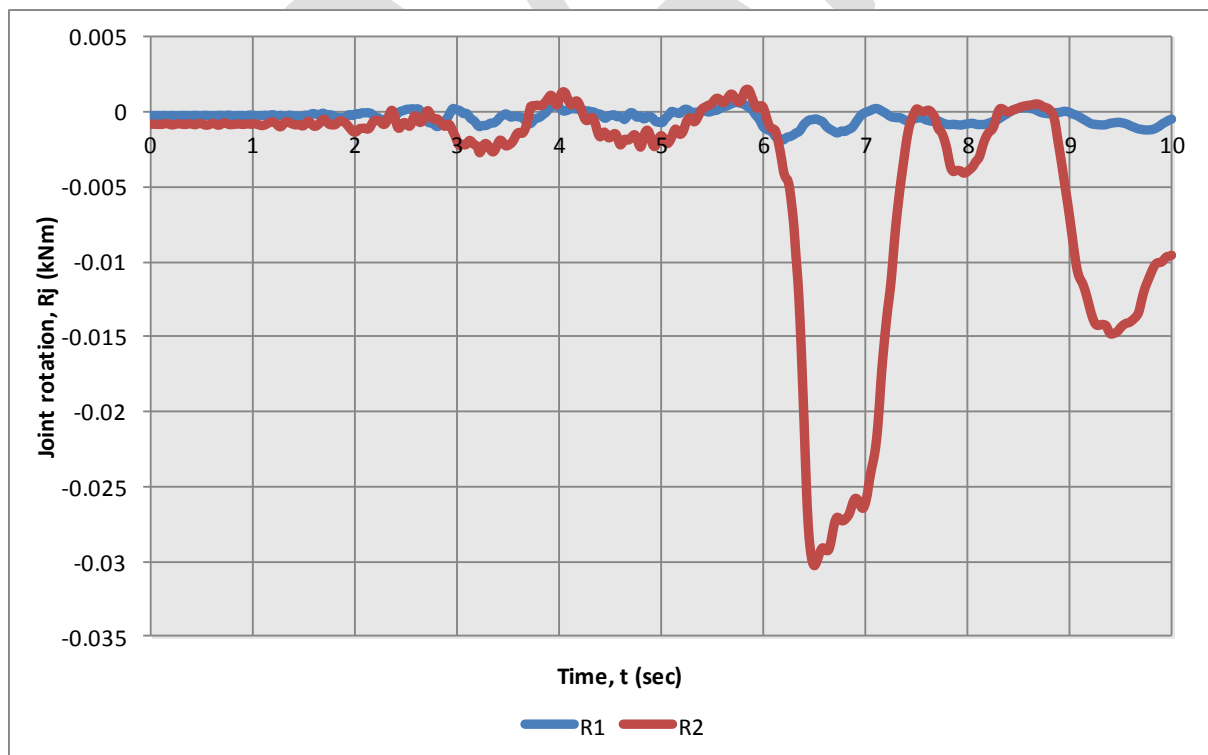


Figure 113: Max GL A BCJ R2 rotations: Column A4 level 3 rotations vs time - CHHC, Lyttelton

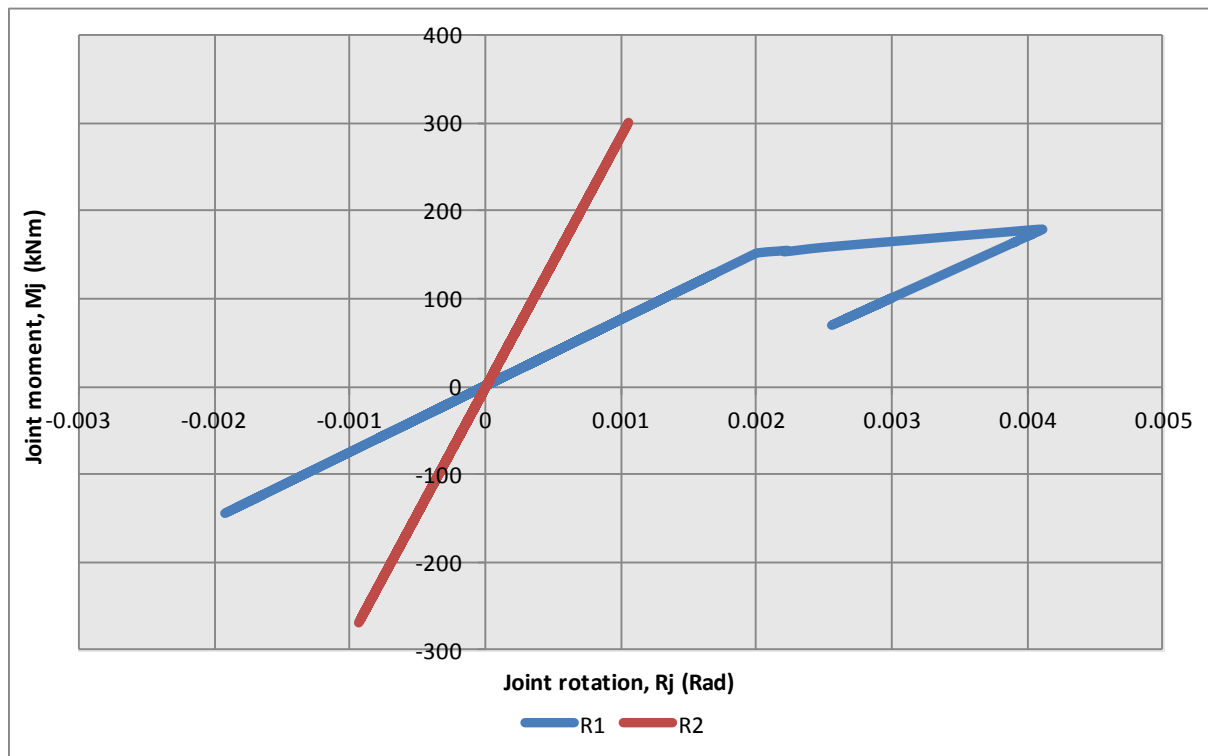


Figure 114: Max GL F BCJ R1 rotations: Column F2 level 6 hysteretic behaviour - CHHC, Lyttelton

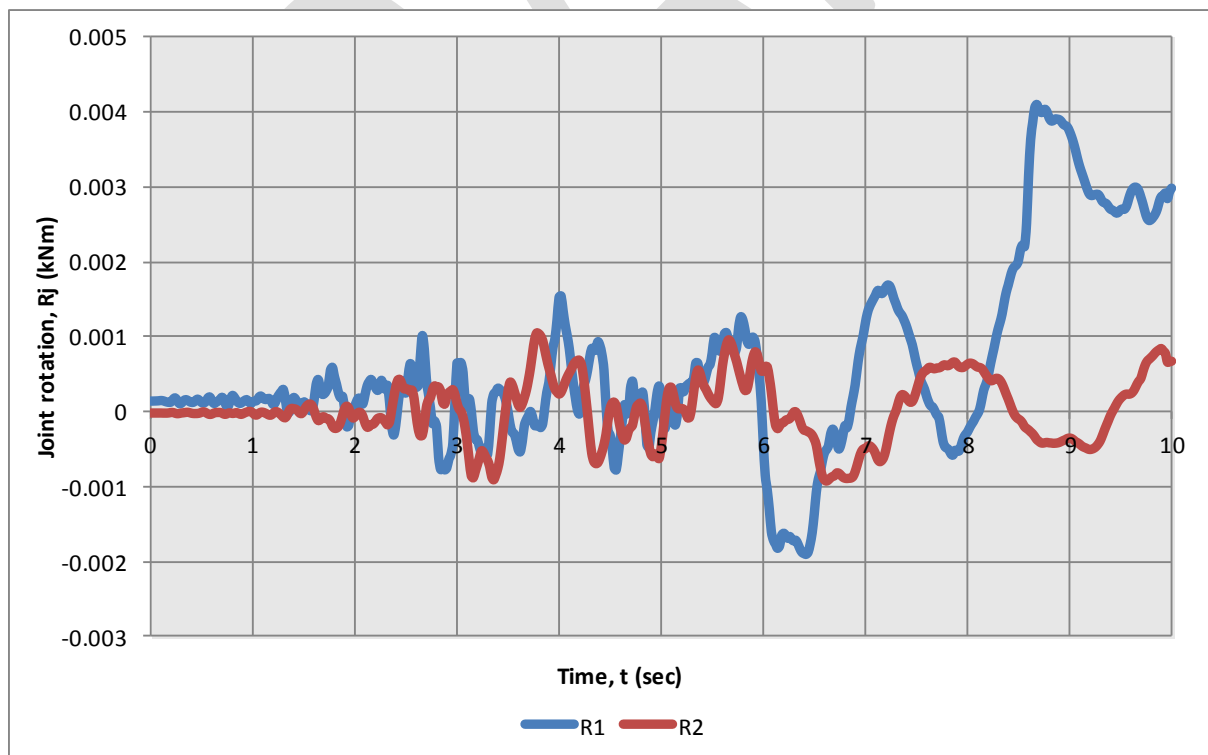


Figure 115: Max GL F BCJ R1 rotations: Column F2 level 6 rotations vs time - CHHC, Lyttelton

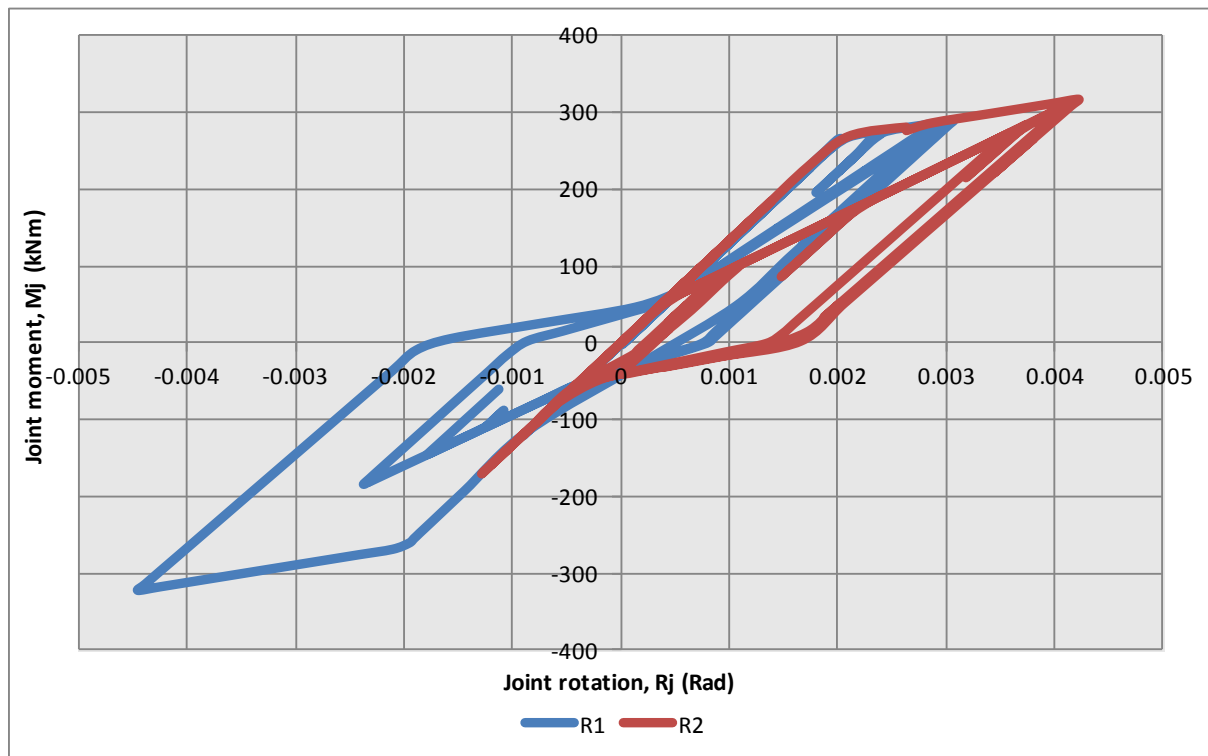


Figure 116: Max GL F BCJ R2 rotations: Column F1 level 5 hysteretic behaviour - CHHC, Lyttelton

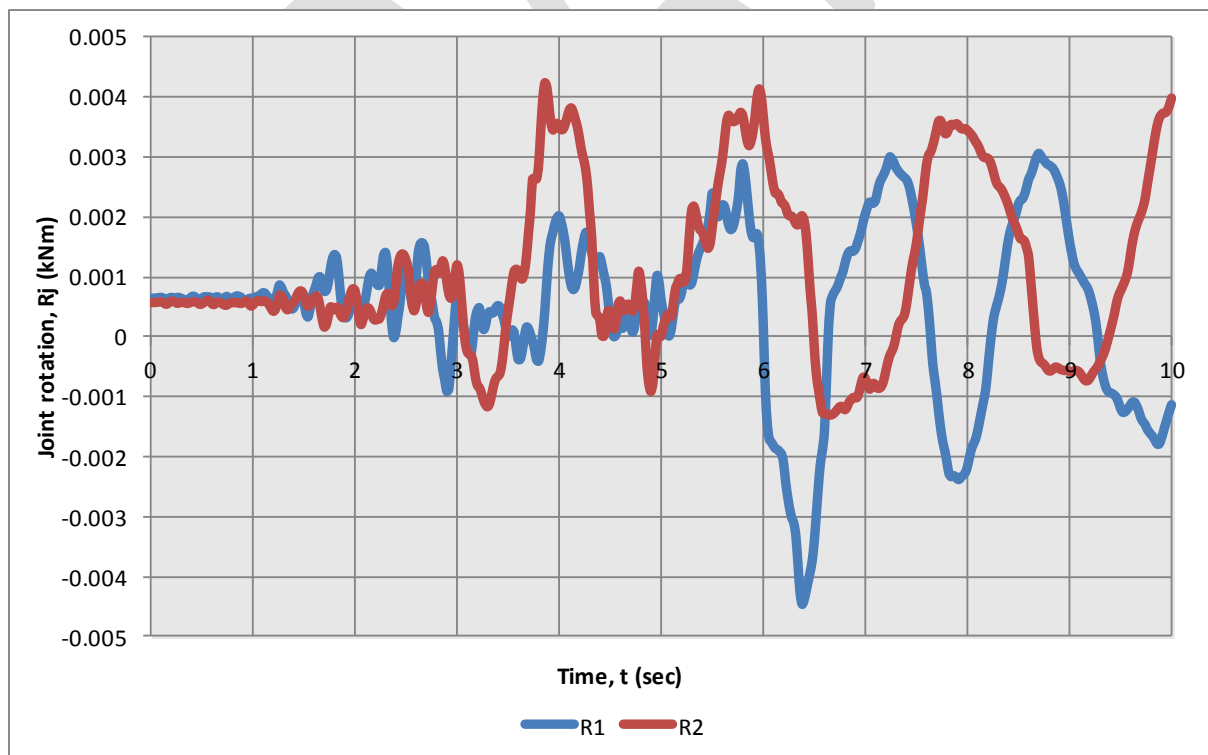


Figure 117: Max GL F BCJ R2 rotations: Column F1 level 5 rotations vs time - CHHC, Lyttelton

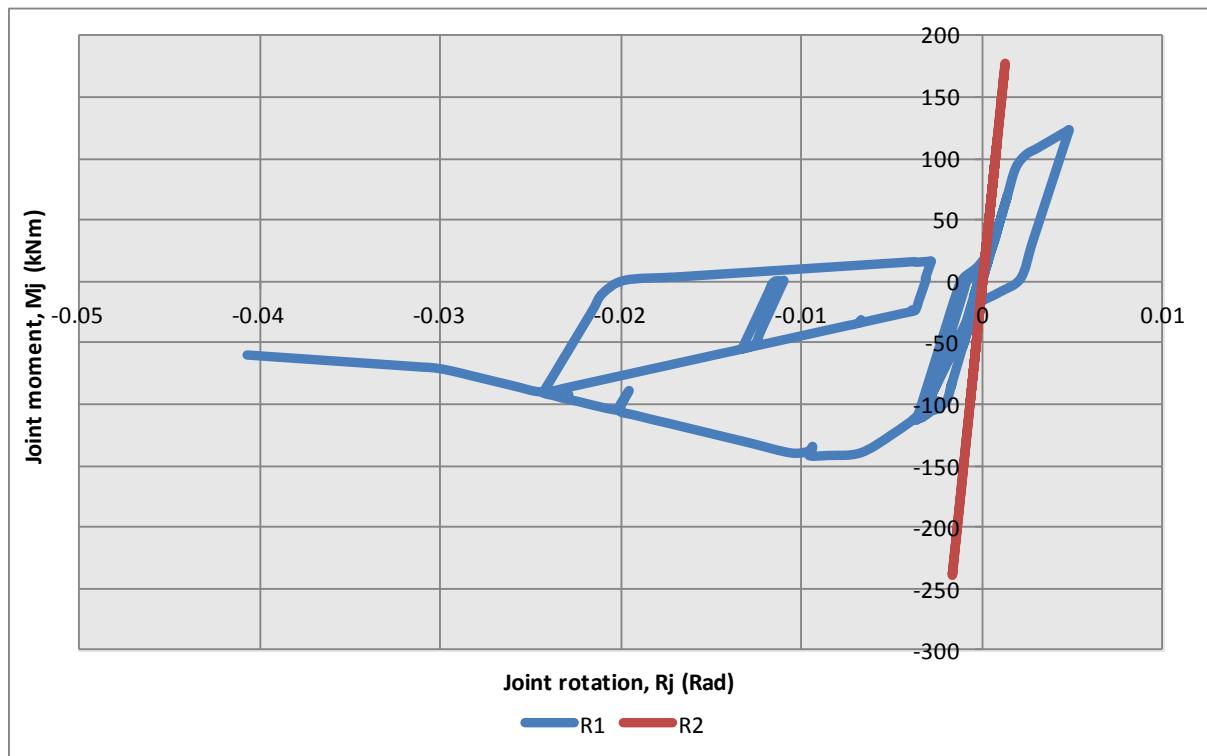


Figure 118: Max GL A BCJ R1 rotations: Column A2 level 4 hysteretic behaviour - REHS, Lyttelton

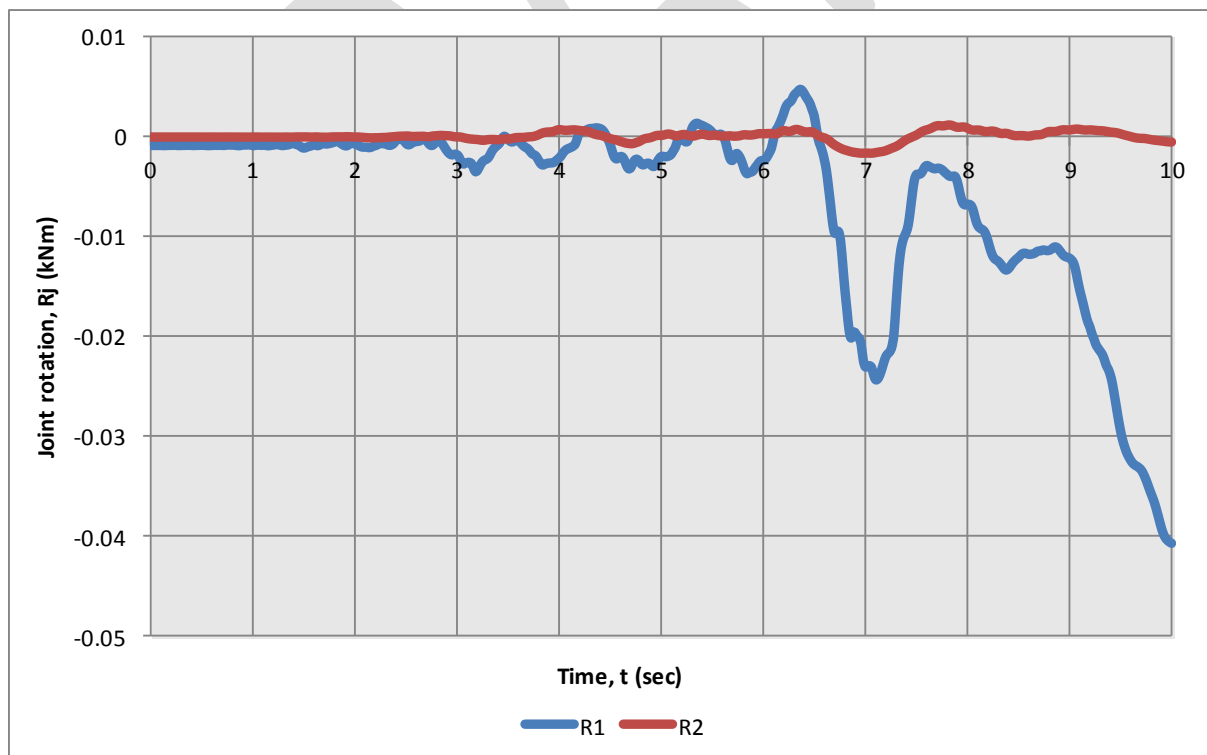


Figure 119: Max GL A BCJ R1 rotations: Column A2 level 4 rotations vs time - REHS, Lyttelton

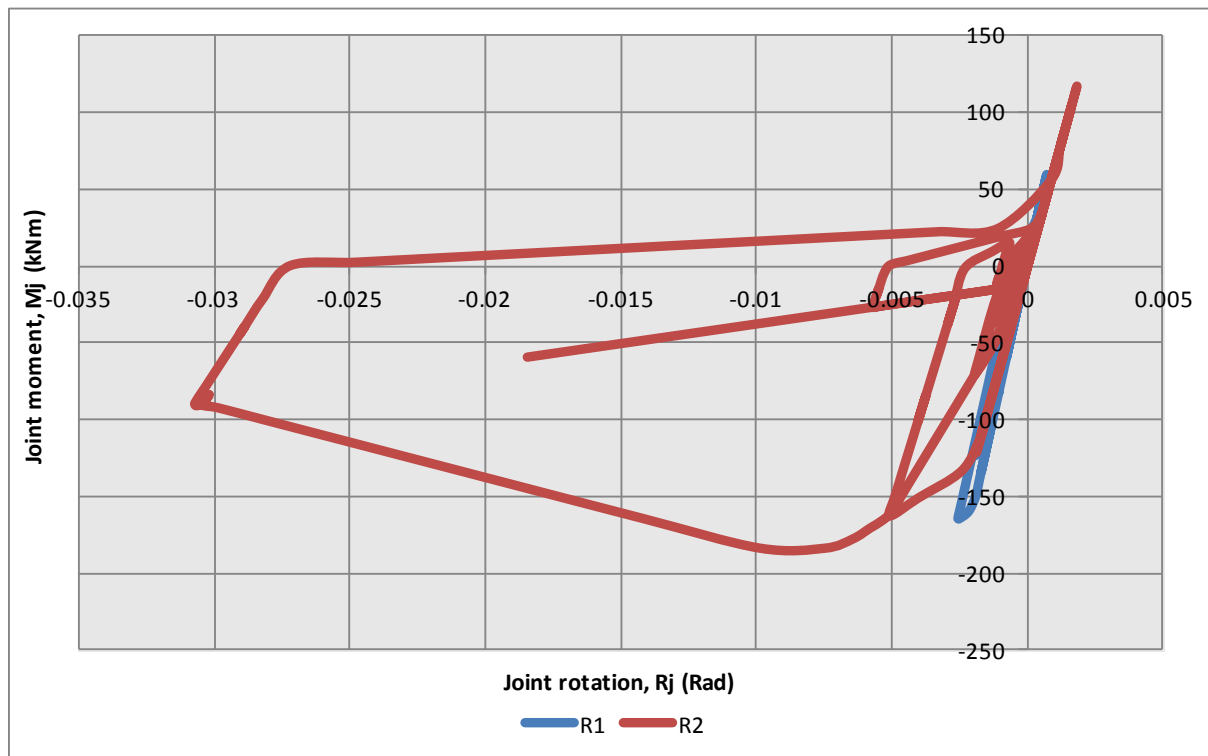


Figure 120: Max GL A BCJ R2 rotations: Column A4 level 3 hysteretic behaviour - REHS, Lyttelton

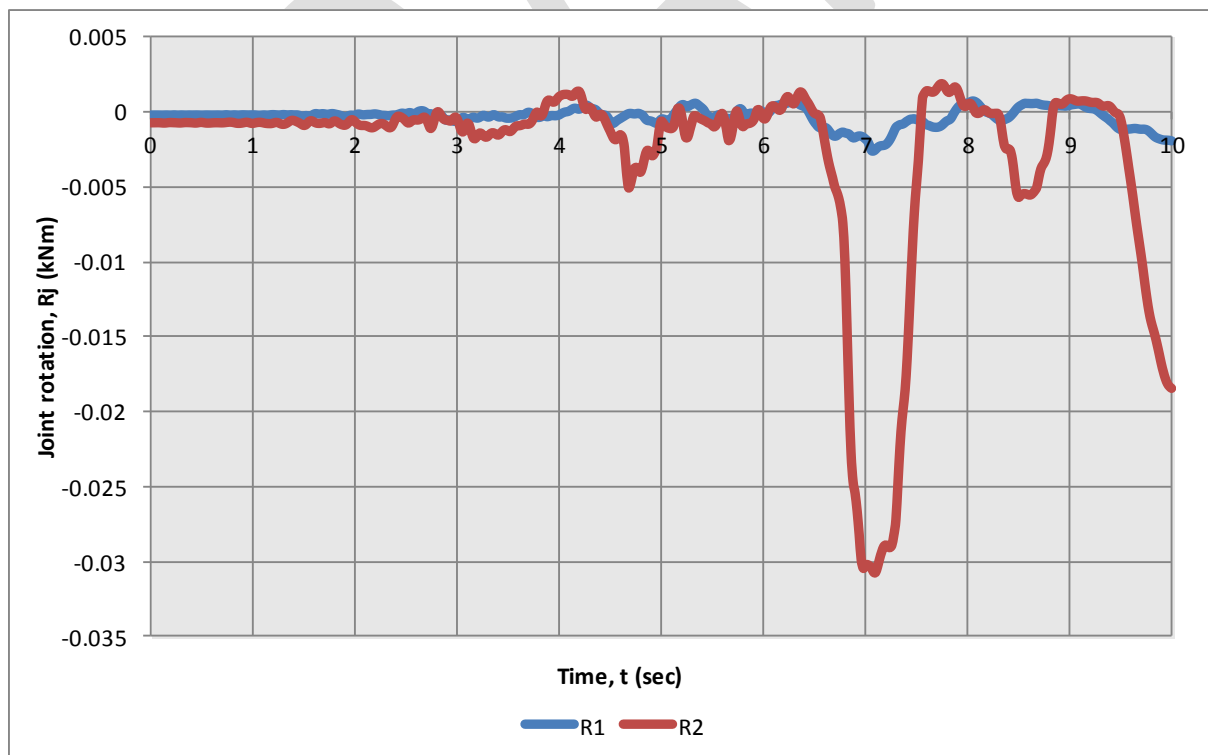


Figure 121: Max GL A BCJ R2 rotations: Column A4 level 3 rotations vs time - REHS, Lyttelton

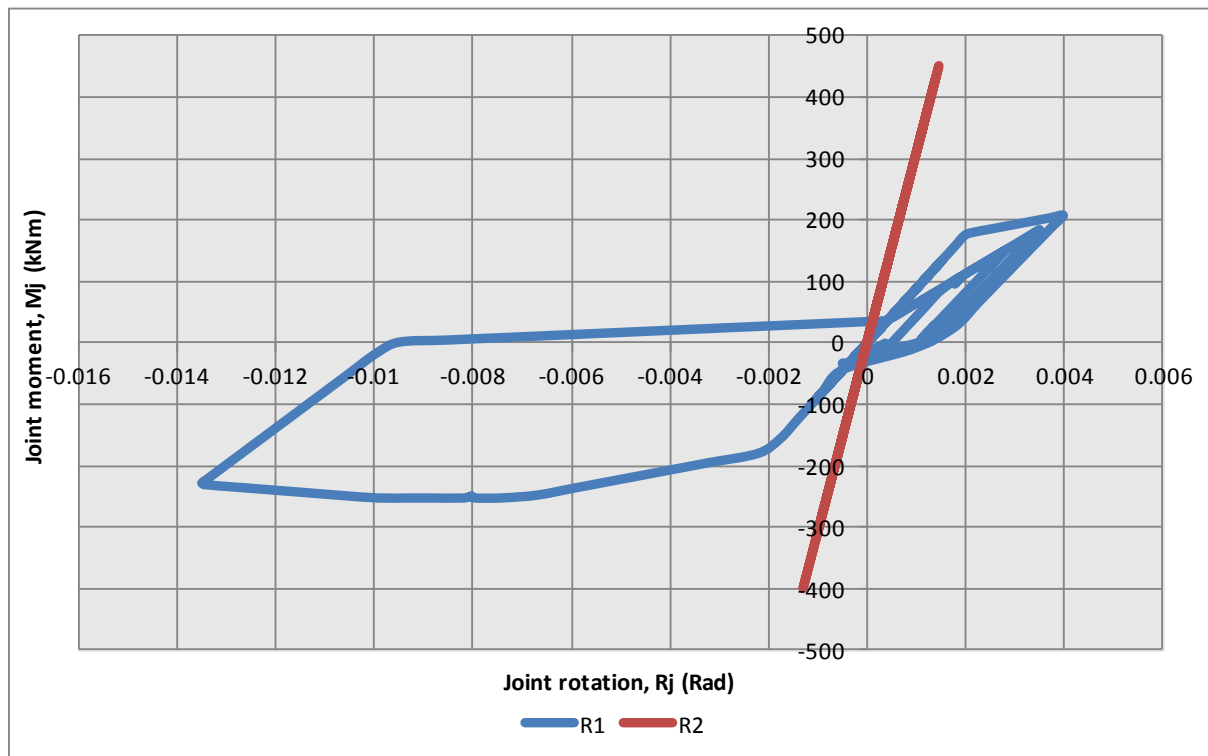


Figure 122: Max GL F BCJ R1 rotations: Column F2 level 5 hysteretic behaviour - REHS, Lyttelton

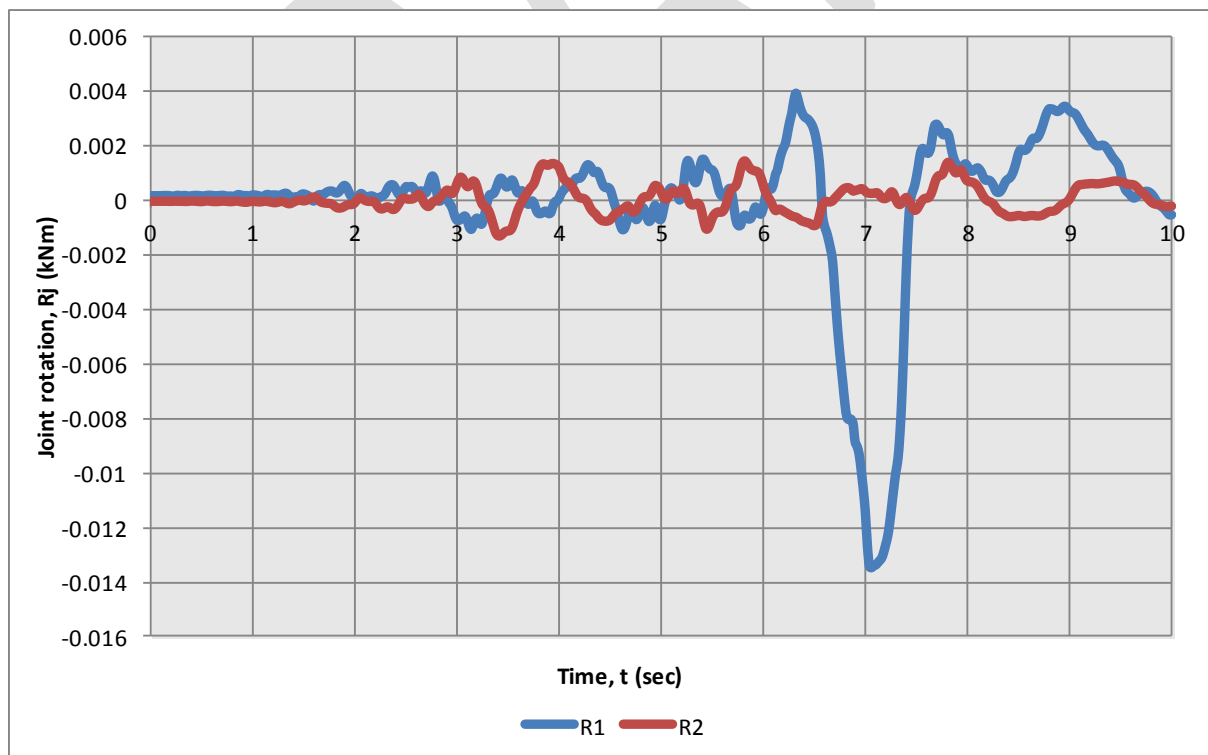


Figure 123: Max GL F BCJ R1 rotations: Column F2 level 5 rotations vs time - REHS, Lyttelton

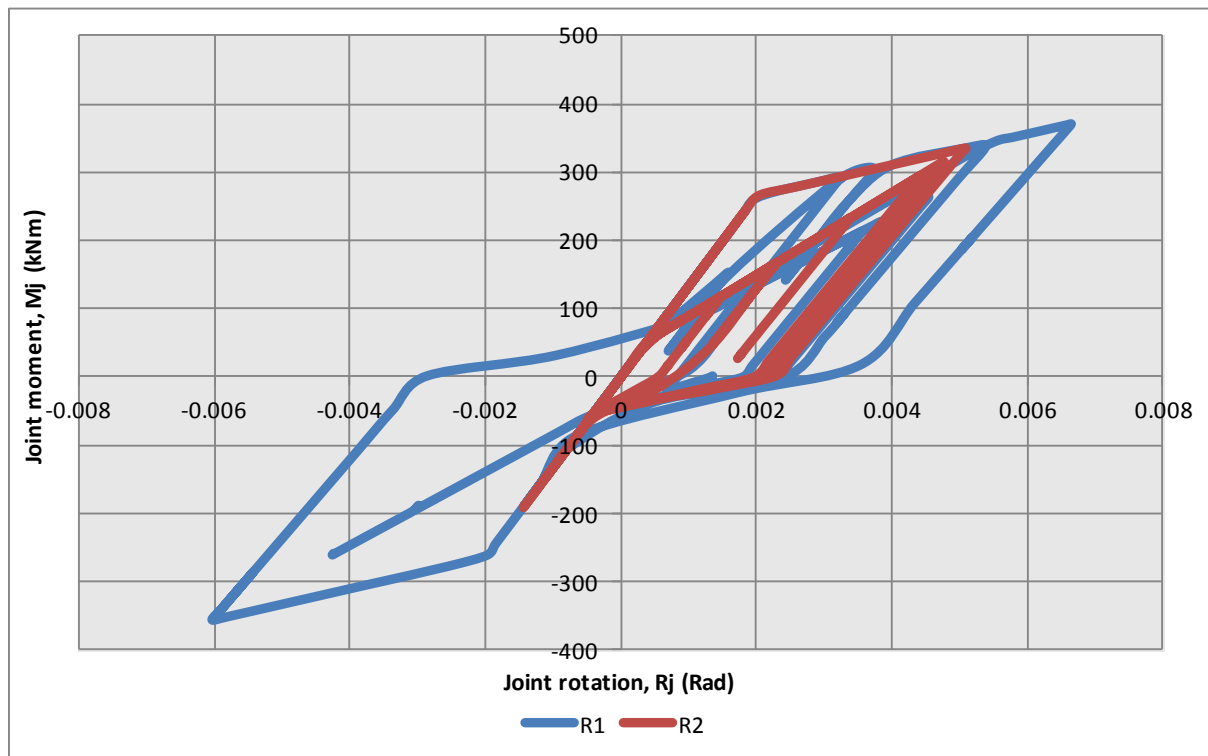


Figure 124: Max GL F BCJ R2 rotations: Column F1 level 5 hysteretic behaviour - REHS, Lyttelton

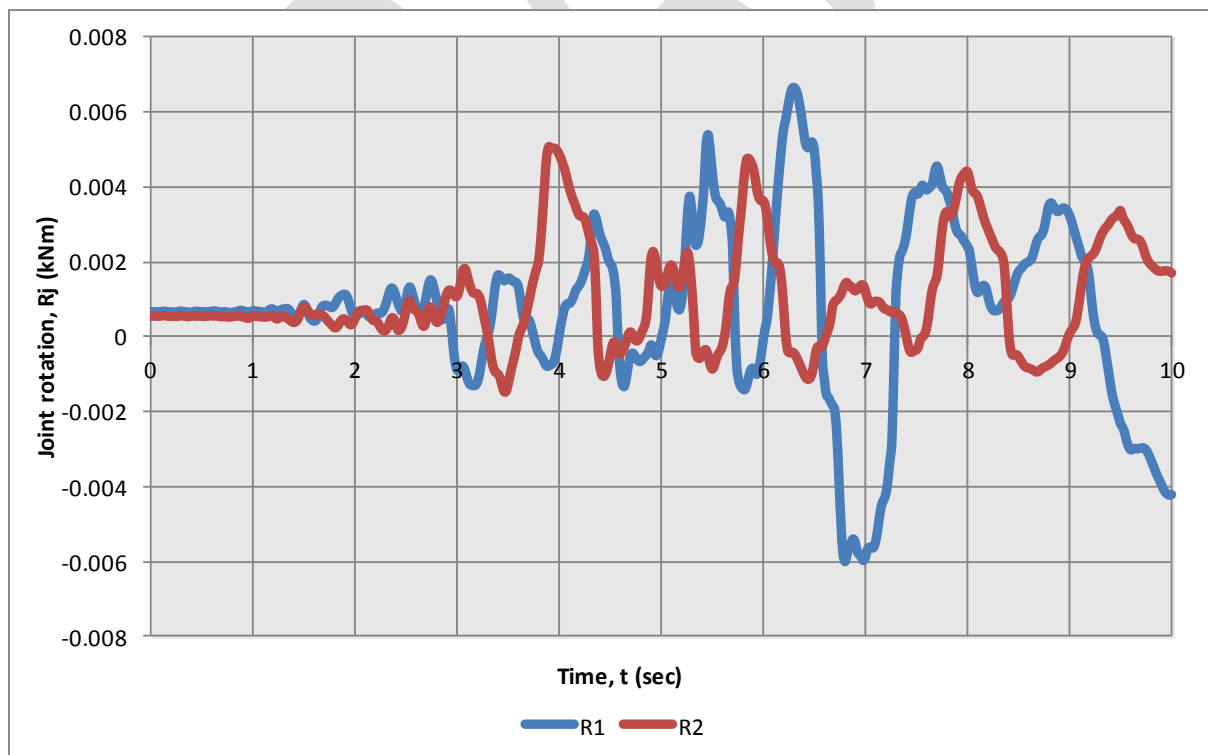


Figure 125: Max GL F BCJ R2 rotations: Column F1 level 5 rotations vs time - REHS, Lyttelton

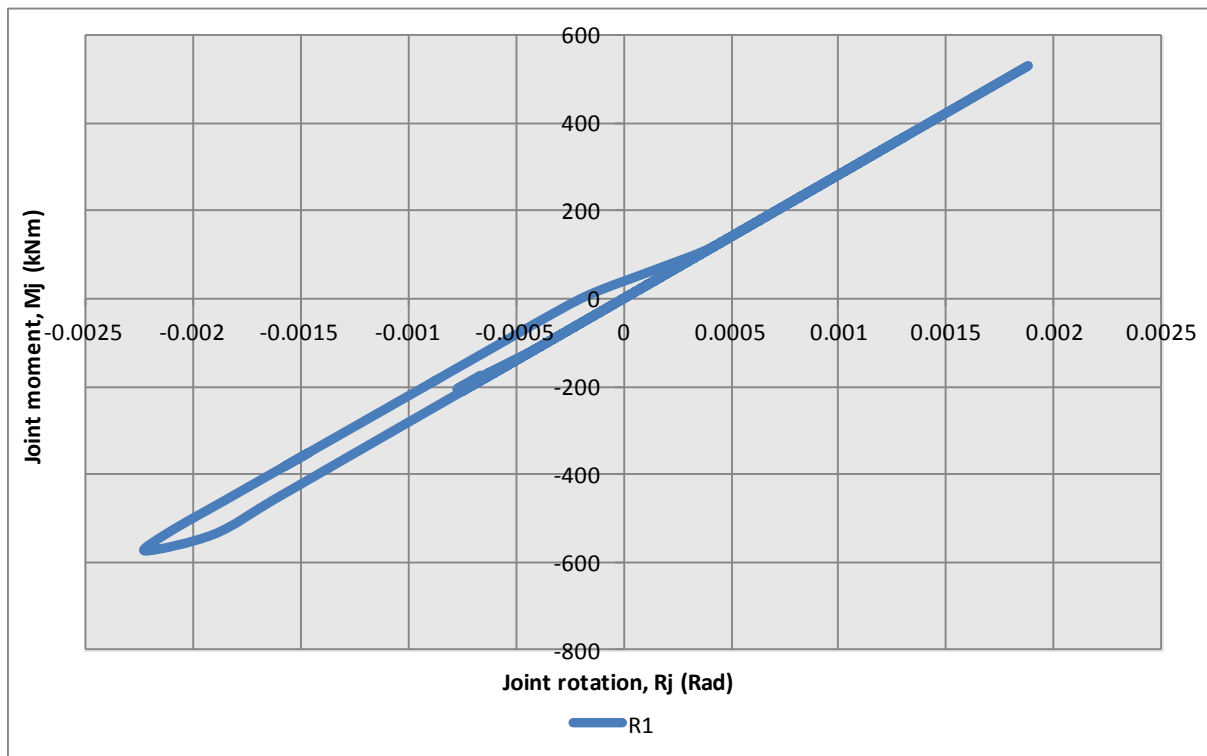


Figure 126: Max one-way BCJ R1 rotations: Column E2 level 3 hysteretic behaviour - REHS, Lyttelton

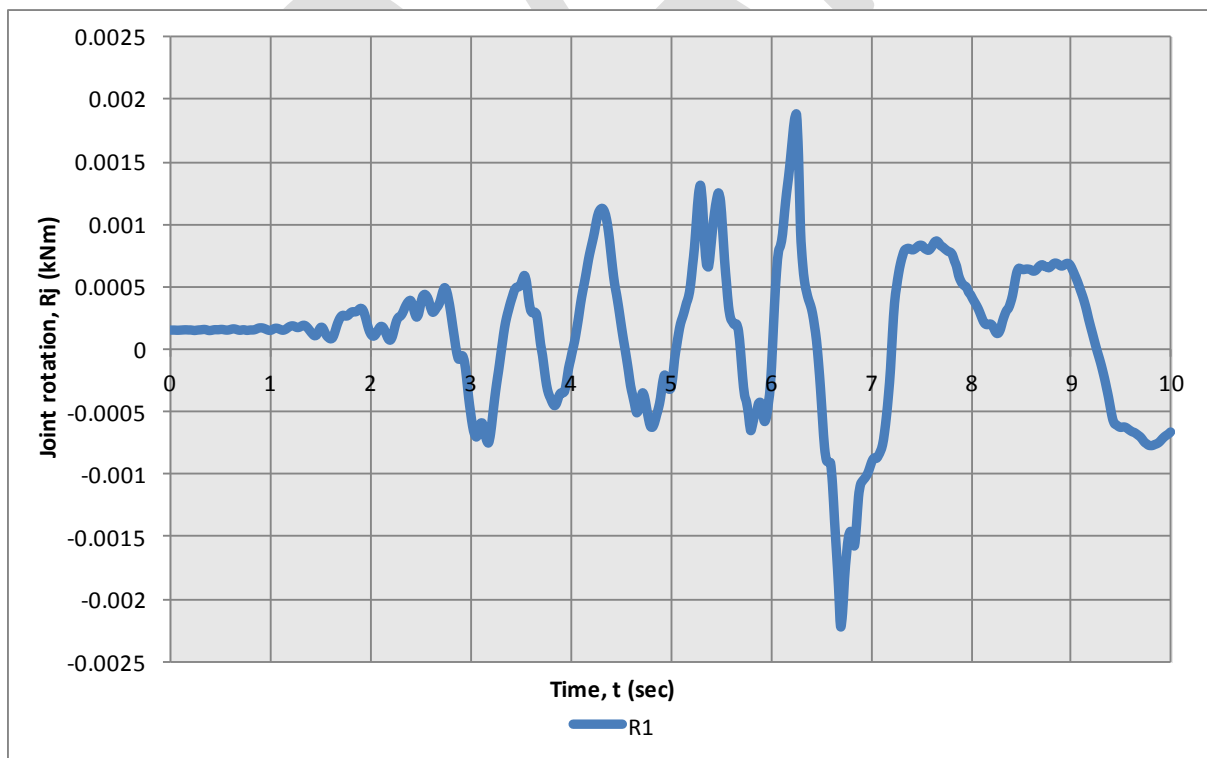


Figure 127: Max one way BCJ R1 rotations: Column E2 level 3 rotations vs time - REHS, Lyttelton

11.5. Beam Bar Pullout.

Hooked beam reinforcement anchorage capacity has been assessed at each time step for the CBGS ground motion record. Figure 128 and Figure 129 present the demand capacity ratios for the joints where bar pullout is shown to occur.

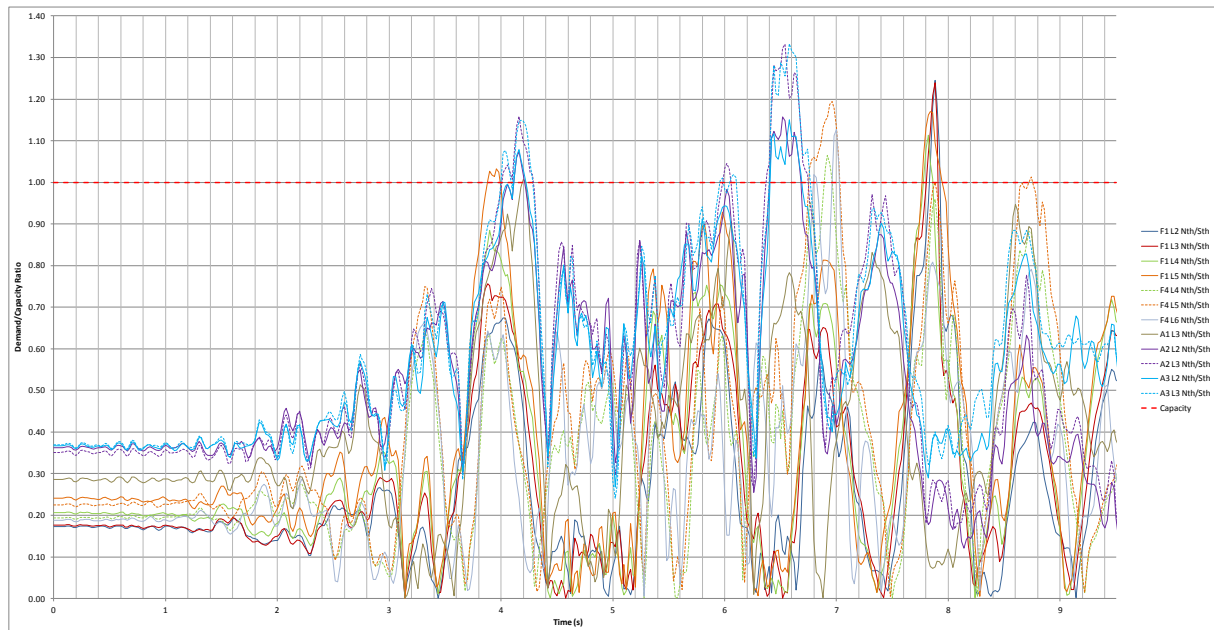


Figure 128: Beam bar pullout demand capacity ratios for north/south translation, CBGS, Lyttelton

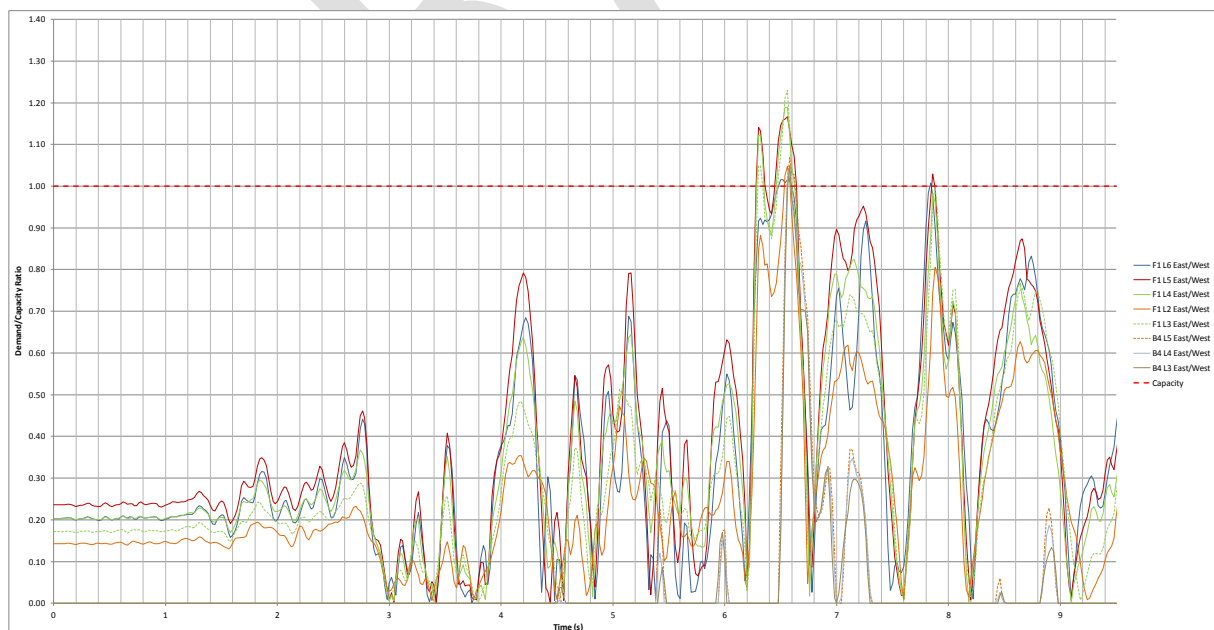


Figure 129: Beam bar pullout demand capacity ratios for east/west translation, CBGS, Lyttelton

12. Vertical Earthquake Effects

12.1. Axial Load Effects

Figure 130 and Figure 131 present the maximum variation in axial force obtained during the analysis for columns on grids C2 and F2 under the CBGS and CCCC record demands.

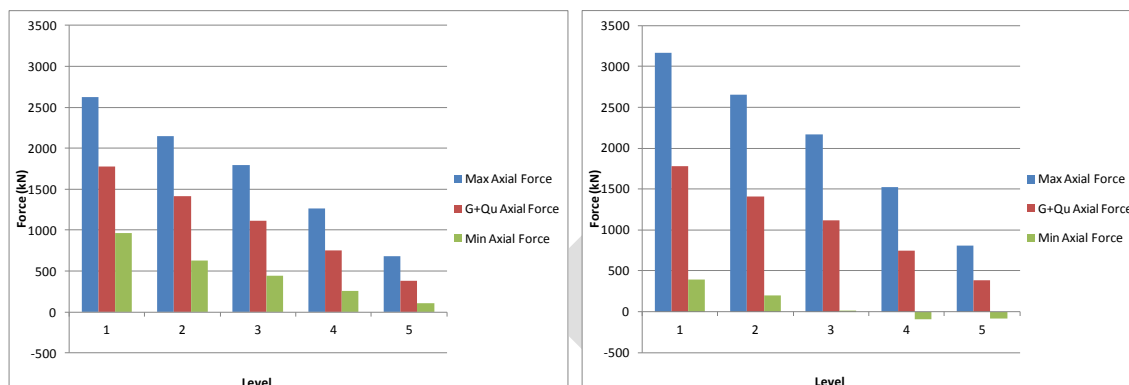


Figure 130: Column C2 axial load variation - CBGS (left) & CCCC (right), Lyttelton

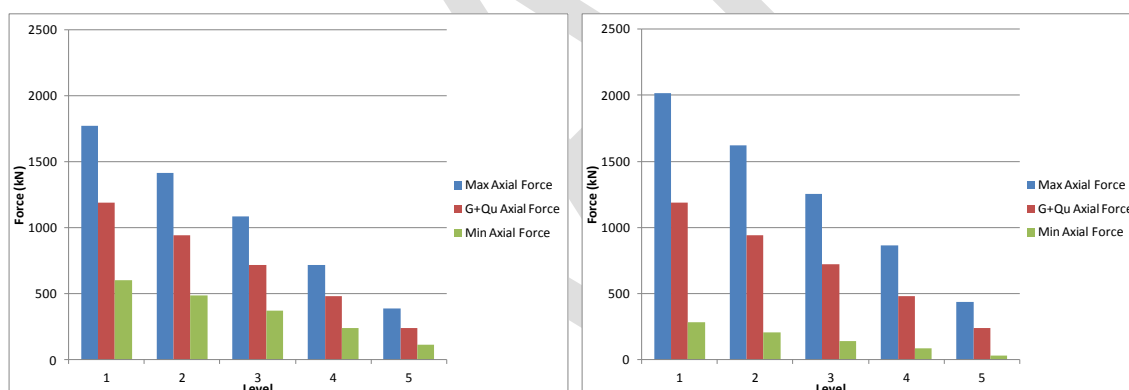


Figure 131: Column F2 axial load variation - CBGS (left) & CCCC (right), Lyttelton

Columns with a larger tributary area of floor slab such as column C2 exhibit a larger variation in axial force than columns with a smaller axial load contribution from the slabs e.g. column F2. In addition to the slab component some of the axial load variation can be attributed to the stiffness of the beams spanning onto the column.

It can be seen that the CCCC record produces a much larger variation in axial load in the elements considered than the CBGS record. This can be attributed to the difference in frequency components between the two records and the magnitude of the vertical accelerations present in each. Figure F.3 and Figure F.4 contain the vertical acceleration time

history records for the CBGS and the CCCC stations. From these it can be seen that the vertical accelerations were considerably higher at the CCCC station than for the CBGS station.

It should also be noted that the peak axial demands may not be concurrent with the peak bending actions that occur as a result of building drift. Consequently, when assessing vertical earthquake demands, consideration should be given to the concurrency of actions.

DRAFT

13. Conclusions

Conclusions will be published at the time of production of the first formal issue of this report.

DRAFT

14. Additional Work

It is important to note that the analyses this report presents were undertaken with significant time pressures.

Additional analyses can be undertaken using the current analysis model without any physical changes to the model. These additional analyses can consider registered concerns relating to the input ground motions that were not able to be considered in this report due to time constraints. The items of interest are as follows (in increasing level of time effort):

1. Consideration of only the horizontal components for the currently adopted earthquake accelerograms (i.e. without the vertical component of ground motion) to investigate more readily the influence of vertical excitation to element demands.
2. Consideration of the currently adopted earthquake accelerograms in their entirety (i.e. without the truncation presented in Table 15).
3. Consideration of sequential earthquake analyses for all of the currently adopted earthquake accelerograms in order to more accurately investigate potential cumulative damage effects for the considered seismic events.
4. Consideration of additional seismic events that occurred between September 2010 and February 2011 to investigate potential cumulative damage effects more rigorously.

Because no physical change to the model is required to undertake the above items they can be implemented with relative ease (save computational, post-processing and reporting time).

Beyond those items listed above it is possible to also make changes to the physical model to either consider individual element behaviour in more detail or consider variations to the inputs. Items could include the following:

1. The effect of the masonry on grid A has been completely disregarded in the current analyses. An additional model could consider the masonry in the form

as detailed on the construction drawings which may alter the response of the building for seismic events that are early in the sequence.

2. The column hinge model does not currently explicitly consider the effect of compression buckling of longitudinal reinforcement. An additional model could make some consideration of this which may affect the performance of the column hinge elements.
3. The potential for the diaphragm to exhibit inelastic behaviour at a location beyond the extent of the saddle bars has not been explicitly modelled. An additional model could consider the inelastic behaviour of the slab in this region on the basis of that the metal decking is either fully or partially bonded to the slab.
4. There is debate over the strength of the “drag bars” that connect the floor slabs to the north core and as such a sensitivity analysis on these strengths could be warranted.
5. The capacity of beam-column joints are considered to have significant unknowns and have been the subject of much debate. An additional model could consider a variation to the methodology adopted in these analyses, ideally with consideration of physical testing of a similarly detailed beam-column joint assemblage.

15. References

- Alire, D. A. (2002). *Seismic Evaluation of Existing Unconfined Reinforced Concrete Beam-Column Joints*. University of Washington, Seattle, Washington, 306p.
- Andriono, T., and Park, R. (1986). "Seismic Design Considerations of the Properties of New Zealand Manufactured Steel Reinforcing Bars." *Bulletin of the New Zealand National Society for Earthquake Engineering*, 19(3), pp.213–246.
- AS/NZS 1170.0. (2002). *Structural design actions, Part 0: General Principles*. Standards New Zealand/Standards Australia, Wellington, New Zealand, 36p.
- ASCE. (2006). *ASCE 41-06 Seismic Rehabilitation of Existing Buildings*. American Society of Civil Engineers, Reston, Virginia, 411p.
- Birely, A., Lowes, L. N., and Lehman, D. E. (2012). "A Model for the Practical Nonlinear Analysis of Reinforced-Concrete Frames Including Joint Flexibility." *Engineering Structures*, 34, pp.455–465.
- Carr, A. J. (1994). "Dynamic Analysis of Structures." *Bulletin of the New Zealand Society for Earthquake Engineering*, 27(2).
- Clyde, C., Pantelides, C. P., and Reaveley, L. D. (2000). *Performance-Based Evaluation of Exterior Reinforced Concrete Building Joints for Seismic Excitation*. Pacific Earthquake Engineering Research Center, Berkeley, California, 50p.
- Concrete Design Committee P3101. (1994). *Revisions to the New Zealand Standard for the Design of Concrete Structures NZS 3101*. New Zealand Concrete Society, Wellington, New Zealand, 168p.
- CSI Berkeley. (2011). *Computer program SAP2000 v14.2.5*. Computers and Structures Inc., Berkeley, California.
- DBH. (2011). "Changes for Christchurch Seismicity: Changes to Verification Method B1/VM1 - Hazard Factor for Christchurch." Accessed at: <http://www.dbh.govt.nz/UserFiles/File/Publications/Building/Guidance-information/pdf/information-sheet-on-seismicity-changes.pdf> (Aug. 22, 2011).
- Design Engineer. (1986a). *Structural Drawings: Office Building - 249 Madras Street*. Set No. 7, Issued 30 September, 39p.
- Design Engineer. (1986b). *Structural Drawings: Office Building - 249 Madras Street*. Set No. 7, Issued 30 September, 39p.
- Dowell, R. K., Seible, F., and Wilson, E. L. (1998). "Pivot Hysteresis Model for Reinforced Concrete Members." *ACI Structural Journal*, 95(5), pp.607–616.
- Geonet. (2010a). "M 7.1, Darfield (Canterbury), September 4 2010." Accessed at: www.geonet.org.nz/earthquake/historic-earthquakes/top-nz/quake-13.html (Aug. 5, 2011).
- Geonet. (2010b). "Darfield Mainshock Records." Accessed at: [ftp.geonet.org.nz/strong/processed/Proc/2010/09_Darfield_mainshock_extended_pass_band/Vol2/data/](ftp://ftp.geonet.org.nz/strong/processed/Proc/2010/09_Darfield_mainshock_extended_pass_band/Vol2/data/) (Aug. 5, 2011).
- Geonet. (2011a). "M 6.3, Christchurch, February 22 2011." Accessed at: www.geonet.org.nz/earthquake/historic-earthquakes/top-nz/quake-14.html (Aug. 5, 2011).

- Geonet. (2011b). "Christchurch Mainshock Records." Accessed at: ftp.geonet.org.nz/strong/processed/Proc/2011/02_Christchurch_mainshock_extended_pass_band/Vol2/data/ (Aug. 5, 2011).
- Hakuto, S., Park, R., and Tanaka, H. (2000). "Seismic Load Tests on Interior and Exterior Beam-Column Joints with Substandard Reinforcing Details." *ACI Structural Journal*, 97(1), pp.11–25.
- Hindi, R. A., and Hassan, M. A. (2004). "Shear Capacity of Diagonally Reinforced Coupling Beams." *Engineering Structures*, 26(10), pp.1437–1446.
- Hyland, C. (2011). *CTV Building Site Examination and Materials Tests*. Hyland Fatigue and Earthquake Engineering, Auckland, New Zealand, 158p.
- Joh, O., Goto, Y., and Shibata, T. (1993). "Anchorage of Beam Bars with 90-Degree Bend in Reinforced Concrete Beam-Column Joints." *Tom Paulay Symposium "Recent Developments in Lateral Force Transfer in Buildings"*, University of California, San Diego, La Jolla, California, 97–116p.
- Joh, O., and Shibata, T. (1996). "Anchorage Behaviour of 90-Degree Hooked Beams in Reinforced Concrete Beam-Column Joints." *Eleventh World Conference on Earthquake Engineering*, Acapulco, Mexico.
- Karthik, M. M., and Mander, J. B. (2011). "Stress-Block Parameters for Unconfined and Confined Concrete Based on a Unified Stress-Strain Model." *Journal of Structural Engineering*, 137(2), pp.270–273.
- Kurose, Y. (1987). *Recent Studies on Reinforced Concrete Beam-Column Joints in Japan*. Phil M. Ferguson Structural Engineering Laboratory, The University of Texas, Austin, Texas, 164p.
- LaFave, J. M., and Shin, M. (2005). "Discussion of 'Modelling Reinforced-Concrete Beam-Column Joints Subjected to Cyclic Loading' by Laura N. Lowes and Arash Altoontash." *Journal of Structural Engineering*, 131(6), pp.992–993.
- Lehman, D. E., Stanton, J. F., Anderson, M., Alire, D. A., and Walker, S. G. (2004). "Seismic Performance of Older Beam-Column Joints." *13th World Conference on Earthquake Engineering*, Vancouver, Canada.
- Mander, J. B. (2012). "RE: Compusoft Request for Information."
- Mander, J. B., Priestley, M. J. N., and Park, R. (1988). "Theoretical Stress-Strain Model for Confined Concrete." *ASCE Journal of Structural Engineering*, 114(8), pp.1804–1826.
- Mitra, N., and Lowes, L. N. (2007). "Evaluation, Calibration, and Verification of a Reinforced Concrete Beam-Column Joint Model." *ASCE Journal of Structural Engineering*, 133(1), pp.105–120.
- Moehle, J. P., Lehman, D., and Lowes, L. N. (2006). "Beam-Column Connections." *PEER/EERI Seminar on Nonductile Concrete*, Accessed at: peer.berkeley.edu/research/powerpoint/non_ductile_concrete/Joints-Moehle.c.ppt (Jun. 15, 2012).
- NZS 1170.5. (2004). *Structural design actions, Part 5: Earthquake Actions - New Zealand*. Standards New Zealand, Wellington, New Zealand, 154p.
- NZS 3101. (2006). *Concrete Structures Standard*. Standards New Zealand, Wellington, New Zealand, 646p.

- NZSEE. (2006). *Assessment and Improvement of the Structural Performance of Buildings in Earthquakes*. New Zealand Society for Earthquake Engineering, Wellington, New Zealand, ~400p.
- Pampanin, S., Calvi, G. M., and Moratti, M. (2002). "Seismic Behaviour of RC Beam-Column Joints Designed for Gravity Loads." *12th European Conference on Earthquake Engineering*, Elsevier Science Ltd., London, England.
- Pantelides, C. P., Hansen, J., and Nadeau, J. (2002). *Performance-Based Evaluation of Exterior Reinforced Concrete Building Joints for Seismic Excitation*. Pacific Earthquake Engineering Research Center, Berkeley, California, 103p.
- Park, S. (2010). *Experimental and Analytical Studies on Old Reinforced Concrete Buildings with Seismically Vulnerable Beam-Column Joints*. University of California, Berkeley, 260p.
- Paulay, T., and Priestley, M. J. N. (1992). *Seismic Design of Reinforced Concrete and Masonry Buildings*. John Wiley & Sons, New York, 744p.
- Priestley, M. J. N. (1997). "Displacement-Based Seismic Assessment of Reinforced Concrete Buildings." *Journal of Earthquake Engineering*, 1(1), pp.157–192.
- Priestley, M. J. N., Calvi, G. M., and Kowalsky, M. J. (2007). *Displacement-Based Seismic Design of Structures*. IUSS Press, Pavia, Italy, 721p.
- Sharma, A., Eligehausen, R., and Reddy, G. R. (2011). "A New Model to Simulate Joint Shear Behaviour of Poorly Detailed Beam-Column Connections in RC Structures Under Seismic Loads, Part 1: Exterior Joints." *Engineering Structures*, 33, pp.1034–1051.
- Sinclair, T. (2011). *CTV Geotechnical Advice (11 July)*. Tonkin & Taylor, Auckland, New Zealand, 14p.
- Sinclair, T. (2012). *CTV Building Geotechnical Advice - Addendum 2 (14 June)*. Tonkin & Taylor, Auckland, New Zealand, 9p.
- Takeda, T., Sozen, M. A., and Nielsen, N. N. (1970). "Reinforced Concrete Response to Simulated Earthquakes." *Journal of Structural Engineering*, 96(12), pp.2257–2273.
- Vecchio, F. J., and Collins, M. P. (1986). "The Modified Compression-Field Theory for Reinforced Concrete Elements Subjected to Shear." *Journal of the American Concrete Institute*, 83(2), pp.219–231.
- Walker, S. G. (2001). *Seismic Performance of Existing Reinforced Concrete Beam-Column Joints*. University of Washington, Seattle, Washington, 326p.
- Weng Yuen, K. (2010). *Selective Weakening and Post-Tensioning for the Seismic Retrofit of Non-Ductile RC Frames*. The University of Canterbury, Christchurch, New Zealand, 672p.

List of appendices

Appendix A	Nonlinear analysis of diagonally reinforced coupling beams.....	130
A.1	Considered model	130
A.2	Example structure	130
A.3	Analysis model definition	131
A.4	Analysis results	133
A.5	Strain penetrations	135
Appendix B interaction	Nonlinear analysis of columns with consideration of axial-moment (P-M) 136	
B.1	Introduction	136
B.2	Proposed model	136
B.3	Axial-moment (P-M) interaction relationship	136
B.4	Moment-curvature relationship – monotonic loading	136
B.5	Moment-curvature relationship – cyclic loading	136
Appendix C	Development of a model for beam-column joints of the CTV building.....	137
C.1	Introduction	137
C.1.1	CTV Building beam-column joints in relation to New Zealand Standards	137
C.1.2	Issues related to modelling of deficient beam-column joints	138
C.2	Implementation	139
C.3	Definition of relative stress vs deformation backbone curve	140
C.4	Definition of maximum joint shear strength	143
C.5	Issues and limitations of the adopted joint degradation implementation	146
C.5.1	Limitations of the method used to implement the joint shear spring	146
C.5.2	Geometry of the exterior beam-column joints.....	148
C.5.3	Relationship of joint strength and deformation characteristics to deformation imposed on adjacent members.....	149
C.6	Calculations showing basis for relating joint moment to shear stress for modelling purposes	151
Appendix D	Hook anchor capacity	153
Appendix E	Foundation Modelling Properties.....	155

Appendix F	Acceleration Time History Records.....	156
F.1	Darfield CBGS	156
F.2	Darfield CCCC	157
F.3	Lyttelton CBGS	158
F.4	Lyttelton CCCC	159
F.5	Lyttelton CHHC	160
F.6	Lyttelton REHS	161
Appendix G	Analysis Results - Darfield Event: CBGS Record.....	163
G.1	Building Displacements and Drifts.	163
G.2	Diaphragm Connection Forces	166
G.3	Column Hinge Actions	172
Appendix H	Analysis Results - Darfield Event: CCCC Record.....	178
H.1	Building Displacements and Drifts.	178
H.2	Diaphragm Connection Forces	181
H.3	Column Hinge Actions	188
Appendix I	Analysis Results - Lyttelton Aftershock: CBGS record	194
I.1	Building Displacements and Drifts.	194
I.2	Diaphragm Connection Forces	200
I.3	Column Hinge Actions	206
Appendix J	Analysis Results - Lyttelton Aftershock: CCCC record	217
J.1	Building Displacements and Drifts.	217
J.2	Diaphragm Connection Forces	224
J.3	Column Hinge Actions	235
Appendix K	Analysis Results - Lyttelton Aftershock: CHHC record.....	242
K.1	Building Displacements and Drifts.	242
K.2	Diaphragm Connection Forces	245
K.3	Column Hinge Actions	251
Appendix L	Analysis Results - Lyttelton Aftershock: REHS record.....	257
L.1	Building Displacements and Drifts.	257
L.2	Diaphragm Connection Forces	260

L.3 Column Hinge Actions

266

DRAFT

Appendix A Nonlinear analysis of diagonally reinforced coupling beams

A.1 Considered model

A method for considering the nonlinear load-deformation behaviour of diagonally reinforced coupling beams is proposed by Hindi and Hassan (2004). In this method a simple truss mechanism is considered to provide all strength and stiffness to the system. When the system is subjected to sway actions the resulting shear force and bending moment is carried via two diagonal members with one in compression and one in tension. The compression member includes the confined concrete core and the diagonal reinforcing bars whereas the tension member includes only the diagonal reinforcing bars. It is considered that the concrete core provides sufficient stiffness to ensure that the member cannot buckle in compression. The proposed truss model is as presented in Figure A.1 below.

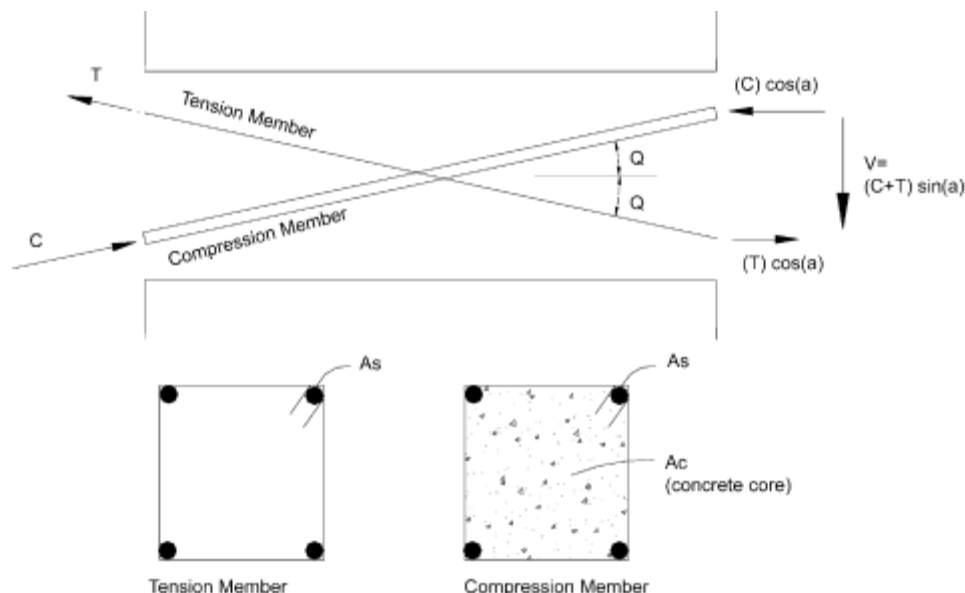


Figure A.1: Proposed model (from Hindi and Hassan 2004)

A.2 Example structure

The proposed model has been implemented for an example structure as presented in Figure A.2 below. In this structure two 2050 mm long reinforced concrete walls are joined by a coupling beam measuring 900 mm long by 1650 mm high. The wall thickness is 400 mm throughout.

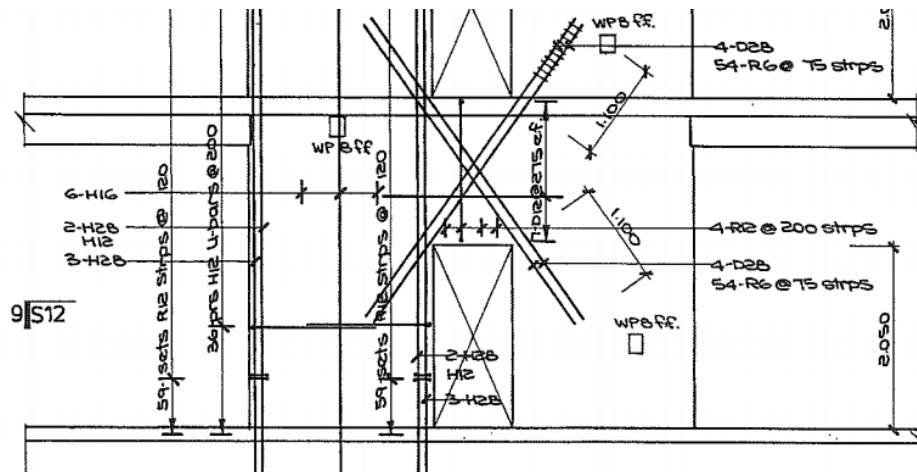


Figure A.2: Example wall reinforcement

A.3 Analysis model definition

The example structure has been analysed considering the proposed model using SAP2000 (v14). In this model axially “stiff” diagonal struts (oriented at 54° to the horizontal from Figure A.2) are included to consider the behaviour of the coupling beam following the model presented in Section A.1. The strut dimensions are taken as 150 mm square. Axial deformation in the struts is provided via fibre type hinge element which incorporates both concrete and reinforcement fibres. The walls are modelled using membrane elements that have sufficient stiffness to ensure that deformation is restricted to the coupling beam. As the conventional beam reinforcement also present in the coupling beam is not included, this modelling analogy will underestimate the stiffness of the coupling beam for elastic response, but will provide a reasonable representation of the wall response in the inelastic range. The analysis model is presented in Figure A.3 below.

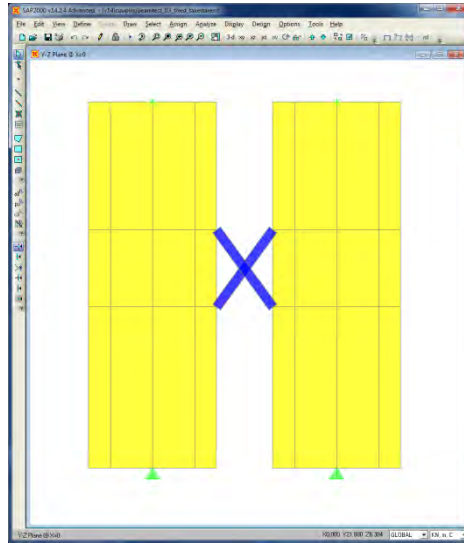


Figure A.3: SAP2000 analysis model

The reinforcement in the diagonal struts is included as a fibre type element with stress-strain behaviour as defined by Park and is presented in Figure A.4 below. The hysteretic form of the reinforcing is taken as kinematic type. The area of the reinforcing steel is taken as the sum of all longitudinal reinforcement present in the strut (i.e. $A_s=4\text{-D}28=2463\text{ mm}^2$). Strain penetration of the diagonal reinforcement into the walls has been excluded in this model.

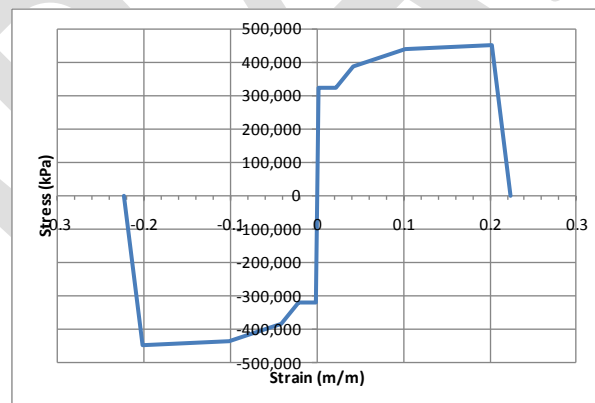


Figure A.4: Reinforcing nonlinear steel stress-strain plot

The concrete core of the diagonal strut elements is included fibre type element with material behaviour based on a Mander confined concrete model (Mander et al. 1988) with an unconfined compressive strength, $f'_c=33.5\text{ MPa}$, $\epsilon_{c0}=0.002$, ultimate unconfined strain capacity given as 0.004, and confining reinforcing as presented in Figure A.4 above (i.e. R6@75crs confining hoops). The hysteretic form of the concrete fibre is considered exhibit Takeda type behaviour. The area of the concrete is taken as the total concrete core area (i.e.

$A_c = A_g - A_s = 150^2 - 2,464 = 20,036 \text{ mm}^2$). The nonlinear stress-strain behaviour for the concrete is as presented in Figure A.5 below (note that the tensile capacity has been taken as zero).

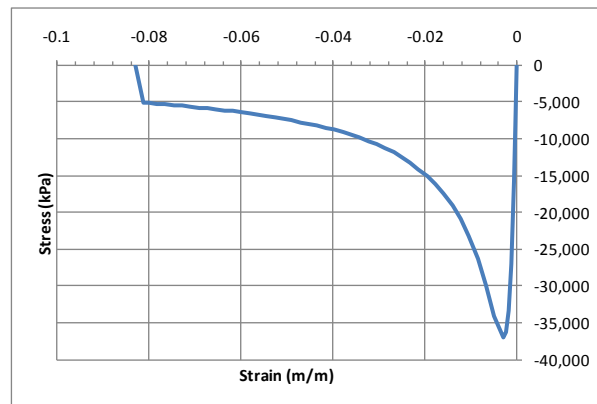


Figure A.5: Concrete nonlinear stress-strain plot

A.4 Analysis results

A nonlinear analysis has been undertaken to derive the force-deformation behaviour of the system. The backbone curve for the coupling beam system plotted as wall rotation (=drift) vs coupling beam shear force is presented in Figure A.6 below.

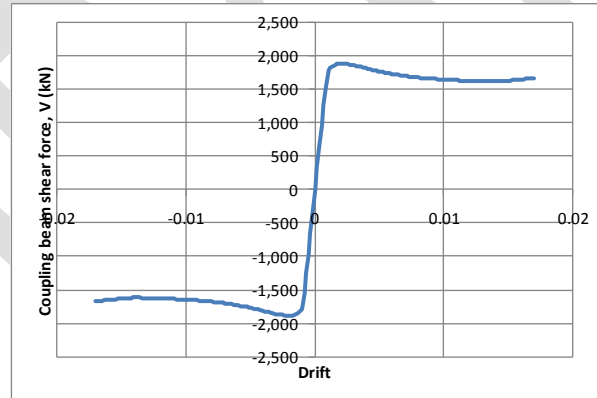


Figure A.6: Nonlinear backbone curve

A qualitative comparison of the resulting backbone curve and those presented by Hindi and Hassan (2004) indicates that the model adequately predicts the force-displacement behaviour for monotonic loading.

In order to assess the hysteretic form, a non-linear displacement time history analysis has been undertaken. Figure A.7 below plots the wall rotation (=drift) vs coupling beam shear force for the cyclic analysis.

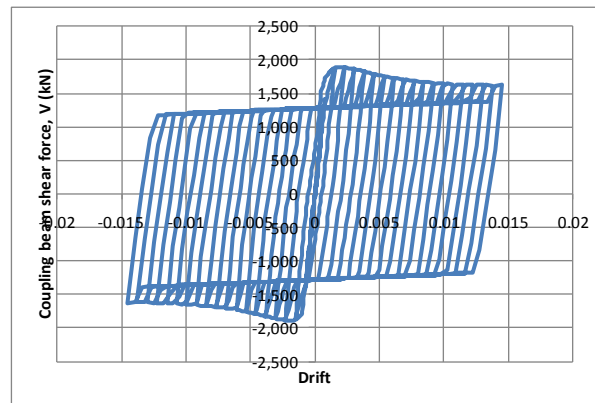


Figure A.7: Coupling beam hysteretic response

It can be seen that for the level of drift considered the analysis model behaves essentially in an elastic-perfectly plastic manner due to the reinforcing with additional strength enhancement as a result of the concrete. A limitation of the analysis undertaken is that the hysteretic behaviour does not reflect the softening that would normally be expected under cyclic loading due to the Bauschinger effect, and other mechanisms such as concrete spalling etc.

In an attempt to approximate these effects an additional analysis model has been developed whereby the hysteresis type for the reinforcement has been changed from the default kinematic type to instead be a Takeda type. The resulting hysteretic response is presented in Figure A.8 below which plots the wall rotation (=drift) vs coupling beam shear force.

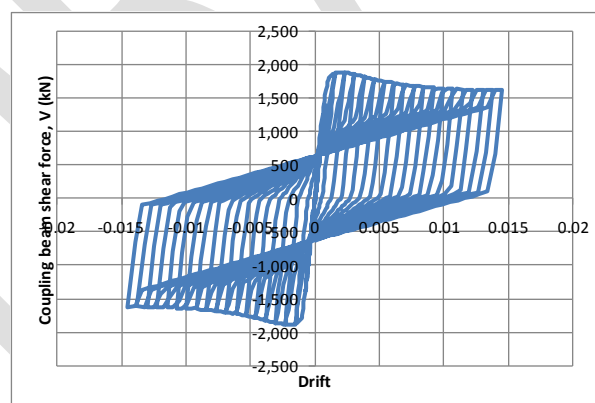


Figure A.8: Coupling beam hysteretic response (Takeda reinforcement)

It can be seen that whilst the hysteretic behaviour is not perfect, the total amount of energy dissipated for the considered loading history is reduced by approximately 50%.

A.5 Strain penetrations

The effects of strain penetration of the diagonal reinforcement into the wall have not been directly incorporated into the analysis models. In order to incorporate these effects, the non-linear stress-strain curve for the reinforcing steel element as presented in Figure A.4 has instead been scaled in the strain domain based on the following:

$$\varepsilon'_s = \varepsilon_s \left(\frac{L + 2L_{SP}}{L} \right)$$

Where ε'_s is the scaled strain, ε_s is the material strain obtained from Figure A.4, L is the length of the element as considered in the model, and L_{SP} is the strain penetration length, determined using the equation below taken from Paulay and Priestley (1992):

$$L_{SP} = 0.022f_s d_b$$

where f_s and d_b are the stress and diameter of the longitudinal reinforcement respectively.

For the example structure the modelled length of the strut is given as 1531 mm and the diagonal bar is given as 28 mm diameter which then gives a modified non-linear stress-strain curve for the reinforcing fibre as presented in Figure A.9 below.

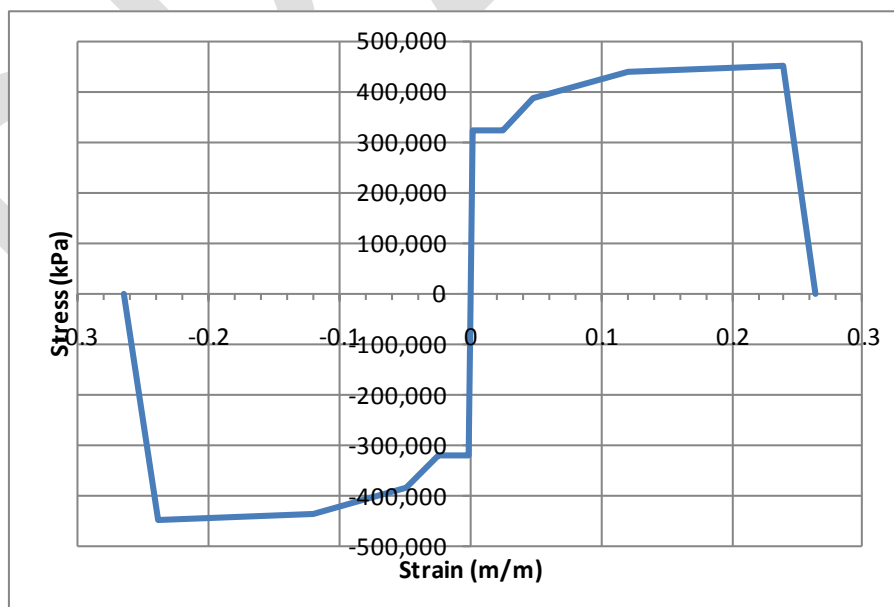


Figure A.9: Reinforcing nonlinear stress-strain plot (modified for strain penetrations)

Appendix B Nonlinear analysis of columns with consideration of axial-moment (P-M) interaction

B.1 Introduction

B.2 Proposed model

B.3 Axial-moment (P-M) interaction relationship

B.4 Moment-curvature relationship – monotonic loading

B.5 Moment-curvature relationship – cyclic loading

Appendix C Development of a model for beam-column joints of the CTV building

C.1 Introduction

In typical modern reinforced concrete structures beam-column joints are designed so that they are stronger than the beam and column members framing into the joint. Such joints can reasonably be assumed to respond elastically during an earthquake, and thus it is not necessary to specifically model the beam-column joint beyond allowing some elastic deformation to occur in the joint core. In contrast, the beam-column joints of the CTV Building are significantly deficient in relation to modern design procedures, and cannot be assumed to respond elastically. Thus the potential for beam-column joint core failure to occur prior to or in conjunction with beam and/or column hinging must be considered when assessing the performance of the CTV Building. During the original time history analyses of the structure the possibility of joint failure was assessed by post-processing of output data. During discussions regarding alterations and enhancements to the CTV Building non-linear analysis model it was made clear that some members of the Royal Commission Expert Panel on Non-linear Time History Analysis (NLTHA) considered this post-processing approach to be inadequate and that implementation of non-linear beam-column joint behaviour in the analysis model would be preferred. This appendix discusses the beam-column joints of the CTV Building and the procedures developed to model them.

C.1.1 CTV Building beam-column joints in relation to New Zealand Standards

Beam-column joints require both horizontal and vertical reinforcement in order to develop the require mechanisms for reliable resistance of earthquake induced forces. Horizontal reinforcement is generally provided by stirrup or spiral reinforcement placed specifically for this purpose, while in New Zealand practice vertical joint shear reinforcement is typically assumed to be provided by the intermediate column longitudinal reinforcing bars, which are expected to behave elastically during earthquakes.

The CTV Building was designed during the mid 1980s, and as such would be assumed to have beam-column joints that met or exceeded (Concrete Design Committee P3101 1994) the detailing requirements of the current New Zealand Concrete Structures Standard (NZS 3101 2006). However, review of the structural drawings indicates that this is not the case. The beam-column joints are instead effectively unreinforced, and hence likely to perform in a

manner similar to joints typical of much older structures designed prior to the adoption of “modern” design standards. The reasons for considering the joints to be effectively unreinforced are twofold:

- The CTV Building drawings are unclear about whether the column transverse reinforcement continues through the joint core; however, the wide spacing of this transverse reinforcement means that even if it did continue through the joint core it would be equivalent to only a small fraction of the horizontal joint reinforcement required.
- The joints also lack effective vertical reinforcement, as the intermediate column longitudinal reinforcing bars of the CTV Building cannot generally be assumed to remain elastic during significant earthquakes. Instead the intermediate column longitudinal reinforcement would be expected to yield because many of the beam-column joints are expected to perform in a “strong beam-weak column” manner, i.e. with plastic hinge formation in the columns rather than the beams. Thus the intermediate column longitudinal bars would not possess reserve capacity with which to reinforce the joint.

C.1.2 Issues related to modelling of deficient beam-column joints

Realistic non-linear modelling of deficient concrete beam-column joints is unfortunately not a trivial exercise. Several factors make it difficult to accurately model the joints of the CTV building. These include:

- The response of deficient joints is still a highly active research topic;
- There are fundamental international disagreements regarding the mechanics and behaviour of concrete beam-column joints;
- Simple models of deficient beam-column joints available in the literature are typically intended for assessment of existing structures, and are thus considered to be unduly conservative for forensic engineering purposes;
- Rigorous joint models available in the literature are not suitable for implementation in commercial finite element software, particularly for a model containing multiple beam-column joints such as that of the CTV building.
- The joints of the CTV building contain many features that are not well covered by the available research literature. These features include circular columns,

“weak column-strong beam” behaviour, biaxial loading, and deficient hooked anchorages in interior joints.

The remainder of this document presents discussion related to the adopted analysis model for the CTV beam-column joints. This discussion is divided into a number of topics. Discussion of some of these topics includes non-comprehensive review of relevant literature where this has been used as the basis for defining the beam-column joint model.

C.2 Implementation

A number of methods can be used to incorporate beam-column joint response within a structural finite element model. The method adopted by Compusoft Engineering Limited for the CTV structural model is to develop a non-linear rotational spring representing the beam-column joint shear stress-shear strain response, with this spring located at the node representing the intersection of beams and columns at the beam-column joint. The moment applied to the joint can be related to the shear stress in the joint based on the geometry of the structure. Details of the calculations defining this relationship are presented in Appendix C.6.

The rotational spring used to model the joints has the following features:

- Independent, non-interacting properties for orthogonal axes of loading.
- No moment-axial load interaction.
- A moment-rotation backbone curve based on the joint shear stress-shear strain backbone curve described in the following sections and the calculations presented in Appendix C.6.
- Hysteretic response based on a “Pivot” hysteresis model (Dowell et al. 1998).

Review of relevant literature has shown that there is significant disagreement between sources with regards to both the peak strength of deficient beam-column joints, and also the force-deformation relationship that is appropriate for deficient joints. This document considers these two issues separately, first considering an appropriate backbone curve defining the relationship between joint deformation and relative or normalised strength, and then considering the peak strength expected from deficient beam-column joints.

C.3 Definition of relative stress vs deformation backbone curve

In this section various backbone curves relating joint deformation to joint stress presented in the literature are discussed, and from these curves an appropriate curve is defined for use in the CTV Building non-linear analyses. In order to clarify the discussion, the backbone curves are defined based on relative joint stress, with a relative joint stress of 1.0 being taken as equal to the maximum joint shear strength.

Figure C.1 shows a number of backbone curves for the relative stress-strain response of deficient beam-column joints. As indicated, these curves have been drawn from a wide variety of sources. It is evident from the plot that there is considerable variance between the postulated curves. Brief details of each curve are as follows:

- The FEMA 356/ASCE 41 curve is taken from a widely used U.S. document outlining procedures for assessment of existing buildings.
- The curve recommended by Park (2010) was based on testing of four exterior beam-column joints. The deformation at peak stress is determined based on joint geometry.
- The curve proposed by Weng Yuen (2010) is for exterior joints, and is a modification of similar curves published widely by other researchers.
- Sharma et al. (2011) specified in the paper that “the plot of principal tensile stress vs. joint shear deformation ... seems appropriate”, but did not show supporting experimental data. Review of the referenced data (Clyde et al. 2000; Pantelides et al. 2002) suggests that the adopted curve was a “lower bound” appropriate for assessment but less so for prediction.
- Birely et al. (2012) provided no data regarding the descending branch of the backbone curve. They calibrated their curve against data from interior beam-column joint tests.
- The final curve plotted was developed by Compusoft Engineering Limited based on review of data presented by Walker (2001) and Alire (2002). It represents an approximate average of the stress-deformation response measured during 11 tests on interior beam-column joints. Data from these 11 tests is shown in Figure C.2.

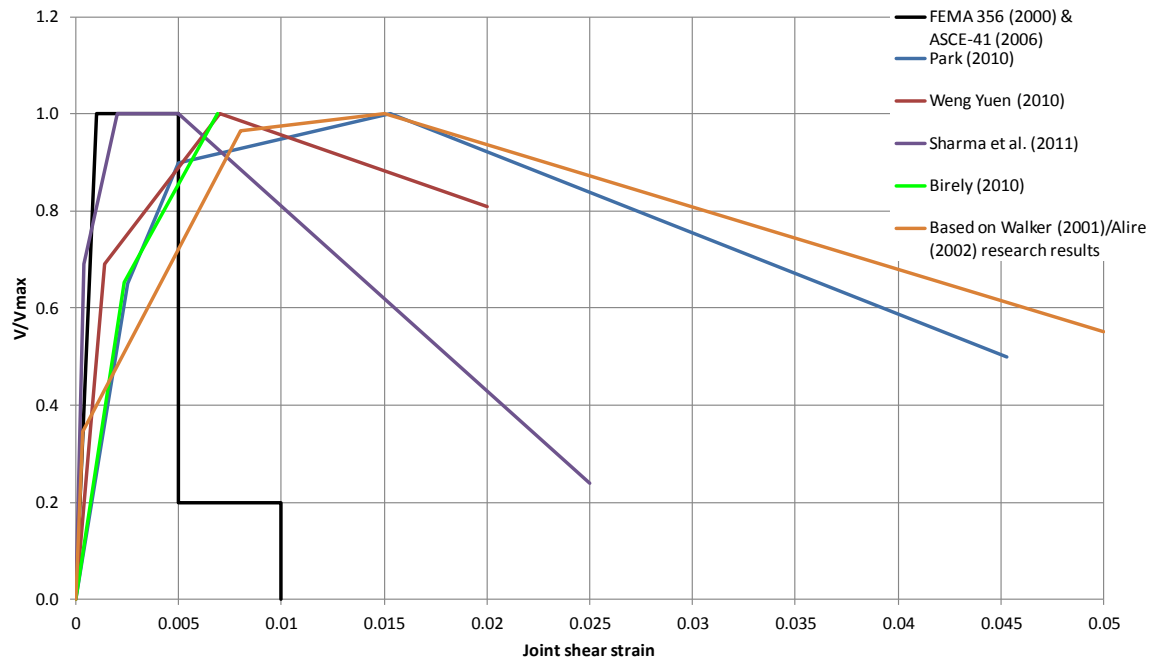


Figure C.1: Backbone curves from various sources (Alire 2002; ASCE 2006; Birely et al. 2012; S. Park 2010; Sharma et al. 2011; Walker 2001; Weng Yuen 2010)

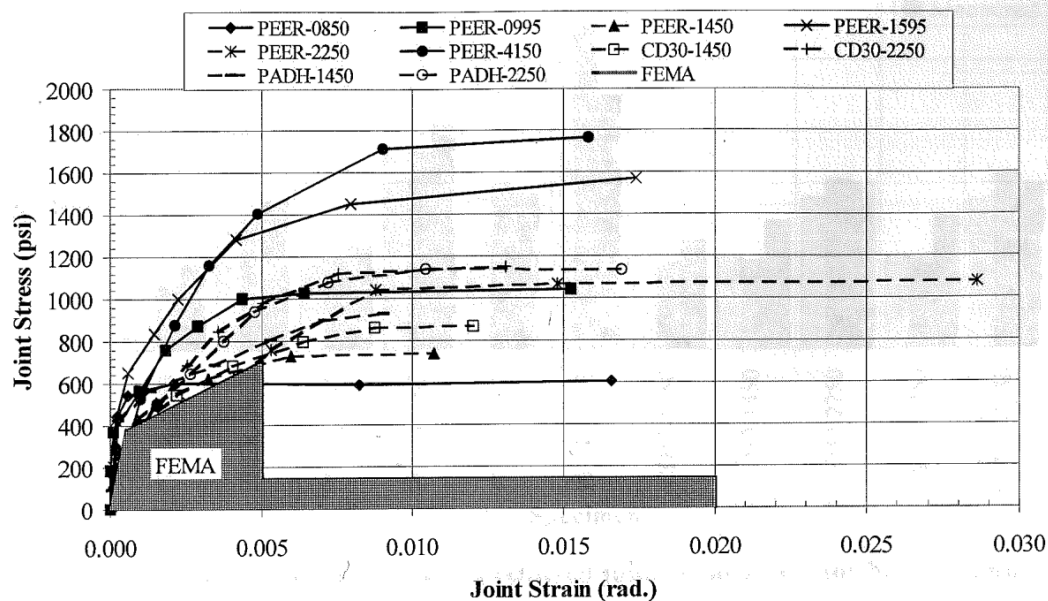


Figure C.2: Joint shear stress vs strain until 3% drift for tests by Walker (2001) and Alire (2002) of interior unreinforced joints with axial load of $\approx 0.1A_{gfc}$

It is clear from consideration of the data presented in Figure C.1 that the backbone curve presented in FEMA 356/ASCE 41 is significantly conservative. Further evidence supporting this statement can be seen in Figure C.3, which shows the stress-deformation response of other deficient beam-column joints. Similarly, it seems that the curve proposed by Sharma et al. (2011) is unduly conservative for forensic purposes. A backbone curve based on

consideration of the remaining four backbone curves has been developed and is presented in Figure C.4. It can be seen that this curve is similar to the curve presented by Weng Yuen (2010).

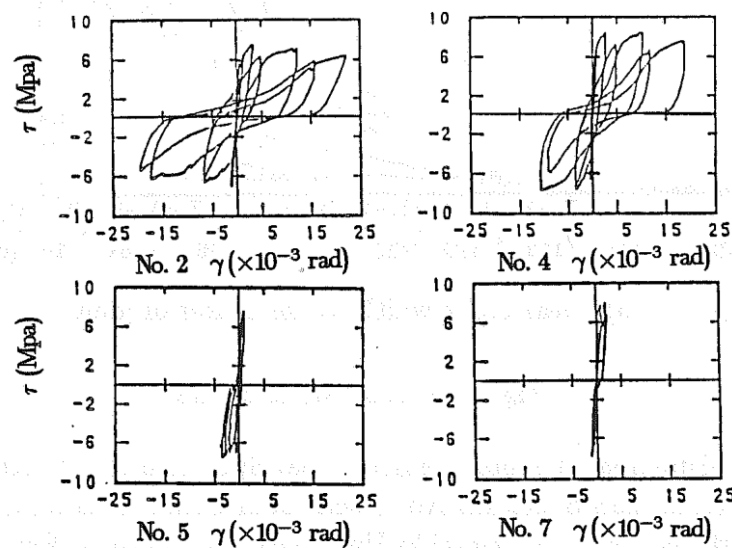


Figure C.3: Joint shear stress-deformation response of deficient beam-column joints (from Kurose 1987)

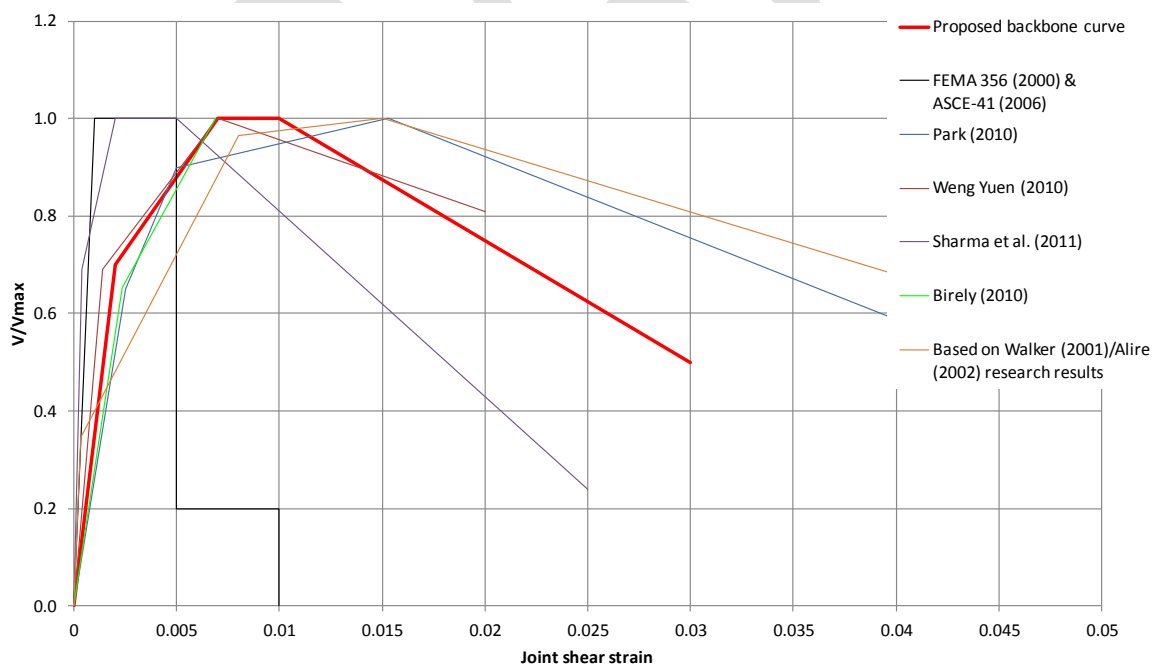


Figure C.4: Proposed backbone curve for joint deformation

Members of the Royal Commission Expert Panel have stated to Compusoft Engineering Limited that the provision of any “plasticity” in the backbone curve for the beam-column joints is unrealistic, as any such plasticity is a result of yielding of beams and/or columns.

Thus it is their opinion that strength decay should begin immediately following the development of peak joint strength, particularly if the joint is not strong enough to sustain yielding of the framing members. Compusoft Engineering Limited does not believe that this view is correct. Figure C.5 shows experimental behaviour of specimen PEER-4150 (Alire 2002; D. E. Lehman et al. 2004) with the proposed backbone curve overlaid. This joint was designed so that the joint shear strength should be exceeded prior to significant yielding of either beams or columns, with this being found to be the case during testing. Despite this it is evident that the stress resisted by the joint core remained essentially constant until quite large deformations were reached. In comparison, the proposed backbone curve appears to underestimate the ability of the joint core to resist stresses at large deformations.

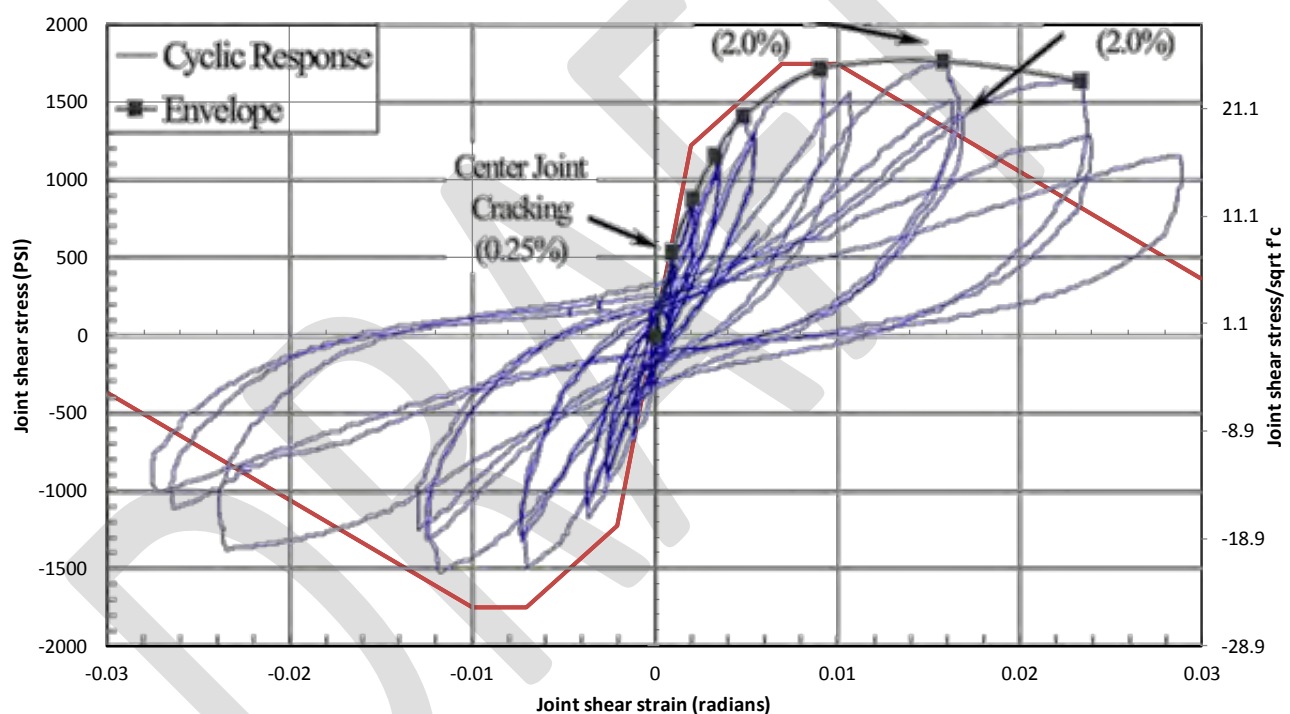


Figure C.5: Comparison of PEER-4150 (Alire 2002; D. E. Lehman et al. 2004) against proposed backbone curve

C.4 Definition of maximum joint shear strength

Two proposals for joint shear strength have been considered. These correspond broadly to the methods used in New Zealand and the U.S.A. for determination of deficient joint core strength.

The New Zealand method for determining joint core strength is based on checking that limiting values of joint principal tension and compression stresses are not exceeded (Hakuto

et al. 2000; NZSEE 2006; Priestley 1997; Weng Yuen 2010). The limits on the principal stresses are dependent on joint detailing, and whether the joint is of the interior or exterior kind. The method inherently leads to joint shear strength being dependent on column axial load.

In U.S. practice, joint shear strength is typically assumed to be independent of column axial load. The limiting joint shear stress is assumed to be proportional to the square root of concrete compressive strength. The constant relating joint shear strength and square root of concrete compressive strength is typically referred to as “ v ”, and its value is dependent on the type of joint (interior/exterior) and the presence of members framing into the joint on the orthogonal axes. Refinements of this method have recently been proposed by Park (2010), who suggested that joint aspect ratio affected shear strength.

Figure C.6 shows a comparison of the joint shear strength coefficient for interior joints according to U.S. practice, New Zealand practice, and with modification to U.S. practice based on the work of Park (2010). Figure C.7 shows similar data for exterior joints. It is clear that there is a marked difference between these strengths for interior joints. It is notable that Lehman et al. (2004) and Moehle (2006) have noted that the strengths given by ASCE 41 can be conservative by a factor of two, with coefficients as high as 25 being observed for interior joints. These observations support the method used in NZ practice as being more realistic, and for this reason this approach has been adopted for the analyses discussed in the body of the report. The approach taken has been based on determining appropriate limits for joint core principal tension and principal compression stresses. The limit value for the principal tension stress was calculated as $f_{tp,max} = k \sqrt{f'_c}$ (NZSEE 2006), with the value of k dependent on whether the joint was an interior or exterior joint and with the curvature ductility of the adjacent member being taken as zero (see Figure C.8). The limiting value for the principal compression stress in the joint core was taken as $f_{cp,max} = 0.5f'_c$ based on a recommendation made by Priestley (1997).

The principal tension and compression stresses existing in the joint core were calculated as $0.5f_a \pm \sqrt{(0.5f_a)^2 + (v_{jh})^2}$, where f_a is the column axial stress and v_{jh} is the horizontal joint shear stress. Consideration of the principal stresses shows that the joint shear stress required to cause tensile failure increases as the column axial compressive stress increases, while the

joint shear stress required to cause compression failure in the joint decreases as the column axial compressive stress increases.

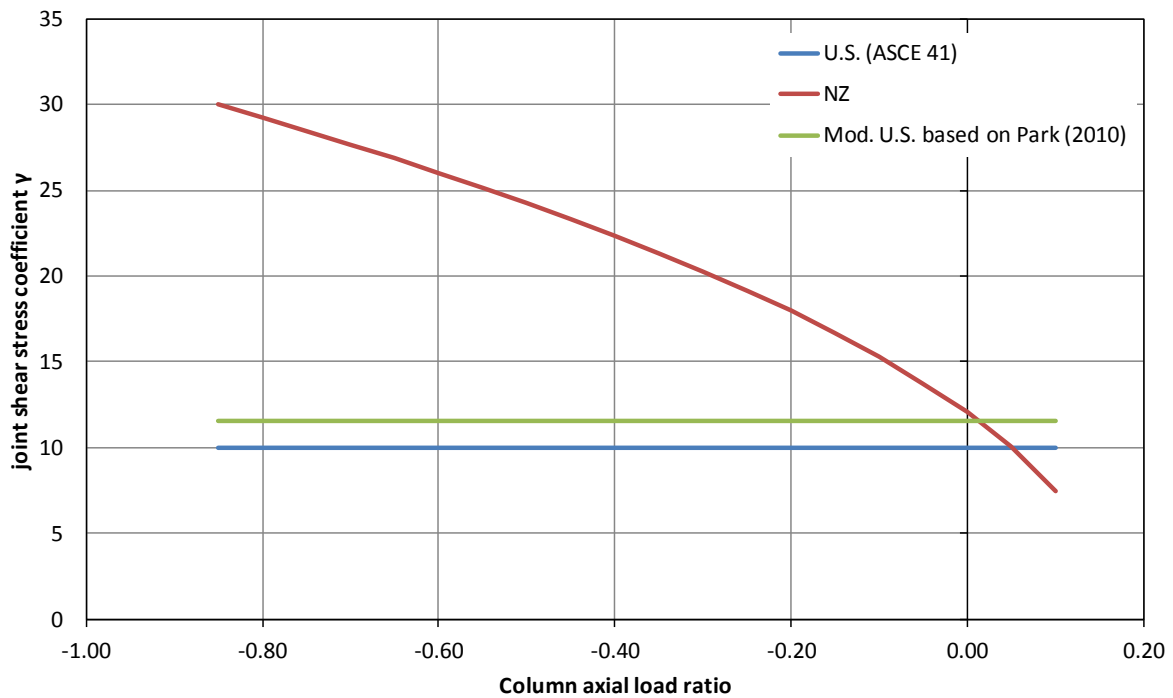


Figure C.6: Column axial load ratio against joint shear strength coefficient for interior joints

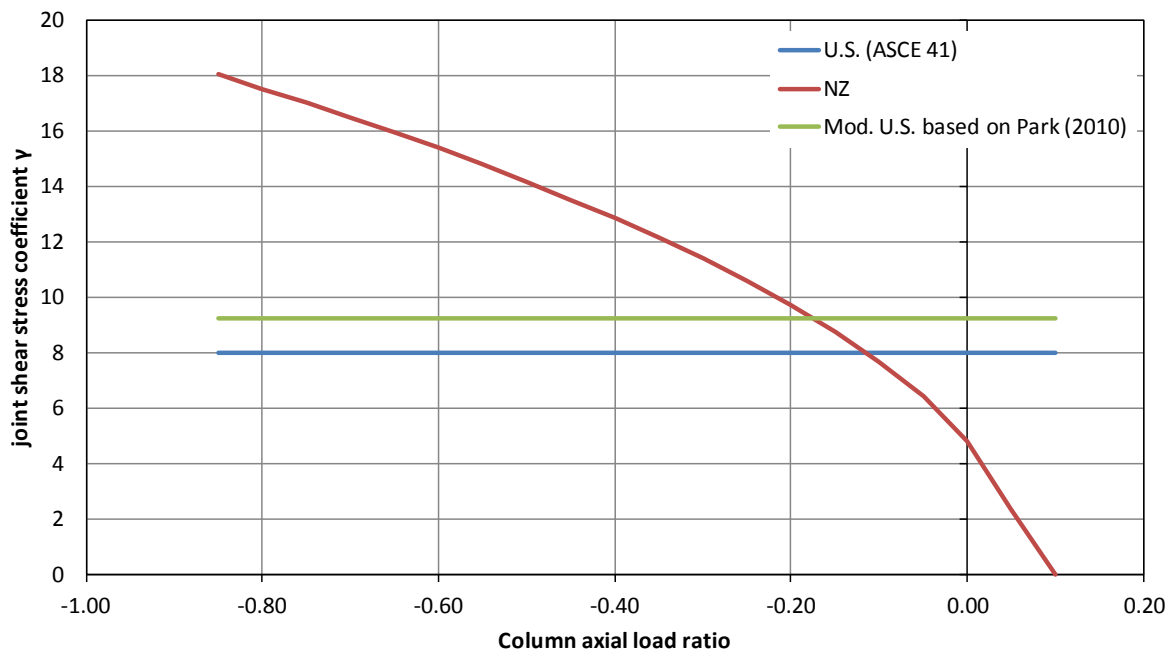


Figure C.7: Column axial load ratio against joint shear strength coefficient for exterior joints

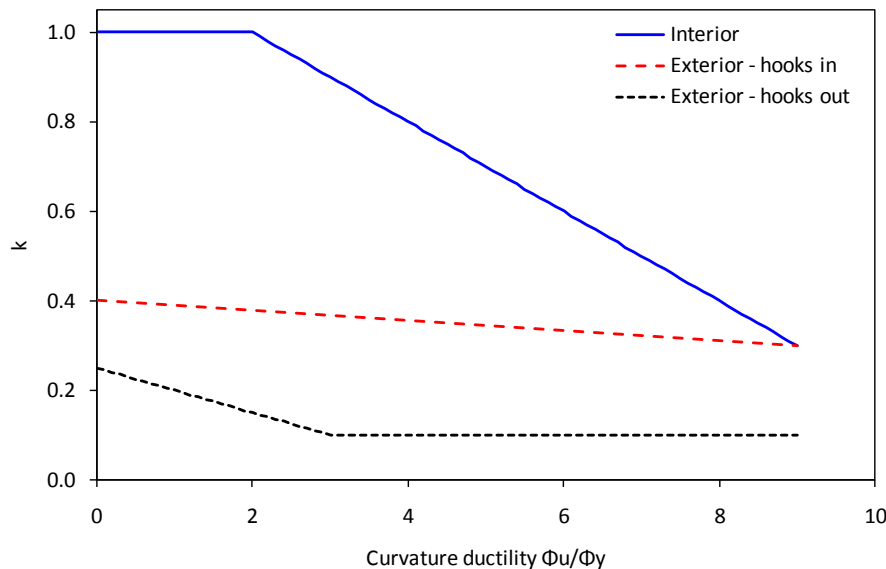


Figure C.8: Relationship of factor K to curvature ductility for different joint types (after NZSEE 2006)

A suggestion was made by members of the Royal Commission Expert Panel that a formulation for joint shear strength based on the Modified Compression Field Theory (“MCFT”, Vecchio and Collins 1986) or related approaches could be appropriate. Such an approach was not pursued due to the wide range of such formulations available, and the observation that MCFT models typically underestimate the strength of deficient beam-column joints (LaFave and Shin 2005; Mitra and Lowes 2007).

C.5 Issues and limitations of the adopted joint degradation implementation

Aside from the issues related to uncertainty of the actual behaviour of joints evident from the scatter of data in the literature, there are a number of limitations to the joint degradation behaviour implemented in the CTV Building finite element model. It is important that these limitations be considered when the output of the finite element model is being used to assess the probable behaviour of the structure.

C.5.1 Limitations of the method used to implement the joint shear spring

As stated in section C.2, the non-linear behaviour of beam-column joints has been implemented in the CTV Building analysis model through use of a moment-rotation spring, with behaviour determined by the sum of moments occurring at the node representing the beam-column joint. In reality, the stress generated in a beam-column joint is not a function of the moment at the joint centroid; rather the stress that develops is determined from the beam

and column internal flexural forces and shears. Accurate representation of this behaviour in a finite element model is challenging to achieve, as it would require implementation of an element with behaviour influenced by multiple spatially separated nodes (for example see Figure C.9).

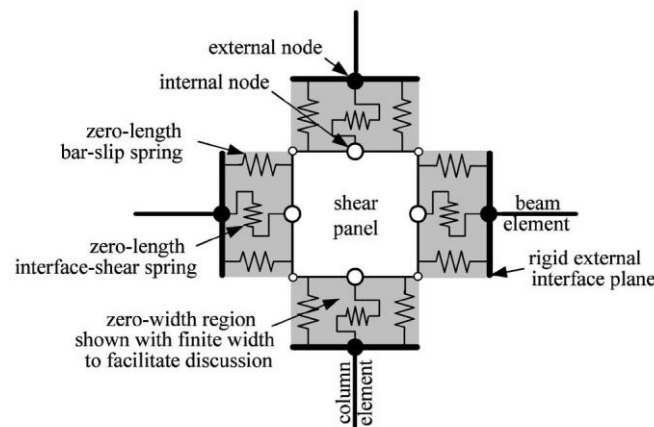


Figure C.9: Example of beam-column joint finite element model relying on inputs from multiple nodes (from Mitra and Lowes 2007)

Consideration was given to implementing a model of the type shown in Figure C.9, but the concept was ultimately not pursued for three reasons:

6. While implementation was considered possible, it was not felt that reliable calibration of the model could be achieved in the time available.
7. The addition of the required number of (non-linear) springs to the model would have prevented completion of the required analyses in the available timeframe.
8. Extension of the model shown to accommodate three-dimensional joints was not reported in literature reviewed by Compusoft Engineering Limited.

The implemented model avoids the difficulties outlined above by calibrating the moment-rotation spring to represent the shear stress-deformation response using calculations outlined in Appendix C.6. However, this process introduces other limitations due to the number of assumptions inherent in the outlined calculations. Principle amongst these is the assumption of equal beam and column moments and shears on opposite sides of the joints (see Figure C.10). While appropriate for typical laboratory test specimens, this assumption are clearly not usually correct in a complete structure. The effect of the assumption made will generally be to overestimate the demands placed on the beam-column joint. The calculations shown in Appendix C.6 are also based on an assumption of equal member spans above and below and

to either side of the joint; this limitation has been mitigated for the implementation used in the final analysis model by conducting the calibration of the spring using more complex calculations accounting for different member lengths at each side of the joint core.

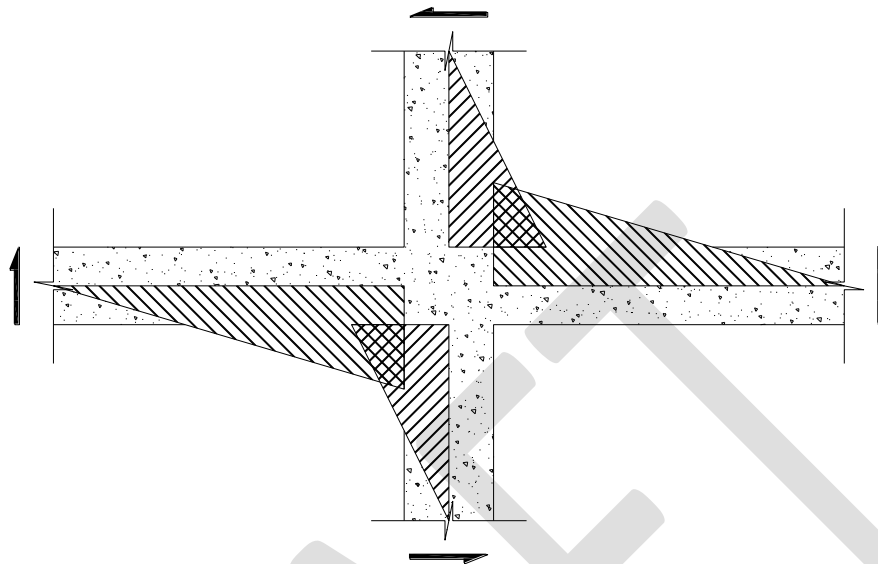


Figure C.10: Moment diagram assumed for development of joint spring

C.5.2 Geometry of the exterior beam-column joints

The consequences of shear failure are generally considered to be more serious for exterior joints than for interior joints, and the strength of exterior joints is generally lower than the strength of interior joints. Both of these points are largely due to the propensity for a wedge of concrete to dislodge from the rear side of the joint after cracking of the joint has occurred and as shown in Figure C.11. The dislodgement of this wedge is liable to result in loss of column axial load capacity.

The strengths of the exterior joints of the CTV Building have been calculated on the basis that their geometry is superficially similar to that shown in Figure C.11, with an inherent assumption that the rear face of the joint (opposite the beam) is relatively poorly confined and prone to dislodgement. However, for many of the joints this assumption is not accurate. As shown in Figure C.12 many of the exterior joints of the CTV Building in fact have a significant volume of concrete located at the rear face of the joint core, with this concrete extending a significant distance beyond the column cross section. This concrete could be expected to provide additional confinement to the rear side of the joint core, and would hence

be likely to enhance the strength of the joint core. This effect has not been accounted for in the analyses undertaken.

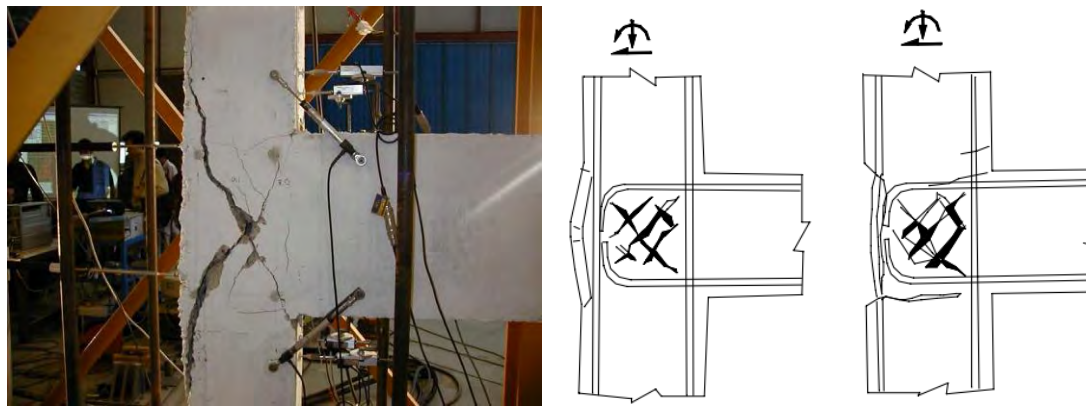


Figure C.11: Damage of exterior joint (left) observed during testing and (right) illustrated schematically (from Pampanin et al. 2002)

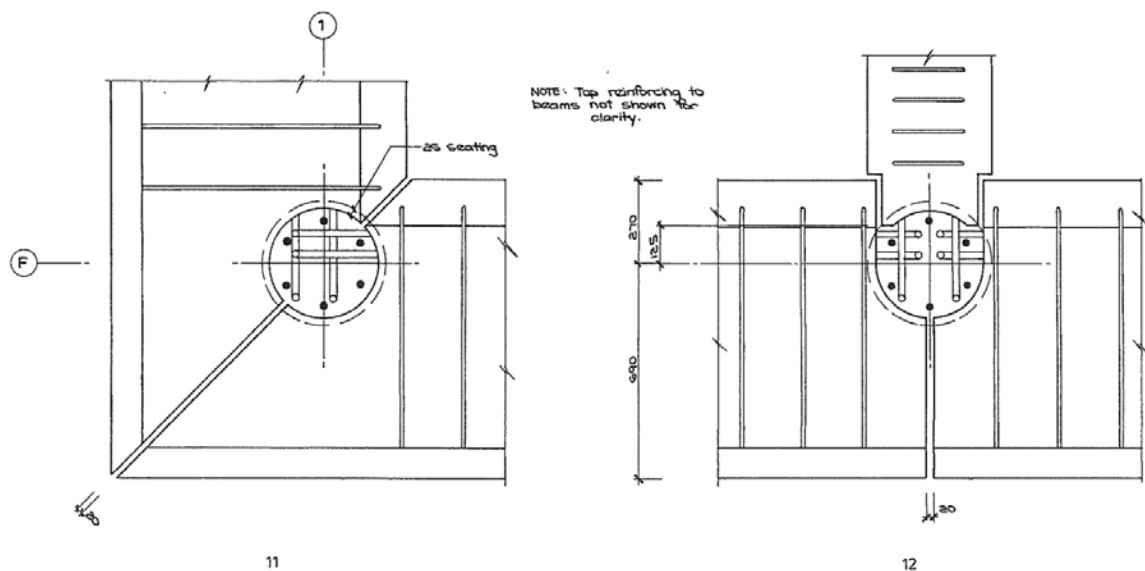


Figure C.12: Plan views of CTV Building exterior joints (Design Engineer 1986a)

C.5.3 Relationship of joint strength and deformation characteristics to deformation imposed on adjacent members

A further complexity is added to definition of the strength of deficient beam-column joints because it is acknowledged in the literature that the strength is not in fact a unique value dependent only on joint core properties (dimensions, concrete strength etc.). Rather, the strength is also dependent on the plastic deformation of the members framing into the beam-column joint (Hakuto et al. 2000; D. E. Lehman et al. 2004; Priestley 1997). The significance of this relationship can be seen in Figure C.13, which indicates that the joint shear capacity of

interior joints drops by 60% as the curvature ductility imposed on the adjacent members is increased from two or less to nine.

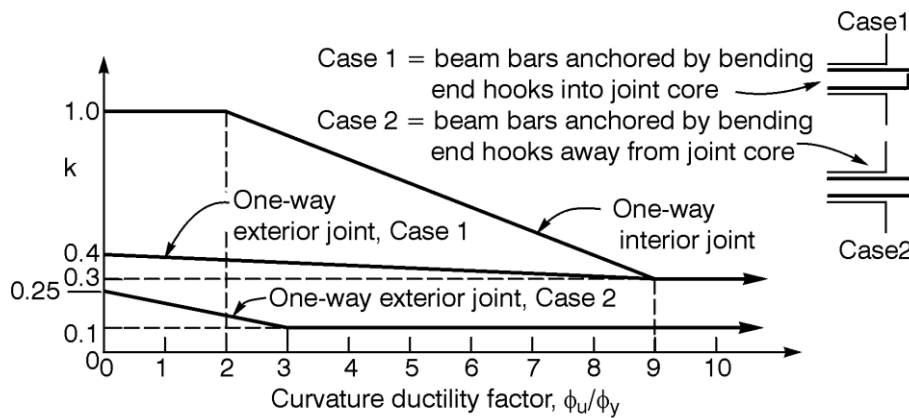


Figure C.13: Relationship between joint shear capacity and framing member curvature ductility (from NZSEE 2006)

The joint model implemented in the CTV Building model does not implement this relationship between member curvature and joint capacity. While technically achievable, the behaviour was not included based on concerns similar to those listed in section C.5.1 that guided the decision not to use a multi-node joint model.

C.6 Calculations showing basis for relating joint moment to shear stress for modelling purposes

COMPUSOFT
ENGINEERING

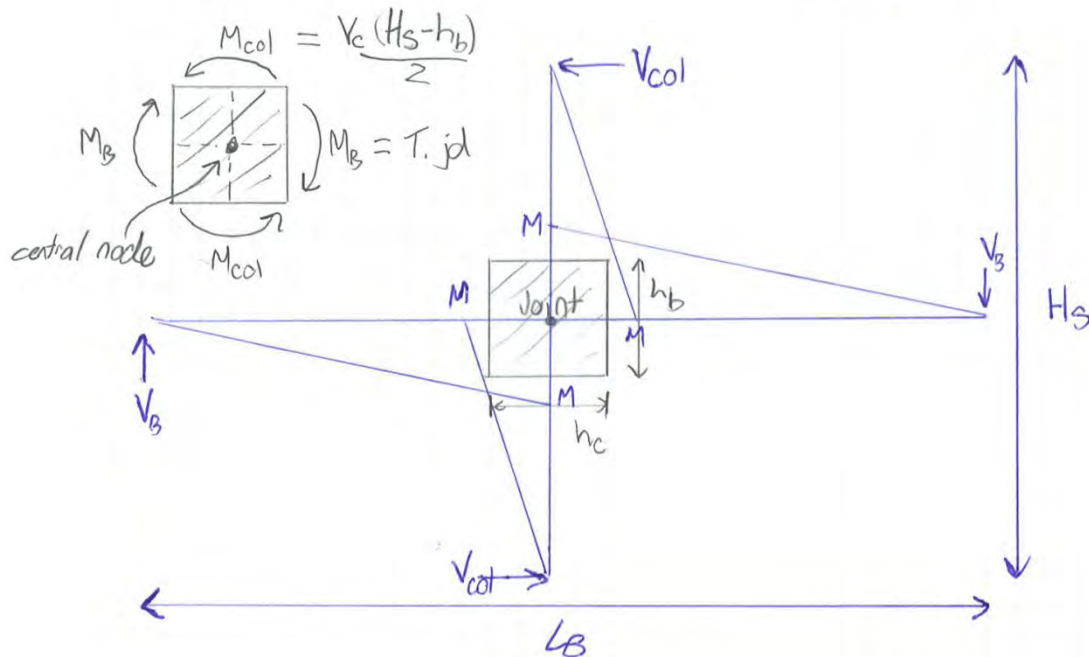
Project: CTV Joints

Date: 19/06 Page: 1

CALCULATIONS

Section:

By: NJB Checked:



Report joint capacity as moment resistance at central node
- ie '2M'

Joint capacities based on principal stresses are calculated
as V_{jh} (horizontal joint shear capacity)

First consider conversion between:

$$V_{jh} = 2T - V_{col}$$

$$T = \frac{M_B}{jd} = \frac{M_{col}}{jd} \cdot \frac{H_s}{L_B} \cdot \frac{L_B - h_c}{H_s - h_b} = \frac{V_{col} H_s}{2jd L_B} (L_B - h_c)$$

$$\therefore V_{jh} = V_{col} \left(\frac{H_s (L_B - h_c)}{L_B \frac{jd}{2}} - 1 \right)$$

COMPUSOFT
ENGINEERING

Project: CTV Joints

Date: 19/06 Page: 2

CALCULATIONS

Section:

By: NJB Checked:

$$\begin{aligned} \text{Now, } 2M &= V_{col} H_s \\ \text{substituting } V_{col} &= \frac{2M}{H_s} \\ V_{jh} &= \frac{2M}{H_s} \left(\frac{H_s}{L_B} \left(\frac{L_B - h_c}{jd} - 1 \right) \right) \\ 2M &= \frac{V_{jh}}{\frac{L_B - h_c}{L_B jd} - \frac{1}{H_s}} \end{aligned}$$

For CEL example plots, dimensions taken were:

$$L_B = 7000 \text{ mm} \quad H_s = 3240 \text{ mm}$$

$$h_c = 400 \text{ mm} \quad jd = 445 \text{ mm}$$

$$\text{therefore } 2M = 0.553 V_{jh} \quad (\text{KN-m})$$

Appendix D Hook anchor capacity

The method of construction used for the CTV building required that the bottom reinforcement of the beams typically be terminated at each column, with reinforcement being hooked into the joint at these locations. Based on engineering drawings (see Figure D.1) the hook length for either H28 or H24 bars from the column face was approximately 275 mm. Similar conditions applied for anchorage of top steel into corner columns. The hook length provided is not adequate to develop the full strength of the reinforcement according to the provisions of the New Zealand Concrete Structures Standard (NZS 3101 2006). Assuming the joint core concrete strength was 25 MPa (i.e. that the beam-column joint was poured at the same time as the floor slab and the upper parts of the beams) and the yield strength of the HD28 reinforcing bars was 448 MPa, the hooked development length required by NZS 3101:2006 would be $L_{dh} = 602$ mm (cl. 8.6.10.3.1) if the beam was to be designed with a ductile hinge adjacent to the columns face. This hook length would be required to be placed the lesser of $8d_b$ or $0.5h_c$ from the column face (cl. 9.4.3.2), which in this case is 200 mm from the face. Thus the total anchor length inside the joint would need to be at least 800 mm to sustain ductile yielding of the beam steel.

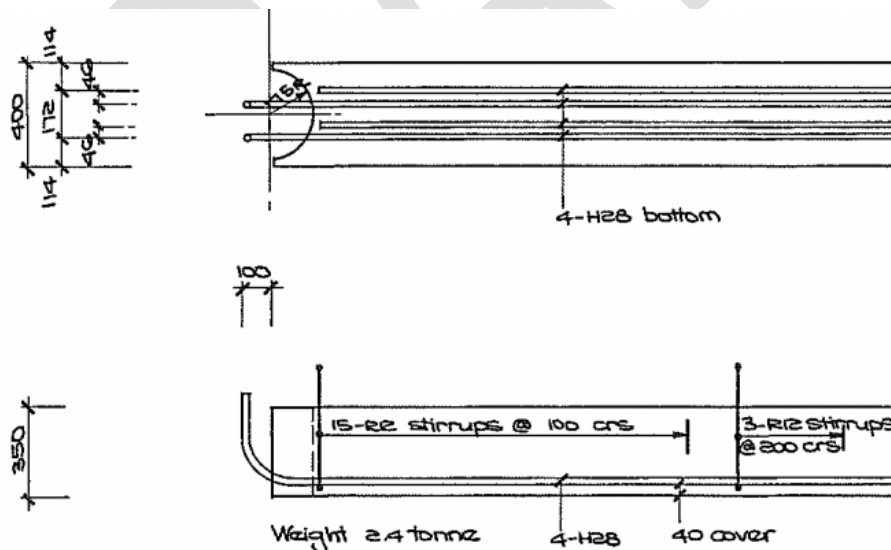


Figure D.1: CTV building hook detail (Design Engineer 1986b)

The behaviour of the CTV Building hook anchorages has been assessed by post-processing of data from the analysis model. Capacities of the anchorages have been determined based on work published by Joh et al. (Joh and Shibata 1996; Joh et al. 1993). Joh et al. identified three failure modes for hooked anchorages, namely side splitting, local compression failure at the bar bend, and “raking-out” failure or pullout of the entire bar group (see Figure D.2). Based

on experimental tests they suggest a method for determining the capacity of hooks based on raking-out failure. According to their method the anchor strength is dependent on the column axial force, the embedment length, and the amount of joint core reinforcement. The assessment method suggests significant bar anchorage can be expected even when hook lengths are severely deficient according to NZS 3101:2006. For example, calculation indicates that the CTV beam bar anchorages could develop the yield strength of the beam reinforcement providing the column axial load on a circular column exceeded 265 kN compression.

Consideration has not been given to the potential for “side split” failure in the CTV Building joints due to a lack of guidance on how to determine the side split strength for circular columns. Preliminary calculations have been undertaken to determine whether local compression failure at the inside of the hooked anchor would be expected. The procedures of NZS 3101:2006 cl.8.4.2.1 indicate that prevention of local crushing at the inside of the hook would require a bend radius of approximately 250 mm, which is smaller than the bend radius provided. It therefore seems reasonable to assume localised crushing at the inside of the hooks was not likely.

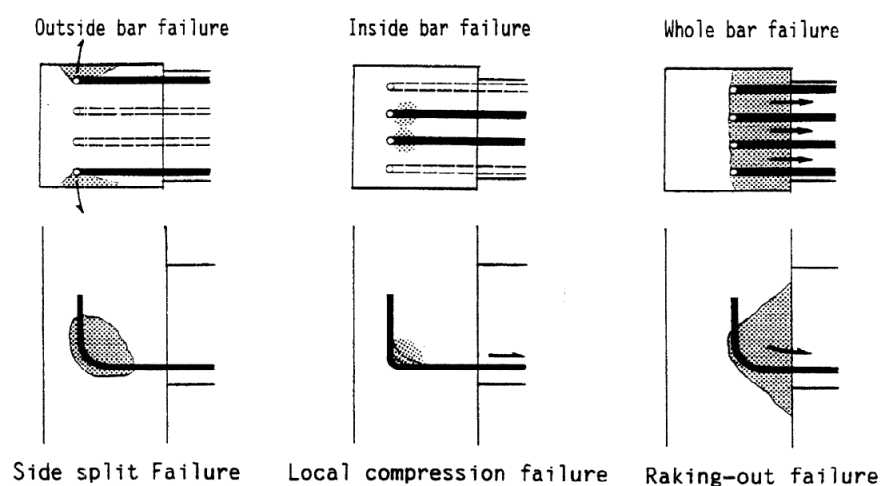


Figure D.2: Hooked anchorage failure modes (from Joh and Shibata 1996)

Appendix E Foundation Modelling Properties

Figure E.1 below shows the foundation stiffness information used as the basis of the CTV analysis model representation of the foundations.

CTV BUILDING FOUNDATION SPRING STIFFNESS

31/05/2011 16:02

Most likely values

Shear wave velocity:

Stiff area 300 m/s
Soft area 200 m/s

Shear modulus:

Stiff area 162.00 MPa
Soft area 70.00 MPa

Density:

Stiff area 1800 kg/m³
Soft area 1750 kg/m³

Poissons Ratio:

Stiff area 0.3
Soft area 0.4

Footing type	B (m)	L (m)	D (m)	L/B	D/B	Depth factor	Barcan: β_s	Spring (MN/m ³)	Comment
1	4	4	1	1.00	0.25	1	2.12	122.71	
1a	4.5	4.5	1	1.00	0.22	1.2	2.12	130.89	
1b	4.5	4.5	1	1.00	0.22	1.2	2.12	65.98	Soft area
2	7.3	7.7	1.8	1.05	0.25	1.3	2.13	85.40	
2a	5.4	7.7	1.8	1.43	0.33	1.35	2.18	53.14	Soft area
3	3.3	5.8	1	1.76	0.30	1.33	2.22	117.22	
3a	3.3	5.8	1	1.76	0.30	1.33	2.22	78.59	Soft area
4	2.5	9.8	1	3.92	0.40	1.4	2.44	159.69	
4a	2.5	12.5	1	5.00	0.40	1.4	2.53	73.94	Soft area
5	3	21.6	1	7.20	0.33	1.35	2.69	104.35	
6	1.7	20	1	10.00	0.59	1.5	2.87	185.42	

Figure E.1: Expected Soil Stiffness (Sinclair 2011)

Appendix F Acceleration Time History Records.

F.1 Darfield CBGS

Christchurch Botanical Gardens (CBGS) time history records (Geonet 2010b) used to determine the structural response for the Darfield event are presented in Figure F.1 below.

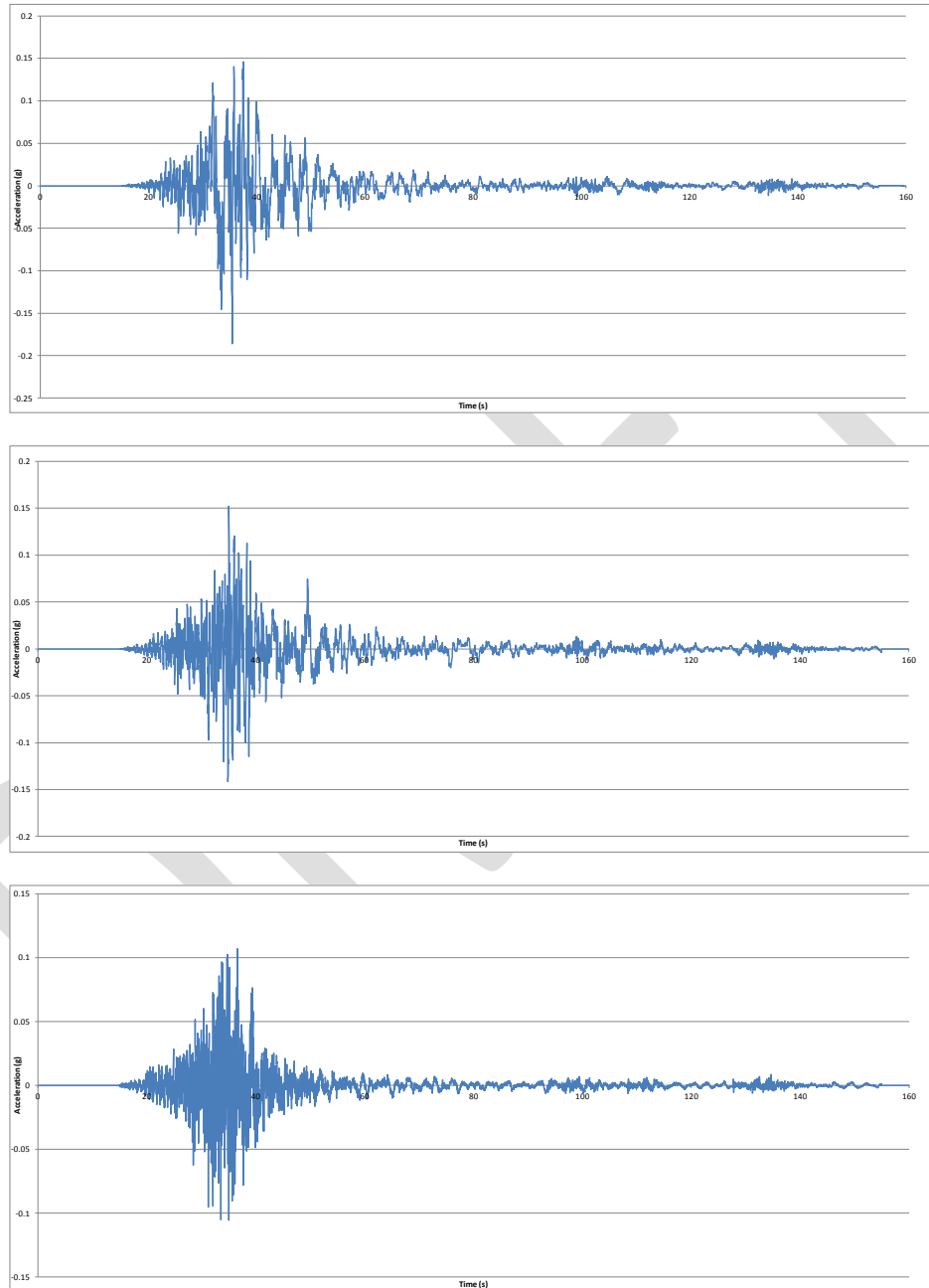


Figure F.1: Darfield 20100903_163541_CBGS N00E (top), N90E (middle), and Vertical (bottom) acceleration time history record plots

F.2 Darfield CCCC

Christchurch Cathedral College (CCCC) time history records (Geonet 2010b) used to determine the structural response for the Darfield event are presented in Figure F.1 below.

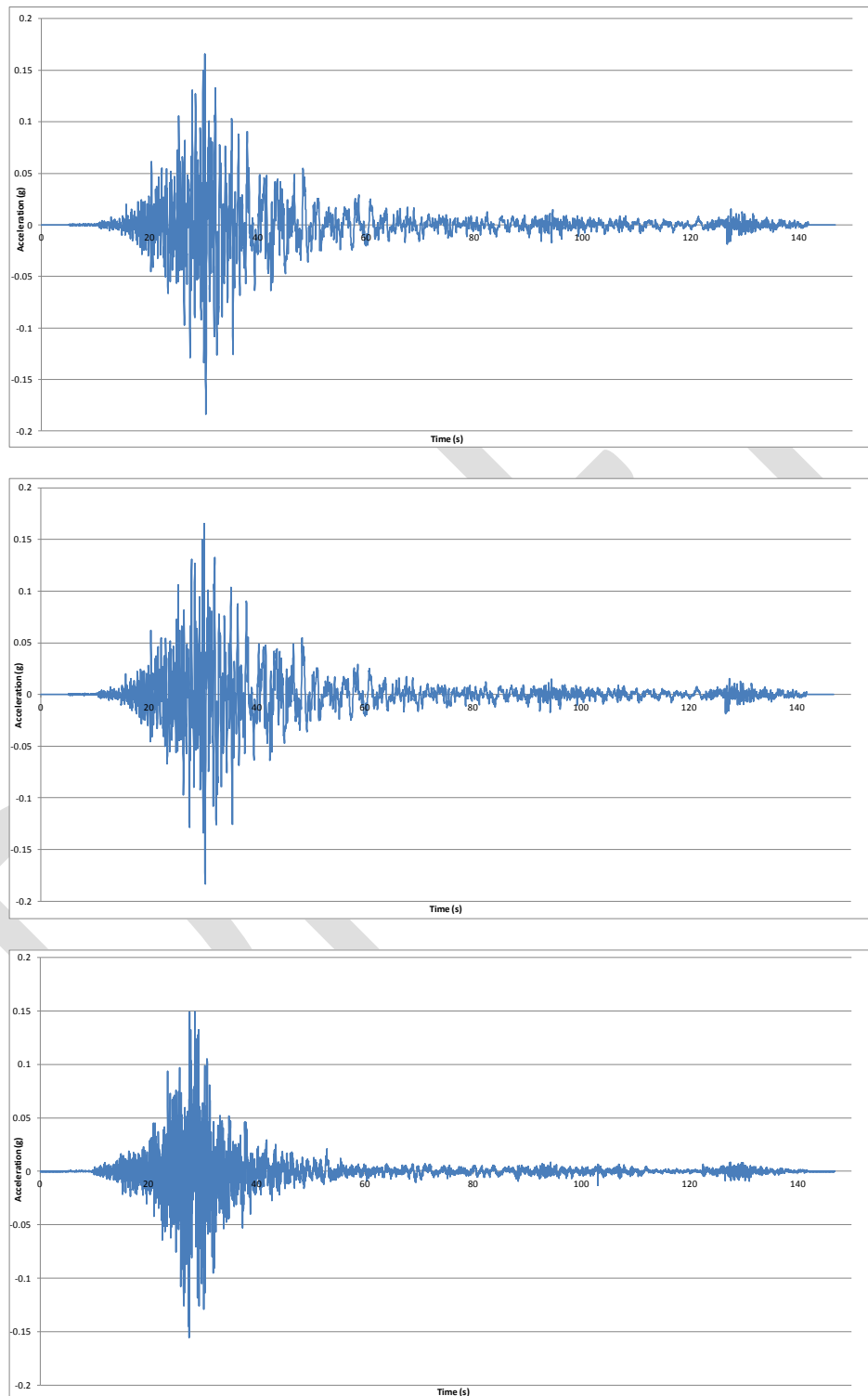


Figure F.2: Darfield 20100903_163541_CCCC N00E (top), N90E (middle), and Vertical (bottom) acceleration time history record plots

F.3 Lyttelton CBGS

Christchurch Botanical Gardens (CBGS) time history records (Geonet 2011b) used to determine the structural response for the Lyttelton aftershock are presented in Figure F.3 below.

DRAFT

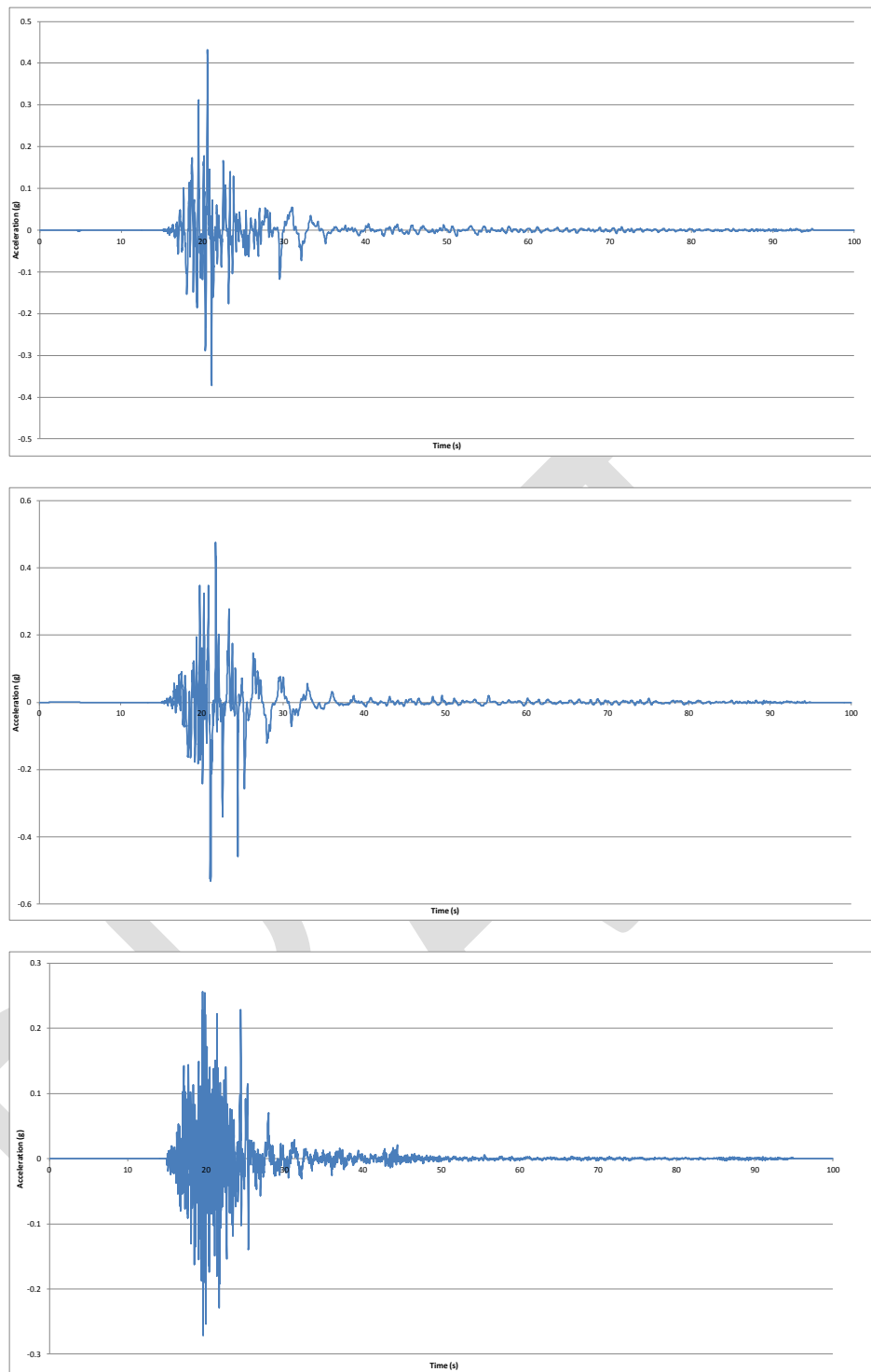


Figure F.3: Lyttelton 20110221_235142_CBGs N00E (top), N90E (middle), and Vertical (bottom) acceleration time history record plots

F.4 Lyttelton CCCC

Christchurch Cathedral College (CCCC) time history records (Geonet 2011b) used to determine the structural response for the Lyttelton aftershock are presented in Figure F.4 below.

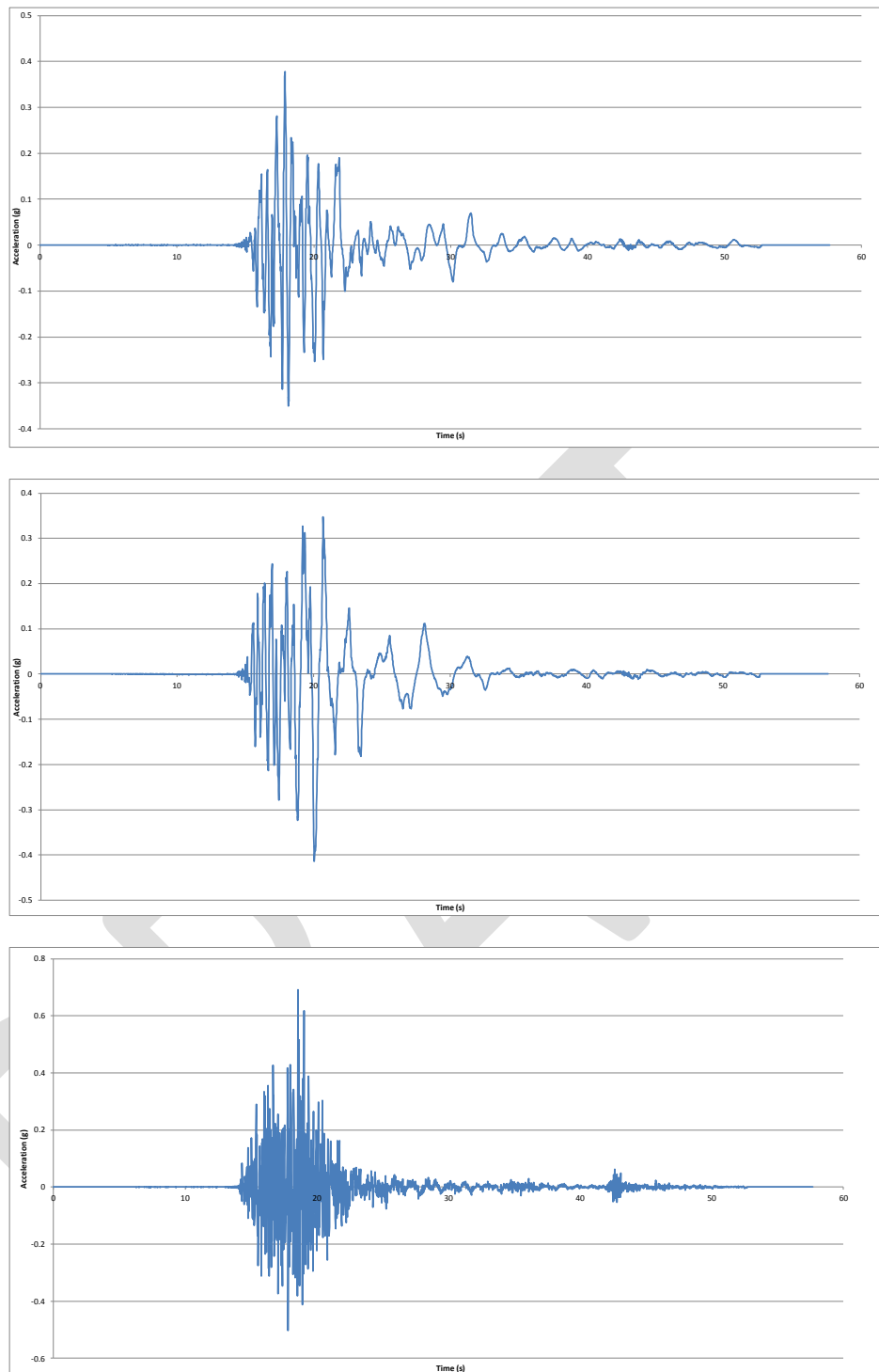


Figure F.4: Lyttelton 20110221_235142_CCCC N00E (top), N90E (middle), and Vertical (bottom) acceleration time history record plots

F.5 Lyttelton CHHC

Christchurch Hospital (CHHC) time history records (Geonet 2011b) used to determine the structural response for the Lyttelton aftershock are presented in Figure F.5 below.

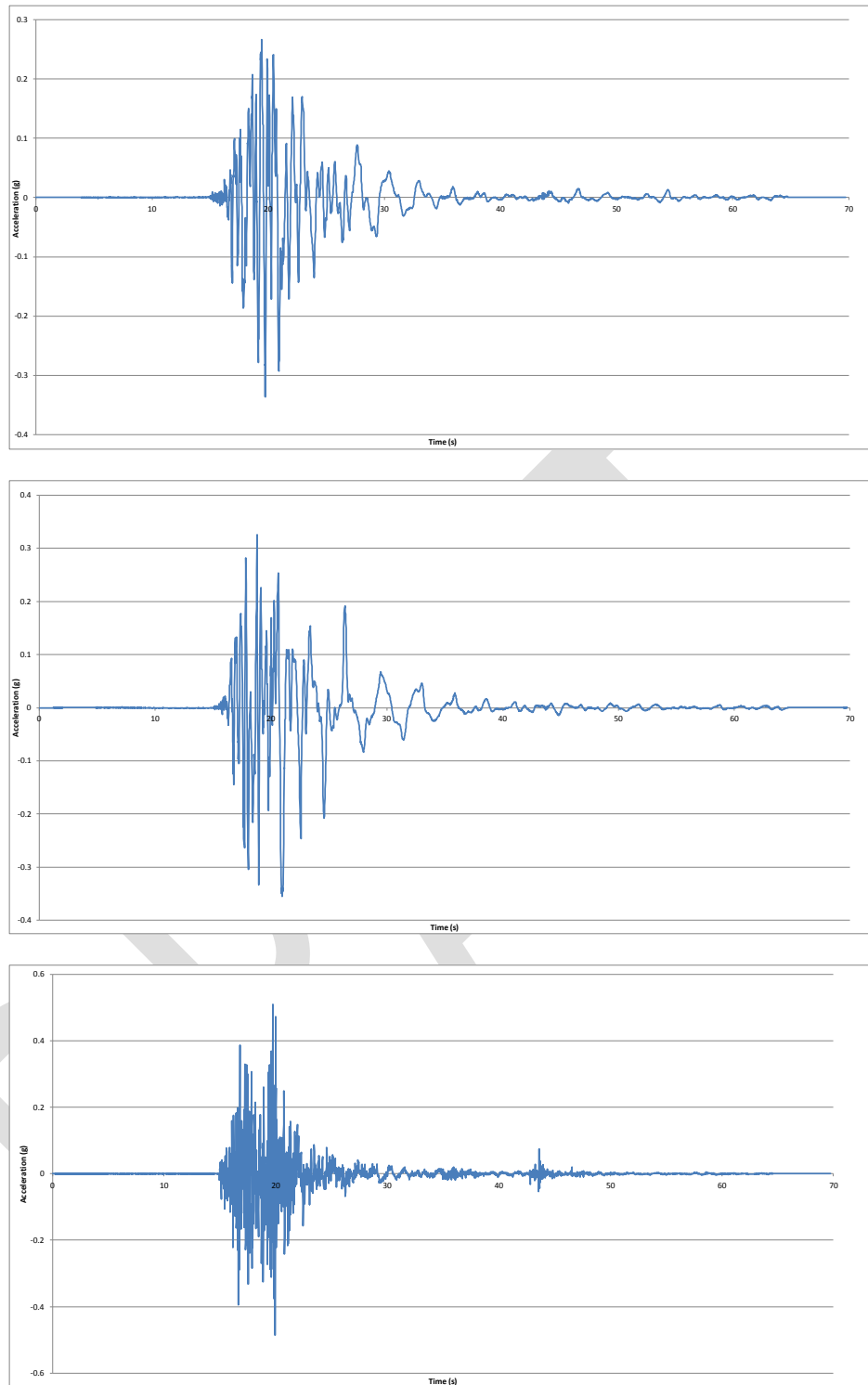


Figure F.5: Lyttelton 20110221_235142_CHHC N00E (top), N90E (middle), and Vertical (bottom) acceleration time history record plots

F.6 Lyttelton REHS

Resthaven (REHS) time history records (Geonet 2011b) used to determine the structural response for the Lyttelton aftershock are presented in Figure F.5 below.

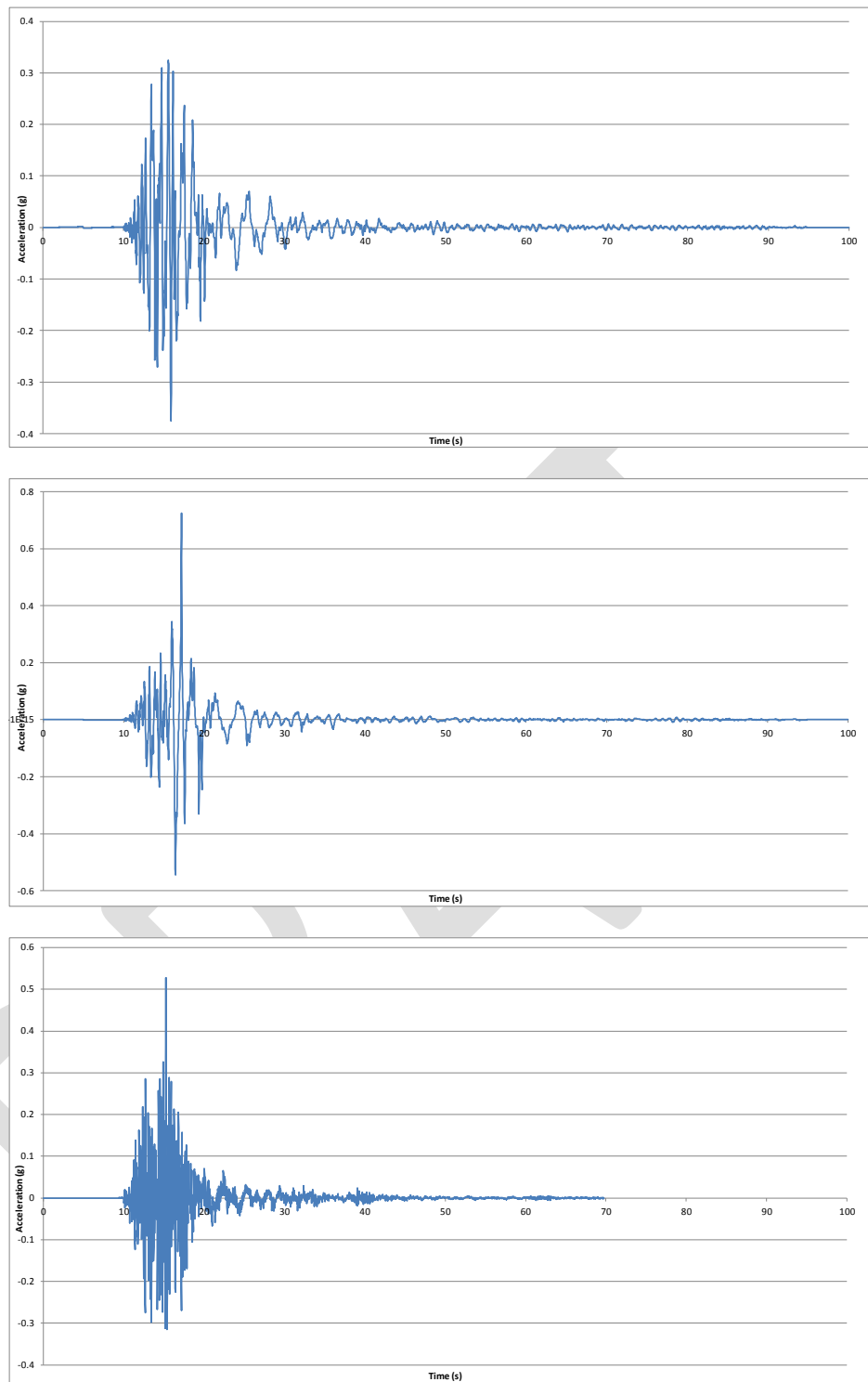


Figure F.6: Lyttelton 20110221_235142_REHS N00E (top), N90E (middle), and Vertical (bottom) acceleration time history record plots

Appendix G Analysis Results - Darfield Event: CBGS Record

The following details the structural actions reported by the analysis as a function of time, for the Darfield event using the acceleration time history recorded at the CBGS station using all components of the record.

G.1 Building Displacements and Drifts.

Building Level 6 displacements are presented in Figure G.1 and Figure G.2 below for the Southeast and Northwest corners of the building respectively.

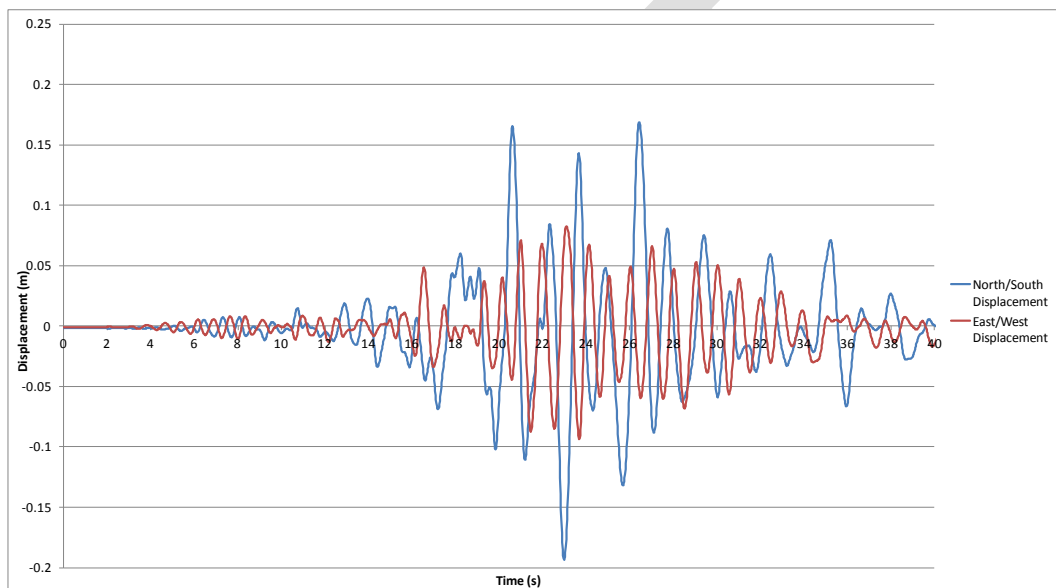


Figure G.1: Level 6 Southeast corner displacements, Darfield, CBGS

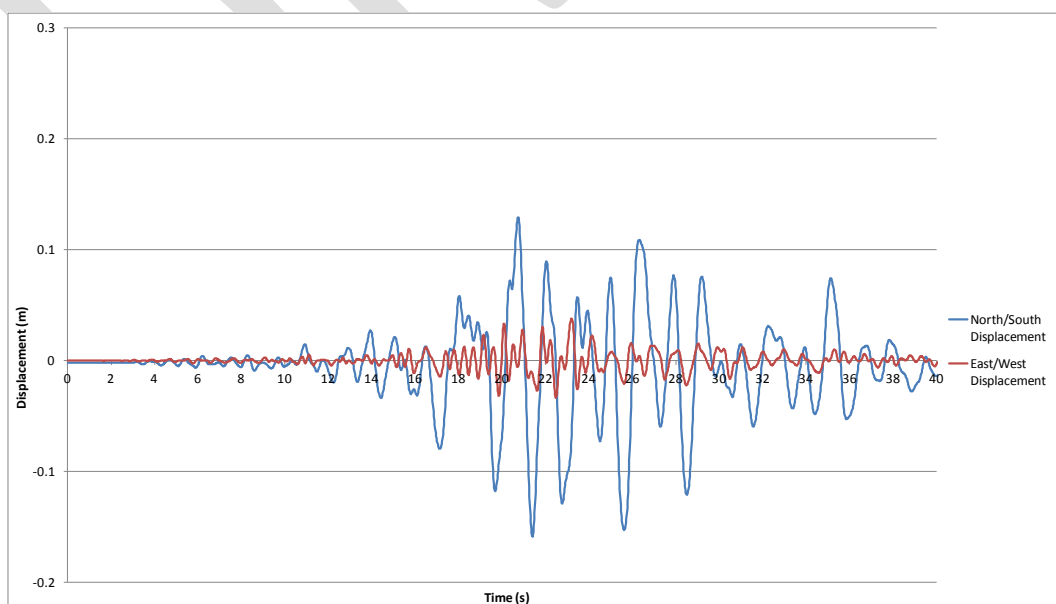


Figure G.2: Level 6 Northwest corner displacements, Darfield, CBGS

As can be seen in Figure G.1 and Figure G.2 the predominant building displacements are in the north/south direction. No drag bars are predicted to fail under the CBGS demands (assuming an upper bound drag bar capacity). Table G.1 presents the sequence of failure of the north core wall ties throughout the record.

Table G.1: Wall D and D/E diaphragm disconnection times, Darfield, CBGS

Level	Wall D Failure (sec)	Wall D/E Failure (sec)
6	No disconnection	No disconnection
5	No disconnection	No disconnection
4	No disconnection	No disconnection

Inter-storey displacements for the perimeter frame lines A and F in the north/south direction are presented in Figure G.3, and Figure G.4 below.

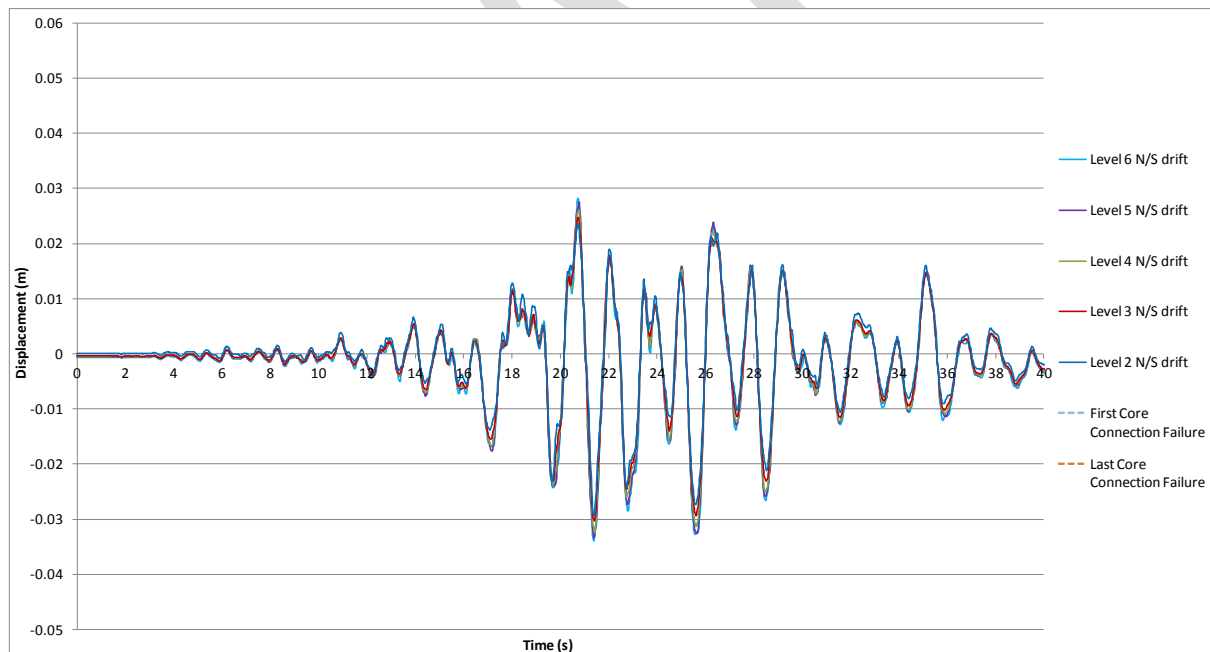


Figure G.3: Frame A north/south inter-storey displacements, Darfield, CBGS

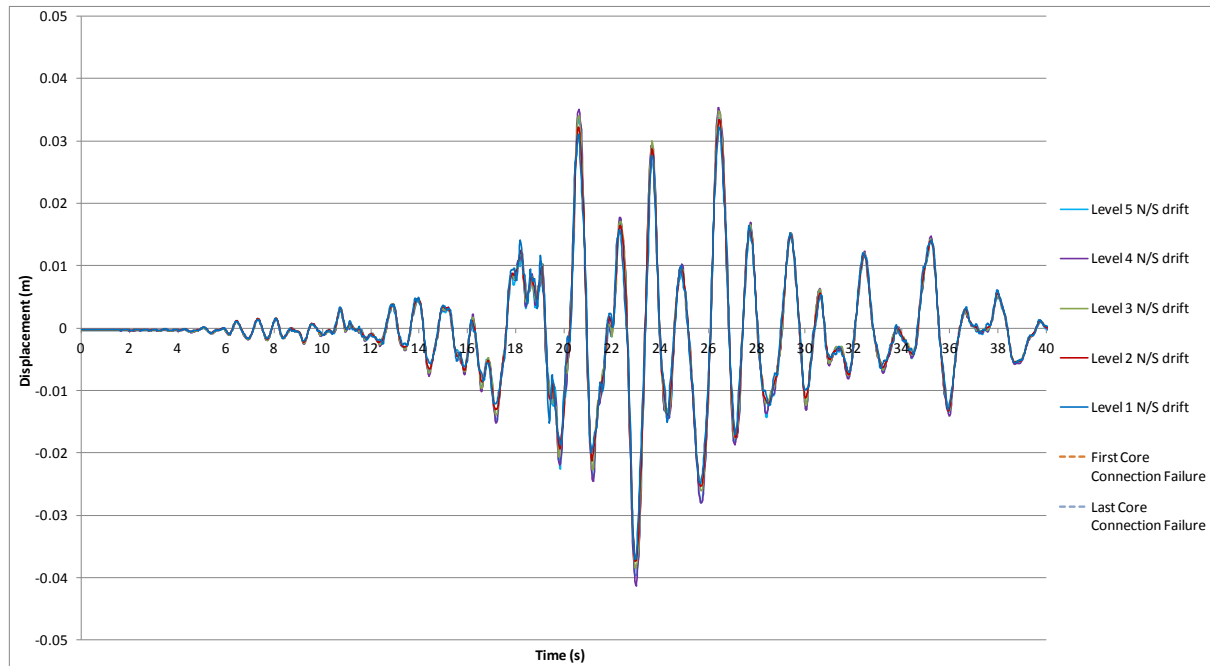


Figure G.4: Frame F north/south inter-storey displacements, Darfield, CBGS

Inter-storey displacements for the perimeter frame lines 1 and 4 in the east/west direction are presented in Figure G.5, and Figure G.6 below.

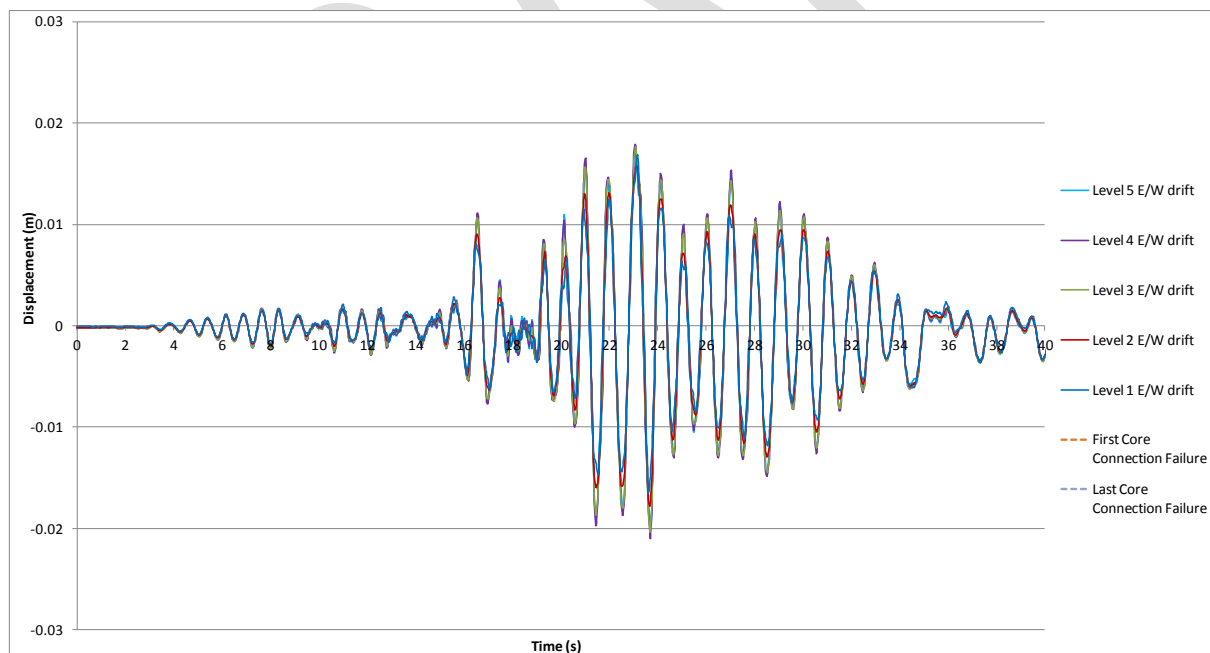


Figure G.5: Frame 1 east/west inter-storey displacements, Darfield, CBGS

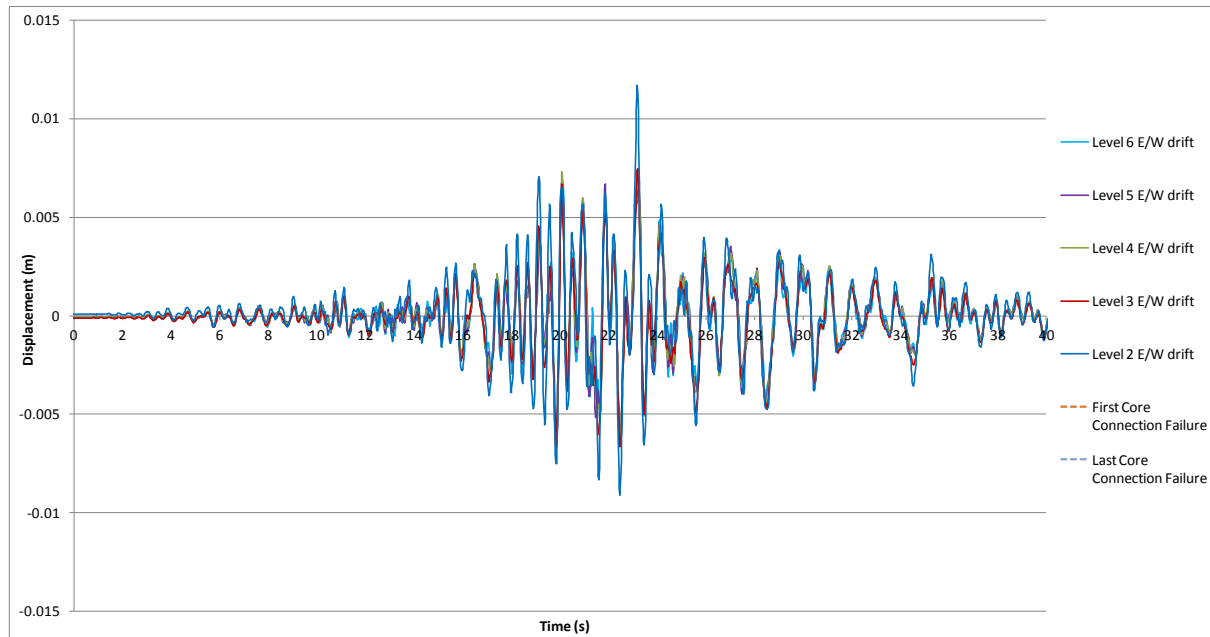


Figure G.6: Frame 4 east/west inter-storey displacements, Darfield, CBGS

G.2 Diaphragm Connection Forces

Diaphragm connection forces are presented in Figure G.7 to Figure G.18 below. Note that moments are reported about the geometric centroid of the element being considered.

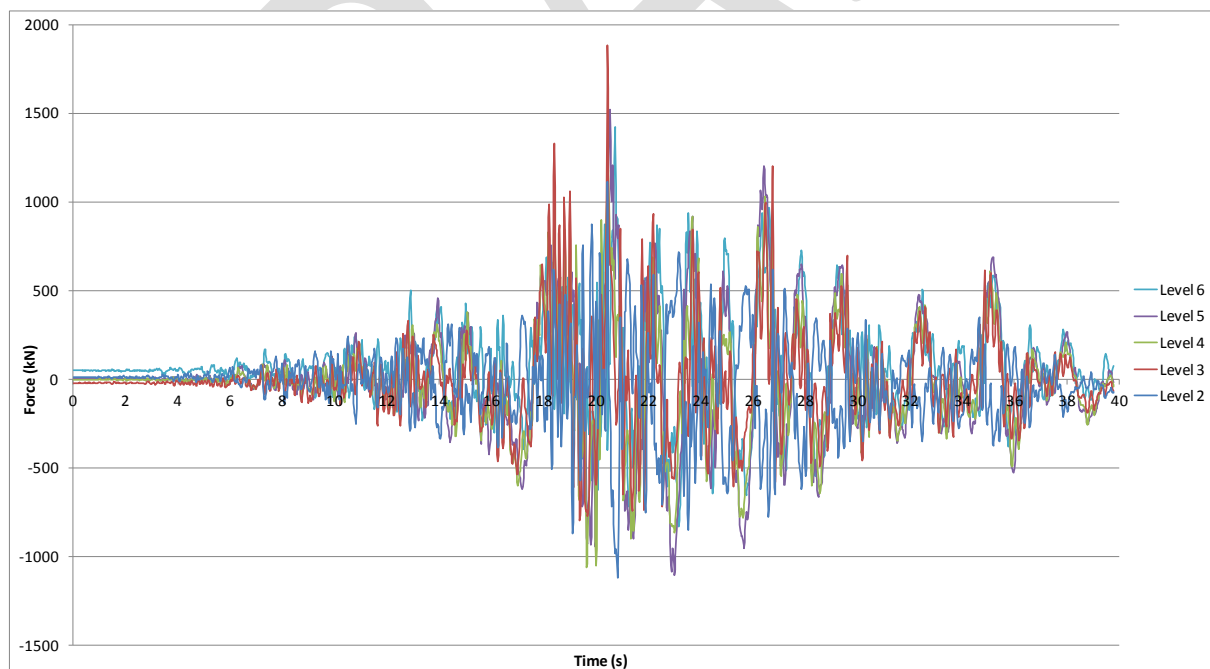


Figure G.7: North core total diaphragm north/south actions, Darfield, CBGS

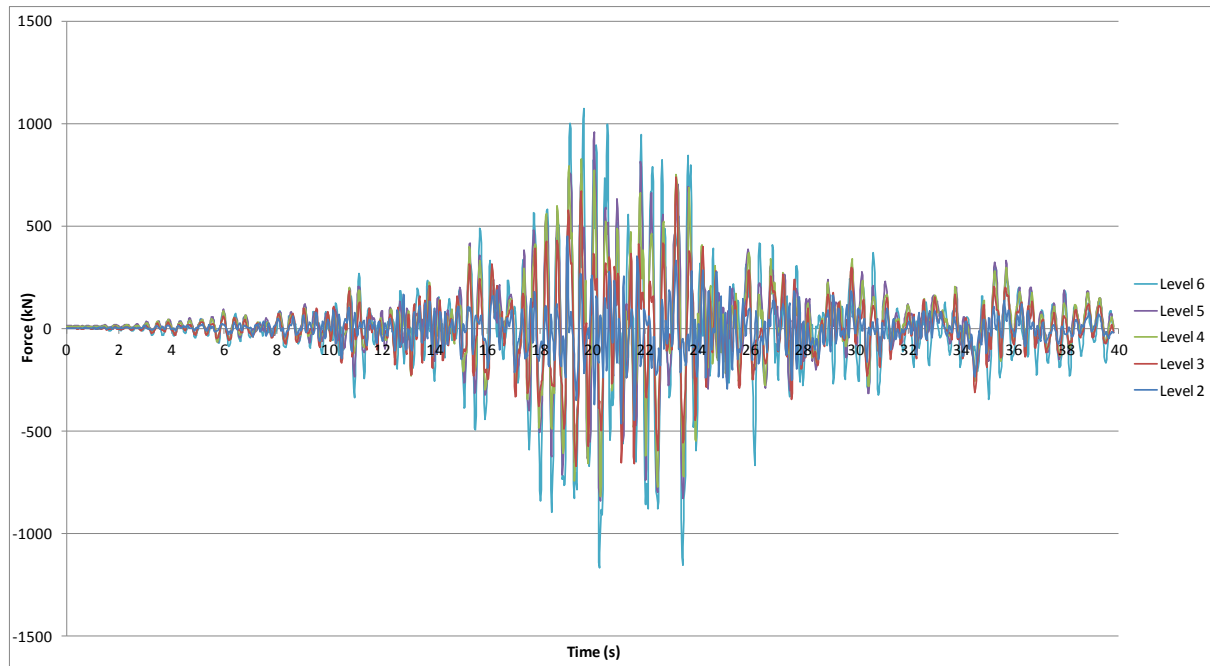


Figure G.8: North core total diaphragm east/west actions, Darfield, CBGS

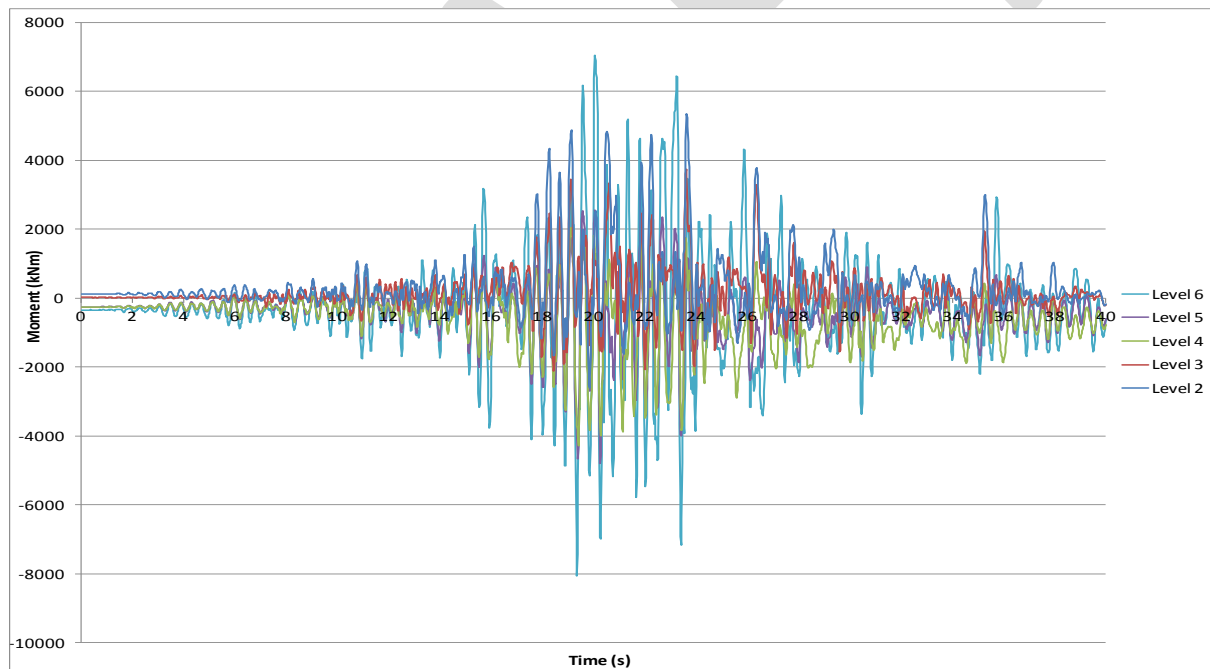


Figure G.9: North core total diaphragm in-plane moments, Darfield, CBGS

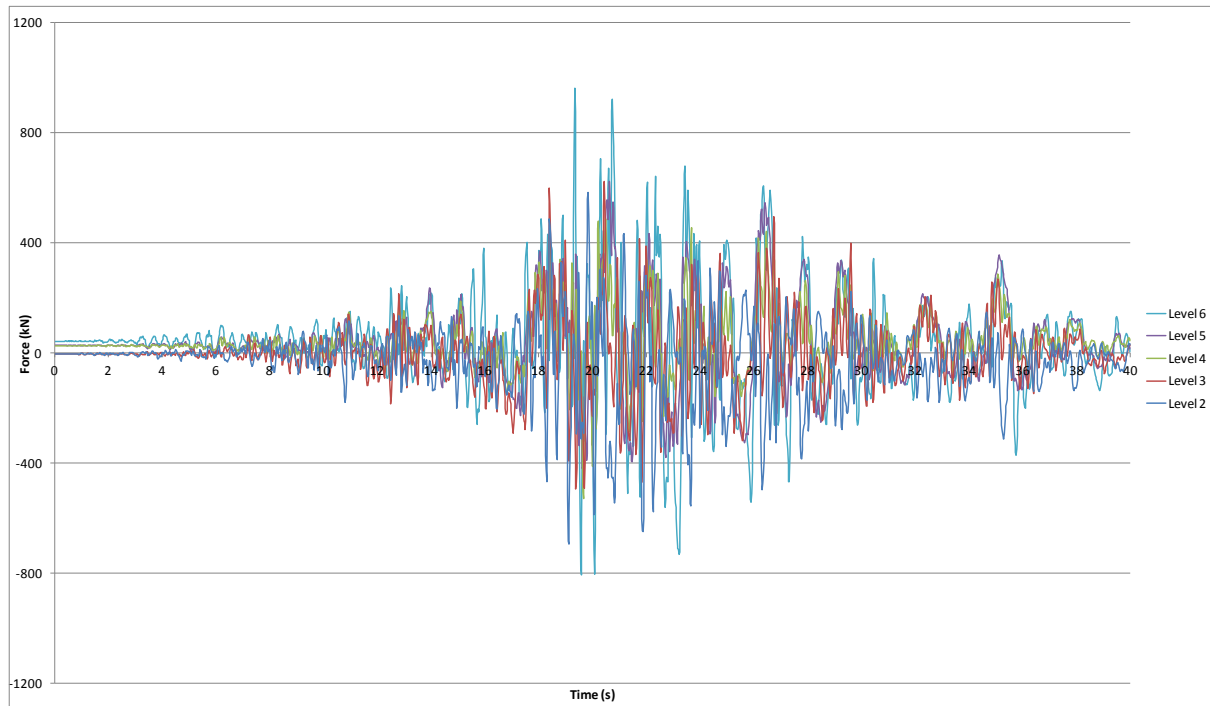


Figure G.10: North core Wall C diaphragm north/south actions, Darfield, CBGS

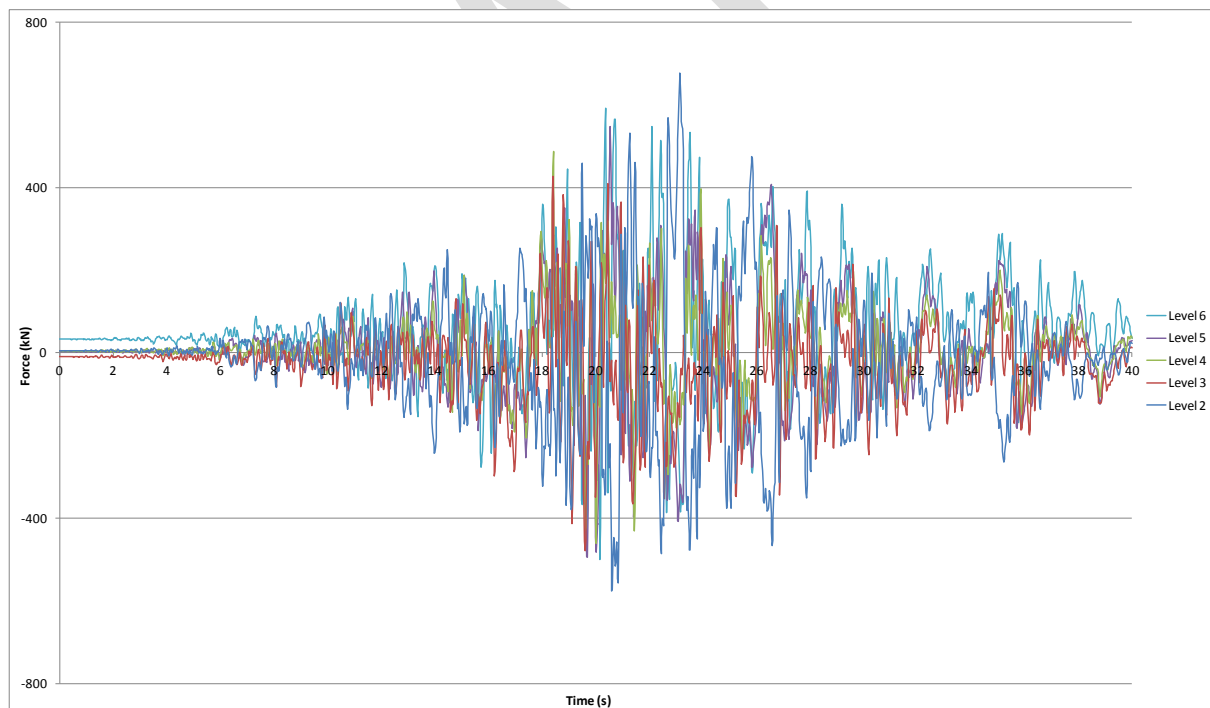


Figure G.11: North core Wall C/D diaphragm north/south actions, Darfield, CBGS

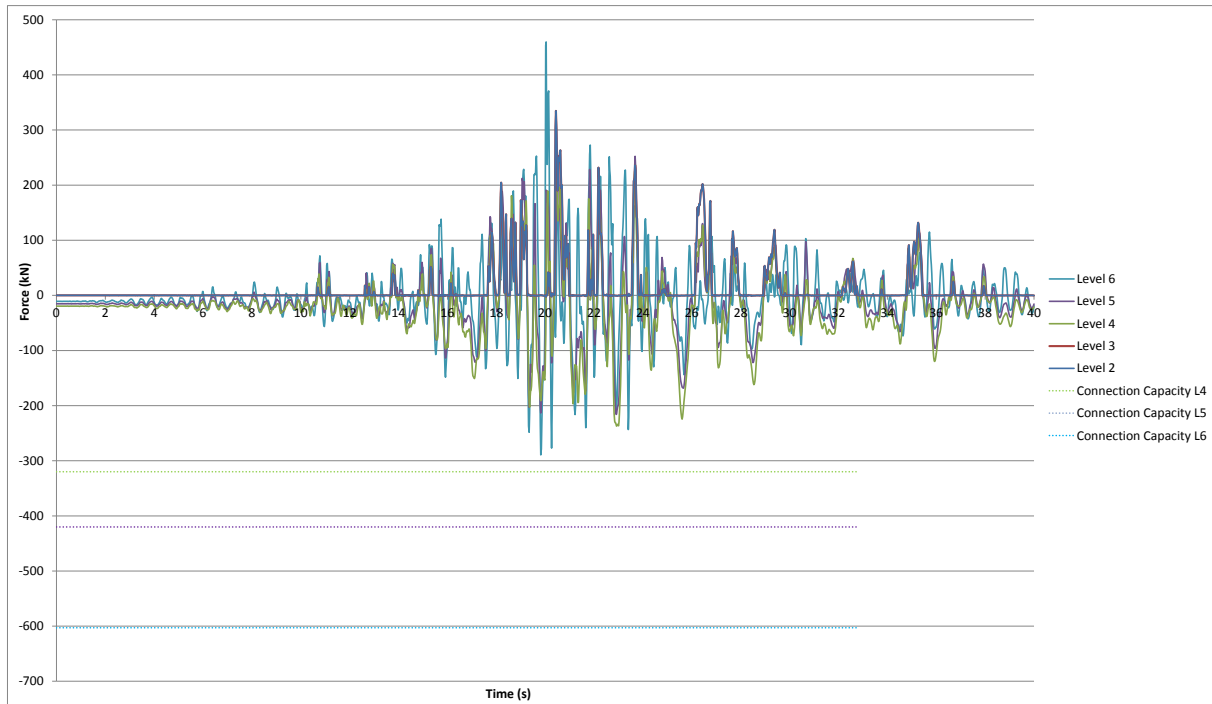


Figure G.12: North core Wall D diaphragm north/south actions, Darfield, CBGS

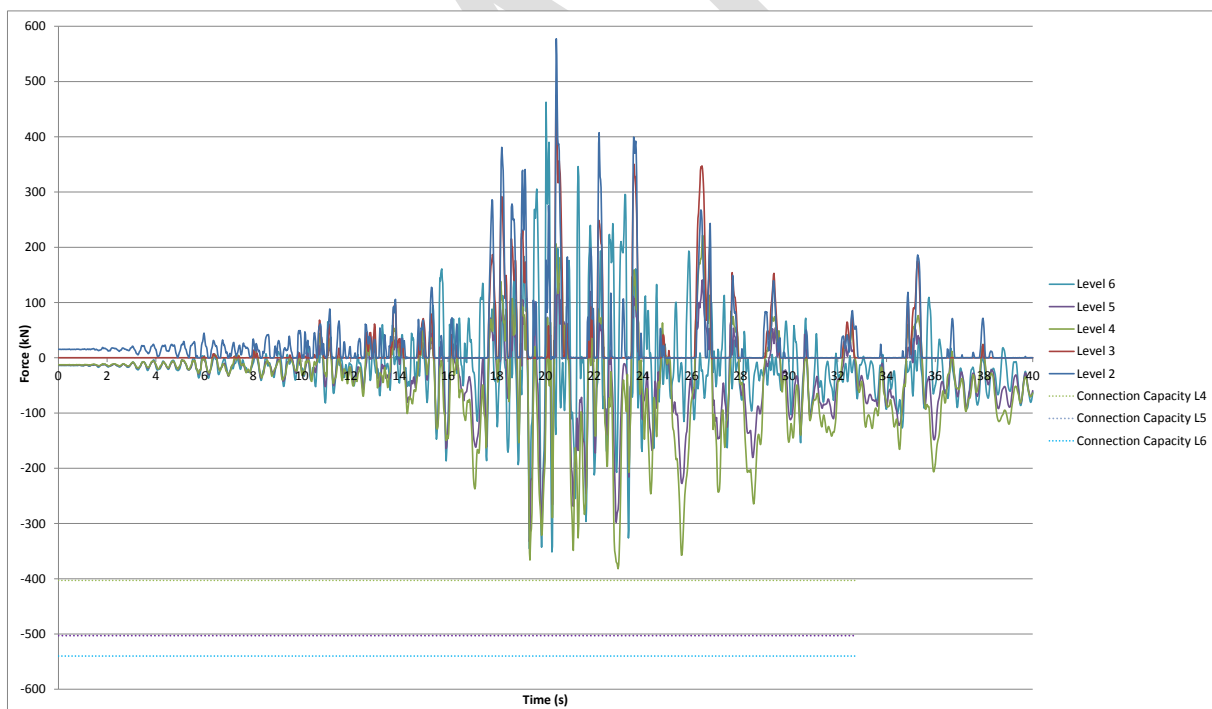


Figure G.13: North core Wall D/E diaphragm north/south actions, Darfield, CBGS

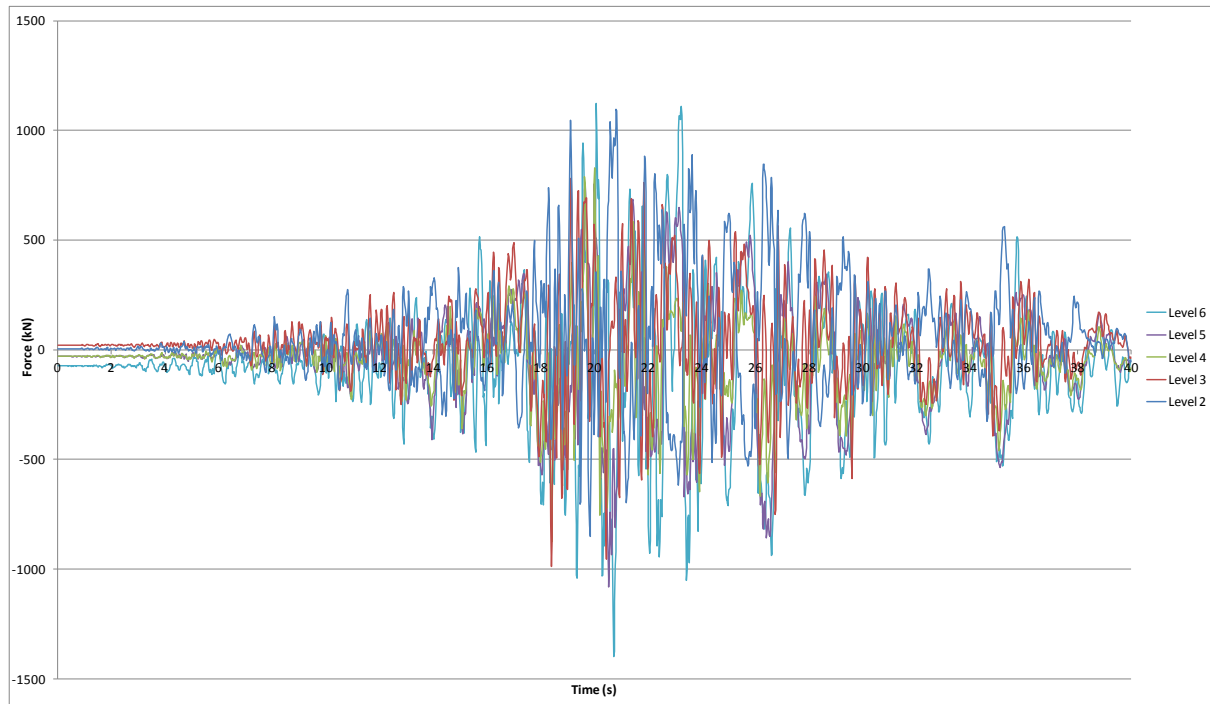


Figure G.14: North core Slab 4/C to C/D diaphragm north/south actions, Darfield, CBGS

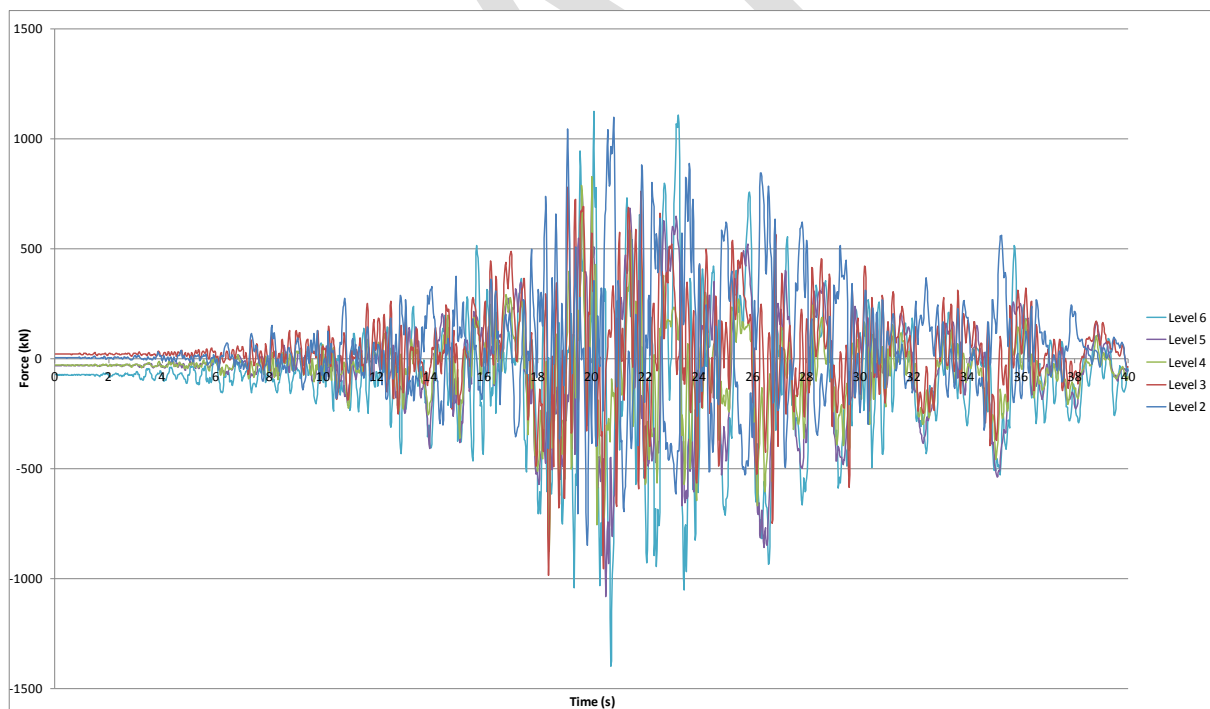


Figure G.15: North core Slab 4/C to C/D diaphragm east/west actions, Darfield, CBGS

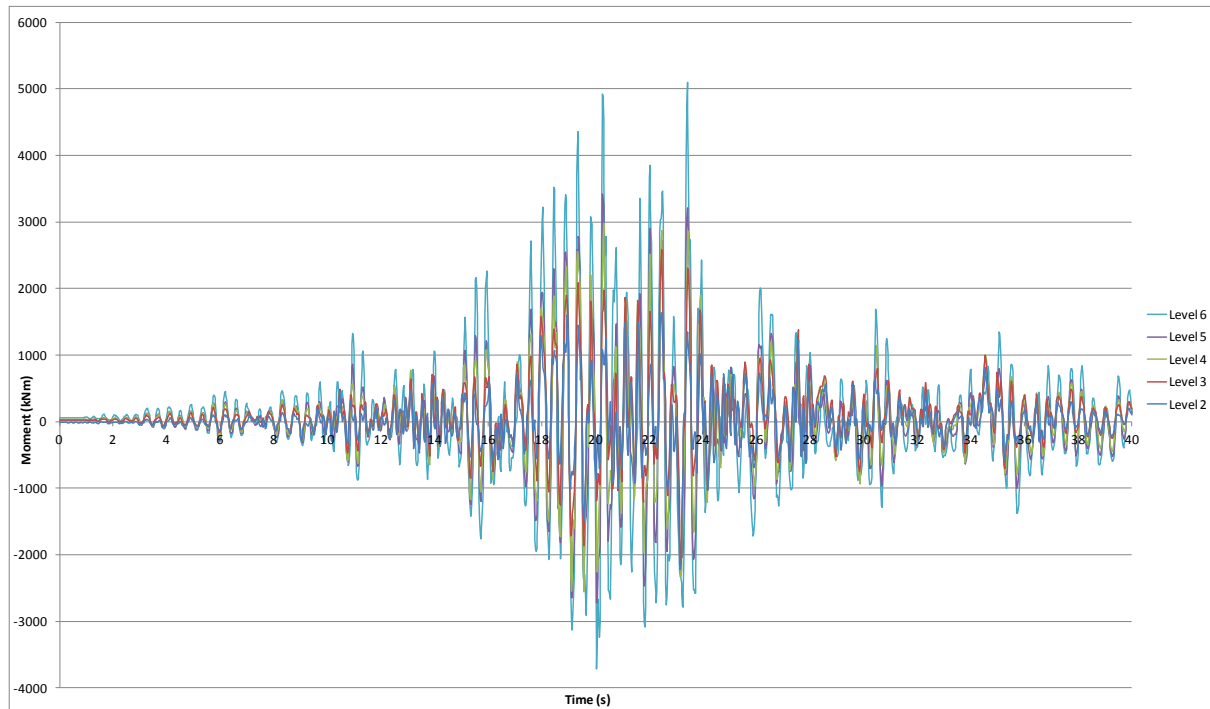


Figure G.16: North core Slab 4/C to C/D diaphragm in-plane moments, Darfield, CBGS

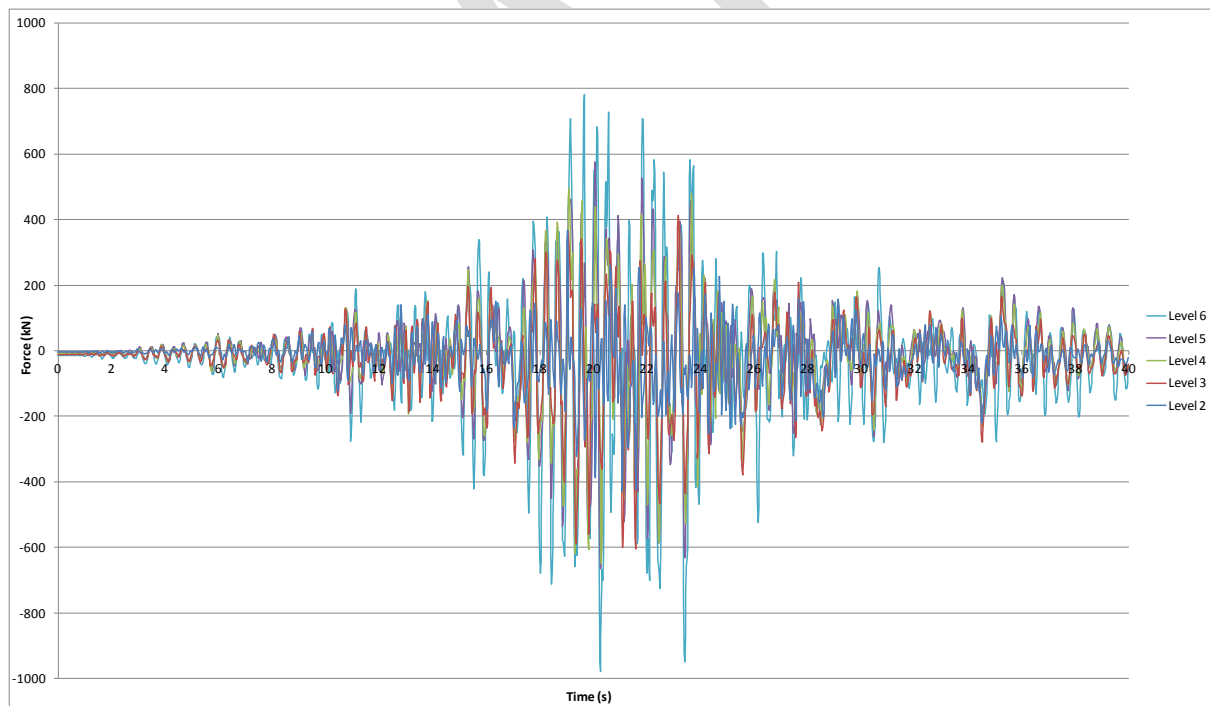


Figure G.17: North core Wall 5 diaphragm east/west actions, Darfield, CBGS

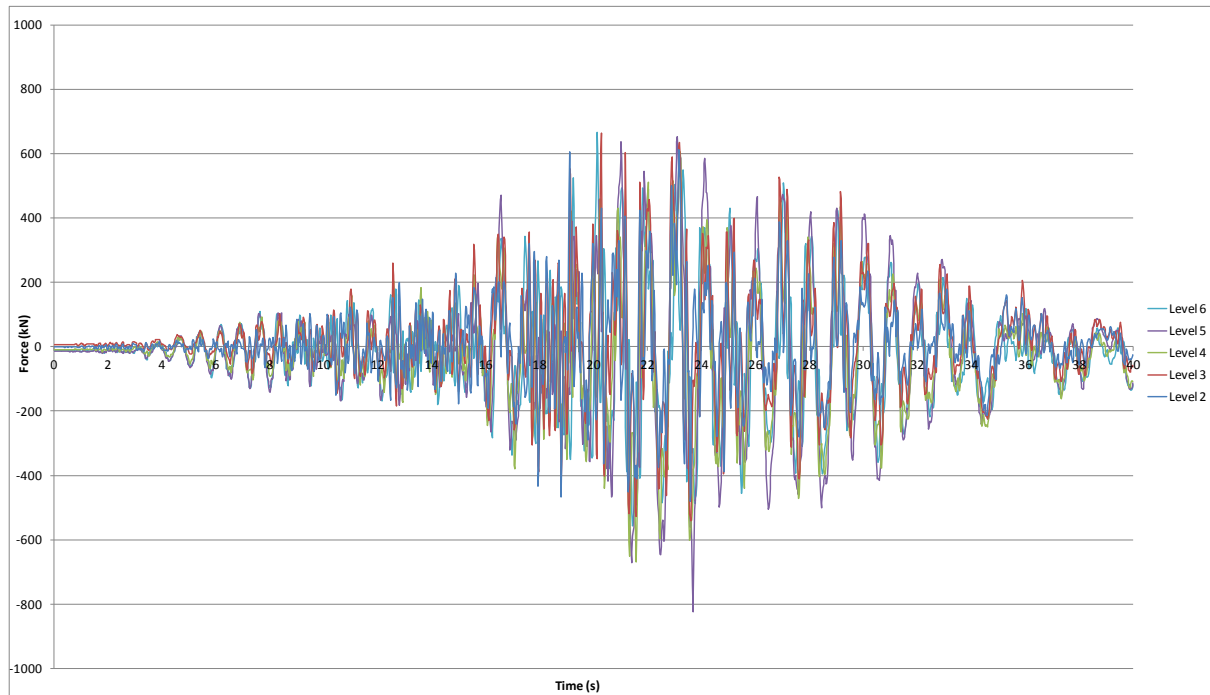


Figure G.18: South wall diaphragm east/west actions, Darfield, CBGS

G.3 Column Hinge Actions

Figure G.19 to Figure G.23 present a selection of column hinge rotations, elongations, and concrete strains for a selected number of critical columns. Strains reported are the maximum that occur at the extreme concrete fibre. Plots are presented for individual columns and are orientated so that the top row of plots relate to the level 5 hinges with each row below corresponding to the hinges in the column below i.e. from the top level to the bottom level. Results presented are for the worst case hinge at each floor level, with hinge rotation and elongation shown in the left hand plot and hinge concrete strain shown in the right hand plot.

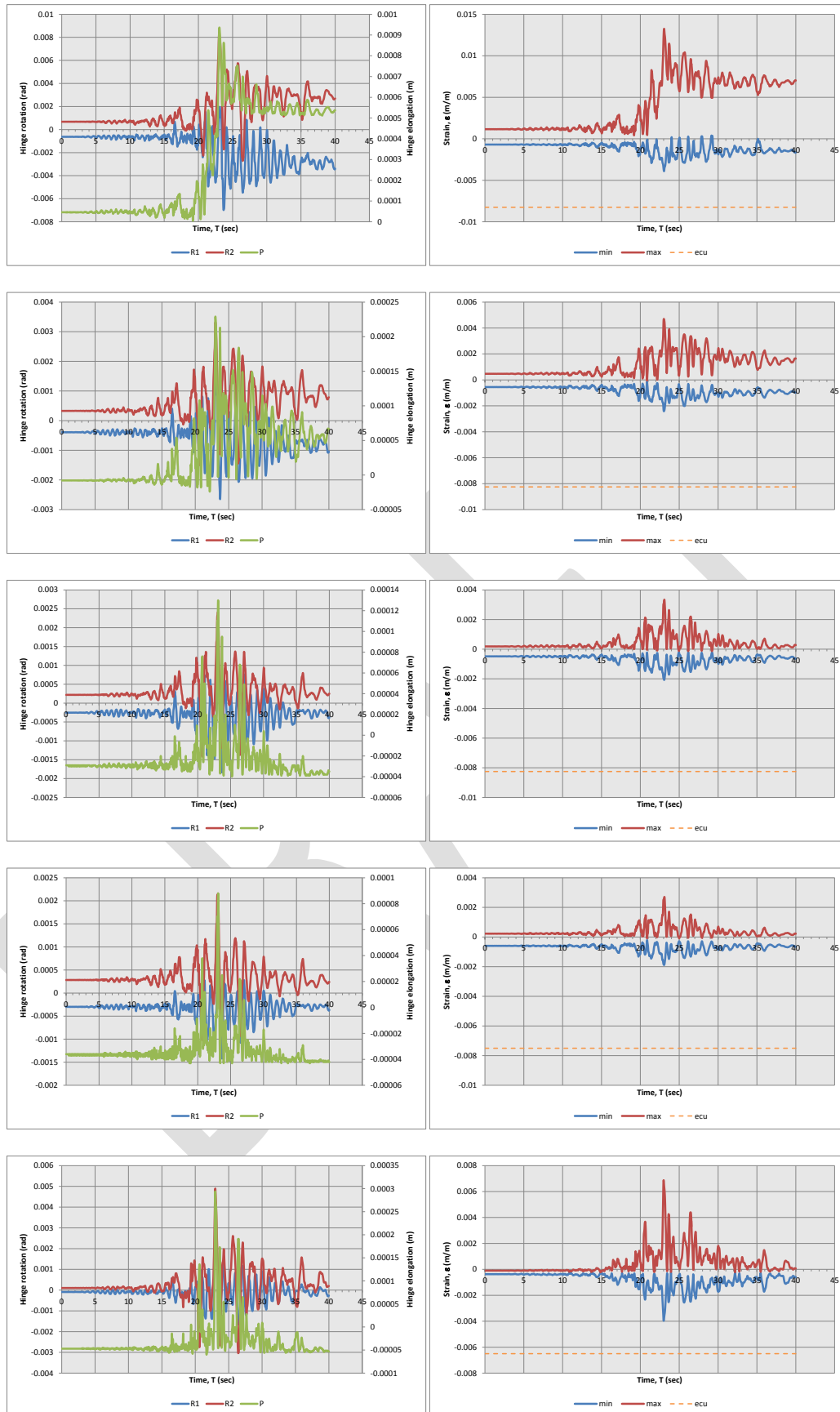


Figure G.19: Column F1 Levels 1 (bottom) to 5 (top) hinge actions, Darfield, CBGS

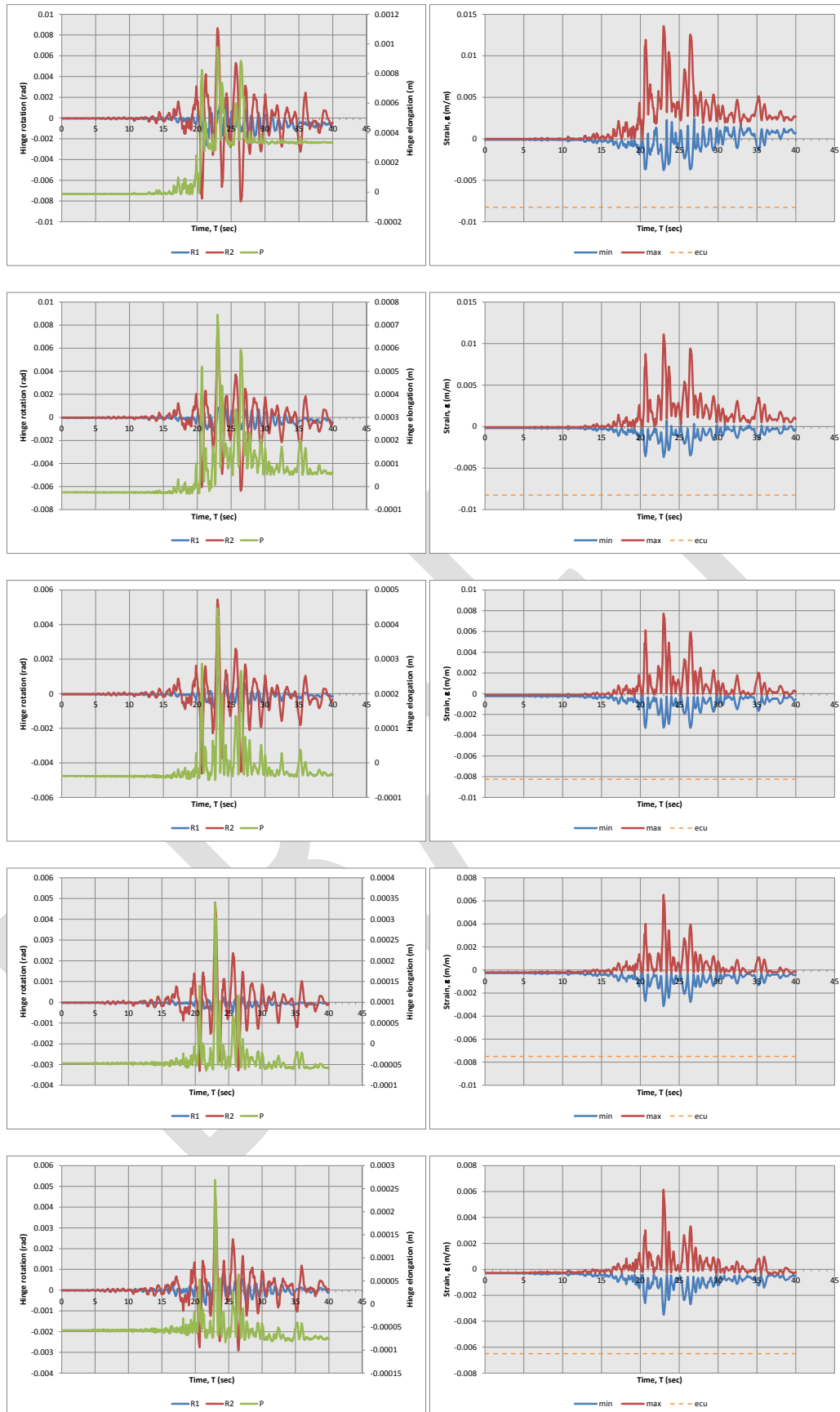


Figure G.20: Column F2 Levels 1 (bottom) to 5 (top) hinge actions, Darfield, CBGS

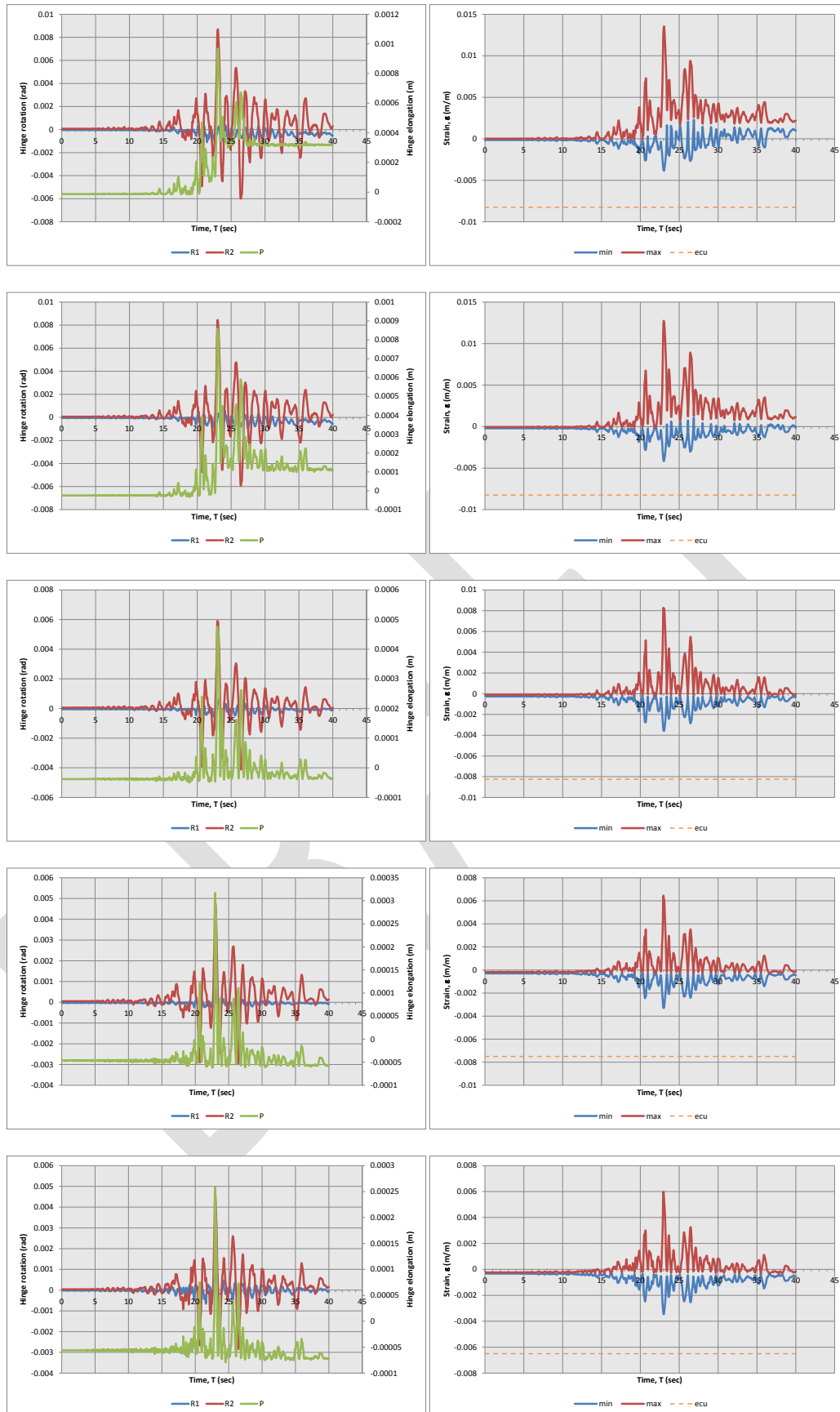


Figure G.21: Column F3 Levels 1 (bottom) to 5 (top) hinge actions, Darfield, CBGS

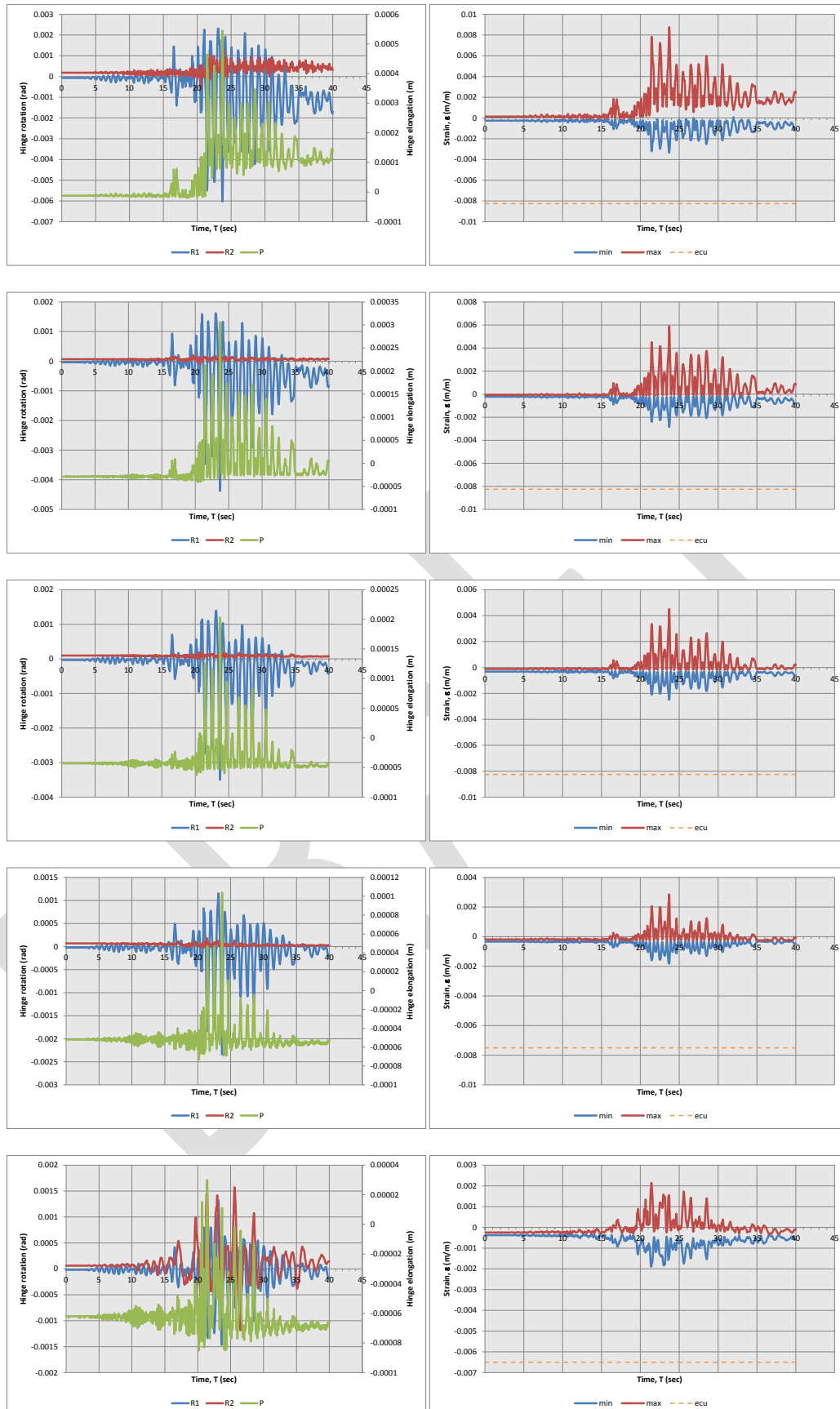


Figure G.22: Column C1 Levels 1 (bottom) to 5 (top) hinge actions, Darfield, CBGS

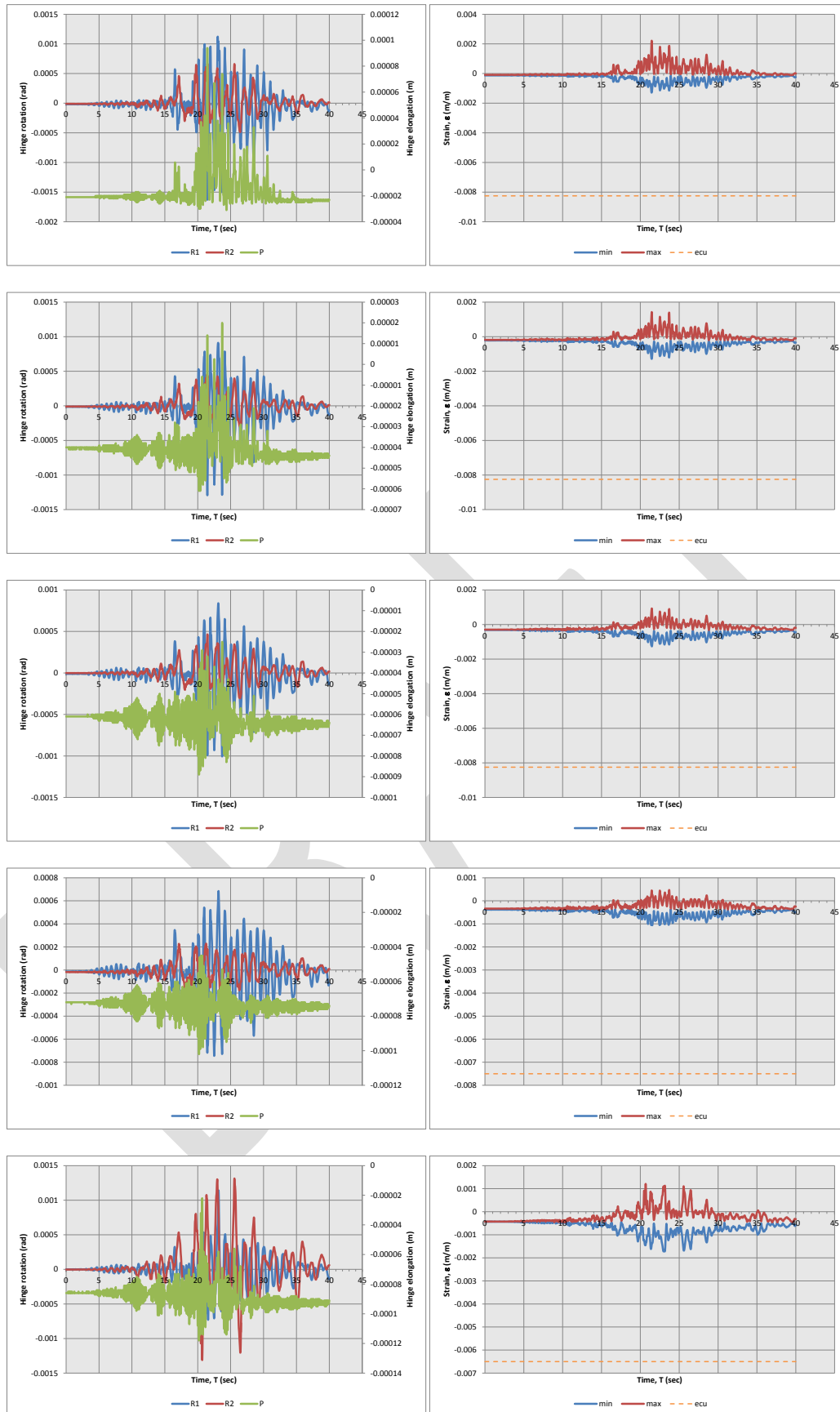


Figure G.23: Column C2 Levels 1 (bottom) to 5 (top) hinge actions, Darfield, CBGS

Appendix H Analysis Results - Darfield Event: CCCC Record

The following details the structural actions reported by the analysis as a function of time, for the Darfield event using the acceleration time history recorded at the CCCC station using all components of the record.

H.1 Building Displacements and Drifts.

Building Level 6 displacements are presented in Figure H.1 and Figure H.2 below for the Southeast and Northwest corners of the building respectively.

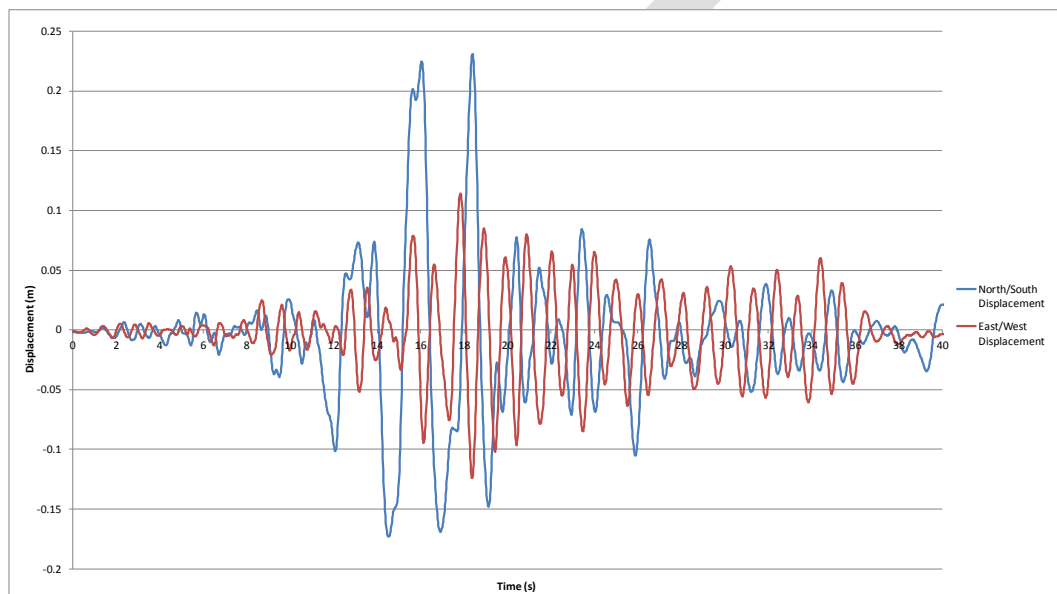


Figure H.1: Level 6 Southeast corner displacements, Darfield, CCCC

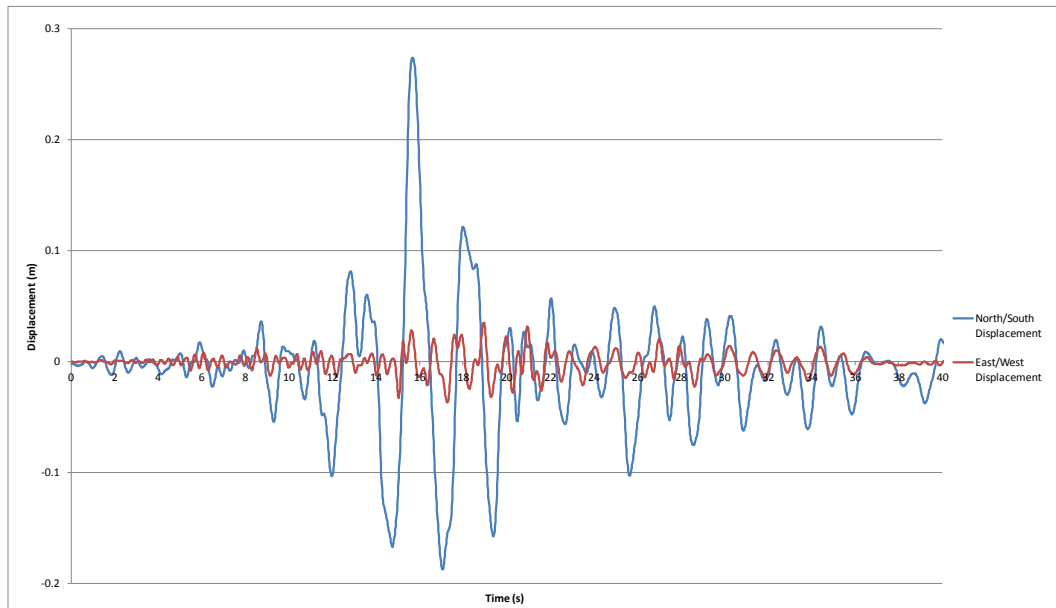


Figure H.2: Level 6 Northwest corner displacements, Darfield, CCCC

As can be seen in Figure H.1 and Figure H.2 above a significant increase in the northward building displacement is observed in the northwest corner of the building between 14 and 20 seconds of the record. The peak displacement corresponds to a clockwise rotation in conjunction with a net northward building translation. Table H.1 presents the sequence of failure of the north core wall ties throughout the record.

Table H.1: Wall D and D/E diaphragm disconnection times, Darfield, CCCC.

Level	Wall D Failure (sec)	Wall D/E Failure (sec)
6	No disconnection	No disconnection
5	No disconnection	No disconnection
4	14.44	14.40

Inter-storey displacements for the perimeter frame lines A and F in the north/south direction are presented in Figure H.3 and Figure H.4 below.

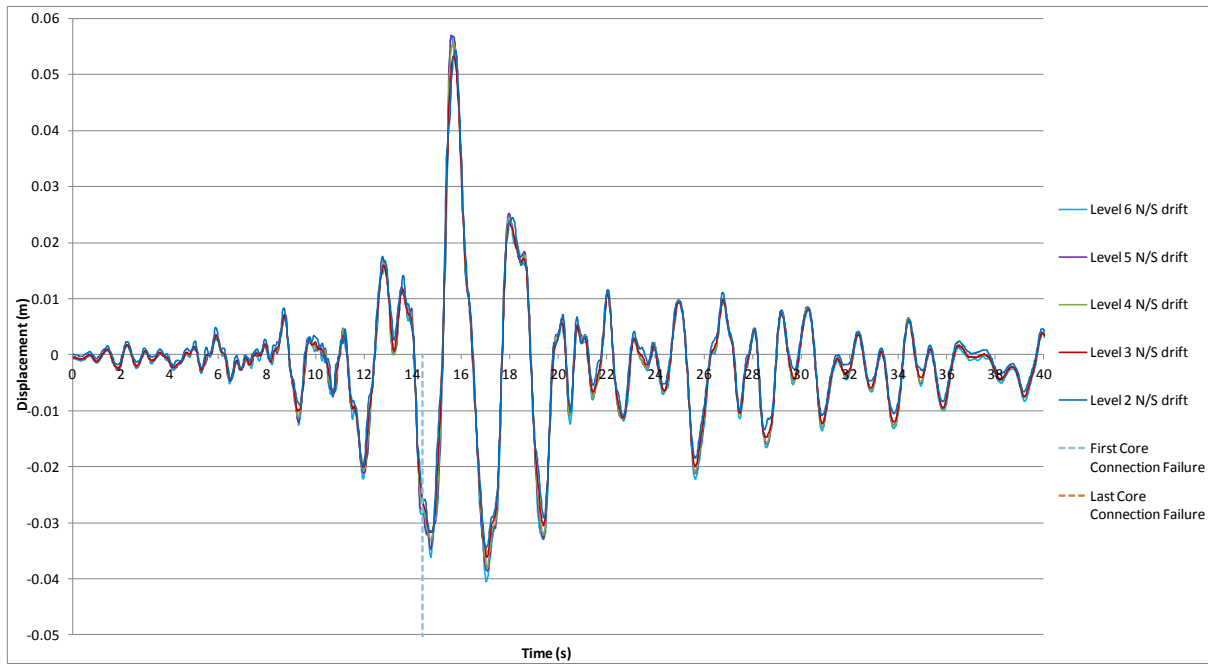


Figure H.3: Frame A north/south inter-storey displacements, Darfield, CCCC

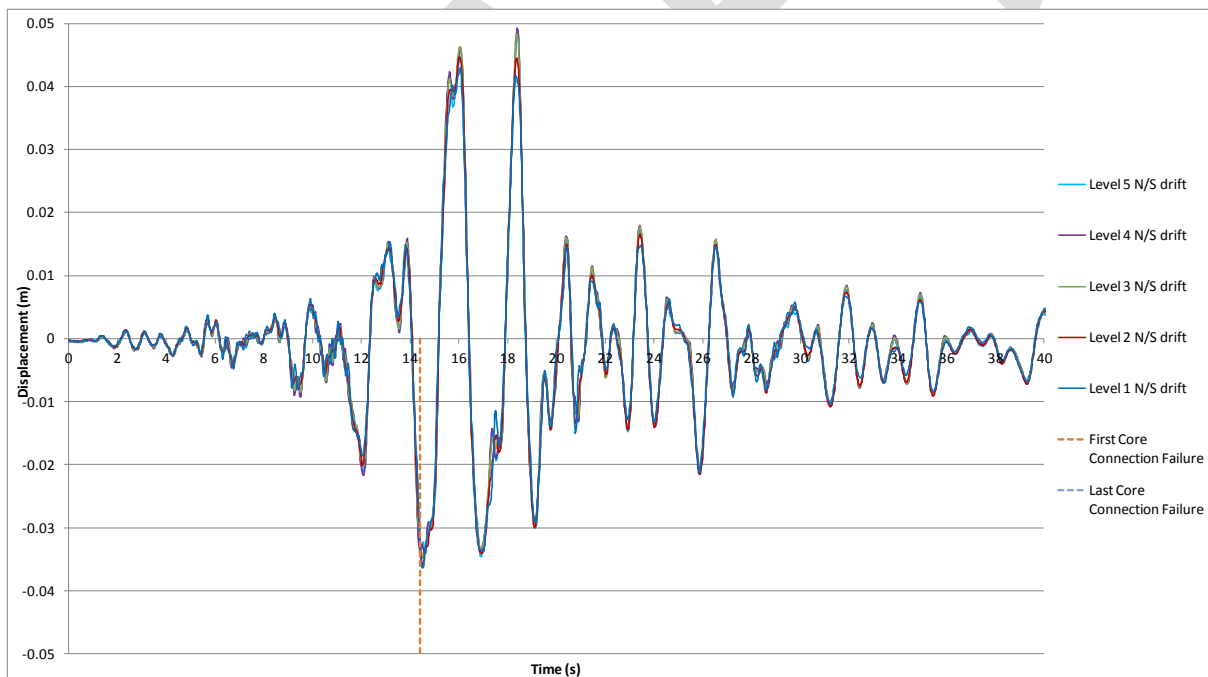


Figure H.4: Frame F north/south inter-storey displacements, Darfield, CCCC

Inter-storey displacements for the perimeter frame lines 1 and 4 in the east/west direction are presented in Figure H.5, and Figure H.6 below.

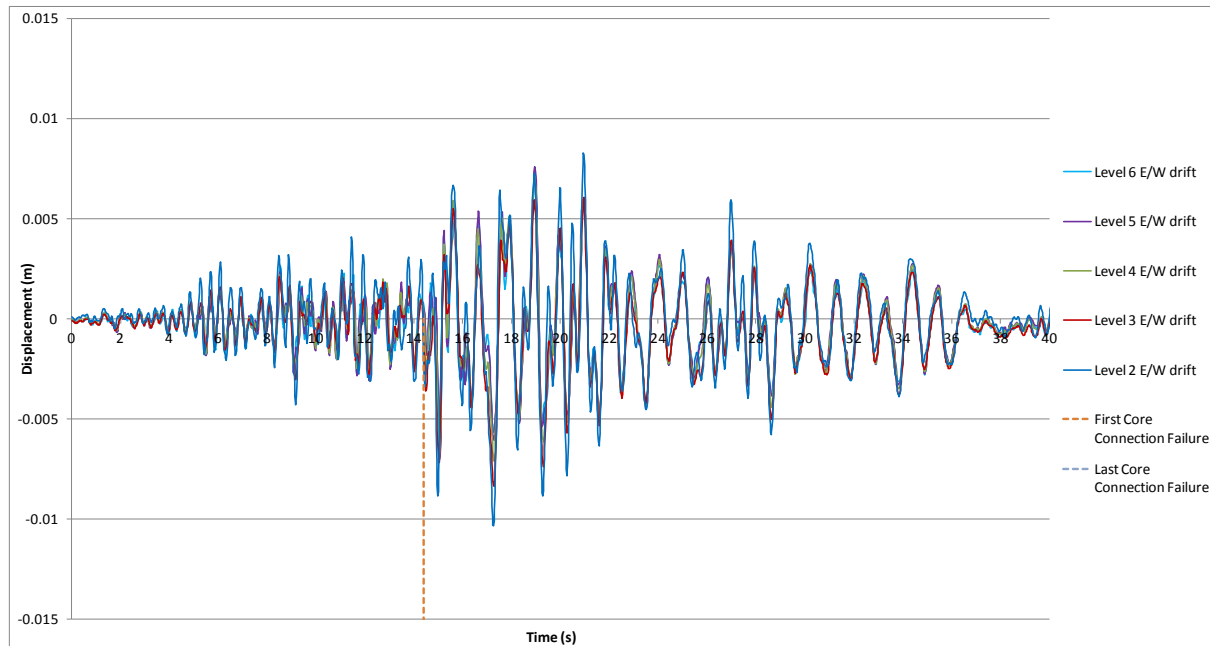


Figure H.5: Frame 1 east/west inter-storey displacements, Darfield, CCCC

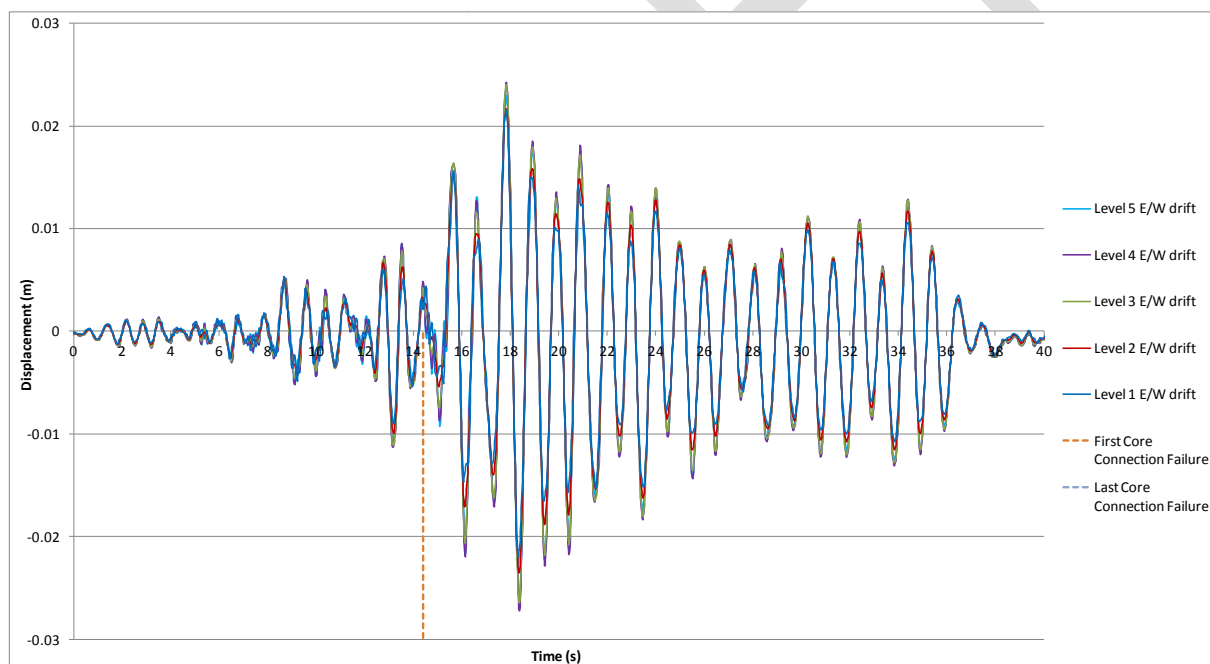


Figure H.6: Frame 4 east/west inter-storey displacements, Darfield, CCCC

H.2 Diaphragm Connection Forces

Diaphragm connection forces are presented in Figure H.7 to Figure H.18 below. Note that moments are reported about the geometric centroid of the element being considered.

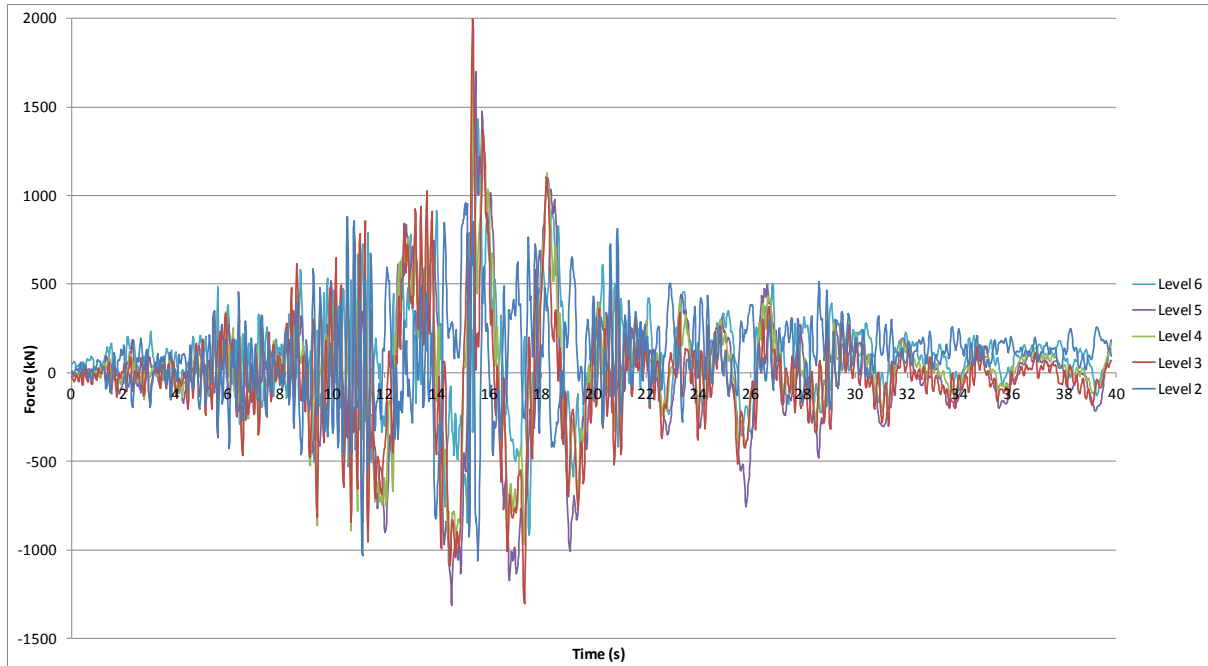


Figure H.7: North core total diaphragm north/south actions, Darfield, CCCC

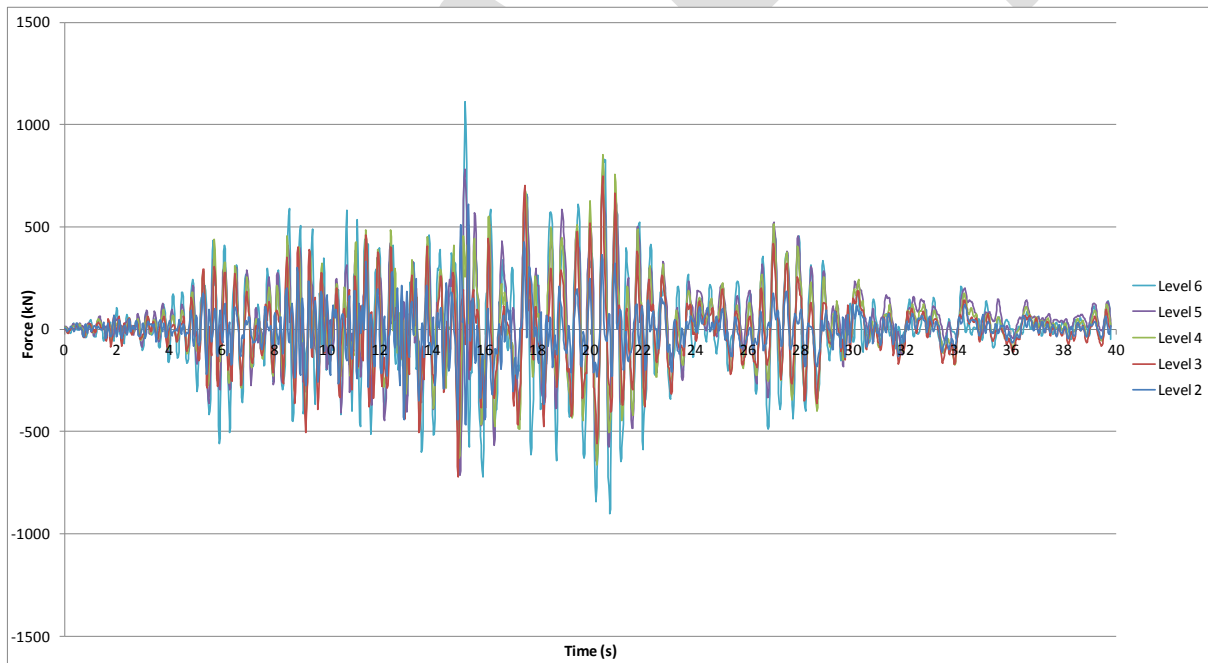


Figure H.8: North core total diaphragm east/west actions, Darfield, CCCC

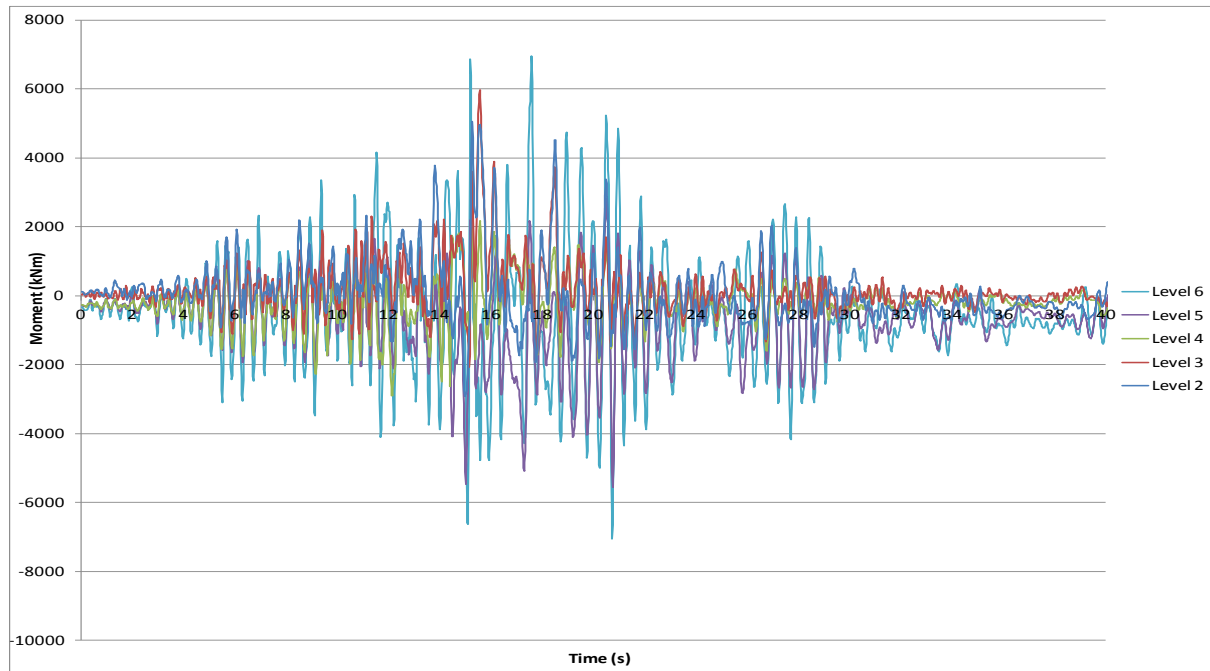


Figure H.9: North core total diaphragm in-plane moments, Darfield, CCCC

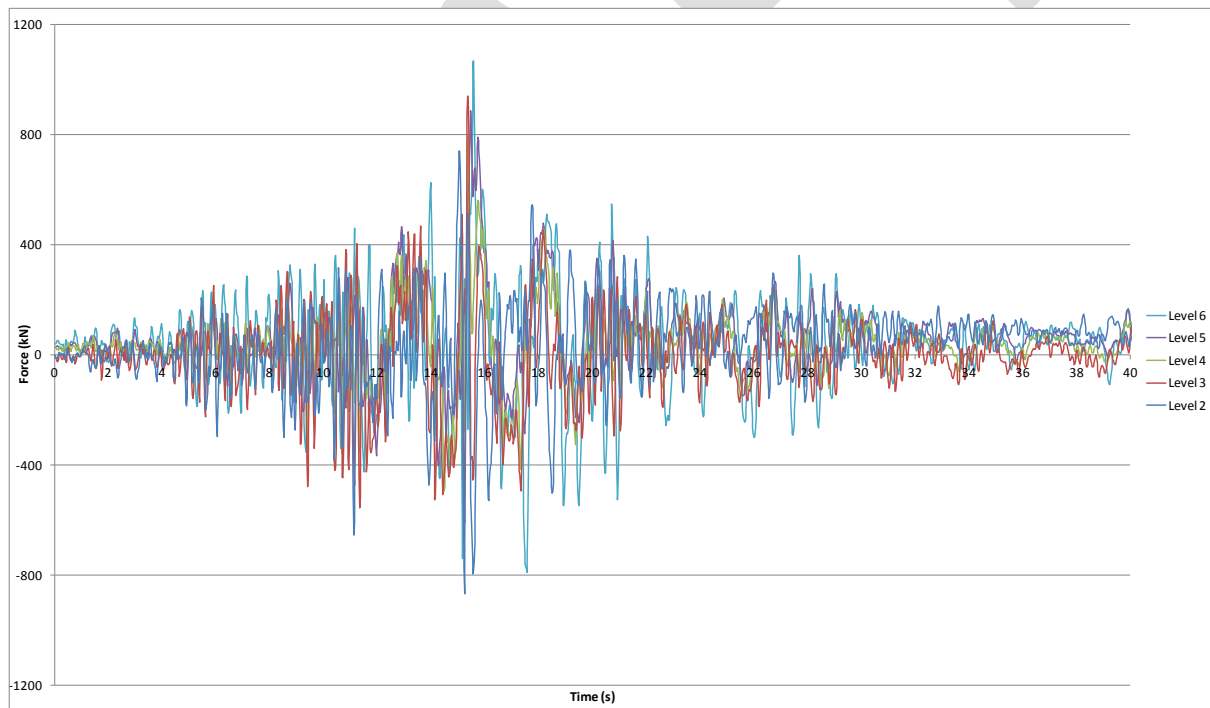


Figure H.10: North core Wall C diaphragm north/south actions, Darfield, CCCC

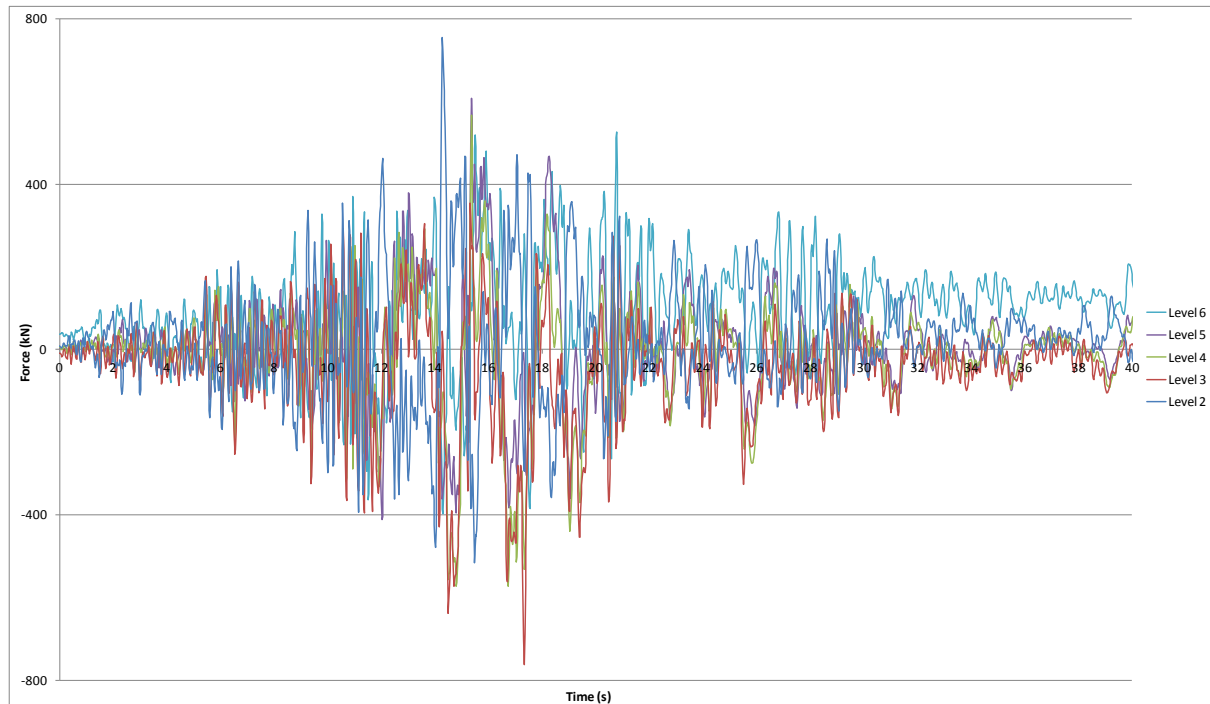


Figure H.11: North core Wall C/D diaphragm north/south actions, Darfield, CCCC.

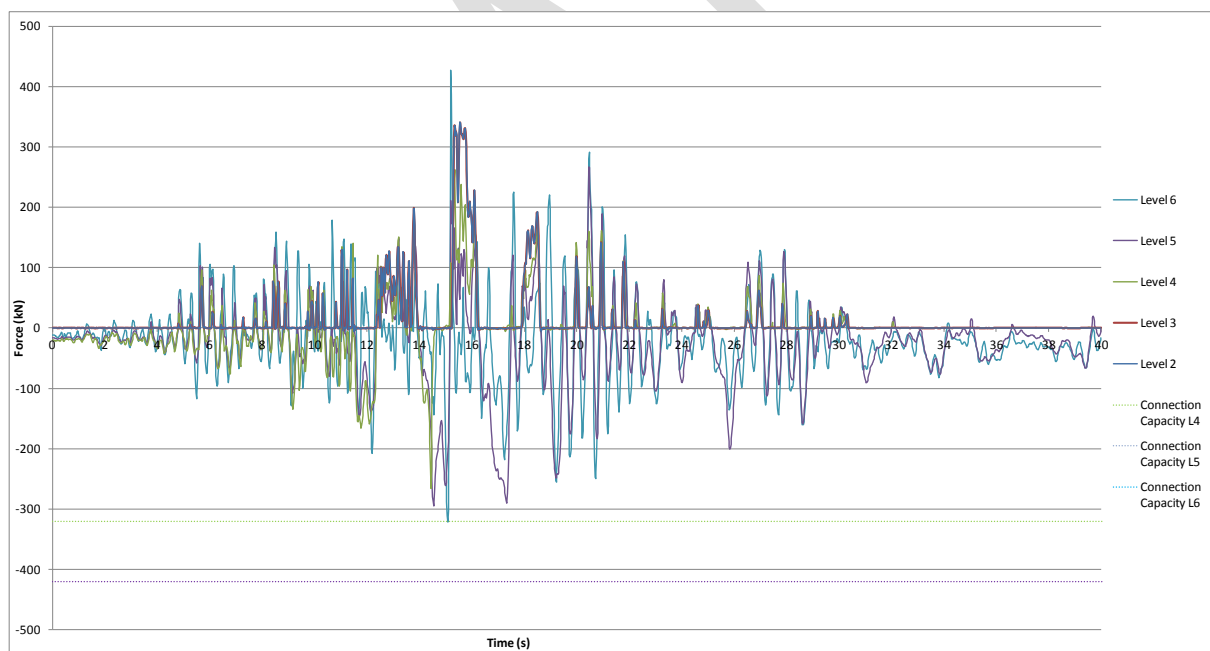


Figure H.12: North core Wall D diaphragm north/south actions, Darfield, CCCC.

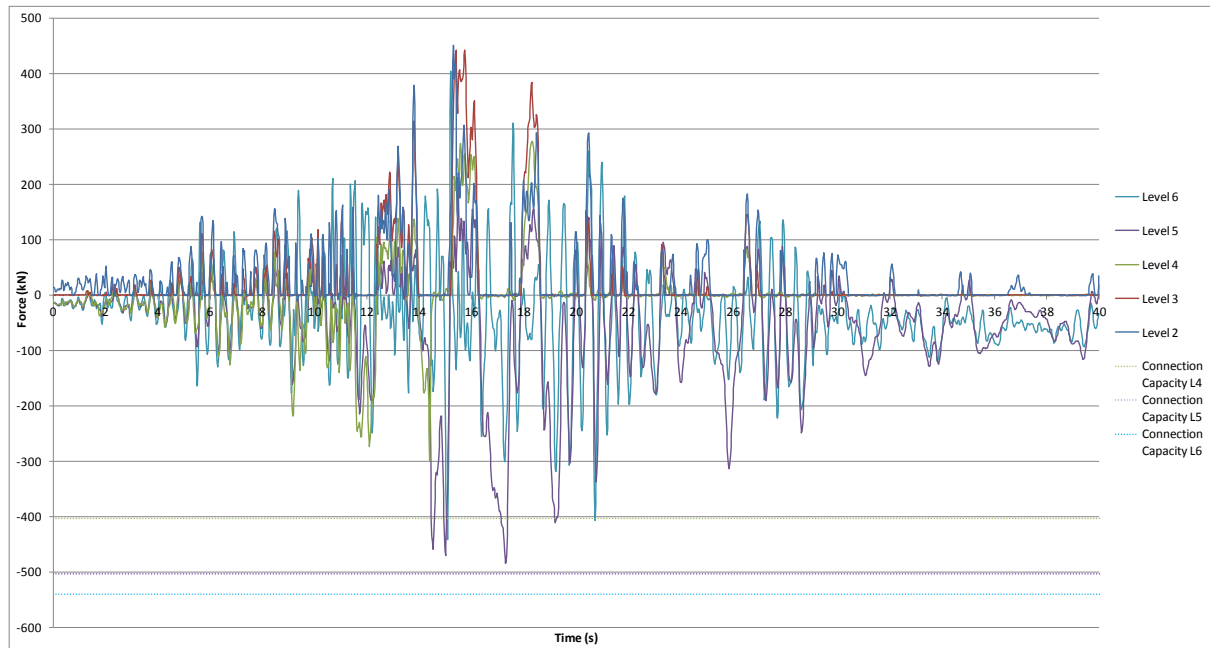


Figure H.13: North core Wall D/E diaphragm north/south actions, Darfield, CCCC.

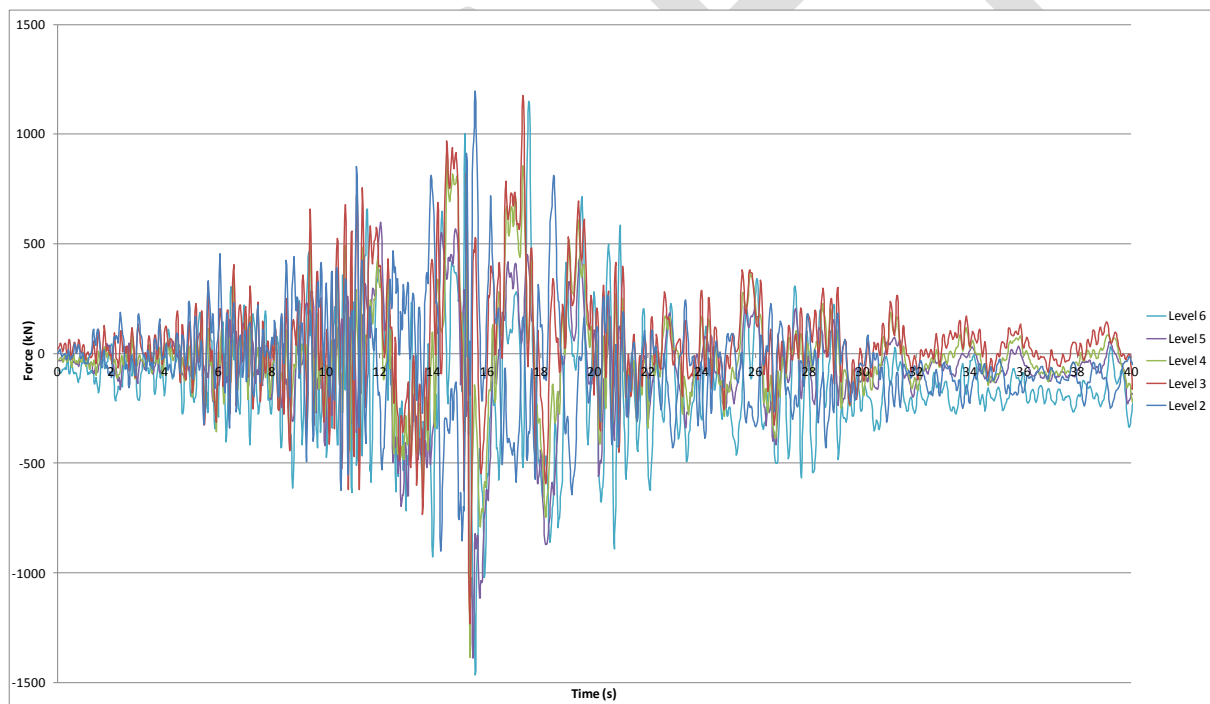


Figure H.14: North core Slab 4/C to C/D diaphragm north/south actions, Darfield, CCCC.

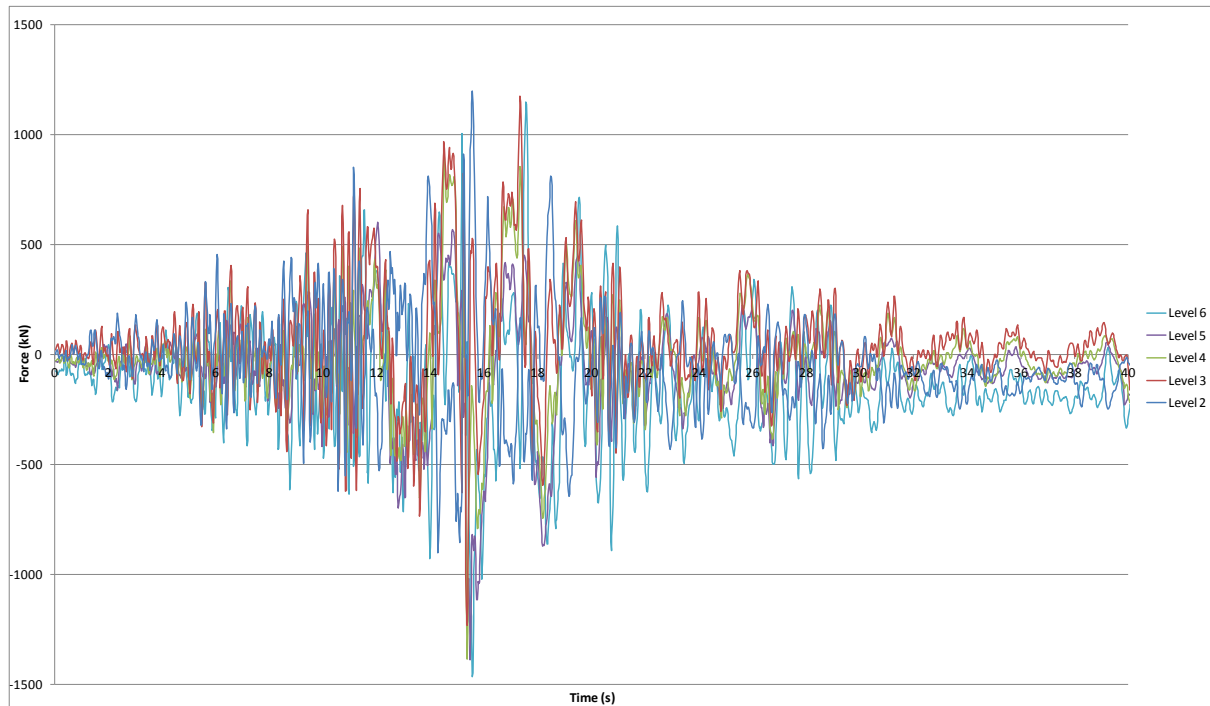


Figure H.15: North core Slab 4/C to C/D diaphragm east/west actions, Darfield, CCCC.

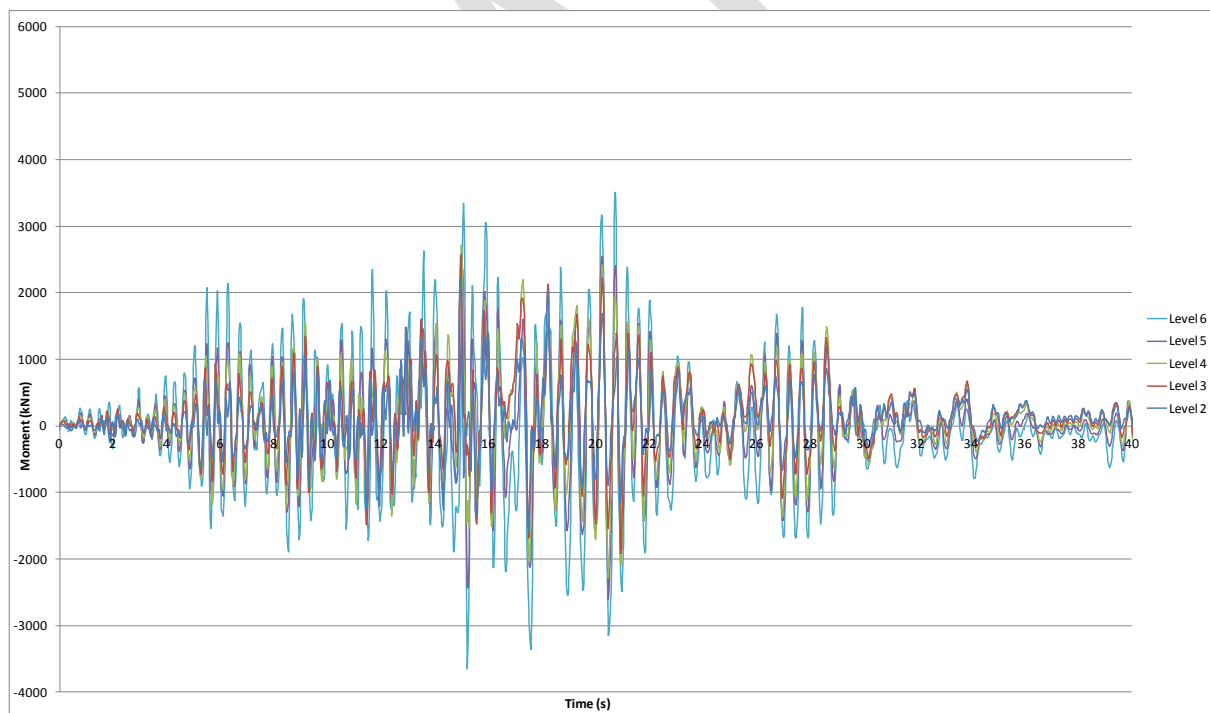


Figure H.16: North core Slab 4/C to C/D diaphragm in-plane moments, Darfield, CCCC.

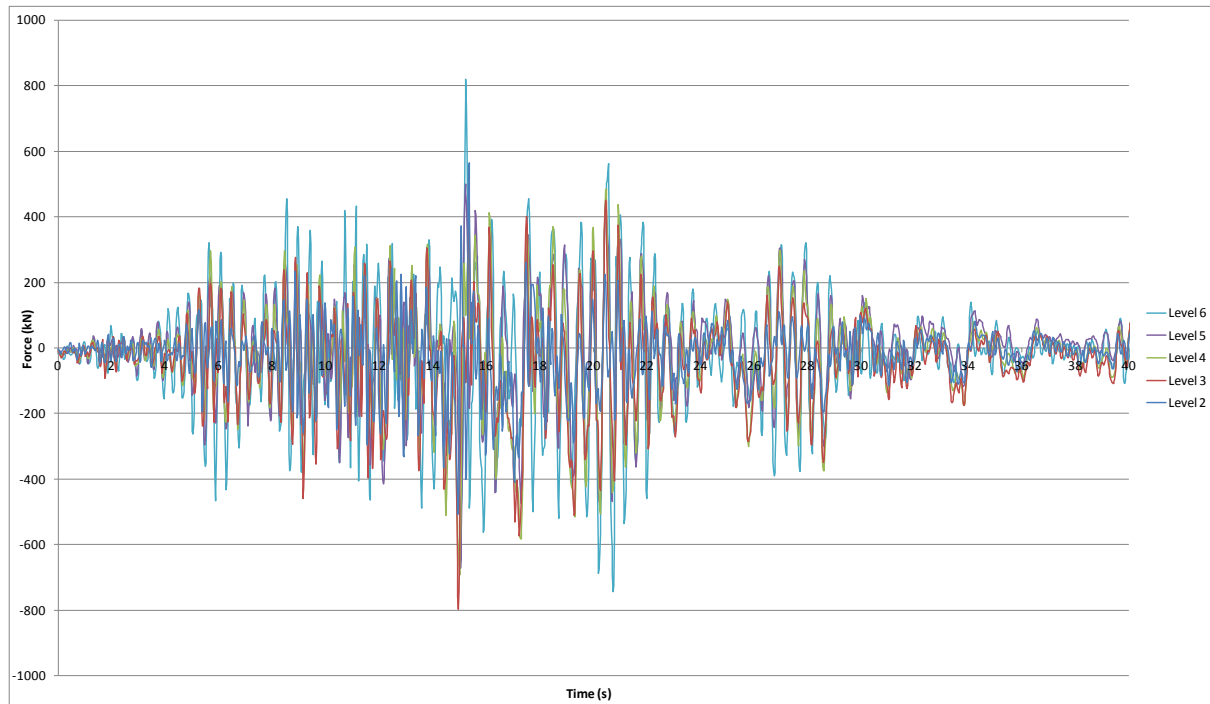


Figure H.17: North core Wall 5 diaphragm east/west actions, Darfield, CCCC.

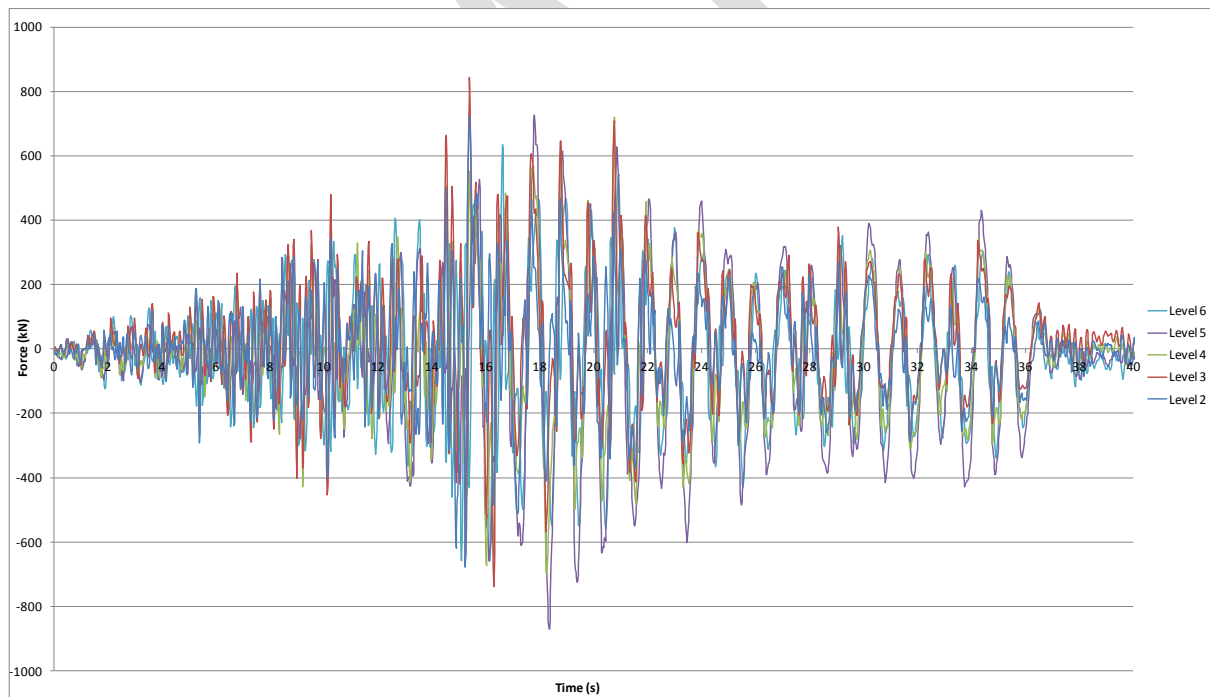


Figure H.18: South wall diaphragm east/west actions, Darfield, CCCC.

H.3 Column Hinge Actions

Figure H.19 to Figure H.23 present a selection of column hinge rotations, elongations, and concrete strains for a selected number of critical columns. Strains reported are the maximum that occur at the extreme concrete fibre. Plots are presented for individual columns and are orientated so that the top row of plots relate to the level 5 hinges with each row below corresponding to the hinges in the column below i.e. from the top level to the bottom level. Results presented are for the worst case hinge at each floor level, with hinge rotation and elongation shown in the left hand plot and hinge concrete strain shown in the right hand plot.

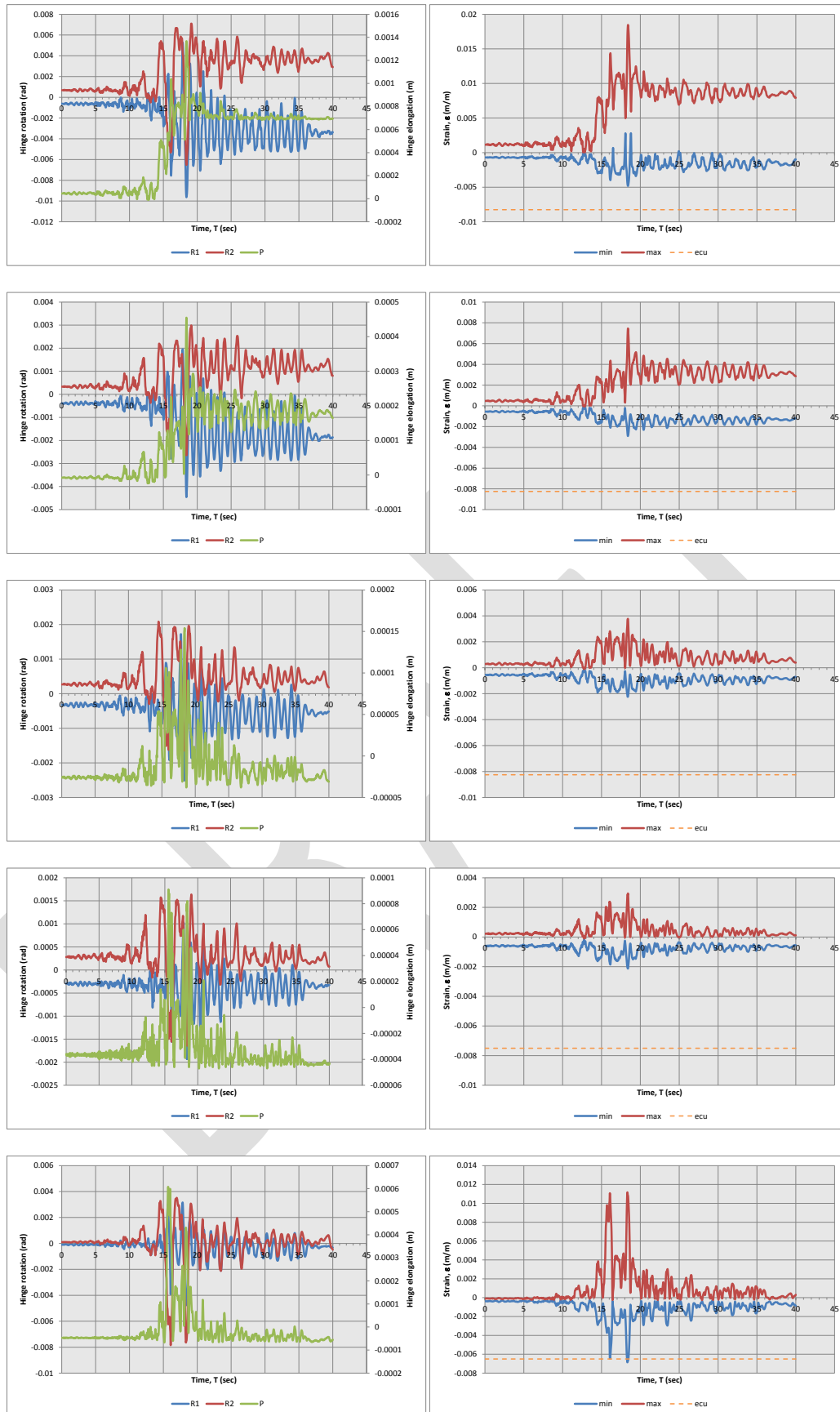


Figure H.19: Column F1 Levels 1 (bottom) to 5 (top) hinge actions, Darfield, CCCC

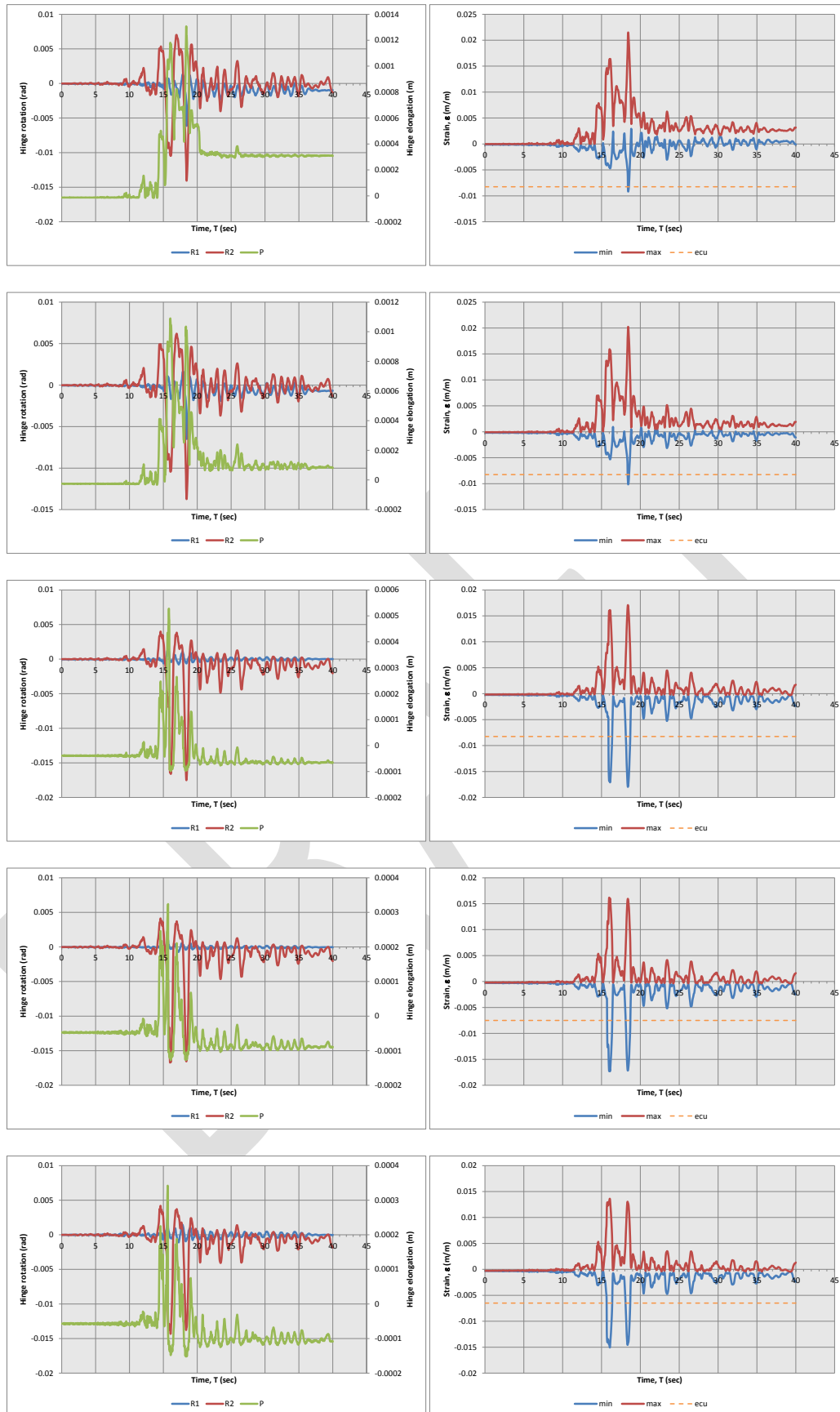


Figure H.20: Column F2 Levels 1 (bottom) to 5 (top) hinge actions, Darfield, CCCC

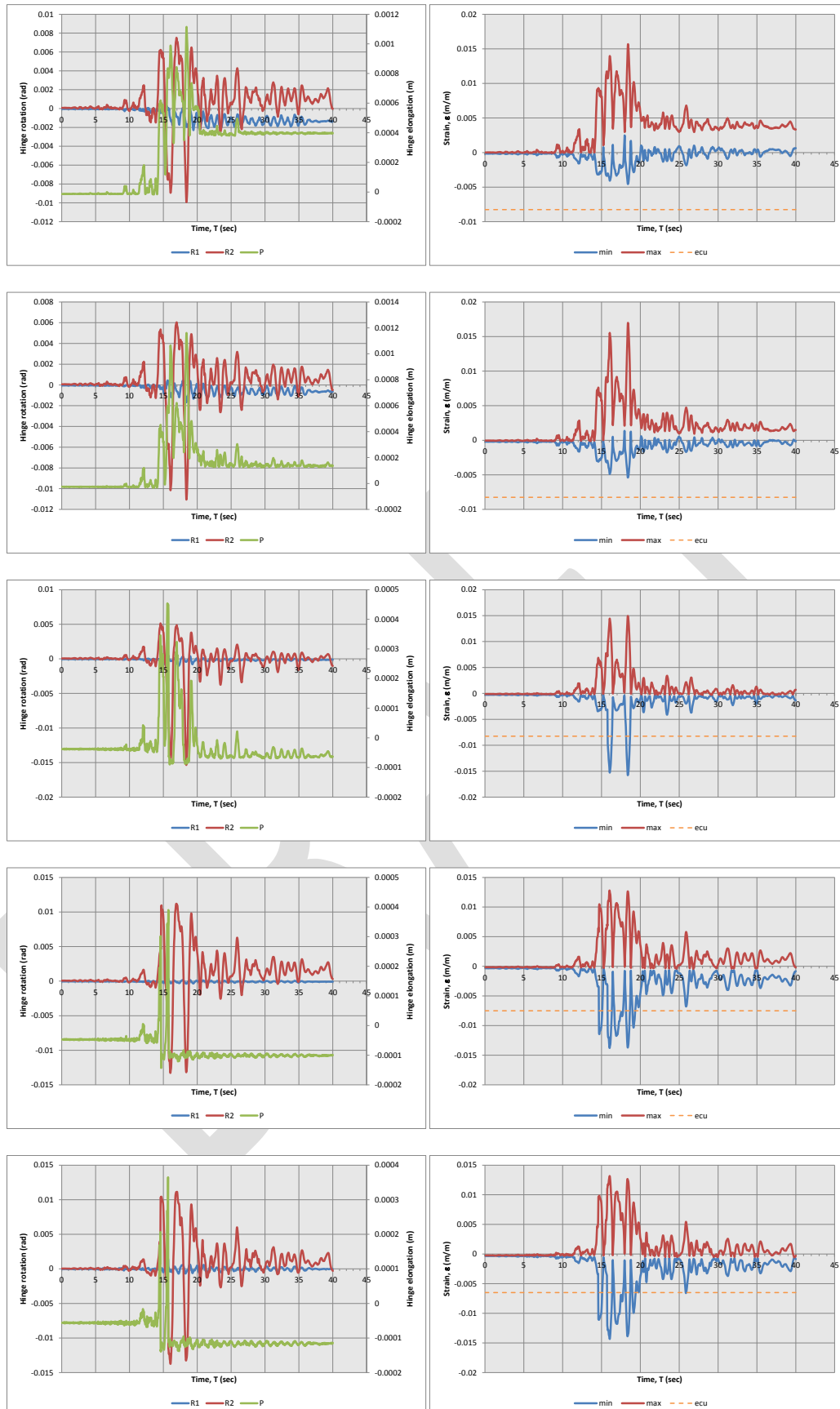


Figure H.21: Column F3 Levels 1 (bottom) to 5 (top) hinge actions, Darfield, CCCC

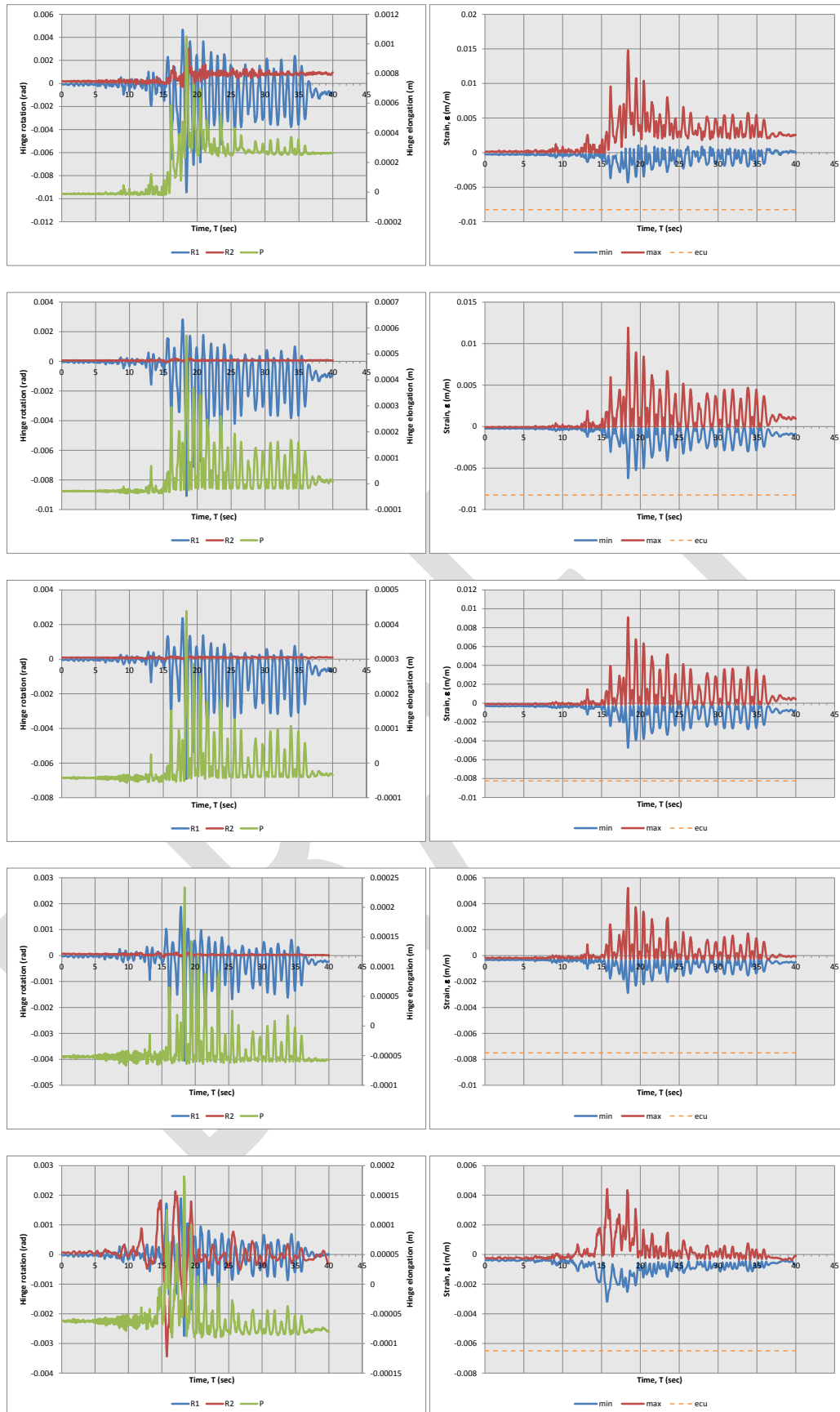


Figure H.22: Column C1 Levels 1 (bottom) to 5 (top) hinge actions, Darfield, CCCC

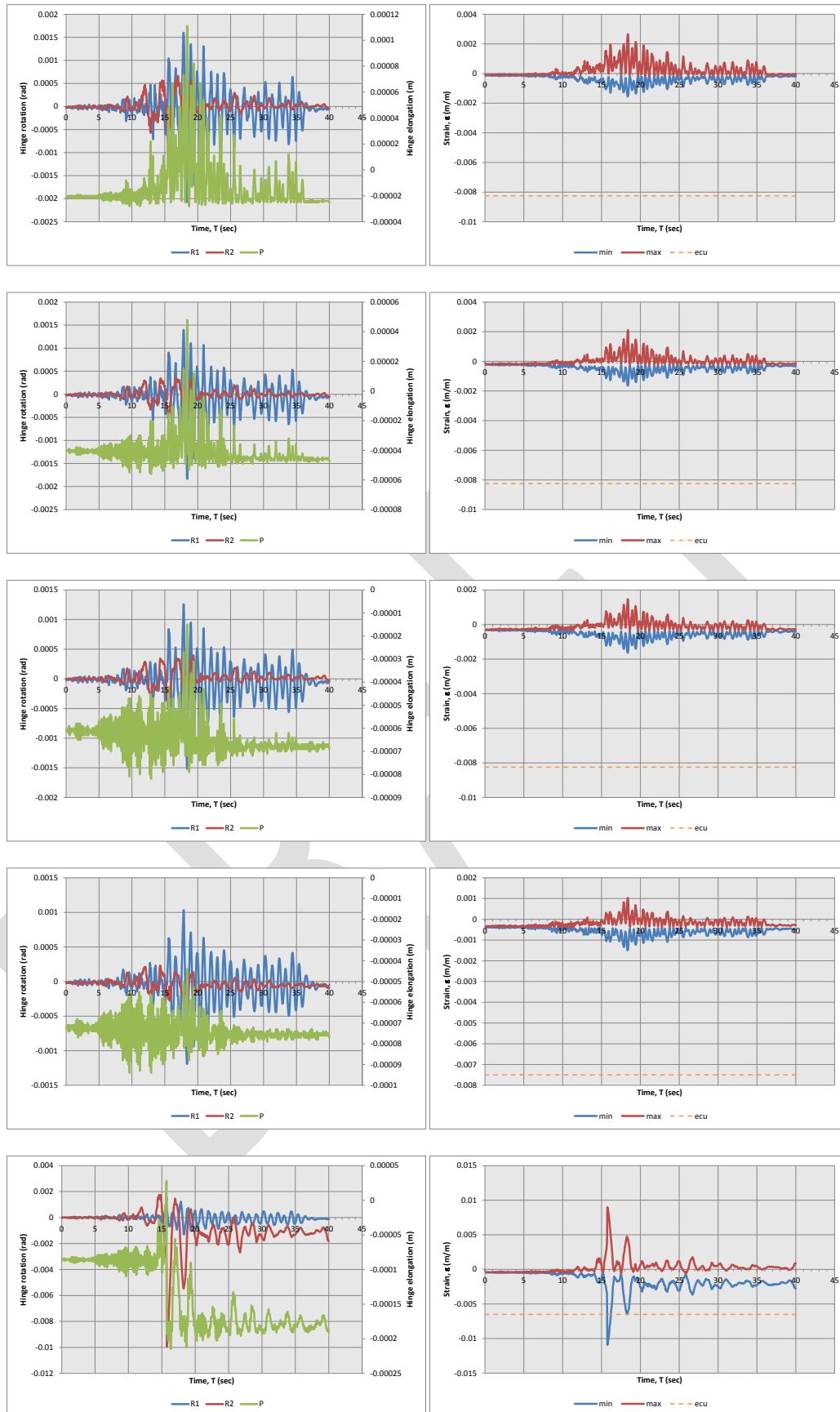


Figure H.23: Column C2 Levels 1 (bottom) to 5 (top) hinge actions, Darfield, CCCC

Appendix I Analysis Results - Lyttelton Aftershock: CBGS record

The following details the structural actions reported by the analysis as a function of time, for the Lyttelton aftershock using the acceleration time history recorded at the CBGS station using all components of the record. Results presented in this section include those assuming that the CTV Building was in an undamaged state, and those for the sequential analyses following on from stiffness state at the end of the Darfield event (denoted '*sequential*').

I.1 Building Displacements and Drifts.

Building Level 6 displacements are presented in Figure I.1 to Figure I.4 below for the southeast and northwest corners of the building respectively.

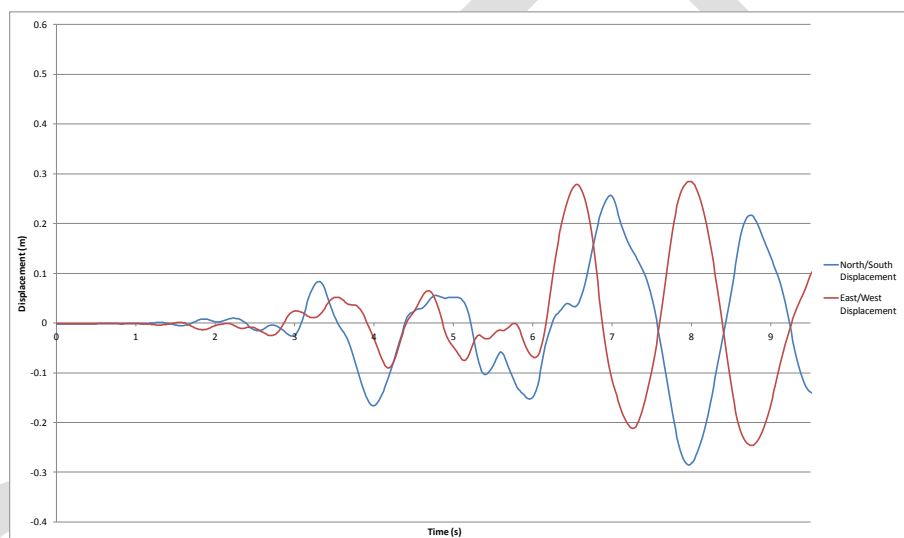


Figure I.1: Level 6 Southeast corner displacements, Lyttelton, CBGS

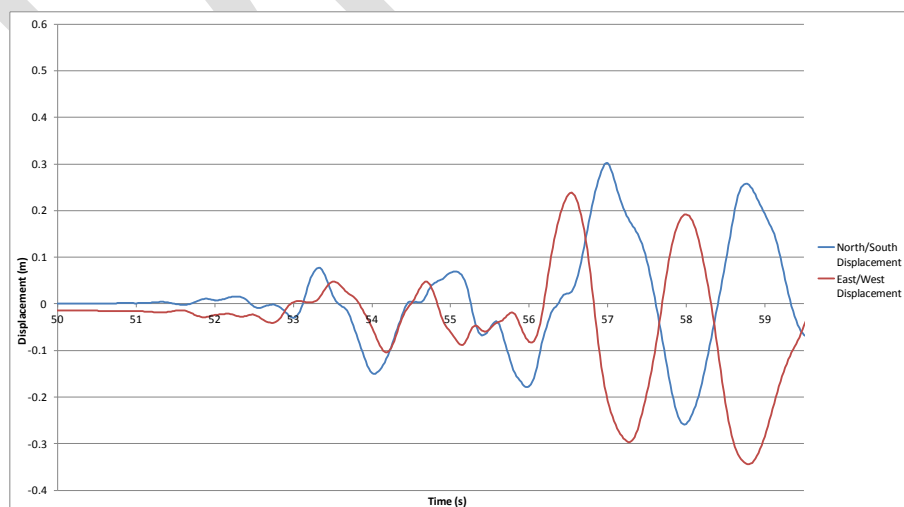


Figure I.2: Level 6 Southeast corner displacements, Lyttelton, CBGS Sequential.

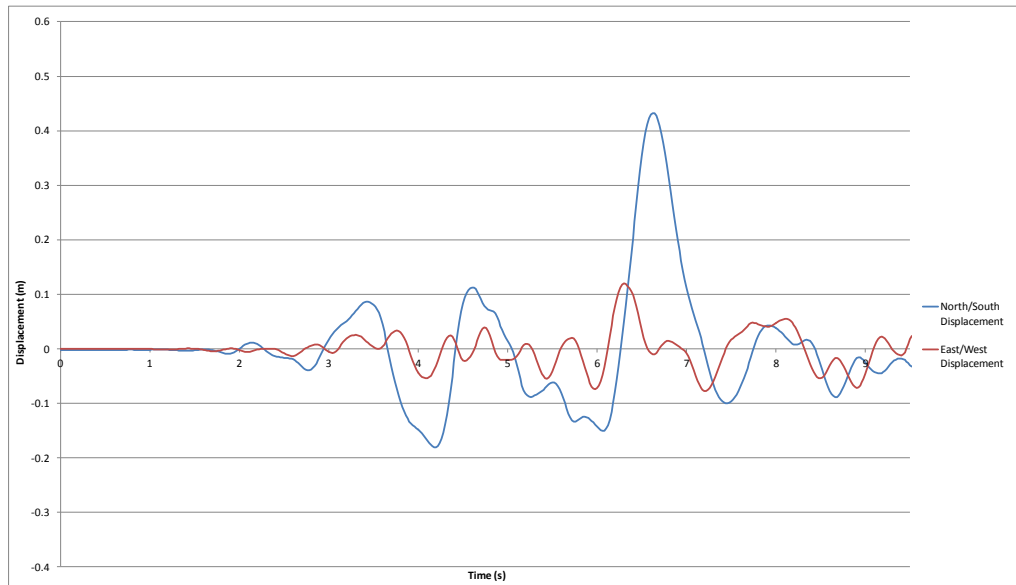


Figure I.3: Level 6 Northwest corner displacements, Lyttelton, CBGS

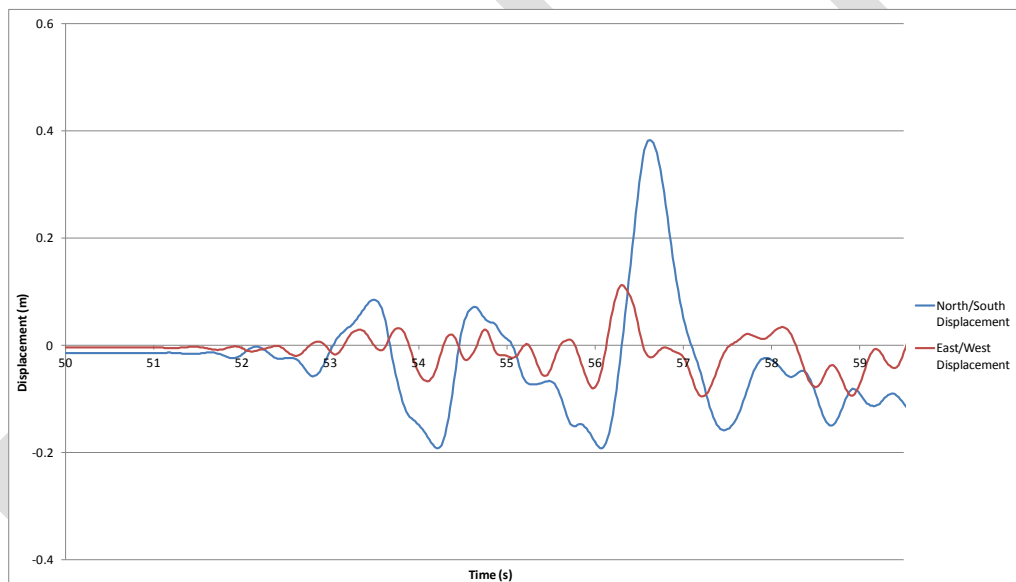


Figure I.4: Level 6 Northwest corner displacements, Lyttelton, CBGS Sequential.

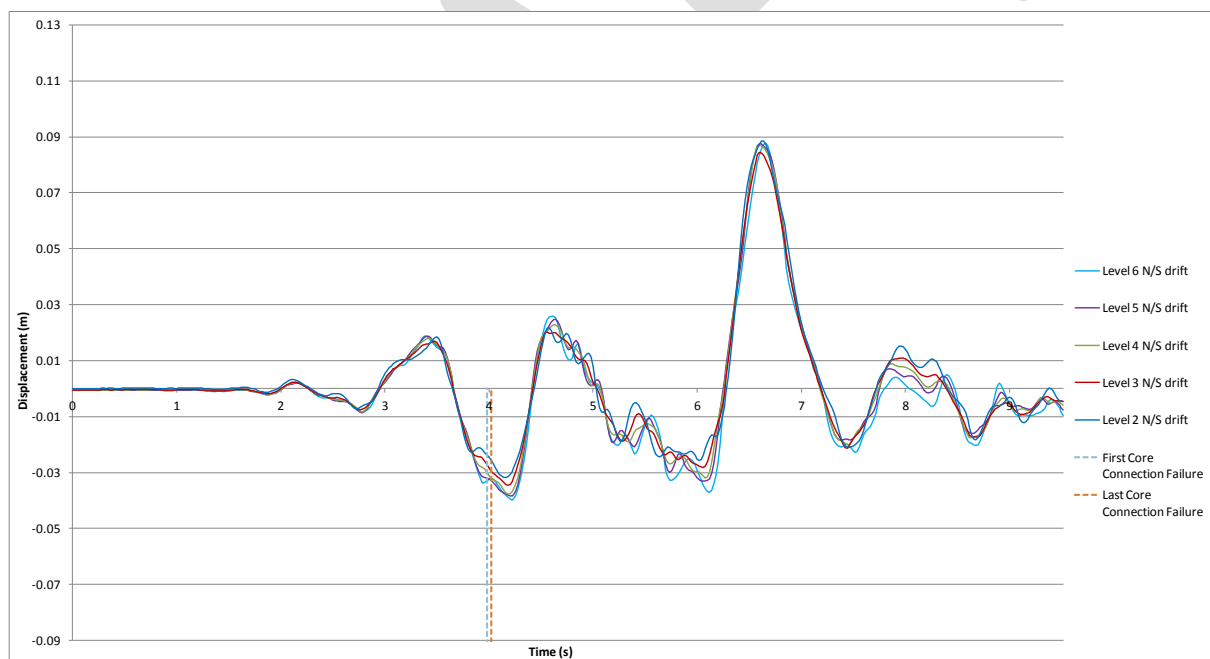
As can be seen in Figure I.3 and Figure I.4 above a significant increase in the northward building displacement is observed in the northwest corner of the building approximately 6.5 seconds into the of the record. This occurs after the tension ties capacities on levels 4 to 6 of the core are exceeded allowing increased building rotation clockwise from west to north. The peak displacement corresponds to a clockwise rotation in conjunction with a net northward building translation. Table I.1 presents the sequence of failure of the north core wall ties throughout the record.

Table I.1: Wall D and D/E diaphragm disconnection times, Lyttelton, CBGS.

Level	Undamaged Analysis		Sequential Analysis	
	Wall D Disconnection (sec)	Wall D/E Disconnection (sec)	Wall D Disconnection (sec)	Wall D/E Disconnection (sec)
6	4.06	4.00	4.06	4.00
5	4.04	4.00	4.04	4.00
4	4.02	3.98	4.02	3.98

It can be seen from Table I.1 that the sequential analysis continuing from the end of the Darfield CBGS record has no impact on the performance of the diaphragm ties.

Inter-storey displacements for the perimeter frame lines A and F in the north/south direction are presented in Figure I.3 to Figure I.8 below. North core tie tensile failure is identified on the plots for reference.

**Figure I.5: Frame A north/south inter-storey displacements, Lyttelton, CBGS**

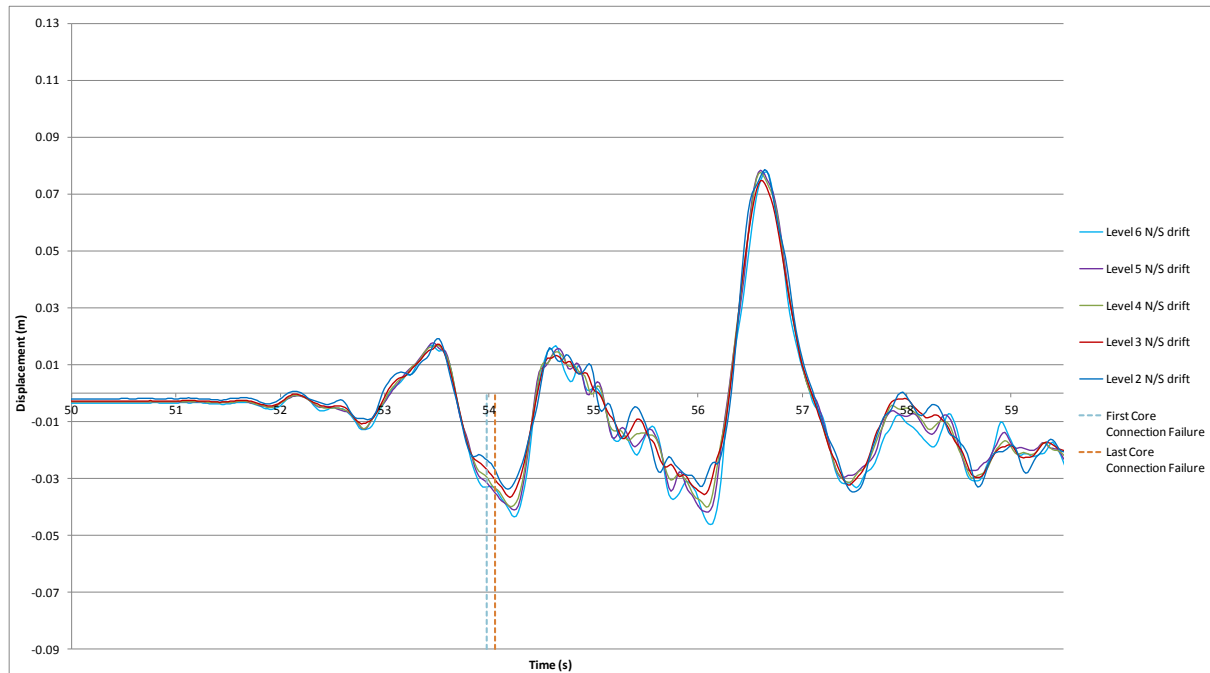


Figure I.6: Frame A north/south inter-storey displacements, Lyttelton, CBGS Sequential.

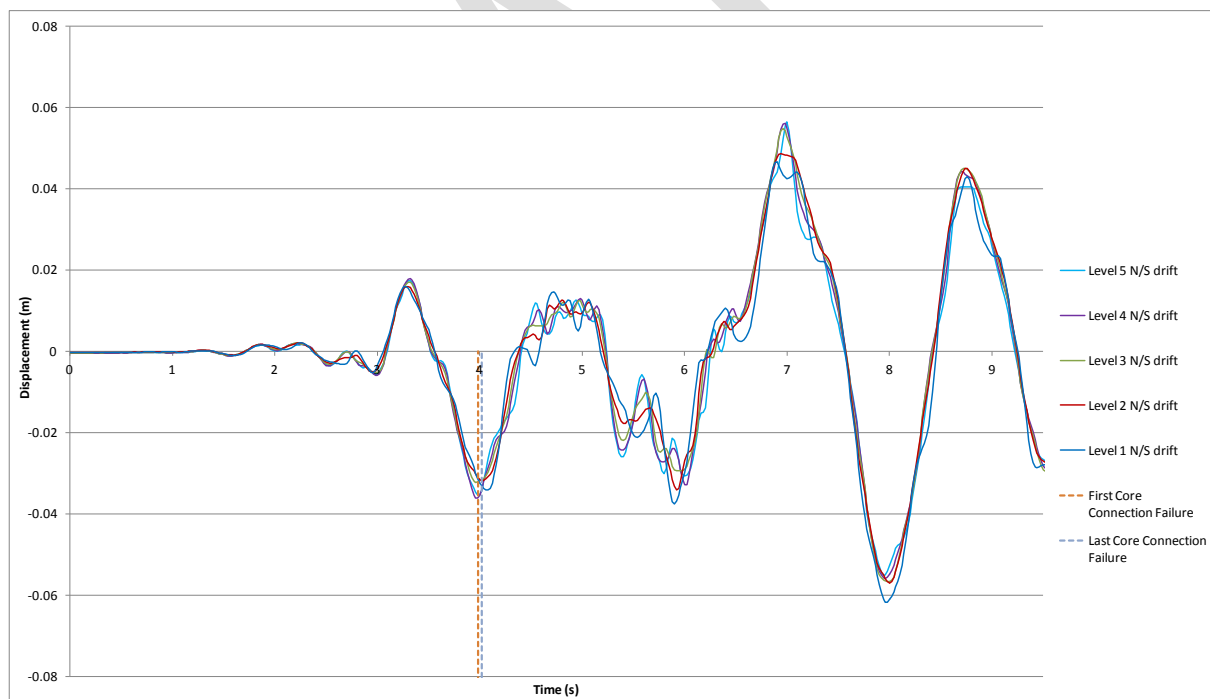


Figure I.7: Frame F north/south inter-storey displacements, Lyttelton, CBGS

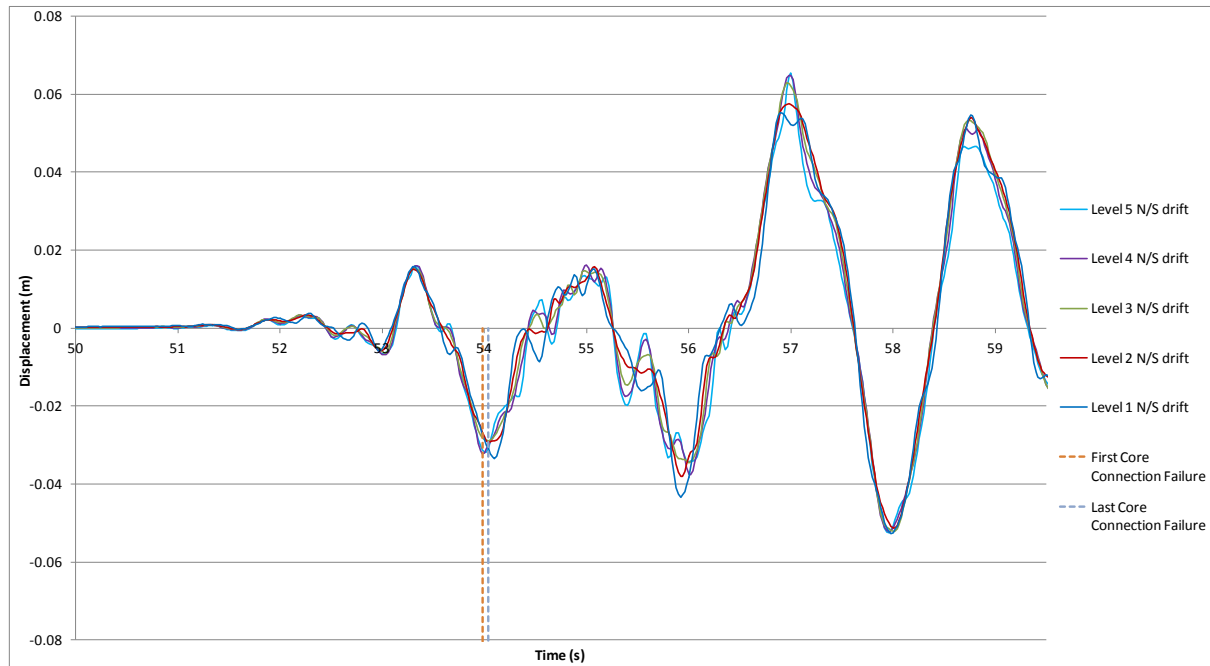


Figure I.8: Frame F north/south inter-storey displacements, Lyttelton, CBGS Sequential.

Inter-storey displacements for the perimeter frame lines 1 and 4 in the East/West direction are presented in Figure I.9, to Figure I.12 below.

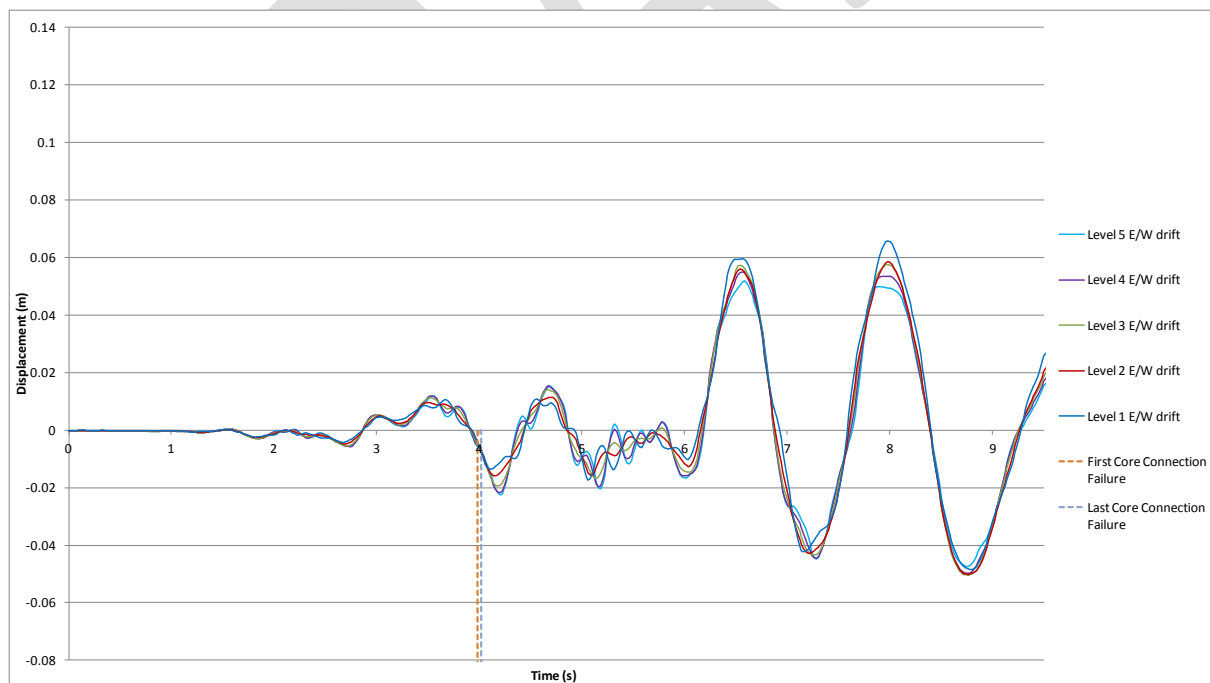


Figure I.9: Frame 1 east/west inter-storey displacements, Lyttelton, CBGS

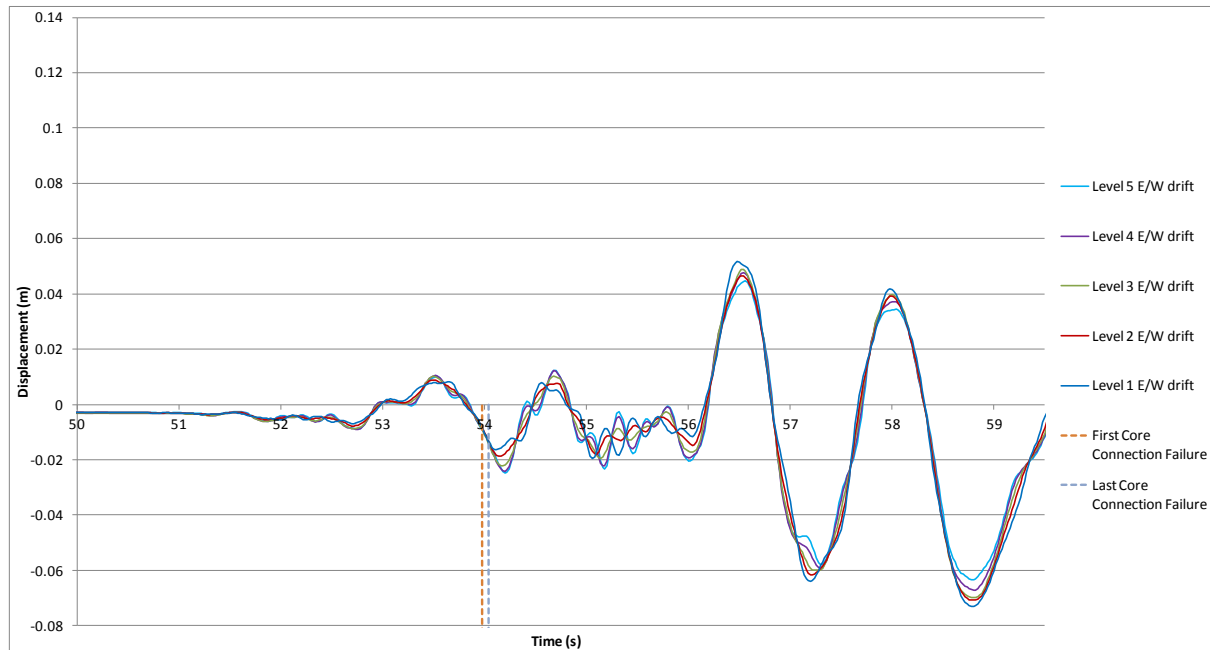


Figure I.10: Frame 1 east/west inter-storey displacements, Lyttelton, CBGS Sequential.

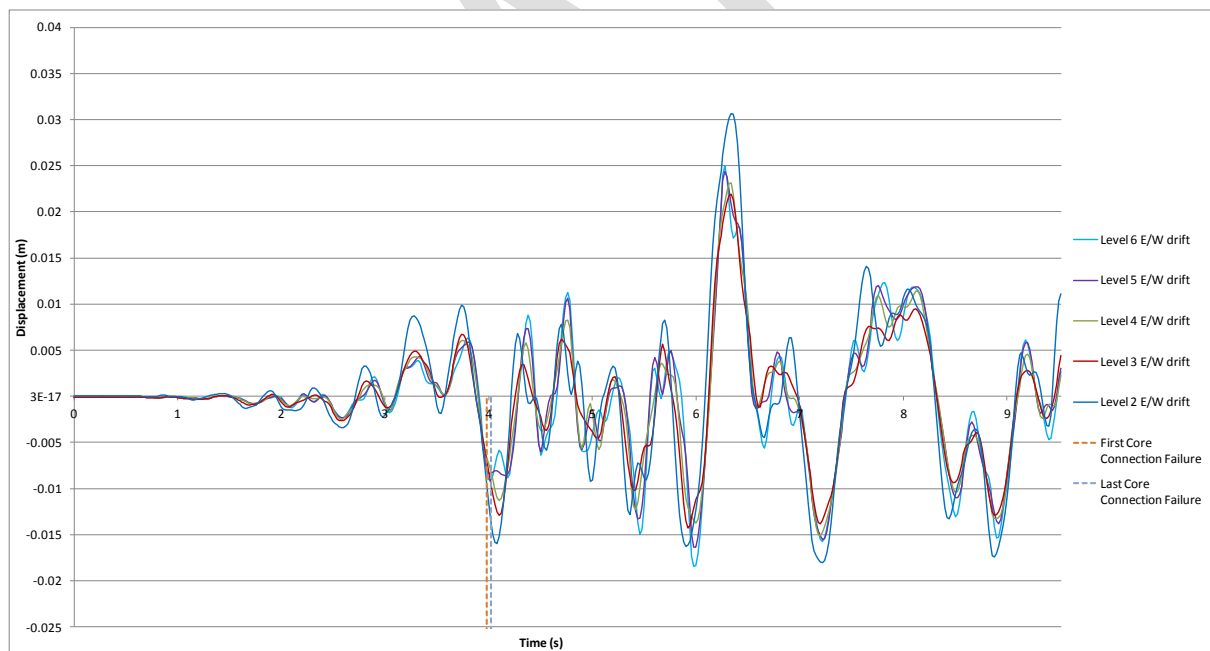


Figure I.11: Frame 4 east/west inter-storey displacements, Lyttelton, CBGS

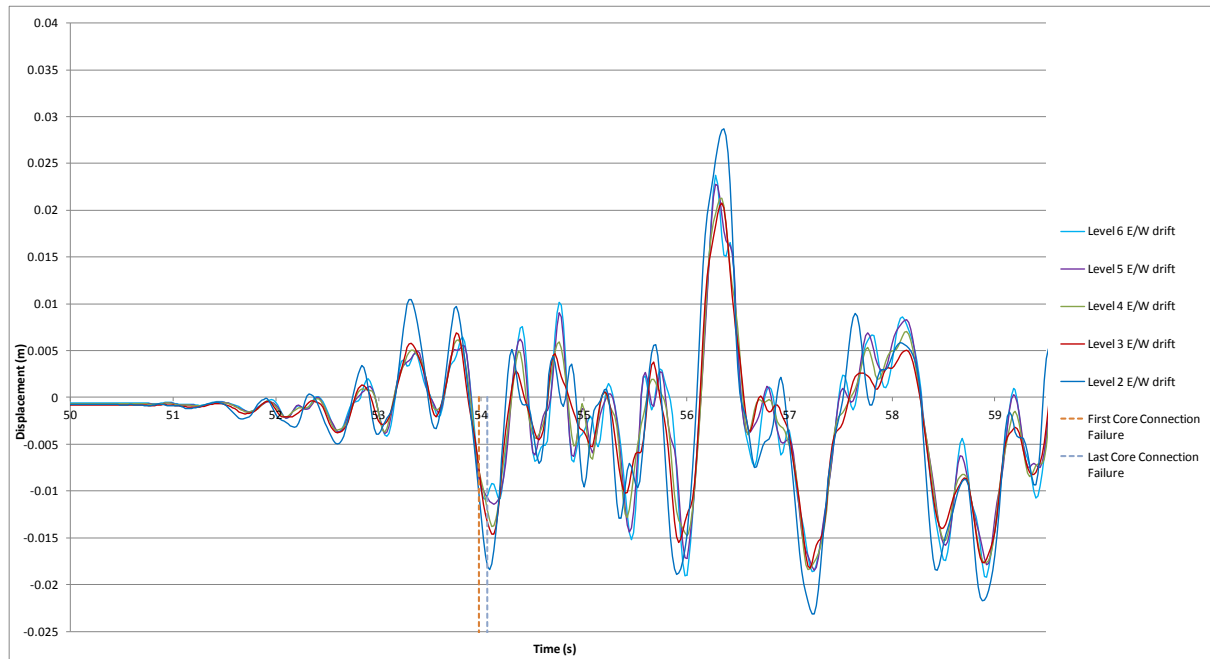


Figure I.12: Frame 4 east/west inter-storey displacements, Lyttelton, CBGS Sequential.

I.2 Diaphragm Connection Forces

Diaphragm connection forces are presented in Figure I.13 to Figure I.24 below. Note that moments are reported about the geometric centroid of the element being considered.

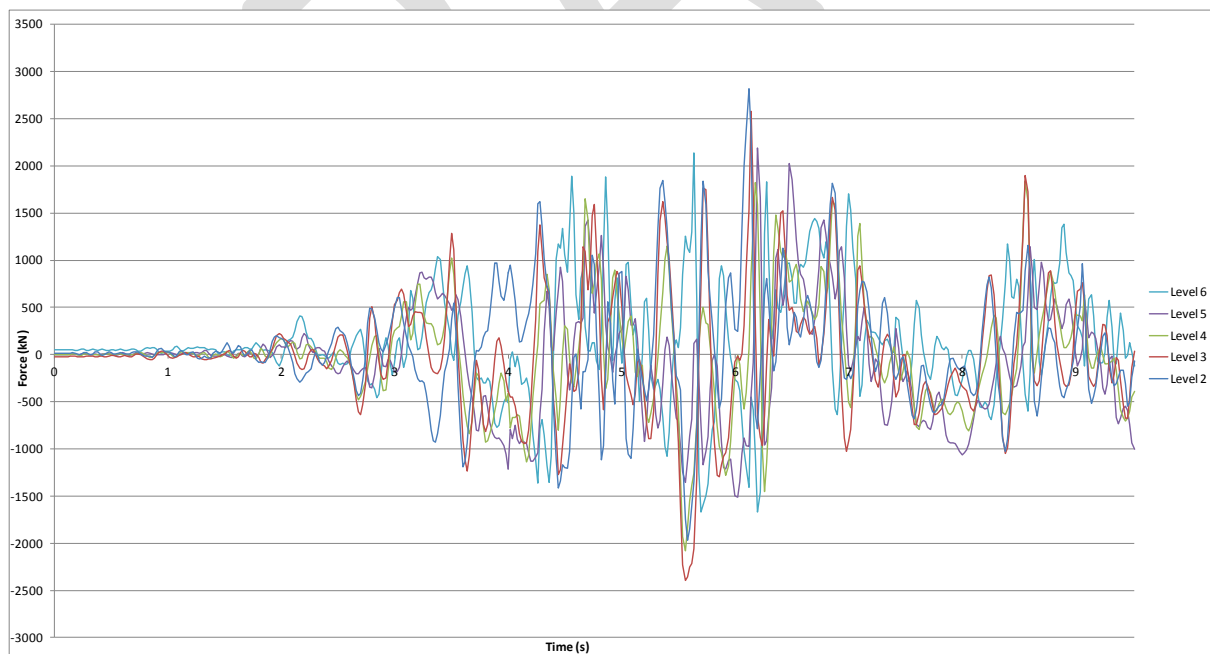


Figure I.13: North core total diaphragm north/south actions, Lyttelton, CBGS

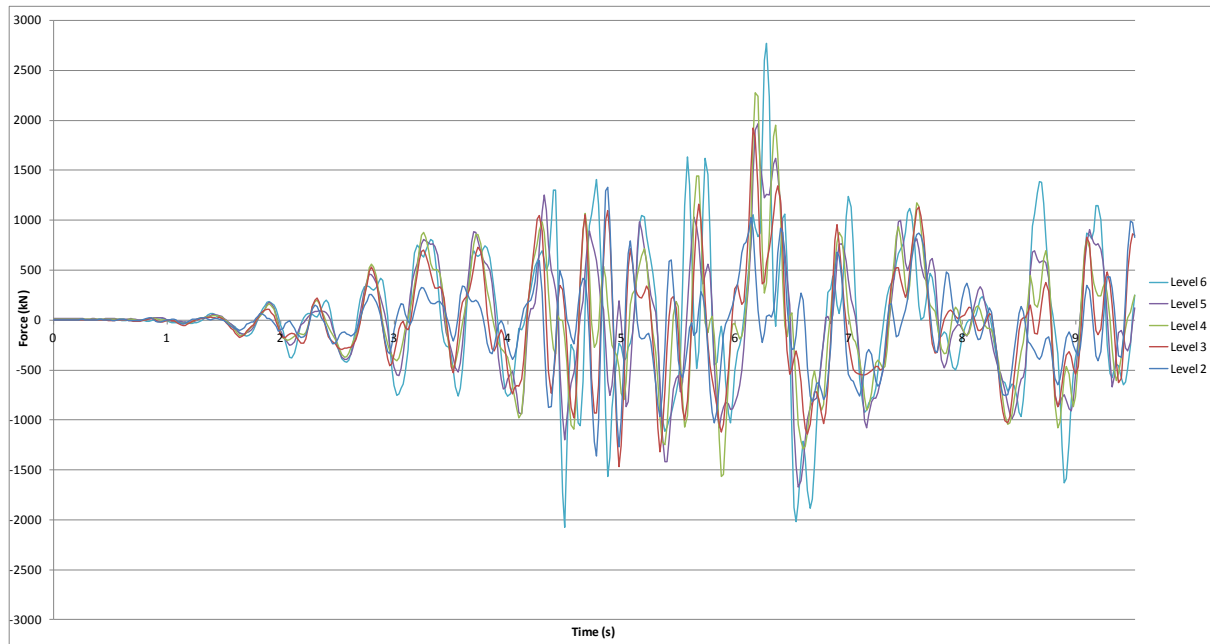


Figure I.14: North core total diaphragm east/west actions, Lyttelton, CBGS

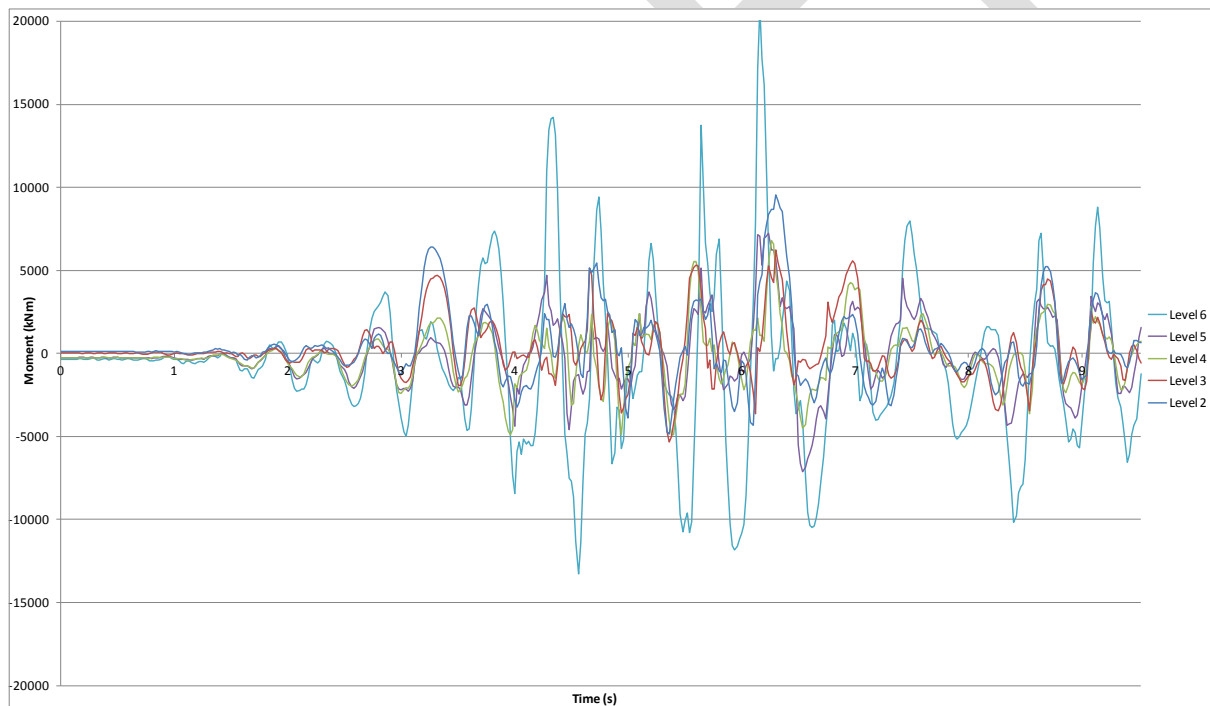


Figure I.15: North core total diaphragm in-plane moments, Lyttelton, CBGS

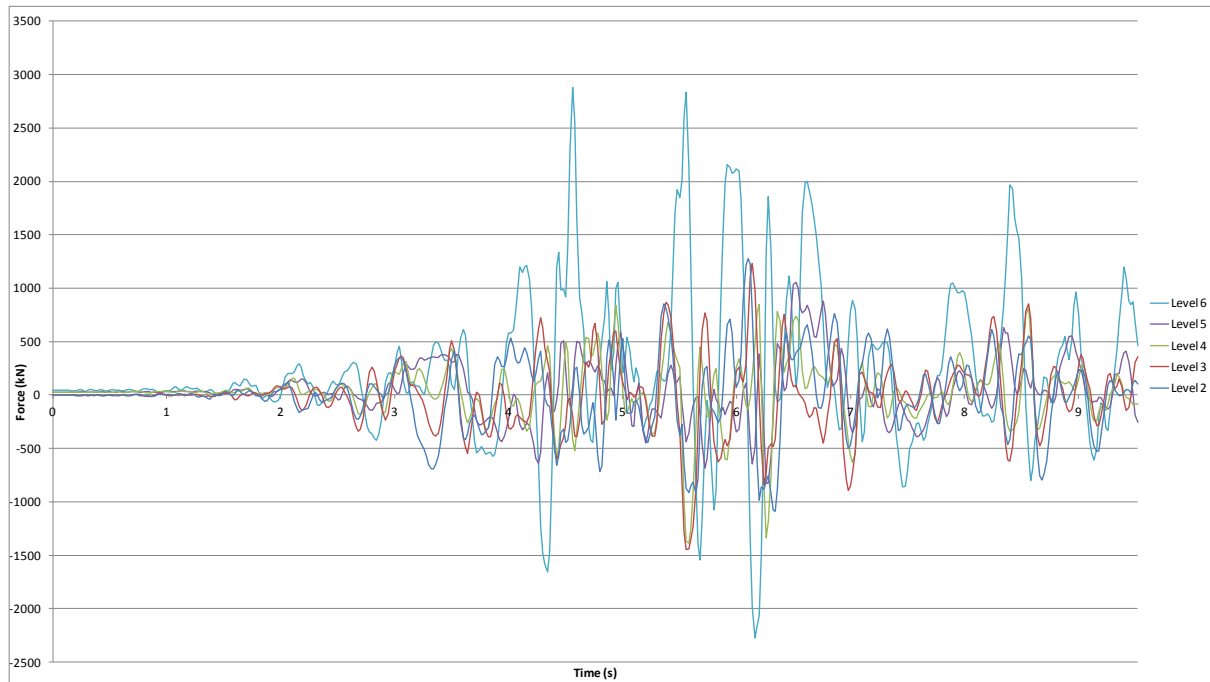


Figure I.16: North core Wall C diaphragm north/south actions, Lyttelton, CBGS

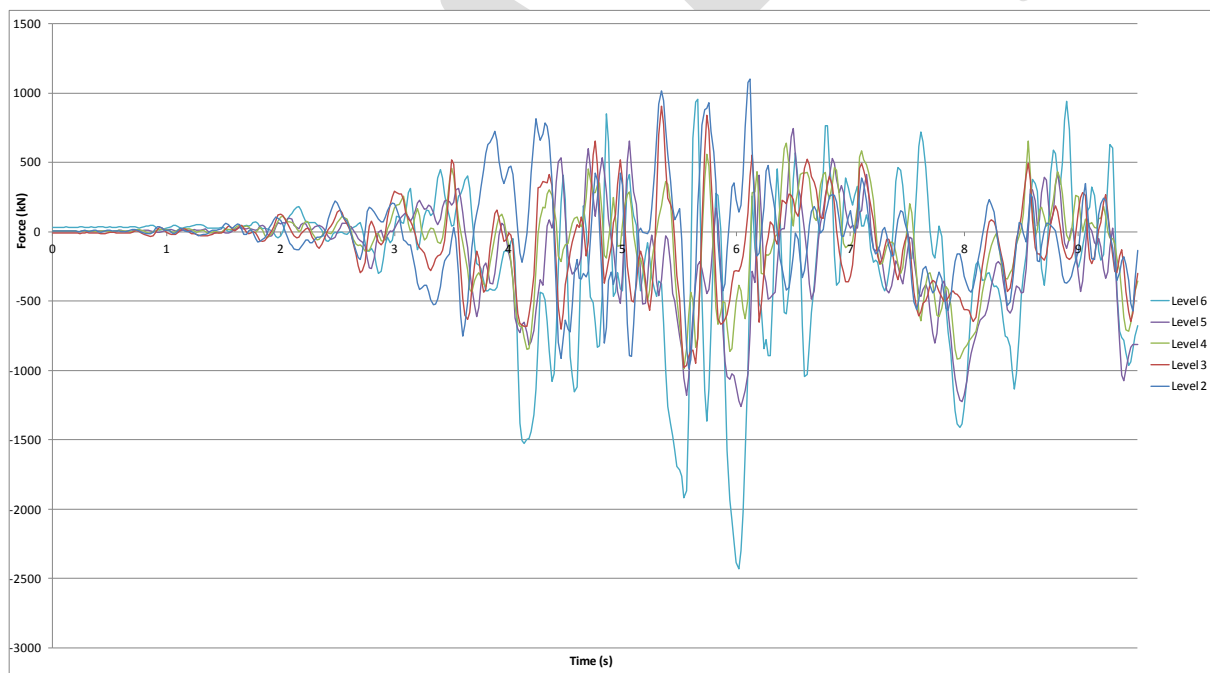


Figure I.17: North core Wall C/D diaphragm north/south actions, Lyttelton, CBGS

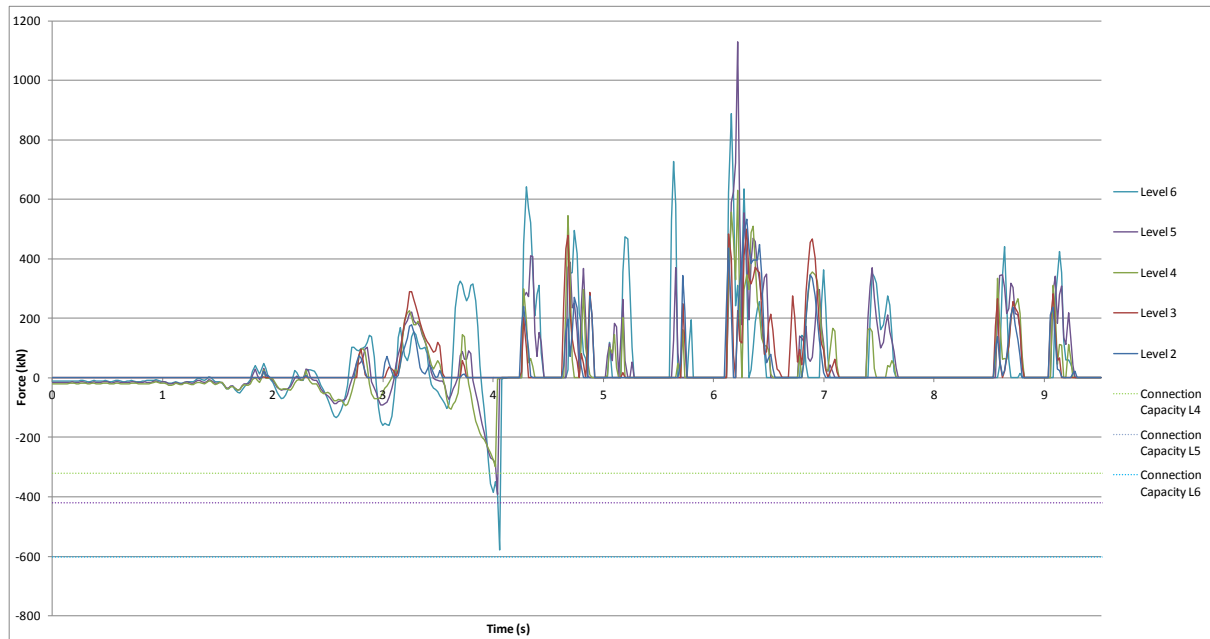


Figure I.18: North core Wall D diaphragm north/south actions, Lyttelton, CBGS

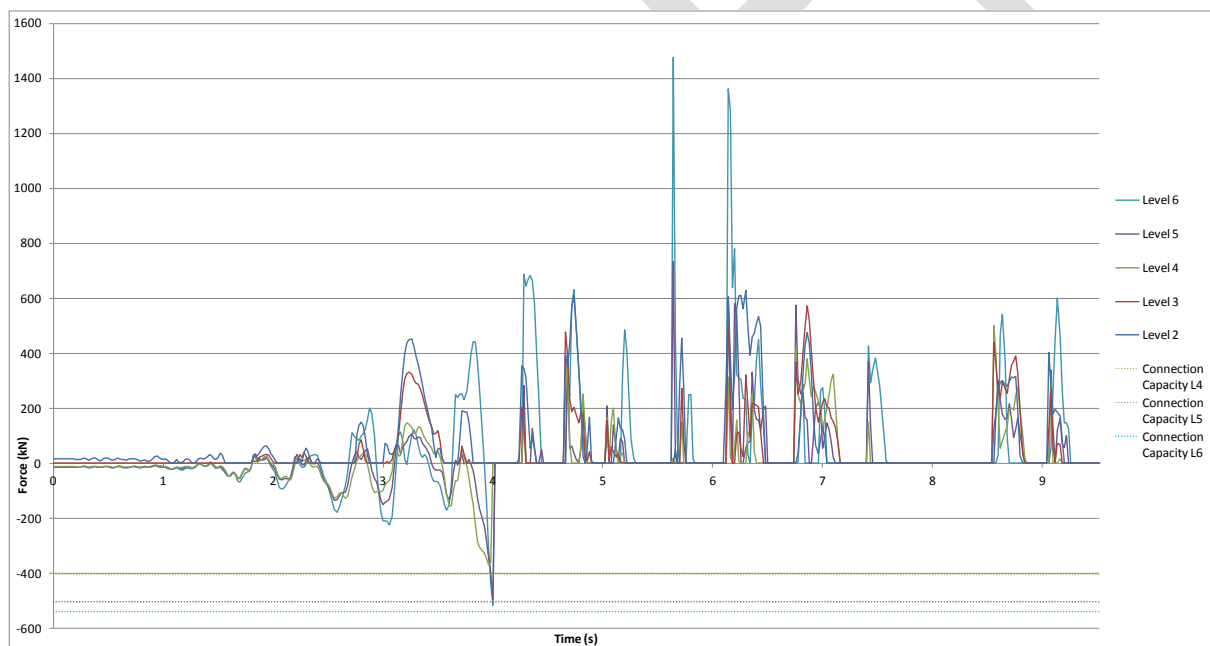


Figure I.19: North core Wall D/E diaphragm north/south actions, Lyttelton, CBGS

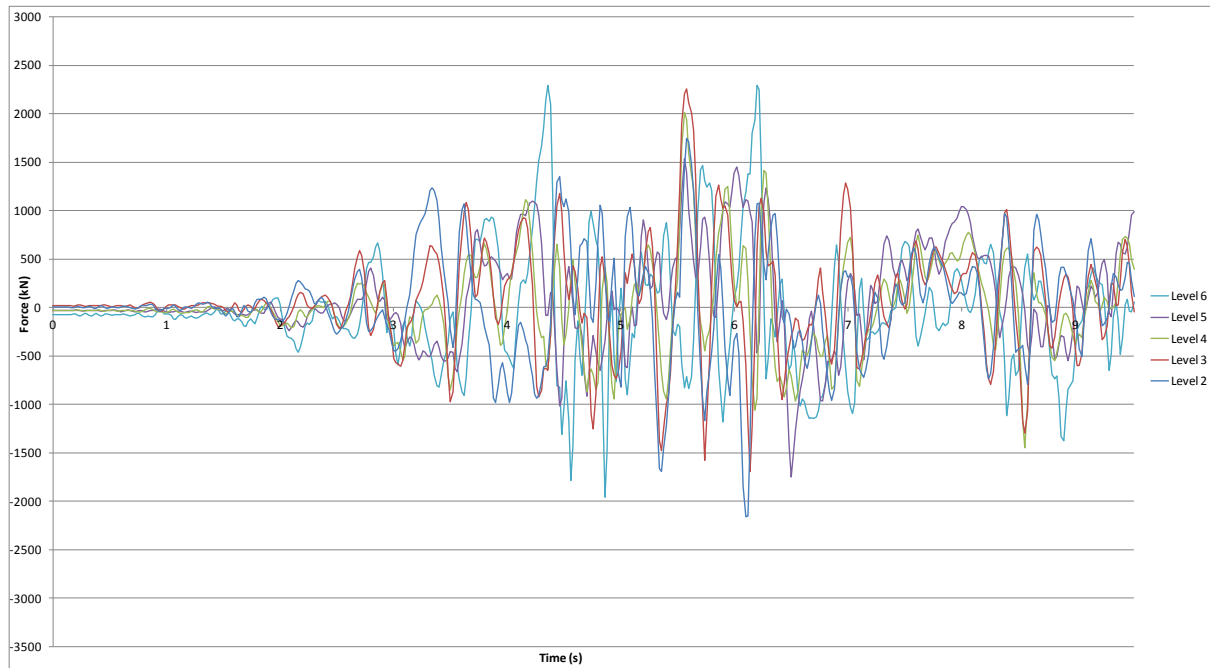


Figure I.20: North core Slab 4/C to C/D diaphragm north/south actions, Lyttelton, CBGS

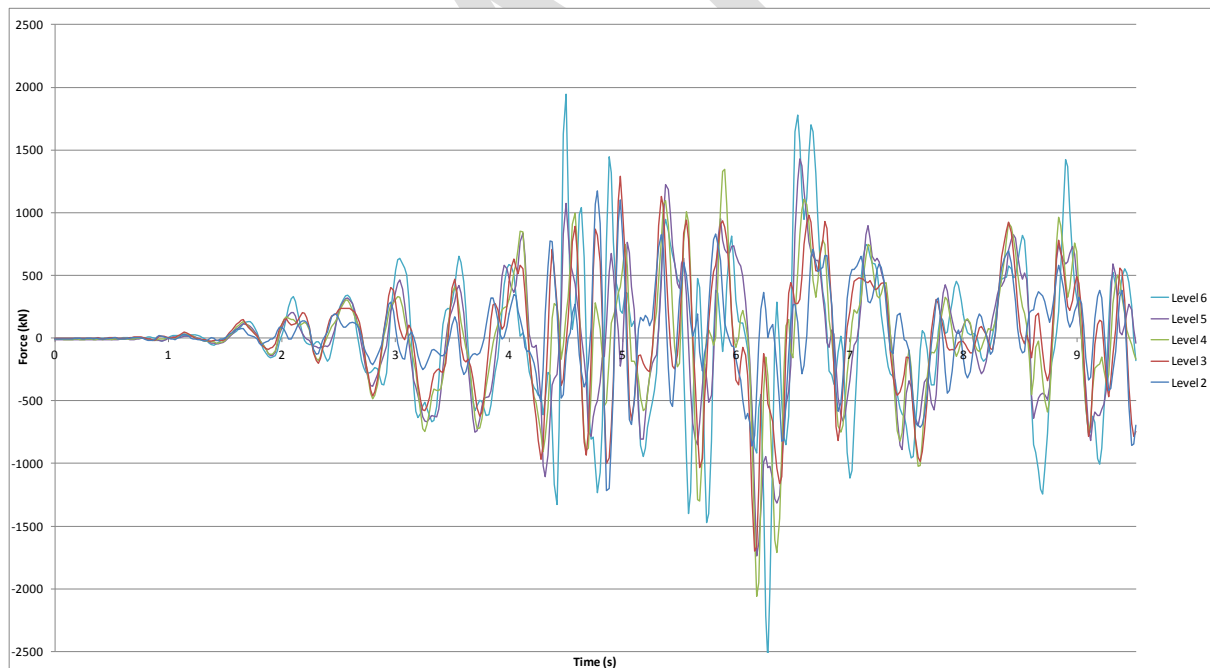


Figure I.21: North core Slab 4/C to C/D diaphragm east/west actions, Lyttelton, CBGS

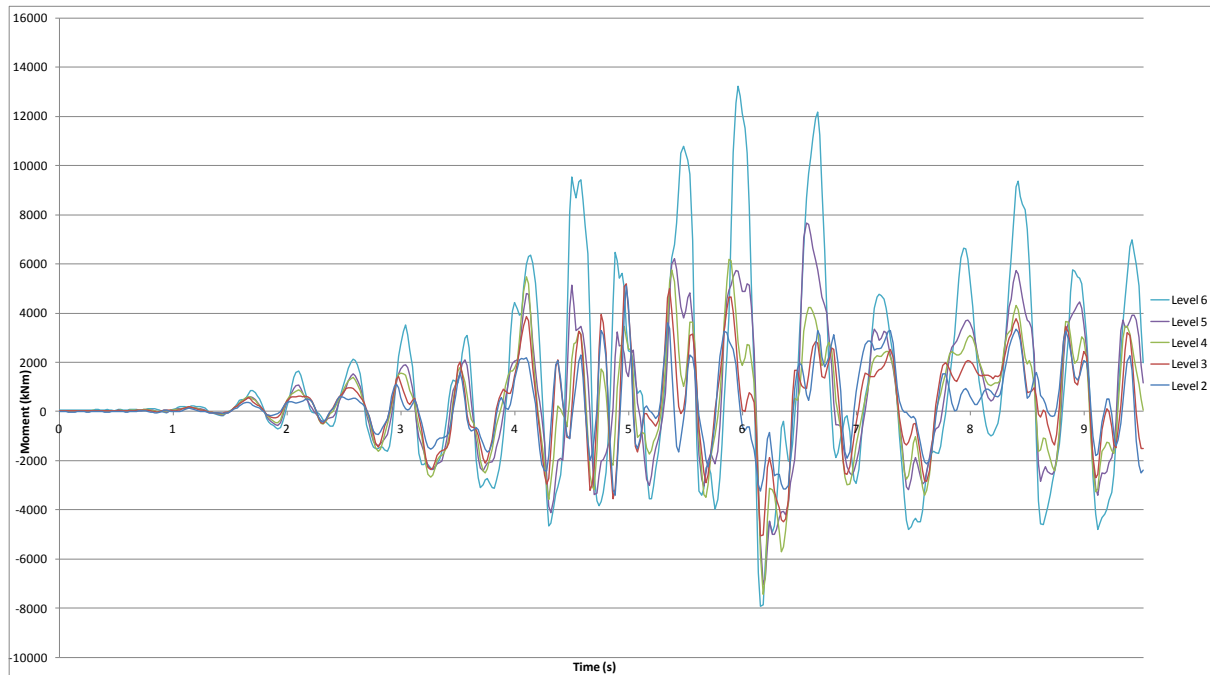


Figure I.22: North core Slab 4/C to C/D diaphragm in-plane moments, Lyttelton, CBGS

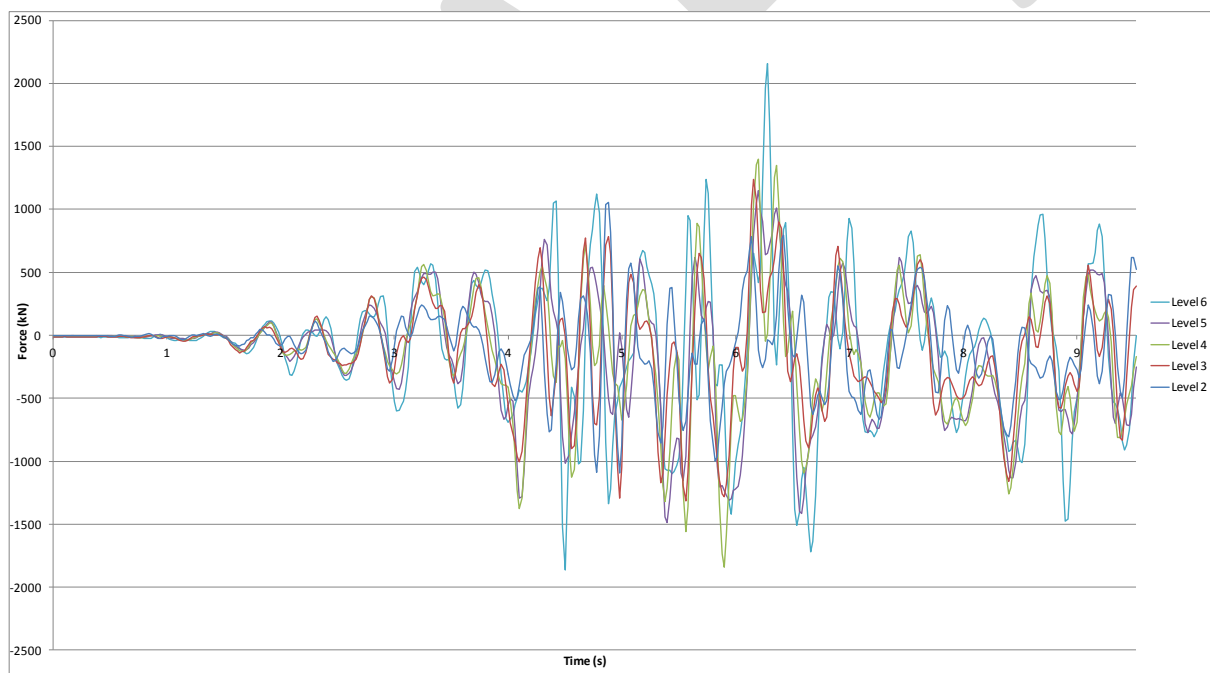


Figure I.23: North core Wall 5 diaphragm east/west actions, Lyttelton, CBGS

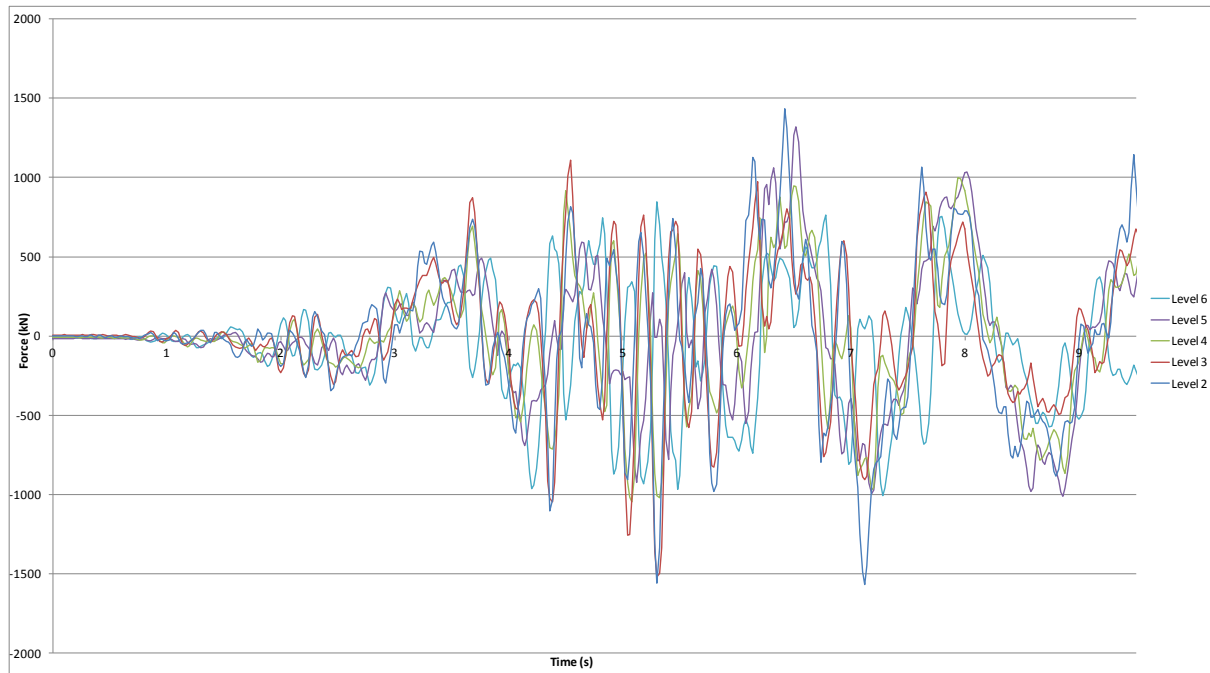


Figure I.24: South wall diaphragm east/west actions, Lyttelton, CBGS

I.3 Column Hinge Actions

Figure I.25 to Figure I.29 present a selection of column hinge rotations, elongations, and concrete strains for a selected number of critical columns. Strains reported are the maximum that occur at the extreme concrete fibre. Plots are presented for individual columns and are orientated so that the top row of plots relate to the level 5 hinges with each row below corresponding to the hinges in the column below i.e. from the top level to the bottom level. Results presented are for the worst case hinge at each floor level, with hinge rotation and elongation shown in the left hand plot and hinge concrete strain shown in the right hand plot.

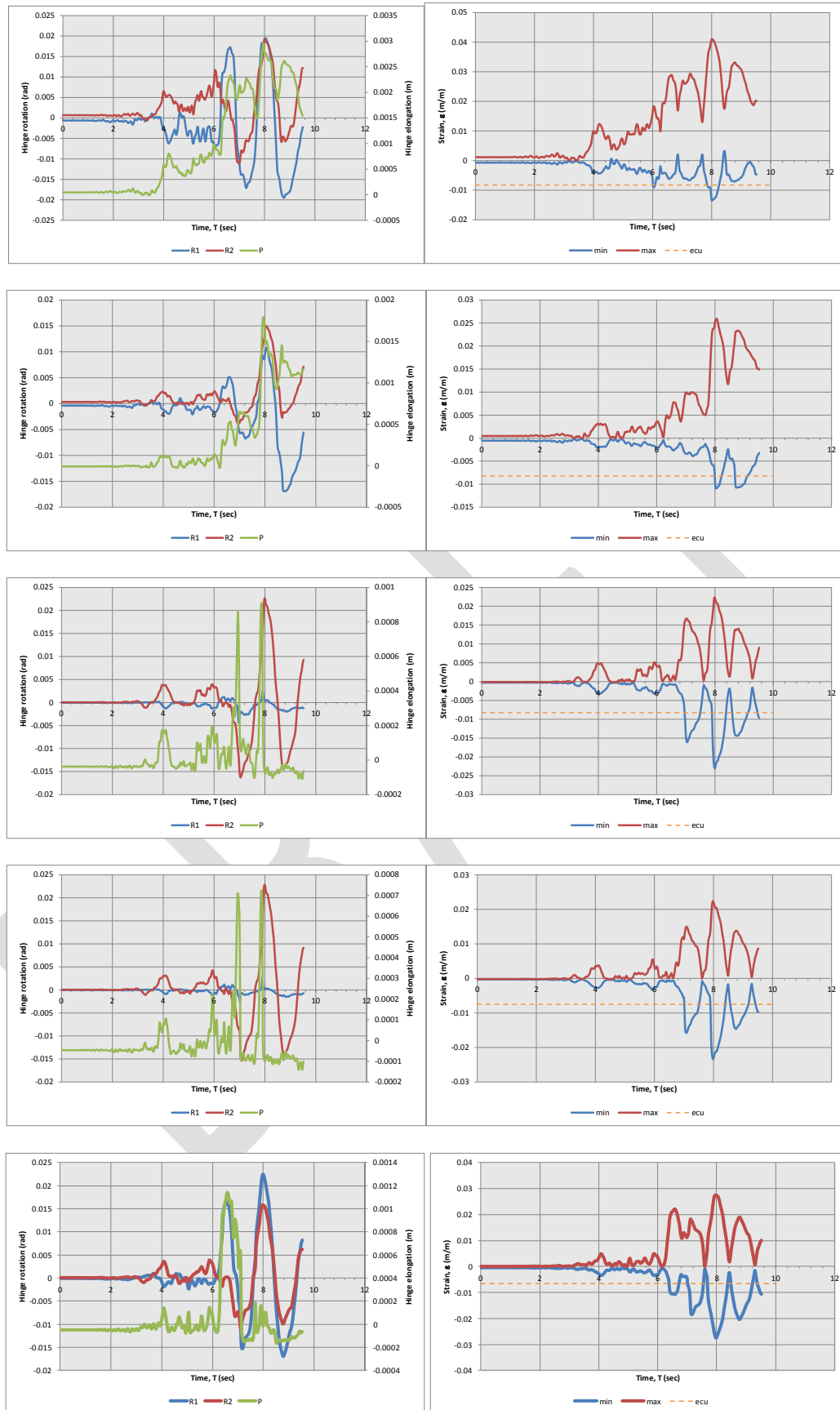


Figure I.25: Column F1 Levels 1 (bottom) to 5 (top) hinge actions, Lyttelton, CBGS

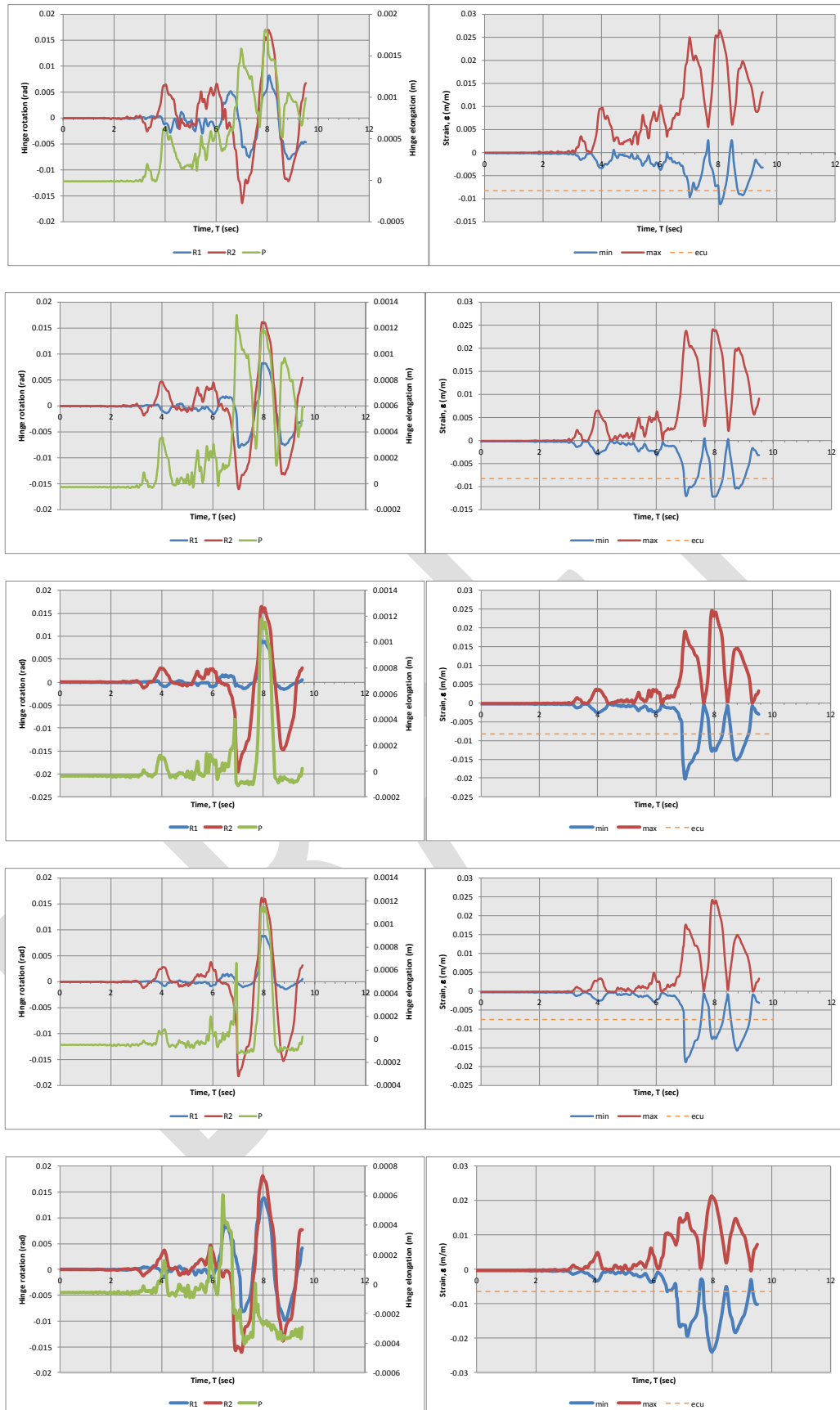


Figure I.26: Column F2 Levels 1 (bottom) to 5 (top) hinge actions, Lyttelton, CBGS

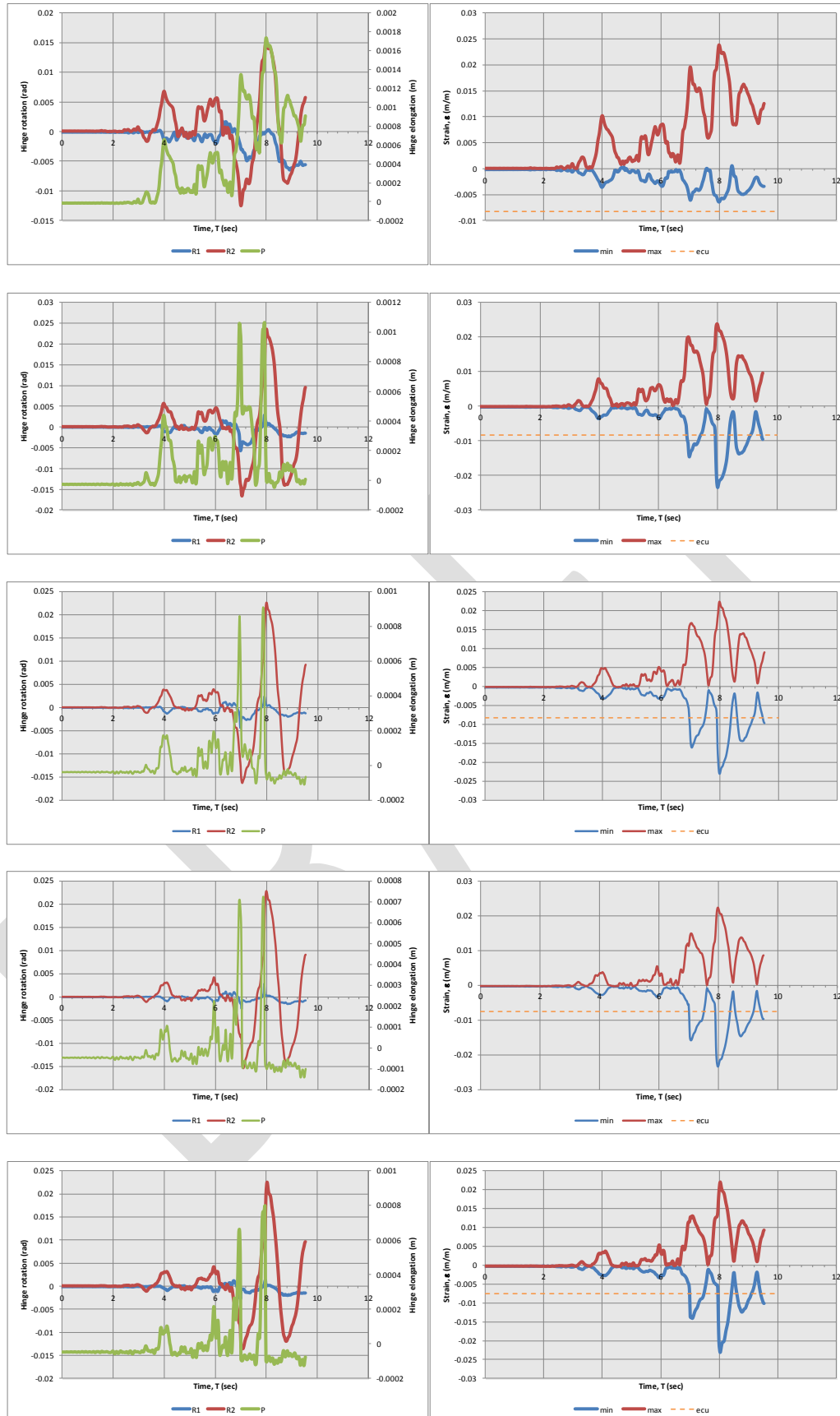


Figure I.27: Column F3 Levels 1 (bottom) to 5 (top) hinge actions, Lyttelton, CBGS

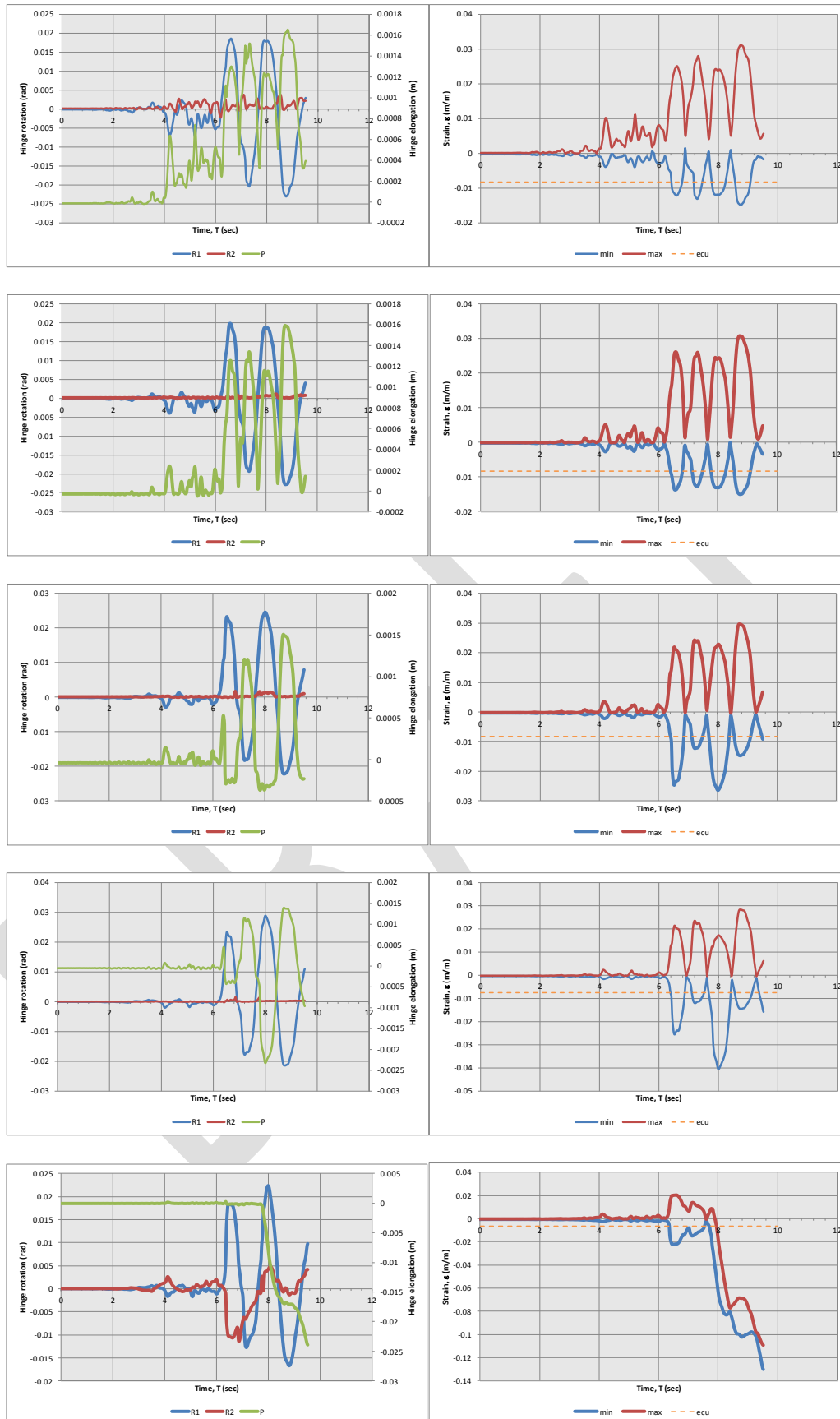


Figure I.28: Column C1 Levels 1 (bottom) to 5 (top) hinge actions, Lyttelton, CBGS

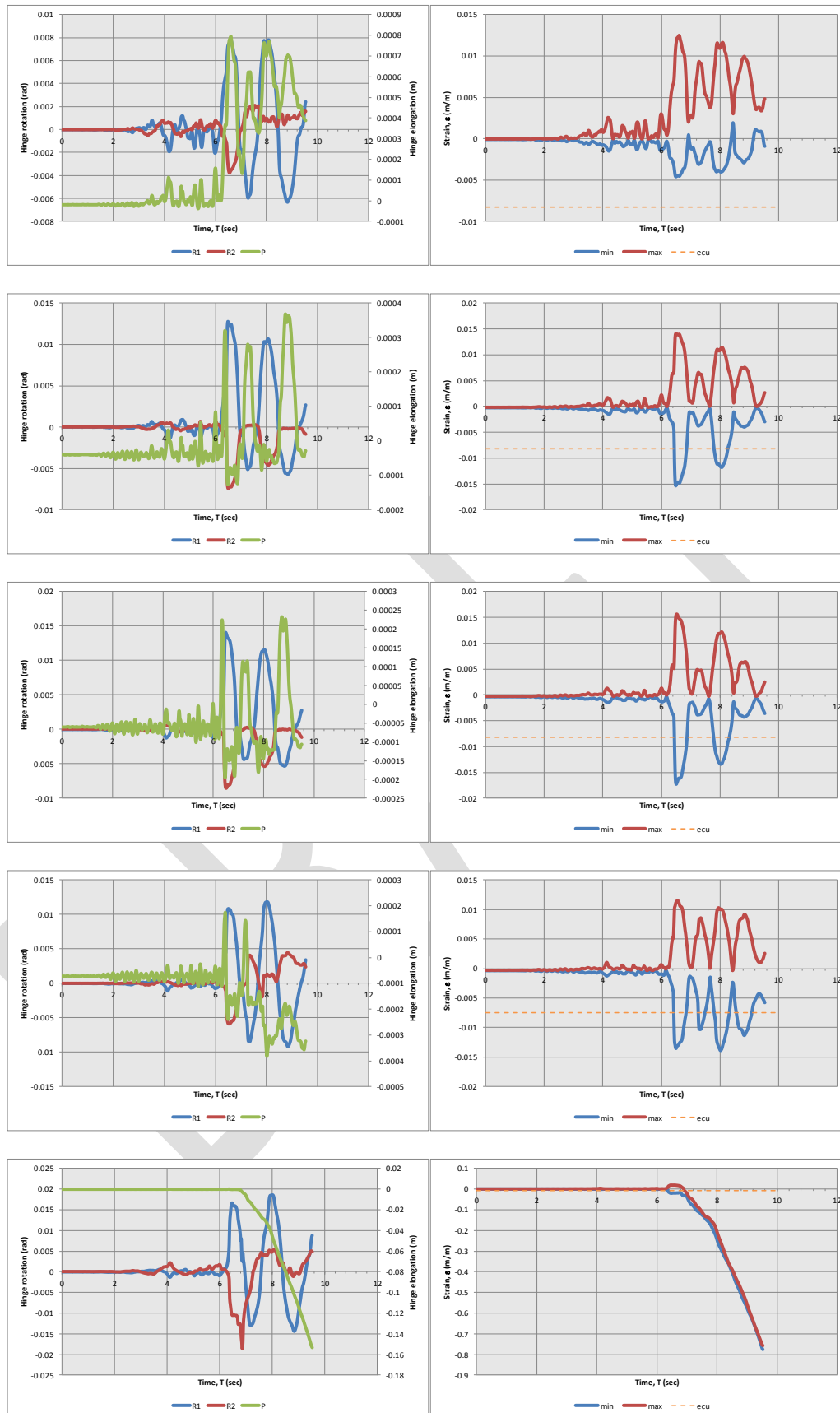


Figure I.29: Column C2 Levels 1 (bottom) to 5 (top) hinge actions, Lyttelton, CBGS

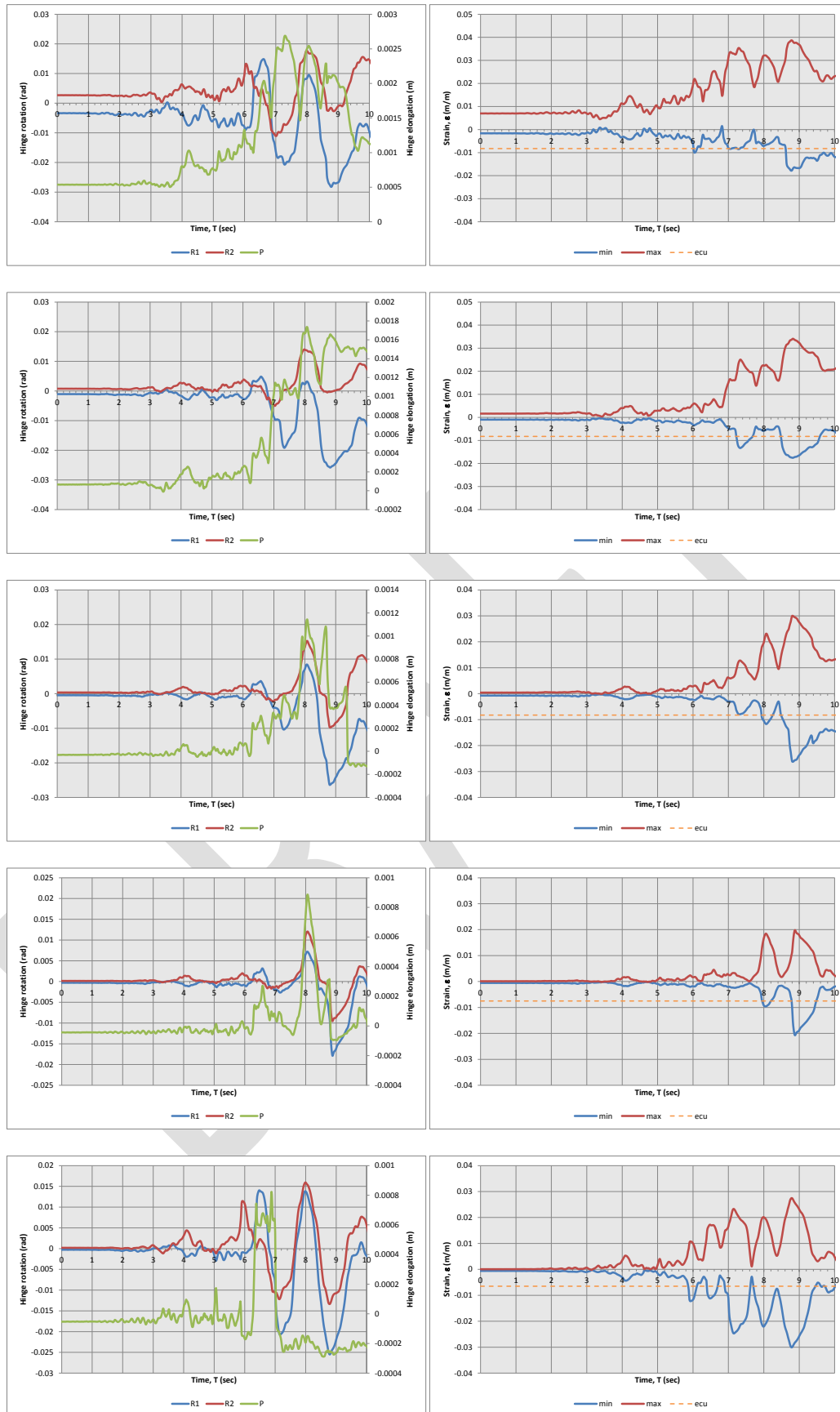


Figure I.30: Column F1 Levels 1 (bottom) to 5 (top) hinge actions, Lyttelton, CBGS Sequential

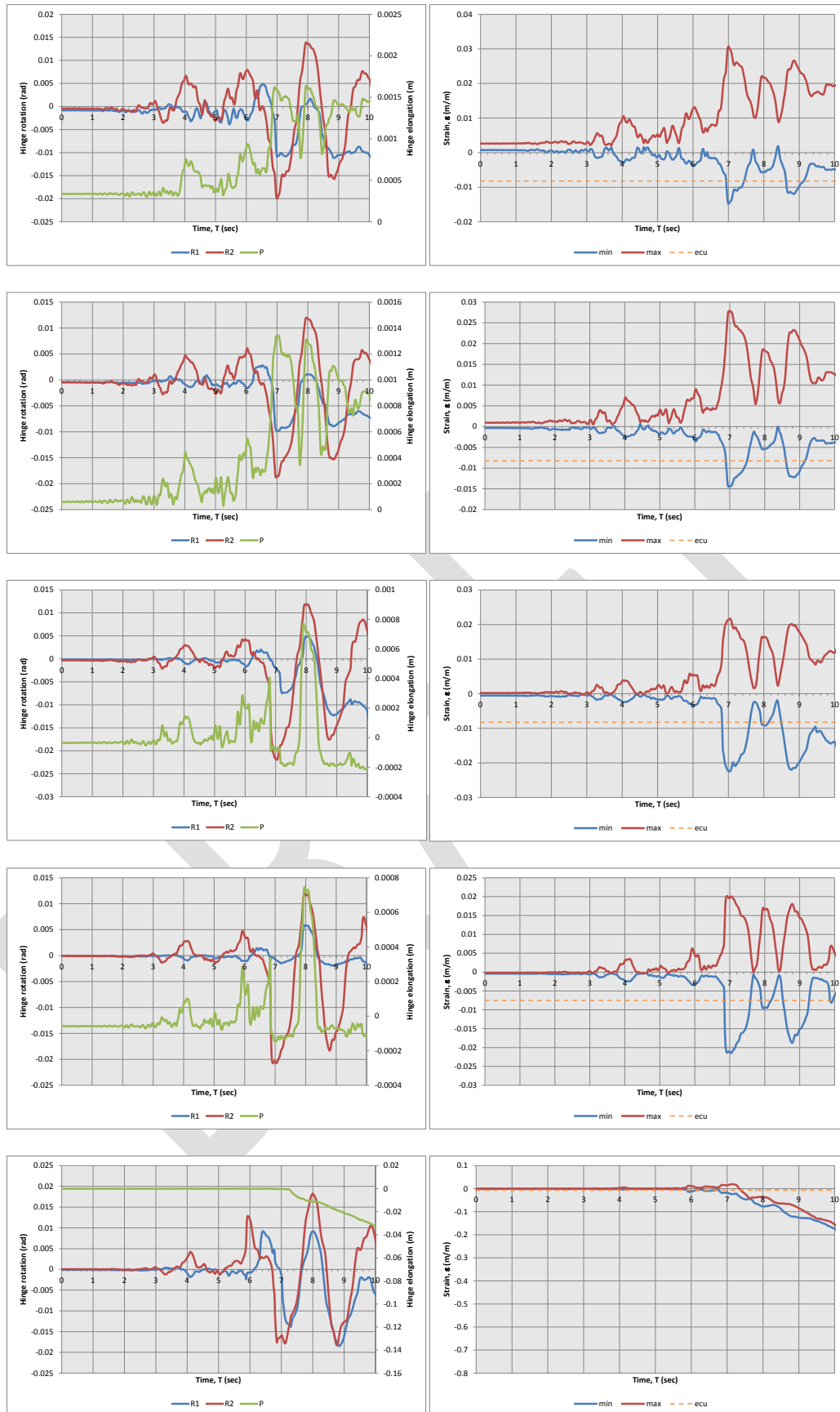


Figure I.31: Column F2 Levels 1 (bottom) to 5 (top) hinge actions, Lyttelton, CBGS Sequential

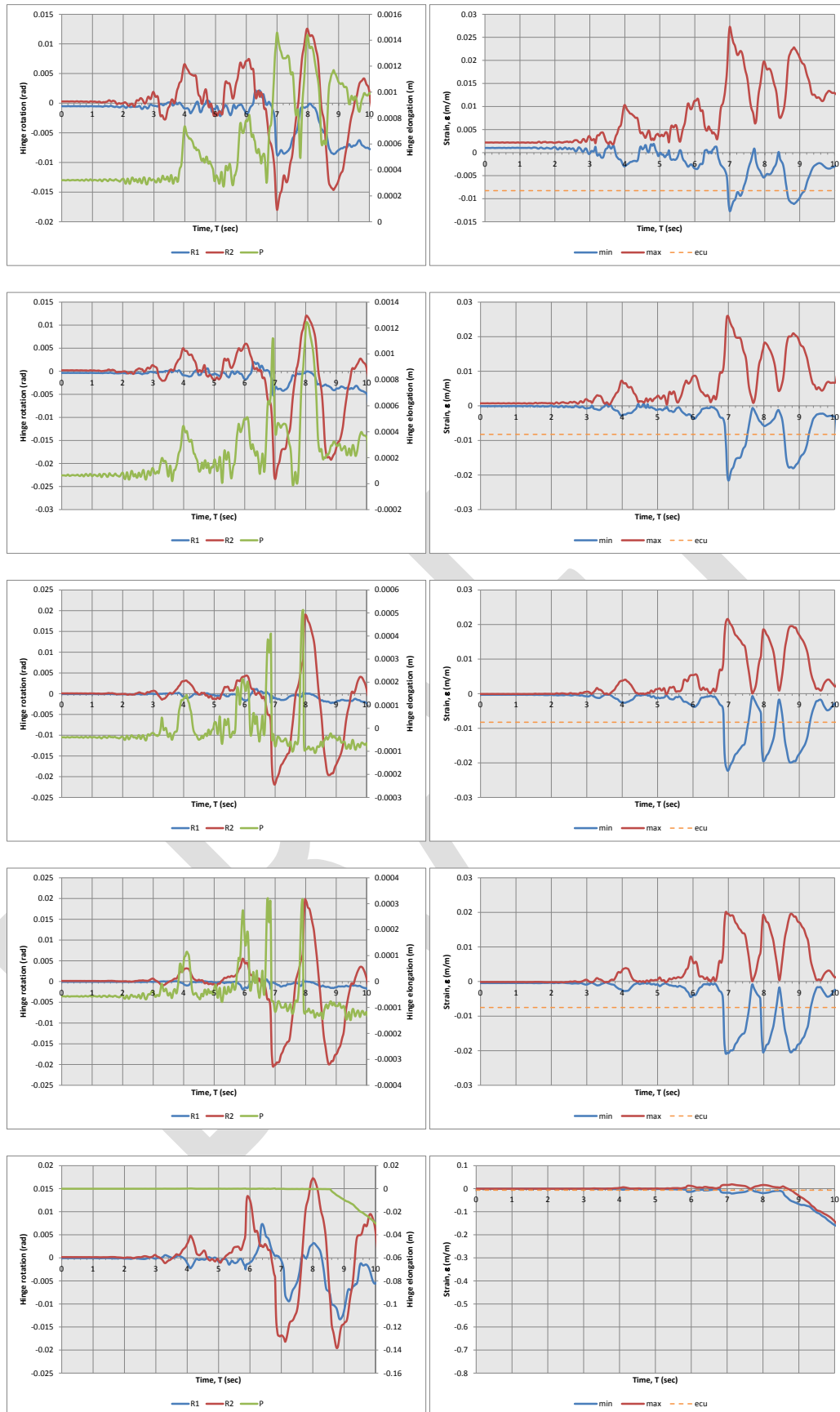


Figure I.32: Column F3 Levels 1 (bottom) to 5 (top) hinge actions, Lyttelton, CBGS Sequential.

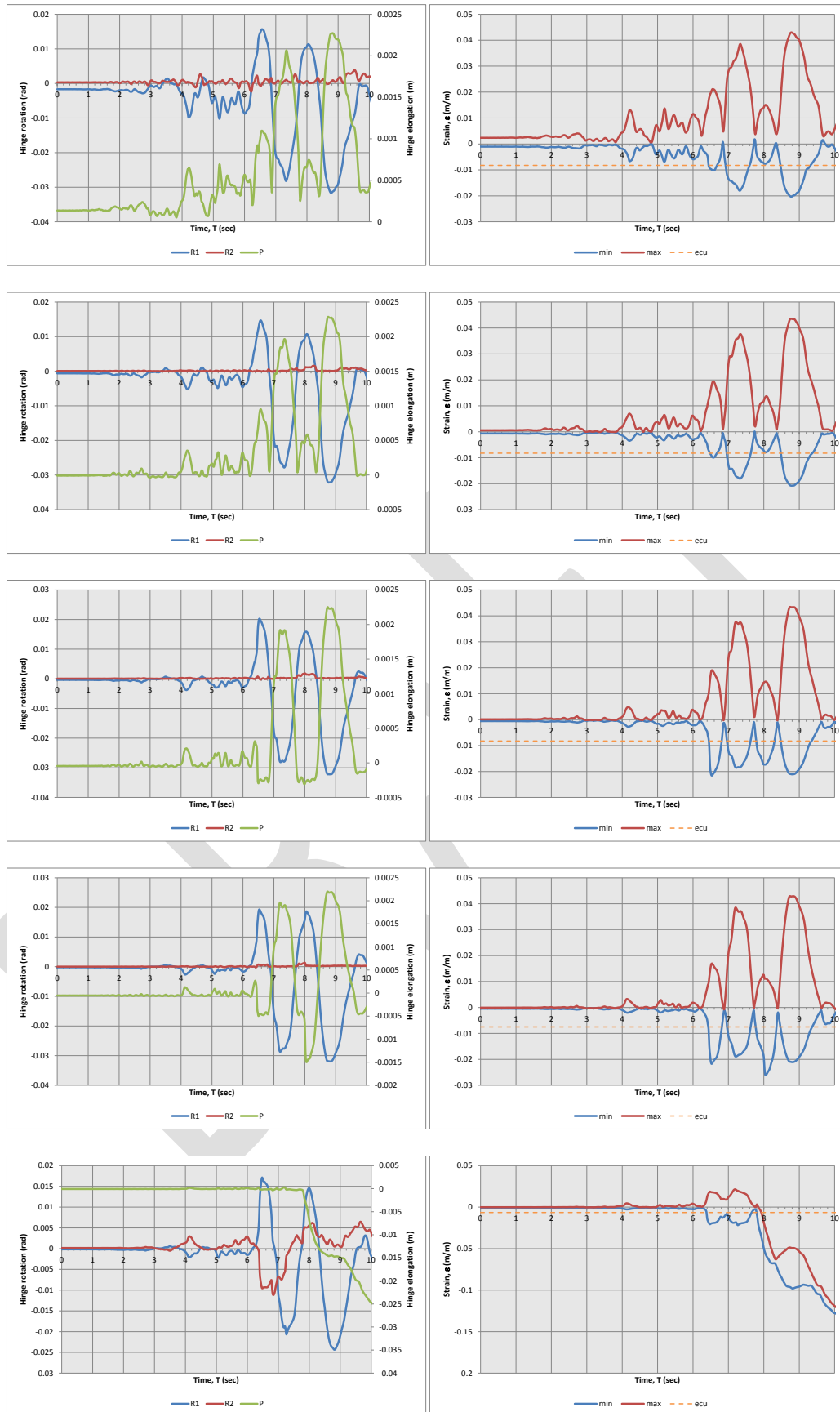


Figure I.33: Column C1 Levels 1 (bottom) to 5 (top) hinge actions, Lyttelton, CBGS Sequential.

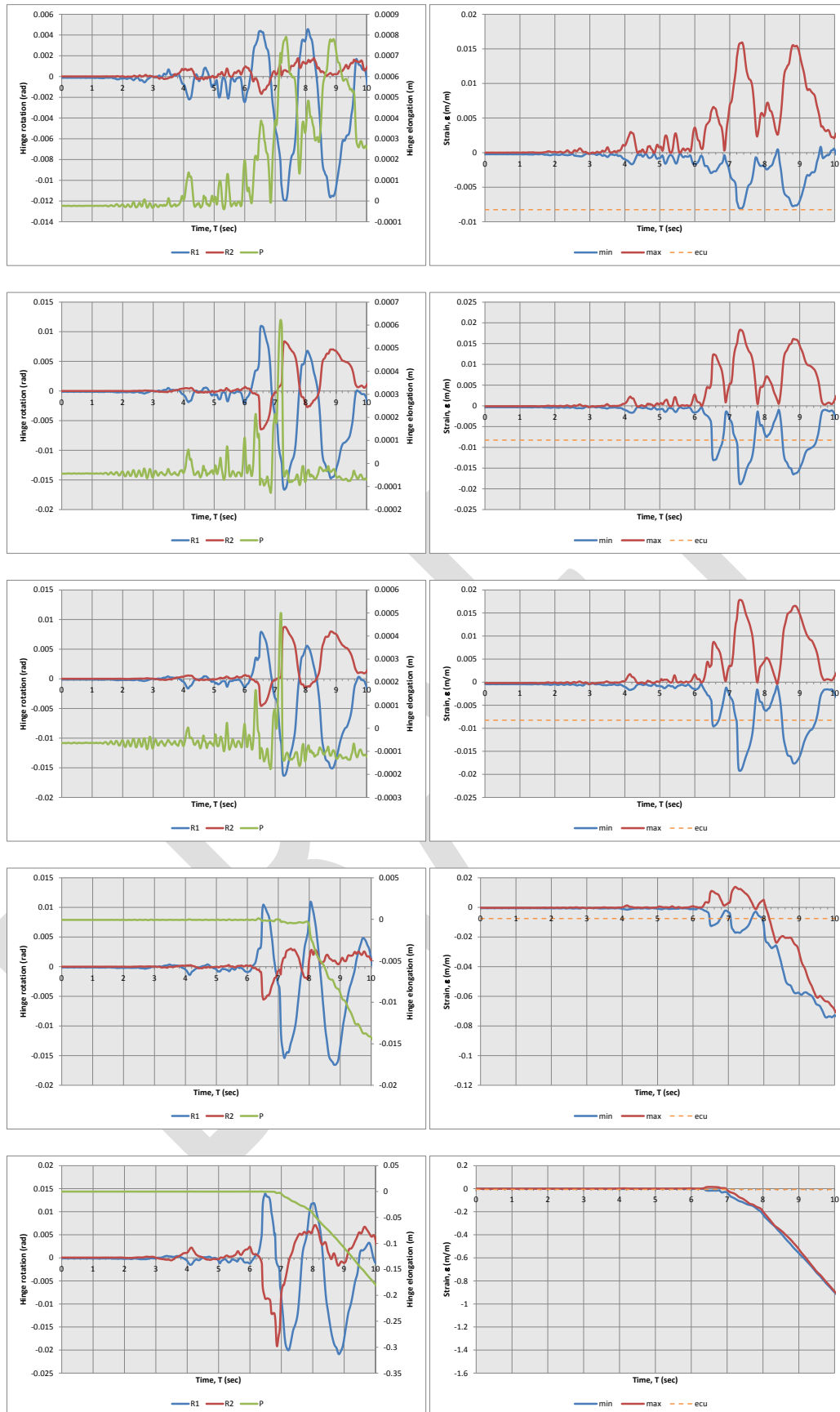


Figure I.34: Column C2 Levels 1 (bottom) to 5 (top) hinge actions, Lyttelton, CBGS, Sequential.

Appendix J Analysis Results - Lyttelton Aftershock: CCCC record

The following details the structural actions reported by the analysis as a function of time, for the Lyttelton aftershock using the acceleration time history recorded at the CCCC station using all components of the record. Results presented in this section include those assuming that the CTV Building was in an undamaged state, and those for the sequential analyses following on from stiffness state at the end of the Darfield event (denoted '*sequential*').

J.1 Building Displacements and Drifts.

Building Level 6 displacements are presented in Figure J.1 and Figure J.4 below for the southeast and northwest corners of the building for both the damaged and undamaged states.

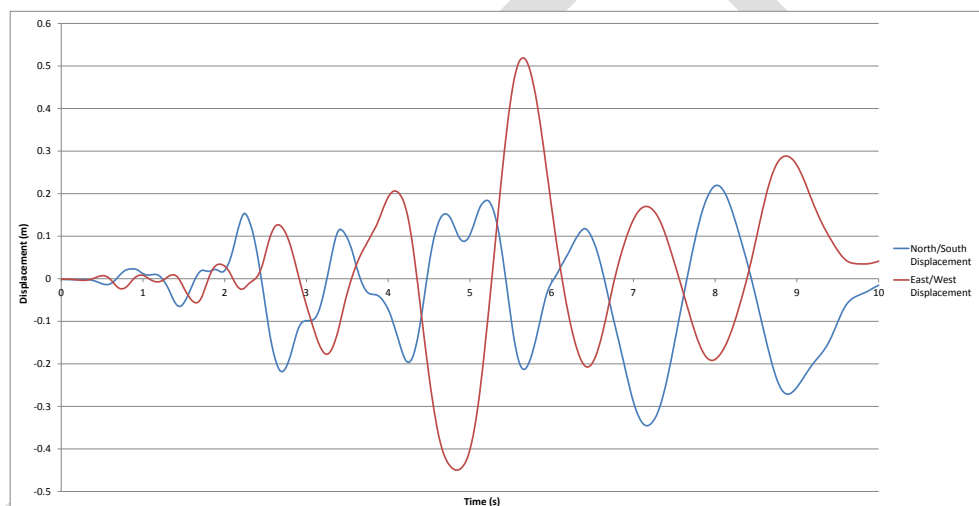


Figure J.1: Level 6 Southeast corner displacements, Lyttelton, CCCC

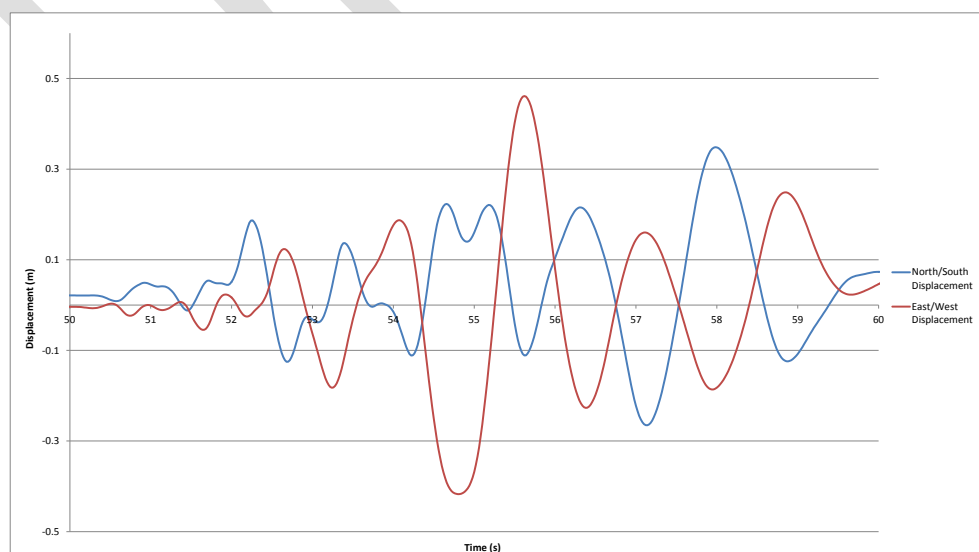


Figure J.2: Level 6 Southeast corner displacements, Lyttelton, CCCC Sequential.

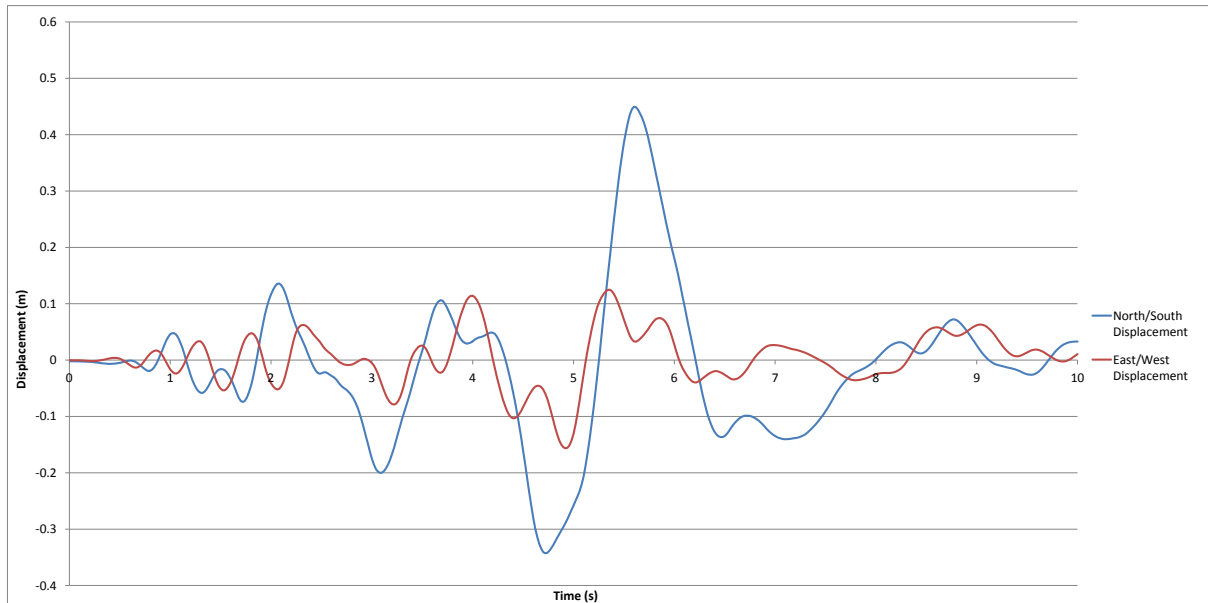


Figure J.3: Level 6 Northwest corner displacements, Lyttelton, CCCC

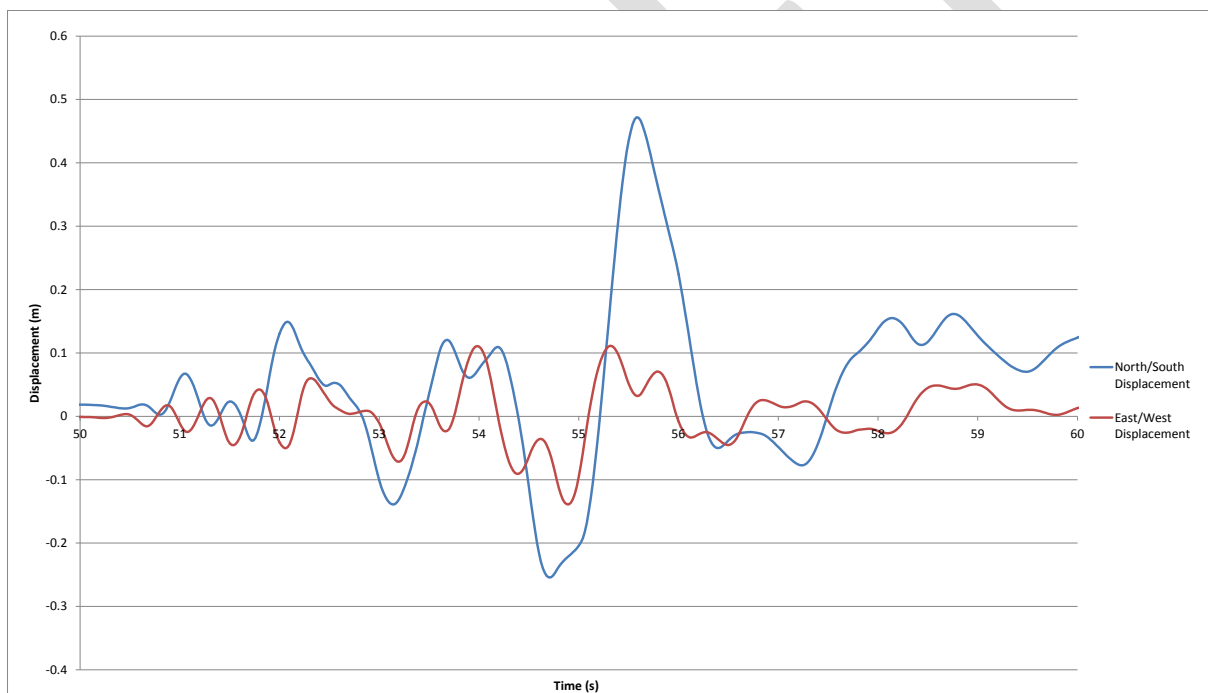


Figure J.4: Level 6 Northwest corner displacements, Lyttelton, CCCC Sequential

As can be seen in Figure J.3 and Figure J.4 above a significant increase in the northward building displacement is observed in the northwest corner of the building approximately 5.5 seconds into the record. This occurs after the tension ties capacities on levels 4 to 6 of the core are exceeded allowing increased building rotation clockwise from west to north. The peak displacement corresponds to a clockwise rotation in conjunction with a net northward building translation. Table J.1 presents the sequence of failure of the north core wall ties

throughout the record (note that time are presented relative to the start of the Lyttelton component of record).

Table J.1: Wall D and D/E diaphragm disconnection times, Lyttelton, CCCC.

Level	Undamaged Analysis		Sequential Analysis	
	Wall D Disconnection (sec)	Wall D/E Disconnection (sec)	Wall D Disconnection (sec)	Wall D/E Disconnection (sec)
6	1.52	1.46	3.18	1.48
5	2.58	1.46	4.18	1.50
4	1.62	1.48	disconnected	disconnected

It can be seen from Table J.1 that the sequential analysis continuing from the end of the Darfield CCCC record influences the performance of the diaphragm ties on wall D, but has little influence on the wall D/E connections.

Inter-storey displacements for the perimeter frame lines A and F in the north/south direction are presented in Figure J.5 to Figure J.8 below. North core tie tensile failure is identified on the plots for reference.

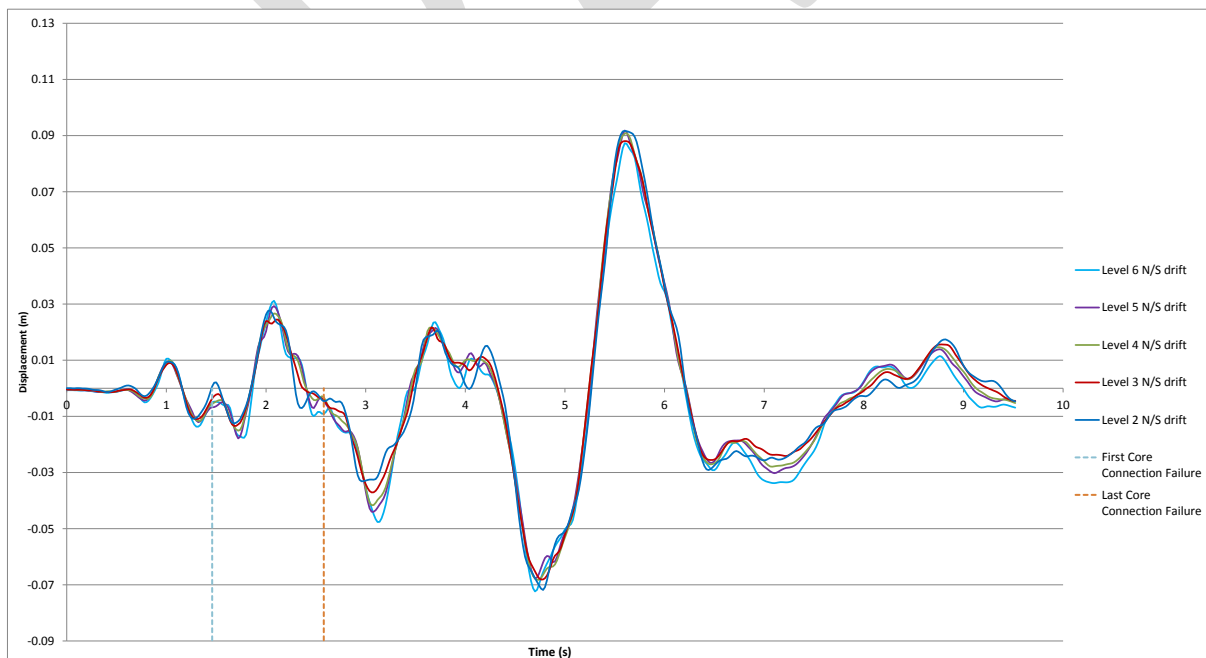


Figure J.5: Frame A north/south inter-storey displacements, Lyttelton, CCCC.

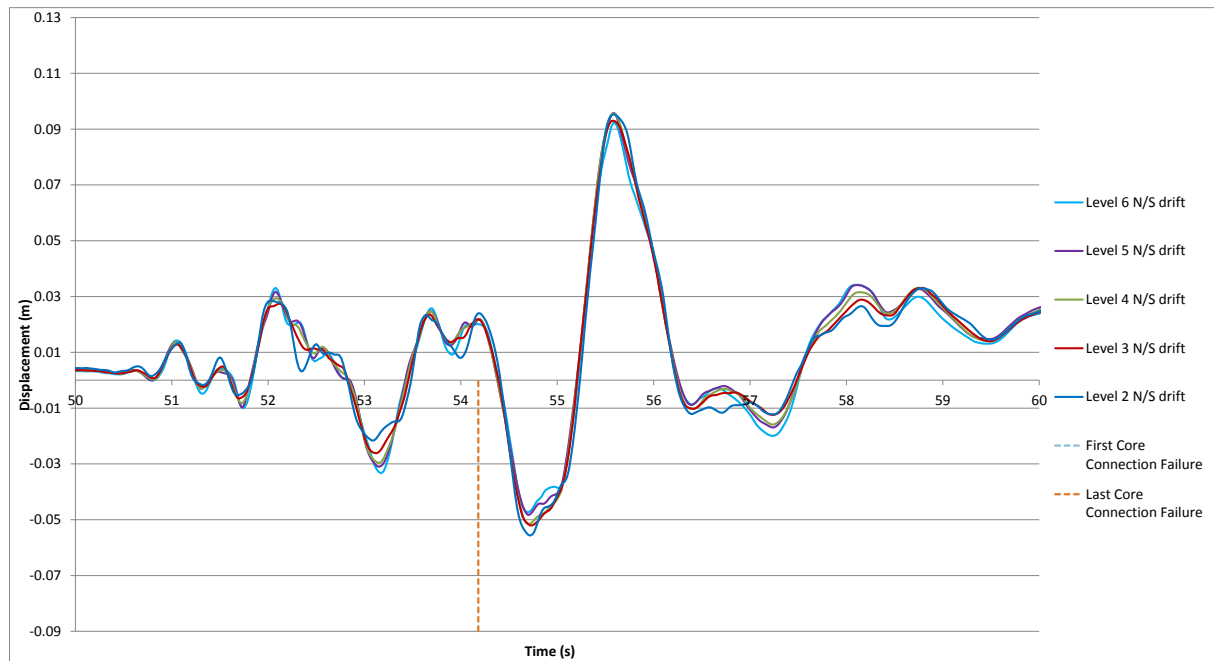


Figure J.6: Frame A north/south inter-storey displacements, Lyttelton, CCCC Sequential.

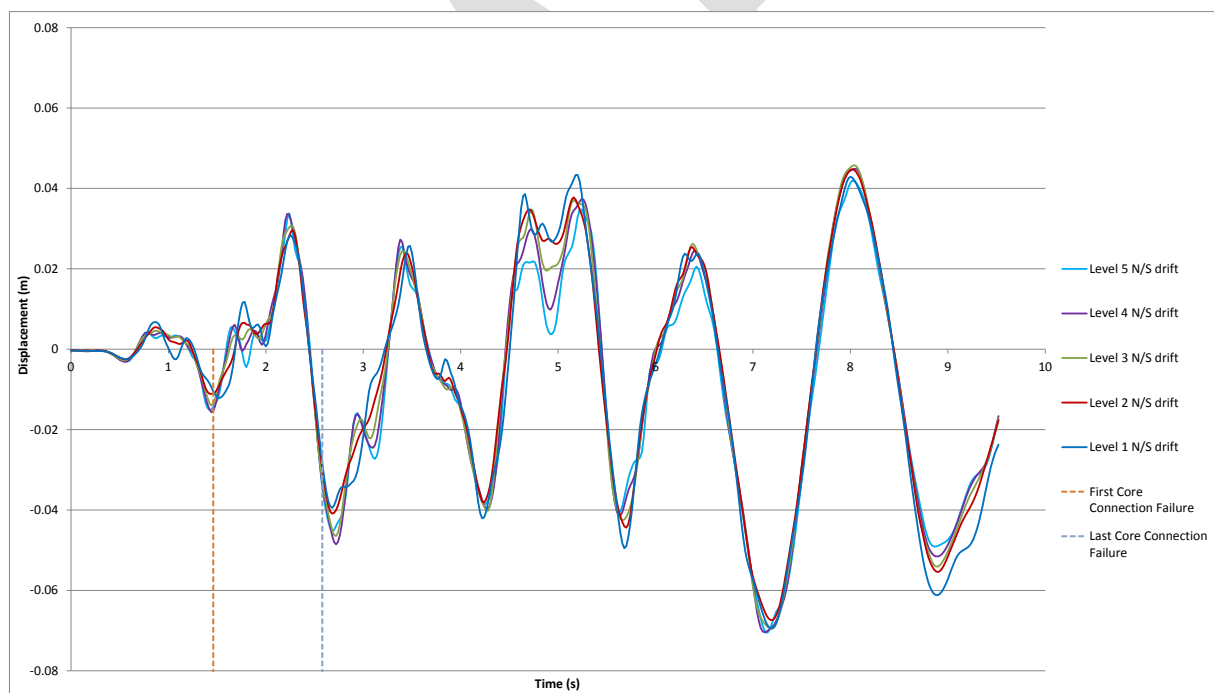


Figure J.7: Frame F north/south inter-storey displacements, Lyttelton, CCCC

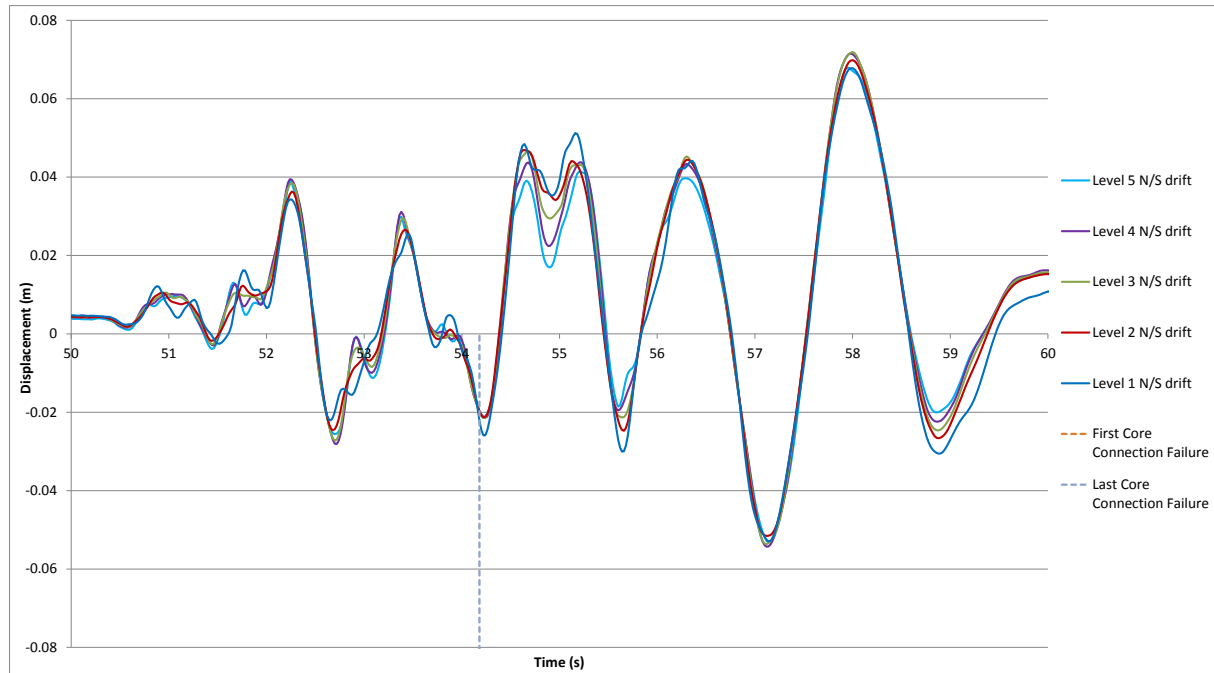


Figure J.8: Frame F north/south inter-storey displacements, Lyttelton, CCCC Sequential.

Inter-storey displacements for the perimeter frame lines 1 and 4 in the East/West direction are presented in Figure J.9 to Figure J.12 below.

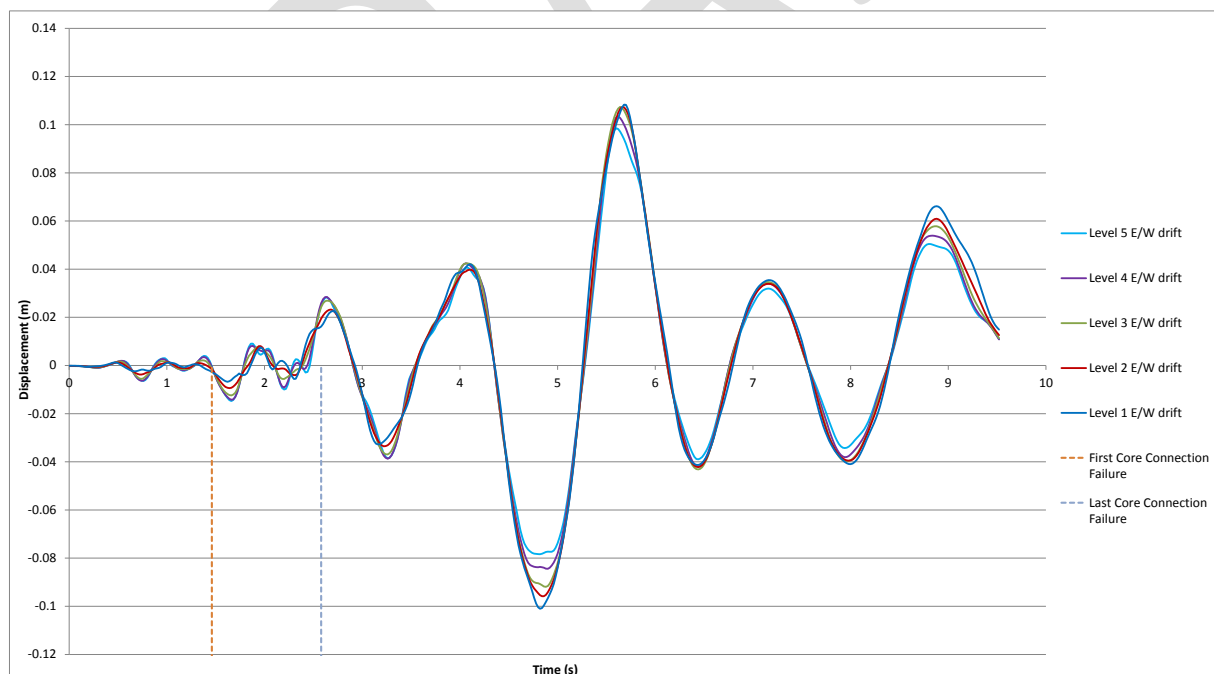


Figure J.9: Frame 1 east/west inter-storey displacements, Lyttelton, CCCC.

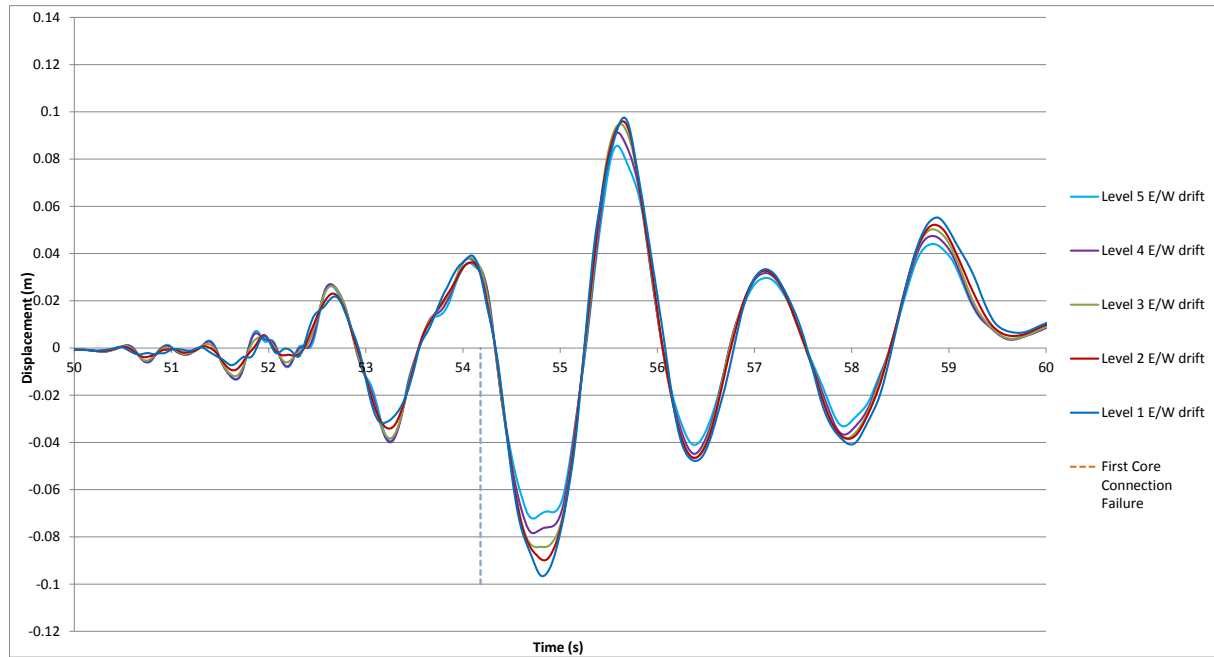


Figure J.10: Frame 1 east/west inter-storey displacements, Lyttelton, CCCC Sequential.

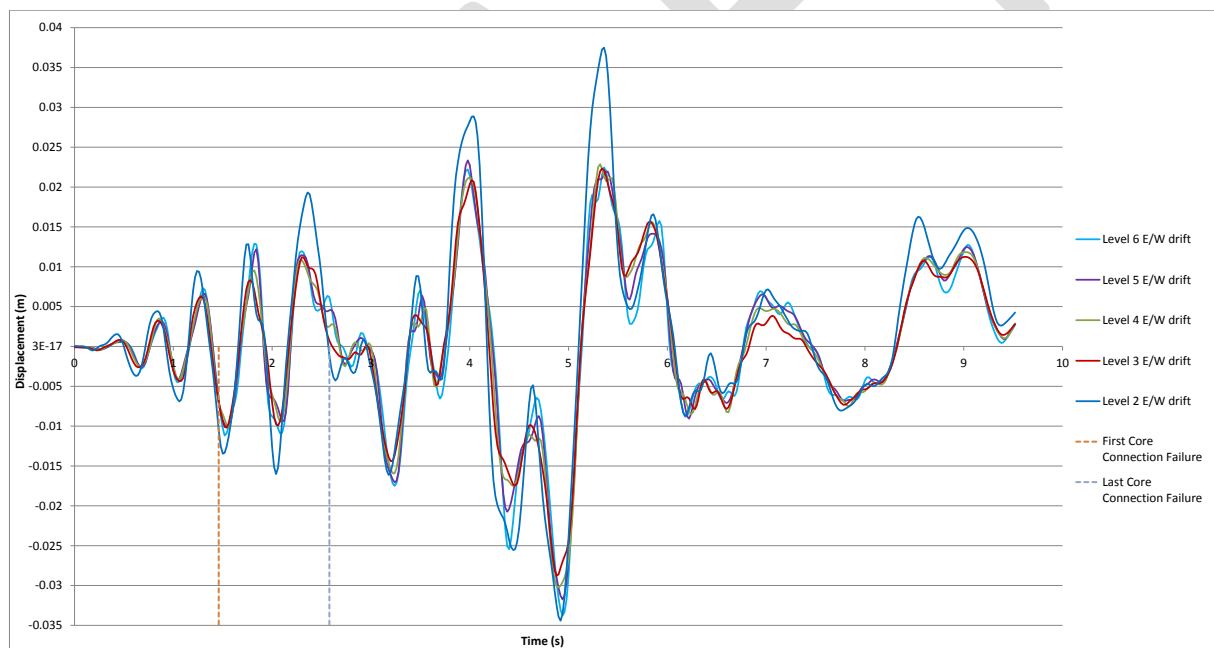


Figure J.11: Frame 4 east/west inter-storey displacements, Lyttelton, CCCC

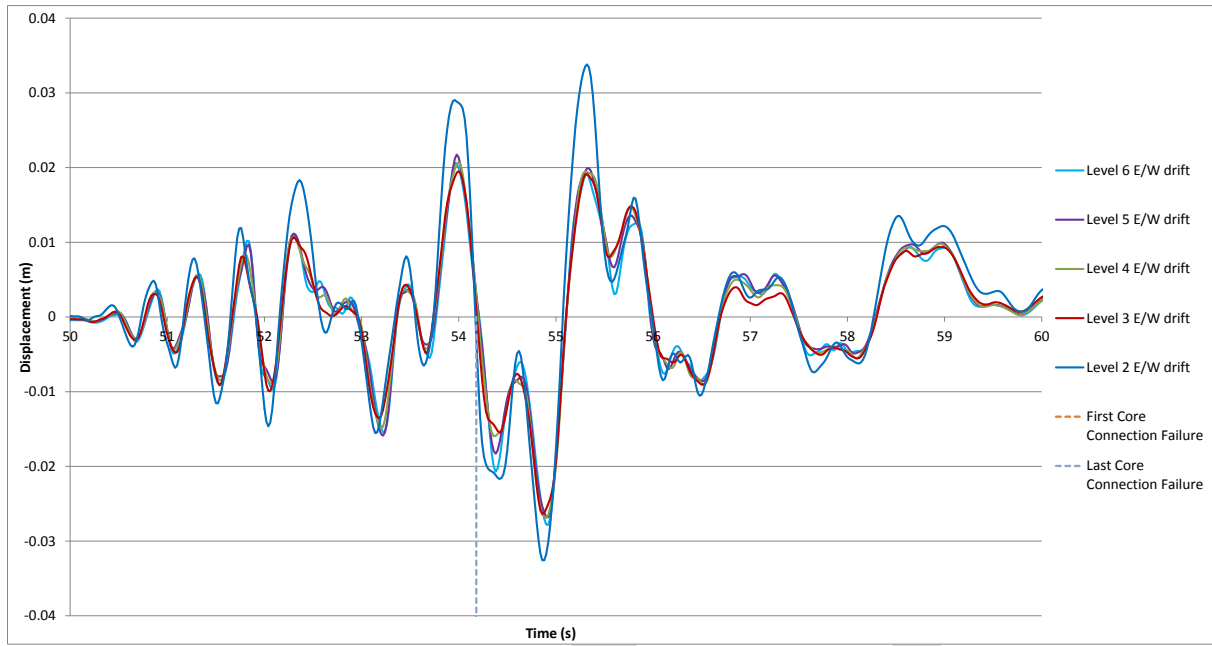


Figure J.12: Frame 4 east/west inter-storey displacements, Lyttelton, CCCC Sequential

J.2 Diaphragm Connection Forces

Diaphragm connection forces are presented in Figure J.13 to Figure J.35 below. Note that moments are reported about the geometric centroid of the element being considered.

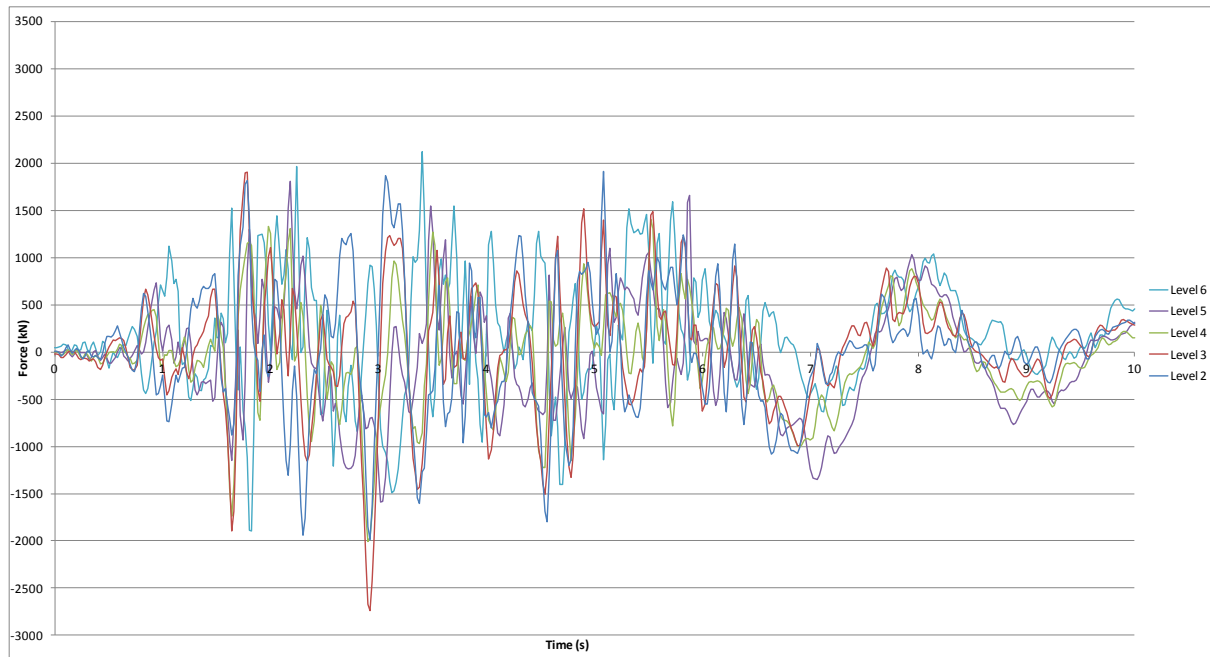


Figure J.13: North core total diaphragm north/south actions, Lyttelton, CCCC

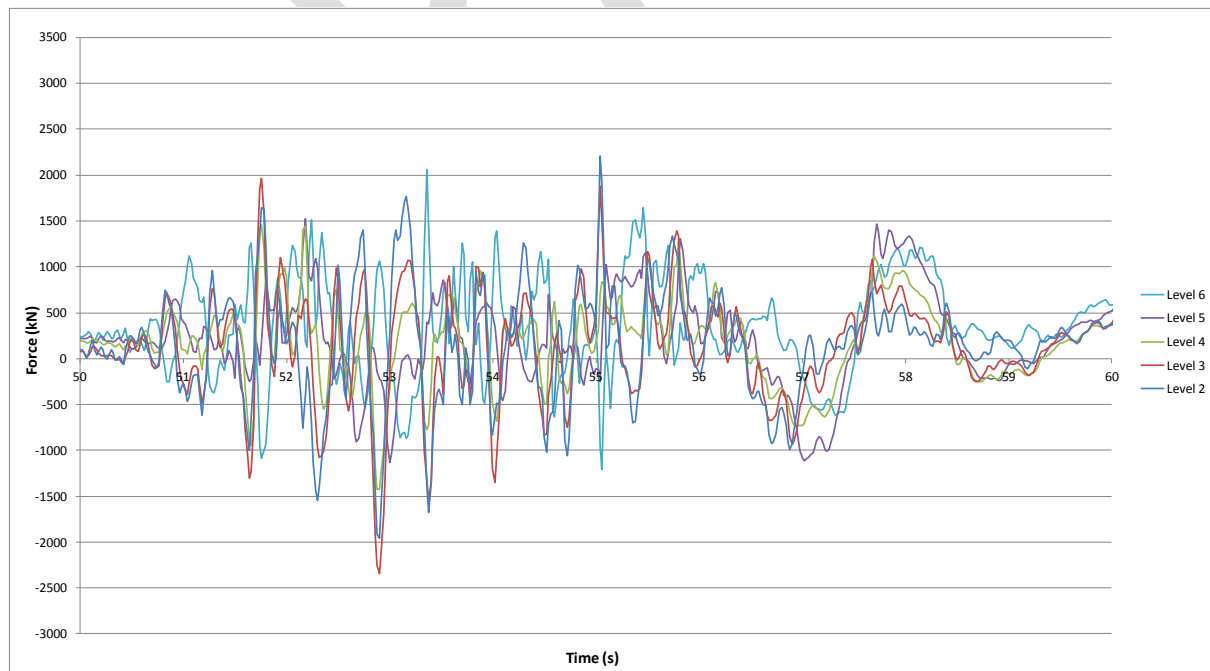


Figure J.14: North core total diaphragm north/south actions, Lyttelton, CCCC Sequential

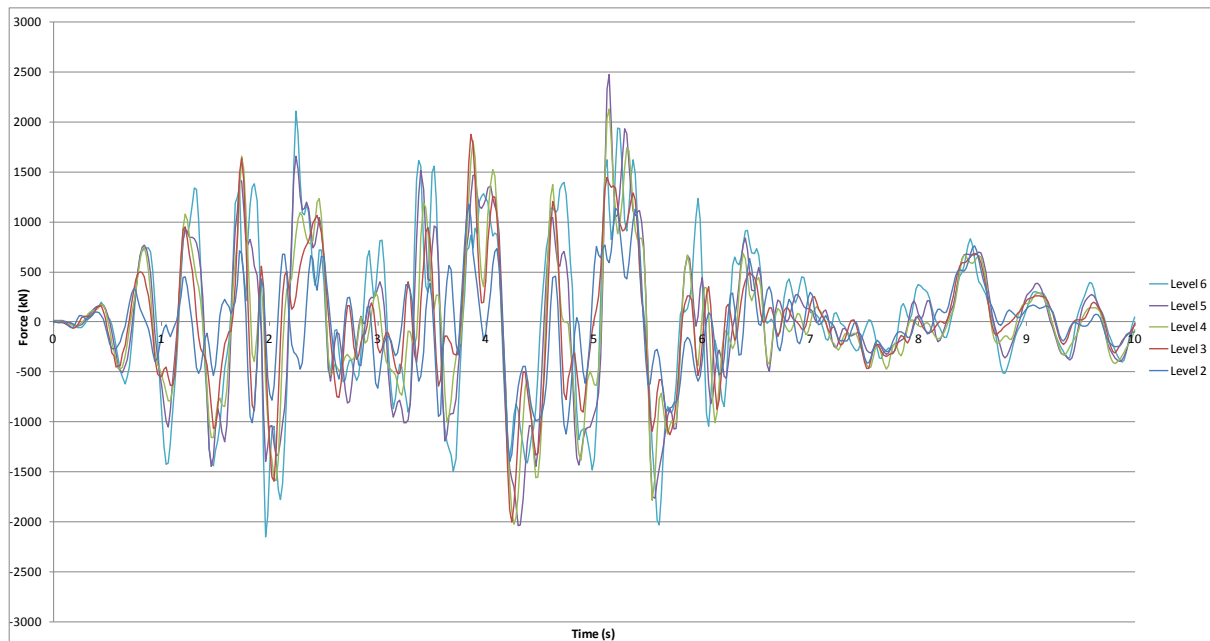


Figure J.15: North core total diaphragm east/west actions, Lyttelton, CCCC

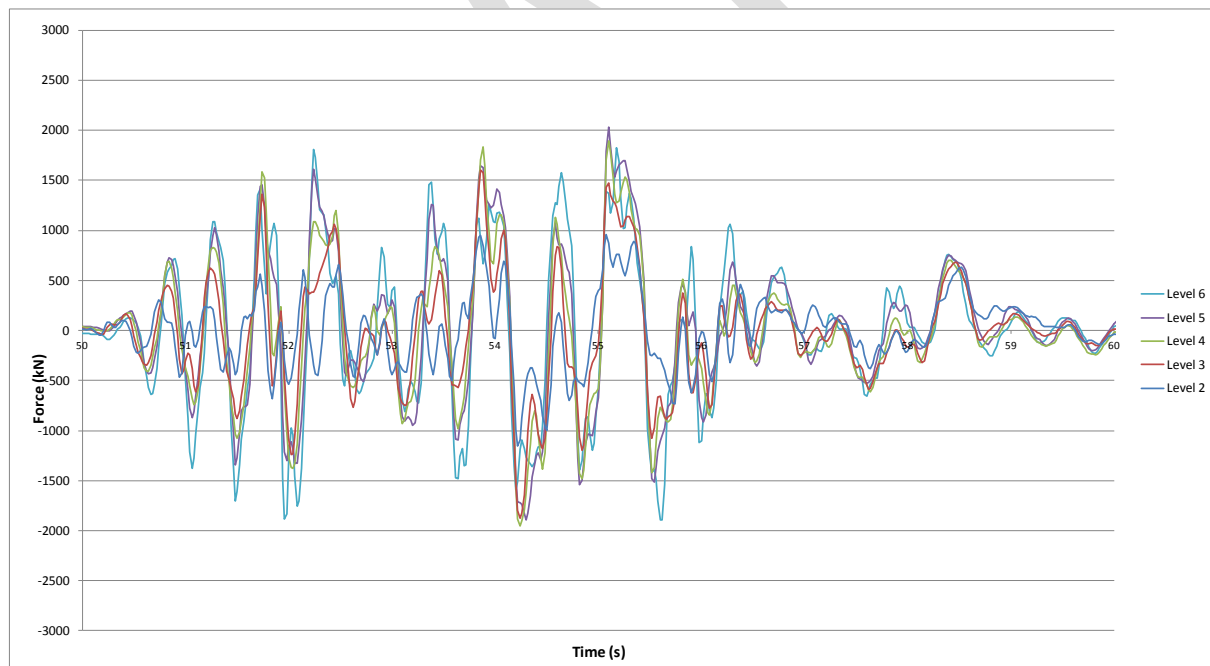


Figure J.16: North core total diaphragm east/west actions, Lyttelton, CCCC Sequential

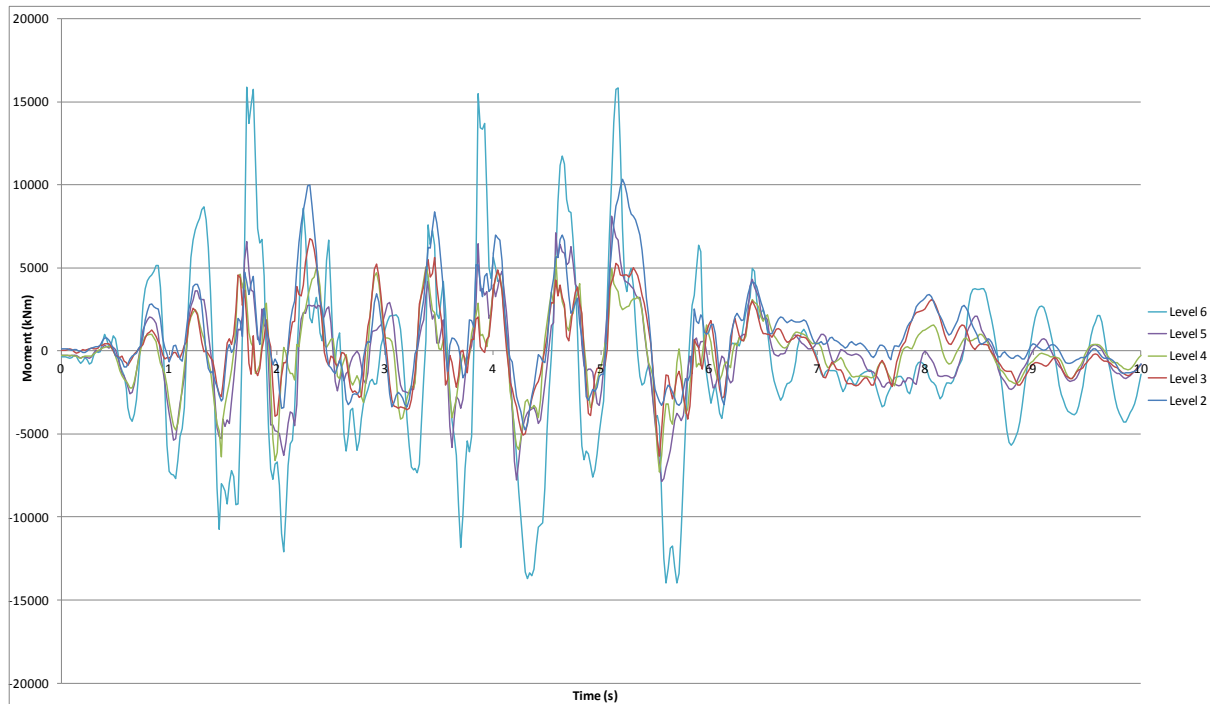


Figure J.17: North core total diaphragm in-plane moments, Lyttelton, CCCC

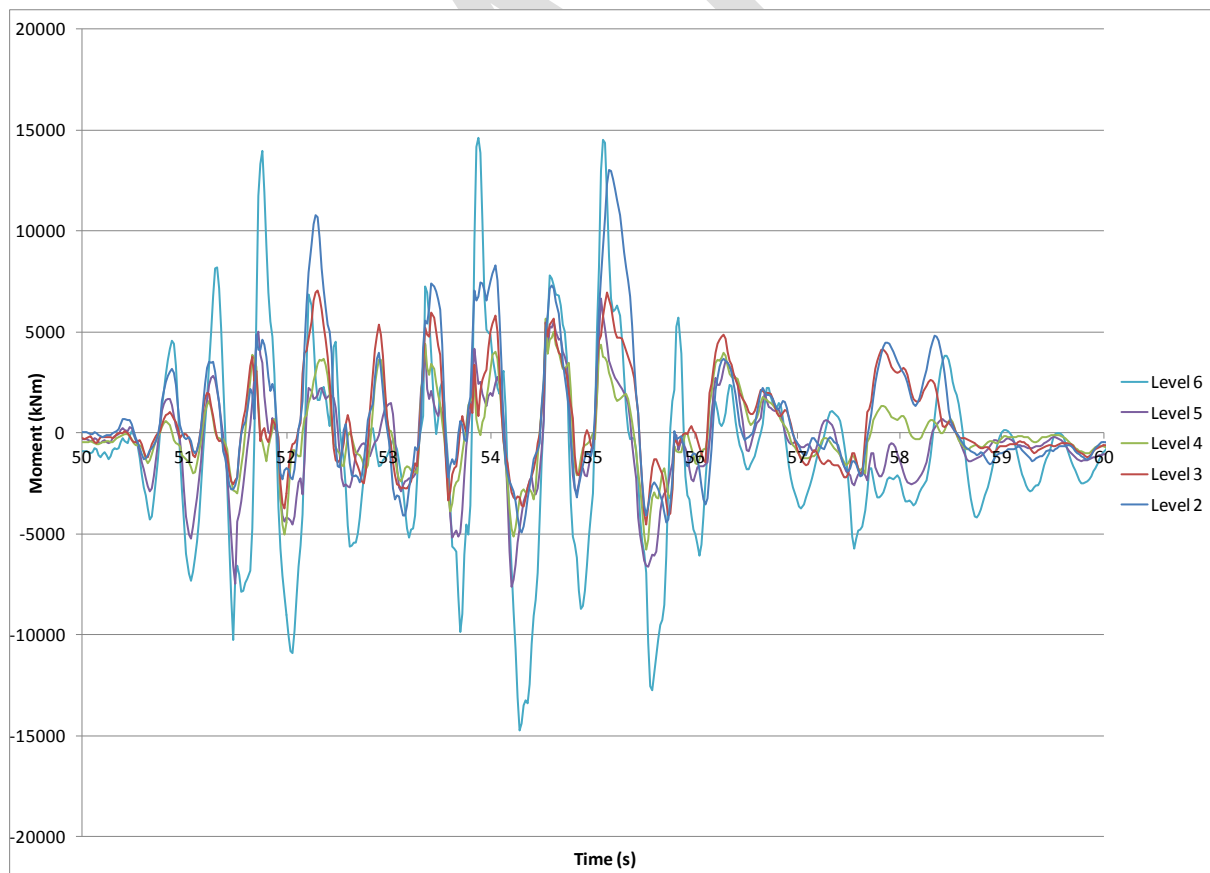


Figure J.18: North core total diaphragm in-plane moments, Lyttelton, CCCC Sequential

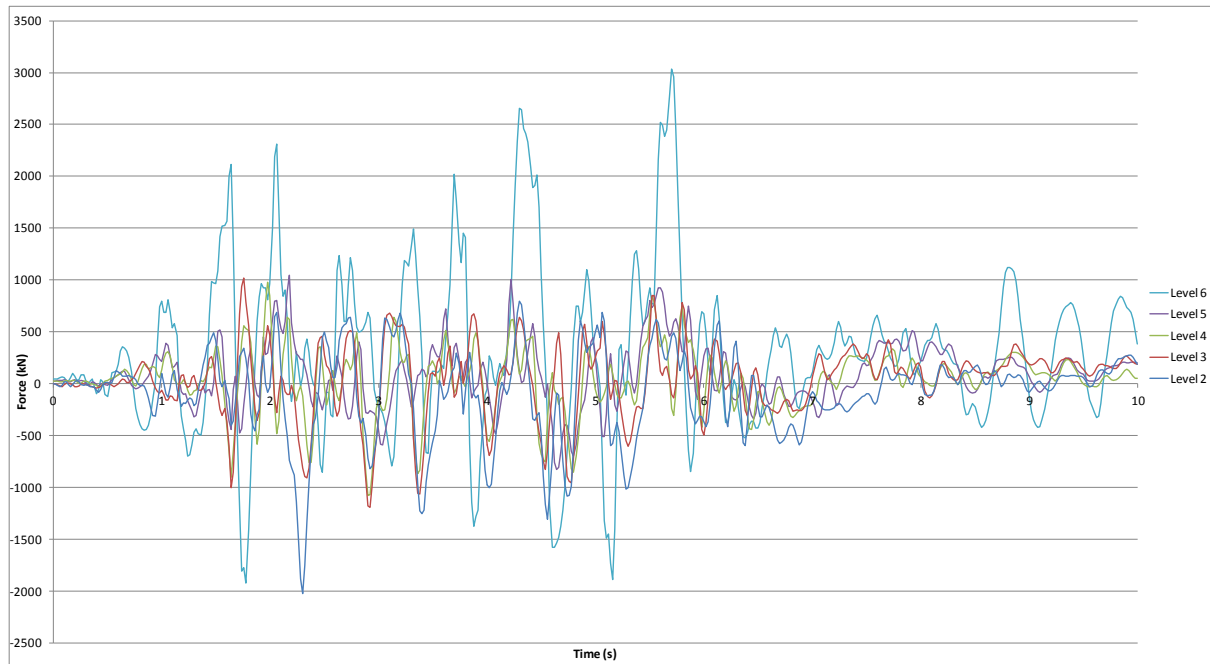


Figure J.19: North core Wall C diaphragm north/south actions, Lyttelton, CCCC

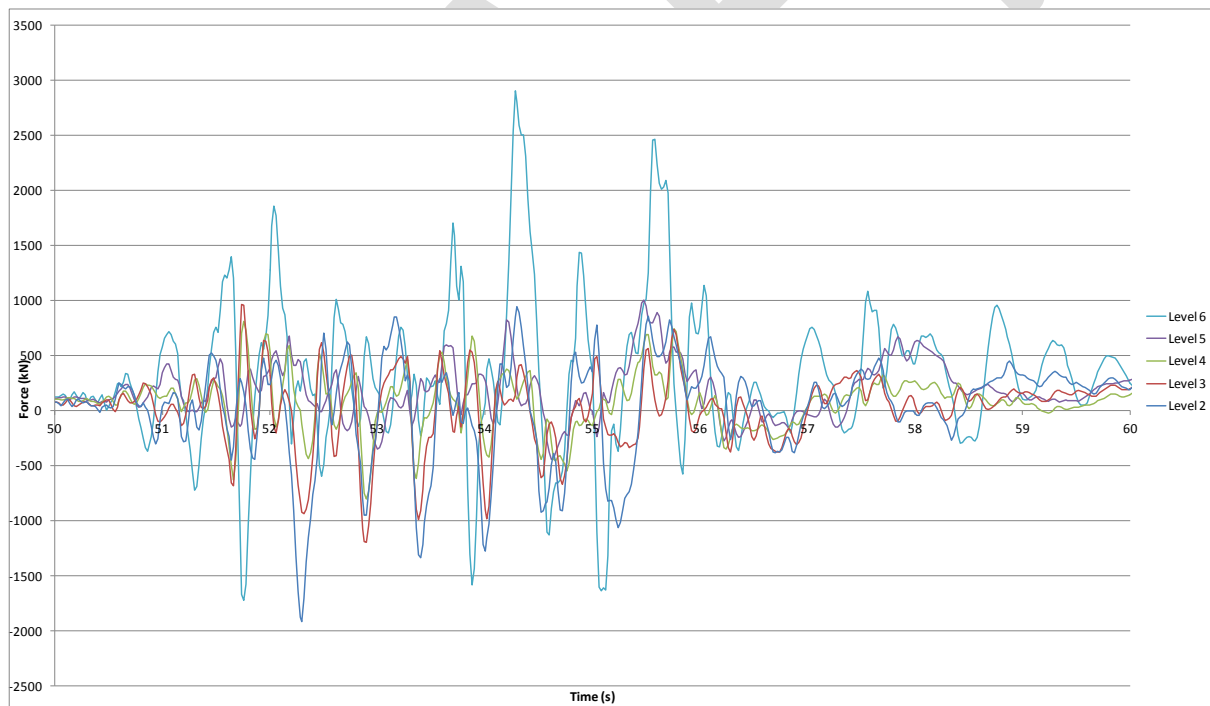


Figure J.20: North core Wall C diaphragm north/south actions, Lyttelton, CCCC Sequential

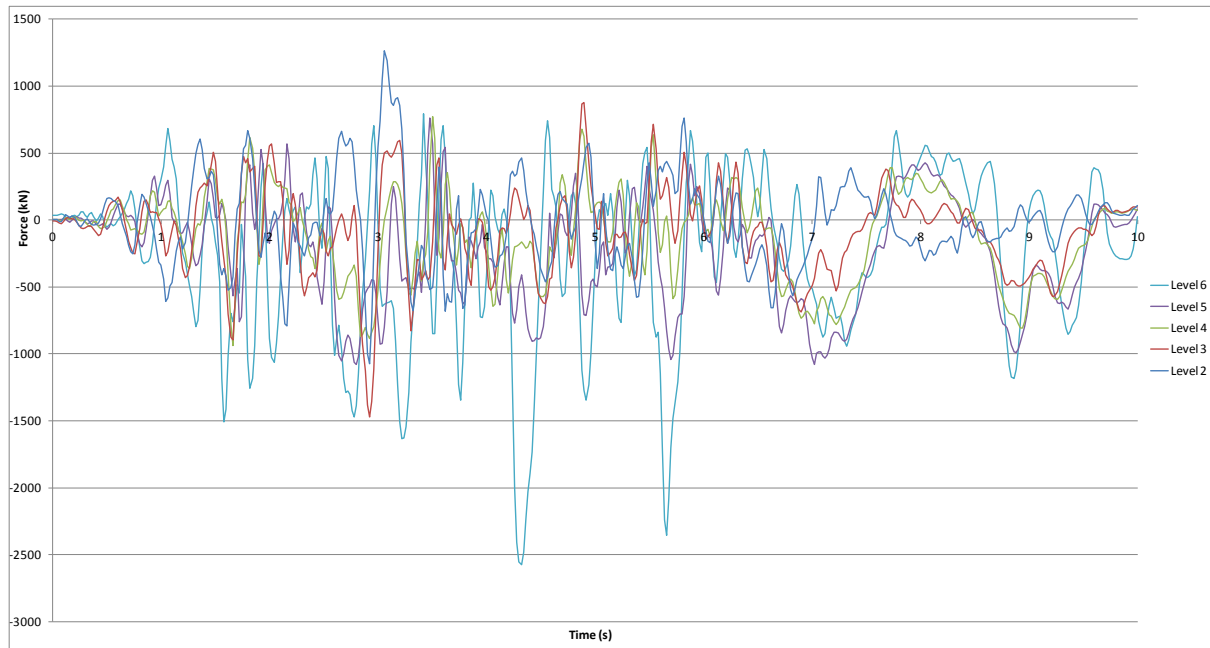


Figure J.21: North core Wall C/D diaphragm north/south actions, Lyttelton, CCCC

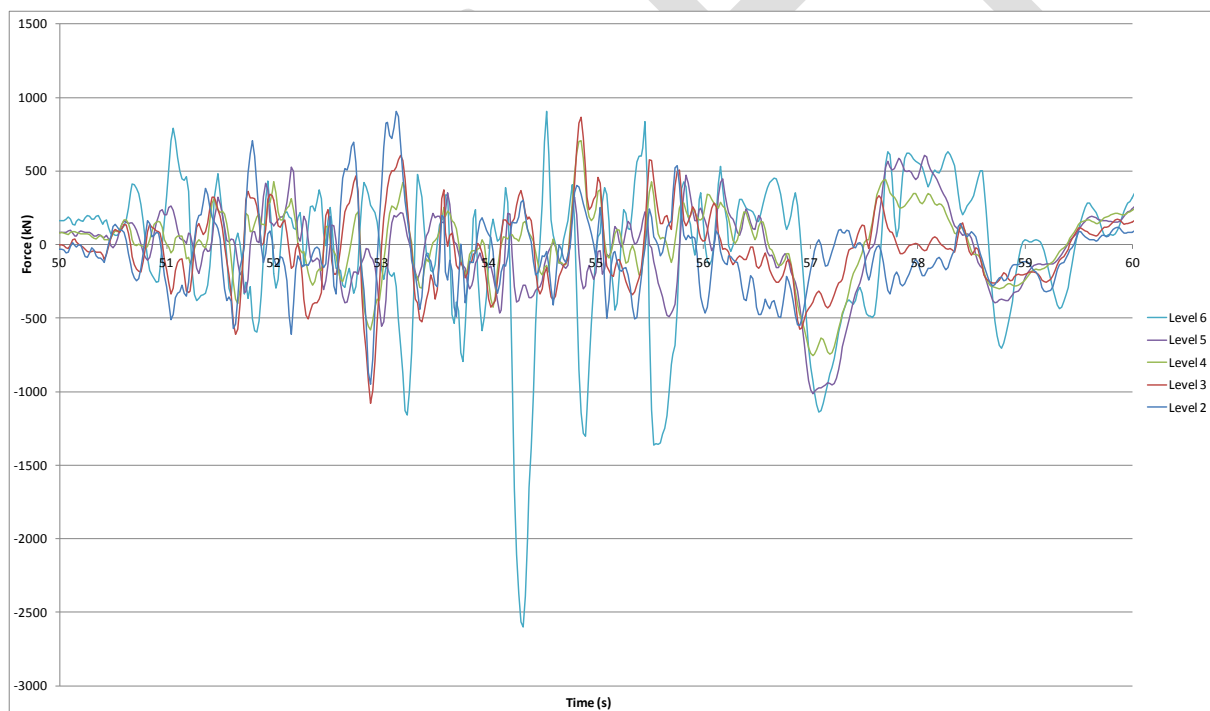


Figure J.22: North core Wall C/D diaphragm north/south actions, Lyttelton, CCCC Sequential

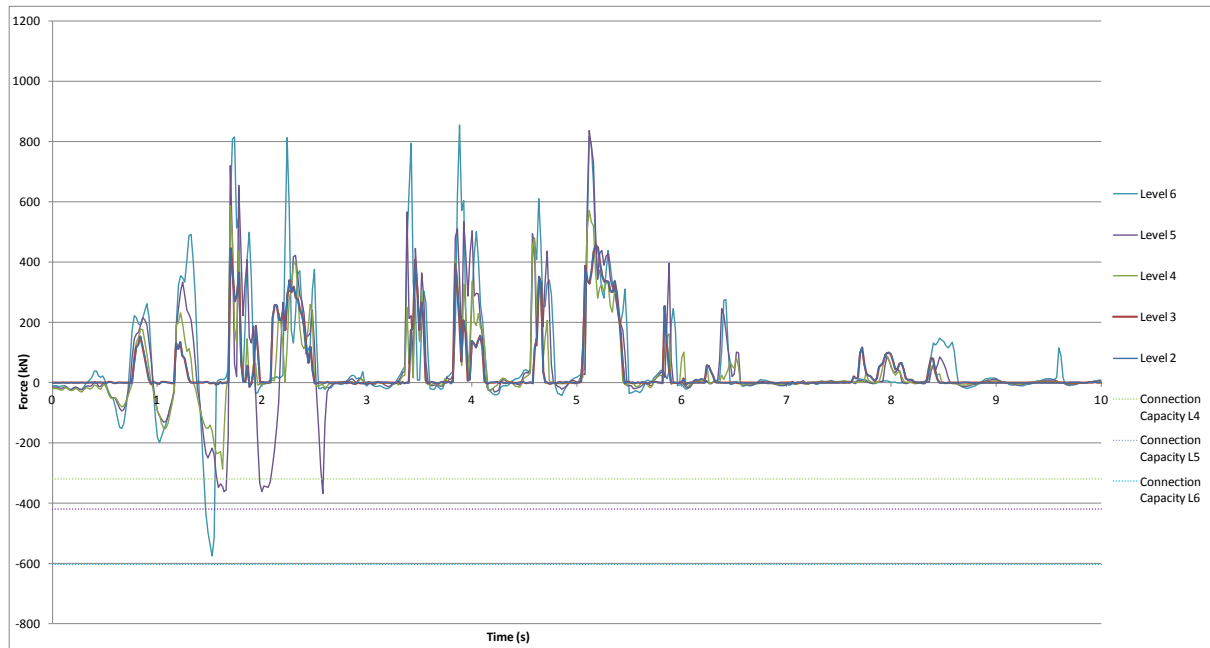


Figure J.23: North core Wall D diaphragm north/south actions, Lyttelton, CCCC

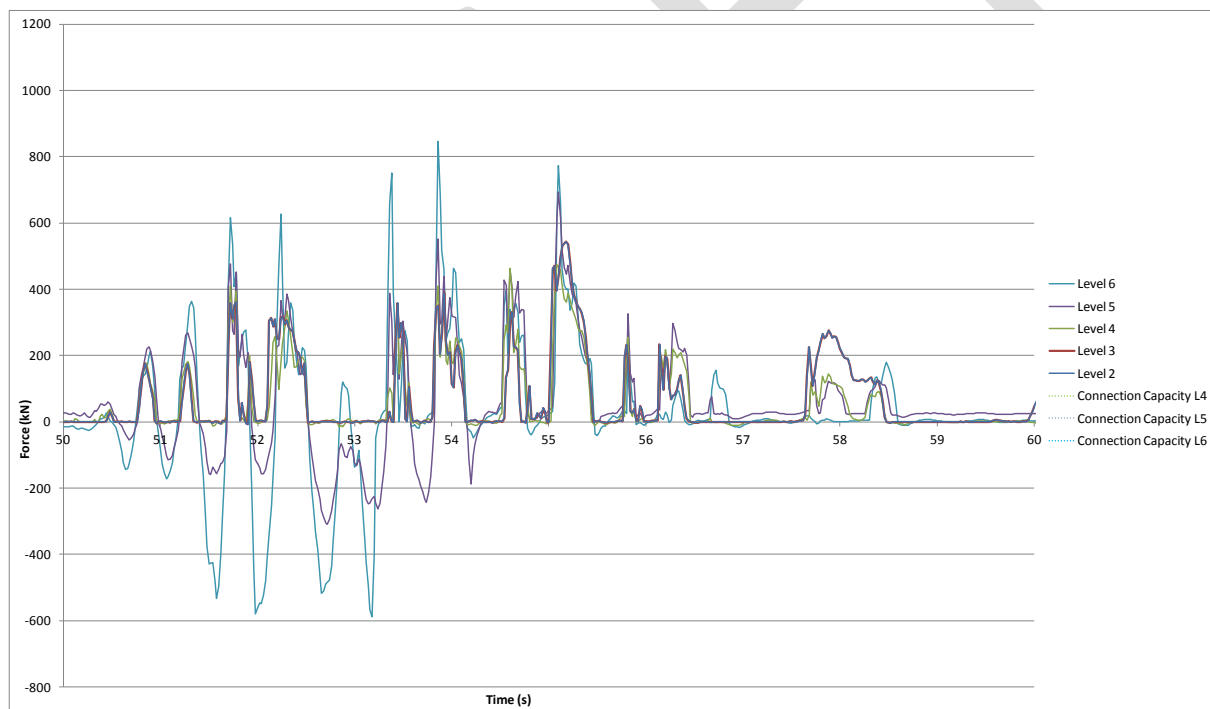


Figure J.24: North core Wall D diaphragm north/south actions, Lyttelton, CCCC Sequential

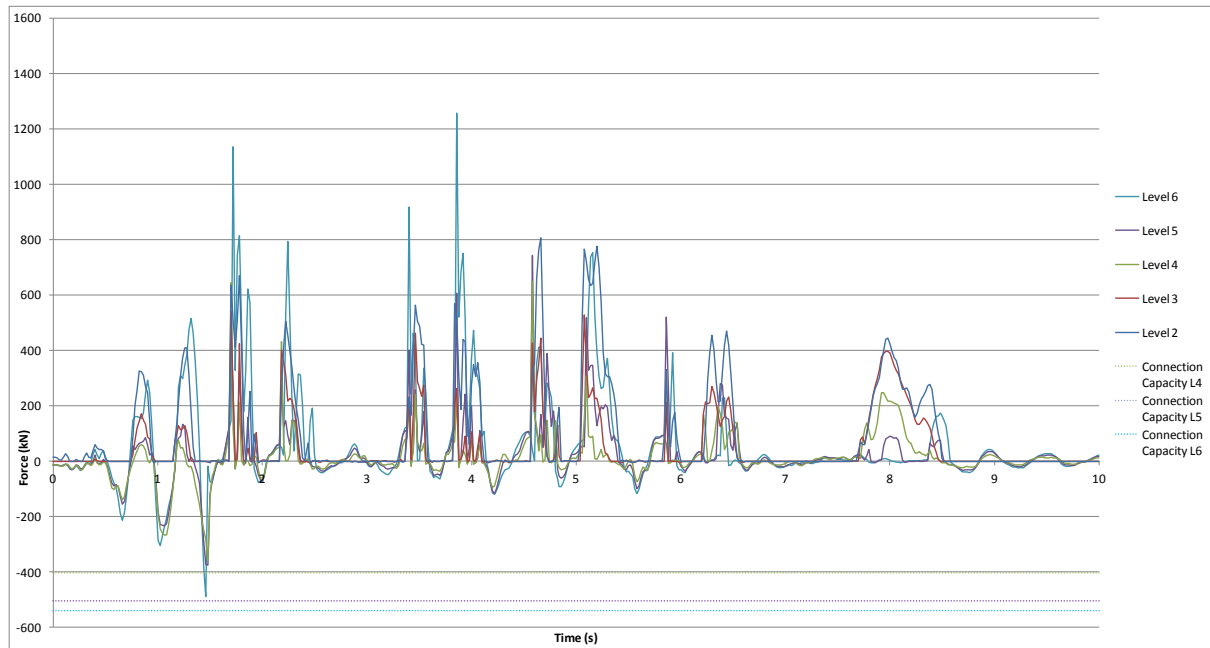


Figure J.25: North core Wall D/E diaphragm north/south actions, Lyttelton, CCCC

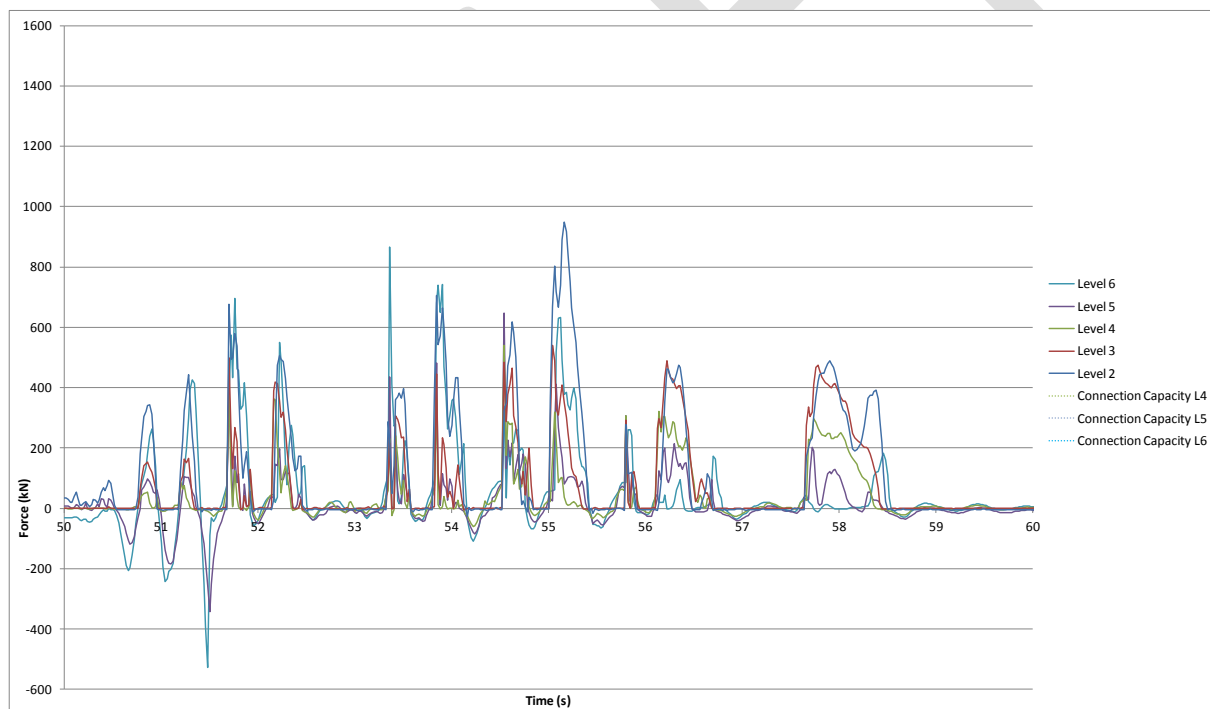


Figure J.26: North core Wall D/E diaphragm north/south actions, Lyttelton, CCCC Sequential

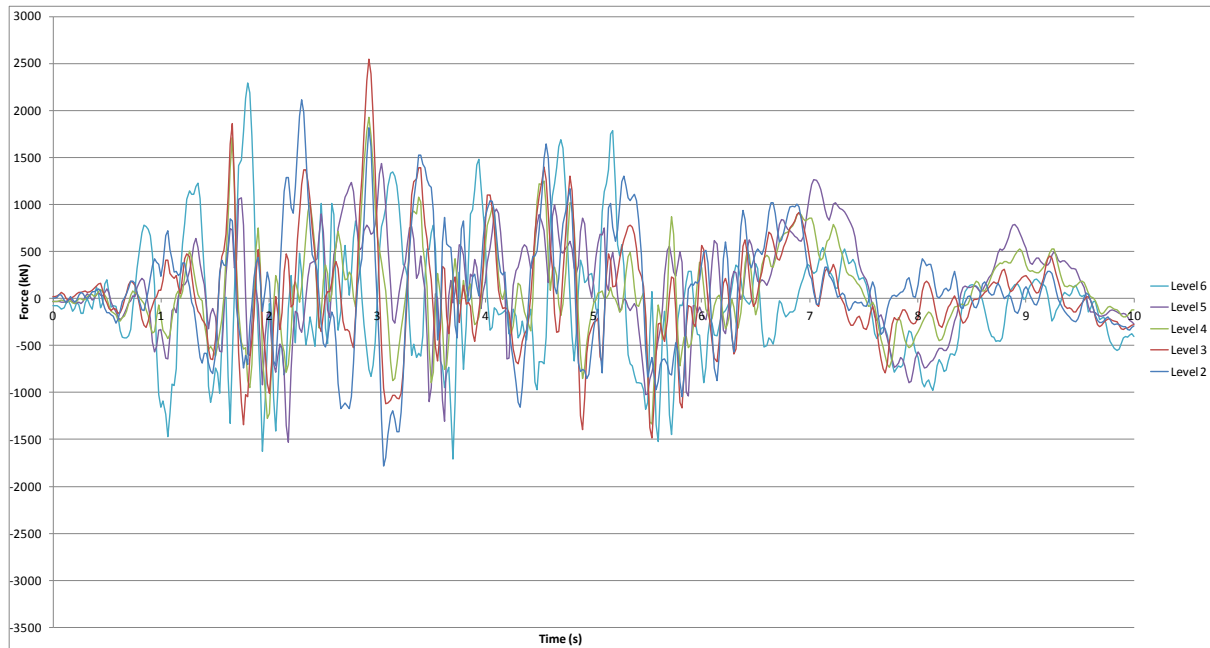


Figure J.27: North core Slab 4/C to C/D diaphragm north/south actions, Lyttelton, CCCC

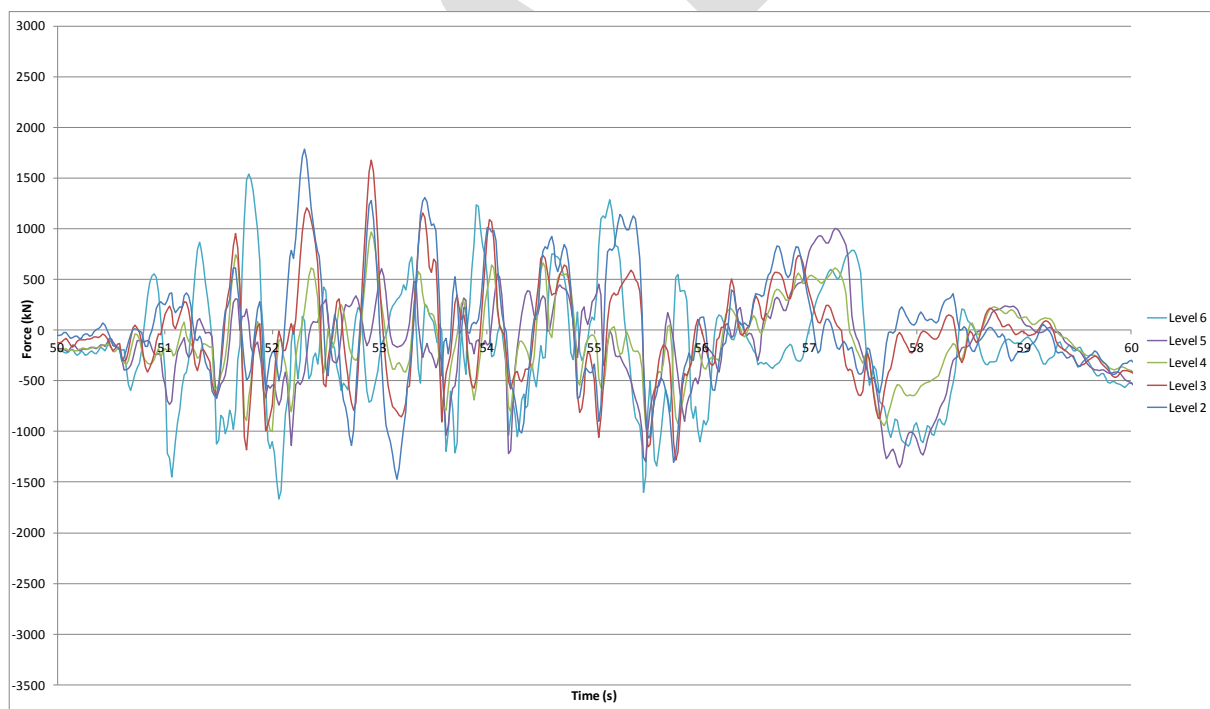


Figure J.28: North core Slab 4/C to C/D diaphragm north/south actions, Lyttelton, CCCC Sequential

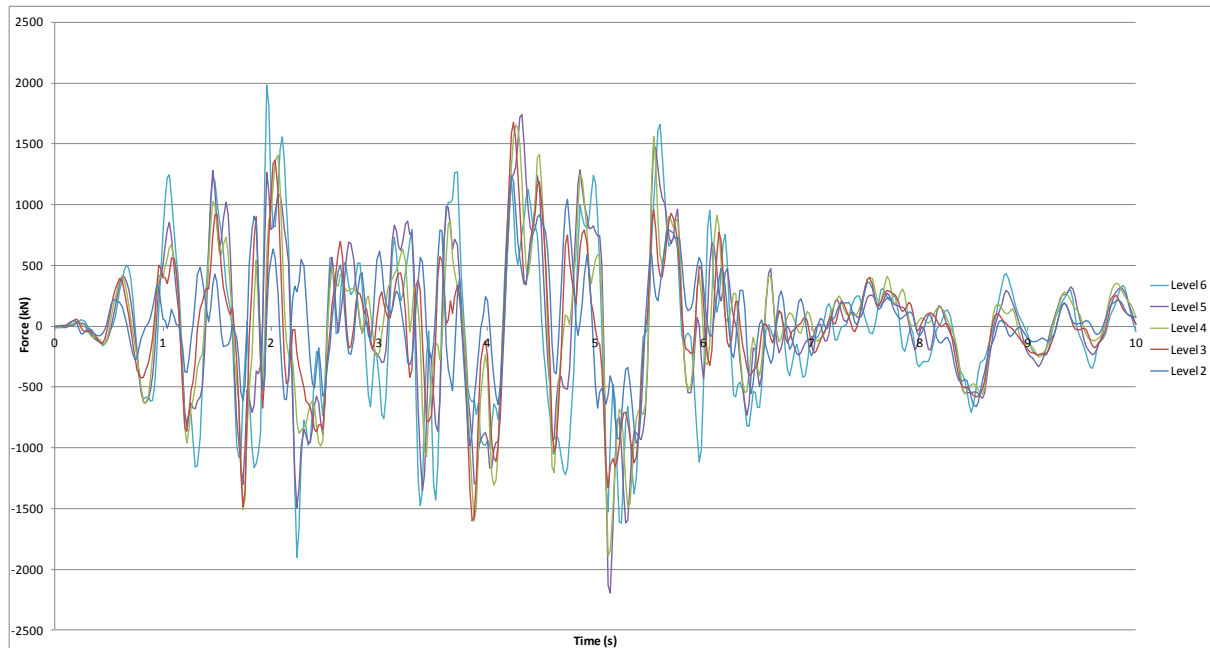


Figure J.29: North core Slab 4/C to C/D diaphragm east/west actions, Lyttelton, CCCC

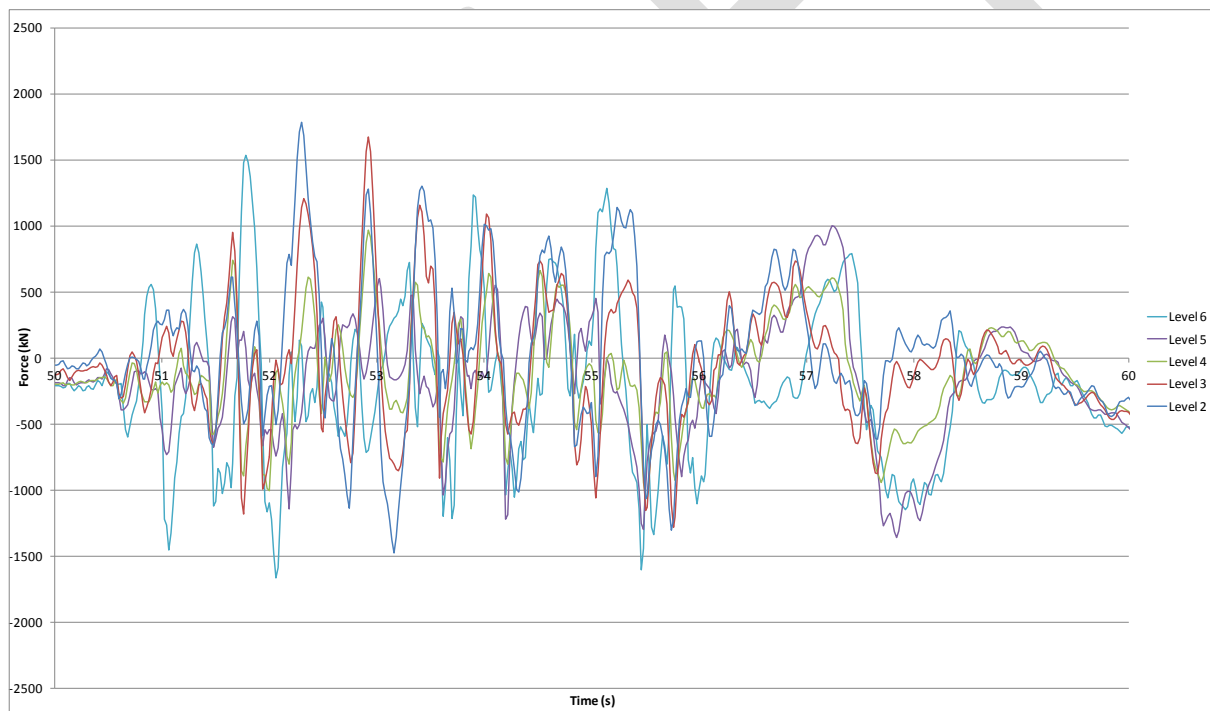


Figure J.30: North core Slab 4/C to C/D diaphragm east/west actions, Lyttelton, CCCC Sequential

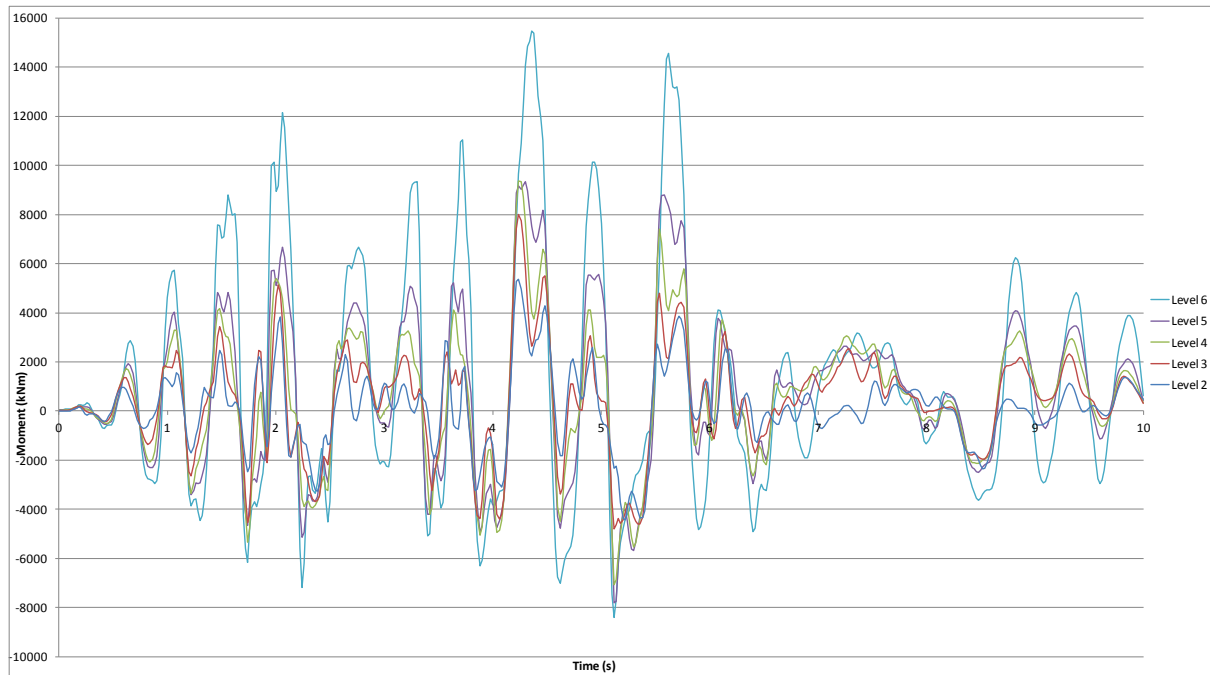


Figure J.31: North core Slab 4/C to C/D diaphragm in-plane moments, Lyttelton, CCCC

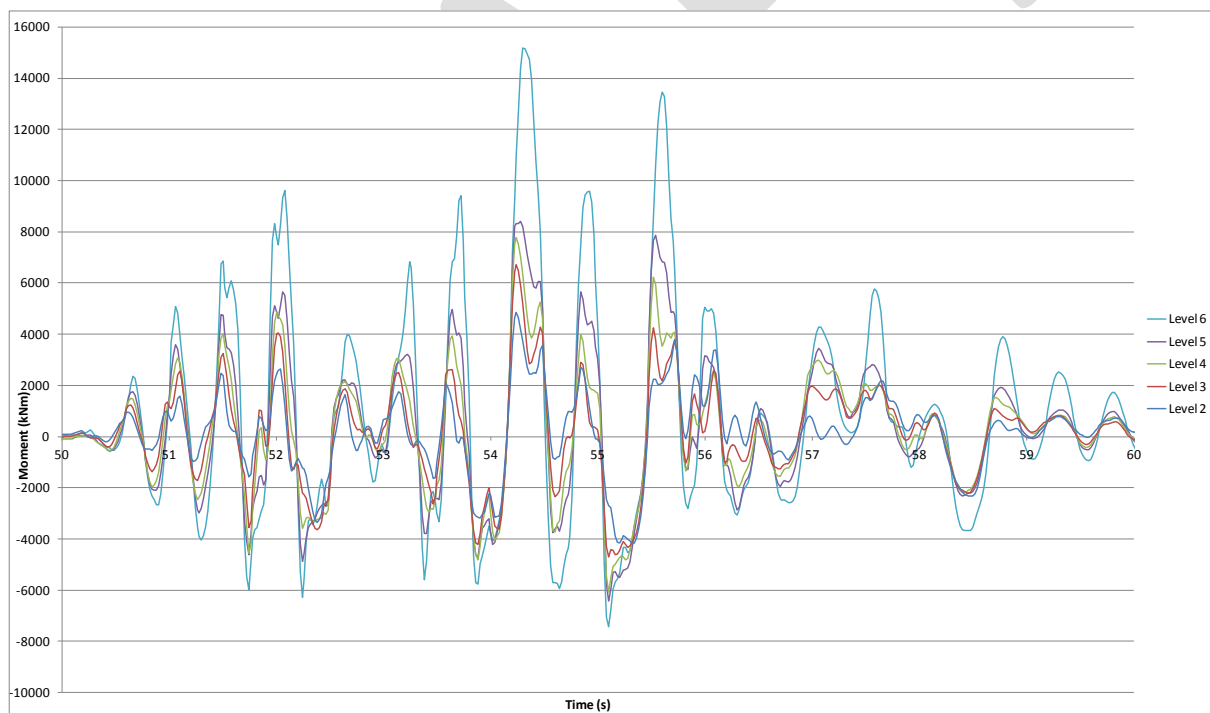


Figure J.32: North core Slab 4/C to C/D diaphragm in-plane moments, Lyttelton, CCCC Sequential

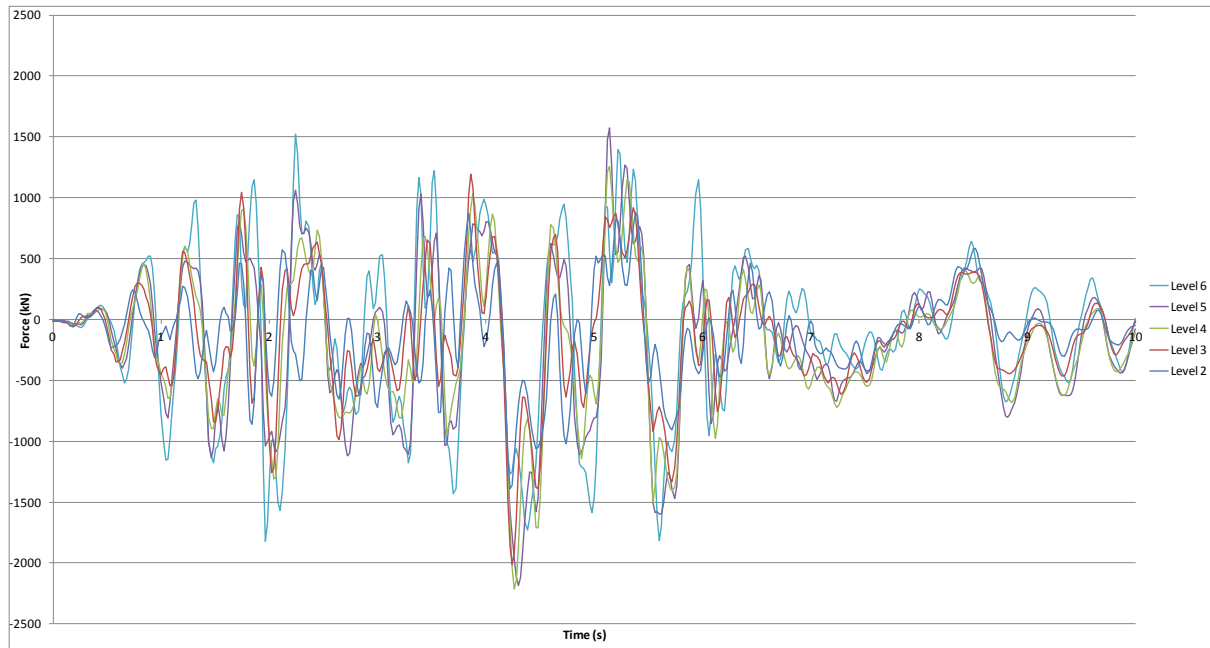


Figure J.33: North core Wall 5 diaphragm east/west actions, Lyttelton, CCCC

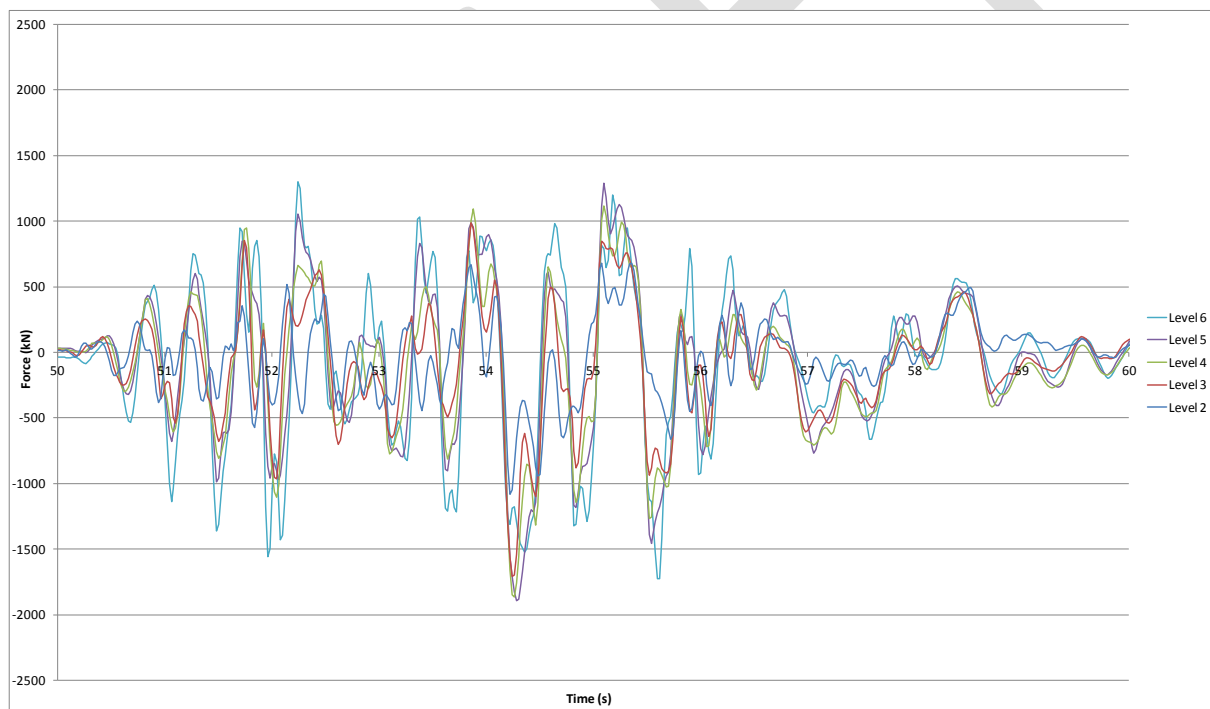


Figure J.34: North core Wall 5 diaphragm east/west actions, Lyttelton, CCCC Sequential

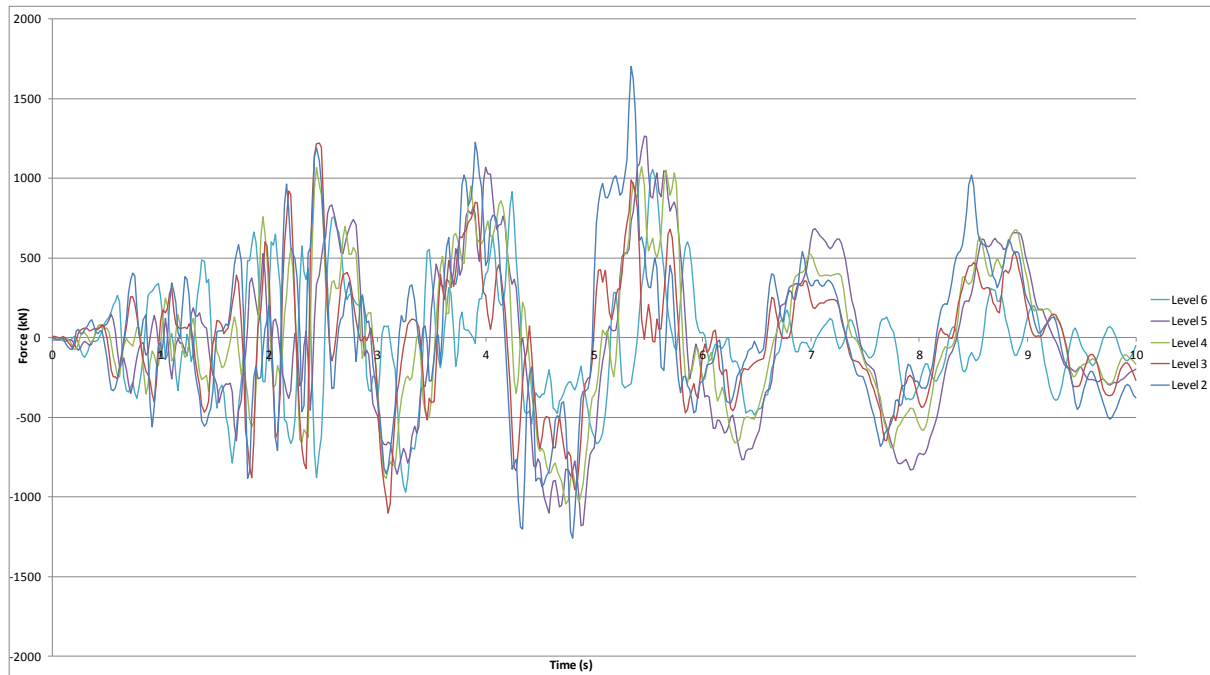


Figure J.35: South wall diaphragm east/west actions, Lyttelton, CCCC

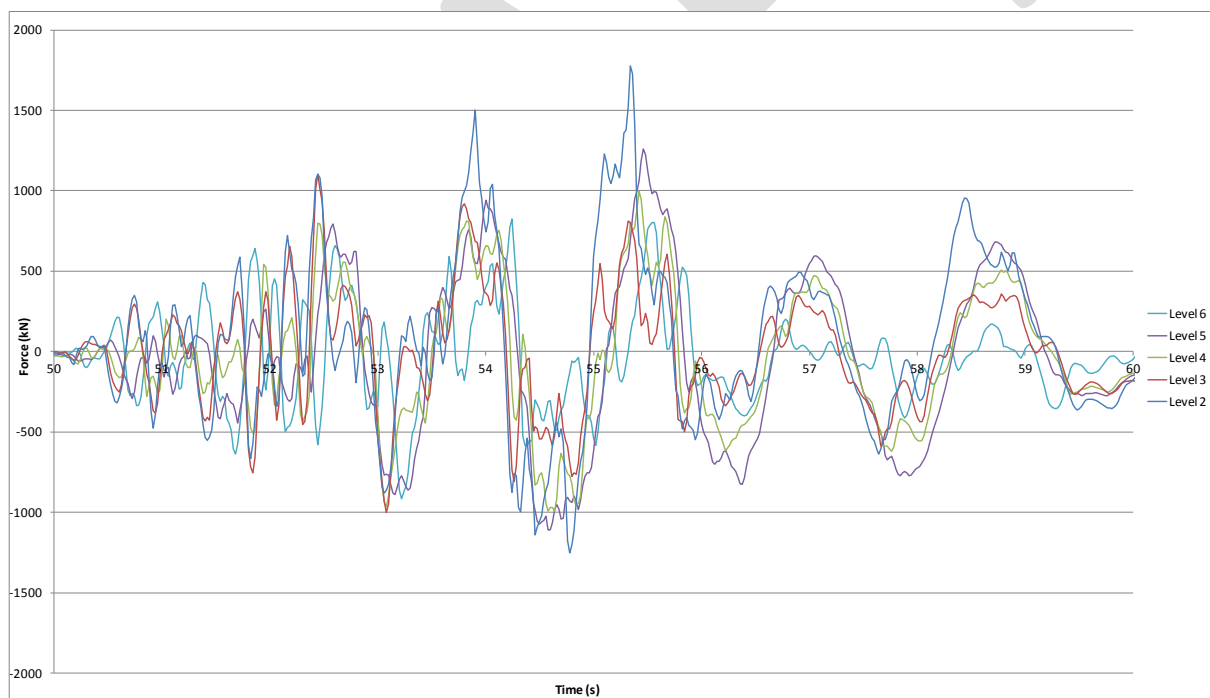


Figure J.36: South wall diaphragm east/west actions, Lyttelton, CCCC Sequential

J.3 Column Hinge Actions

Figure J.37 to Figure J.41 present a selection of column hinge rotations, elongations, and concrete strains for a selected number of critical columns. Strains reported are the maximum that occur at the extreme concrete fibre. Plots are presented for individual columns and are

orientated so that the top row of plots relate to the level 5 hinges with each row below corresponding to the hinges in the column below i.e. from the top level to the bottom level. Results presented are for the worst case hinge at each floor level, with hinge rotation and elongation shown in the left hand plot and hinge concrete strain shown in the right hand plot.

DRAFT

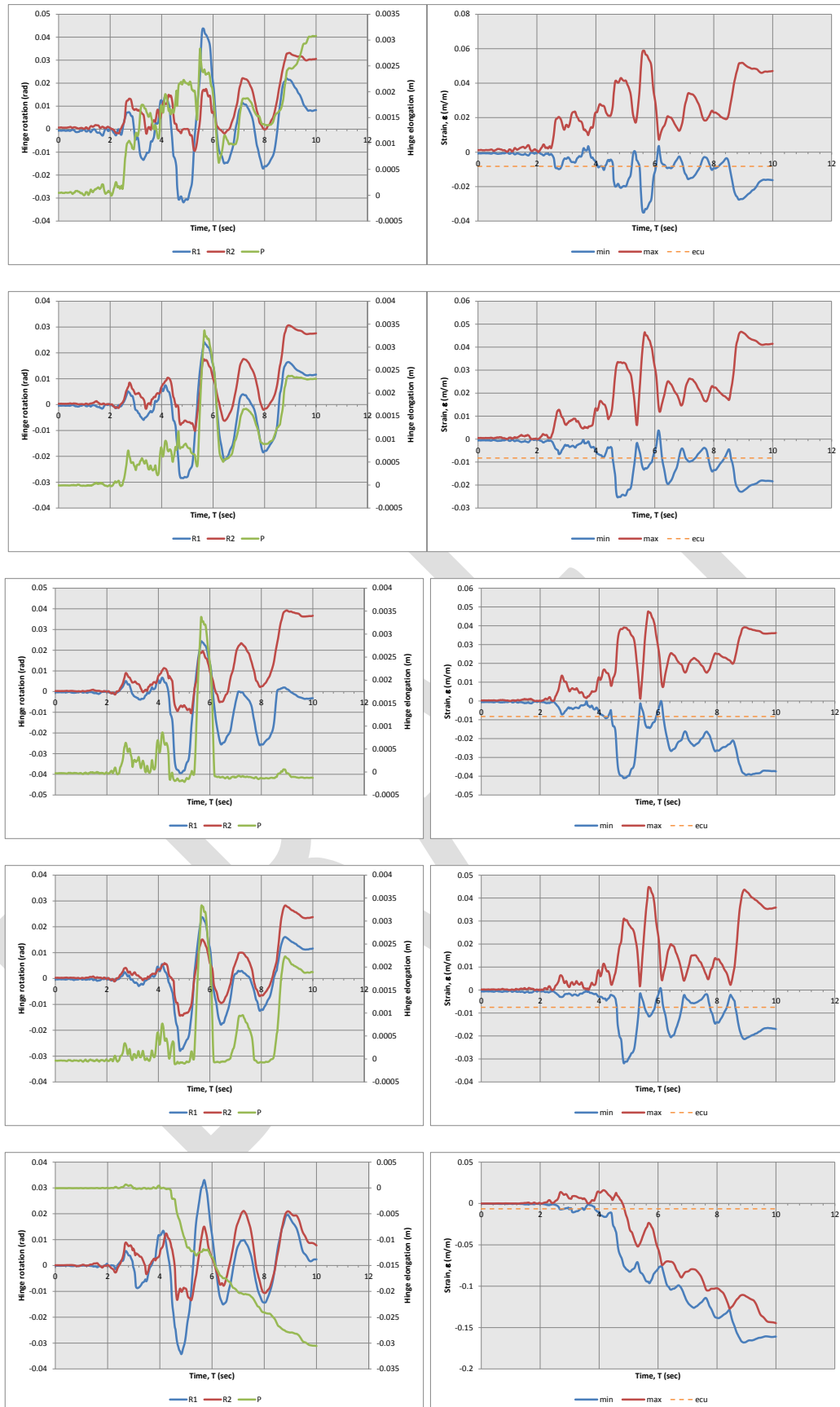


Figure J.37: Column F1 Levels 1 (bottom) to 5 (top) hinge actions, Lyttelton, CCCC

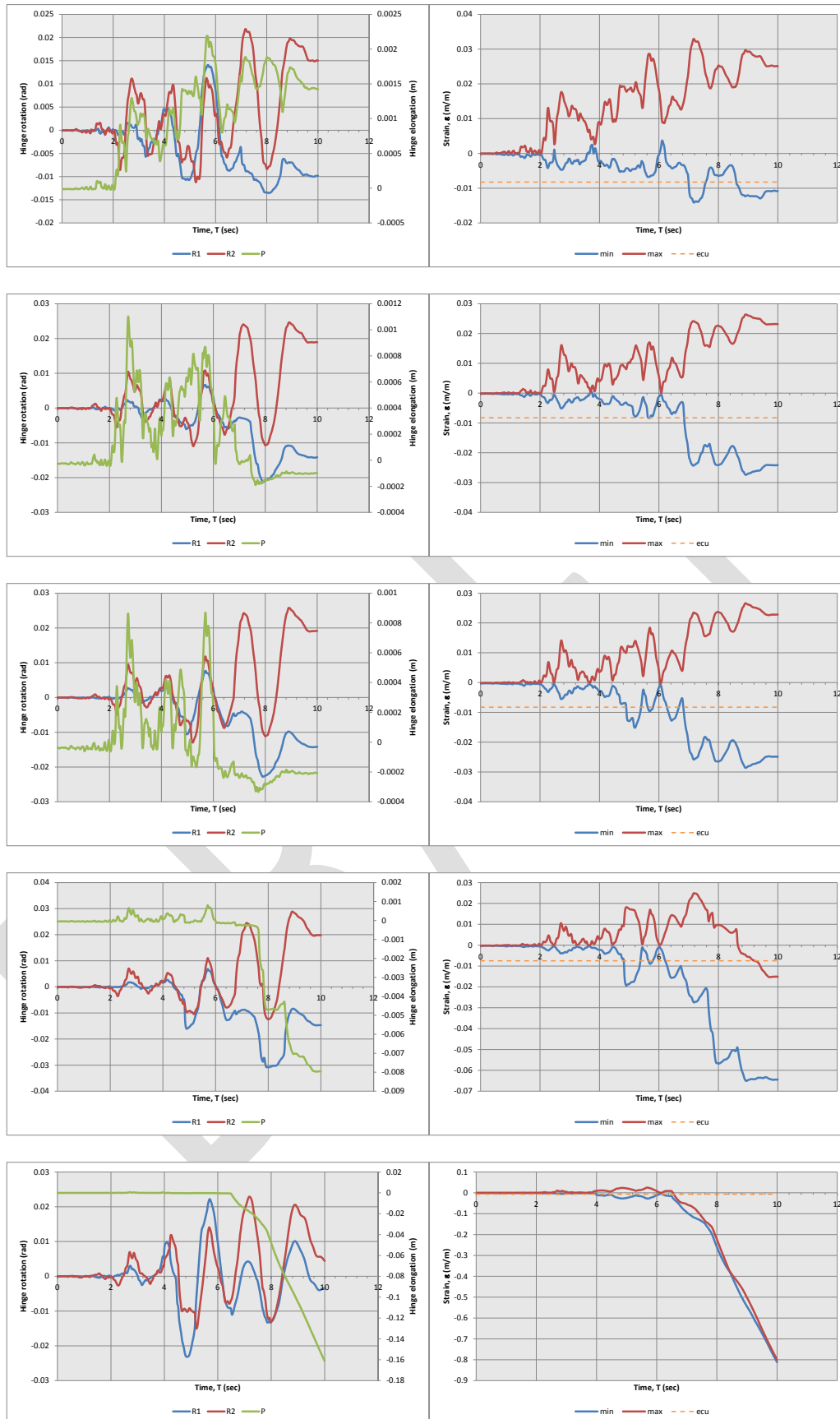


Figure J.38: Column F2 Levels 1 (bottom) to 5 (top) hinge actions, Lyttelton, CCCC

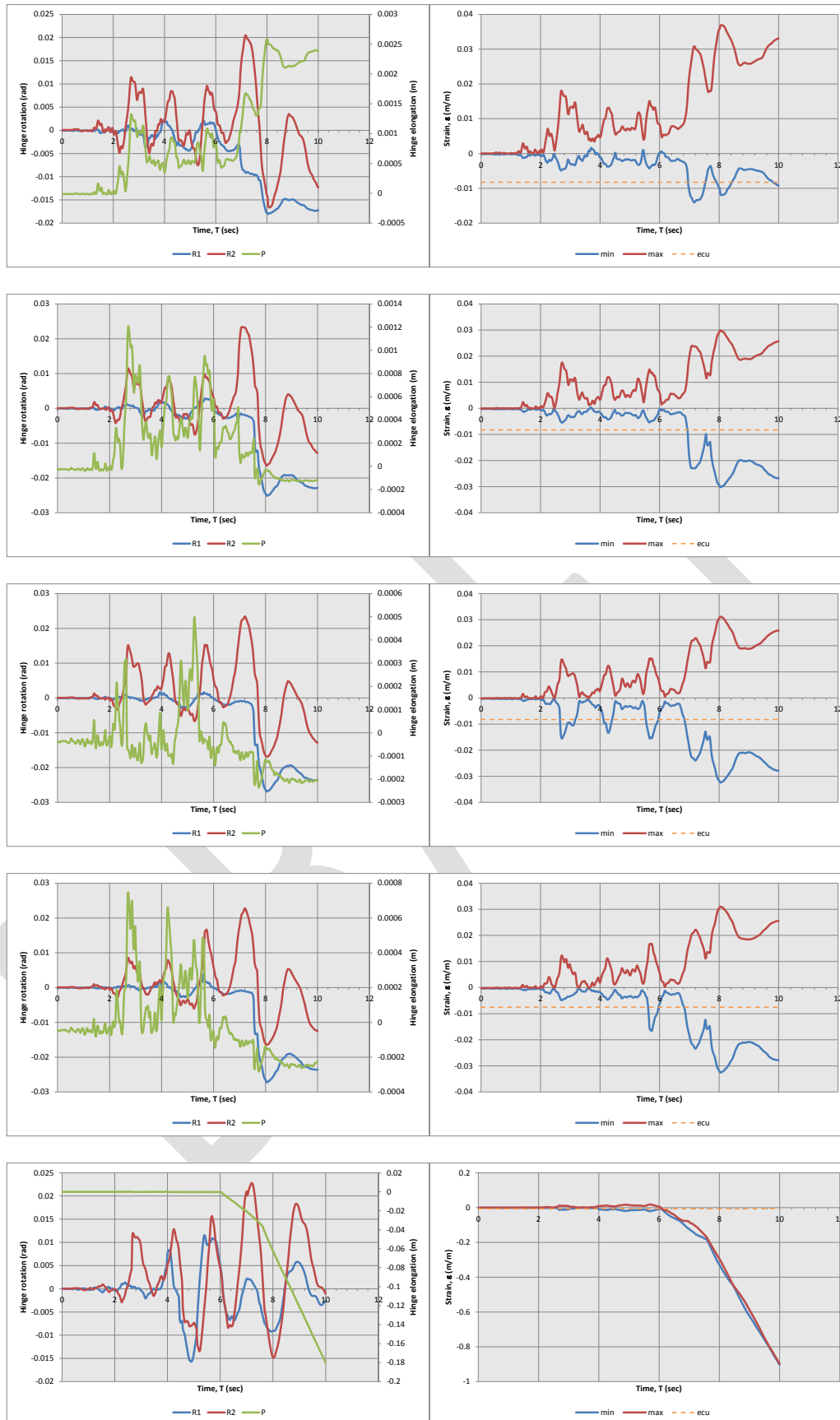


Figure J.39: Column F3 Levels 1 (bottom) to 5 (top) hinge actions, Lyttelton, CCCC

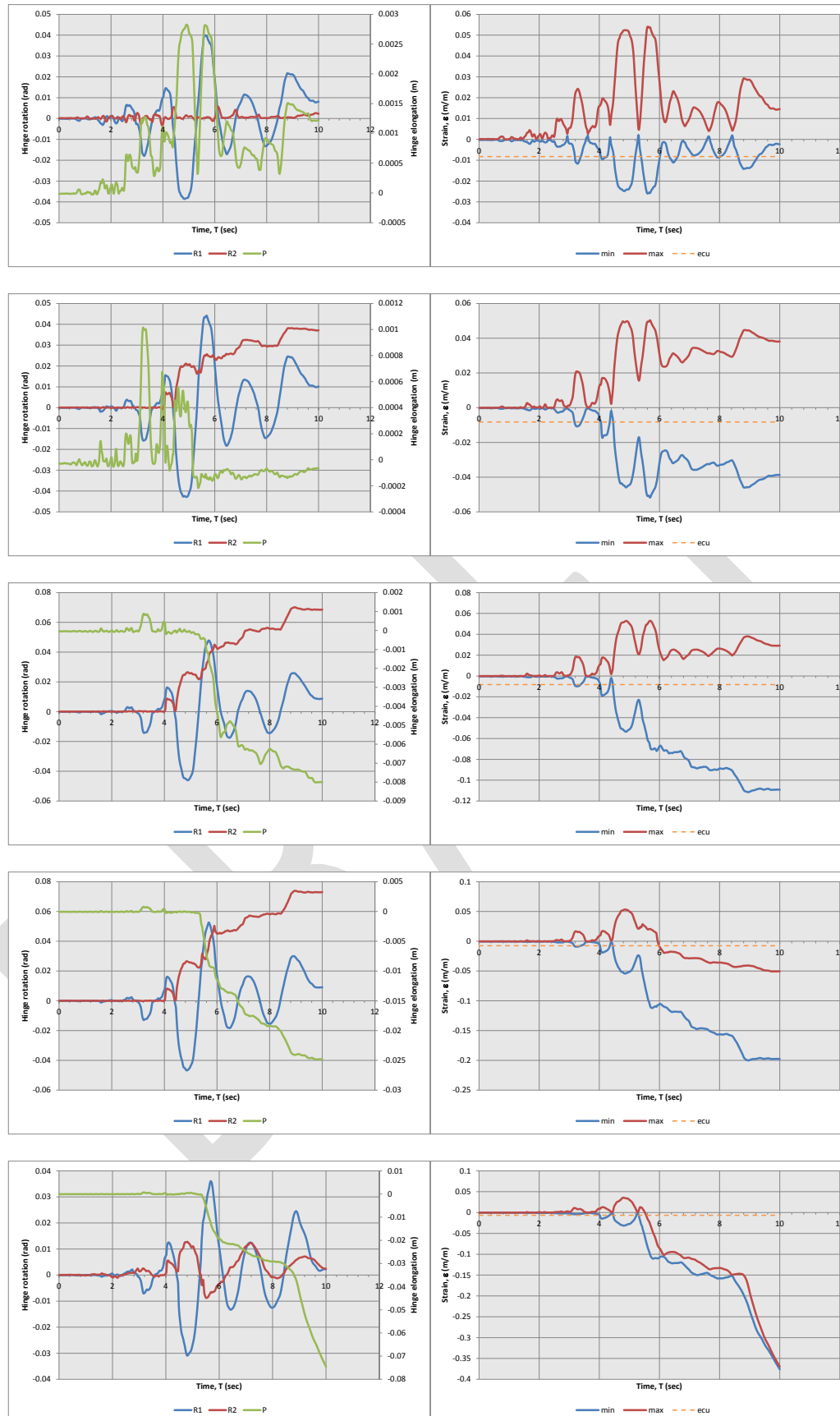


Figure J.40: Column C1 Levels 1 (bottom) to 5 (top) hinge actions, Lyttelton, CCCC

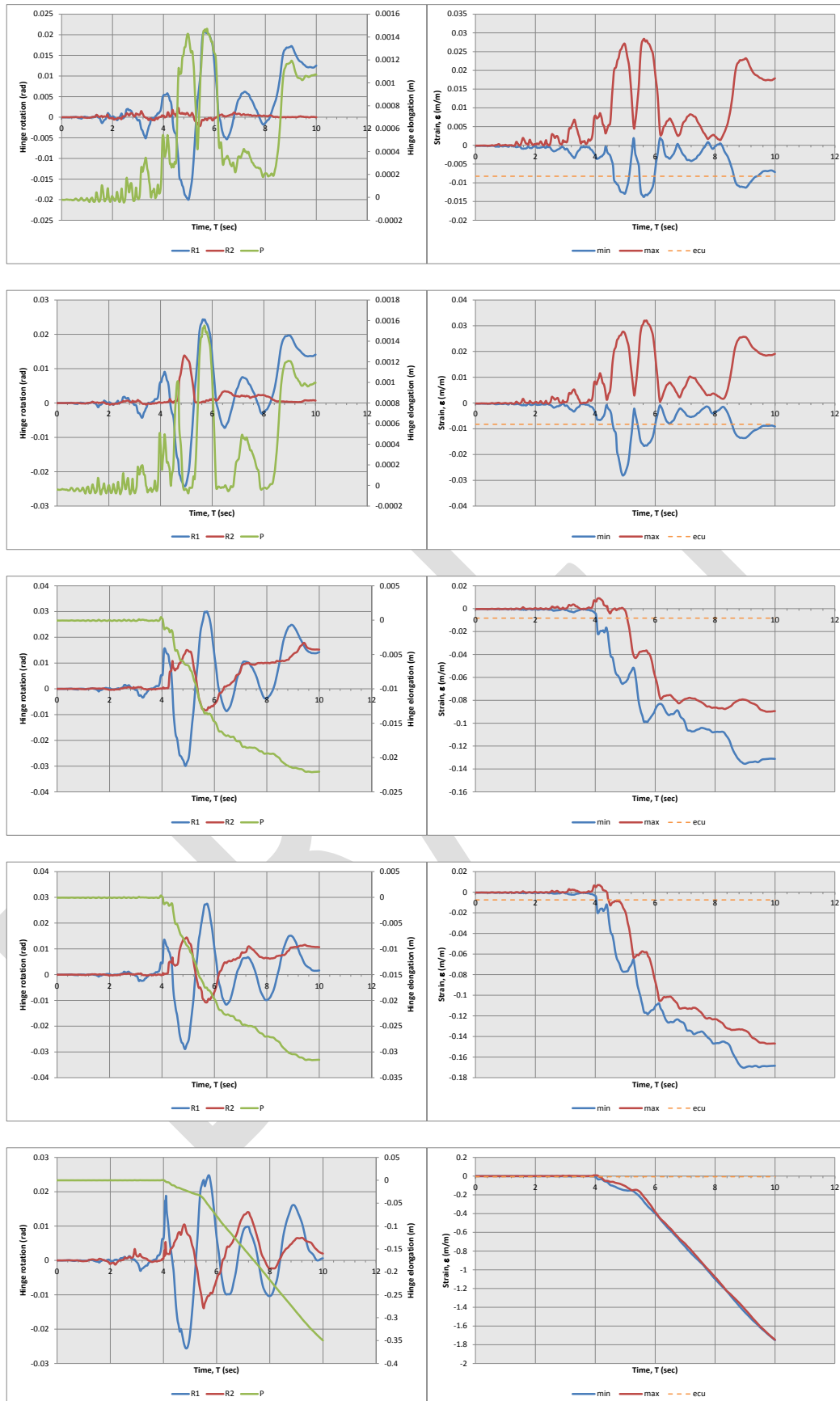


Figure J.41: Column C2 Levels 1 (bottom) to 5 (top) hinge actions, Lyttelton, CCCC

Appendix K Analysis Results - Lyttelton Aftershock: CHHC record

The following details the structural actions reported by the analysis as a function of time, for the Lyttelton aftershock using the acceleration time history recorded at the CHHC station using all components of the record.

K.1 Building Displacements and Drifts.

Building Level 6 displacements are presented in Figure K.1 and Figure K.2 below for the southeast and northwest corners of the building respectively.

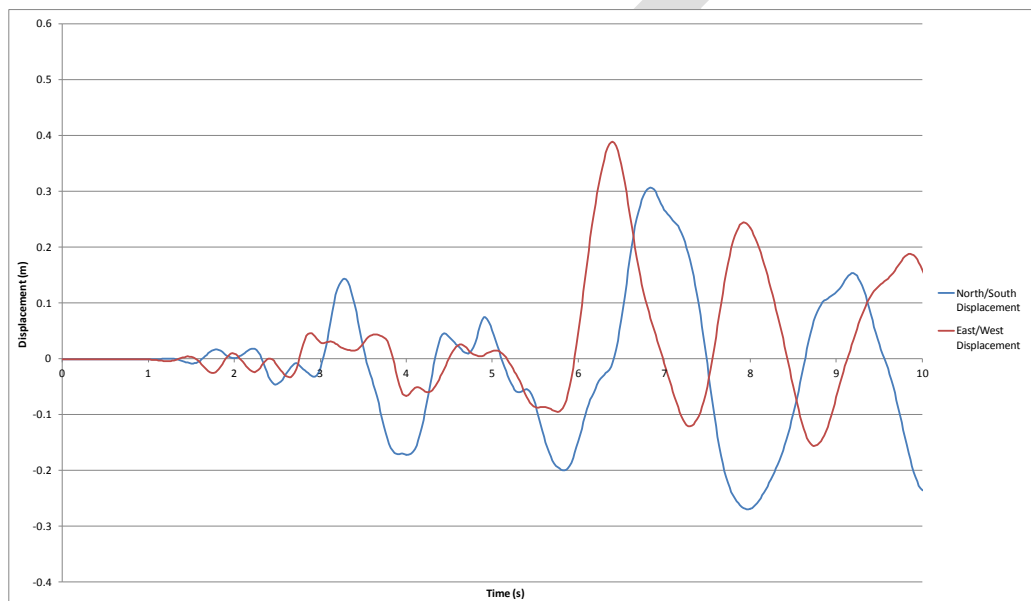


Figure K.1: Level 6 Southeast corner displacements, Lyttelton, CHHC

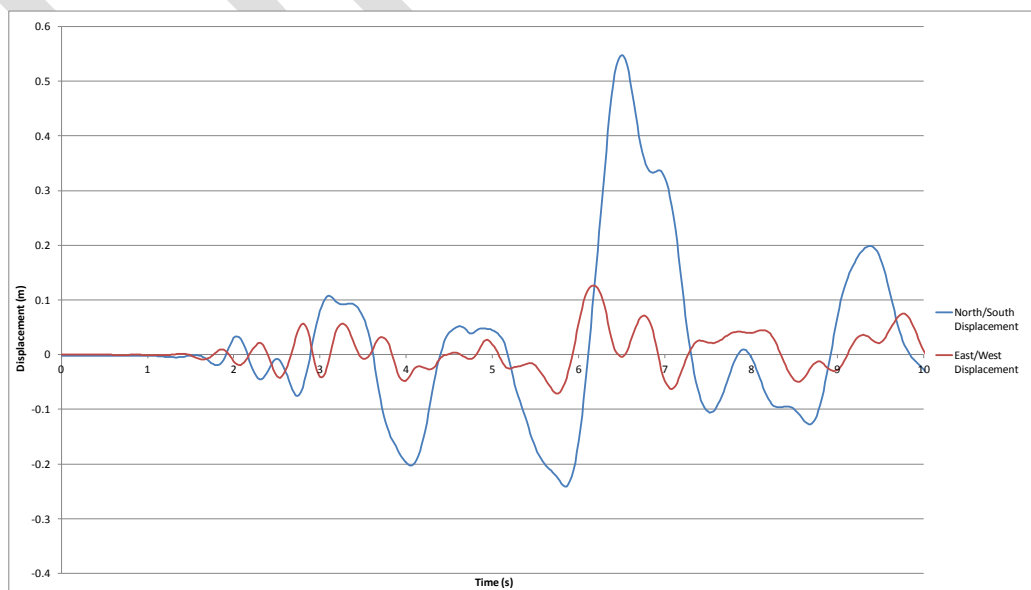


Figure K.2: Level 6 Northwest corner displacements, Lyttelton, CHHC

As can be seen in Figure K.2 above a significant increase in the northward building displacement is observed in the northwest corner of the building between 6.2 and 7.2 seconds of the record. This occurs after the tension ties capacities on levels 4 to 6 of the core are exceeded allowing increased building rotation clockwise from west to north. The peak displacement corresponds to a clockwise rotation in conjunction with a net northward building translation Table K.1 presents the sequence of failure of the north core wall ties throughout the record.

Table K.1: Wall D and D/E diaphragm disconnection times, Lyttelton, CHHC.

Level	Wall D Failure (sec)	Wall D/E Failure (sec)
6	2.96	2.50
5	3.90	2.50
4	3.86	2.50

Inter-storey displacements for the perimeter frame lines A and F in the north/south direction are presented in Figure K.3 and Figure K.4 below. North core tie tensile failure is identified on the plots for reference.

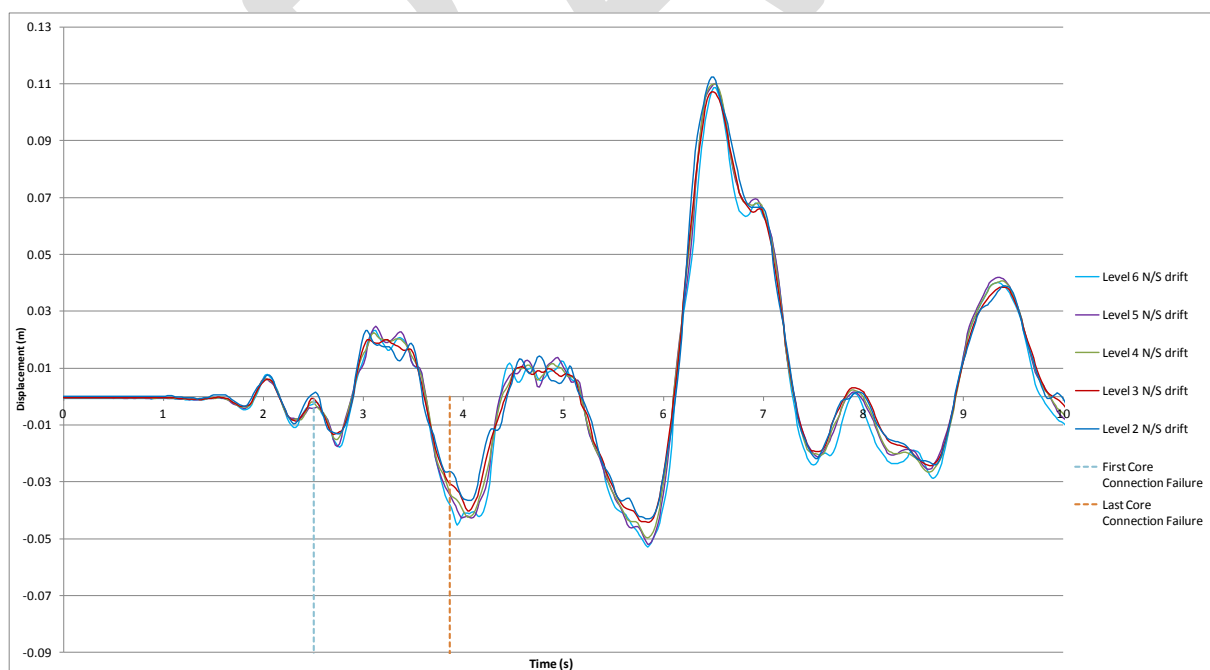


Figure K.3: Frame A north/south inter-storey displacements, Lyttelton, CHHC

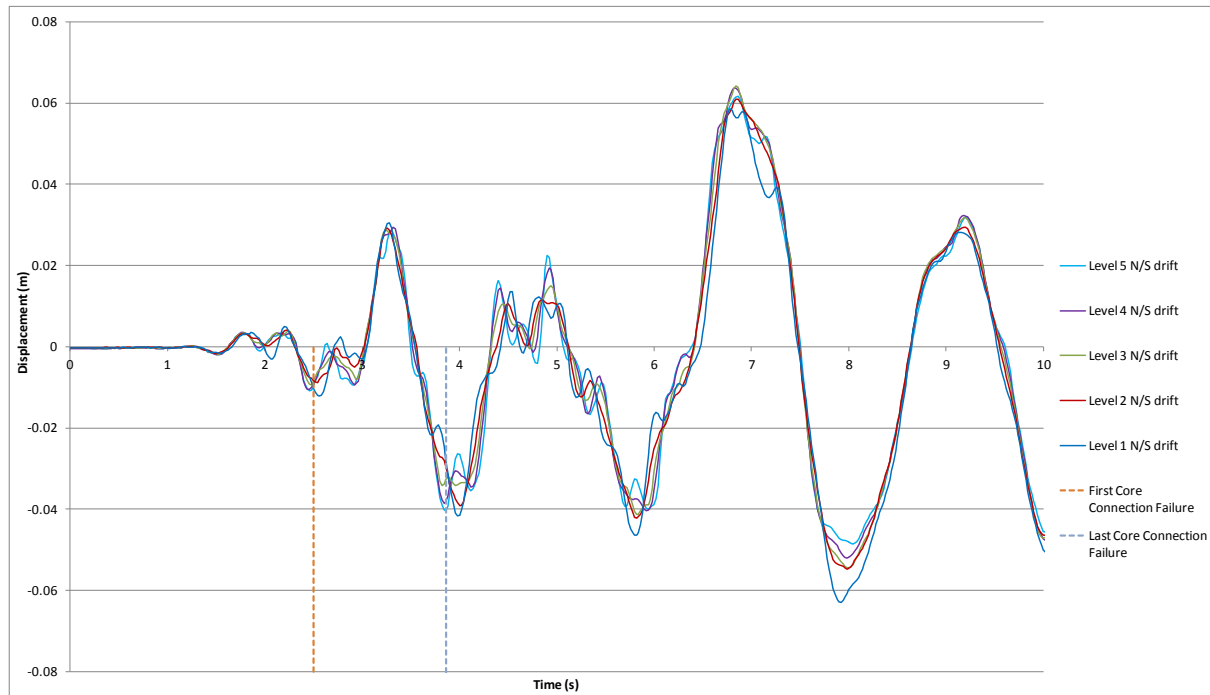


Figure K.4: Frame F north/south inter-storey displacements, Lyttelton, CHHC

Inter-storey displacements for the perimeter frame lines 1 and 4 in the East/West direction are presented in Figure K.5 and Figure K.6 below.

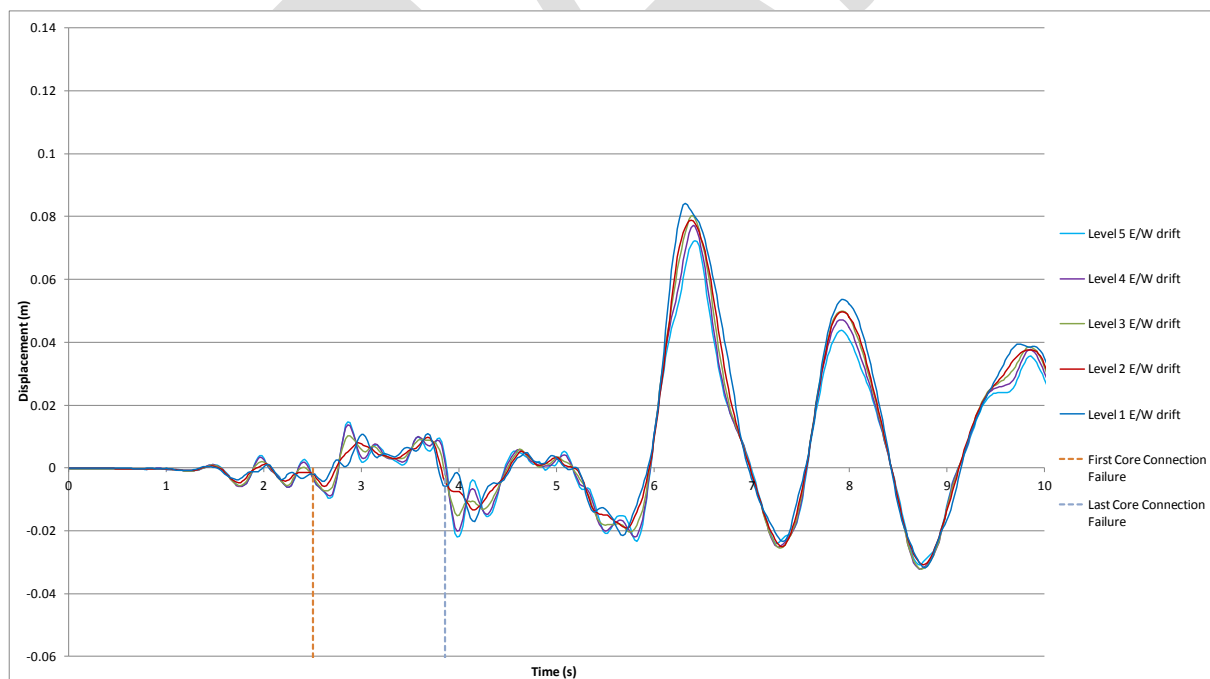


Figure K.5: Frame 1 east/west inter-storey displacements, Lyttelton, CHHC

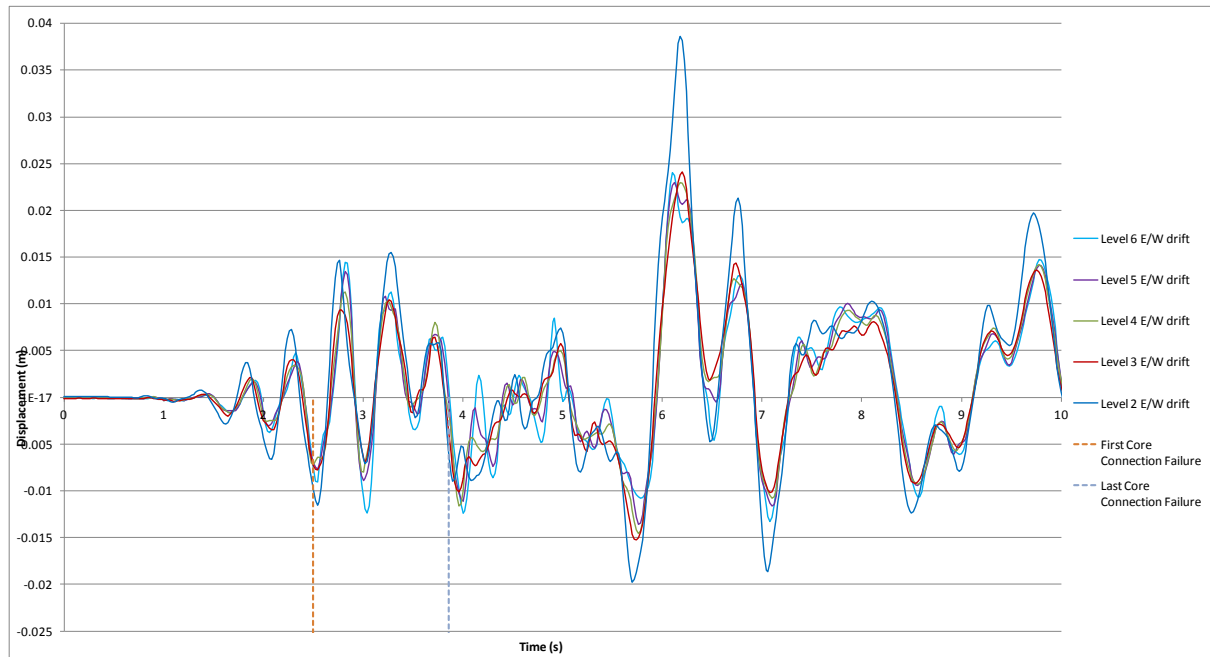


Figure K.6: Frame 4 east/west inter-storey displacements, Lyttelton, CHHC

K.2 Diaphragm Connection Forces

Diaphragm connection forces are presented in Figure K.7 to Figure K.18 below. Note that moments are reported about the geometric centroid of the element being considered.

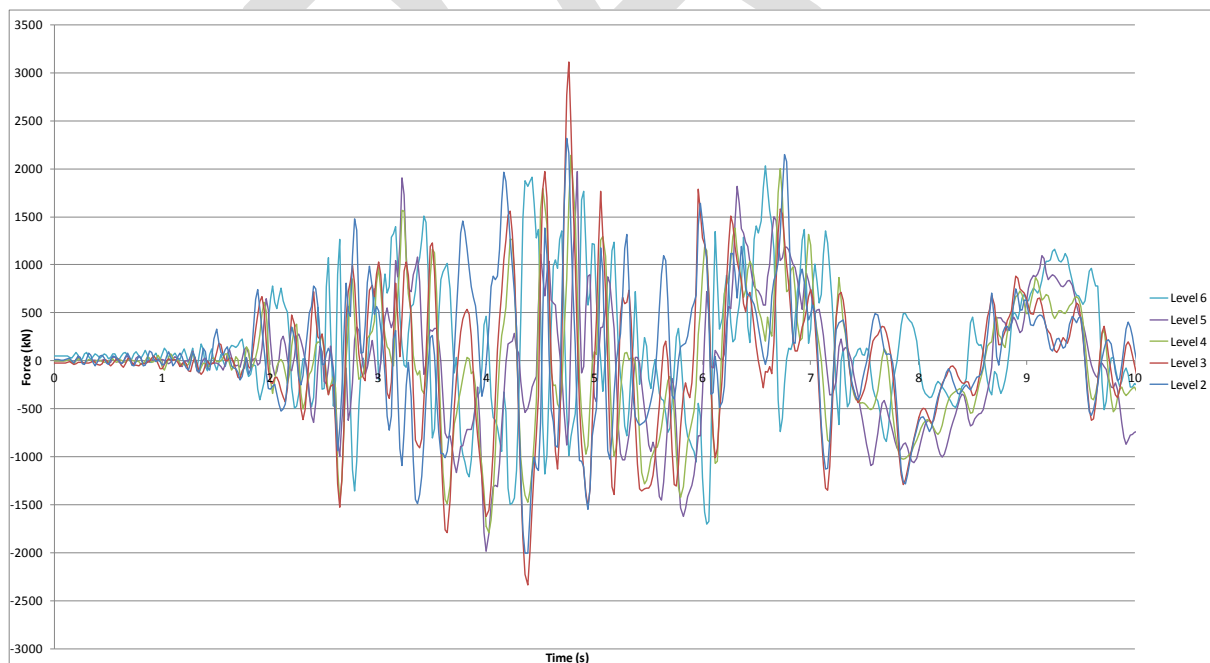


Figure K.7: North core total diaphragm north/south actions, Lyttelton, CHHC

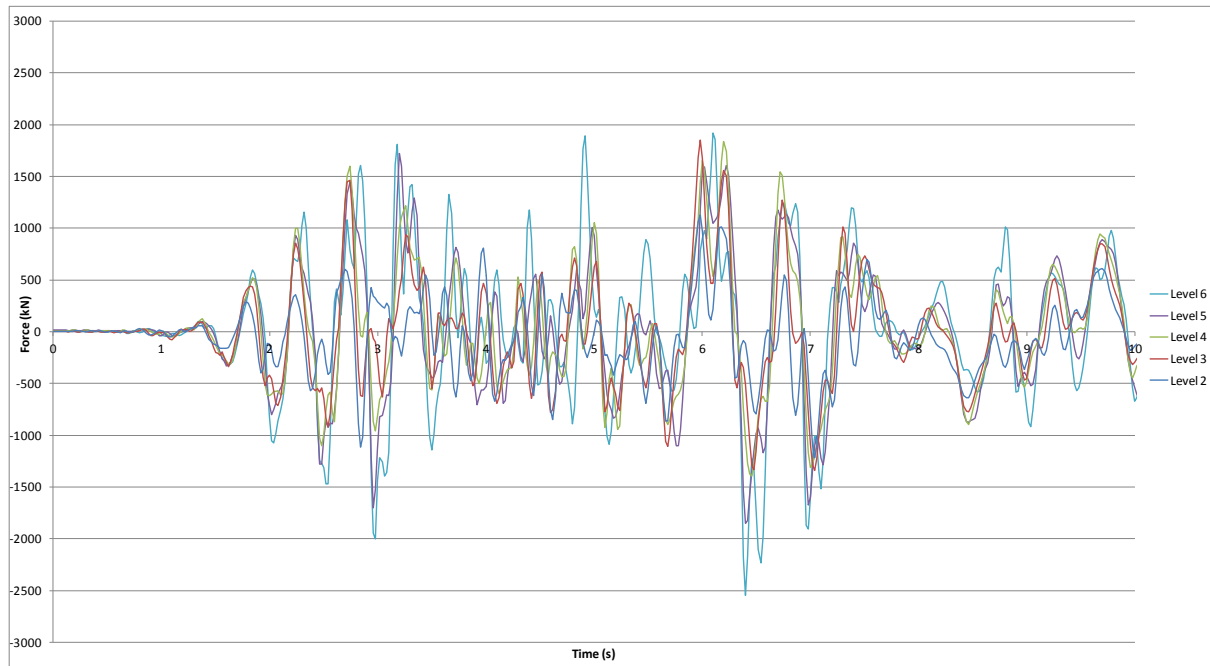


Figure K.8: North core total diaphragm east/west actions, Lyttelton, CHHC

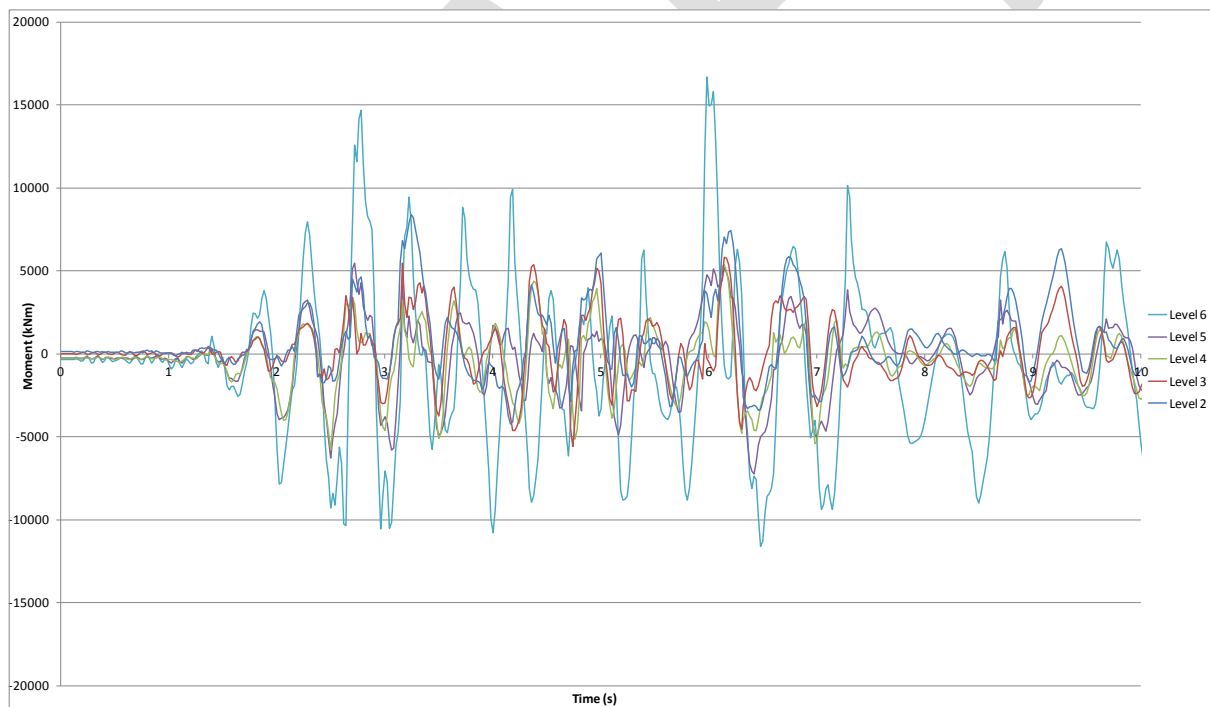


Figure K.9: North core total diaphragm in-plane moments, Lyttelton, CHHC

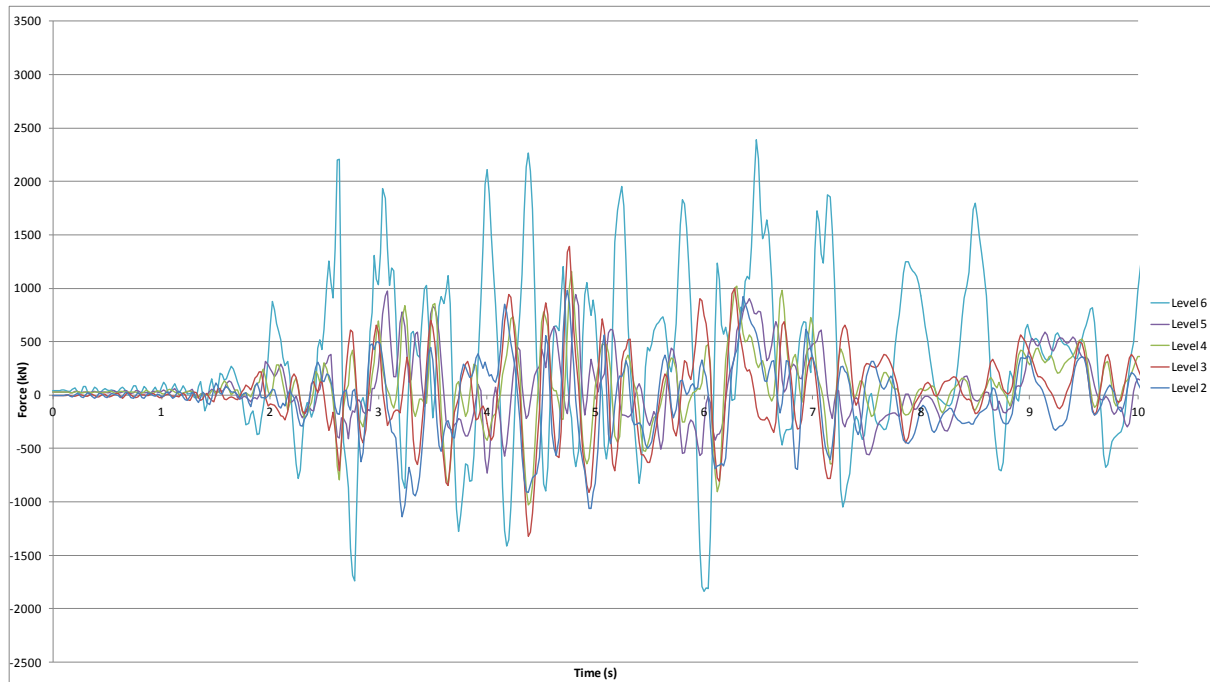


Figure K.10: North core Wall C diaphragm north/south actions, Lyttelton, CHHC

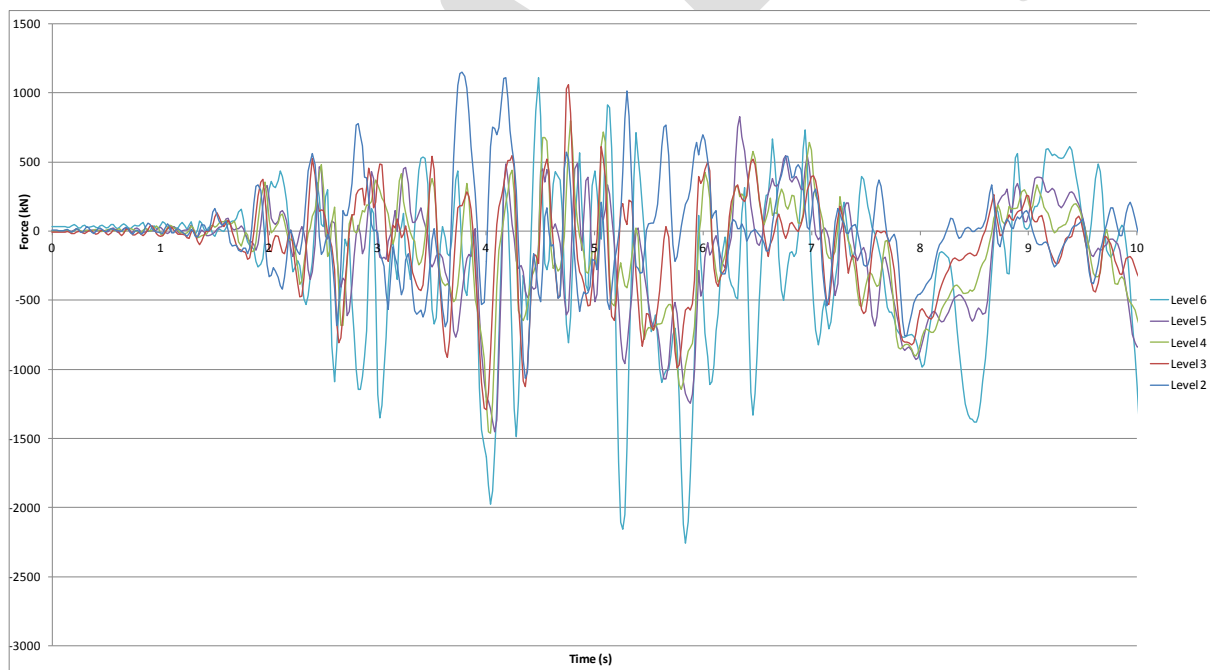


Figure K.11: North core Wall C/D diaphragm north/south actions, Lyttelton, CHHC

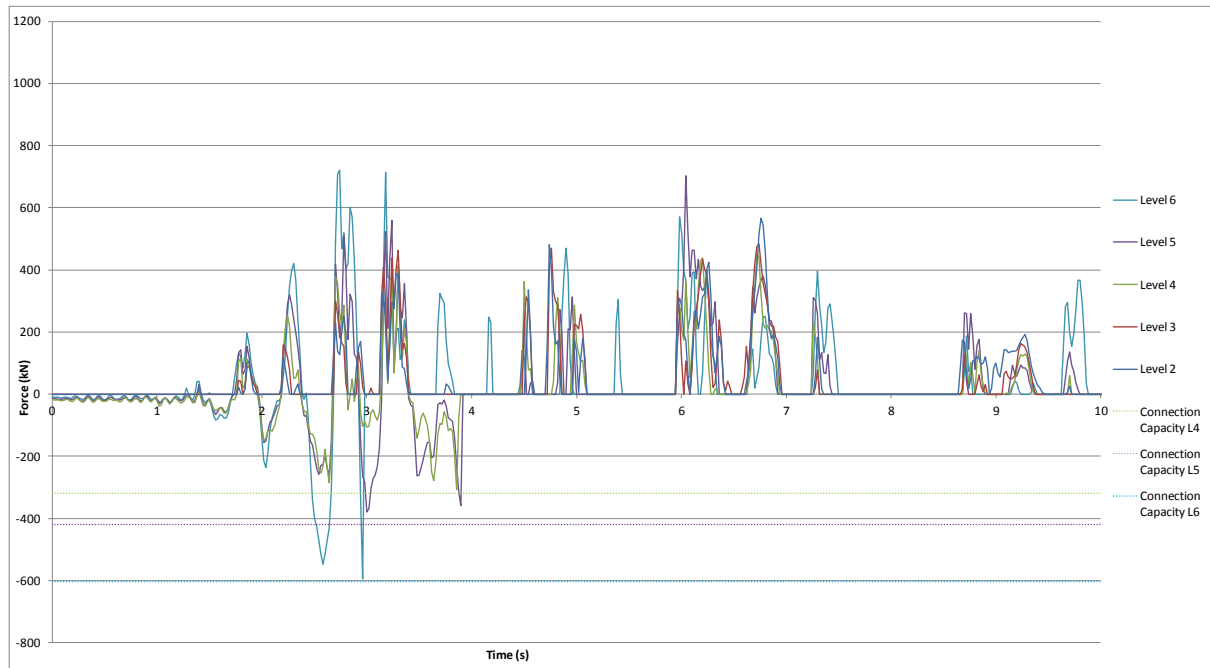


Figure K.12: North core Wall D diaphragm north/south actions, Lyttelton, CHHC

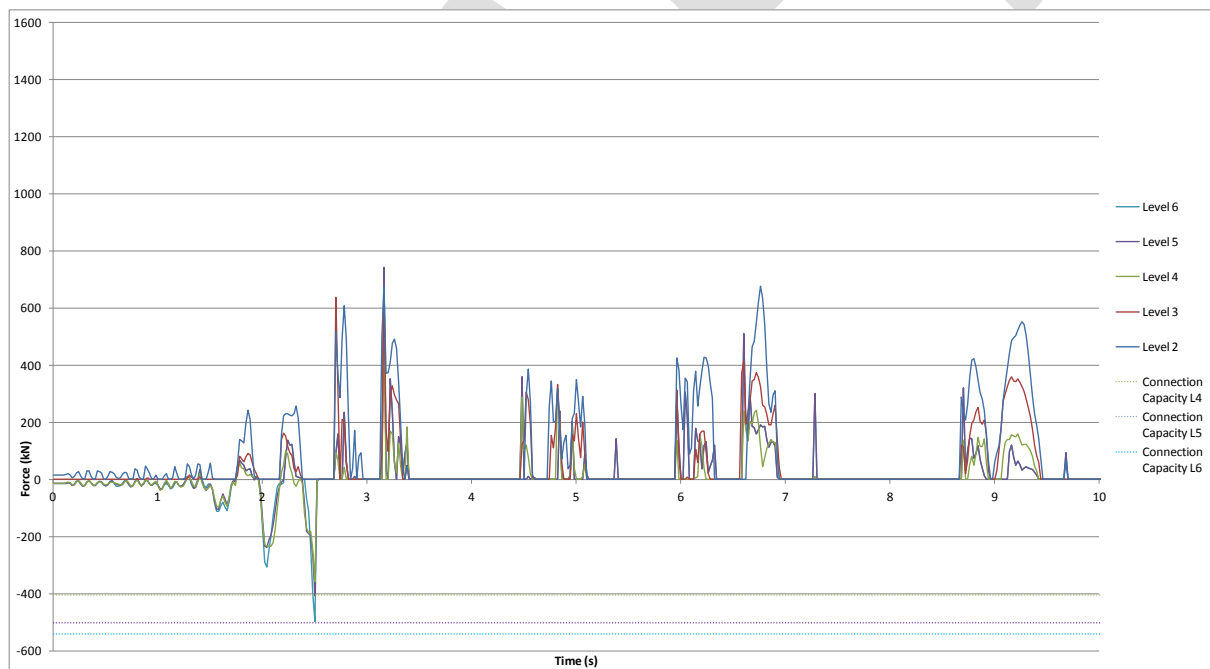


Figure K.13: North core Wall D/E diaphragm north/south actions, Lyttelton, CHHC

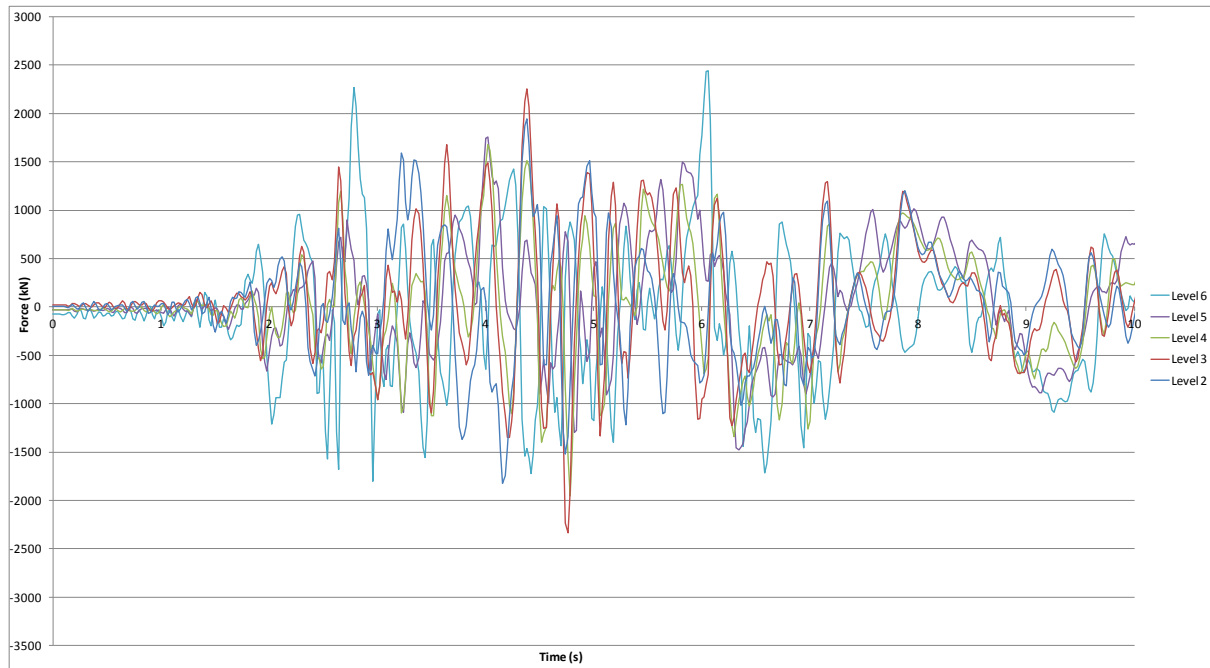


Figure K.14: North core Slab 4/C to C/D diaphragm north/south actions, Lyttelton, CHHC

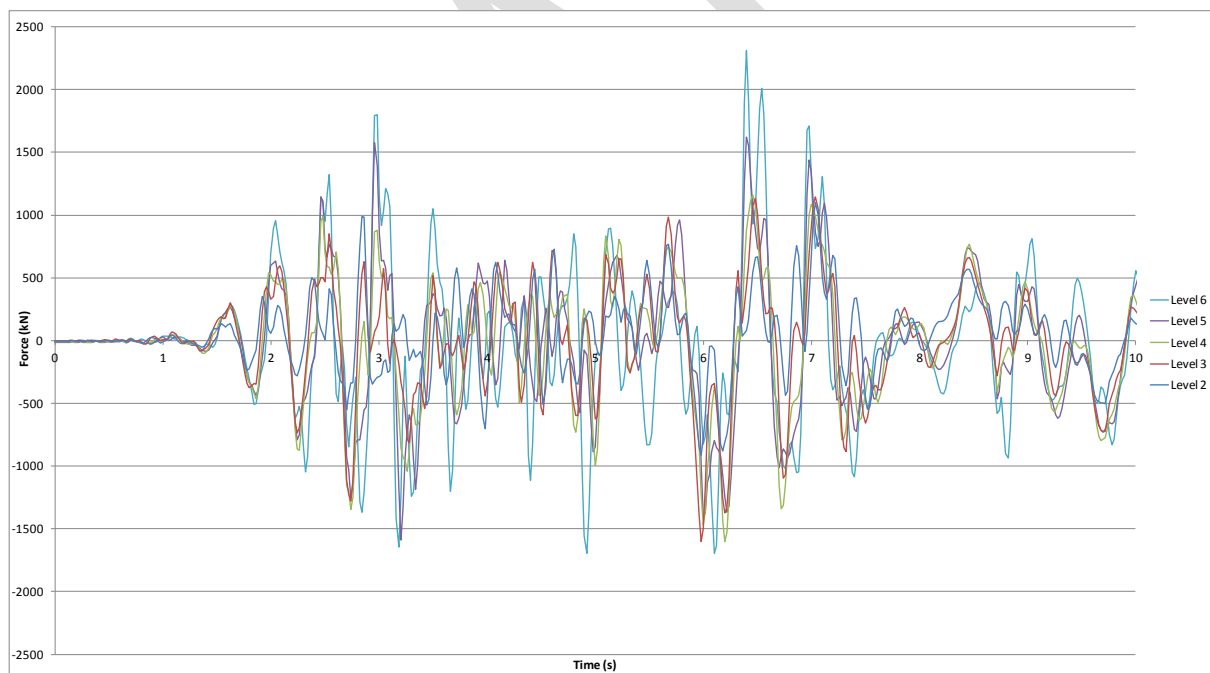


Figure K.15: North core Slab 4/C to C/D diaphragm east/west actions, Lyttelton, CHHC

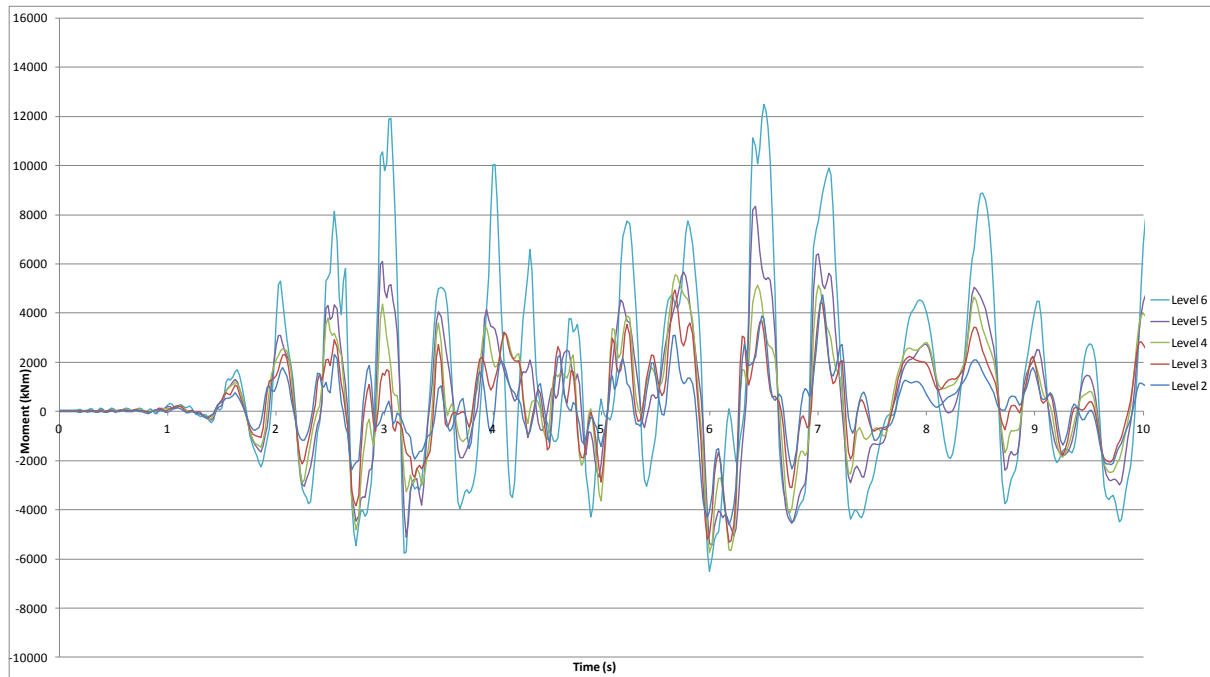


Figure K.16: North core Slab 4/C to C/D diaphragm in-plane moments, Lyttelton, CHHC

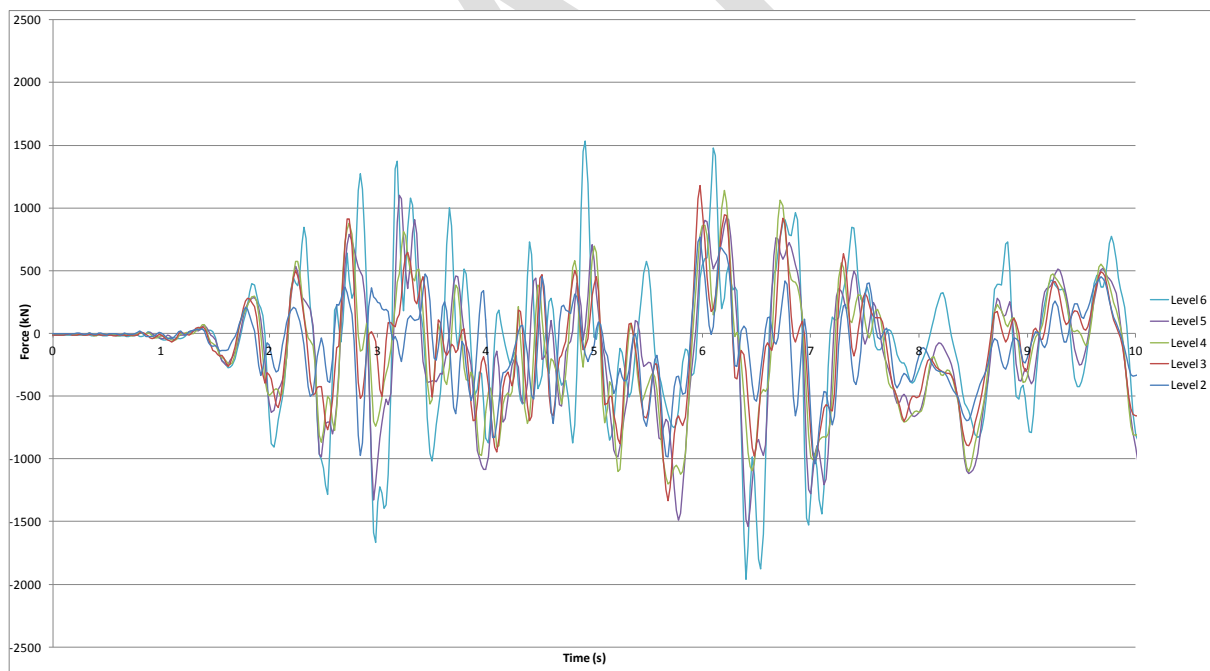


Figure K.17: North core Wall 5 diaphragm east/west actions, Lyttelton, CHHC

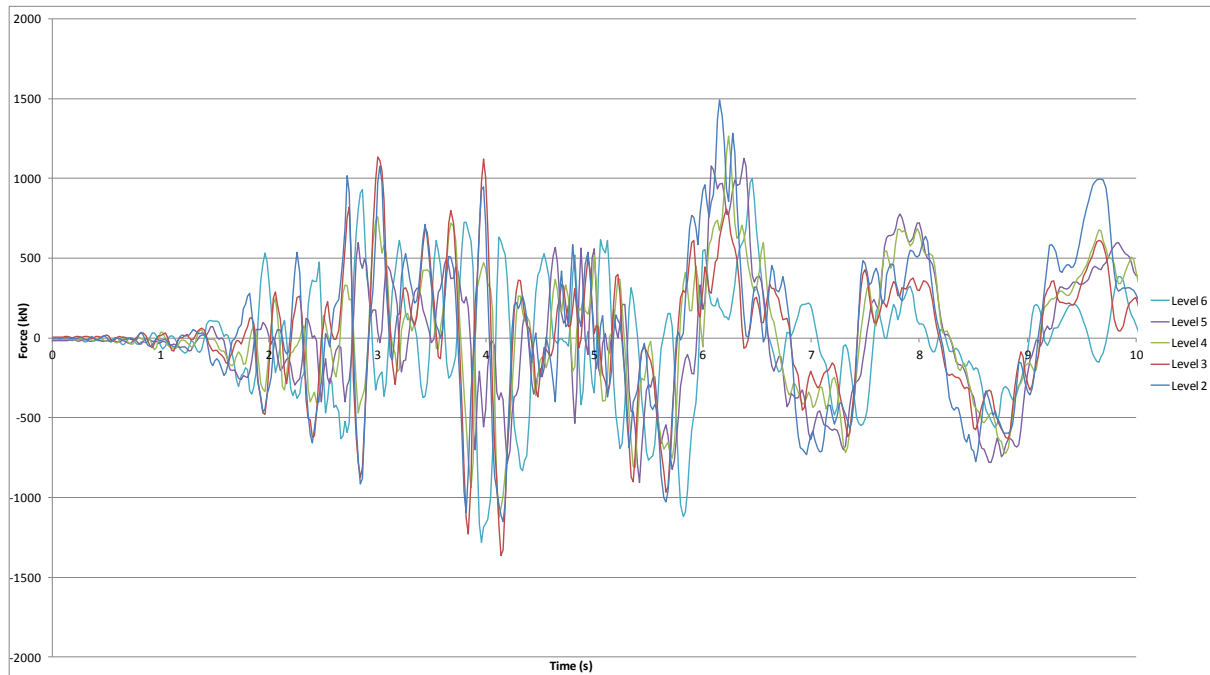


Figure K.18: South wall diaphragm east/west actions, Lyttelton, CHHC

K.3 Column Hinge Actions

Figure K.19 to Figure K.23 present a selection of column hinge rotations, elongations, and concrete strains for a selected number of critical columns. Strains reported are the maximum that occur at the extreme concrete fibre. Plots are presented for individual columns and are orientated so that the top row of plots relate to the level 5 hinges with each row below corresponding to the hinges in the column below i.e. from the top level to the bottom level. Results presented are for the worst case hinge at each floor level, with hinge rotation and elongation shown in the left hand plot and hinge concrete strain shown in the right hand plot.



Figure K.19: Column F1 Levels 1 (bottom) to 5 (top) hinge actions, Lyttelton, CHHC

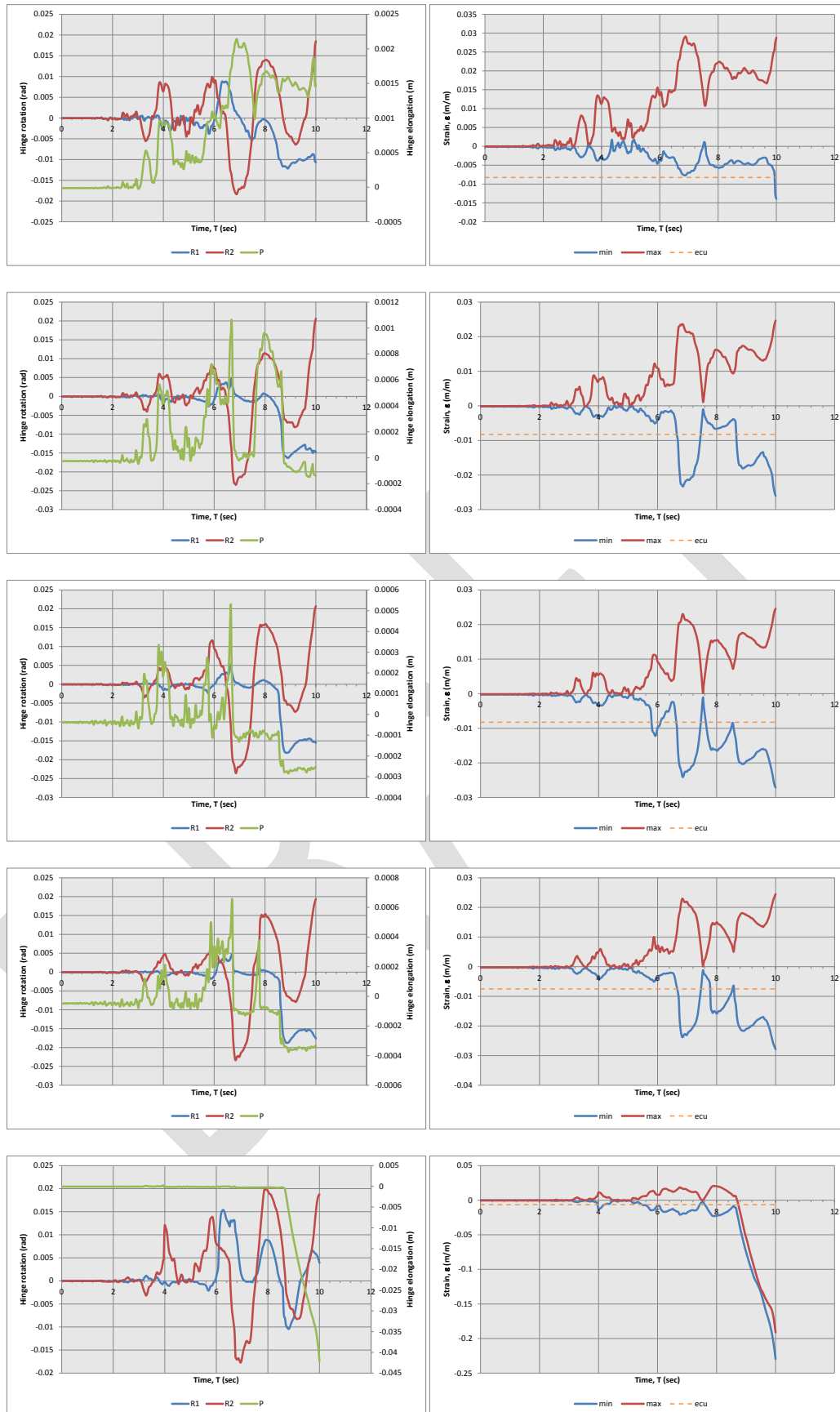


Figure K.20: Column F2 Levels 1 (bottom) to 5 (top) hinge actions, Lyttelton, CHHC

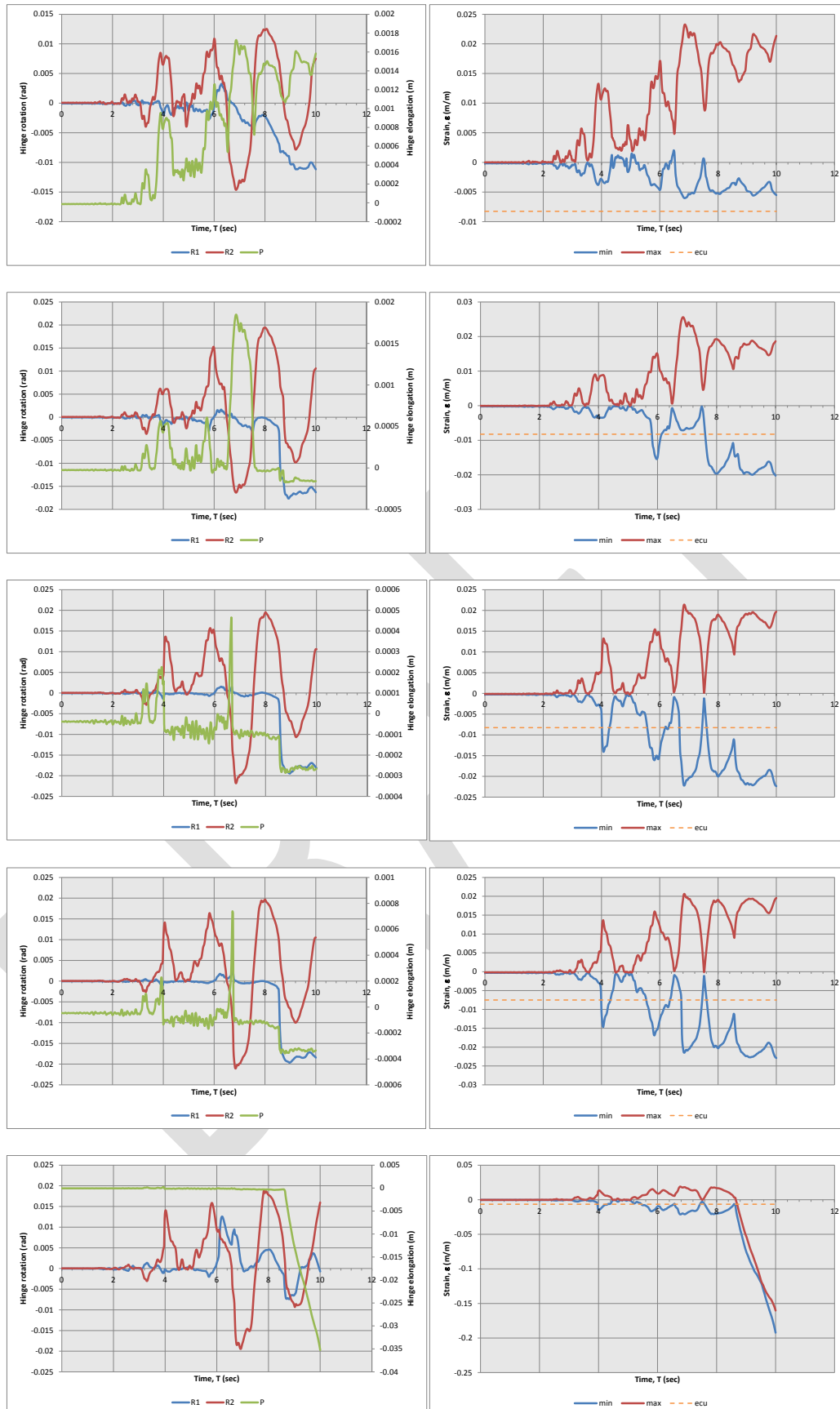


Figure K.21: Column F3 Levels 1 (bottom) to 5 (top) hinge actions, Lyttelton, CHHC

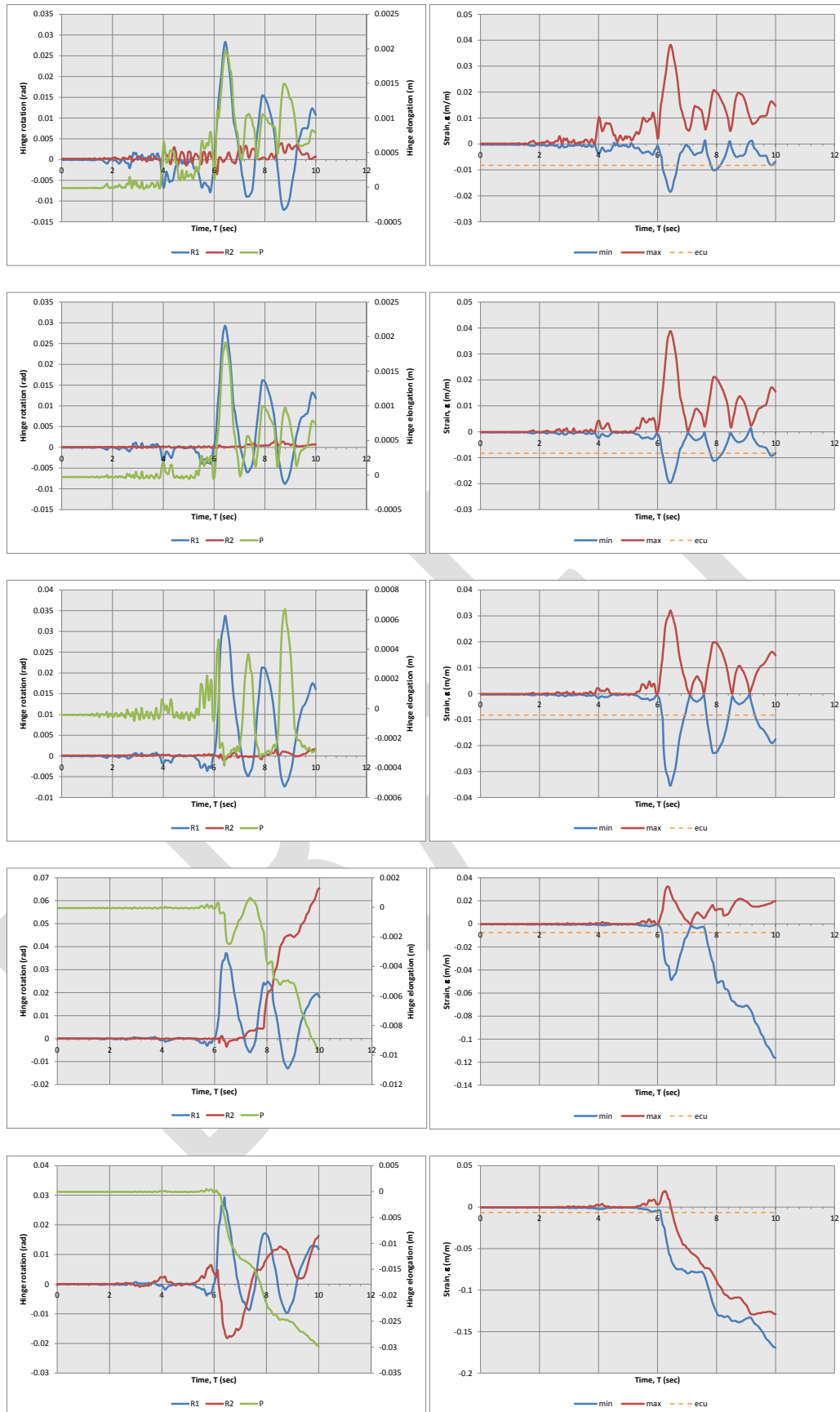


Figure K.22: Column C1 Levels 1 (bottom) to 5 (top) hinge actions, Lyttelton, CHHC

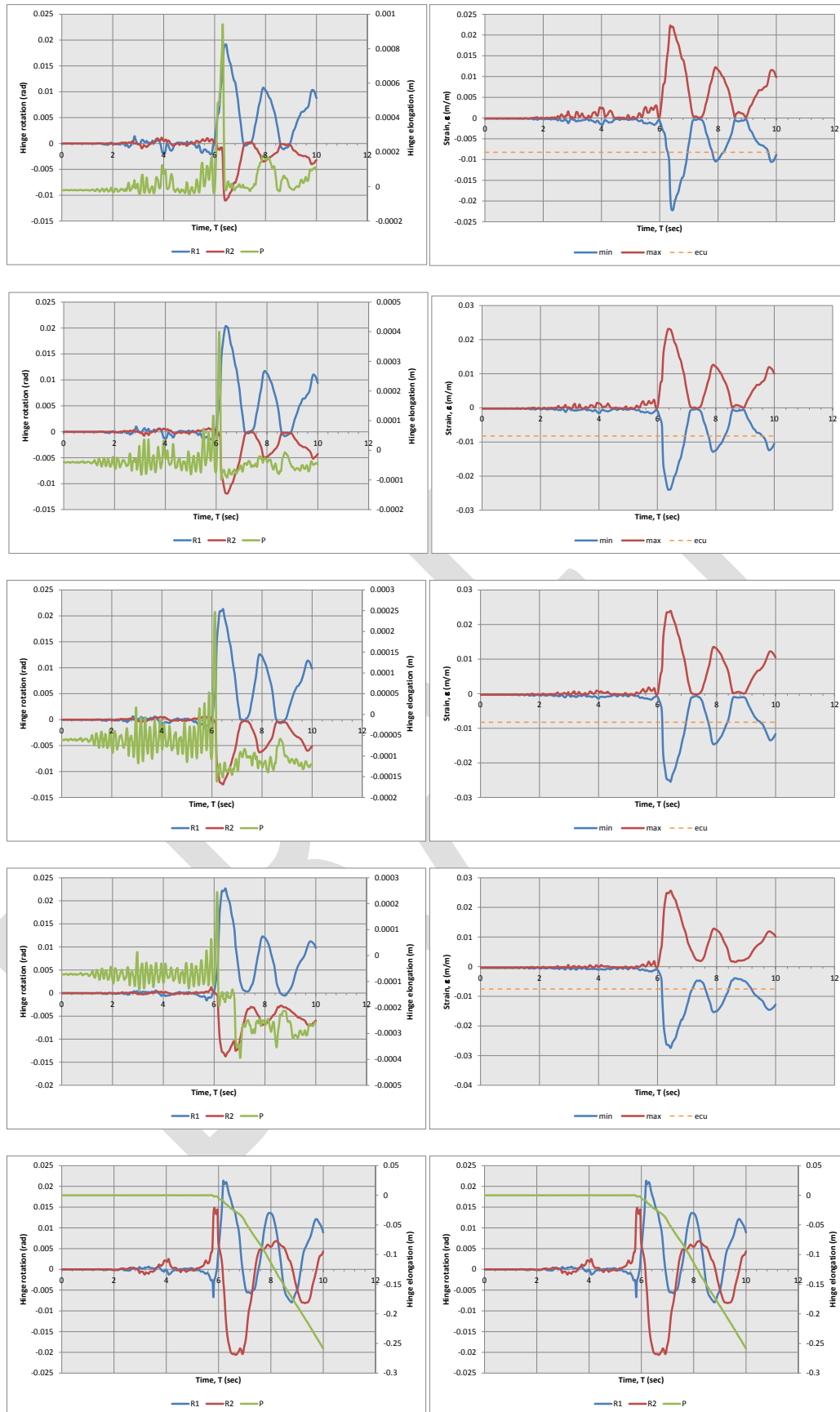


Figure K.23: Column C2 Levels 1 (bottom) to 5 (top) hinge actions, Lyttelton, CHHC

Appendix L Analysis Results - Lyttelton Aftershock: REHS record

The following details the structural actions reported by the analysis as a function of time, for the Lyttelton aftershock using the acceleration time history recorded at the REHS station using all components of the record.

L.1 Building Displacements and Drifts.

Building Level 6 displacements are presented in Figure L.1 and Figure L.2 below for the southeast and northwest corners of the building respectively.

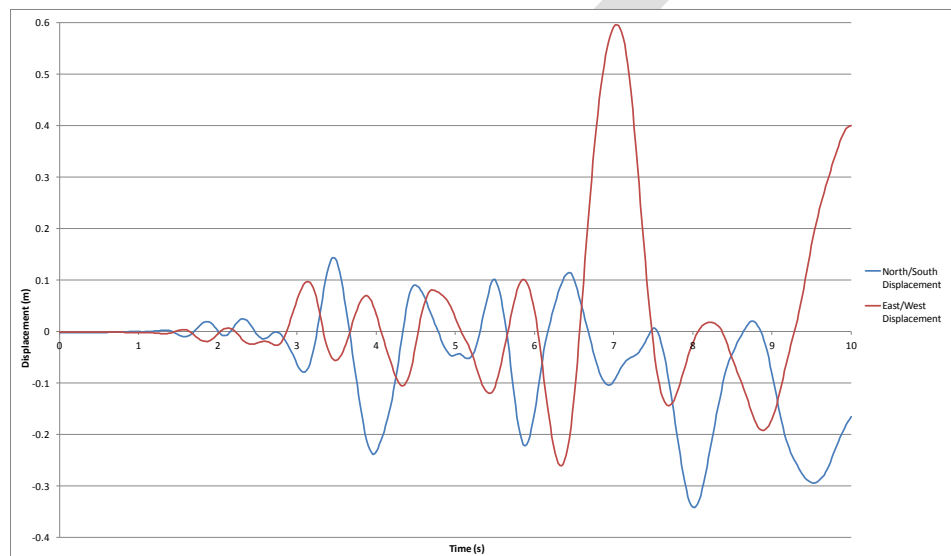


Figure L.1: Level 6 Southeast corner displacements, Lyttelton, REHS

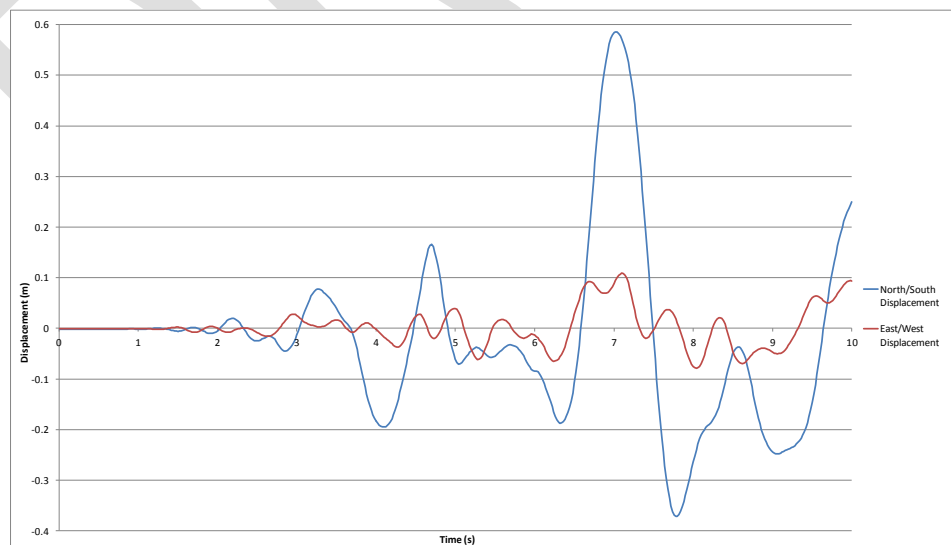


Figure L.2: Level 6 Northwest corner displacements, Lyttelton, REHS

As can be seen in Figure L.2 above a significant increase in the northward building displacement is observed in the northwest corner of the building between 6.5 and 7.5 seconds of the record. Similarly, a significant increase in the westward building displacement is observed in the southeast corner of the building over the same time period. This occurs after the tension ties capacities on levels 4 to 6 of the core are exceeded allowing increased building rotation clockwise from west to north. The peak displacement corresponds to a clockwise rotation in conjunction with a net northward building translation Table L.1 presents the sequence of failure of the north core wall ties throughout the record.

Table L.1: Wall D and D/E diaphragm disconnection times, Lyttelton, REHS

Level	Wall D Failure (sec)	Wall D/E Failure (sec)
6	5.18	4.68
5	5.20	3.80
4	3.76	3.70

Inter-storey displacements for the perimeter frame lines A and F in the north/south direction are presented in Figure L.3 and Figure L.4 below. North core tie tensile failure is identified on the plots for reference.

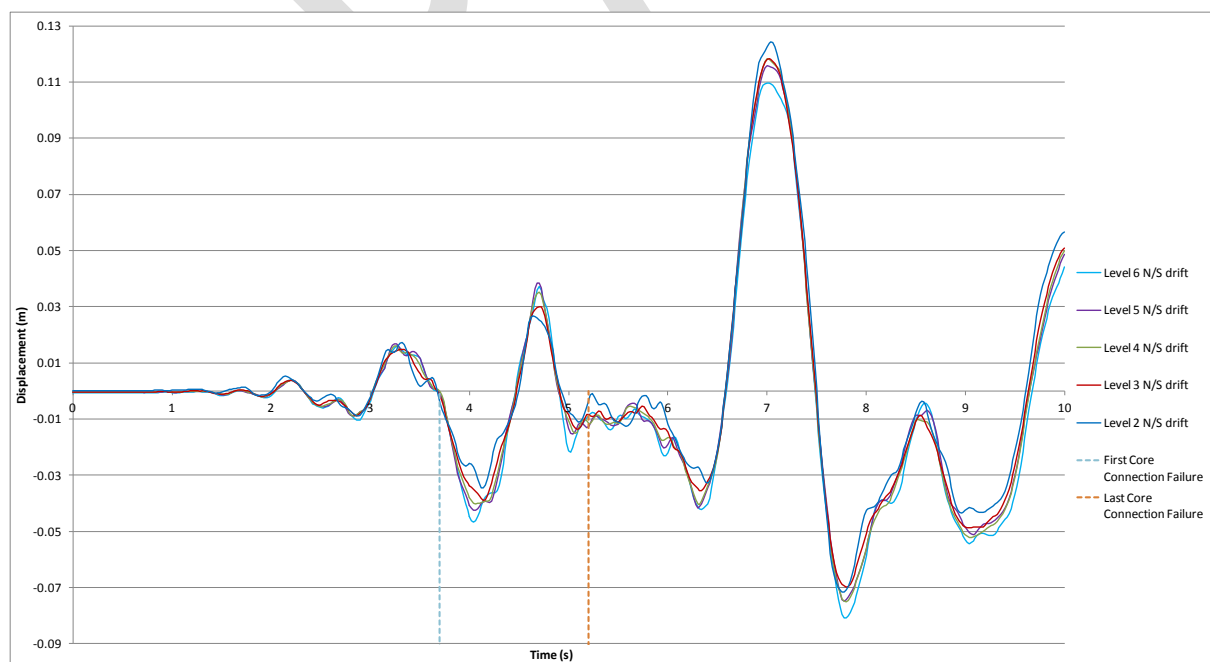


Figure L.3: Frame A north/south inter-storey displacements, Lyttelton, REHS

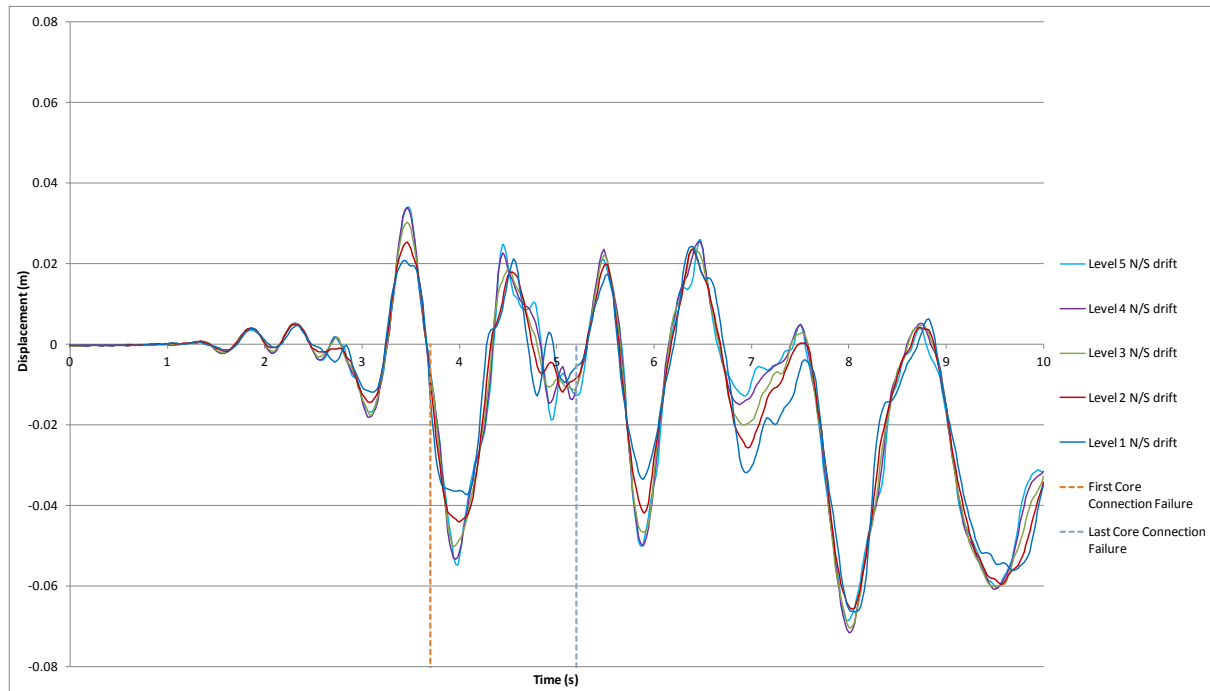


Figure L.4: Frame F north/south inter-storey displacements, Lyttelton, REHS

Inter-storey displacements for the perimeter frame lines 1 and 4 in the East/West direction are presented in Figure L.5 and Figure L.6 below.

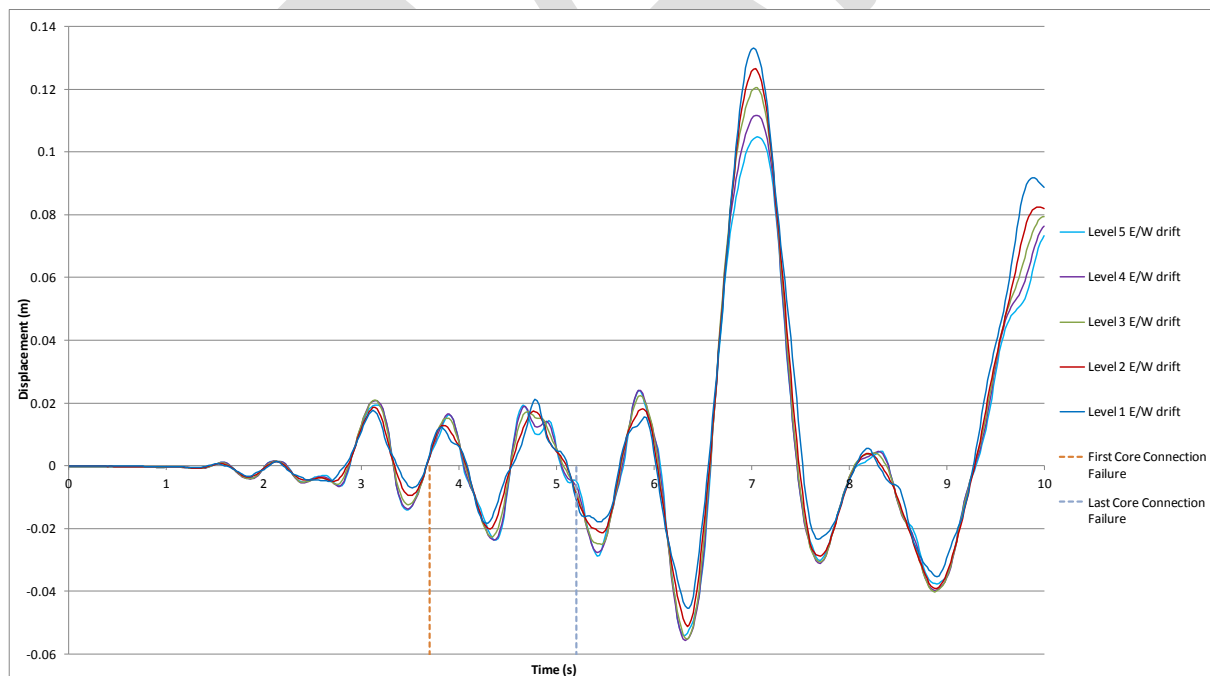


Figure L.5: Frame 1 east/west inter-storey displacements, Lyttelton, REHS

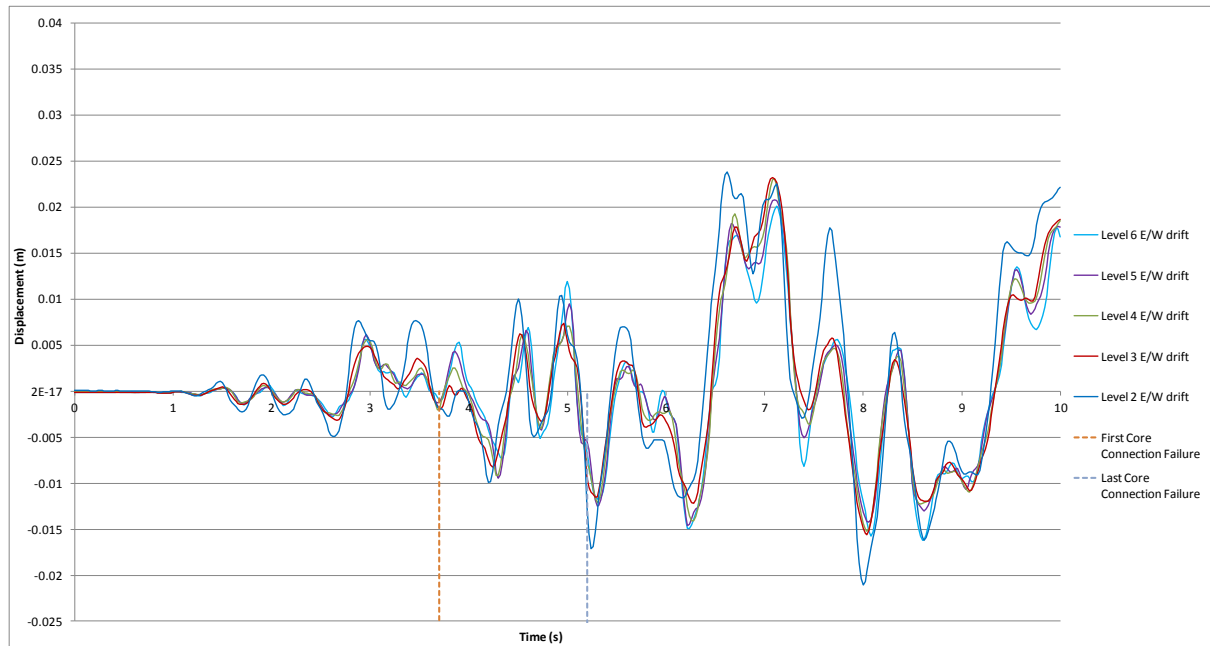


Figure L.6: Frame 4 east/west inter-storey displacements, Lyttelton, REHS

L.2 Diaphragm Connection Forces

Diaphragm connection forces are presented in Figure L.7 to Figure L.18 below. Note that moments are reported about the geometric centroid of the element being considered.

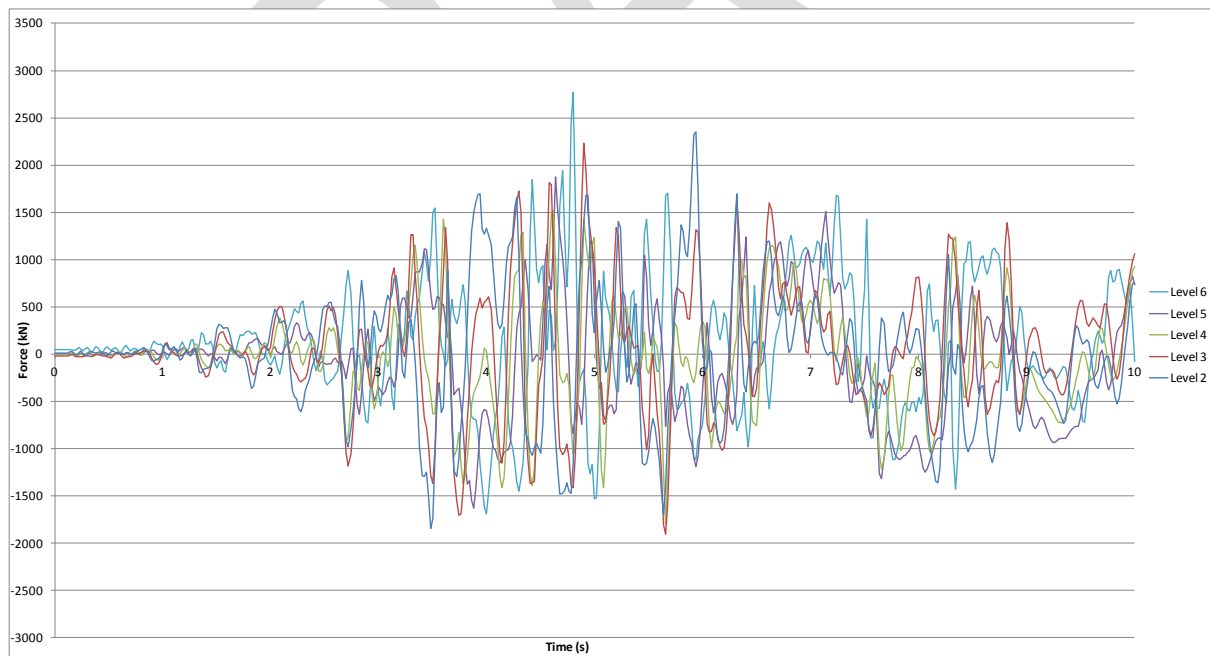


Figure L.7: North core total diaphragm north/south actions, Lyttelton, REHS

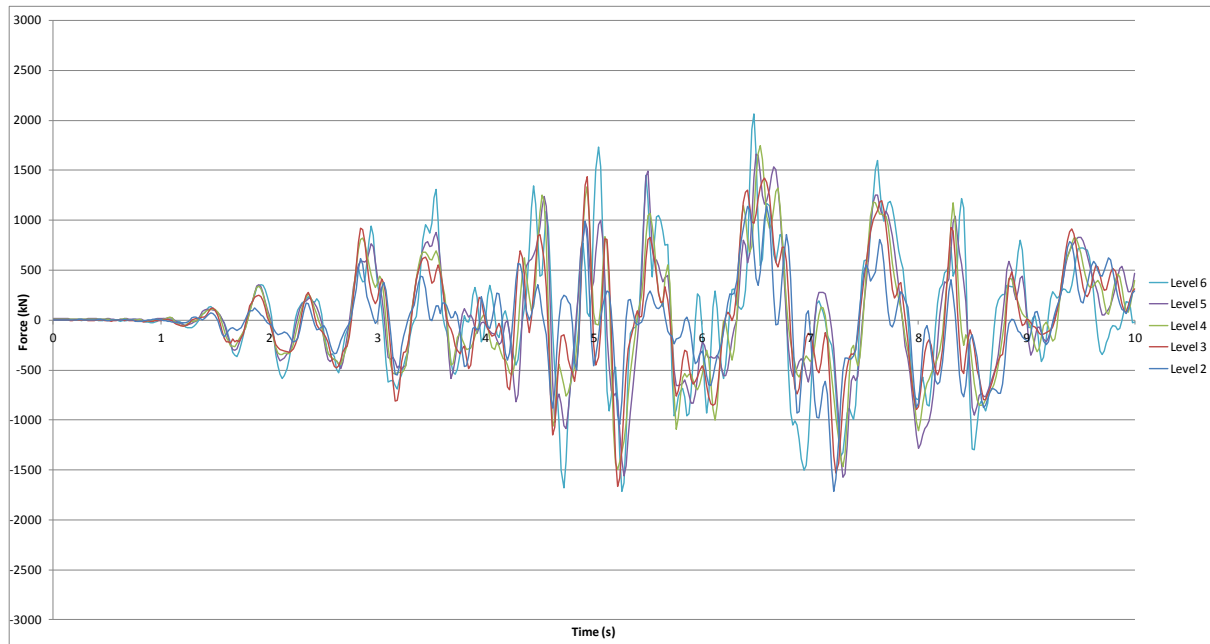


Figure L.8: North core total diaphragm east/west actions, Lyttelton, REHS

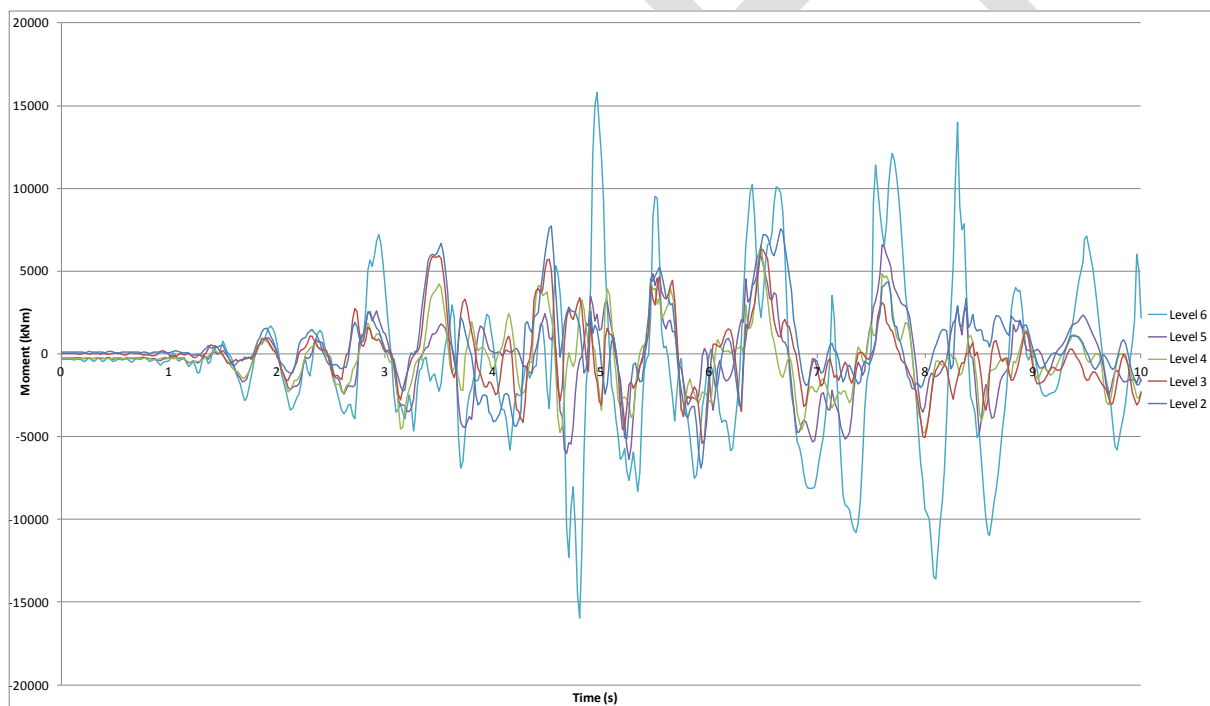


Figure L.9: North core total diaphragm in-plane moments, Lyttelton, REHS

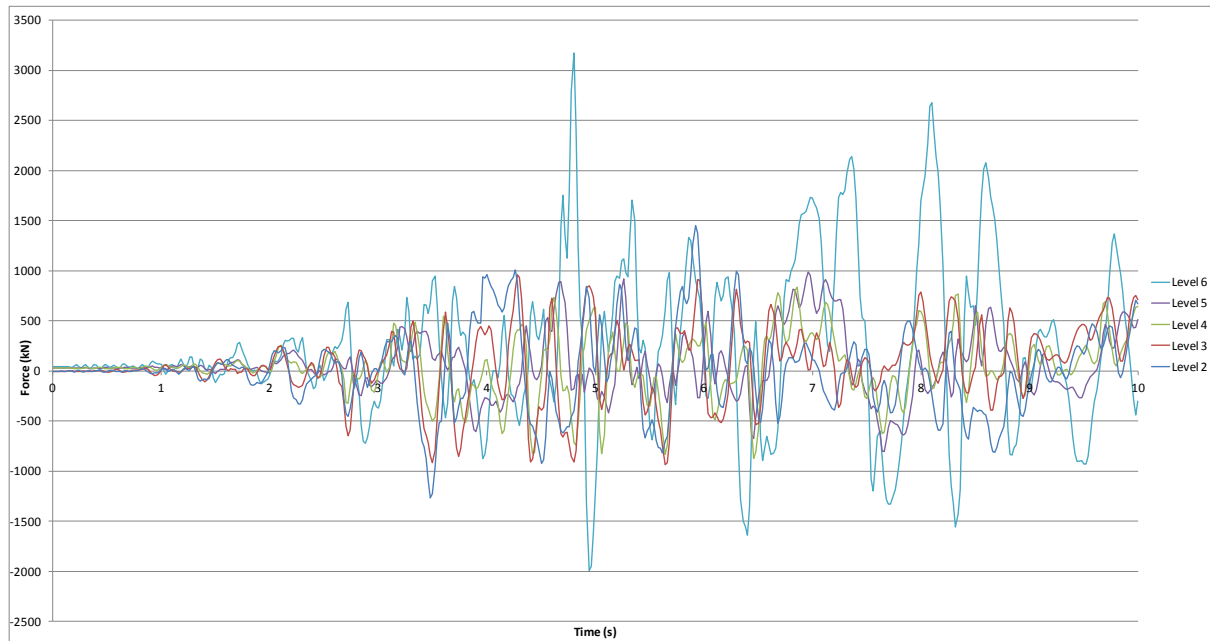


Figure L.10: North core Wall C diaphragm north/south actions, Lyttelton, REHS

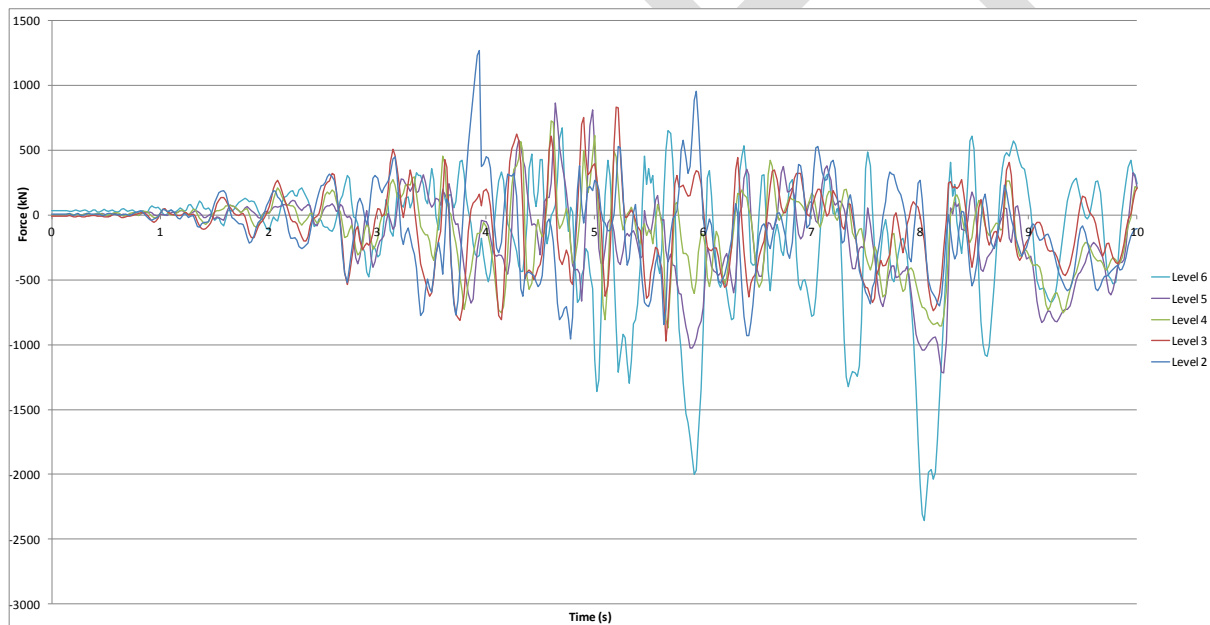


Figure L.11: North core Wall C/D diaphragm north/south actions, Lyttelton, REHS

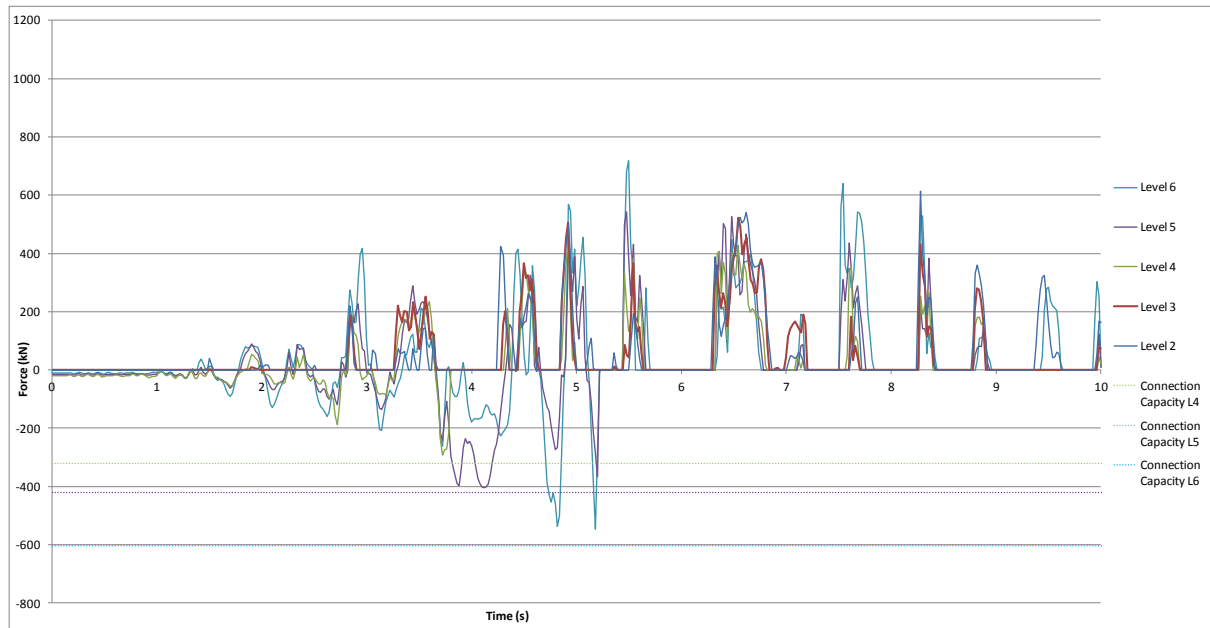


Figure L.12: North core Wall D diaphragm north/south actions, Lyttelton, REHS

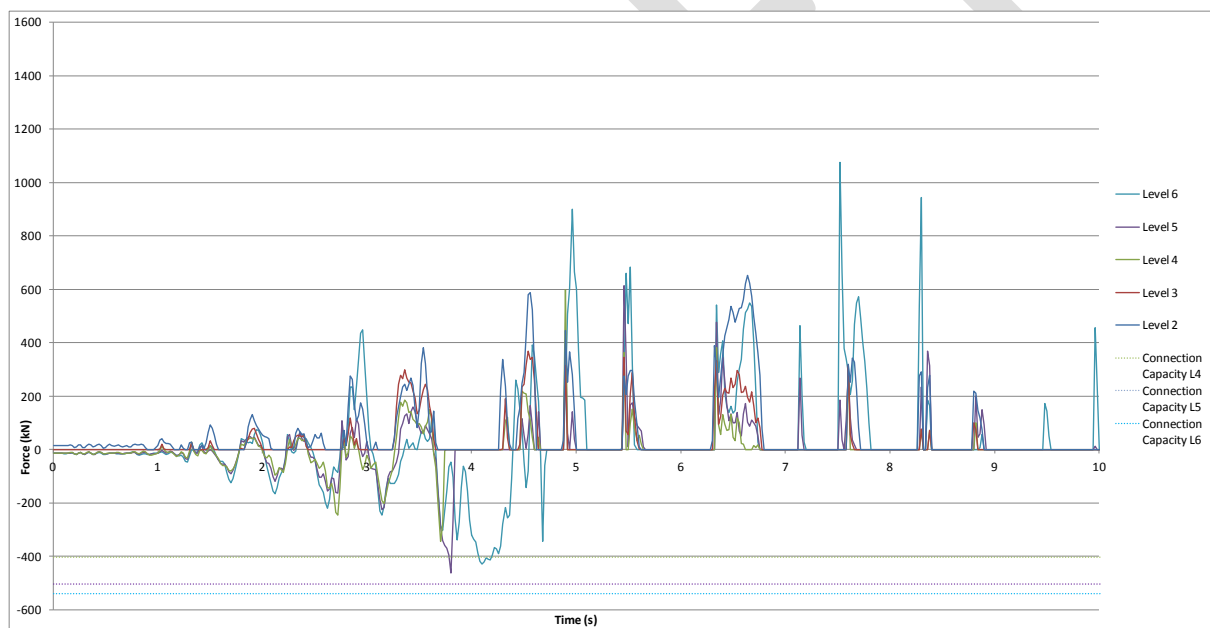


Figure L.13: North core Wall D/E diaphragm north/south actions, Lyttelton, REHS

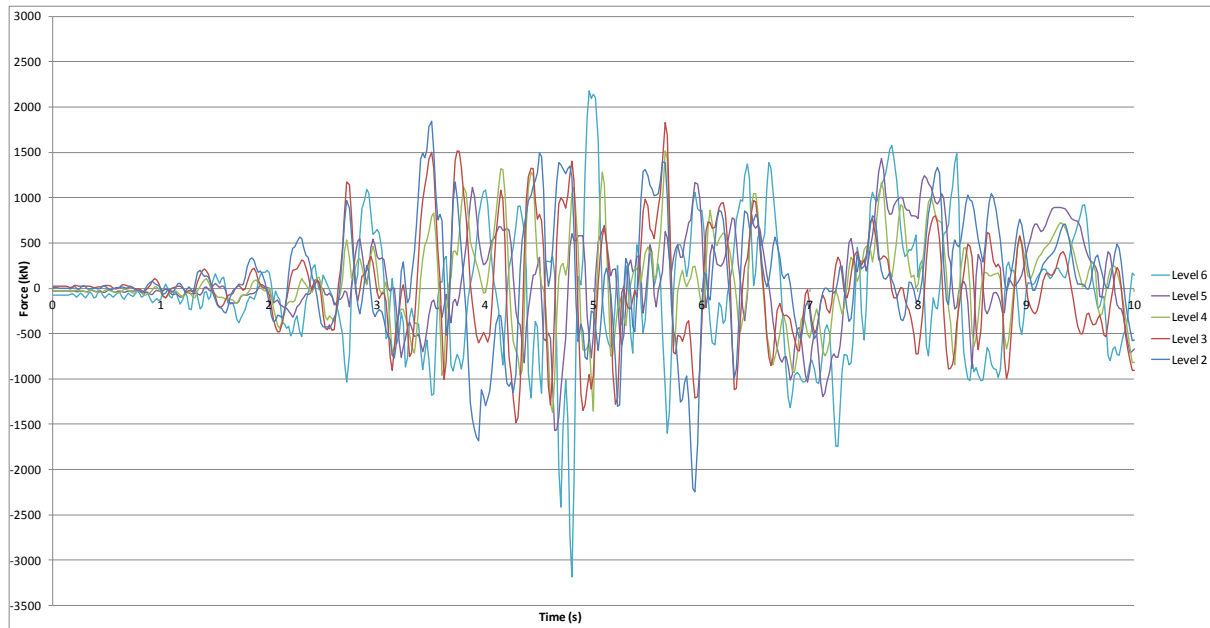


Figure L.14: North core Slab 4/C to C/D diaphragm north/south actions, Lyttelton, REHS

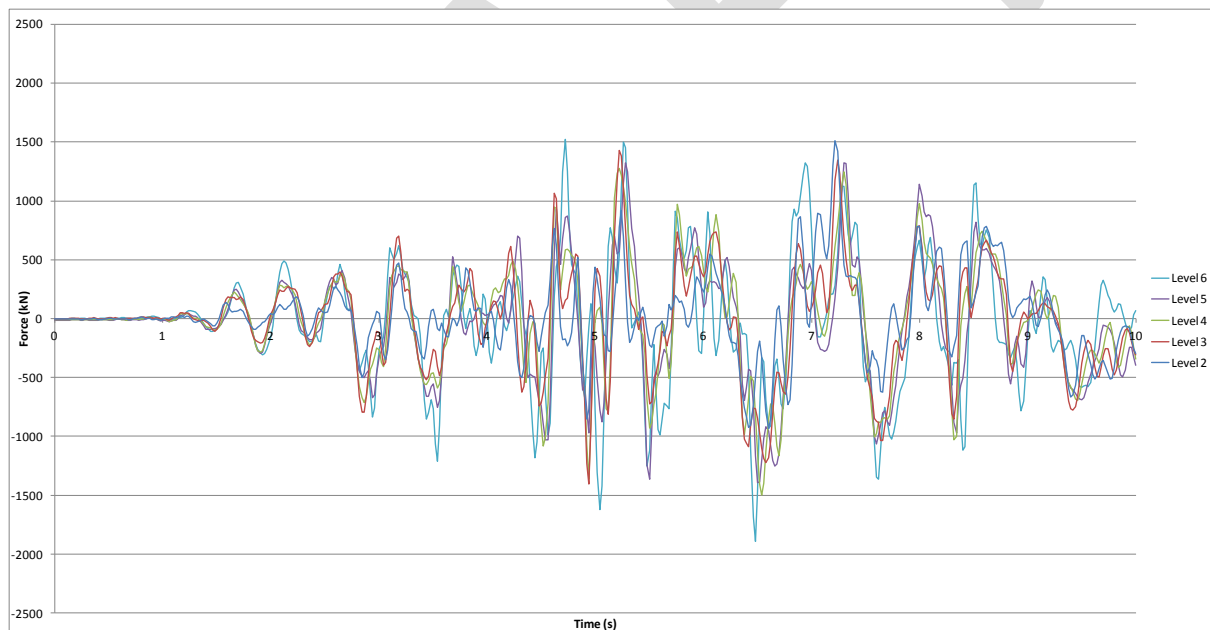


Figure L.15: North core Slab 4/C to C/D diaphragm east/west actions, Lyttelton, REHS

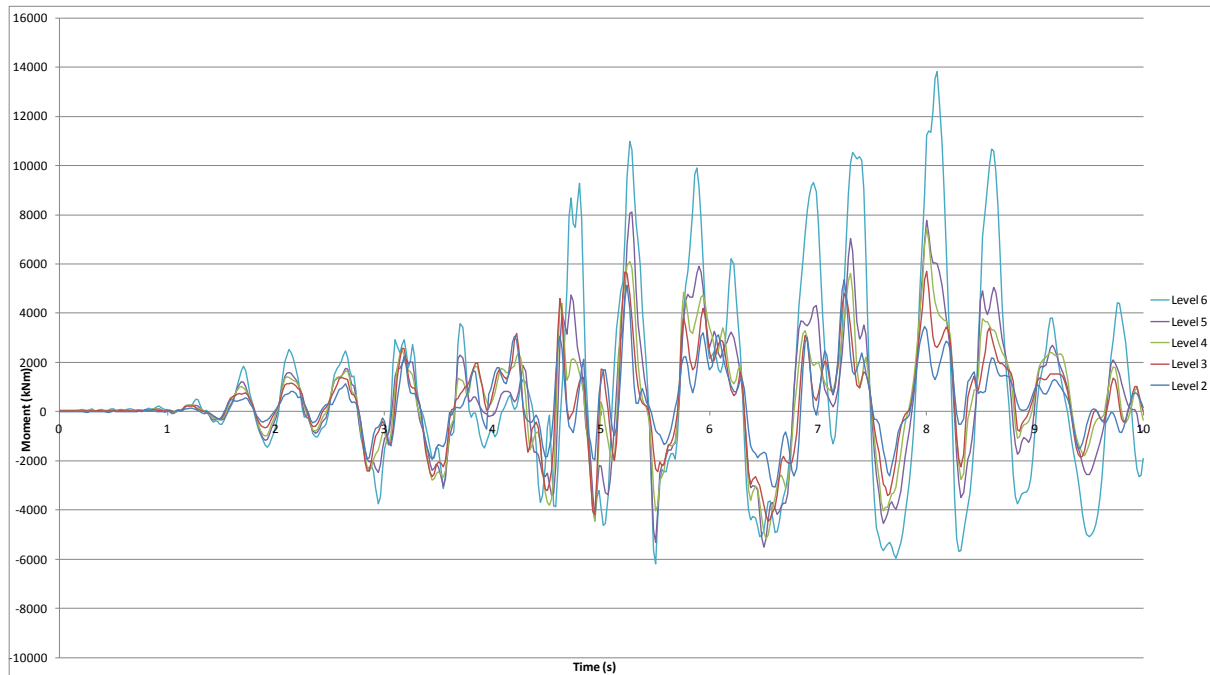


Figure L.16: North core Slab 4/C to C/D diaphragm in-plane moments, Lyttelton, REHS

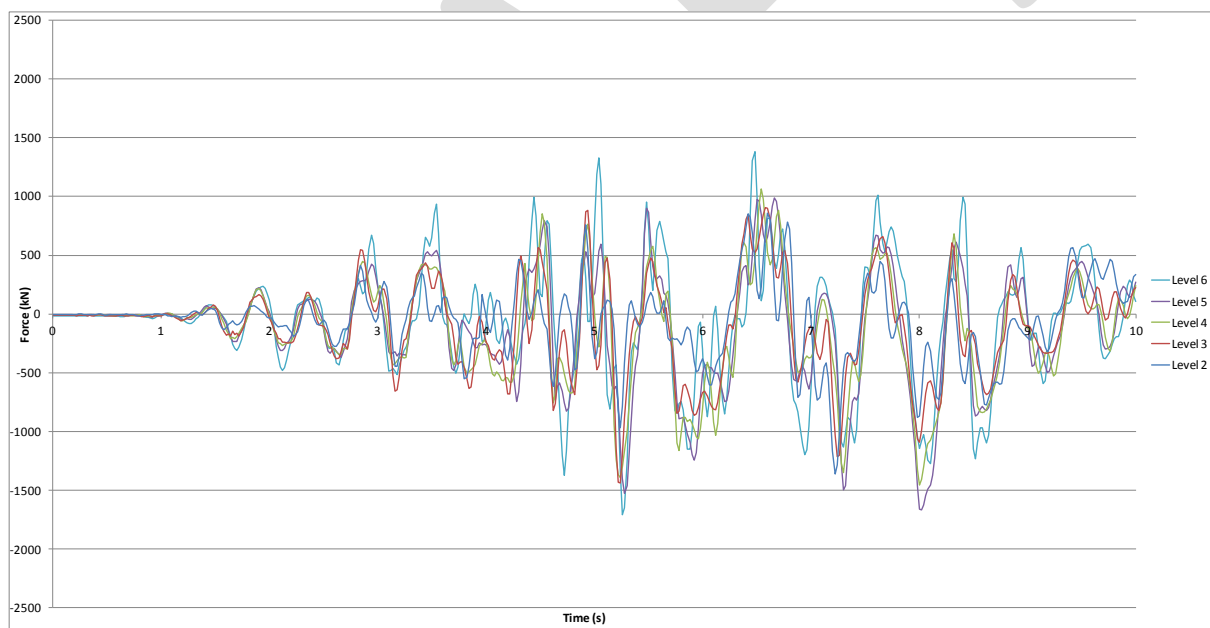


Figure L.17: North core Wall 5 diaphragm east/west actions, Lyttelton, REHS

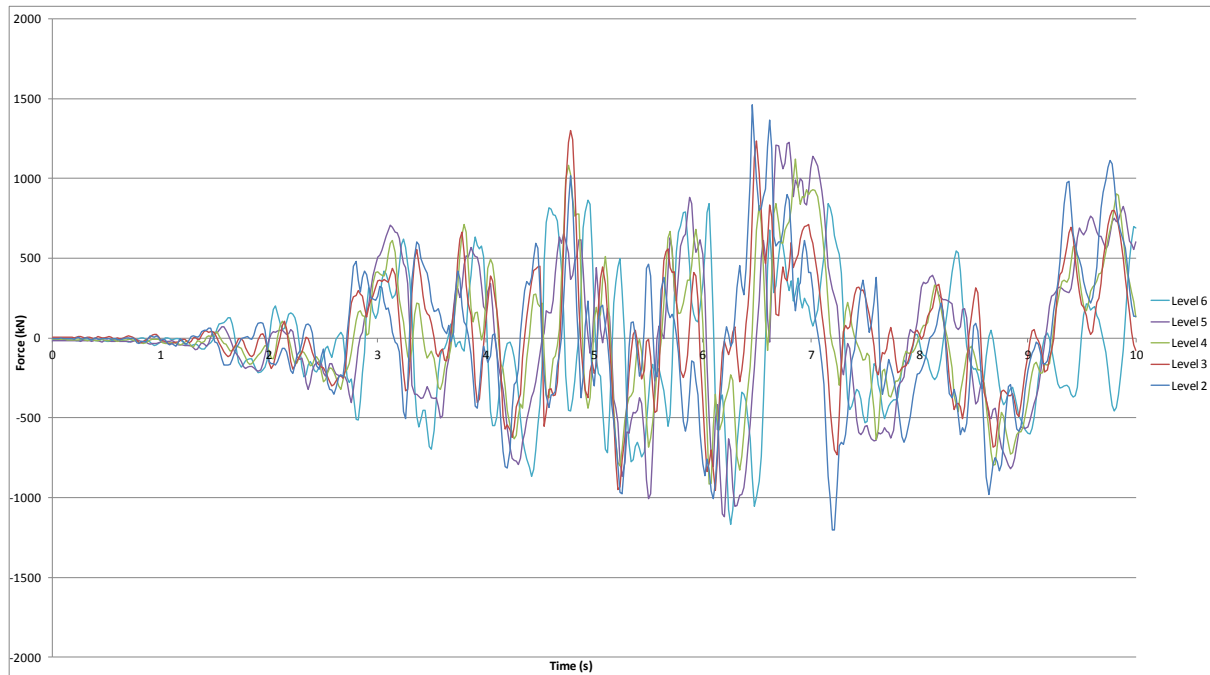


Figure L.18: South wall diaphragm east/west actions, Lyttelton, REHS

L.3 Column Hinge Actions

Figure L.19 to Figure L.23 present a selection of column hinge rotations, elongations, and concrete strains for a selected number of critical columns. Strains reported are the maximum that occur at the extreme concrete fibre. Plots are presented for individual columns and are orientated so that the top row of plots relate to the level 5 hinges with each row below corresponding to the hinges in the column below i.e. from the top level to the bottom level. Results presented are for the worst case hinge at each floor level, with hinge rotation and elongation shown in the left hand plot and hinge concrete strain shown in the right hand plot.

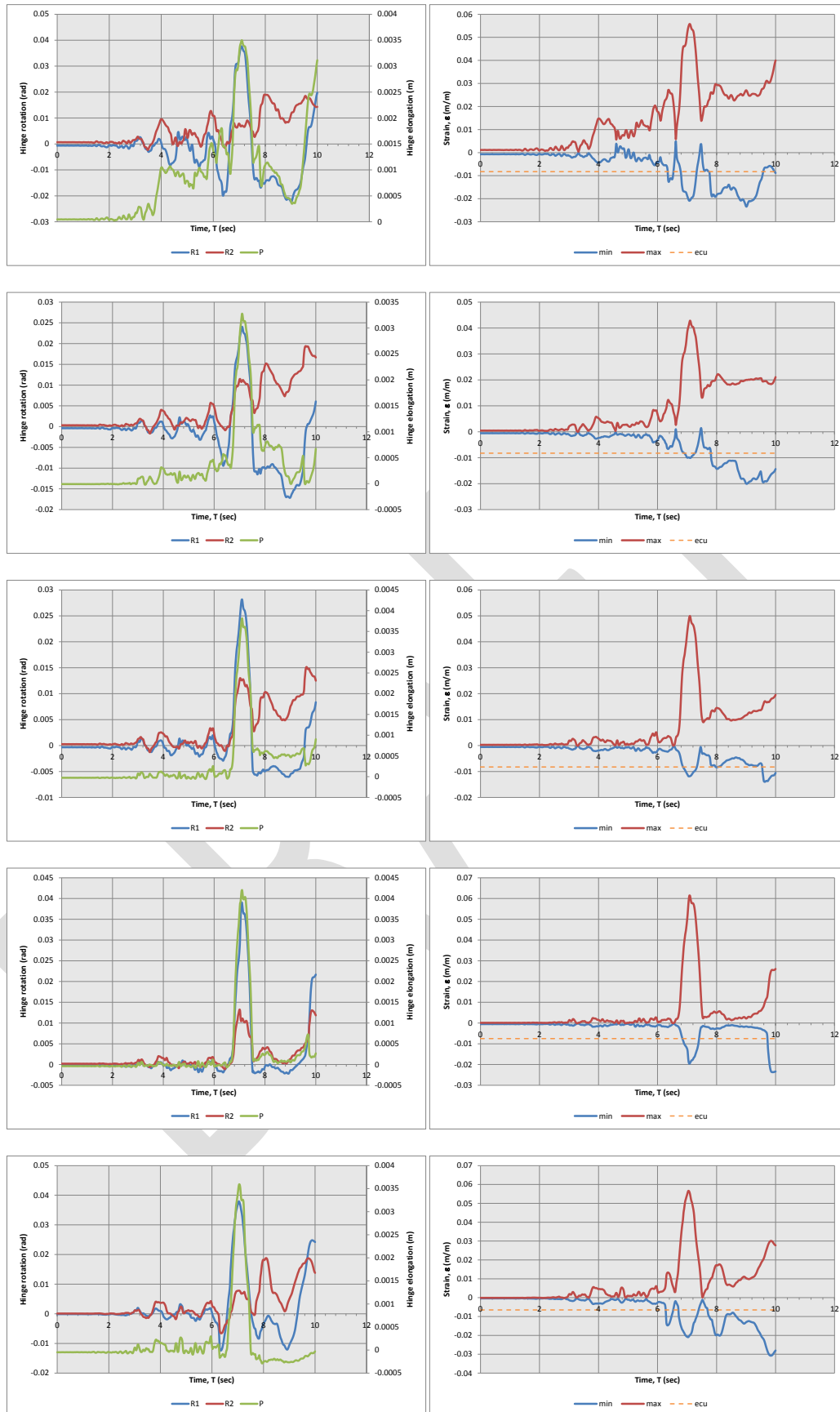


Figure L.19: Column F1 Levels 1 (bottom) to 5 (top) hinge actions, Lyttelton, REHS

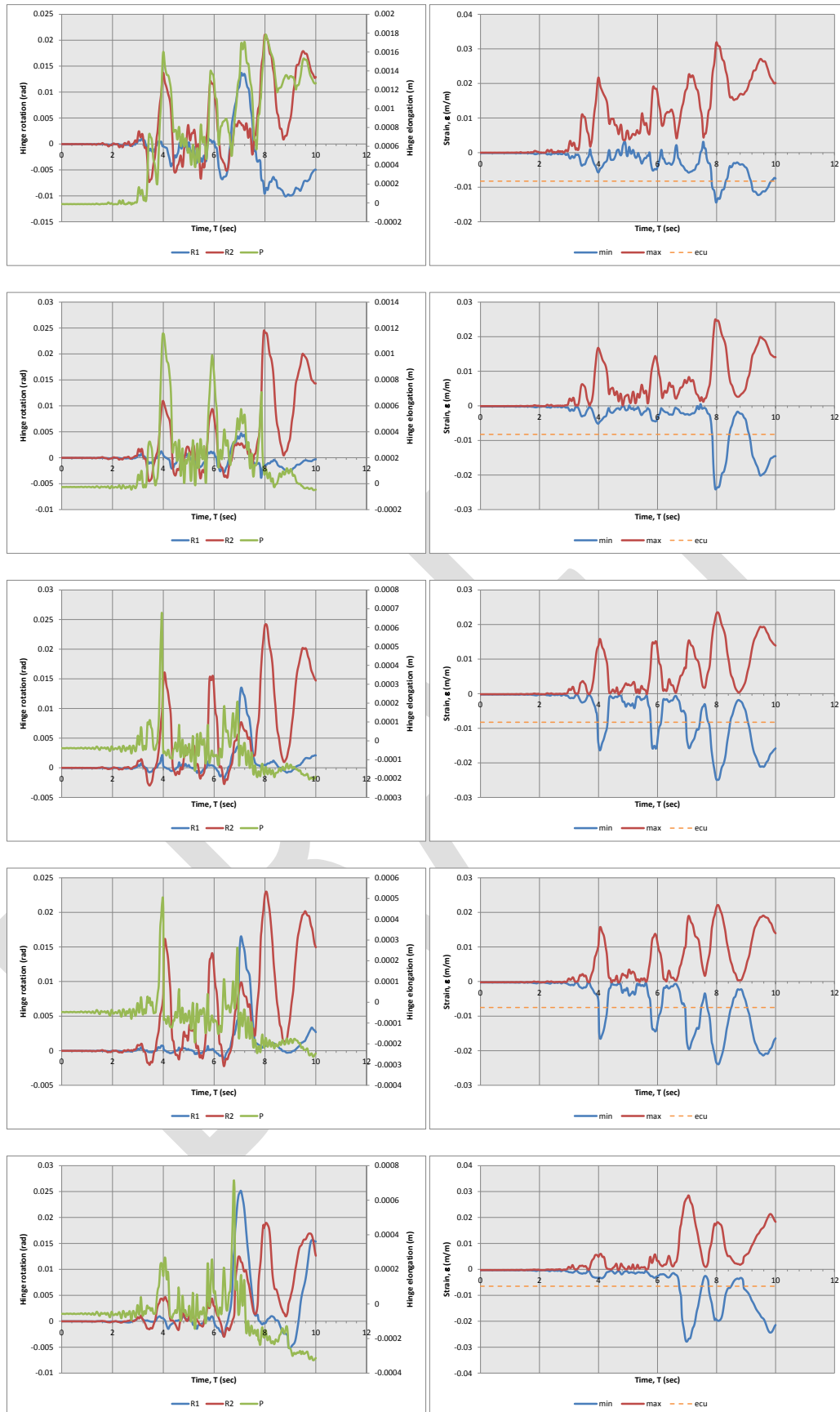


Figure L.20: Column F2 Levels 1 (bottom) to 5 (top) hinge actions, Lyttelton, REHS

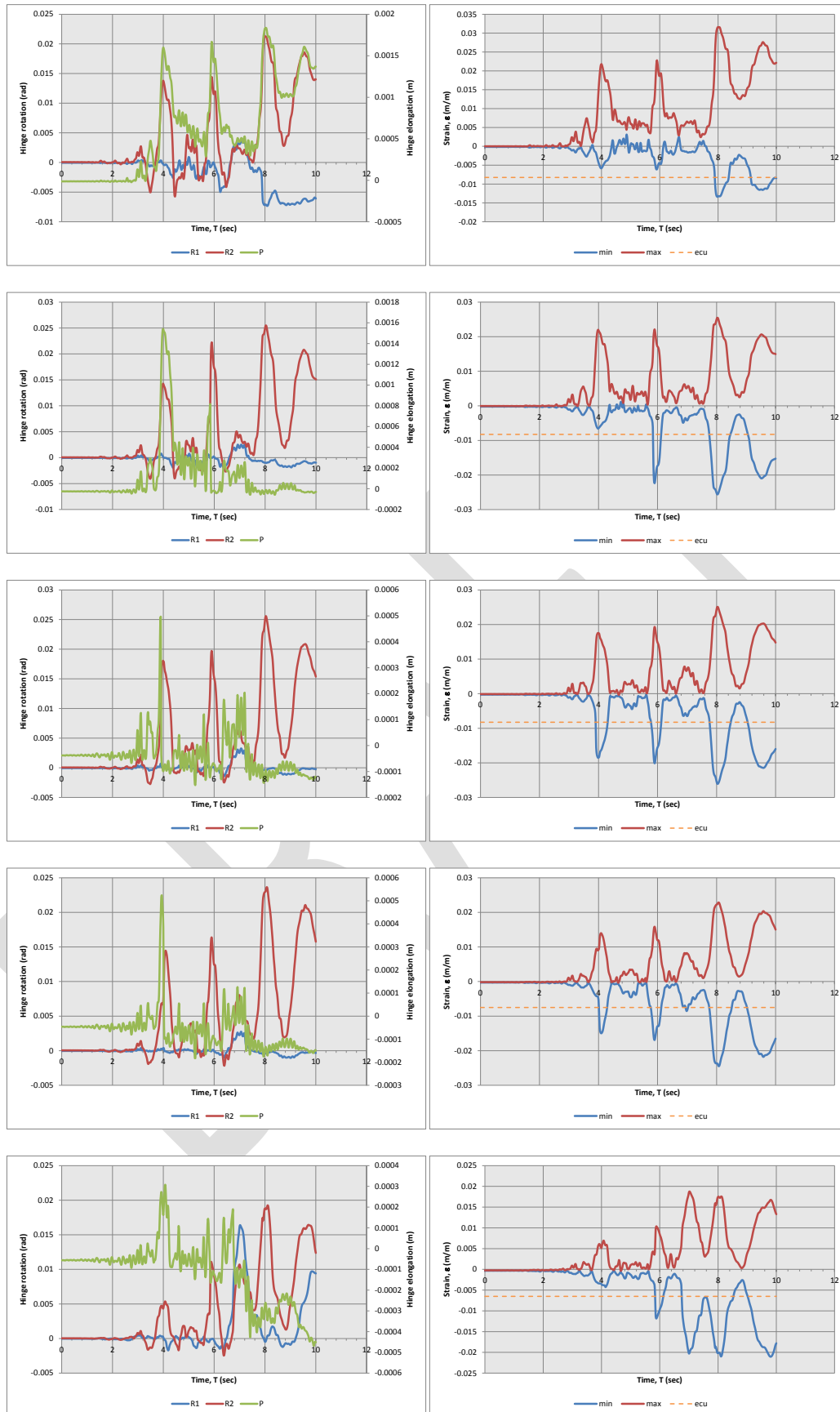


Figure L.21: Column F3 Levels 1 (bottom) to 5 (top) hinge actions, Lyttelton, REHS

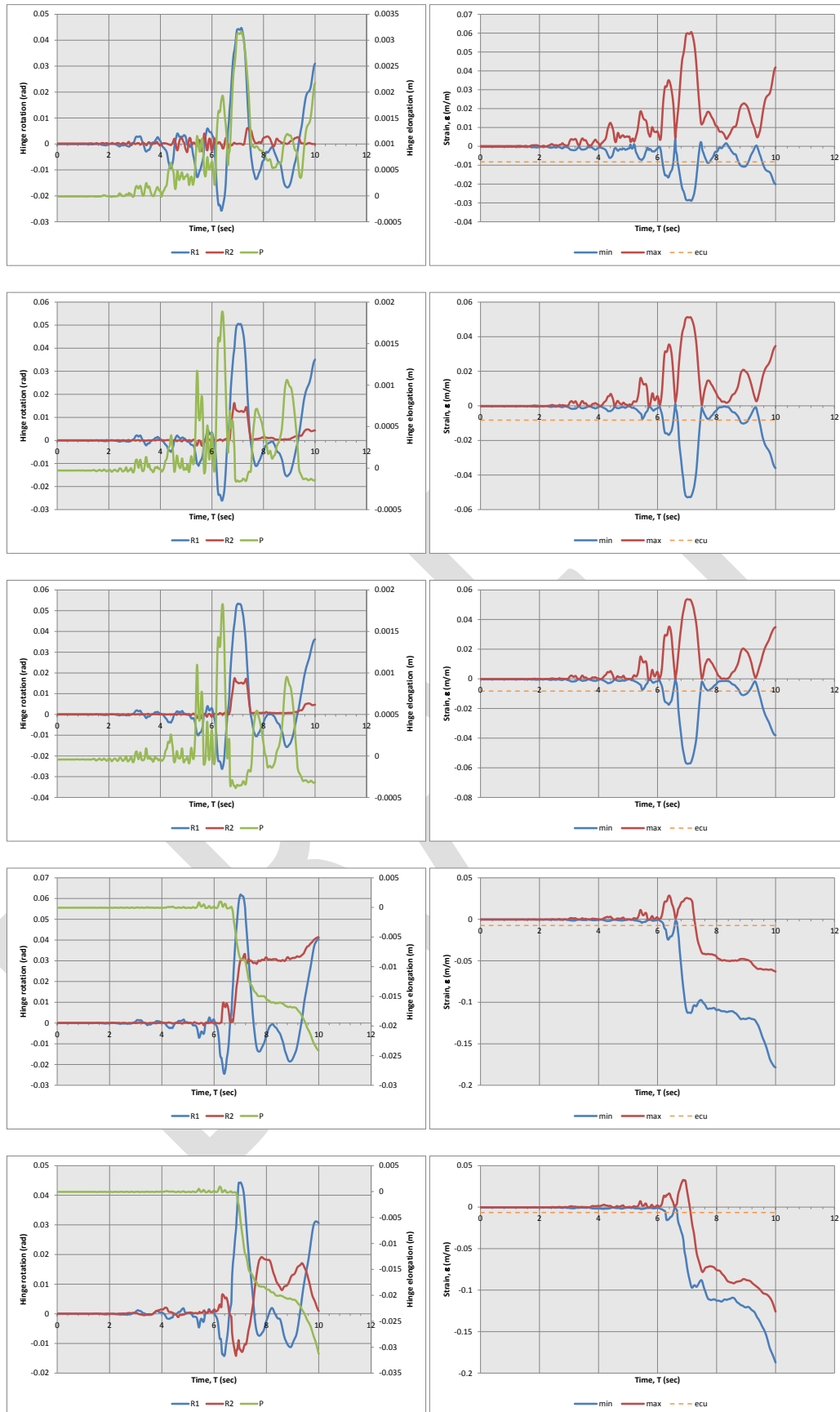


Figure L.22: Column C1 Levels 1 (bottom) to 5 (top) hinge actions, Lyttelton, REHS

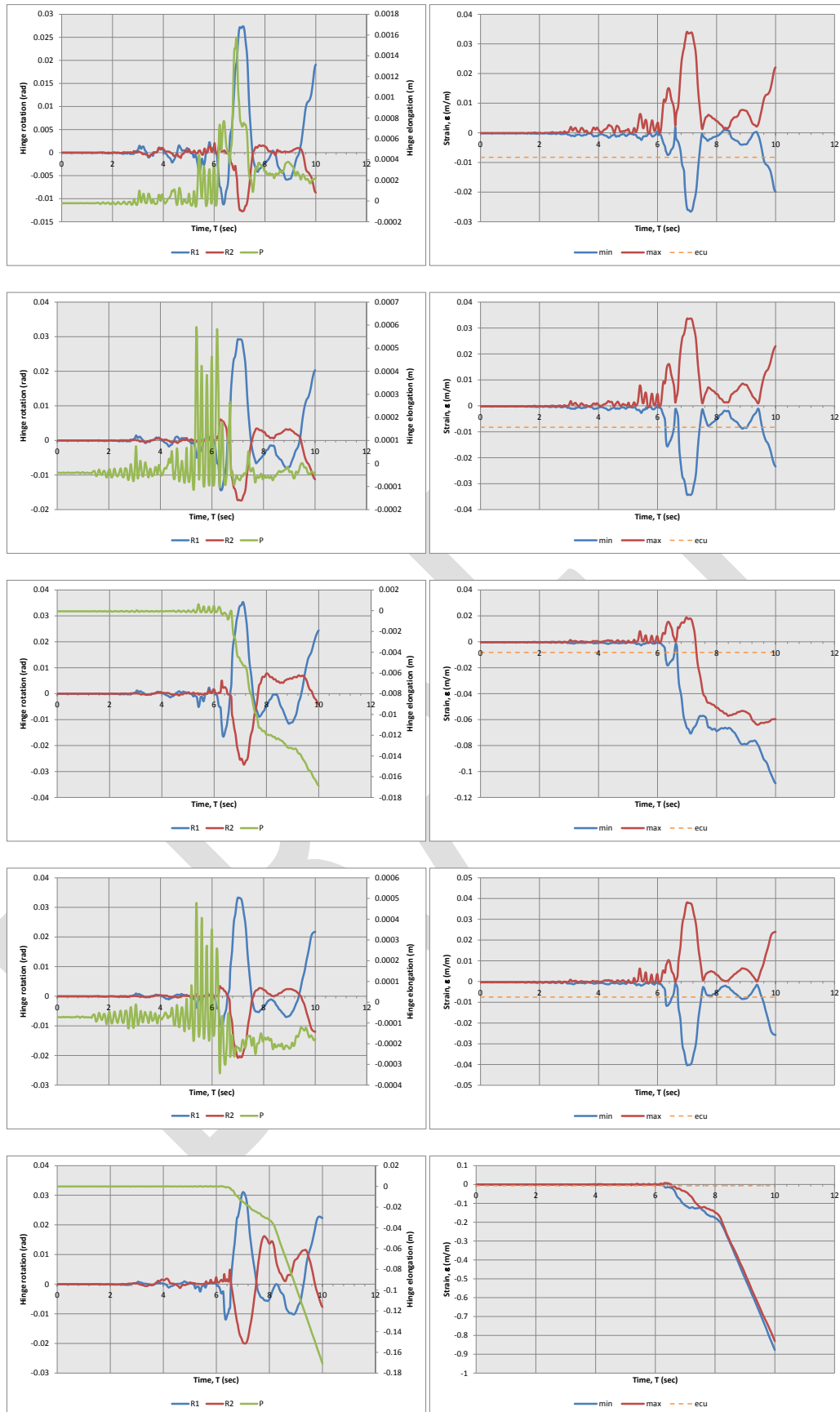


Figure L.23: Column C2 Levels 1 (bottom) to 5 (top) hinge actions, Lyttelton, REHS